AN APPROACH FOR LANDSLIDE RISK ASSESMENT BY USING GEOGRAPHIC INFORMATION SYSTEMS (GIS) AND REMOTE SENSING (RS)

A THESIS SUBMITTED TO
THE GRADUATE SCHOOL OF NATURAL AND APPLIED SCIENCES
OF
MIDDLE EAST TECHNICAL UNIVERSITY

BY

ARZU ERENER

IN PARTIAL FULFILLMENT OF THE REQUIREMENTS
FOR
THE DEGREE OF DOCTOR OF PHILOSOPHY
IN
GEODETIC AND GEOGRAPHIC INFORMATION TECHNOLOGIES

DECEMBER 2009

Approval of the thesis:

AN APPROACH FOR LANDSLIDE RISK ASSESMENT BY USING GEOGRAPHIC INFORMATION SYSTEMS (GIS) AND REMOTE SENSING (RS)

Submitted by **ARZU ERENER** in partial fulfillment of the requirements for the degree of **Doctor of Philosophy in Geodetic and Geographic Information Technologies Department, Middle East Technical University by,**

Prof. Dr. Canan Özgen _____
Dean, Graduate School of **Natural and Applied Sciences**

Assoc. Prof Dr. Mahmut Onur Karslıoğlu _____
Head of Department, **Geodetic and Geographic Information Technologies Department**

Assoc. Prof Dr. Şebnem Düzgün _____
Supervisor, **Geodetic and Geographic Information Technologies Department**

Examining Committee Members:

Prof. Dr. M. Semih Yücemen _____
Civil Engineering Dept., METU

Assoc. Prof. Dr. Şebnem Düzgün _____
Mining Engineering Dept., METU

Prof. Dr. Candan Gökçeoğlu _____
Geological Engineering Dept., Hacettepe University

Assoc. Prof. Dr. Zuhal Akyürek _____
Civil Engineering Dept., METU

Asst. Prof. Dr. Nejan Huvaj Sarıhan _____
Civil Engineering Dept., METU

Date: December 17, 2009

I hereby declare that all information in this document has been obtained and presented in accordance with academic rules and ethical conduct. I also declare that, as required by these rules and conduct, I have fully cited and referenced all material and results that are not original to this work.

Name, Last name : Arzu Erener

Signature :

ABSTRACT

AN APPROACH FOR LANDSLIDE RISK ASSESMENT BY USING GEOGRAPHIC INFORMATION SYSTEMS (GIS) AND REMOTE SENSING (RS)

Arzu Erener
PHd., Geodetic and Geographic Information Technologies
Supervisor : Assoc. Prof. Dr. Şebnem Düzgün

December 2009, 414 pages

This study aims to develop a Geographic Information Systems (GIS) and Remote Sensing (RS) Based systematic quantitative landslide risk assessment methodology for regional and local scales. Each component of risk, i.e., hazard assessment, vulnerability, and consequence analysis, is quantitatively assessed for both scales. The developed landslide risk assessment methodology is tested at Kumluca watershed, which covers an area of 330 km^2, in Bartın province of the Western Black Sea Region, Turkey.

GIS and RS techniques are used to create landslide factor maps, to obtain susceptibility maps, hazard maps, elements at risk and risk maps, and additionally to compare the obtained maps.

In this study, the effect of mapping unit and mapping method upon susceptibility mapping method, and as a result the effect upon risk map, is evaluated. Susceptibility maps are obtained by using two different mapping units, namely slope unit-based and

grid-based mapping units. When analyzing the effect of susceptibility mapping method, this study attempts to extend Logistic Regression (LR) and Artificial Neural Network (ANN) by implementing Geographically-Weighted Logistic Regression (GWR) and spatial regression (SR) techniques for landslide susceptibility assessment.

In addition to spatial probability of occurrence of damaging events, landslide hazard calculation requires the determination of the temporal probability. Precipitation triggers the majority of landslides in the study region. The critical rainfall thresholds were estimated by using daily and antecedent rainfalls and landslide occurrence dates based on three different approaches: Time Series, Gumble Distribution and Intensity Duration Curves.

Different procedures are adopted to obtain the element at risk values and vulnerability values for local and regional scale analyses. For regional scale analysis, the elements at risk were obtained from existing digital cadastral databases and vulnerabilities are obtained by adopting some generalization approaches. On the other hand, on local scale the elements at risk are obtained by high resolution remote sensing images by the developed algorithms in an automatic way.

It is found that risk maps are more similar for slope unit-based mapping unit than grid–based mapping unit.

Keywords: Risk Assessment, GIS, RS, Hazard, Susceptibility, Consequence Analysis, Mapping Unit, Mapping Method

ÖZ

COĞRAFİ BİLGİ SİSTEMLERİ VE UZAKTAN ALGILAMA KULLANILARAK HEYELAN RİSKİ BELİRLEME YAKLAŞIMI

Arzu Erener
Doktora, Jeodezi ve Coğrafi Bilgi Teknolojileri
Tez Yöneticisi : Doç. Dr. Şebnem Düzgün

Aralık 2009, 414 sayfa

Bu çalışma local ve bölgesel ölçekler için Coğrafi Bilgi Sistemlerine (CBS) ve Uzaktan Algılamaya (UA) dayalı sayısal ve sistematik bir risk metodolojisi geliştirmeyi amaçlamaktadır. Riskin her bir bileşeni olan tehlike, duyarlılık ve sonuç analizleri her bir ölçek için nitel olarak değerlendirilmiştir. Geliştirilen heyelan riski belirleme metodolojisi 330 km^2 alan kaplayan Türkiye'nin batı karadeniz bölgesinde bulunan Bartın ilinin Kumluca havzasında test edilmiştir.

Duyarlılık haritalarını oluşturmak için gerekli olan faktörleri ve duyarlılık, tehlike, risk altındaki elemanların belirlenmesi, risk haritalamaları ve elde edilen haritaların karşılaştırma aşamalarında CBS ve UA teknikleri kullanılmıştır. Bu çalışmada haritalama unitesi ve metodun heyelan duyarlılık haritalarına olan etkisi ve sonuç olarakta risk haritalarına olan etki değerlendirilecektir. Duyarlılık haritaları eğim birimi-esaslı ve hücre birimi-esaslı olmak üzere iki farklı haritalama biriminden elde edilmiştir. Oluşturulacak duyarlık haritalarına duyarlılık metodlarının etkisini araştırmak amaçlı, bu çalışma, Lojistik Regrasyon (LR) ve Yapay Sinir Ağları (YSA) metodlarını, Coğrafi Ağırlıklandırılmış Lojistik Regrasyon (CAR) ve Mekansal Regrasyon (MR) teknikleri ile iyileştirmiştir.

Heyelan tehlikesinin tahmininde mekansal olasılık yanında, zamansal olasılığın da belirlenmesi gerekmektedir. Çalışma alanında meydana gelen çoğu heyelan yağışların tetiklemesi ile meydana geldiği için, bu tez çalışmasında da yağışın neden olduğu heyelanlara odaklanılmıştır. Kritik yağış eşikleri günlük ve geçmiş yağış bilgisi ve heyelan olma tarihleri kullanılarak zaman serisi, gumble dağılımı ve siddet ve süre eğrileri kullanılarak üç farklı yaklaşımla tahmin edilmiştir.

Risk altındaki elemanların ve bunların duyarlılıklarının belirlenmesinde local ve bölgesel ölçekte farklı prosedürler uygulanmıştır. Bölgesel ölçekteki analizler için risk altındaki elemanlar var olan dijital kadastral veri tabanından elde edilmiştir ve duyarlılıklar bazı genelleştirme yaklaşımları ile oluşturulmuştur. Diğer taraftan, local ölçekte risk altındaki elemanlar geliştirilen algoritmalarla otomatik olarak yüksek çözünürlüğe sahip uzaktan algılama görüntülerinden elde edilmiştir.

Sonuç risk haritalarının karşılaştırılması sonrası, eğim birimi-esaslı risk haritalarının hücre birimi-esaslı risk haritalarına göre daha çok benzediği görülmüştür.

Anahtar Kelimeler: Risk Belirleme, CBS, UA, Tehlike, Duyarlılık, Sonuç Analizleri, Haritalama Birimi, Haritalama metodu.

To My Family

ACKNOWLEDGEMENTS

Many people have contributed to this thesis, and to the editing process. Were it not for the aid, support and encouragement of these people, this thesis would not be what it is. I would like to express my sincere gratefulness; nevertheless I know that the words are not enough to express their contributions and support.

Among all, I wish to express my wholehearted thanks to my supervisor, Assoc. Prof. Dr. Şebnem Düzgün, for her supervision, patience, wisdom, insight, guidance motivation and kindness in every stage of this thesis. Her guidance was most helpful during the development process of this thesis. I am grateful for her continuous support. She was not only a supervisor but also a friend, who will always be close to me in my future life.

I am grateful to the members of the examining committee, Prof Dr. Candan Gökçeoğlu, Assoc. Prof. Dr. Zuhal Akyürek for their support and invaluable comments. Moreover, I would like to express my thanks to my instructors Assoc. Prof Dr. Nurünnisa Usul and Assoc. Prof. Dr. Mahmut Karslıoğlu.

I would like to thank to Asst. Prof. Dr. İlkay Ulusoy in Electrical and Electronics Eng. Department and especially to Orsan Aytekin for his endless support at Matlab for the collaborated study.

I express my grateful acknowledgements to my close friends, who have been like my sisters, Ayten Koç and Gülcan Sarp. We were always together during our Ph.D. adventure and academic studies, and also very close friends. They always gave me positive energy with their presence in my life. Besides, I would also like to thank Ayten, again for her kind hospitality, kindness and patience during my stay at her room. Thank you Ayten, not living me alone in the last days of the thesis study.

Additionally, thanks for the unsleeping nights to help me to finish the last formats of the thesis. I would also like to show my deep gratitude to the GGIT family, Dilek Koç, Aslı Özdarıcı, and Reşat Gecen for the encouragement they offered throughout my academic study and my special appreciation goes to Pınar Aslantaş Bostan, Kıvanç Ertugay, Serkan Kemeç, for their help in different stages of the thesis and to Ali Özgün Ok for his technical supports and help.

I wish to express heartfelt thanks to my wonderfully supportive husband Gündüz Ayhan Erener for his endless love, motivation, understanding, and encouragement throughout my study. I always felt his support beside me in each step of my thesis from the beginning till the end. His support and sensibility gave me extra strength to overcome the difficulties I faced throughout my study. Furthermore, special thanks go to my little doughter Damla Melis Erener. She stayed away from me during the last four months of my thesis study and she was so brave during these days that she never cried behind me. I would also express my sincere thanks to my husband's family, Saliha and Raif Erener, who looked after my little daughter when I was away for my studies, for their understanding in these hard times.

Last, but not least, I owe my deepest gratitude to my parents Gönül and Hüseyin Daşcı, who encouraged me throughout my life with their endless patience and love and also with their unswerving support in each step of my life. Finally, a special thank you is reserved for my brother Mustafa Daşcı for his presence and support in all my life.

This research was supported by ÖYP research foundation No: BAP-08-11-DPT.2002K120510 and partly supported by TÜBİTAK 1002 project No: 109Y003. The author would also like to thank to the International Centre for Geohazards for financing her stay at Norwegian Geotechnical Institute (NGI).

TABLE OF CONTENTS

ABSTRACT iv
ÖZ vi
DEDICATION viii
ACKNOWLEDGMENTS ix
TABLE OF CONTENTS xi
LIST OF TABLES xvi
LIST OF FIGURES xix

CHAPTER

1. INTRODUCTION 1
1.1 Background 1
1.2 General Terminology 7
1.3 Purpose and Scope of Thesis 10
1.4 Outline of the Thesis 11

2. METHODOLOGY 13
2.1 Introduction 13
2.2 Data Collection 14
2.2.1 Data Collection and Processing for the Proposed Methodology 18
2.3 Hazard Assessment 23
2.3.1 Literature Review on Susceptibility Mapping 24
2.3.1.1 Susceptibility Mapping Methods 24
2.3.1.1.1 Qualitative Methods 26
2.3.1.1.2 Quantitative Methods 31
2.3.1.2 Mapping Unit 43

2.3.1.3 Scale 46
2.3.2 The Susceptibility Assessment Methods in the Thesis 48
2.3.2.1 Logistic Regression 50
2.3.2.2 Artificial Neural Network (ANN) 51
2.3.2.3 Spatial Models 54
2.3.3 Analysis of Triggers 59
2.3.3.1 Literature Review on Analysis of Triggers 59
2.3.3.2 The Proposed Approach for the Analysis of Triggers 62
2.3.3.2.1 Time Series Analyis of Rainfall pattern with ARIMA model fitting.. 63
2.3.3.2.2 Critical Rainfall analysis with Gumble Approach 64
2.3.3.2.3 Intensity Duration Curves 66
2.3.4 Hazard Assessment 66
2.3.4.1 Literature Review on Hazard Assessment 66
2.3.4.2 Obtaining Hazard Maps from Susceptibility and Trigger Analysis 68
2.3.5 Consequence Analysis 69
2.3.5.1 Literature Review of Consequence Analysis 69
2.3.5.1.1 Literature Review of Elements at Risk 69
2.3.5.1.2 Literature Review of Vulnerability Assessment 70
2.3.5.2 The Adopted Methodology for Consequence Analysis 74
2.3.5.2.1 The Adopted Methodology for Element at Risk 76
2.3.5.2.2 The Adopted Methodology for Vulnerability 76
2.3.6 Risk Analysis 77
2.3.6.1 Literature Review of Risk Analysis 77
2.3.6.2 The Adopted Methodology for Risk Analysis 81

3. IMPLEMENTATION FOR REGIONAL SCALE RISK ASSESSMENT .....
3.1 Description of the Study Area 84
3.2 Data Collection 90
3.3 Susceptibility Assessment 94
3.3.1 Data Preparation 95
3.3.1.1 Processing of Topographical Data 97
3.3.1.2 Processing of Geological Data 115

3.3.2 Analyzed Landslide Influencing Factors 123
3.3.3 Statistical Analysis of Data for Each Mapping Unit 124
3.3.3.1 Statistical Analysis of Data for Grid Mapping Unit 125
3.3.3.1.1 Assigning the Data Set to Grid-Based Mapping Unit 125
3.3.3.1.2 Pre-Analysis of Database 128
3.3.3.2 Statistical Analysis of Data for Slope Unit 135
3.3.3.2.1 Creation of Slope Unit-based Mapping Unit and Assigning the Data Set to Each Mapping Unit 135
3.3.3.2.2.Pre-Analysis of Data Set 141
3.3.4 Quantitative Susceptibility Mapping Models 144
3.3.4.1 Logistic Regression (LR) 144
3.3.4.2 Artificial Neural Network (ANN) 150
3.3.4.3 Spatial Regression (SR) 152
3.3.4.4 Geographically Weighted Regression 155
3.3.4.5 Performance Testing and Accuracy Assessment for Susceptibility Assessment Models 166
3.3.4.6 Field Evaluation of Landslide Susceptibility Maps 170
3.4 Comparison of Susceptibility Maps 175
3.5 Relative Comparison of the Susceptibility Maps with the Landslide Map in terms of Accuracy 184
3.5.1 Comparison of the Similarity Between the Prediction Maps 187
3.6 Analysis of Triggers 192
3.6.1 Analysis of Data used for Triggering Analysis 194
3.6.1.1 Determination of Critical Rainfall Thresholds 201
3.6.1.2 Time Series Analyis of Rainfall Pattern with ARIMA Model Fitting . 201
3.6.1.3 Critical Rainfall analysis with Gumble Distribution Approach 208
3.6.1.4 Antecedent Rainfall Model Construction and the Threshold Approach 210
3.6.1.4.1 Critical Rainfall Threshold for Antecedent Days by Gumble Distribution Approach 213
3.6.1.4.2 Estimation of Threshold Values by Using Intensity-Duration Curves 214

3.6.1.5 Evaluation Rainfall Thresholds obtained from Various Methods..... 216
3.7 Hazard Assessment 218
3.8 Consequence Analysis 223
3.8.1 Probability of Spatial impact..... 224
3.8.2 Probability of Temporal Impact 225
3.8.3 Vulnerability Analysis..... 225
3.8.4 Element at Risk 226
3.9 Risk Assessment..... 235
3.9.1 Risk Analysis for Property 234
3.9.2 Risk Analysis for Loss of Life 241
3.10 Comparison of Risk Maps..... 247

4. IMPLEMENTATION FOR LOCAL SCALE RISK ASSESSMENT 253
4.1 Determination of High Hazard Zone 253
4.2 Characteristics of the Study Area: Hepler Village..... 256
4.3 Data Acquisition and Preparation 256
4.4 Consequence Analysis 262
4.4.1 Probability of Spatial Impact 262
4.4.2 Identification of Elements at Risk by Remote Sensing..... 267
4.4.3 Vulnerability Assessment..... 278
4.4.4 Risk Assessment..... 281
4.4.4.1 Risk Assessment for Property 281
4.4.4.2 Risk Assessment for Loss of Life 287
4.5 Comparison of Risk Maps on Local Scales 292

5. CONCLUSION..... 304
5.1 Overview of the Results 304
5.2 Conclusions 314
5.3 Future Work and Recommendations..... 317

REFERENCES 320

APPENDICES

APPENDIX A 360
APPENDIX B 367
APPENDIX C 379
APPENDIX D 386
APPENDIX E 391
LIST OF ABBREVIATIONS 408

VITA 412

LIST OF TABLES

TABLES

Table 1.1 Different risk and hazard definitions proposed in the literature 9
Table 2.1 Review of geomorphologic analysis for susceptibility mapping..... 26
Table 2.2 Review of index based analysis for susceptibility mapping 27
Table 2.3 Review of bivariate susceptibility mapping methods. 32
Table 2.4 Review of discriminant analysis for susceptibility mapping 35
Table 2.5 Review of logistic regression and conditional probability for Susceptibility mapping in the literature 36
Table 2.6 Review of ANN for susceptibility mapping in the literature..... 40
Table 2.7 Review of Geotechnical slope stability analysis in the literature 41
Table 2.8 Comparison of the main susceptibility mapping methods on different mapping scales (Huabin et al., 2005; Glade, 2005) 48
Table 2.9 Heuristics proposed in the literature 53
Table 2.10 The existing hazard mapping approach in the literature..... 67
Table 2.11 Landslide risk assessment methods 78
Table 3.1 Characteristics of data for Kumluca basin..... 92
Table 3.2 RMSE of DEM 100
Table 3.3 Variables considered as landslide influencing factors..... 123
Table 3.4 Correlation matrix for continuous landslide influencing factors..... 130
Table 3.5 Correlation between nominal landslide influencing factors 131
Table 3.6 Logistic regression modeling for correlation analysis between Continuous and nominal landslide influencing factors..... 133
Table 3.7 Multicollinearity analysis of factors 142
Table 3.8 LR Model test results for grid-based and slope unit-based mapping units. 146
Table 3.9 The statistics of the susceptibility models for different mapping units 148
Table 3.10 Descriptive statistics of GWR parameter estimations for grid-based mapping unit 159

Table 3.11 Descriptive Statistics of GWR parameter estimations for slope unit-basedmapping unit 160
Table 3.12 Area under the curve for grid-based mapping unit 169
Table 3.13 Area under the curve for slope-based mapping unit 170
Table 3.14 Error Matrix resulting from the Model prediction classification..... 172
Table 3.15 Paired samples correlations for cell-based and slope unit-based model pairs..... 188
Table 3.16 Paired samples test..... 189
Table 3.17 Characteristics of meteorological stations which are available for analysis..... 197
Table 3.18 Stationary analysis of data 203
Table 3.19 Auto correlation values of daily rainfall 205
Table 3.20 Maximum Likelihood Estimation 206
Table 3.21 The outliers detected for the model ARIMA(1,0,0) 207
Table 3.22 Calculated Plot positions (pp) for daily precipitation of landslides..... 208
Table 3.23 Rainfall values estimated from the Gumbel distribution diagram for different return periods for daily data 210
Table 3.24 The rainfall values for different Return Periods, RP (year)..... 214
Table 3.25 Absolute antecedent rainfall from 1 to 60 days and corresponding return periods for 16 landslide events 216
Table 3.26 The critical rainfall thresholds obtained from Gumbel analytical process and Intensity Duration Curves. 218
Table 3.27 Model summary of logistic regression for rainfall values greater than the thresholds 219
Table 3.28 Parameters required for the creation of probabilistic Hazard Maps 220
Table 3.29 The statistics obtained from the hazard maps 224
Table 3.30 Classification of economic value with loss estimation of the principal elements at risk in TL/pixel 228
Table 3.31 Risk calculation for property. Hazard values are mean value and loss value according to Table 3.30. 236
Table 3.32 The statistics of the property risk maps for different methods and mapping units (TL/per pixel) 241
Table 3.33 Risk calculation for life. Hazard values are mean value obtained from

Table 3.30 242
Table 3.34 The statistics of the risk maps of life for different methods and mapping units (Loss of Life/per pixel) 246
Table 4.1 Characteristics of data for local slope analysis 256
Table 4.2 Accuracy Components 277
Table 4.3 Damage Probability Matrix for Building 279
Table 4.4 Damage Probability Matrix for Road 279
Table 4.5 Damage Probability Matrix for Loss of Life 281
Table 4.6 The statistics of the risk maps of loss of property for different methods and mapping units 286
Table 4.6 The statistics of the risk maps of loss of life for different methods and mapping units (Loss of Life/Pixel) 292
Table A-1 The Q-Q plot for factors considered in grid-based mapping unit..... 261
Table A-2. The Q-Q plot for factors considered in slope unit-based mapping unit 262
Table E-1. Overland Flow Manning's n Roughness Value. 1Adapted from COE, 1997..... 391

LIST OF FIGURES

FIGURES

Figure 1.1 Frequency of natural disasters in the world (OFDA/CRED, 2007) 1
Figure 1.2 Frequency of natural disasters in Turkey (OFDA/CRED, 2007) 2
Figure 1.3 Damages caused by disasters in Turkey (Ergunay et al., 2003)..... 3
Figure 1.4 Basic steps in landslide risk assessment..... 8
Figure 2.1 Basic steps in landslide risk assessment..... 14
Figure 2.2 Schematic overview of the data sets (adopted from van Westen et al., 2006) involved in landslide risk assessment..... 15
Figure 2.3 Data collection and data processes framework 19
Figure 2.4 Landslide susceptibility assessment classifications..... 25
Figure 2.5 Grid or raster representation of the terrain at Kumluca watershed, Bartın (Turkey) 44
Figure 2.6 Unique condition unit of the of the Riomaggiore catchment Northern Apennines (Italy) (Ermini et al., 2005)..... 45
Figure 2.7 Slope unit representation of the terrain at Kumluca watershed, Bartın (Turkey) 46
Figure 2.8 Data characteristics for different mapping scales..... 47
Figure 2.9 The adopted procedure for landslide susceptibility assessment..... 50
Figure 2.10 Architecture of the ANN used in this thesis..... 52
Figure 2.11 Delaunay triangularization approach..... 56
Figure 2.12 Conceptual 3-D vulnerability framework (Düzgün and Lacasse, 2005)73
Figure 2.13 The adopted conceptual 3-D vulnerability framework (adopted from Düzgün and Lacasse, 2005) 75
Figure 2.14 Example of possible calculation methods for specific risk to buildings and persons in buildings (van Westen et al., 2005) 80
Figure 3.1 Study region, Kumluca watershed, in the south-western part of Bartin city and the map showing the landslide locations with two types of

slides, Type 1: Non active and depth >5m, Type 2: Active and depth >5m. 84
Figure 3.2 The damages observed at the rural settlements during field surveys 85
Figure 3.3 The damages observed at the road embankments and roads 86
Figure 3.4 Generalized geological map of the study area adopted from Ercanoğlu, 2005 (simplified from Timur et al., 1997)..... 87
Figure 3.5 A small site in the south-west part of the study region vulnerable to both flooding and landslides with different types (A: mass flow, B: debris flow). 88
Figure 3.6 Landslides in Bartın Kumluca region: a. rotational slide, b. debris flow, c. shallow complex slide, d. rotational slide 89
Figure 3.7 Interpretation of landslide boundaries from aerial photo 91
Figure 3.8 The procedure followed for susceptibility assessment methodology.... 95
Figure 3.9 The main input data set and processed data to obtain influencing factors 96
Figure 3.10 The contour map of the study area 97
Figure 3.11 DEM of the study region overlaid with the landslide locations and the frequency distribution of values..... 98
Figure 3.12 Histogram showing the relationship between elevation and landslide frequency..... 99
Figure 3.13 Slope map of study region overlaid with landslide locations b. frequency distribution of slope variable 101
Figure 3.14 Histogram showing the relationship between slope angle and landslide frequency..... 102
Figure 3.15 a. Aspect map of the study region and b. frequency distribution of values 103
Figure 3.16 Histogram showing the relationship between aspect and landslide frequency..... 104
Figure 3.17 The positive and negative curvature..... 104
Figure 3.18 Statistics for curvature, plan curvature and profile curvature map (%) 105
Figure 3.19 Histogram showing the relationship between curvature and landslide frequency..... 106

Figure 3.20 Topographic wetness index (TWI) overlaid with landslide locations zoomed in the north-eastern part of study region 107
Figure 3.21 Histogram showing the relationship between curvature and landslide frequency..... 108
Figure 3.22 a. Road network map overlaid with the villages and b. Stream network map showing the names of rivers..... 109
Figure 3.23 a. Distance to road network map and b. Frequency distribution of distance to road network 110
Figure 3.24 a. Distance to stream network map and b. Frequency distribution of distance to stream network..... 110
Figure 3.25 a. Density of Road Network map b. Frequency distribution of Road Density 111
Figure 3.26 a. Density of stream network map b. Frequency distribution of stream density 111
Figure 3.27 Histogram showing the relationship between distance to road network and landslide frequency 112
Figure 3.28 Histogram showing the relationship between distance to stream network and landslide frequency 112
Figure 3.29 Histogram showing the relationship between road density and landslide frequency 113
Figure 3.30 Histogram showing the relationship between stream network density and landslide frequency 113
Figure 3.31 a. Vegetation Index Map of the study region calculated from Aster Image b. The percent of vegetation cover after classification of data into 2 classes with threshold 0.3. 114
Figure 3.32 Histogram showing the relationship between NDVI and landslide frequency..... 115
Figure 3.33 Geological map of the study region overlaid with road network and fault lines. The legend refers to 1: Alluvial, 2: Andesite, 3: Sandstone-Mudstone, 4: Marl 5: Limestone, 6: Conglomerate (GDMRE, 2007) 116
Figure 3.34 Histogram showing the relationship between Geologic units and landslide frequency 116

Figure 3.35 Fault line map with three different types where Type 1 represents the actual faults, Type 3 and 4 represents half and half approximate fault, overlaid by the landslide map 117
Figure 3.36 a. Distance to fault line map b. Frequency distribution of distance to fault line 118
Figure 3.37 Histogram showing the relationship between distance to fault lines and landslide frequency 118
Figure 3.38 Soil Map showing 5 different types in the study region..... 119
Figure 3.39 Histogram showing the relationship between soil type and landslide frequency where: 1= Alluvial Soil, 2= Brown Forest Soil, 3= Colluvial Soil, 4= Grey Brown Podzol Soil, 5= Brown forest soil without lime 119
Figure 3.40 a. Land use map of the study region b. The percent frequency of land-use types..... 120
Figure 3.41 Histogram showing the relationship between soil type and landslide frequency where: 1= Rock And Debris, 2= River Flooding Regions, 3= Dry Farming, 4= Forest, 5= Settlement..... 120
Figure 3.42 Soil depth map showing 4 different classes of thickness 121
Figure 3.43 Histogram showing the relationship between soil type and landslide frequency where: 1=None, 2=Very Deep, 3=Very Shallow, 4=Deep, 5=Shallow 121
Figure 3.44 Erosion map showing 4 different classes of the erosion b. Percent frequency of each erosion class 122
Figure 3.45 Histogram showing the relationship between soil type and landslide frequency where 1=Less, 2=Middle 3=Severe 4= Very Severe 122
Figure 3.46 Conversion of categorical data to raster format a. The vector layer in the categorical format b. Vector layer converted to raster format c. The raster data is reclassified for each category in the layer and assigned 0 or 1 value d. Each category layer in raster format is assigned to a database..... 126
Figure 3.47 Point mesh overlaid with factor layers 127
Figure 3.48 The resultant variables considered for grid-based analysis..... 134
Figure 3.49 Flow chart showing the steps to create slope unit 137

Figure 3.50 a) Watershed boundaries determined using the DEM. b) Drainage line overlaid with watershed of the region c) Watershed boundaries determined using the reverse DEM (shown with red lines) overlaid with watershed boundaries present the left (L) or right (R) side of a sub-basin. d) Slope unit of region obtained in 3D. 138
Figure 3.51 a. Landslide boundaries and slope unit boundary b. DEM overlaid with landslide boundaries 139
Figure 3.52 Slope Unit map showing landslide and landslide-free regions zooming in the south-western part to show the logic to assign landslide values. 140
Figure 3.53. a) Slope map of the region ranges between 0 and 65.55 b) Slope unit map showing the mean slope values assigned to each mapping unit 140
Figure 3.54. a. Road distance computed for each cell unit b. Road distance assigned to each slope unit by computation of mean value. 141
Figure 3.55 The resultant influencing parameters after the statistical analysis 144
Figure 3.56 LR Model prediction map created for landslide susceptibility for grid-based mapping unit (LR_GRD_SUSCP)..... 147
Figure 3.57. LR Model prediction map created for landslide susceptibility for slope unit-based mapping unit (LR_SU_SUSCP)..... 148
Figure 3.58. The relations between RMSE and number of training cycle for different combinations of hidden neurons 150
Figure 3.59. ANN prediction map created for landslide susceptibility for grid-based mapping unit (ANN_GRD_SUSCP) 151
Figure 3.60 ANN prediction map created for landslide susceptibility for slope unit-based mapping unit (ANN_SU_SUSCP) 151
Figure 3.61 SR prediction map created for landslide susceptibility for grid-based mapping unit (SR_GRD_SUSCP) 154
Figure 3.62 SR prediction map created for landslide susceptibility for slope unit-based mapping unit (SR_SU_SUSCP) 154
Figure 3.63 The R^2 result map of GWR model for grid-based mapping unit..... 157
Figure 3.64 The GWR prediction map created for landslide susceptibility for grid-based mapping unit (GWR_GRD_SUSCP)..... 157
Figure 3.65 The R^2 result map of GWR model for slope unit-based mapping unit ....

..... 158
Figure 3.66 GWR prediction map created for landslide susceptibility for slope unit-based mapping unit (GWR_GRD_SUSCP)..... 158
Figure 3.67 GWR parameter variation accross the study area for vegetation (Veg)... 161
Figure 3.68 GWR parameter variation accross the study area for Land-Use Dry Farming (LU_DF)..... 162
Figure 3.69 GWR parameter variation accross the study area for Land-Use Dry Settlement (LU_S)..... 162
Figure 3.70 Spatial distribution of testing (TEST_LS) and training (TRAIN_LS) landslide inventory data..... 167
Figure 3.71 Prediction accuracy assessment of models by using ROC curve..... 168
Figure 3.72 Predictive performance of different susceptibility methods for slope unit-based mapping unit..... 169
Figure 3.73 Konuklu village showing first degree of risk where the terrain show a clear movement with some indicators as house cracks..... 171
Figure 3.74 a. Ground truth data represented with ”H” was overlaid to the DEM of the study region and existing landslide location b. The density map of the ground truth observed through field surveys with the landslide polygons obtained from MTA. 171
Figure 3.75 Accuracy assessment of the prediction models by kappa and overall accuracy 174
Figure 3.76 The classified LR Model prediction map created for landslide susceptibility for grid-based mapping unit (LR_GRD_SUSCP)..... 176
Figure 3.77 The classified LR Model prediction map created for landslide susceptibility for slope unit-based mapping unit (LR_SU_SUSCP).. 177
Figure 3.78 The classified SR model prediction map created for landslide susceptibility for grid-based mapping unit SR_GRD_SUSCP)..... 178
Figure 3.79 The classified SR model prediction map created for landslide susceptibility for slope unit-based mapping unit SR_SU_SUSCP).... 178
Figure 3.80 The classified ANN model prediction map created for landslide susceptibility for grid-based mapping unit (ANN_GRD_SUSCP) ... 179
Figure 3.81 The classified ANN model prediction map created for landslide

susceptibility for slope unit-based mapping unit (ANN_SU_SUSCP) 180
Figure 3.82 The classified GWR model prediction map created for landslide susceptibility for grid-based mapping unit (GWR_GRD_SUSCP)... 181
Figure 3.83 The classified GWR model prediction map created for landslide susceptibility for slope unit-based mapping unit (GWR_SU_SUSCP) 181
Figure 3.84 Evaluation of grid and slope unit-based models for different classes 182
Figure 3.85 Evaluation of grid-based models for different classes 183
Figure 3.86 Evaluation of slope unit-based models for different classes 184
Figure 3.87 Bar graphs showing the relative distribution of landslide densities at various classes of the LR, SR, ANN, GWR susceptibility maps for grid-based mapping unit 187
Figure 3.88 Bar graphs showing the relative distribution of landslide densities at each 187
Figure 3.89 The area and percentage of different and similar regions between the pair of maps for cell-based mapping unit. 191
Figure 3.90. The area and percentage of different and similar regions between the pair of maps for slope unit-based mapping unit..... 191
Figure 3.91. The methodology adopted for analysis of triggers 193
Figure 3.92. a.Spatial distribution of the conveyed house frequency after devastating landslide events b. Showing the year and the frequency of each devastating landslide event..... 194
Figure 3.93. The landslide events distribution over months and daily rainfalls on each event day..... 196
Figure 3.94 Meteorological stations distributed around the study region for station see Table 3.17for station characteristics. Legend 1 indicates that the meteorological station measurements are available for analysis. 2 indicate the station measurements are not present or the station is closed 197
Figure 3.95. Hypsometric Curve of Bartın Kumluca watershed 198
Figure 3.96. The daily rainfall pattern of each station in 1998 May 199
Figure 3.97. The graph showing the correlation between the meteorological

stations for 1998 May 199
Figure 3.98. The lowest and the highest monthly rainfall average from mean 200
Figure 3.99. The annual maximum precipitation in Bartın (reference meteorological station) from 1975 to 2006. The horizontal line indicates the mean annual maximum precipitation (MAMP) Legend: triangles indicate landslide events triggered with flood; squares indicate potential landslide events 200
Figure 3.100. The time series plot of daily rainfall of Bartın station..... 202
Figure 3.101. Autocorrelation plot of daily rainfall..... 204
Figure 3.102. Partial autocorrelation plot of daily rainfall 204
Figure 3.103. Autocorrelogram of residuals of ARIMA(1,0,0)..... 206
Figure 3.104. Partial Autocorrelogram of residuals of ARIMA(1,0,0) 207
Figure 3.105. Gumble distribution diagram for estimation of rainfall with 50 years return period..... 209
Figure 3.106. Plots of normalized accumulated rainfall versus normalized daily rainfall for landslide events shown with pink square and non-landslide events labeled with blue point: a for 3 days; b for 5 days; c for 10 days; d for 15 days ; e for 20 days 212
Figure 3.107. Intensity Duration plot of 16 reported landslide events 216
Figure 3.108. Landslide hazard map of Bartın Kumluca region obtained annually for different mapping methods where a. LR, b. SR and c. ANN, expressed as probability of occurrence for each pixel 222
Figure 3.109. Landslide hazard map of Bartın Kumluca region obtained annually for different mapping methods where a. LR, b. SR and c. ANN, expressed as probability of occurrence for each slope unit 223
Figure 3.110. Category of the buildings and their spatial distribution over the stream network..... 229
Figure 3.111. The road network categories 230
Figure 3.112. The power and road network overlaid on to hillshade of study region 231
Figure 3.113. Land Use map of the study region..... 232
Figure 3.114. Elements at risk map generated with monetary terms at pixel basis

(TL/per pixel) 233
Figure 3.115. The spatial pattern of residents that are points on the map 234
Figure 3.116. The risk to property for grid-based mapping unit for different methods, a. LR, b. SR and c. ANN 238
Figure 3.117 The risk to property for slope unit-based mapping unit for different methods, a. LR, b. SR and c. ANN 240
Figure 3.118. The risk to population for grid-based mapping unit for different methods, a. LR, b. SR and c. ANN 244
Figure 3.119. The risk to population for slope unit-based mapping unit for different methods, a. LR, b. SR and c. ANN 246
Figure 3.120. Risk to property for LR model and grid-based mapping unit (LR_GRD) 248
Figure 3.121. Risk to life for LR model and grid-based mapping unit (LR_GRD) 249
Figure 3.122. Bar graphs showing the relative distribution of risk levels for property for different class ranges 249
Figure 3.123. Bar graphs showing the relative distribution of risk levels for life for different class ranges 250
Figure 3.124. Bar graphs showing the percentage difference of risk levels based on different models and mapping units for property 251
Figure 3.125. Bar graphs showing the percentage difference of risk levels based on different models and mapping units for life 251
Figure 4.1. The grid-based LR hazard map levels for Hepler district 253
Figure 4.2. The grid-based SR hazard map levels for Hepler district 254
Figure 4.3. The grid-based ANN hazard map levels for Hepler district 254
Figure 4.4. The slope unit-based LR hazard map levels for Hepler district 254
Figure 4.5. The slope unit-based SR hazard map levels for Hepler district 255
Figure 4.6. The slope unit-based ANN hazard map levels for Hepler district 255
Figure 4.7. Location of the study region in 3D View 257
Figure 4.8. The cracks and scarps observed and mapped through field survey at 6-7 June 2009 259
Figure 4.9. The photos of the terrain with scarps and crowns 260
Figure 4.10 The anomalies investigated through the field surveys, the photos are

overlaid to the remote sensing image of the region a. A fracture representation of the region b. The protection wall of a house in the region c. The cracks inside the house 260
Figure 4.11 Some photos from the field survey a. The crack on the terrain, b. The toe of the upper scarp c. The main scarp and head of the upper scarp d. The deformation observed at the column of the building e. The cracks observed outside the building 261
Figure 4.12 The daily rainfall pattern of Bartın station in 1998 May..... 263
Figure 4.13 Rainfall distribution at Bartın Station May 17-23, 1998..... 264
Figure 4.14 The velocity map of the simulation result 266
Figure 4.15 The spatial distribution of velocity values over the 3D image of the study region..... 266
Figure 4.16 Flowchart of the Methodology 268
Figure 4.17 The subregions used for the building detection algorithm 269
Figure 4.18 Vegetation mask and shadow mask are summed and overlaid onto the original image a. Subregions 1 and 2 b. Subregions 3 and 4.. 271
Figure 4.19 The segmentation result of the original image 272
Figure 4.20 Linear Features extracted by the algorithm 273
Figure 4.21 The candidate buildings extracted at the end of the algorithm overlaid on the ground truth..... 274
Figure 4.22 The local main road in the study region 275
Figure 4.23 The road detection outputs in sequence where 1: The vegetation and shadow mask; green is the vegetation and shadow mask, red is the man-made features (road and buildings) 2: The result map obtained from the linear feature detection algorithm. 3: The result map after PCA algorithm. 4: The result map of both linear feature detection and PCA is overlaid to obtain the road feature 5: The morphological processes (imfill imopen, erode, close) implemented to road feature 6: The road feature overlaid to the remote sensing image 276
Figure 4.24 Risk to property for grid-based mapping unit for different methods, a. LR, b. SR and c. ANN 284
Figure 4.25 Risk to property for slope unit-based mapping unit for different methods, a. LR, b. SR and c. ANN 286

Figure 4.26 Risk of loss of life for grid-based mapping unit for different methods, a. LR, b. SR and c. ANN 289
Figure 4.27 Risk of loss of life for slope unit-based mapping unit for different methods, a. LR, b. SR and c. ANN 291
Figure 4.28 Risk to property map created based on the LR model at grid-based mapping unit (LR_GRD) 293
Figure 4.29 Risk to property map created based on the LR model at slope unit-based mapping unit (LR_SU) 294
Figure 4.30 Bar graphs showing the relative distribution of risk levels for property 294
Figure 4.31 Difference of risk to property maps between SR and LR models at grid-based mapping unit (SR_LR_GRD) 295
Figure 4.32 Difference of risk to property maps between SR and LR models at slope unit-based mapping unit (SR_LR_SU) 296
Figure 4.33 Bar graphs showing the percentage difference of risk levels based on different models and mapping units for property 297
Figure 4.34 Risk to life map created based on the LR model at grid-based mapping unit (LR_GRD) 299
Figure 4.35. Risk to life map created based on the LR model at slope unit-based mapping unit (LR_SU) 300
Figure 4.36 Bar graphs showing the relative distribution of risk levels for life 300
Figure 4.37 Difference of risk to life maps between SR and LR models at grid-based mapping unit (SR_LR_GRD) 301
Figure 4.38 Difference of risk to life maps between SR and LR models at slope unit-based mapping unit (SR_LR_SU) 302
Figure 4.39 Bar graphs showing the percentage difference of risk levels based on different models and mapping units for life 303
Figure B-1. GWR parameter variation across the study area for Greybrown Podzolic Soil (S_GBPdz) for grid-based mapping unit 367
Figure B-2. GWR parameter variation across the study area for Brown Forest Soil (S_BFS) for grid-based mapping unit 368
Figure B-3. GWR parameter variation across the study area for Sandstone-Mudstone unit of Geology (Geo_SM) for grid-based mapping unit 368

Figure B-4. GWR parameter variation across the study area for Slope (Slp) for grid-based mapping unit 369
Figure B-5. GWR parameter variation across the study area for Distance to Road (DisttoRoad) for grid-based mapping unit 369
Figure B-6. GWR parameter variation across the study area for Colluvial Soil (S_Colv) for grid-based mapping unit 370
Figure B-7. GWR parameter variation across the study area for very shallow soil depth (SD_VS) for grid-based mapping unit 370
Figure B-8. GWR parameter variation across the study area for Elevation (Elev) for grid-based mapping unit 371
Figure B-9. GWR parameter variation across the study area for Aspect (Asp) for grid-based mapping unit 371
Figure B-10. GWR parameter variation across the study area for Distance to Stream (DisttoStrm) for grid-based mapping unit..... 372
Figure B-11. GWR parameter variation across the study area for Distance to Fault (DisttoFault) for grid-based mapping unit 372
Figure B-12. GWR parameter variation across the study area for Land use Dry Farming (LU_DF) for slope unit-based mapping unit..... 373
Figure B-13. GWR parameter variation across the study area for Forest (LU_F) for slope unit-based mapping unit 373
Figure B-14. GWR parameter variation across the study area for the Conglomerate unit of Geology (Geo_C) for slope unit-based mapping unit 374
Figure B-15. GWR parameter variation across the study area for the Sandstone Mudstone unit of geology (Geo_SM) for slope unit-based mapping unit 374
Figure B-16. GWR parameter variation across the study area for the Grey brown podzolic soil (S_GBPdz) for slope unit-based mapping unit..... 375
Figure B-17. GWR parameter variation across the study area for the brown forest soil (S_BFS) for slope unit-based mapping unit..... 375
Figure B-18. GWR parameter variation across the study area for the brown forest soil without lime (S_BFSWL) for slope unit-based mapping unit 376
Figure B-19. GWR parameter variation across the study area for the distance to stream network (DisttoStrm) for slope unit-based mapping unit..... 376

Figure B-20. GWR parameter variation across the study area for the distance to vegetation (Veg) for slope unit-based mapping unit..... 377
Figure B-21. GWR parameter variation across the study area for the distance to Slope (Slp) for slope unit-based mapping unit 377
Figure B-22. GWR parameter variation across the study area for the distance to distance to road network (DisttoRoad) for slope unit-based mapping unit 378
Figure B-23. GWR parameter variation across the study area for the distance to topographic wetness index (Wtns) for slope unit-based mapping unit 378
Figure C-1. Map similarity computed for SR_GWR for grid-based mapping unit. 379
Figure C-2. Map similarity computed for SR_LR for grid-based mapping unit 380
Figure C-3. Map similarity computed for SR_ANN for grid-based mapping unit.. 380
Figure C-4. Map similarity computed for LR_ANN for grid-based mapping unit . 381
Figure C-5. Map similarity computed for LR_GWR for grid-based mapping unit. 381
Figure C-6. Map similarity computed for ANN_GWR for grid-based mapping unit 382
Figure C-7. Map similarity computed for SR_LR slope unit-based mapping unit. 382
Figure C-8. Map similarity computed for SR_GWR slope unit-based mapping unit. 383
Figure C-9. Map similarity computed for SR_ANN slope unit-based mapping unit. 383
Figure C-10. Map similarity computed for LR_ANN slope unit-based mapping unit 384
Figure C-11. Map similarity computed for LR_GWR slope unit-based mapping unit. 384
Figure C-12. Map similarity computed for ANN_GWR slope unit-based mapping unit. 385
Figure D-1. Risk to property for SR model and grid-based mapping unit (SR_GRD) 386
Figure D-2. Risk to property for ANN model and grid-based mapping unit (ANN_GRD) 386
Figure D-3. Risk to property for LR model and slope unit-based mapping unit

(LR_SU) 387
Figure D-4. Risk to property for SR model and slope unit-based mapping unit (SR_SU) 387
Figure D-5. Risk to property for ANN model and slope unit-based mapping unit (ANN_SU) 388
Figure D-6. Risk to life for SR model and grid-based mapping unit (SR_GRD) 388
Figure D-7. Risk to life for ANN model and grid-based mapping unit (ANN_GRD) 389
Figure D-8. Risk to life for LR model and slope unit-based mapping unit (LR_SU) 389
Figure D-9. Risk to life for SR model and slope unit-based mapping unit (SR_SU) 390
Figure D-10. Risk to life for ANN model and slope unit-based mapping unit (ANN_SU) 390
Figure E-1. Risk to property map created based on the SR model at grid-based mapping unit (SR_GRD) 392
Figure E-2. Risk to property map created based on the ANN model at grid-based mapping unit (ANN_GRD) 393
Figure E-3. Risk to property map created based on the SR model at slope unit-based mapping unit (SR_SU) 394
Figure E-4. Risk to property map created based on the ANN model at slope unit-based mapping unit (ANN_SU) 395
Figure E-5. Difference of risk to property maps between SR and ANN models at grid-based mapping unit (SR_ANN_GRD) 396
Figure E-6. Difference of risk to property maps between LR and ANN models at grid-based mapping unit (LR_ANN_GRD) 397
Figure E-7. Difference of risk to property maps between SR and ANN models at slope unit-based mapping unit (SR_ANN_SU) 398
Figure E-8. Difference of risk to property maps between LR and ANN models at slope unit-based mapping unit (LR_ANN_SU) 399
Figure E-9. Risk to life map created based on the SR model at grid-based mapping unit (SR_GRD) 400

Figure E-10. Risk to life map created based on the ANN model at grid-based mapping unit (ANN_GRD) 401
Figure E-11. Risk to life map created based on the SR model at slope unit-based mapping unit (SR_SU) 402
Figure E-12. Risk to life map created based on the ANN model at slope unit-based mapping unit (ANN_SU) 403
Figure E-13. Difference of risk to life maps between SR and ANN models at grid-based mapping unit (SR_ANN_GRD)..... 404
Figure E-14. Difference of risk to life maps between LR and ANN models at grid-based mapping unit (LR_ANN_GRD) 405
Figure E-15. Difference of risk to life maps between SR and ANN models at slope unit-based mapping unit (SR_ANN_SU) 406
Figure E-16. Difference of risk to life maps between LR and ANN models at slope unit-based mapping unit (LR_ANN_SU) 407

CHAPTER 1

INTRODUCTION

1.1 BackGround

Natural disasters may pose severe threat to life, property and infrastructure, which results in human suffering, property losses, and environmental degradation. Systematic risk assessment procedures decrease these losses due to natural hazards and provide effective strategies for disaster preparedness.

The data collected between 1903 and 2007 in Emergency Disaster Database (EM-DAT) (OFDA/CRED, 2007) shows that landslide is the fifth most frequently occurring natural disaster among all natural hazard types (Figure 1.1). In many countries, the economic losses and casualties are considerably high and landslides generate a yearly loss of property larger than property losses from earthquakes, floods and windstorms (Schuster and Fleming, 1986; Alexander, 1989; Swanston and Schuster, 1989; Olshansky, 1990; Schuster, 1995; Glade, 1998).

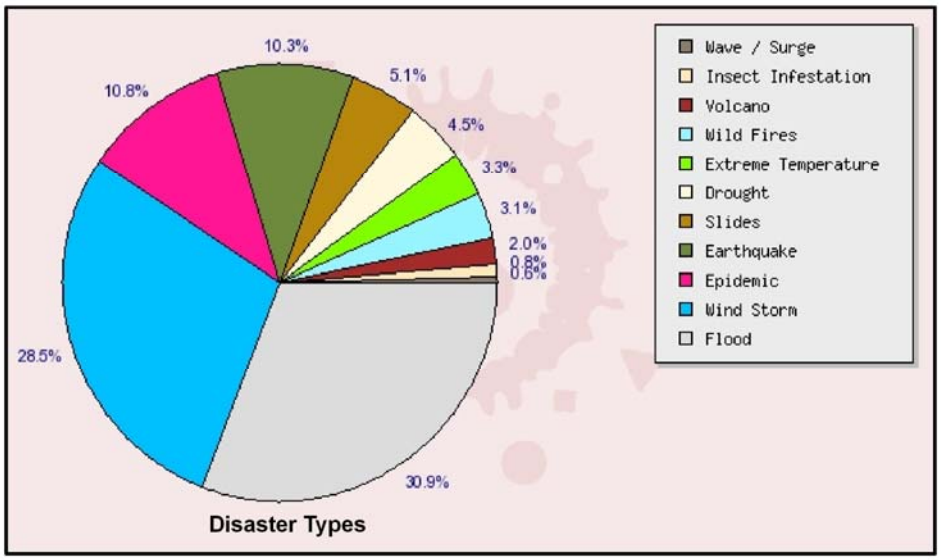

Figure 1.1. Frequency of natural disasters in the world (OFDA/CRED, 2007).

In the United States, landslides cause an estimated economic loss of US$1–2 billion and about 25–50 deaths annually, which exceeds the average losses due to earthquakes (Schuster and Fleming, 1986). When the EM-DAT database (OFDA/CRED, 2007) is analyzed for the number of fatalities and the cost of damage from landslides between 1903 and 2007, it is found that around US$2,5 million of damage occurred in Europe. Asia follows Europe with a damage of more than US$1,5 million and then America comes with more than US$1 million of damage. Furthermore, as reported by EM-DAT, landslides are the seventh leading cause of death among all the natural disaster types in the database.

In Turkey, landslides are one of the most devastating natural hazards. The Black Sea Region is particularly vulnerable to such hazards. 89% of the middle and the eastern parts of the region are reported to be susceptible to landslides (Toprak Su, 1978; Öztürk, 2002). The frequency analyses of the EM-DAT database for natural disasters in Turkey between 1903 and 2007 (OFDA/CRED, 2007) show that the frequency of the landslides is the fourth in order (Figure 1.2). Landslides are the second most common natural disasters that cause damages in Turkey (Figure 1.3). Between 1959 and 1994, landslides damaged 76,995 buildings, killed hundreds of people, and destroyed farming lands and roads throughout Turkey (Ildir, 1995). Thus, landslide risk assessment is of crucial importance in decreasing the potential losses.

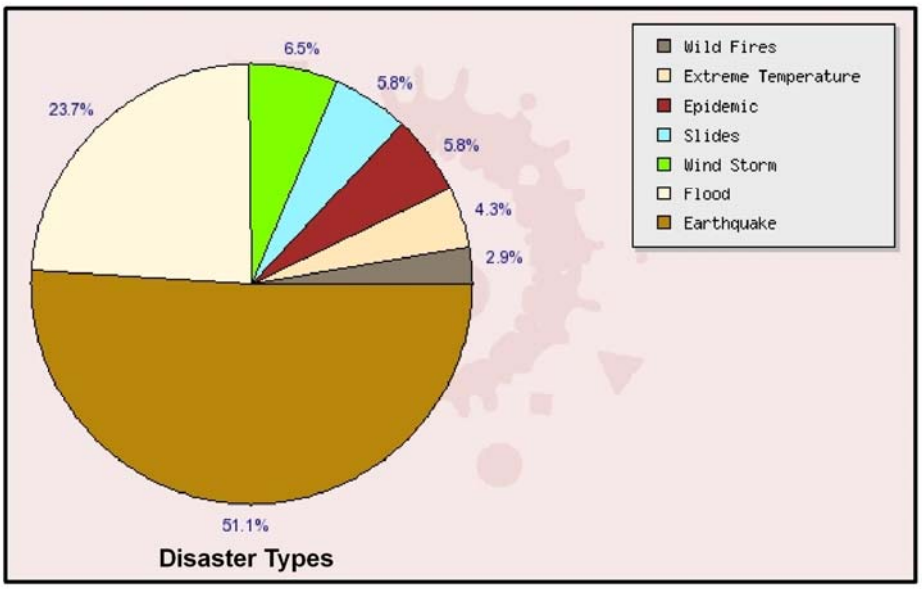

Figure 1.2. Frequency of natural disasters in Turkey (OFDA/CRED, 2007)

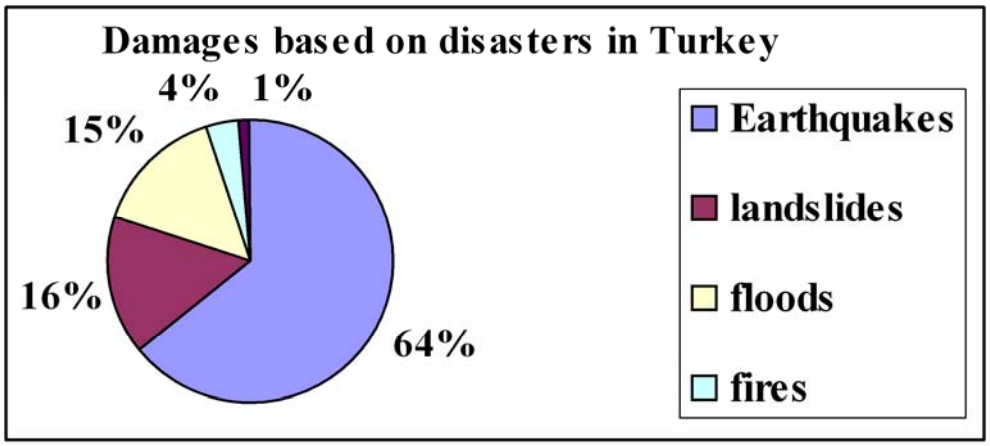

Figure 1.3. Damages caused by disasters in Turkey (Ergunay et al., 2003)

Risk is defined in terms of the expected degree of loss due to a particular natural phenomenon (Varnes, 1984). It is the product of two main elements: landslide hazard and consequences of the landslide events. In most of the publications, the risk is assessed qualitatively (Lateltin 1997; Blake et al. 2002; Cardinali et al. 2002b; Glassey et al. 2003; Leiba et al. 2003; Catani et al., 2005) because of the fact that obtaining quantitative data is more difficult. However, the qualitative risk assessment has some weaknesses. The main shortcoming is that, the results are incomparable due to the verbal expression of risk for various cases. Since most of the time these verbal risk levels reflect the experts' opinions, they are subjective in nature.

Being reproducible, justifiable and meaningful, quantitative landslide risk assessment methods have received increased focus on regional and local scales in recent years. Risk assessment on regional scale is necessary to support decisions for urban development and land-use planning, and also it provides important information for hazard mitigation. Local scale risk assessments are required to carry out more detailed analysis and risk management. Therefore, there have been considerable efforts on developing quantitative risk assessment for landslides (e.g. Varnes, 1984; Einstein, 1988; Wang and Unwin, 1992; Fell, 1994; Chung et al., 1995; Carrara et al., 1995; Chowdhury and Flentje, 1996; Leroi, 1996; Aleotti and Chowdhury, 1999; Chung and Fabbri, 1999; Jibson et al., 1998; Ho et al., 2000; Dai et al., 2002; Bell and Glade, 2004; Remondo et al. 2008). However, most of these studies appeared not to have a well-developed systematic approach. Hence, the present study aims to develop a systematic methodology to quantitatively assess the landslide risk. The

proposed methodology relies on two different scales: regional and local. The methodology developed for regional scale involves the application of the risk assessment procedure to numerous mapped landslides. On the other hand, the methodology for local scale is adapted to a single slope. Each component of risk, i.e., hazard assessment, vulnerability and consequence analysis, is quantitatively assessed for both scales. In this way, the decision makers will be able to perform cost-benefit analysis for proper land-use planning and to develop effective disaster preparedness strategies.

Hazard mapping, which is one of the main components of risk assessment, should contain information about probability of occurrence of a landslide in a given area over a specified period of time (Varnes, 1984). Because of the lack of complete landslide inventory maps (especially temporal) and oversimplifications related to landslide influencing factors and triggers (Van Westen et al., 2006, Guzetti et al 2005), it is difficult to make temporal predictions of landslide occurrence (Ohlmacher and Davis, 2003). Few attempts have been made to establish the temporal occurrence of landslides (Hansen, 1984; Keaton et al., 1988; Hutchinson, 1995; Grunert and Hardenbicker, 1997; Dikau and Schrott, 1999; Lang et al., 1999; Coe et al., 2000; Corsini et al., 2000; Barnard et al., 2001; Derbyshire, 2001; Cardinali et al, 2002b; Vanacker et al., 2003; Carrasco et al., 2003; Catani et al. 2005), and also there is yet not a wide range of studies on integration of these parameters. Hence, most of the hazard maps in the literature basically determine the susceptibility (lsao, 1996; Uromeihy et al., 2000; Lee et al., 2004; Chen and Wang, 2006; Fourniadis, 2007*)*, which aims to predict where failures are likely to occur without any clear indication of when they will occur.

In this thesis, the developed risk assessment methodology propose a systematic approach for transforming susceptibility maps into hazard maps by integrating susceptibility maps with landslide trigger probabilities. Susceptibility maps have an utmost importance in risk assessment as they are the first stage in hazard mapping. It is evident that an accurate assessment of susceptibility model is crucially important for the accuracy of hazard and also ultimately of the risk map. The choice of an inappropriate model for the analysis may result in probabilities which over or underestimate the occurrence of future events. There exist several reviews on

landslide hazard and susceptibility zonation methods as Carrara (1983), Hansen (1984), Van Westen (1993), Leroi (1996), Soeters and Van Western (1996), Guzetti et.al (1999), Aleotti and Chowdhury (1999), and Huabin et al., (2005). At present, there is no agreement or any guide on how to choose susceptibility mapping method (Brabb, 1984; Carrara, 1989; Nieto, 1989). The majority of the papers concerning hazard assessment deal with data preparation and the methods used; Varnes (1984), Anagnosti and Lesevic, (1991), Van Westen (1997), Chung and Fabbri (1999), Dai and Lee (2001), Baeza and Corominas (2001), Lee and Min (2001), Pistocchi et al. (2002), Lee and Dan (2005), Yeşilnacar and Topal (2005), Lee and Pradhan (2006). Most of the studies in the literature deal with the application of the conventional methods and there is not yet a common consensus on the appropriate susceptibility method to be applied in susceptibility assessment. Very few deal with the comparison of different methods and none describe its effect on the resultant risk maps.

In this thesis, the influence of different susceptibility models on the resultant risk maps was investigated to develop guidelines on the selection of appropriate susceptibility mapping. In addition to the existing methods, a new approach to enhance the performance of susceptibility assessment method, which considers the spatial correlation structure of the parameters, was proposed as it has better explanation level for the phenomenon of landslide occurrence. In addition to the utilization of different models on regional scale, the effects of the mapping unit and the scale on the resultant risk maps were analyzed. Prediction capabilities of models were evaluated by using validation tests comparing susceptibility maps and past landslides occurrences. Such analyses also provide a guideline for the choice of suitable mapping units and scale for risk maps.

Spatial probability maps were converted into the hazard maps by combining the temporal probability with susceptibility map. Precipitation is the main trigger for landsliding in the study region. Therefore, rainfall data were analyzed to obtain the critical thresholds for exceedance probabilities.

Another important aspect of quantitative risk assessment is the characterization of consequence scenarios, which are based on elements at risk and vulnerability of

elements at risk. Consequences are the potential outcomes arising from the occurrence of a natural phenomenon (Bell and Glade, 2004) and the vulnerability reflects the degree of loss of an element within the landslide-affected area (Fell, 1994). Difficulties in the modeling of run-out zone and damage data shortage are the main limitations of consequence mapping (van Westen et al., 2006).

In this thesis study, a loss estimation approach due to landslides was developed for regional and local scales. The procedures followed for regional and local scales to obtain the elements at risk and vulnerability differs from each other. On regional scale, a more general approach was followed, whereas on local scale a more specific methodology was developed to obtain quantitative vulnerability and elements at risk. The quantitative risk maps were obtained for both local and regional scale by the developed methodology for risk assessment through combination of hazard maps with the consequence maps.

Geographic information systems (GIS) and remote sensing (RS) have recently become important tools for handling and analyzing spatial data, which facilitates the application of quantitative techniques in landslide hazard and risk assessment (Turrini and Visintainer, 1998; Chung and Fabbri, 1995, 1999; Guzzetti et al., 1999; Gökceoglu et al., 2000; Luzi et al., 2000; Lee and Min, 2001; Huabin et. al., 2005).

In the developed methodology an integrated approach of RS and GIS was used for risk assessment. RS is mostly used for capturing, displaying and determining the relevant data which may be required at different stages of the risk assessment procedure. A medium-resolution Aster remote sensing data was used to obtain the vegetation cover of the whole study region which may contribute to landslide. Moreover, a semiautomatic algorithm was developed to extract the buildings and roads from Quickbird, which is a high resolution satellite image, for determining the elements at risk.

GIS technology provide more objective maps than a comparable laborious and time-consuming hand-made product in landslide hazard assessment (Turrini and Visintainer, 1998; Chung and Fabbri, 1999; Guzzetti et al., 1999; Gökçeoğlu et al., 2000; Luzi et al., 2000; Lee and Min, 2001). GIS was used in each step of the quantitative risk assessment to store, monitor, evaluate, process, and manage the

data. In the thesis, the raw data was stored, monitored and projected in the GIS environment to determine the influencing factors that lead to landslides. Besides, the mapping and visualization of the spatial distribution of the maps, and the evaluation of simple statistics of the data were done in GIS environment. Data is usually transformed into external software products for core analyses to obtain susceptibility maps due to deficiency in GIS technology (Ayalew et al., 2005). Despite these difficulties, GIS technology provides high efficiency and convenience in most of the steps in risk assessment processes. The final quantitative susceptibility, hazard, consequence and risk maps were produced by stepwise combination of relevant components in GIS environment.

1.2 General Terminology

Risk assessment is comprised of risk analysis and evaluation. The former is based on hazard analysis and consequence analysis (Cascini et al., 2005). The latter, on the other hand focuses on the stage at which the risk analysis values are evaluated. As a result of this judgment enter the decision process, explicitly or implicitly, by including consideration of the importance of the estimated risks and the associated social, environmental, and economic consequences, in order to identify a range of alternatives for managing the risks (AGS, 2000). This study mainly focuses on the risk analysis, rather than the risk evaluation.

The risk assessment approaches can be generated qualitatively by expert knowledge or quantitatively via complex mathematical or statistical analysis (Chung and Fabbri, 2003). Qualitative risk assessment uses word form, hence the components of risk, which are basically hazard, element at risk, and vulnerability are expressed verbally (Düzgün and Lacasse, 2005). Quantitative risk assessment, on the other hand, is based on numerical values of the probability, resulting in a numerical value of the risk (JTC, 2008). Thus, the use of quantitative risk assessment allows better risk communication and the use of systematic decision making methods (Lee and Jones 2004).

In a simple form, for the evaluation of quantitative landslide risk assessment process the following questions which were discussed in detail by AGS (2000), Ho et

al. (2000) and Lee and Jones (2004), and Düzgün, (2006) should be answered:

- Where will the landslide occur? [Susceptibility Assessment]
- What type of failures will occur? [Susceptibility Assessment]
- What would be the magnitude of landslide? [Hazard Assessment]
- When will the landslide occur? [Hazard Assessment]
- What damage or injury may result? [Vulnerability]
- What are the elements at risk and the possible consequences? [Consequence/Elements at Risk Identification]
- How important is the damage caused by landslide? [Risk Evaluation]
- What precautions could be taken to prevent similar cases? [Risk Management]

The quantitative risk assessment frameworks differ depending on the characteristics of the landslide, the available data, scale of the investigation and the nature of consequences; as a result, each stage can use different approaches (Düzgün, 2008).

Risk assessment involves hazard assessment and consequence (C) analysis (Bell and Glade, 2004). The hazard assessment is comprised of spatial and temporal probability, whereas consequence analysis involves elements at risk and vulnerability assessment (Figure 1.4). The main elements of a risk assessment procedure are shown in Figure 1.4.

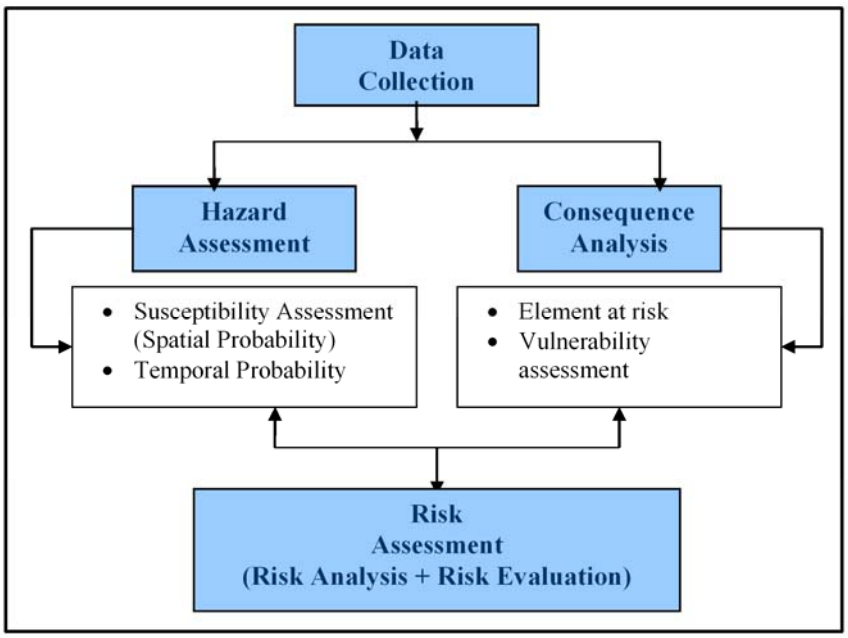

Figure 1.4. Basic steps in landslide risk assessment

Risk mapping can be carried out separately for each type of element at risk (specific risk) and then combined into a total risk by adding all maps of specific risk (Remondo et al., 2008). The risk assessment process is followed by landslide evaluation, where it may be possible to define "acceptable risk". Acceptable risk is the possible social, economic, and environmental consequences that a society or a component of it can implicitly or explicitly tolerate.

Terms like susceptibility, hazard, vulnerability, consequence, and risk can be found with different definitions that can be referenced to many technical papers (Yong et al., 1977; Brabb, 1984; Varnes, 1984, Brand, 1988; Carrara et al., 1991; van Westen, 1993; Fell, 1994; Guzzetti et al., 1994; Scheidegger, 1973, Ibsen and Brunsden, 1996; Leone et al., 1996; Cruden and Fell, 1997; Wong et al., 1997; Glade, 1998; Aleotti and Chowdhury, 1999; Dai and Lee, 2002). The most widely adopted set of definitions regarding risk and its components is presented in Table 1.1. There is a need for a unified terminology in susceptibility, hazard, and risk, which is essential for authorities to compare and discuss common studies on a similar basis. JTC-1, the Joint Technical Committee on Landslides and Engineered Slopes, proposed international guidelines for landslide susceptibility, hazard and risk zoning for land-use planning, which are acceptable for the international community. The guideline provides definitions, terminology and international standards for methods, levels, scales, and types of zoning. The basic terminology adopted in this thesis is listed in Table 1.1.

Table 1.1. Different risk and hazard definitions proposed in the literature

Term	Definition	Source
Risk	"The expected number of lives lost, persons injured, damage to property and distribution of economic activity due to a particular damaging phenomenon for a given area and reference period."	Varnes (1984)
Risk Analysis	"The use of available information to estimate the risk to individuals, population, property, or the environment, from hazards. "	JTC (2008)
Risk Management	"The complete process of risk assessment and risk control (or risk treatment)."	JTC (2008)
Risk Control or Risk Treatment	"The process of decision making for managing risk, and the implementation or enforcement of risk mitigation measures and the re-evaluation of its effectiveness from time to time, using the results of risk assessment as one input."	JTC (2008)
Risk Assessment	"The process of risk analysis and risk evaluation. "	JTC (2008)

Table 1.1. Different risk and hazard definitions proposed in the literature (Continued)

Term	Definition	Source
Risk Estimation	"The process used to produce a measure of the level of health, property, or environmental risks being analyzed. Risk estimation contains the following steps: frequency analysis, consequence analysis, and their integration."	JTC (2008)
Risk Evaluation	"The stage at which values and judgments enter the decision process, explicitly or implicitly, by including consideration of the importance of the estimated risks and the associated social, environmental, and economic consequences, in order to identify a range of alternatives for managing the risks."	JTC (2008)
Societal Risk	"The risk of multiple fatalities or injuries in society as a whole: one where society would have to carry the burden of a landslide causing a number of deaths, injuries, financial, environmental, and other losses."	AGS (2000)
Individual Risk	"The risk of fatality or injury to any identifiable (named) individual who lives within the zone impacted by the landslide; or who follows a particular pattern of life that might subject him or her to the consequences of the andslide."	AGS (2000)
Acceptable Risk	"A risk for which, for the purposes of life or work, we are prepared to accept as it is with no regard to its management. Society does not generally consider expenditure in further reducing such risks justifiable."	JTC (2008)
Tolerable Risk	"A risk within a range that society can live with so as to secure certain net benefits. It is a range of risk regarded as non-negligible and needing to be kept under review and reduced further if possible."	JTC (2008)
Landslide hazard	"The probability of occurrence within a specified period of time and within a given area of a potentially damaging phenomenon"	Varnes (1984)
Consequence	"The outcomes or potential outcomes arising from the occurrence of a landslide expressed qualitatively or quantitatively, in terms of loss, disadvantage or gain, damage, injury or loss of life. "	AGS (2000)
Vulnerability	"The degree of loss to a given element or set of elements within the area affected by the landslide hazard. It is expressed on a scale of 0 (no loss) to 1 (total loss). "	AGS (2000)
Element at Risk	"Population, properties, economic activities, including public services, etc. at risk in a given area."	Varnes (1984)

1.3 Purpose and Scope of the Thesis

The main objective of this thesis is to develop a GIS- and RS-based quantitative risk assessment methodology for landslides. The methodology was developed for two different scales: Landslide risk assessment for a region with numerous landslides (regional scale) and landslide risk assessment for a single landslide (local scale). While developing the methodology, the thesis involves several subobjectives:

- To investigate the effect of different susceptibility assessment models, mapping units and scales on resultant risk maps to develop guidelines for risk mapping.
- To enhance the performance of landslide susceptibility mapping by using spatial regression and geographic weighted regression.
- To compare various methods for determining rainfall trigger threshold for landslides
- To propose a new hazard assessment methodology to estimate the spatial and temporal probability of rainfall triggered landslides.
- To develop a new RS- and GIS-based consequence assessment approach to estimate the vulnerability of elements at risk on regional and local scales.
- To implement and validate the proposed methodology in Bartın Kumluca Basin, Turkey on regional and local scales.

1.4 Outline of the Thesis

The thesis study is organized in four main chapters as follows;

The second chapter is the "Methodology" chapter. In this chapter, in addition to the theoretical overview and the literature, the general methodology adopted for this thesis is presented. The literature survey and the methodology adopted are presented for each component of risk, which involves data collection, susceptibility mapping, triggering, hazard assessment, consequence, and risk assessment. Each component is described by considering two different scales, local and regional scale.

The third and the fourth chapters contain the "Implementation" part. These chapters are organized for the implementation of the methodology for two different scales, regional and local respectively. In the regional scale risk assessment part, a comprehensive landslide risk assessment considering data collection, susceptibility, hazard, vulnerability, elements at risk and risk assessment was conducted for Bartın Kumluca region. In this part, four different mapping methods and two different mapping units were considered to analyze the differences between the resultant maps and their affects on the resultant risk maps. In the last part of this chapter, the susceptibility maps obtained from different mapping units and methods were

compared in addition to the risk map comparison. High hazard regions on regional scale were interpreted for more detailed risk assessment and Hepler region was identified as a high risk zone to adopt the local scale risk assessment methodology. In the local scale implementation part, the hazard value obtained from the regional scale maps was used and the vulnerability and elements at risk were conducted to produce local scale risk maps. The resultant risk maps were compared and the similarities and dissimilarities for different risk maps obtained by using different mapping methods and mapping units were evaluated and discussed.

In the "Conclusion" chapter, an evaluation is given regarding the aim, the objective of the study, and the analysis of these objectives. Finally, the recommendations and the conclusion of the study are presented and some suggestions are put forward for the future studies.

CHAPTER 2

METHODOLOGY

2.1 Introduction

The objective of this study is to develop a GIS- and RS-based methodology for quantitative landslide hazard and risk mapping on local and regional scale and to investigate the effects of several landslide hazard mapping procedures on final risk maps. The methodology of this study is composed of six consecutive steps including data collection, susceptibility assessment, analysis of triggers, hazard assessment, consequence analysis and risk assessment (Figure 2.1.).

In this thesis, the proposed methodology involves two different scales: local and regional scales. The landslide risk assessment procedure at each scale requires the following issues to be addressed: (1) probability of landsliding, (2) consequence of landslide, (3) vulnerability of property and people to landslide, (4) landslide risk to property and people (Dai et al., 2002). The type of data and methods adopted in each stage depends on the scale of the risk assessment framework, i.e. whether it is applied at the regional level for numerous slides or at the local level for a single slope. Therefore, it is better first to introduce the data requirement for the components of the risk and then describe each component individually.

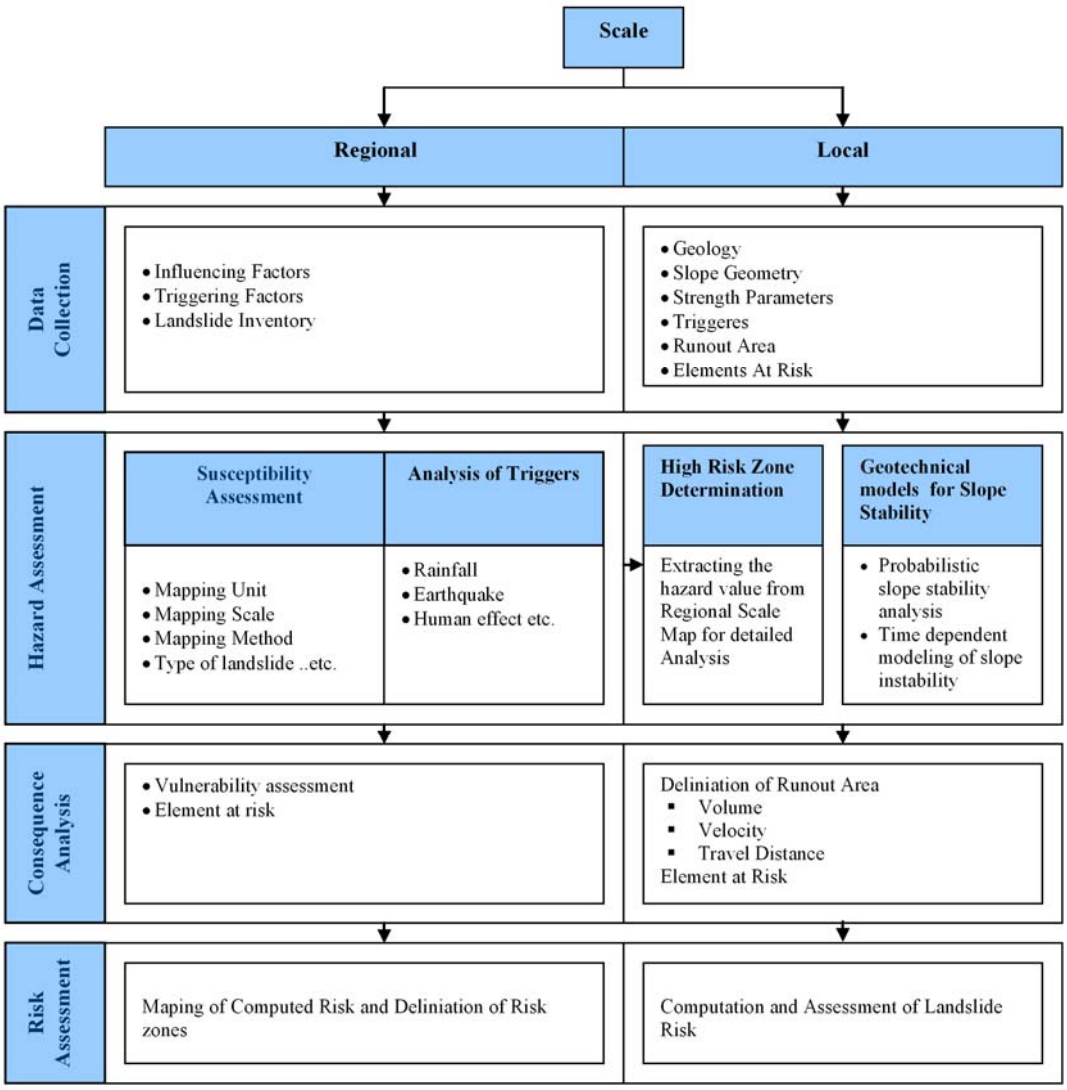

Figure 2.1. Basic steps in landslide risk assessment

2.2 Data Collection

Data collection is required for susceptibility assessment, hazard analysis, and consequence analysis. Figure 2.2 gives a schematic overview of the main data sets required for components of landslide risk assessment. While both the landslide inventory and the influencing factors are necessary to obtain susceptibility maps, triggers are the required data for hazard assessment of temporal probability, and in order to create a consequence map, the list of elements at risk will be required.

The data collection is directly related to the scale. The regional scale hazard and risk assessment require data in the form of maps whereas the local scale hazard and risk

assessment demand specific geotechnical investigations including observational procedures.

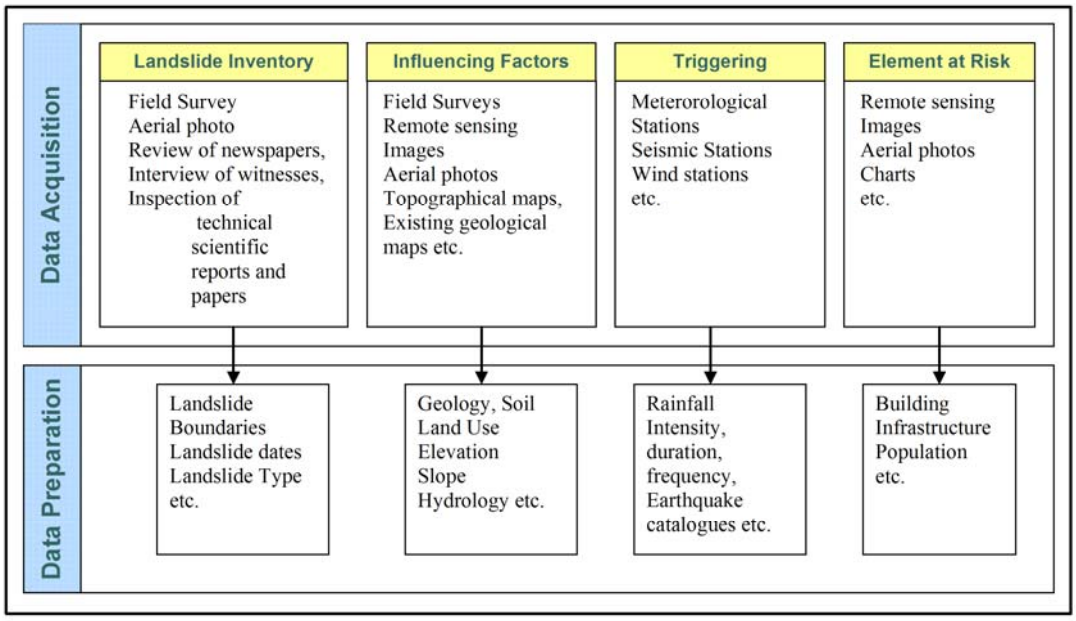

Figure 2.2. Schematic overview of the data sets (adopted from van Westen et al., 2006) involved in landslide risk assessment

The most straightforward initial approach to any regional scale landslide hazard analysis is compilation of a landslide inventory map. This map generally shows the spatial distribution of landslides in an area and provide information about the characteristics, type of slope movement, dates of activity, thickness of material, and so on. These maps are based on the interpretation of aerial photo in different time periods with geomorphologic field checking (Dai et al., 2002; Guzzetti et al., 2000). The landslide locations are imported into GIS environment and represented with vector file, forming the cumulative landslide inventory map.

When assessing the probability of landslides for a specified period of time and within a given area, the priority is given to the recognition of the conditions that cause the slope to become unstable and to the identification of the processes that trigger the movement. The factors that are responsible for creating a landslide on a particular slope or in a particular area may be categorized into two groups: the influencing (preparatory, intrinsic) factors that make the slope susceptible to failure without actually initiating it, such as slope, aspect, geology, lithology, topographical

elevation, vegetation triggers, and geotechnical properties and so on, and the triggering (extrinsic) factors that cause the failure, such as heavy rainfall, earthquakes, and human activities and so on.

Lithology and slope gradient are important contributing factors leading to landslide activity. Most assessments of susceptibility utilize slope angle and/or lithology as commonly-used independent variables for susceptibility mapping (Carrara, 1983; Anbalagan, 1992; Campbell and Bernknopf, 1993; Maharaj, 1993; Jager and Wieczorek, 1994; Atkinson and Massari, 1998; Zezere et al., 1999; Guzzetti et al., 2000; Lee and Min, 2001; Ohlmacher and Davis, 2003; Ayalew, and Yamagishi, 2005, Ayalew et. al., 2005). Topographical elevation is also significant due to its property of controlling the degree and the type of erosion (Dai and Lee, 2002). Human activities, however, are rarely referred to in the literature (Pachauri and Pant, 1992; Gritzner et al., 2001; Ercanoğlu and Gökçeoğlu, 2002; Can et al., 2005; Ayalew, and Yamagishi, 2005; Ayalew et. al., 2005). Aspect can influence the concentration of soil moisture; hence it can have an impact on the distribution and density of landslides (Wieczorek et al., 1997). Although its relation to mass movement has long been investigated, several authors (e.g., Carrara et al., 1991; Maharaj, 1993; Gökçeoğlu and Aksoy, 1996; Atkinson and Massari, 1998; Jakob, 2000; Nagarajan et al., 2000; Ayalew, and Yamagishi, 2005; Can et al., 2005; Akgün and Bulut, 2007) have considered aspect as a factor in landslide activity. Planar and profile curvatures are the second and the first derivative of a surface, hence they are mostly found to be redundant in the susceptibility analysis; however, it's taken into consideration by a few researchers (Lee and Min, 2001; Lee, 2004; Can et al., 2005). Land use refers to the type of vegetation cover on the slope, which may cause slope instability for shallow landslides. Several researchers emphasized the importance of vegetation cover in landslide activity (Carrara, 1983; Gökçeoğlu and Aksoy, 1996; Luzi and Pergalani, 1999; Can et al., 2005; Guzetti at al. 2005 and 2006; Nagarajan et al., 2000; Baeza and Corominas 2001; Fernández et al. 2003). Rivers, roads and lineaments are linear features whose influences are spatially limited; however, by using distance or density analysis in GIS, it's worth analyzing their contribution to slope movements (Yeşilnacar and Topal, 2005; Ayalew et al., 2005).

In order to generate the necessary variables to identify the influencing factors, remote

sensing products (multispectral satellite imagery and aerial photographs), topographical maps, and existing geological maps are used (Süzen and Doyuran, 2004; Weirich and Blesius, 2007). Furthermore, data from meteorological stations, seismic stations, and wind stations will be required in order that the variables can be obtained to discover the triggering factors. If no data is available from meteorological stations, generally rainfall estimates from satellite imagery can be used for larger regions. The data can also be grouped into two as static or dynamic. The basic static data sets are stable, which are generally seen in geology, soil types and geomorphology (van Westen et al., 2008). Yet, dynamic data sets need to be updated regularly and may range from hours to years such as meteorological data, land use and elements at risk data. Generally, the influencing factors and historical landslide information will be analyzed for cause-effect relationships by using heuristic or statistical methods. This analysis leads to susceptibility map production. Landslide susceptibility maps combined with frequency analysis of triggering factors transform susceptibility maps into hazard maps.

In developing a method for landslide risk assessment, it is of fundamental importance to collect data about consequences of landslides (losses due to landslides). The analysis of consequences involves determination of elements at risk and vulnerability of elements at risk. The vulnerability of elements at risk depends on the understanding of the interaction between a given landslide and the affected elements. Elements at risk for a regional scale analysis refer to the population, buildings, road networks, services, utilities and infrastructure and so on (van Westen, 2005). Most of these features can often be derived from existing cadastral databases, and population data may be derived from existing census data. If there is no existing digital cadastral database, it may be possible to digitize the elements at risk from the satellite images (van Westen, 2008). However, due to the size of the study region, digitizing may be cumbersome. Automatic extraction of features from high resolution images requires acquisition of various satellite images for a large region, which makes this solution unpractical in economical terms. Even though digital information for elements at risk exists, the development of a GIS database for these features requires considerable effort since it is complex to define. In addition, in regional risk assessment studies, it is generally difficult to obtain information about the vulnerability of elements at risk from landslide initiation. Therefore,

generalization approaches are adopted - as in the study of Glade et al., 2003- where it is assumed that if an element at risk is affected by a landslide, then its totality will be destroyed.

On the other hand, specific slope situations usually do not require high amount of data collection for vulnerability and consequence analyses, as the elements at risk can be relatively easy to determine (Düzgün and Lacasse, 2005). Local slope instability problems widely employ geotechnical models, which involve application of mainly slope stability models. These models require input data from field work with some laboratory testing, where the evaluation area changes from several hectares to several tens of square kilometers. Therefore, these methods are normally applied only in small areas. In order to perform a stability analysis, the data required for a single slope involve topographic attributes (e.g. slope angle, vertical and horizontal curvatures, slope aspect, distance to divide or channel, contributing area, etc.), hydrological conditions (e.g. soil saturation, permeability, hydraulic conductivity), geometry (height, width and inclination of slope) and generalized geotechnical information of soil properties (e.g. cohesion, angle of internal friction, specific weight). In addition, the creation of hazard maps on local scale will need triggers (rainfall intensity, ground water level, seismic load magnitudes, etc.) and the creation of consequence maps involves the location and characteristics of elements at risk with more detail, such as the number of buildings, length of transportation, the number of people, farm lands on the slope and in the runout zone and the like (Thomas and Michael, 2004; Düzgün, 2008). In addition to the field surveys on local scale, the remote sensing data is mostly preferred to obtain the elements at risk like buildings and road features.

2.2.1 Data Collection and Processing for the Proposed Methodology

Data collection and processing is the first stage of the proposed methodology. The data collection framework in this thesis was adopted from Düzgün (2008). For regional scale risk assessment, data collection and related data processing has three main parts: Data for susceptibility mapping, data for analysis of triggers and data for consequence analysis (Figure 2.3).

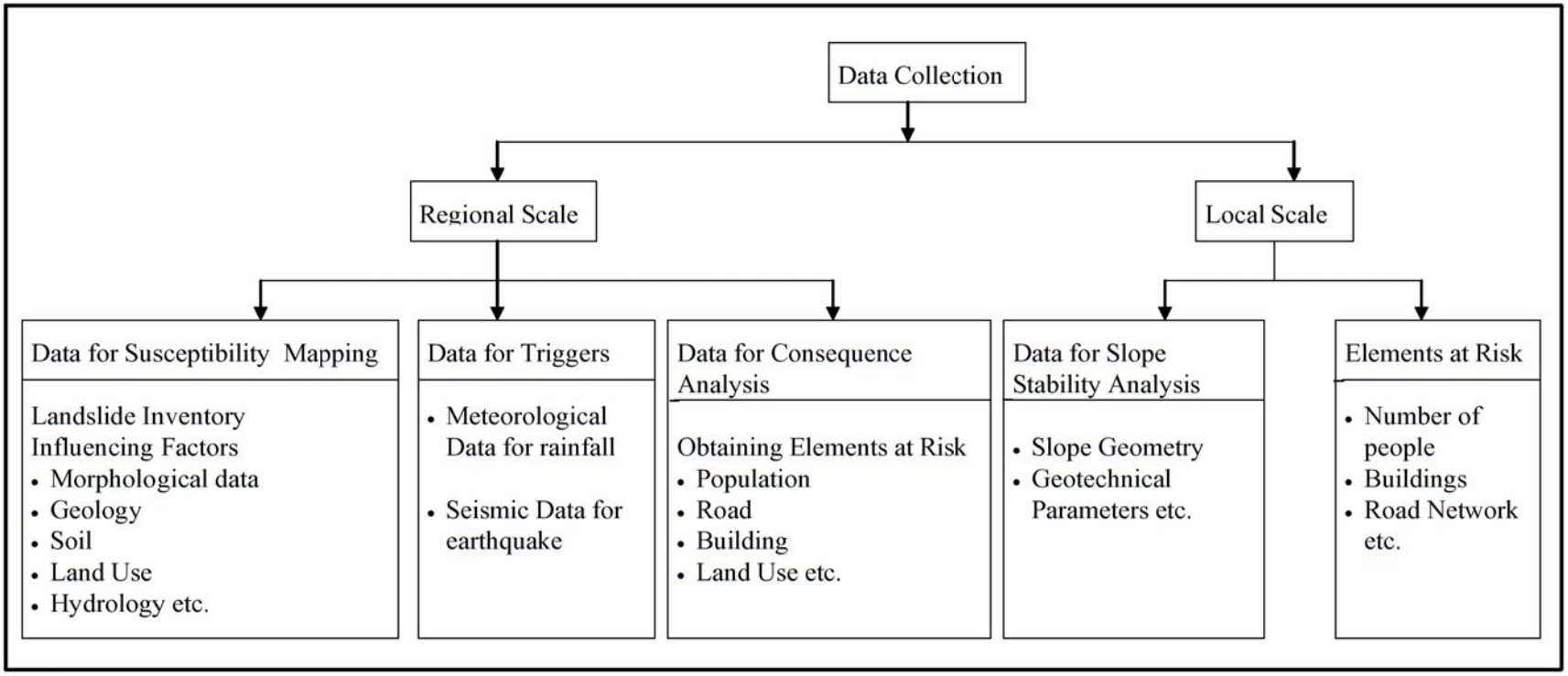

Figure 2.3. Data collection and data processes frame work

In addition, for local scale analysis, data collection has two main parts: data for slope stability analysis and elements at risk for consequence analysis (Figure 2.3). Slope stability analysis can adopt two different approaches. The first approach follows the regional scale analysis. After determination of the high-risk areas, a more specific study is carried out at a slope where the hazard value is obtained from the regional scale. This approach has been adopted in this thesis study, in which Hepler village is interpreted as the high risk zone based on the regional scale analysis. The second approach follows individual slope analysis. This analysis involves application of geotechnical studies for hazard analysis, which require enormous data sets from field and laboratory tests.

The landslide inventory usually involves the locations of past landslides as well as their types, dates etc. The types of data layers for influencing factors can be divided into five main groups; i.e., morphological data (maps of digital elevation model (DEM), slope, aspect, curvature, etc.), geology (lithology, faults, etc.), soil (soil type, soil depth, erosion, etc.), land use (land use map, vegetation cover, road, etc.), and hydrology (soil moisture, stream network, etc.). In order to obtain relevant input such as vegetation cover, land-use maps, wetness index data etc., medium resolution satellite images are often used.

Influencing factors are required to predict the spatial probability of future landslides and the GIS is used to store, monitor, evaluate, compile, manipulate and manage data. There are few studies in the literature which supplement clear information as to the preparation and processing of the data (Baeza and Corominas, 2001; Ercanoğlu et al., 2004; van Westen et al., 2008). In most published studies, the type of analysis conducted on the raw data set and the related statistical analyses are not described clearly. They mostly indicate the dataset used and the description of the raw data only. In this thesis study, in addition to the detailed description of raw input data set and the analysis of the relationship between each influencing factor and landslide frequency, the statistical analysis of the influencing factors contributing to landslides was described in detail. The statistical process comprises pre-analysis of the data set before constructing the database for further analysis. The statistical treatment of the influencing factors changes depending on the adopted procedure. Hence, the partition of the land surface into mapping unit may be determined initially. In this study, two

different mapping units, grid and slope units, were adopted for the analysis. For each mapping unit, (i) transformation of qualitative variables, and (ii) selection of independent variables by multicolinearity analysis, (iii) testing for normal distribution for each variable was carried out. As a result, two different spatial databases were constructed. These databases were used to predict the future landslide locations by using different methods for each mapping unit on regional scale.

Spatial probability maps can be converted into hazard maps by combining temporal probability with susceptibility map. Temporal behavior of landslides is estimated by means of frequency of landslides for a region. The frequency of landslides can be obtained from historical landslide data, triggering event frequencies (eg. rainfall, earthquakes) with known annual exceedance probabilities (Cascini et al., 2005). In this thesis study, the frequency was assessed with the landslide occurrence dates to obtain the temporal probability.

On regional scale, the procedure followed to obtain the consequence analysis differs from the local scale procedure, which also causes a change in the data collection procedure. On regional scale, it is more difficult to identify elements at risk and determine the vulnerabilities of each element at risk. The main reason is that run-out should be predicted to determine the elements which may be exposed to landslides. However, it is a challenging issue to define the run-outs for a number of landslides on regional scale. The vulnerabilities of elements at risk may change depending on their geographical and temporal existence with respect to landslides. In addition, the value or cost of each element at risk may vary depending on its type. Therefore, mostly quantitative assumptions can be adopted for estimation of vulnerabilities and the elements at risk can be obtained by overlaying the existing hazard maps with the land-use maps on regional scale. In this study, the elements at risk were determined from the existing topographic maps, and the inhabitants were estimated per house in rural areas using the population density of Kumluca settlement. The vulnerability level was evaluated as 1 for all elements at risk.

For local slope analysis, two different approaches were proposed in the methodology for slope stability analysis, which requires different data sets. If a quick risk map following a regional scale analysis is required for a local slope, then the hazard

values of that slope can be obtained from the regional scale hazard map. Therefore, there is no need to collect data for hazard analysis. This approach was followed in this thesis study and it is not present in the literature yet. On the other hand, a comprehensive local slope study requires geotechnical modeling, which can be encountered in the literature. This geotechnical modeling contains the assessment of deterministic models or probabilistic analysis. The analysis of slope stability for a single slope requires extensive data including geometrical data, shear strength parameters (cohesion and angle of internal friction), depth below the terrain surface, soil layer thickness, angle of internal friction, slope angle, pore water pressure and the like, which are mostly determined in the field or in the laboratory.

On local scale, it can be relatively easier to determine the elements at risk, but a more detailed data collection procedure is required such as a detailed survey of the elements at risk, type of the elements at risk, its usage, size, and the number of inhabitants in each building, and seasonal or temporal movement of the population. If no digital data exist on local scale, remote sensing products can be used to extract the element at risk data, such as road network and buildings. It might be possible to digitize the elements at risk from high resolution images, which entails considerable amount of work. On the other hand, the elements at risk can be automatically extracted from images using various image processing and enhancement techniques. The population data is required for each individual building to estimate the loss of life. The population data can be collected through field inquires which are time-consuming and costly. On the other hand, recently remote sensing has had potential for predicting the population with low cost and up-to-date data. Wang (1990), Zhang (2003), Lu et al. (2006), Morton and Yuan (2008), and Erener and Düzgün, (2009) has examined residential population dynamics from satellite remote sensing images. In the thesis study, an algorithm was developed to obtain the elements at risk and the number of inhabitants per house was obtained by field surveys.

Moreover, the estimation of the run-out of the area for the slope is required, which is governed by the volume, velocity, and topography of the region (Düzgün, 2008). The Digital Elevation Model (DEM) is the most crucial factor in the modeling of the run-out distance for landslides on local scale. Hence, in field, a detailed survey of topography is mostly required, which can be done by using Lidar, GPS instruments

or other engineering surveys.

The damage is related to the temporal occurrence of landslides. Thus, daily and seasonal movements of dynamic elements (residents of the buildings, cars, trains etc.) are also required for a reliable estimation. Consideration of the dynamic property of elements is also another difficulty to estimate the vulnerability.

To quantify the elements at risk, the exposure of each element is needed for consequence analysis. This requires compilation of data from different organizations through interviews with the employees, which is a time-consuming process.

2.3 Hazard Assessment

Varnes et al. (1984) proposed the most widely adopted definition of landslide hazard as "the probability of occurrence of a potentially damaging phenomenon (landslide) within a given area and in a given period of time". Hence, basically, a landslide hazard assessment methodology is composed of two important aspects. The first one is susceptibility mapping, which involves assessing the spatial probability of a landslide-prone area. The other aspect is determining the probability of occurrence of a specific triggering event.

In the literature, there is confusion over the concepts of hazard and susceptibility. Most hazard maps in the literature are in fact susceptibility maps, where landslide-prone areas are determined based on the correlating influencing factors with the landslide inventory. By definition, hazard mapping should contain information about the probability of landslide occurrence for a given area in a specified period of time (Varnes 1984). Hence, effective landslide hazard maps can be constructed based on the combination of spatial and temporal prediction of the landslide occurrence probability. In this study, susceptibility was considered as the relative indication of the spatial probability.

2.3.1 Literature Review on Susceptibility Mapping

Susceptibility mapping forms the basis of any hazard mapping, which is an essential part of quantitative risk mapping. These maps can be expressed as relative hazard (Einstein, 1988; Hartlen and Viberg, 1988), landslide-deposits inventory (van Westen, 1993), and total landslide density or likely frequency (Evans and King, 1998; Evans et al., 1997). A landslide susceptibility map ranks the slope stability from stable to unstable in categories in order to determine zones of landslide-prone areas without any temporal implication. These maps represent the occurrence of landslides (Chacon et al., 2006) and they are useful for areas where there is lack of information about the triggering events of landslide and not enough information concerning historical records.

The choice of susceptibility mapping method depends on a variety of factors, which are the type of susceptibility method, the mapping unit, scale, the type of landslide, and availability of data, triggers, and the purpose of mapping.

2.3.1.1 Susceptibility Mapping Methods

Numerous efforts have been devoted in the last three decades to evaluating landslide susceptibility and no agreement has been reached either on the procedure or the scope of producing landslide susceptibility maps (Brabb, 1984).

The proposed methods for susceptibility assessment are based on widely accepted principles or assumptions as the following (Varnes and IAEG, 1984; Carrara et al., 1991; Hutchinson et al., 1991; Hutchinson, 1995; Aleotti and Chowdhury, 1999):

i. The past and present landslides are keys to the future landslides

ii. The future landslides will always occur in the same conditions as in the past

iii. The main conditions that cause landslides are controlled by identifiable physical factors.

The susceptibility assessment methodologies can be classified mainly as qualitative

or quantitative approaches as presented in Figure 2.4, similar to those proposed by such authors as Carrara (1988), Hutchinson (1995), Leroi (1996) and Soeters and van Westen (1996).

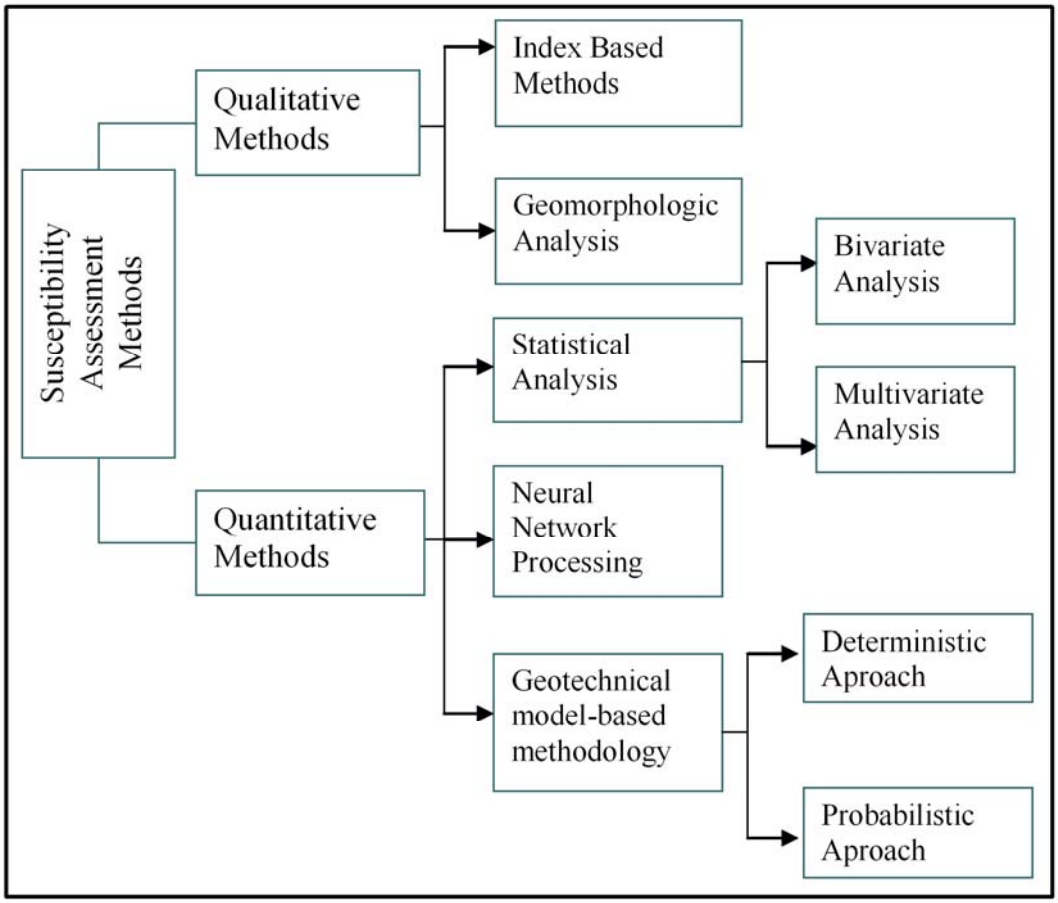

Figure 2.4 Landslide susceptibility assessment classifications

Some significant contributions to general review of the concepts, principles, techniques, and methodologies for susceptibility assessment and evaluations of subsequent approaches are given in: Brabb et al. (1972), Carrara et al. (1978), Cotecchia (1978), Carrara (1983), Brabb (1984), Varnes (1984), Crozier (1986), Einstein (1988), Hartlen and Viberg (1988), Mulder (1991), van Westen (1993) (1994), Leroi (1996), Soeters and van Westen (1996), Aleotti and Chowdhury (1999), Guzzetti et al. (1999), Miles and Ho (1999), Wu and Abdel-Latif (2000), Carrara et al. (2001), Chung and Fabbri (2003), Remondo et al. (2003), Van Westen et al. (2003), van Westen (2004), Chung and Fabbri (2005), Huabin et al. (2005), Chaco´n et al. (2006).

2.3.1.1.1 Qualitative Methods

Qualitative methods are subjective and portray the susceptibility zoning in descriptive terms. The qualitative methods involve mapping of spatial distribution of mass movements based on one way or a combination of ways: the aerial photo-interpretation, field survey, and catalogue of historical landslides in the region (Demek, 1972; Demek and Embleton, 1978). An overview of qualitative methods is illustrated in Table 2.1 and Table 2.2. Table 2.1 and Table 2.2 include information as to where and upon what size of an area they are applied and by whom they are implemented. Table 2.1 summarizes the photo-interpretive analysis for landslide inventory mapping and/or susceptibility zoning by geomorphological analyses. Table 2.2 summarizes the index based methods for susceptibility mapping. The regions reviewed here range between 30 and 8456 km^2.

Table 2.1 Review of geomorphologic analysis for susceptibility mapping

Region	Area (km^2)	Source
Staffora river basin, (Italy)	280	Carrara et al. (2003)
La Honda basin, California	17	Carrara et al. (1992)
Southern Apennines (Italy)	30	Parise (2001)
Lands between Kelso and Woodland	275	Wegmann, (2002)
Umbria (Italy)	8456	Cardinali et al. (2002b)
San Mateo County, California, (USA)	Not defined	Brabb and Pampeyan (1972)
Kathmandu, (Nepal)	Not defined	Ives and Messerli, (1981)
Zonguldak (Turkey)	39.081	Duman et al. (2005a)
Umbria (Italy)	8456	Ardizzone (2005)
Flemish Ardennes (Belgium).	125	Van Den Eeckhaut et al. (2007)
Andorra, Pyrenees Mountains (between Spain and France)	5	Copons and Vilaplana (2008)
Gran Canaria island, (Spain)	49	Jose et al. (2000)
Tuscan-Emilian Apennines (Italy)	Not defined	Zanutta et al. (2006)

Table 2.2 Review of index based analysis for susceptibility mapping

Region	Area (km^2)	Data Used	Source
Colorado Plateau, the Appalachian Highlands, the Coast Ranges of California, and the Southern Rocky Mountains, (USA)	Not defined	Rock types, structures, topography, precipitation, landslide type, and landslide incidence	Radbruch et al. (1982)
La Cabrera Sierra (Madrid)	Not defined	Reach angle, run-out distance	Ayala-Carcedo et al. (2003)
Southeast Umbria, East of Spoleto (Perugia)	18	Distance from faults, parallelism between the fractures and the landslide scarps, land use, lithology, distance from the streams, orientation and steepness of slopes, orientation of layers compared to the slope.	Donati and Turrini (2002)
Wushan–Badong area in theThree Gorges (China)	Not defined	Slope angle in relation to lithology; distance to drainage network in relation to stream order; and distance to tectonic lineament in relation to lineament length.	Fourniadis et. al. (2007)
YangSan area, (Korea)	339.67	Lithology, elevation, slope gradient, slope aspect, lineament, drainage, vegetation, and land use	Nguyen and Bui, (2004)
Alpago, (Italy)	20.8	Geomorphological maps, lithology, structural geology, surficial materials, slope, land use, distance from streams, roads and houses	Van Westen et al., (2003)
Swabian Alb (SW-Germany)	500	Soil type, Geological units, Distance-escarpment, Hydro-geological units, Lineament-density, Lineament-distance, Geomorphological units, Slope angle, Curvature	Neuhäuser and Terhorst (2007)
Jurassic escarpment in the Swabian Alb (SW-Germany)	500	Geology, lineament-density,curvature, slope angle, distance-escarpment and soil type.	Neuhäuser and Terhorst (2007)
Rio Mendoza Valley, (Argentina)	1600	Lithology, slope angle, landslide distribution and landslide activity	Moreiras (2005)
Texas, (USA)	Not defined	Slope, geology, vegetation, and proximity to faults.	Wachal and Hudak (2000)
Pena Canyon and Big Rock Canyon, Santa Monica, CA	1.90 1.80	Slope angle, dip angle, dip angle versus the slope angle factor, distance to faults factor, distance to roads factor, distance to streams factor, lithology factor, soil permeability factor, land cover factor.	Weirich and Blesius (2007)
Dessie area, (Ethiopia)	16	Geological, geotechnical, geomorphological, hydrogeological, and anthropogenic factors	Ayenew and Barbieri (2005)
Tsugawa area of Agano River, Niigata Prefecture, (Japan)	53	Elevation, slope gradient, aspect and curvature.	Ayalew et al. (2004)
Yomra and Arsin (Trabzon)	38.87	Slope angle, slope aspect, distance from drainage, distance from roads and the weathered lithological units	Akgün and Bulut (2007)
Guizhou(China)	176,167	Slope, lithology, landslide inventory, tectonic activity, drainage distribution and annual precipitation	Wang, et al. (2008)
More and Romstal (Norway)	12,168	Slope, aspect,curvature, lineaments, vegetation index and elevation	Erener and Düzgün (2008)

Since the late 1960's, a number of maps have been made on qualitative landslide

susceptibility by various researchers: Blanc and Cleveland (1968), Pomeroy (1974), Scott (1972), Brabb and Pampeyan (1972), Brabb (1976), Radbruch et al. (1982), Mahr and Malgot (1978), Kienholtz (1978), Rodriguez Ortiz et al. (1978), Hinojosa and Leon (1978), Ives and Messerli (1981), Van Den Eeckhaut et al. (2007), Parise (2001), Cardinali et al. (2002a), Zanutta et al. (2006); Schädel and Stober (1988), Thein (2000), Neuhäuser and Terhorst (2007). These methodologies are also defined as expert evaluation approaches (Leroi, 1996; Jose, 2000), in which an expert of geomorphology decides on the type and degree of hazard for each area. They can be divided into two types, direct mapping or indirect mapping. In the direct mapping approach, the degree of hazard is mapped based on the field geomorphologic analysis. The indirect mapping approach utilizes the combination or overlaying of index maps with or without weighting.

Qualitative methods are usually geomorphologic mapping, in which an expert identifies past and present landslides as well as making predictions for future failures which are likely to occur (Carrara et al., 1995; Aleotti and Chowdhury, 1999). The expert-driven approach or the direct approach involves assessment and/or zonation of the degree of hazard directly in the field based on the experience of earth scientist, or evolving it after the fieldwork on the basis of a detailed geomorphological map. Overviews of conventional geomorphological mapping systems on medium and large scale are presented by Demek and Embleton (1978) and Van Zuidam (1986).

The major drawback of these types of maps is that it is a time-consuming process due to the requirement of lengthy field surveys. Besides, the maps are hardly reproducible because of subjectivity (Dai and Lee, 2001). Examples of susceptibility maps based on field analysis can be frequently found between the 1970's and early 1990's (Carrara and Merenda, 1976; Fenti et al., 1979; Kienholz, 1978; Ives and Messerli, 1981; Rupke et al., 1988; Carmassi et al., 1992; Terhorst, 1997, 2001; Jose, 2000; Parise, 2001).

The historical aerial photos are of fundamental importance for qualitative analysis as given in Brabb and Pampeyan (1972), Wegmann (2002), Van Westen et al., 2003, Ardizzone (2005), Zanutta et al. (2006), Duman et al. (2005a). Carrara et al. (1992) and (2003) compare the landslide maps produced independently by different

investigators for the same region (Table 2.1). In addition to aerial photos, with the development of technology, Van Den Eckhaut et al. (2007) maps old landslides by using Lidar (Light Detection and Ranging) images with the help of the expert knowledge of seven geomorphologists (Table 2.1).

In addition to medium and regional scale analysis, for large slopes Rouiller and Marro (1997), Rouiller et al. (1998) and Jaboyedoff et al. (2004) use rating methods based several factors such as structural geology, weathering, seepages, etc. to assess the propensity of large rock falls. Copons and Vilaplana (2008) obtained the records of rock falls by means of geomorphologic analysis to analyze the susceptibility of minor rock falls on large scale (Table 2.1).

Index based methods are also called heuristic methods. Heuristic methods involve ranking and weighting of instability factors according to their assumed or expected importance based on their effects on landsliding (Nilsen and Brabb, 1977; Amadesi and Vianello, 1978; Hollingsworth and Kovacs, 1981; Neeley and Rice, 1990; Montgomery et al., 1991; Mejıa-Navarro et al., 1994; Jose et al. 2000). GIS-based overlay functions have strongly facilitated the use of a combination or an overlay of index-based maps with or without weighting on any scale to assess landslide susceptibility (Huabin et al., 2005). The main reason is that GIS allows easier application of arithmetic procedures and overlay analysis. Examples of these studies can be found in Pachauri and Pant (1992), Maharaj (1993), Gökçeoğlu and Aksoy (1996), Hylland and Lowe (1997), Pachauri et al. (1998), Turrini and Visintainer (1998), Dhakal et al. (1999), Luzi and Pergalani (1999), Wachal and Hudak (2000), Donati and Turrini (2002), Sarkar and Kanungo (2004), Moreiras (2005) and Ayenew and Barbieri (2005).

As geomorphological analysis depends on the expert subjective criteria and the appropriate interpretation of the landscape, in the study of Moreiras (2005) each parameter conditioning landslide occurrence is analyzed and ranked according to the slope instability conditions in order to reduce subjectivity and to quantify the degree of susceptibility (Table 2.2). Qualitative ranking was applied in this methodology to create susceptibility. Wachal and Hudak (2000) and Erener and Düzgün (2008) applied a scoring method (Table 2.2). In these studies, a numerical rating system is

applied first by grouping the data into categories, then assigning a value to each category, and then assigning weights to each factor between 0.0 and 1.0 based on their relative importance to slope instability in the study area.

To provide qualitative maps Bonham-Carter (1994), Van Westen et al. (2003), Nguyen and Bui (2004), and Neuhäuser and Terhorst (2007) use the weights-of-evidence method (Table 2.2). In this method, a pair of positive and negative weights is calculated for each causative factor. This calculation is done by applying the log-linear form of the Bayesian probability, which describes how probably a landslide will occur in the case of present factor and in the case of absent factor. Wang et al. (2008) assess the susceptibility with trapezoidal fuzzy number weighting (TFNW) approach (Table 2.2). The weighting procedure showed that the TFNW is an efficient method for landslide causal factors weighting. Ayalew et al. (2004) and Akgün and Bulut (2007) use the weighted linear combination model (Table 2.2), which is a hybrid method between qualitative and quantitative methods in landslide susceptibility assessments. This technique has been described by Saaty (1988, 1994) and Saaty and Vargas (2001) in the context of decision making processes and it is likely to be the best known and commonly used multicriteria-GIS method (Eastman 1999; Jiang and Eastman 2000). In the weighted linear combination (WLC) model, the class weights of landslide triggering factors are determined using the analytical hierarchy process (AHP) and then each factor is multiplied with the determined weight values and so the weighted factor maps are obtained for the studied area. Finally, all the weighted factor maps are overlaid and a landslide susceptibility map is produced. Akgün and Bulut (2007) compared Logistic regression (LR) and WLC methods and the results showed that the WLC model is more suitable than the LR model.

Most susceptibility maps are performed on small or medium scales, in general lower than a scale of 1:25,000. Ayala-Carcedo et al. (2003) explore the problems and possibilities of large scale mapping. They analyze a rock fall front in the Sierra de la Cabrera (Madrid, Spain) by a heuristic approach (Table 2.2).

2.3.1.1.2 Quantitative Methods

The quantitative methods include statistical methods, neural network analysis, geotechnical approaches, and fuzzy set-based approaches. Quantitative methods produce numerical estimates for probability of landslide occurrence phenomena for areas currently free of landslides, and have conditions similar to the past landslide occurrence areas (Guzetti et al., 1999; Chung and Fabbri, 1993; Huabin et al., 2005). Examples of quantitative or semi-quantitative analysis using these methods in the literature are Reger (1979), Carrara (1983), Bernknopf et al. (1988), Carrara et al. (1991, 1992, 1995, 2003), Jade and Sarkar (1993), Chung et al. (1995), Baeza and Corominas (1996, 2001), Wieczorek et al. (1996), Van Westen et al. (1997), Atckinson and Massari (1998), Rowbotham and Dudycha (1998), Nagarajan et al. (2000), Sakellariou and Ferentinou (2001), Baeza and Corominas (2001), Ardizzone et al. (2002), Bianchi and Catani (2002), Cardinali et al. (2002b), Dai and Lee (2002, 2003), Ercanoğlu and Gökçeoğlu (2002, 2004), Lee et al. (2003), Lu and Rosenbaum (2003), Olhmacher and Davis (2003), Santacana et al. (2003), Süzen and Doyuran (2004), Ayalew and Yamagishi (2005), Guzetti et al. (2005), Ermini et al. (2005), Gomez and Kavzoglu (2005), Düzgün (2008, 2009). The summary of quantitative methods is listed in Table 2.3-Table 2.6.

Among quantitative methods, the statistical methods are the most popular ones. They can easily be implemented in GIS. GIS allows extraction of parameters such as slope gradient, slope aspect, slope convexity, watershed area, drainage network, and so on. These parameters can easily be included for susceptibility analyses in GIS environment. Complete overviews of the use of GIS for landslide susceptibility assessment can be found in Van Westen (1994) and Carrara et al. (1995), and the statistical methods applied by using GIS involve studies of van Westen (1993), Carrara et al. (1990), Carrara et al. (1995), Carrara et al. (1999), van Westen et al. (1997), Thurston and Degg (2000), Ohlmacher and Davis (2003), Melelli andTaramelli (2004), Çan et al. (2005), Duman et al. (2006), Erener et al. (2007) and Akgün and Bulut (2007).

Statistical approaches are based on the observed relationship between each factor and the distribution of landslides (Huabin et al., 2005). This requires a landslide inventory map, which is used in combination with a series of

environmental factors, and is based on the assumption that landslides are likely to occur under the same conditions as those under which they occurred in the recent past (Van Westen et al. 2005). Since the instability determinants and their interrelations are evaluated on a statistical basis, susceptibility evaluation becomes an operation as objective as possible.

Statistical techniques are generally considered as the most appropriate approach for landslide susceptibility mapping on medium scales (1:10,000–1:50,000). This can also be seen in Table 2.3, where most of the application scales are on a medium scale. The main reason for this is that it is possible to map the occurrence of past landslides in detail and to collect sufficient information on variables which are considered to be relevant to the occurrence of landslides (Huabin et al. 2005; Dai et al. 2002). Examples of statistical analyses are by Carrara et al. (1991), Jade and Sarkar (1993), Guzzetti et al. (1999), Lee and Min (2001), Ercanoğlu et al. (2004), Ayalew and Yamagishi (2005), Erener and Düzgün (2006) (Table 2.3, Table 2.4, Table 2.5 and Table 2.6).

Table 2.3. Review of bivariate susceptibility mapping methods.

Region	Area (km^2)	Factor	Landslide Type	Cell Size	Source
Konkan Coast, (India)	Not defined	Land cover vegetation, drainage density, slope aspect, relative relief, stratification of rocks, joint discontinuity/lineament, weathering, soil type, soil–rock interface, rainfall.	Not defined	Not defined	Nagarajan et al. (2000)
Kuzulu landslide Sivas (Turkey)	6.9	Geology, slope, aspect, elevation, topographic-wetness index and stream-power index	Earth flow	25x25 m	Gökçeoğlu et al. (2005)
Asarsuyu catchment, Bolu (Turkey)	200	Slope, aspect, lithologic map, fault density, elevation map, land cover map, distance to drainage, distance to lineament, distance to ridge, distance to E-5 highway, distance to power and road network and distance to settlement.	Earth flow and shallow translational slides	25x25 m	Süzen and Doyuran (2004)
Janghung area (South Korea)	Not defined	Landslide location, geological structure and topography	Not defined	20x20 m	Lee et al. (2002)
Janghung area (South Korea)	41	Slope gradient, slope aspect, and curvature of topography, Soil texture, material, drainage, and effective depth forest type, diameter, and density, land cover	Debris flows and shallow soil slips	10 x 10 m	Lee (2004)
Terni basin (Italy)	15.3	Geology, slope, distance from rivers and distance from faults	Debris-flows	25×25m	Melelli and Taramelli (2004)
Contraviesa Area, Granada (Spain)	94	Altitudes, slopes, aspect, hillshading, slope curvature, slope roughness, slope area and qualitative classification of landforms.	Falls, slides, flow	6x6 m	Fernández et al. (2003)

Statistical methods can be divided into two as bivariate and multivariate statistical data analysis methods.

In multivariate methods, all of the factors are treated together and their interactions assist to resolve the phenomena statistically whereas bivariate methods assume that the factors are not correlated with each other. Some examples of bivariate and multi-variate models can be found in Carrara (1983), Wang and Un-win (1992), Van Westen (1993), Baeza and Corominas (2001).

In bivariate statistical analyses, each individual factor is compared to the landslide occurrence data (Aleotti and Chowdhury, 1999) and the role of each individual parameter or that of combinations of parameters with regard to slope failures is statistically evaluated (Van Westen, 1997). The comparison is applied by calculation of the number of landslide locations in primary factors unit divided by the areal extent of that unit. The correlation analysis between landslides and their causal factors made by using bivariate statistical methods constitutes assigning objective weights. There have been many applications of bivariate methods in the literature, some of which can be listed chronologically as Brabb et al. (1972), Brabb (1984), Degraff and Romersburg (1980), Kobashi and Suzuki (1988), Yin and Yan (1988), Gupta and Joshi (1990), Pachauri and Pant (1992), Jade and Sarkar (1993), Chung and Fabbri (1993), Van Westen (1993), Irigaray (1995), Fiener and Haji (1999), Uromeihy and Mahdavifar (2000), Fernández et al. (2003), Melelli and Taramelli (2004). Some of these are listed in Table 2.3. Recently, Suzen and Doyuran, 2004 provided a GIS-based comparison between bivariate and multivariate analysis in terms of performance and accuracy.

As can be seen in Table 2.3, most researchers used slope, aspect, and vegetation parameters for bivariate statistical analysis. The cell sizes range between 6x6 m. and 25x25 m. and the regions range between 15 km^2 and 275 km^2. The method was applied to a variety of slide types such as earth flows, debris flows, and shallow translational slides and flows (Melelli and Taramelli, 2004; Süzen and Doyuran, 2004; Lee, 2004; Van Westen et al., 2003; Fernandez et al., 2003).

Multivariate analysis is one of the most sophisticated techniques for landslide

susceptibility assessment. Multivariate statistical approaches include discriminant analyses and logistic regression. This approach was applied by Neuland (1976), Carrara (1983), Bernknopf et al. (1988), Carrara et al. (1991) Wang and Unwin (1992), Baeza (1994), Chung et al. (1995), Süzen and Doyuran (2004), Ercanoğlu et al. (2004), Melelli andTaramelli (2004), Duman et al. (2006), and Tunusoğlu et al. (2008).

The purpose of discriminant analyses is to classify a set of observations into predefined classes based on their values for a set of predictors or input variables. A detailed description of the discriminant analysis can be found in David et al. (1977), Lebart et al. (1982) and Dillon and Goldstein (1986). The technique constructs a set of linear functions of environmental variables which maximizes the differences between the populations of stable and unstable slopes with minimal error (Guzzetti et al., 2006).

Some examples of the use of discriminant analysis are Reger (1979), Carrara (1983), Carrara et al. (1991), (1992), (1995), Guzzetti et al. (1999), (2006), Nagarajan et al. (2000), Baeza and Corominas, (2001), Ardizzone et al. (2002), Cardinali et al. (2002a), Santacana et al.(2003), Guzetti at al. (2005), (2006).

When using multivariate statistical methods, all parameters related to slope instability can be analyzed by multiple regression techniques or parameter maps, which are overlaid by landslide distribution maps, and the correlation is established for stable and unstable areas through discriminant analysis (Van Westen, 1997). Stepwise discriminant analysis is effectively applied in relation to a particular land surface subdivision in the mentioned hydrological slope units (Carrara et al., 1991, 1992 and 2003; Guzetti at al., 2006) and grid units (Santacana et al., 2003) to classify stable and unstable regions (Table 2.4). Carrara (1983) evaluates the landslide susceptibility by multivariate models for two different regions using both grid unit and slope unit. Most of the researchers summarized in Table 2.4 studied in an area affected by shallow landslides. Among these, Santacana et al. (2003), Baeza and Corominas (2001), and Guzetti et al. (2006) carried out their studies in areas that range between 60 and 275 km^2.

Table 2.4. Review of discriminant analysis for susceptibility mapping

Region	Area (km^2)	Factor	Landslide Type	Mapping Unit	Source
La Pobla de Lillet (Eastern Pyreenes, Spain).	Not defined	Cellheight, slope angle, slope aspect, curvature, transverse curvature, and longitudinalcurvature,sinusoidal slope angle, solar radiation, slope roughness, watershedangle and both watershed length and area of the whole basin and that of the colluvial deposits	Shallow Landslide	Grid (15 × 15 m)	Santacana et al. (2003)
Ferro (Italy)	120	slope elevation, gradient, aspect and curvature, Slong with land use/cover, drainage network	Mass movements Deep Seated landslides	Grid (200 x 200 m) Slope Units	Carrara (1983)
Buonamico (Italy)	91				
Pyrenees (Spain)	Not defined	Height, orientation, slope angle, drainage sub-basin, vegetation, soil width and land use units	Shallow landslides	Not defined	Baeza and Corominas (2001)
The Staffora river basin, (Italy)	280	Land-use data, A digital terrain model, geological–morphological factors, lithological variables	Earth flows and translational slides, large rotational slides	Slope units	Carrara et al. (2003)
La Honda basin, California Tescio, (Italy) Merecchia basin (Italy)	60	Morphometric parameters, lithologic, structural and hydrological data	Slide flow	Slope units	Carrara et al. (1992)
Umbria, Italy	60	40 morphological, geological and vegetational attributes	Translative slides and flows	Slope units (266 units)	Carrara et al. (1991)
Collazzone area in central Umbria, Italy	78.9	46 thematic environmental variables environmental thematic variables, including morphology, hydrology, lithology, structure, bedding attitude and land use.	Shallow landslides	Slope units (894)	Guzetti et al. (2006)
Lombardy region,(Italy)	275	46 thematic variables, including morphology (24 variables), lithology (14 variables), structure (3 variables) and land use (5 variables).	Not defined	Not defined	Guzetti et al. (2005)

LR allows forming a best fitting model to describe the relationship between the occurrence or non-occurrence of landslides and independent parameters (Wrigley, 1985; Upton and Fingleton, 1989; Dobson, 1990; O'Brien, 1992; Ohlmacher and Davis 2003). It uses this relationship to produce a map showing the probability of future landslides that are constrained to fall between 0 and 1 by considering several independent factors. The main advantage of LR over simple multiple regression is that LR allows the use of binary dependent variable types, which are the presence or absence of landslides in landslide susceptibility mapping. LR is one of the most widely applied methods for statistical susceptibility mapping and it is successfully applied by Menard (1995), Bernknopf et al. (1988), Jade and Sarkar (1993), Jager and Wieczorek (1994), Wieczorek et al. (1996), Atkinson and Massari (1998), Guzzetti et al. (1999) Hosmer and Lomeshow (2000) Gorsevski et al. (2000), Dai and Lee (2002), Ohlmacher and Davis (2003), Lee (2004), Guzetti et al. (2005), Yeşilnacar and Topal (2005), Dai and Lee (2001), Dai et al. (2001), Lee and Min

(2001), Dai and Lee (2002), Süzen (2002), Süzen and Doyuran (2004), Ayalew and Yamagishi (2005), Çan et al. (2005), Lee (2005), Duman et al. (2006), Erener and Düzgün (2006), Zhu and Huang (2006), Akgün and Bulut (2007), Erener and Lacasse (2007) and Tunusluoğlu et al. (2008).

As presented in Table 2.5, the application of the LR analysis to produce susceptibility map is encountered for areas with a variable size (38-2668 km^2). The method is mostly used by grid cells with a size ranging from 10 to 90 m. (Atkinson and Massari, 1998; Ohlmacher and Davis, 2003; Akgün and Bulut, 2007). However, few are used for unique condition units (Can et al., 2005; Chen and Wang, 2007). Most of the researchers applied logistic regression to different types of slides such as debris flows and shallow soil slips, rapid slump-earth flow, rotational slides, etc. (Jager, and Wieczorek, 1994; Ohlmacher and Davis, 2003; Lee, 2004; Can et al., 2005; Yeşilnacar and Topal, 2005; Greco et al., 2007) and few to rock falls (Marquinez et al., 2003). The information about influencing factors are provided by few studies such as Atkinson and Massari (1998) (geology and slope angle), Ayalew et al. (2005) (slope) and Ayalew and Yamagishi (2005) (road network). Additionally Can et al. (2005) applied susceptibility mapping to three different regions where most of the influencing factors are obtained for each region.

Table 2.5. Review of logistic regression and conditional probability for susceptibility mapping in the literature

Region	Method	Area (km^2)	Factor	Landslide Type	Mapping Unit	Source
Yomra and Arsin (Trabzon)	LR	38.87	Slope angle, slope aspect, distance from drainage, distance from roads and the weathered lithological units	Not defined	Grid (20 x 20 m)	Akgün and Bulut (2007)
Apennines, (Italy)	LR	65	Geology, dip, strike, strata-slope interaction, aspect, density of lineaments and slope angle	Not defined	Grid (20 x 20 m)	Atkinson and Massari (1998)
Sado Island (Japan)	Analytical hierarchy process (AHP) and the LR	854.6	Elevation, lithology and slope gradient	Deep-seated, rotational and translational slides	Grid (10x10 m)	Ayalew et. al. (2005)
Kakuda-Yahiko Mountains (Japan)	LR	105	Lithology, bed rock-slope relationship, lineaments, slope gradient, aspect, elevation and road network	Slide	Grid (10x10m)	Ayalew, and Yamagishi (2005)

Table 2.5. Review of logistic regression and conditional probability for susceptibility mapping in the literature (Continued)

Region	Method	Area (km^2)	Factor	Landslide Type	Mapping Unit	Source
Tully Valley, (New York)	LR	415	clays, slope angle, and glacial lake levels	Rapid slump-earth flow	Grid (90x90 m)	Jager, and Wieczorek (1994)
Mackenzie Valley, (Canada)	LR	2,668	Bedrock, surface material, elevation, slope, aspect, dip angle, dip direction, distance to water system, and vegetation cover.	Not defined	unique-condition unit	Chen and Wang (2007)
Egerci, Agustu Kelemen catchments (Turkey)	LR	80.4 26.2 79.0	Area and elevation, Aspect, Plan curvature, Slope, Landcover, Geology	Shallow earthflows	unique condition units (UCU)	Can et al. (2005)
Aspromonte case study, Calabria, (Italy)	LR	850	Rock type, land use, elevation, slope angle, aspect, slope profile curvature down-slope and across-slope.	Fall/topple, block slide, slide, complex slide/flow and flow, lateral spreading, sackung (rock flow, debris avalanche.	Grid (10x10 m)	Greco et al. (2007)
Kansas and Missouri (Kansas)	LR	202.3	slope, slope aspect, geology, and soils.	Shallow failures	Grid (10x10 m)	Ohlmacher and Davis, (2003)
Hendek (Turkey)	LR and ANN	290	aspect, distance to drainage network, distance to fault planes, distance to ridges, distance to roads, drainage density, elevation, fault density, geology, land cover, plan curvature, profile curvature, road density, slope, slope length, stream power, surface area ratio, topographic wetness index and subwatershed basins)	Rotational	Grid (25 x 25 m)	Yeşilnacar and Topal (2005)
Janghung, (Korea)	LR and Likelihood Ratio Model	41	Slope gradient, slope aspect, and curvature, Soil texture, material, drainage, and effective depth, while forest type, diameter, and density , Land cover.	Debris flows and shallow soil slips	Grid (10 x 10 m)	Lee (2004)
Yongin, (Korea)	LR and Probability	66	Slope, aspect, curvature, texture, material, drainage, soil thickness, timber type, age, diameter and dendity, Lithology, land use		Grid (10 x10m)	Lee and Min (2001)

Table 2.5. Review of logistic regression and conditional probability for susceptibility mapping in the literature (Continued)

Region	Method	Area (km^2)	Factor	Landslide Type	Mapping Unit	Source
Cantabrian Mountains (Asturias, North Spain)	LR	500	Altitude, sun radiation, slope roughness, slope gradient, anisotropy and lithology.	Rock fall	Grid (25 x 25 m)	Marquinez et al. (2003)
Sivas, (Turkey)	Conditional probability	Not defined	Geology, slope, aspect, elevation, topographic-wetness index and stream-power index	Rapid flow	Grid (25x25 m)	Gökçeoğlu et al. (2005)
Cekmece, İstanbul (Turkey)	Conditional probability	Not defined	Slope, aspect and altitude, lithology, geomorphology, distance from faults, dis20 tance from drainage, distance from roads	Not defined	Grid (25×25 m)	Duman et al., (2005a)
Yomra and Arsin, Trabzon (Turkey)	LR and weighted linear combination (WLC)	38.87	Slope angle, slope aspect, distance from drainage, distance from roads and the weathered lithological units	Not defined	Geotechnical unit	Akgün and Bulut (2007)

A number of studies have utilized a considerable diversity of parameters including morphological factors such as slope geometry (slope angle, slope aspect, plan curvature, profile curvature, topographical elevation), geological factors such as geologic properties (lithological types, fault, anticlines, and bedding), drainage factors (distance to water system and channel gradient), and land use/land cover for landslide analysis (Gupta and Joshi, 1990; Maharaj, 1993; Jager and Wieczorek, 1994; Van Westen, 1994; Carrara et al., 1995; Chung et al., 1995; Hansen et al., 1995; Guzzetti et al., 1999; Donati and Turrini, 2002). Relatively few studies have additionally considered the use of other variables such as topographic wetness index, elevation, slope length and soil type, which may have significant effects on landslide, in landslide susceptibility mapping (Carrara, 1983).

Conditional analysis involves assessment of the probability that event A will occur if event B occurs (Negnevitsky, 2002). In recent years, the conditional probability approach has been successfully applied to produce susceptibility maps by some researchers (Carrara et al., 1995; Chung et al., 1995; Clerici et al., 2002; Süzen and Doyuran, 2004a; Lee, 2004; Duman et al., 2005a, 2005b; Gökçeoğlu et al., 2005). According to the findings of Lee (2004), the logistic regression analysis seems to be

more consistent when compared with the conditional probability (Table 2.5).

Artificial neural networks have been introduced to produce landslide hazard maps under the consideration of the nonlinear characteristics of the sliding process. Neural networks analysis must be considered as a black box model (Aleotti and Chowdhury, 1999). Lees (1996) describes it as follows: "Neural network is a processing device, implemented as an algorithm or in hardware, whose design was motivated by the design and function of mammalian brains; they react to training data input in such a way as to alter their initial state, something no conventional algorithm does: they can learn". The main characteristics of artificial neural networks (ANN) dealing with mixed-type parameters such as categorical and cardinal units (Ermini et al. 2005; Gomez and Kavzoglu, 2005; Huabin et al., 2005) also include large-scale parallel distributed processing, continuously nonlinear dynamics, collective computation, high fault-tolerance, self-organization, self-learning, and real-time treatment (Rumelhart et al., 1986).

Recently, several papers have been published concerning ANN applications in the literature (e.g Emami et al., 1998; Lee et al., 2001, 2003; Bianchi and Catani, 2002; Lu and Rosenbaum 2003; Catani et al., 2005; Ercanoğlu, 2005; Ermini et al., 2005; Gomez and Kavzoglu 2005; Yeşilnacar and Topal, 2005; Tunusluoğlu et al., 2007). Rumelhart et al. (1986) and Binaghi et al. (2004) provide examples of GIS landslide mapping using ANN methods.

Several researchers have compared and evaluated susceptibility maps produced by logistic regression and ANN. While some researchers have found that neural network is superior to LR (Ayalew et. al, 2005; Yeşilnacar and Topal, 2005) (Table 2.5), other authors have found no differences in overall predictive performance (Mahiny and Turner, 2003; Ottenbacher et al., 2001; Manel et al., 1999; Tu, 1996; Schumacher et al., 1996). These comparisons are highly dependent on the nature of the data set used in the analysis.

As presented in Table 2.6, in order to classify stable and unstable regions, ANN is applied to land surface mapping units in the aforementioned Unique Condition Unit, (Ermini et al. 2005; Catani et al., 2005) and grid units (Lee et al., 2003a; Yeşilnacar

and Topal, 2005; Gömez and Kavzoglu, 2005; Neaupane and Piantanakulchai, 2006; Ercanoğlu, 2005). The pixel sizes range between 5 and 230 m^2 and the sizes of areas range from 17 to 9100 km^2. As indicated in Table 2.6. most of the ANN was applied in rotational type landslides.

Table 2.6. Review of ANN for susceptibility mapping in the literature

Region	Factor	Area (km^2)	Landslide Type	Mapping Unit	Source
Arno River (Central Italy)	Slope angle, lithology, profile curvature, land cover and upslope contributing area.	9100	Rotational slides, solifluctions and other shallow slow movements and flows	Unique conditions units (UCU)	Catani et al. (2005)
Hendek (Turkey)	Aspect, distance to drainage network, distance to fault planes, distance to ridges, distance to roads, drainage density, elevation, fault density, geology, land cover, plan curvature, profile curvature, road density, slope, slope length, stream power, surface area ratio, topographic wetness index and subwatershed basins	Not defined	Rotational slides	Grid (25 x25 m)	Yeşilnacar and Topal (2005)
Riomaggiore catchment, Northern Apennines (Italy)	Lithology, slope angle, profile curvature, land cover and upslope contributing area.	17	Rotational-traslational movements associated with earth slides–earth flows.	Unique Condition Unit, UCU)	Ermini et al. (2005)
Jabonosa river (Venezuela)	Land cover, slope angle, slope aspect, elevation, slope length, topographic wetness index, lineaments, geological formations, soil types	110	Shallow landslides	Grid (30x30 m)	Gömez and Kavzoglu (2005)
Boun (Korea)	Slope, aspect, curvature, topographic type, soil texture, soil material, soil drainage, soil effective thickness, timber type, timber age, timber diameter, timber density, geology, and land cover	68	Not defined	Grid (5x5 m)	Lee et al. (2003b)
Himalayas (Nepal)	Slope steepness and aspect, underlying geology, landuse and vegetation cover, channel proximity, groundwater hydrology	Not defined	Not defined	Grid (230×230 m)	Neaupane and Piantanakulchai (2006)
West Black Sea (Turkey)	Slope angle, slope aspect, topographical elevation, topographical shape, wetness index, and vegetation index	879	rotational slides, soil flows, and translational slides.	Grid (25×25 m)	Ercanoğlu (2005)

The geotechnical model, which is deterministic or probabilistic, has been widely employed in civil engineering and engineering geology for slope stability analysis of a single slide. Examples of geotechnical slope stability analysis are presented in Benda and Zhang (1990), Gökçeoğlu and Aksoy (1996), Luzi and Pergalani (1996), VanWesten et al., (1997), Borga et al. (1998), Terlien (1998), Luzi and Pergalani (1999), Preston and Crozier (1999), Miles and Ho (1999), Xie et al., 2004, Wu and

Abdel-Latif, 2000 , Düzgün and Özdemir, (2006), Düzgün and Karpuz (2006), Fall et al. (2006), Düzgün (2008), and Düzgün and Bhasin (2009). Some of these are reviewed in Table 2.7.

Table 2.7. Review of Geotechnical slope stability analysis in the literature

Region	Factor	Method	Area (km^2)	Landslide Type	Mapping Unit	Source
Mengen, (Turkey)	Cohesion, angle of internal friction, slope, relative height, orientation of slopes, proximity to drainage pattern, vegetation cover and proximity to major faults	Deterministic slope stability analyses techniques	120	Rotational, successive shallow landslides	Not defined	Gökçeoğlu and Aksoy (1996)
San Francisco East Bay Hills, Berkeley, California (USA)	Soil parameters, topography, slip surface depth, fault location and acceleration time histories, drained cohesion, friction angle and unit weight of the regional soils	Newmark's analysis	31	Not defined	Not defined	Miles and Ho (1999)
Hawke's Bay, (New Zealand)	Shear Strength, Crıtıcal Slope Angles, Cohesıve Strength	Geotechnical model	Not defined	Earthflows	Not defined	Preston and Crozier (1999)
Dakar	Geology map (lithology, structural geology, etc.), relief maps (slope height and gradient), historical landslides maps, erosion at the study area (material loss, cliff retreat), hydrogeological information layers (groundwater level, natural and domestic source, flow direction of the surface or rain water, convergence zone of the rain water, etc.), geotechnical soils map (soils and their liability to slide, different homogenous sections determined), and safety factors map	Geotechnical field and laboratory works, of GIS, and of mechanical (deterministic and numerical) stability analysis.	Not defined	Not defined	Grid (2 x2 m)	Fall et al. (2006)
Kyushu, (Japan)	Elevation, inclination, slope, groundwater, strata, slip surface and mechanical parameters)	Deterministic Model	3.4	Slide failure	Slope unit	Xie et al. (2004)
Bandırma (Turkey)	Slope, aspect, soil strength	FORM	Not defined	Not defined	Not defined	Düzgün and Karpuz (2006)
Dereköy, (Konya)	Geologic, hydrologic, vegetation and geotechnical information	FORM	Not defined	Old, active and potential slope movements,	Not defined	Düzgün and Özdemir (2006)
Pete King watershed, Clearwater National Forest, northcentral Idaho, (USA)	Climate data, a digital elevation model, soil, and land use data.	Infinite slope model Monte Carlo Simulation	72	Not defined	Not defined	Gorsevski et al. (2006)
West Black Sea Region, (Turkey)	Geological: Closeness to the structural elements and relationship between discontinuities and slopes Topographical : distance to drainage network, topographical elevation, shape of slope and slope aspect, Environmental: vegetation cover and main roads	Fuzzy Relations	275.4	Rotational slide,soil flow and shallow translational slide.	Grid (25x 25 m)	Ercanoğlu and Gökçeoğlu, (2004)

Table 2.7. Review of Geotechnical slope stability analysis in the literature (Continued)

Region	Factor	Method	Area (km^2)	Landslide Type	Mapping Unit	Source
Lombardia (Italy)	Landslides and slopes (localisation, lithology, structural characteristics, morphology, aspect, landuse, slope angle, erosion, hydrology, type of landslide activity, causes, presence of infrastructures. Geotechnic parameters:unit weight , residual effective cohesion , and residual effective angle of internal friction.	Probabilistic Analysis Dynamic Analysis	310	Flows, translational slides, rotational slides, and transla tional slides-flows.	Grid (10x 10 m)	Luzi and Pergalani (1999)

Deterministic approaches are based on a set of physical laws or models controlling slope stability (Montgomery and Dietrich, 1994; Terlien et al. 1995; Xie et al., 2004). Being process-driven models, they may provide significant insight on the causes of landslides.

Deterministic models have been successfully used for many years to evaluate landslide hazards (Ward et al. 1981, 1982; Nash, 1987; Benda and Zhang 1990; Van Westen et al. 1993; Terlien et al., 1995; Terlien 1996; Atkinson and Massari, 1998; Fall and Azzam, 2001 and so on). This method is applicable on a large scale over small areas (Terlien et al., 1995; Wu and Sidle, 1995) due to the need for exhaustive data including geometrical data, shear strength parameters (cohesion and angle of internal friction), depth below the terrain surface, soil layer thickness, angle of internal friction, slope angle, pore water pressure, etc. The parameters used in these models can be determined in the field or in the laboratory. Their limitations include the fact that very few geotechnical data can be collected over a large region at reasonable cost; an example is provided by the Mulder (1991).

In its simplest form, deterministic approaches consist of an estimation of quantitative values of slope stability for each slope, which generally aims to evaluate a safety factor. The factor of safety does not take into consideration the variability of geotechnical material parameters; hence a high degree of simplification is usually necessary for the use of such models (Aleotti and Chowdhury, 1999). The recognition of uncertainties in the slope stability has led to the development of methods of analysis within a probabilistic framework. The probability of failure is usually considered simply as the probability that the factor of safety is less than the threshold value (Dai et. al. 2002; Aleotti and Chowdhury, 1999). Three commonly

used methods of probability are First Order Reliability Method (Luzi et al., 2000; Zhou et al., 2003; Uzelli et al. 2006; Düzgün and Karpuz, 2006; Düzgün and Özdemir, 2006; Düzgün and Grimstad, 2007; Düzgün, 2008), Point Estimate Method, and Monte Carlo Simulation Method (Xie et al., 2004; Gorsevski et al., 2006). These probability methods are described in Chowdhury (1984), Nguyen and Chowdhury (1984, 1985), and Aloetti and Chawroli, (1999) (Table 2.7). Some of the studies presented in Table 2.7 (Gorsevski et al., 2006; Lacasse et al., 2006) use a combination of deterministic and probabilistic slope stability analyses.

Infinite slope stability models may be employed in one-dimensional (1-D) geometry (Aleotti and Chowdhury, 1999; VanWesten et al., 1997; Xie et al., 2001; Zhou et al., 2003), two-dimensional (2-D) geometry (Janbu, 1973; Sarma, 1973; Gökçeoğlu and Aksoy (1996)) or three-dimensional (3-D) geometry (Gens et al., 1988; Leshchinsky and Huang, 1992; Hungr, 1994; Xie et al., 2004). As indicated in Table 2.7, some researchers have considered pixel (Luzi and Pergalani, 1999; Fall et al., 2006) as the mapping unit, and some prefer the slope unit (Xie et al., 2004). Furthermore, rotational slides, translational slides, and earth flows are types of slides mostly studied for deterministic studies.

2.3.1.2 Mapping Unit

Landslide susceptibility mapping requires the preliminary selection of a suitable mapping unit (Guzzetti et al., 2005). Selection of the mapping unit largely influences all the subsequent analyses and modeling. Mapping unit is the process of partitioning the land surface into smaller units such that a unit contains a set of ground conditions which differ from the adjacent units across definable boundaries (Hansen, 1984). After determination of the mapping unit, each unit is assigned a value for each factor that is taken into consideration and each unit is treated as a case or sampling unit in the analysis. Various methods have been proposed to partition the landscape (Meijerink, 1988; Carrara et al., 1995; Leroi, 1996), which has pros and cons that can be enhanced or reduced by choosing the appropriate susceptibility mapping method.

The methods for partitioning the territory can be simply named as (Carrara, 1983;

Meijerink, 1988; Pike, 1988; Carrara et al., 1991; van Westen, 1993; Bonham Carter, 1994; Chung and Fabbri, 1995; Hearn and Griffiths, 2001; Lee and Min, 2001):

- ◊ grid-cells,
- ◊ terrain units,
- ◊ unique-condition units,
- ◊ slope-units, and
- ◊ topographic units

A grid (also known as a raster format) consists of a regular orthogonal pattern that divides the space into small units called cells (Figure 2.5). The advantage of this mapping unit technique is that it can be automatically created with the aid of a GIS and the grids are in the matrix format, which is algorithmically simple. The main disadvantage of grid-based mapping unit, on the other hand, is that they do not bear any physical representation of the land. Besides, the selection of grid-cell size is intrinsically subjective in classifying the region. It is important to determine the adequate grid size for the scale of the analysis. Each cell is assigned the value of the contributing factor at that location; hence the selection of a small cell size may result in a cumbersome computational process while the selection of a large cell size may result in overgeneralization of each factor, which causes a reduction in information.

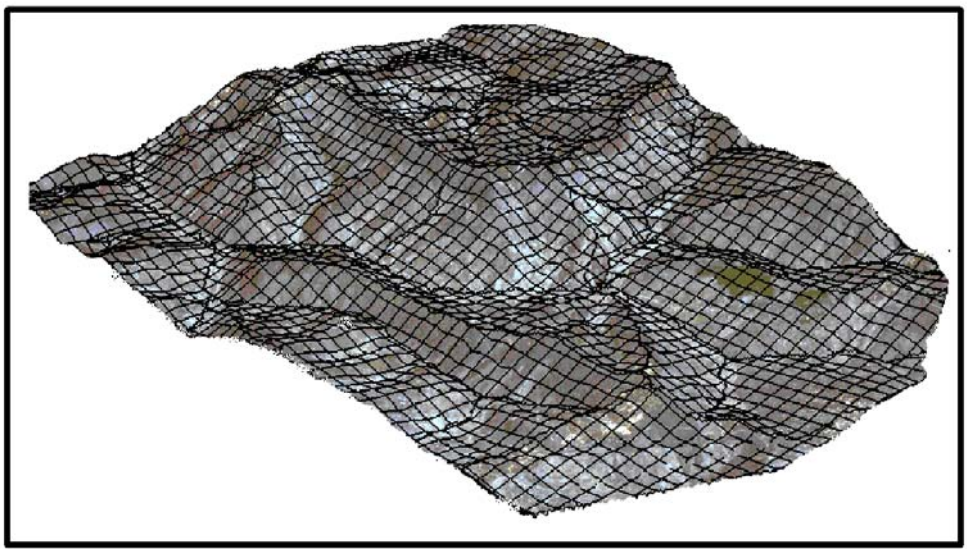

Figure 2.5. Grid or raster representation of the terrain at Kumluca watershed, Bartın (Turkey)

Terrain units are the land-system classification approach. To partition the landscape

into geomorphologic units, maps portraying all the different forms and processes are used. The main drawback lays in the intrinsic subjectivity of the method. This subjectivity occurs due to different perspectives of different experts on the same region.

Unique-condition units are constructed by grouping the grid cells into fewer groups (Can et al., 2005; Chen and Wang, 2006) by the sequential overlay of different categorical maps where all grid cells within one group have the same terrain condition, hence each map unit is defined by a unique homogeneous combination of the attributes (Bonham-Carter, 1994; Chung et al., 1995) (Figure 2.6). Problems arise when linear features, i.e., fault lines or lithological boundaries, are used in the analysis (Guzzetti et al., 1999).

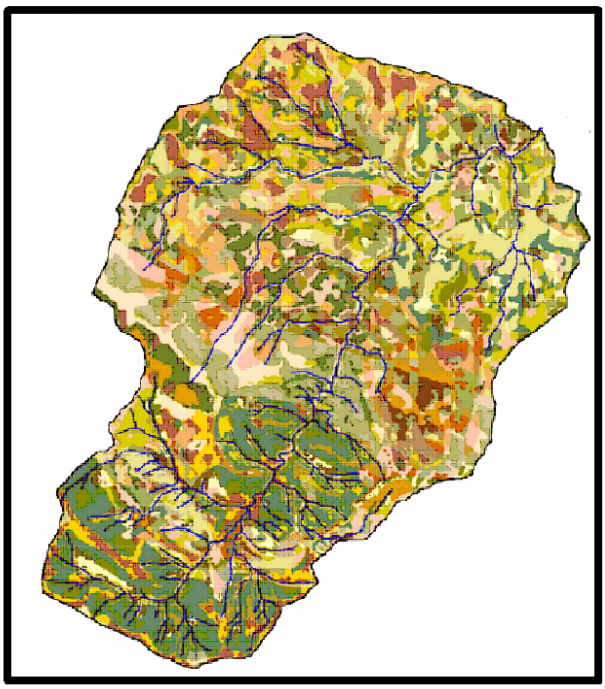

Figure 2.6. Unique condition unit of the of the Riomaggiore catchment Northern Apennines (Italy) (Ermini et al., 2005)

Partition of a region into sub-basins or slope units (Figure 2.7) are obtained from high-quality DEM's and hydrological regions between drainage and divide lines (Carrara et al., 1991). In the nature, there exists a clear physical relationship between landsliding and the fundamental morphological elements of a hilly or mountainous region, namely drainage and divide lines. Therefore, the slope unit-based mapping unit has more representative power for the landslide phenomena. Slope units can be

further subdivided into topographic units, which are based on the intersection of topographical contours and flow lines. Due to the physical relationship between topography and surface and sub-surface hydrology, this approach has higher potential to predict the surface saturation and the occurrence of topographically controlled landslides, such as debris flows (Montgomery and Dietrich, 1994).

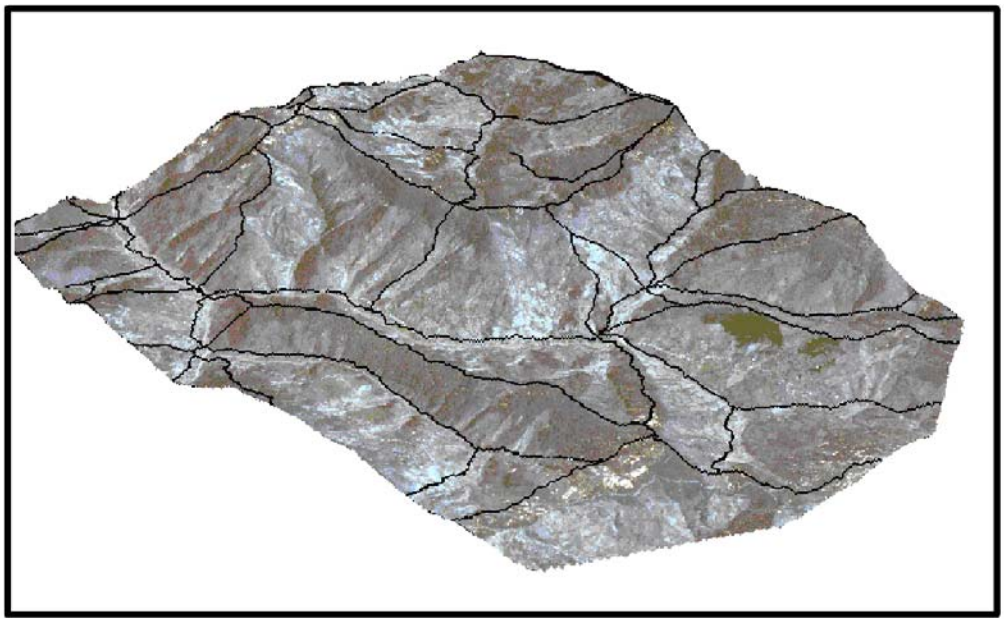

Figure 2.7. Slope unit representation of the terrain at Kumluca watershed, Bartın (Turkey)

2.3.1.3 Scale

Another important aspect of susceptibility mapping is the scale of investigation. Scale determines basically the size of the region to be covered in the analysis. Therefore, it is also a critical factor for the resolution of the analysis and an output of the study. It is chosen on the basis of three factors: the purpose of the assessment, the extent of the studied area and the availability of data. The landslide susceptibility mapping can be grouped as large scale (1:5000–1:10 000), medium scale (1:25 000–1:50 000), and regional scale (1:250 000) (Luzi and Pergalani, 1996). Planning on a regional scale requires a regional scale (1:100.000–1:500.000), whereas for more specific problems such as the implementation of large engineering structures or the identification of priority measures, larger scales are required (medium scale: 1: 25.000–1: 50.000) (Aleotti and Chowdhury, 1999). Furthermore, the quantification of the components of risk assessment may vary depending on different levels

of scale (Figure 2.8). For example, it might not be easy to quantify the elements at risk and assign vulnerability values to them in regional scale analysis. However, it is relatively easier to survey the elements at risk, analyze the vulnerability, or assess the hazard quantitatively on local scale. Hence, on more detailed scales, risk maps require more detailed data and resolution.

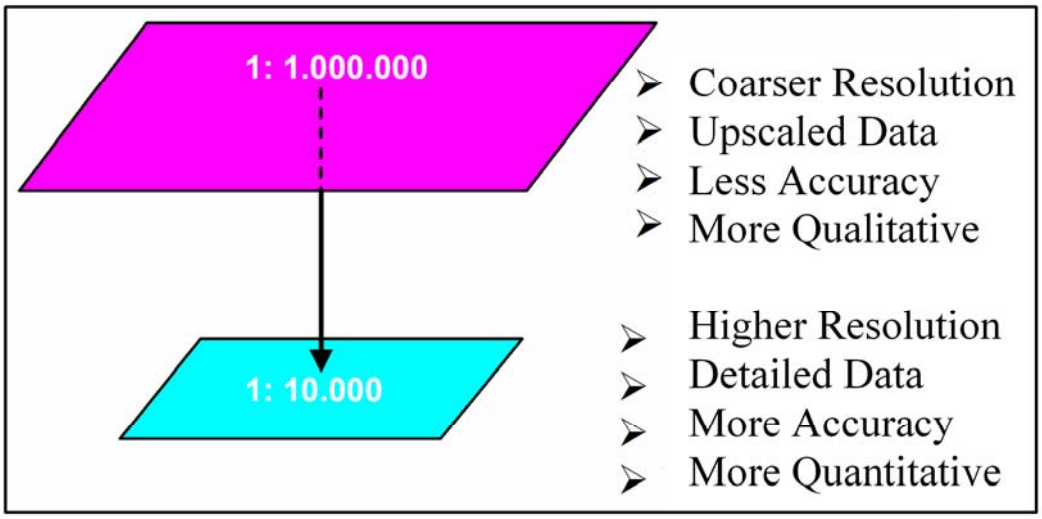

Figure 2.8. Data characteristics for different mapping scales

Another aspect of scale is the scale difference of input data used in the analysis. As a general rule-of-thumb, a regional scale analysis can only be carried out on the scale of the data set with the coarsest resolution (Thomas and Michael, 2004). Therefore, before the analysis, all data should be upscaled to coarser resolution. However, if only one data layer is in the coarser resolution and the rest are in higher resolution, instead of losing information by upscaling, the downscaling process can be applied to obtain high-resolution data. The downscaling process is useful to run the analysis and gain the results; however, because the original data is on the small scale, the content of the data is still dependent on the original data scale. For up scaling or downscaling GIS technology can be easily used.

Moreover, whatever the analysis scale, a different work scale determines the selection of the susceptibility assessment approach. The most appropriate approaches for different work scales are given in Table 2.8. These work scales and selection of

the methodology are defined extensively by Huabin et al. (2005), Glade (2005), and Dai et al. (2002).

Table 2.8. Comparison of the main susceptibility mapping methods on different mapping scales (Huabin et al., 2005; Glade, 2005)

	Type of Analysis	Technique	Scale		
			>1:100000	1:25000-1:50000	<1:10000
Qualitative	Heuristic	Index Based Methods	+	+	-
		Geomorphologic Analysis	-	-	+
Quantitative	Statistical	Bivariate	-	+	-
		Multivariate	-	+	Limited
	Neural Network Processing		-	+	-
	Geotechnical Model-Based Methodologies	Safety Factor	-	-	+
		Probability of Failure	-	-	+

2.3.2 The Susceptibility Assessment Methods in the Thesis

Statistical models are one of the most preferred methods among many landslide susceptibility assessment methods. As landslide occurrences and influencing factors have spatial variations, global models like artificial neural network (ANN) or logistic regression (LR) ignore spatial dependence or autocorrelation characteristics of data between observations in susceptibility assessment. However, to assess the probability of landslide occurrence within a specified period of time and within a given area, it is important to understand the spatial correlation between landslide occurrences and influencing factors. By including these relations, the predictive ability of the developed model increases. In this respect, the techniques of spatial regression (SR) and geographically weighted regression (GWR), which consider spatial variability in the parameters, were proposed in this thesis study for landslide susceptibility assessment to provide better representations of landslide susceptibility.

Most of the studies in the literature deal with the application of conventional methods, yet there is not a common consensus on the best susceptibility assessment method. Hence there is little literature on the comparison of methods related to combination methods and analyzing their affects on resultant maps. In addition, there are few studies in the literature which assess the performance of models in different mapping units. However, the statistical treatment of independent variables changes depending on the adopted mapping unit procedure. Hence, the resultant map may also change depending on the adopted mapping unit procedure. In the thesis, the landslide susceptibility mapping was assessed quantitatively by constructing three global models, LR, SR, NN, and a local model, GWR for two different mapping units, slope unit-based and grid-based mapping unit (Figure 2.9).

The prediction maps were obtained on a continous scale, where the numerical values lie between 0 and 1. In the"implementation part" of the thesis, the prediction maps were analyzed visually and on a statistical basis. Yet, for comparison purposes it is more suitable to change the susceptibility maps from continuous scale into categorical classes. It is not an easy task to categorize continuous data automatically as there are no statistical rules yet. Therefore, a classification method was adopted for comparison of the prediction maps, which was discussed in detail in the last sections of the implementation part.

The validation of prediction results is absolutely the most essential part of risk assessment. Without any validation process, the resultant susceptibility maps are totally useless and have hardly any scientific significance (Chung and Fabbri, 2003). Thus, for validation of the models, two different approaches were used. In the first approach, the dataset was partitioned into two subsets by space-partition technique. The first subset of data was used for obtaining the prediction maps and the second subset was used for validation by performing the relative operating characteristics (ROC).

In the second approach, the validation was performed by field works. Most of the high hazard slopes were checked in the field for the whole region and the model results were compared by these inventories.

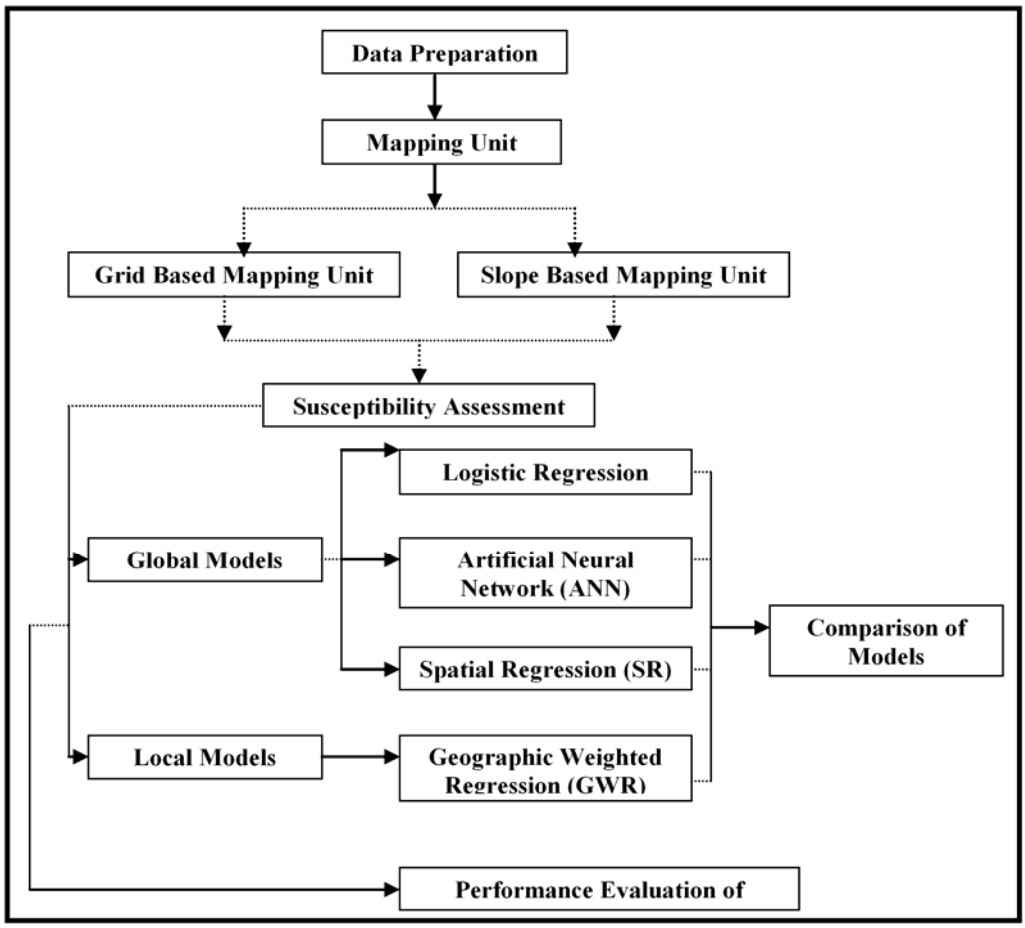

Figure 2.9. The adopted procedure for landslide susceptibility assessment

2.3.2.1 Logistic Regression

Logistic regression (LR) is useful for dichotomous dependent or predictor variables. The advantage of logistic regression is that through the addition of an appropriate link function to the usual linear regression model, the variables may be either continuous or discrete, or any combination of both types (Lee 2005). Using a logistic multiple regression model, the relationship between landslide occurrence (Y, *dependent variable*) and landslide influencing factors ($X_1, X_2, \ldots, X_n$, *independent variable*), is established. Then a mathematical formula of landslide occurrence is obtained. The dependent variable (Y) represents the presence or absence of landslides. Generally, logistic regression involves fitting the dependent variable using an equation in the following form (Bugería and Lorente, 1999):

$$\ln\left(\frac{p_i}{1-pi}\right) = \beta_0 + X_1 * \beta_1 + ... + X_n * \beta_n \quad (1)$$

where p_i is the probability that the event Y occurs, p(Y=1) , $p_i/(1-p_i)$ is the "odds ratio" or likelihood ratio, ln[$p_i/(1-p_i)$] is the log odds ratio, or "logit" ,β_0 is the intercept, and $\beta_1, \beta_2, ...\beta_n$ are coefficients that measure the contribution of independent variables (X_1, X_2,…,X_n), which are landslide influencing factors of the variations in Y (landslide occurrence).

The LR procedure offers several methods for stepwise selection of the "best" predictors to be included in the model. In this thesis study, a forward stepwise procedure was used to introduce the independent variables in the analysis. Forward stepwise methods start with a model that does not include any of the predictors. At each step, the variables which are determined to be significant are added to the model while all the others are withheld. The variables which have a significance level higher than 0.05 are left out of the analysis in the last step. As a result, the procedure selects only the variables that significantly contribute to the improvement of the model.

2.3.2.2 Artificial Neural Networks (ANN)

ANN is an attempt, in the simplest way, to imitate the neural system of the human brain. The attractiveness of ANN is due to its performance in learning and adaptivity, which allows the system to update its internal structure (Jain et al., 1996). Recently, ANN's have been used for various scientific and engineering applications (Emami et al., 1998; Caparrini et al., 1996; Sönmez et al., 2006) and also for landslide susceptibility mapping (Lee et al., 2001; Fernandez-Steeger et al., 2002; Ermini et al., 2005; Yeşilnacar and Topal, 2005; Neaupane and Achet, 2004; Lee et al., 2001; Gomez and Kavzoglu, 2005). In this thesis, the data set was divided into three groups as training, testing, and validation data. Back propagation neural network learning algorithm (BMNN) was used for assessing the landslide susceptibility. BMNN is currently the most widely used algorithm for connectionist learning. Each iteration in the back propagation algorithm has two operations: forward activation and backward propagation. In the forward operation, after the neuron in the first layer receives

its input, it applies the Linear Combiner and the Activation Function to the inputs and maps an input vector $X = [x_1, ..., x_n]$ into an output.

The activation function or, transfer function h (.), determines the relationship between inputs and outputs of neurons in a network, which may be in different types. Any differentiable nonlinear function can be used as an activation function, but the sigmoids activation function, or "S" function, is the most common in the literature (Gomez and Kavzoglu, 2005; Sönmez et al., 2006). A backward propagation step involves the computation of error to modify the weights (Basheer and Hajmeer, 2000). The error is computed and propagated backwards starting at the output layer in order to update the connection weights to reduce the error. At the end of this training procedure, an optimum weight matrix was obtained, which represent the best approximation of the process being modeled (Basheer, 2000). A single-layered network typically consists of input units fully connected to output units, which is only a satisfactory estimator for linear problems, whereas a multi-layered network has one or more hidden layers in between (Neaupane and Achet, 2004), where the complexity increases by the addition of hidden layers. Villiers and Barnard (1992) show no significant statistical differences between one and two hidden layers and they indicate that networks with two hidden layers are often more difficult to train and are affected more by the initial weight set. Therefore, one hidden layer was preferred in the thesis study. The three-layer artificial neural network structure with 3 layers (input, hidden, and output), which was employed in this thesis study, is shown in Figure 2.10.

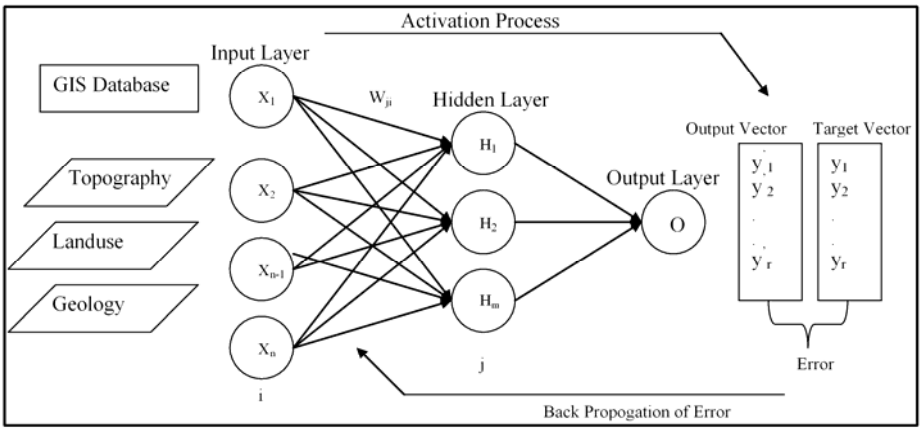

Figure 2.10. Architecture of the ANN used in this thesis

There are n neurons in the first layer, where n equals the number of inputs. There are one neuron in the output layer, which represents the dependent variables (in this case it is the landslide occurrence) (Basheer and Hajmeer, 2000). The compromised number of neurons that may be used in the hidden layer is proposed in the literature with some heuristics. The heuristics used for determination of number of neurons are presented by Sönmez et al. (2006). Depending on Table 2.9, different heuristics are presented to calculate the number of hidden neurons.

Table 2.9. Heuristics proposed in the literature

Hidden Neuron Heuristic	Reference	Learning Rate	Reference
$\sqrt{(N_i \times N_0)}$	Masters (1994)	0.1–10	Wythoff (1993)
$\left(2 + N_0 \times N_i + 0.5 \times N_0 \times (N_0^{\ 2} + N_i) - 3\right)/(N_i + N_0)$	Paola (1994)	1/ d	McClelland and Rumelhart (1986)
$(N_i + N_0)/2$	Ripley (1993)	0.3–0.6	Zupan and Gasteiger (1993)
		0.0–1.0	Fu (1995)
Test Data		**Training Set Number**	
20–30%	Nelson and Illingworth (1990)	30 x n_i x (n_i+1)	Kavzoglu, 2001
25%	Looney (1996)	D*0.65	Looney (1996)
20%	Swingler (1996)		
Initial weights		**Momentum Coefficient**	
-0.30 and +0.30	ASCE (2000)	0.4 and 0.9	Wyhthoff (1993)
[-0.1;0.1]	Paola (1994) and Staufer and Fisher (1997)	0.0 to 1.0	Hassoun (1995) and Fu (1995)
[-0.25;0.25]	Gallahger and Downs (1997) and Kavzoglu (2001)	μ≈1:0	Henseler (1995) and Hertz et al. (1991)
		μ =0.9 and η=0.25	Swingler (1996)

*N_i=Number of input layer, N_0=Number of output layer=, D= parent database d= total number of nodes in the network, n_i=number of input nodes

2.3.2.3 Spatial Models

The spatial data, where several attributes are specified for each spatial zone, contain autocorrelation. The non-spatial regression models lack the ability to include this property in analysis. Consider the linear logistic regression model:

$$Y = BX + e \tag{2}$$

Where,

Y : Vector of dependent variable, (nx1).

X : Matrix of the values of p independent variables in each spatial zone, (nxp).

e : Vector of errors with zero mean and constant variance, (nx1).

B : Regression coefficients to be estimated (px1)

The model given in Eq. 2 does not take the spatial variability of the parameters into account. Hence, for a better treatment of spatial data, spatial regression models are developed. These spatial models have been widely used in broad scientific disciplines, such as analysis of crime, modeling land prices, poverty mapping, epidemiology, air pollution and health, natural and environmental sciences, and so on (Düzgün and Kemeç, 2008). In this way, the main shortcomings of non-spatial regression, which are assumptions of identically and independently distributed (i.i.d.) independent variables (X_i's) and uncorrelated error terms, are tried to be eliminated by relaxing the regression method with the allowance of spatial autocorrelation.

Although spatial regression (SR) models take the spatial variability of the parameters into account, they are not considered as local models since they are developed for modeling the mean of the spatial phenomena. Geographically Weighted Regression (GWR) is a relatively simple and effective technique for explaining the local characteristics of the spatial phenomena, especially when the phenomena vary over the space (Fotheringham et al., 2002). It is one of the most widely used local modeling methods, which is implemented in various disciplines such as natural, environmental, social and, earth sciences.

In the thesis study, the SR and GWR models were developed for assessing landslide susceptibility.

SR is a global spatial modeling technique in which spatial autocorrelation among the regression parameters are taken into account (Düzgün and Kemec, 2008). Spatial autocorrelation or dependence means that observations at location i depend on other observations at locations $j \neq i$. When there is spatial dependence, neighboring units exhibit a high degree of spatial correlation than units located far apart (LeSage, 1999). If the phenomenon has a spatial nature, incorporating the spatial correlation into the model provides better performance, which is reflected by higher R^2 values.
Spatial correlation can be incorporated into the model by modification of the regression equation (Eq. 2) using a contiguity matrix (proximity matrix or geographic weights matrix), in which the neighborhood information about the spatial zones is characterized and used for spatial autocorrelation. There are a large number of ways to construct the contiguity matrix. Some alternative ways can be listed as follows: sharing a common edge (linear contiguity), sharing a common side (Rook contiguity), sharing a common vertex (bishop contiguity), length of shared borders, and inter-centroid distance functions. For spatial regression model, the first task is to construct a spatial contiguity matrix. In this study, in order to obtain a contiguity matrix, a function was developed based on the Delaunay triangularization (Matlab 7.1, 2008). The input variables are the coordinates of x and y, such as n by 1 vector. The Delaunay triangulation is a set of lines connecting each point to its natural neighbours (Figure 2.11). The circle circumscribed around a Delaunay triangle has its centre at the vertex of a Voronoi polygon. It returns a set of triangles such that no data points are contained in any triangles' circumscribed circle for the data points defined by vectors x and y.

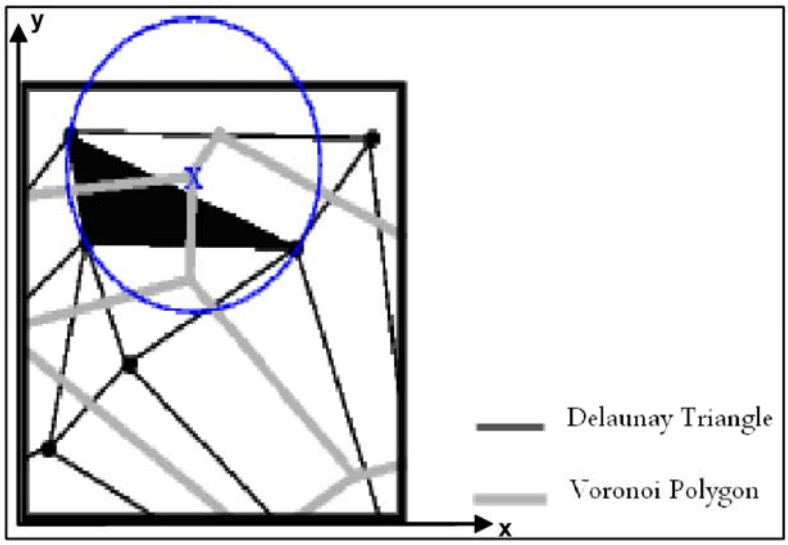

Figure 2.11. Delaunay triangularization approach

After the creation of the Delaunay triangulation, the sum of corners (ssum) that share a common vertex was computed (LeSage, 1999). This sum of corners was used to calculate the weight matrixes (Eq. 4-6) based on Eq. 3. Three different spatial weight matrixes were created as output. These matrixes are:

wmat = sqrt((1/ssum)'); (3)

W1=wmat (4)

W2= wmat*wmat*A (5)

W3= wmat*A*wmat (6)

Where, A represents the adjacency matrix from Delaunay triangles, which depicts the neighbors of each vertexes; ssum is the sum of corners connected to the same vertex; wmat is the standardized 1st-order contiguity matrix, computed based on the sum of corners connected to the same vertex.

There are basically three spatial regression models depending on the formulation of spatial autocorrelation: Simultaneous auto regression (SAR), moving average (MA), and conditional spatial regression (CSR) (Anselin 1988; Dubin, 1988; Dubin 1992; Anselin, 1995; Fotheringham et al., 1996; Fotheringham, 1997; Pace 1997; Brunsdon et al., 1998). In this study, the SAR model for limited dependent variable, which is in the form of binary data, was used. The SAR model (Eq. 4-6) is also called auto correlated error model as the error term in non-spatial regression model is

formulated in such a way that it involves spatial autocorrelation (Bailey, 1994; Anselin, 1995; Pace et al, 1998; Fotheringham et al., 2000; Gamerman and Moreira, 2004).

$$\boldsymbol{Y} = \boldsymbol{X\beta} + \boldsymbol{U} \tag{7}$$

$$\boldsymbol{U} = \boldsymbol{\rho W y} + \boldsymbol{\varepsilon} \tag{8}$$

Then

$$\boldsymbol{Y} = \boldsymbol{X\beta} + \boldsymbol{\rho W y} + \boldsymbol{\varepsilon} \tag{9}$$

Where,

ε : Vector of errors with zero mean and constant variance σ^2

W: Proximity matrix

ρ : Interaction parameter or spatial autoregressive coefficient

β : Parameter to be estimated due to relationship between the variables

Y : Landslide occurrence

As can be seen in Eq. 9, the SAR model requires prediction of an additional parameter of ρ, which accounts for the direction and magnitude of the neighborhood effect. Hence the SAR model is computationally costly as compared to non-spatial regression as it requires the estimation of β and ρ. For more information, refer to Bailey and Gatrell, (1995) and Fotheringham et al. (2000). For individual observation (y_i) Eq. 9 takes the following form:

$$y_i = \rho\left(\sum_j w_{ij} y_j\right) + \varepsilon \tag{10}$$

Incorporating spatial variation using contiguity improves the fit of the model, raising the R^2 statistic. The spatial phenomena have potential variability across space. Global models have inadequacies in exploring the local variations (Fortheringham et al., 2000). Geographically Weighted Regression (GWR) allows local parameters to be estimated, which are specific to each location. Hence, it helps understanding the factors that cause landslide occurrences on a local scale. It arises from the extension of non-spatial regression in Eq. 2. The basic mechanism of GWR relies on obtaining separate regression equations for each spatial zone, in which a kernel centered on the

area is adapted in such a way that neighboring areas are weighted based on a distance decay function (Fotheringham et al., 2002). In GWR:

$$Y = (\beta \otimes X)1 + \varepsilon \tag{11}$$

Where $\otimes$ is a multiplication operator serving the multiplication of each element of β with the corresponding element of X and 1 is vector of 1s (Kazar et al, 2005). For n number of spatial zones with k number of independent variables, β and X have n x (k+1) dimensions and hence 1 has the dimension of (k+1) x 1. Then least square estimates of β_i ($\hat{\beta}_i$) and their variances are:

$$\hat{\beta}_i = \left(X^T W_i X\right)^{-1} X^T W_i Y \tag{12}$$

$$VAR(\hat{\beta}_i) = (X^T W_i^{-1} X)^{-1} \tag{13}$$

Where W_i is n by n weighting matrix whose off-diagonal elements are zero and diagonal elements are the geographical weighting (Eq.14).

$$W_i = \begin{bmatrix} w_{i1} & 0 & \dots & 0 \\ 0 & w_{i2} & \dots & 0 \\ . & . & & . \\ & & & . \\ . & . & & . \\ 0 & 0 & \dots & w_{i3} \end{bmatrix} \tag{14}$$

The choice of W_i depends on the selection of the kernel function, which may be in the form of fixed (i.e. fixed bandwidth) or adaptive kernels (i.e. varying bandwidths). A typical kernel for W_i is given in Eq. (15).

$$w_{ij} = \exp\left[\frac{d_{ij}^{\ 2}}{2b^2}\right] \tag{15}$$

where b is referred to as the bandwidth. The weighting of data will decrease according to a Gaussian curve as the distance d between i and j increases.

2.3.3 Analysis of Triggers

2.3.3.1 Literature Review on Analysis of Triggers

While susceptibility maps provide zonations of areas with similar instability or similar conditions that generate landslides, a true landslide hazard map should offer a zonation of areas with similar probabilities of landslides in a given period of time, based on quantitative analysis of data (Chaco et al., 2006). Hence, the described susceptibility methods suffice to assess the spatial probability but are not adequate to solve the problems in evaluating the temporal probability. To produce real hazard maps by definition, a hazard map should include the consideration of a time dimension (reoccurrence period). A few attempts have been made to establish the temporal occurrence of landslides (Hansen, 1984; Keaton et al., 1988; Hutchinson, 1995; Grunert and Hardenbicker, 1997; Dikau and Schrott, 1999; Lang et al., 1999; Coe et al., 2000; Corsini et al., 2000; Barnard et al., 2001; Derbyshire, 2001; Cardinali et al, 2002b; Vanacker et al., 2003; Carrasco et al., 2003; Catani et al. 2005). The time dimension of a landslide may be estimated by the exceedance probability of landslide occurrence during an established period (Guzzetti et al., 2005). The exceedence probability is most commonly obtained through the analysis of catalogues of historical landslide events (Morgan et al., 1992; Moon et al., 1992; Cruden, 1997; Cardinali et al., 2002b; Catani et al., 2005; Guzzetti et al., 2005).

However, these catalogs, which list the time (or period) of occurrence of a single failure or multiple slope failures, are not available for most regions. In such cases, there are varieties of methods to quantitatively assess the frequency or probability of landslide occurrence from the disparate sets of information (Fell et al., 2005). They may be summarized as follows: judgment based on experience (Foster et al., 1998), inventories, slope instability ranking systems (Koirala and Watkins, 1988; Flentje and Chowdhury, 1999), relation between geomorphology and geology (Hutchinson, 1988; Fell and Hartford, 1997; Moon et al, 1992; Leroi, 1996; and Soeters and Van Westen, 1996), relating a landslide event to a triggering event, e.g. rainfall, snowmelt, earthquake, and the like (Fell et al., 1988; Lumb, 1975; Flentje and Chowdhury, 1999; Brand et al, 1984 and Premchitt et al., 1994), modeling primary variable (Fell et al., 1991; Haneberg, 1991 and Okunushi and Okumura, 1987), and probabilistic methods or a combination of methods (Mostyn and Fell, 1997), where

most of which are limited by data availability (Corominas et al., 2005; AGS Sub-Committee, 2000).

Studies in the literature show that the number of landslide occurrences in a given time or the frequency of landslides is often derived from the temporal occurrence of landslide triggers (e.g. rainfall, earthquake). The statistical analysis of triggering mechanism is significant for hazard assessment due to the evaluation of critical thresholds above which landslides are triggered and the calculation of the frequency with which these thresholds are exceeded (Aleotti and Chowdhury, 1999). Landslides triggered by earthquakes may exhibit different mechanisms and characteristics. Examples of triggered landslides by earthquakes are presented in e.g. Adams (1980), Wieczorek and Jager (1996), Keefer (1999) and Hung (2000). To understand the level of hazard and to evaluate the risk, the return period of earthquakes of different magnitudes must be estimated (Aleotti and Chowdhury, 1999). It may be more difficult to establish a record of seismically-induced landslides due to the low return periods of these sparse events. On the other hand, it is easier to obtain a record of rainfall induced landslides because rainfall records coupled with historical landslide information permit the computation of the temporal probability of rainfall induced landslides (Thomas and Micheal, 2004). Hence, rainfall analysis is the most frequently adopted approach in forecasting the occurrence of landslide events (Crosta, 2004). In the study of Aleotti (2004), Zezere et al. (2004), Carrasco et al. (2003) and Remondo et al. (2005b) rainfall induced landslides are investigated.

Generally two types of rainfall thresholds are proposed in the literature, which are empirical thresholds (historical, statistical) and physical-based (process based, conceptual) thresholds (Corominas, 2000; Aleotti, 2004; Guzetti et al, 2007).

The most widely used empirical thresholds are based on the historical analysis of the relationship between rainfall and landslide occurrence and they depend on studying the results of rainfall events that result in slope failures (Caine ,1980; Crozier and Glade, 1999; Glade et. al., 2000; Aleotti, 2004; Wieczorek and Glade, 2005, Guzzetti et al, 2007) whereas physical-based thresholds are rarely used because they require detailed knowledge, which is difficult to be collected over large areas, about the spatial information on the hydrological, lithological, morphological, and soil

characteristics that control the initiation of landslides (Montgomery and Dietrich, 1994; Salvucci and Entekabi, 1994; Wu and Sidle, 1995; Wilson and Wieczorek, 1995; Crosta, 1998; Terlien, 1998; Iverson, 2000).

Empirical rainfall thresholds are commonly investigated with reference to combinations of different rainfall parameters (Glade et al., 2000; Aleotti, 2004; Guzetti et al., 2007) such as antecedent rainfall ("pre-event"), cumulative rainfall ('total'), and rainfall intensity and duration.

The importance of antecedent rainfall may be related to ground water levels and moisture properties of soil which causes slope failures (Wieczorek, 1996; Wieczorek and Guzetti, 1999; Guzetti et al., 2007). Using antecedent rainfall data in the analysis may be problematic because it is difficult to define the period which is affected by conditions such as climate, soil and, vegetation. In the literature, different studies use different periods ranging from 2-day to 6-month antecedent rainfalls, e.g. Kim et al, 1991; Pasuto and Silvano, 1998; Glade et al, 2000; Aleotti, 2004; Cardinali et al., 2006. Cumulative rainfall versus time is another type of threshold that is frequently used. Examples of cumulative rainfall use as an indicator of debris flow hazard have been reported by Wilson and Wieczorek, 1995; Page et.al. 1993.

Intensity-duration (ID) rainfall thresholds are the most frequently used threshold type proposed in the literature (Caine, 1980; Larsen and Simon, 1992; Wieczorek, 1987; Casini and Versace, 1988; Cancelli and Nova, 1985). In addition, in the study by Guzetti et al., (2007), a summary and comparisons of 52 different intensity-duration thresholds were listed. Intensity-duration rainfall threshold curves are proposed for shallow landslides and debris flows (i.e. Caine 1980; Wieczorek 1987; Cannon 1988) and for mid-sized landslides and mudslides (i.e. Corominas and Moya 1999) in some regions (Corominas et. al., 2005). The literature reveals that these thresholds vary as local thresholds, regional thresholds, and global thresholds.

ID thresholds have the general form (Eq.16):

$$I = c + \alpha * D^{\beta} \qquad (16)$$

where I is (mean) rainfall intensity, D is rainfall duration, and $c \geq 0$, α and β are

parameters.

The objective of this study is to obtain rainfall thresholds for Bartın Kumluca region because owing to its geologic, geomorphologic, and climatic settings, it is highly prone to the occurrence of rainfall induced landslides. Therefore, a series of meteorological events that triggered landslides were studied to define the rainfall thresholds.

2.3.3.2 The proposed Approach for the Analysis of Triggers

Landslides may be triggered by short intense storms or by prolonged rainfall events. Several studies have attempted to define rainfall thresholds both on empirical and on physical bases for the triggering of landslides. Empirical thresholds are defined by collecting rainfall data for meteorological landslide events and for events without landslides, while physical thresholds are based on numerical models that consider the relation between rainfall, pore pressure, and slope stability (Aleotti, 2004). The main objective of this thesis study is the identification of the empirical triggering thresholds for Kumluca Region. Through the systematic review of newspapers, interviews with local witnesses, and the inspection of technical and scientific reports and papers, sixteen meteorological events were selected and analyzed. In most of these meteorological events, which are known to trigger the slides due to extreme rainfall, the rainfall intensities ranged between 20 mm and 94 mm per day. Interviews with the local host revealed that most of the slides were triggered by prolonged and relatively moderate rainfall events. In this thesis, daily rainfall data were analysed for both daily extremes and antecedent rainfalls. In order to explore the extremes for daily data, two different models were adopted. The first approach, which is proposed in this thesis as an alternative way for extreme rainfall methods, is a time series model. The second approach is the graphical gumble approach, which is one of the most preferred methods for extreme analysis. Furthermore, for the antecedent rainfall analysis two different methods were adopted for the study. The first one is the analytical gumble approach and the second one is the adoption of intensity–duration relationships for antecedent rainfall events that trigger landslides.

The thresholds obtained for daily and antecedent rainfall data were compared.

The Gumble approach applied to the antecedent rainfall was selected for further hazard analysis. Three different triggering scenarios for different return periods obtained from Gumble approach were used in order to model the hazard. The triggering scenarios were combined with conditional probability to obtain an ultimate probability of trigger that exceeds a certain threshold for a unique annual hazard.

The motivation for the analysis of the triggering rainfall threshold study was twofold. First, the identification of rainfall amounts for daily extremes and for antecedent rainfalls which lead to landslides may help mitigate the loss of life and property. Second, the motivation was towards developing a quantitative hazard model relating rainfall to landslide.

2.3.3.2.1 Time Series Analysis of Rainfall Pattern with ARIMA Model Fitting

Time series is a set of observations obtained by measuring a single variable regularly over a period of time. The aim of obtaining a time series model is to forecast the outliers.

ARIMA models provide more sophisticated methods for modeling trend and seasonal components and it is the most generally used models in forecasting. There are three basic components in an ARIMA model: autoregression (AR), differencing or integration (I), and moving-average (MA). An ARIMA model is typically expressed as: ARIMA(p,d,q) where p is the order of autoregression, d is the order of differencing (or integration), and q is the order of moving-average involved. These components are used to explain significant correlations found in the autocorrelation (ACF) and partial autocorrelation (PACF) plots to handle trends.

In an autoregressive (AR) process, each value in a series is a linear function of the preceding value or values. In a first-order autoregressive process, only the single preceding value is used. The assumption is that the time series to be modeled should be stationary. The differencing or integration component of an ARIMA model tries, through differencing, to make a series stationary. A stationary series has a constant mean and a constant variance over time (Boverman and O'Connell, 1993). The

moving-average (MA) component of an ARIMA model tries to predict future values of the series based on deviations from the series mean observed for previous values. In practical terms, MA processes are more useful for modeling short-term fluctuations, while AR processes are more useful for modeling longer-term effects.

In the thesis study, the autocorrelation function (ACF) and partial autocorrelation function (PACF) were plotted and the autocorrelation values were examined to determine the decision levels. After the identification of likely models, the ARIMA procedure was applied. In the ARIMA procedure, different combinations of AR and MA levels were evaluated to get the best results. After determination of the suitable model, it was run to predict the outliers.

2.3.3.2.2 Critical Rainfall Analysis with Gumbel Approach

For extreme value analysis, several alternative distributions are suggested to be used most often in hydrology as Normal (Gaussian) distribution, Log-Normal distribution, Gumbel (Type I Extreme Value distribution), and Pearson Type III (Gamma) distribution. Gumbel is one commonly preferred distribution type for extreme value analyses.

Gumbel extreme value diagram is used to plot data for probability distribution. The plotting position of probability values are computed depending on Weibull definition given by the following equation:

$$q = \frac{m}{n+1} \tag{17}$$

Where n is the number of years of recording and m is the rank of the event (smaller to larger) (Usul, 2005). The coefficient of the correlation was computed with the below formulation of Eq.18.

$$R^2 = \frac{\sum (y-\bar{y})^2 - \sum (y-y_s)^2}{\sum (y-\bar{y})^2} \tag{18}$$

where;

y = observed data
$\bar{y}$ = mean of the rainfall data
y_s = simulated data

The Gumbel theoretical distribution considers the distribution of the largest or the smallest value observed in repeated samples. In this extreme distribution, the probability (p) of the occurrence of a magnitude equal to or greater than any value of the observations (x) and the theory of extremes is applied by using the Equation:

$$q = 1 - e^{-e^{-y}} \tag{19}$$

where y= reduced variate and computed with the equation below as:

$$y=a(xi-x0) \tag{20}$$

where a=dispersion parameter (a scale parameter), x_0 is the location parameter of the distribution.

$$a = \frac{\sigma_n}{\sigma_x} \tag{21}$$

$$x_0 = \bar{x} - y_n(a) \tag{22}$$

Where $\bar{x}$ and σ_x is the mean and standard deviation of the observations found with equations as follows:

$$\bar{x} = \frac{\sum x}{n} \tag{23}$$

$$\sigma_x = \sqrt{\frac{\sum (x - \bar{x})^2}{n - 1}} \tag{24}$$

2.3.3.2.3 Intensity Duration Curves

Critical pairs of rainfall amount-duration were defined as proposed by D'Ecclesiis et al. (1991), and by referring to the applied studies of Zezere et al. (2004) and Marques et al. (2007), the critical pair is determined depending on the combination of cumulative rainfall amounts and the corresponding return periods where the extreme combination is decided with the higher return period. The applied assumption is not physically based; however, it provides discrimination between rainfall periods characterized by landslide activity and rainfall periods. After the determination of higher return period for each event, the corresponding antecedent day is determined to compute the intensity with the Eq. 25:

$$I = P_r/X \qquad (25)$$

where;
I= Intensity
Pr= Absolute antecedent precipitation for the day with higher return period,
X=Antecedent day of the higher return period

2.3.4 Hazard Assessment

2.3.4.1 Literature Review of Hazard Assessment

In regional scale analysis, hazard maps can be obtained by combining the susceptibility map and triggering factors. There is yet not a wide range of studies on integration of these parameters.Table 2.10 lists different definitions of hazard for landslides and also indicates the integration of parameters to obtain hazard.

Guzzetti et al. (2005) and Cardinali et al. (2002a) study the historical information on past landslide events to obtain a quantitative estimate of landslide hazard. The definition of landslide hazard by Guzzetti et al. (2005) incorporates the concepts of location and time, in addition to the size of landslides. Poisson model is adopted for the temporal occurrence of landslides as shown in Table 2.10 by considering the landslides as independent random point-events in time. As an alternative to the

Poisson model (Crovelli, 2000), binomial model can be adopted (Coe et al., 2000).

Due to the lack of data, Carrasco et al. (2003) obtain the temporal probability by statistical analysis of precipitation (Table 2.10). The probability map of occurrence of the precipitation conditions is then combined with landslide susceptibility map to generate the hazard map. The hazard map is made by overlaying the reclassified maps (susceptibility and probability). Cardinali et al. (2002b) assess landslide hazard for Umbria, in Central Italy, depending on the frequency of landslide movements (F) and the landslide's intensity (I). The ascertained frequency of occurrence of a single landslide or multiple landslides is based on the number of events recognized during the observation period. The landslide intensity (I) is considered as a measure of the destructiveness of a landslide, which is defined as a function of landslide volume (v) and of landslide expected velocity (s). Likewise, Corominas et al., (2003) determine the landslide magnitude and frequency in susceptible areas in order to produce a hazard map.

Table 2.10. The existing hazard mapping approach in the literature

Mathematical Model	Definition	Source
HL = PAL x PN x S PN = ($e^{-\lambda t}\lambda t^n$)/n!	HL : landslide hazard PAL: conditional probability of landslide size, PN : landslide occurrence in an established period t, S: landslide spatial occurrence, λ: the estimated average rate of occurrence of landslides, which corresponds to 1 /μ, μ : the future mean recurrence interval	Guzzetti et al., (2005) (southern Lombardy region, in northern Italy)
H = f (F, I) I = f (v, s).	H: Landslide hazard F : the frequency of landslide Movements I : the landslide's intensity	Cardinali et al, (2002b) (Umbria, Central Italy)
$H(N) = 1 - (1 - 1/T)^N$	$H(N:$)absolute hazard N : a given time span T: Return time (years)	Catani et al., (2005) (Arno River basin (Italy)
$P = 1 - \left(1 - \frac{T_{afffected}}{T_y} * pred\right)$	$T_{affected}$=Total area to be affected by landslide in a scenario (x) T_y= total area of susceptibility class y pred=prediction value of susceptibility class y	Zezere et al, 2004 (Lisbon (Portugal)

Table 2.10. The existing hazard mapping approch in the literature (continued)

Mathematical Model	Definition	Source
H= landslide susceptible zones, landslide magnitude and frequency.		Coromias et al., (2003) (Principality of Andorra)
H = M x P	H= Hazard M= a description of the magnitude P= probability of occurrence of the landslide(s)	Fell (1994)
$P_V = \frac{\sum_{i=1}^{n} a(H_V - H_{Si}) + P_{Si}}{n}$ Hazard = combination of probability map of occurrence of the precipitation and landslide susceptibility map	*PV:* the average precipitation at a desired location; *HV*: the average altitude of the Valley *Hsi*:the altitude of the desired locations; *a:* the intersection value (constant value, that depends on the quantity of precipitation); *Psi:* is the precipitation value used to calculate the series; and *n* is the number of rain gauges.	Carrasco et al., (2003) (Jerte Valley (Spain))

The frequency of landslides has been obtained from the temporal distribution of rainfall events, and the size of the mobilized mass along with the propagation velocity provides an estimation of the landslide magnitude. As a result, the degree of hazard is obtained from the frequency and magnitude of the landslide events based on hazard matrix.

The temporal prediction is obtained by Catani et al., (2005) through the combination of susceptibility values with information on the state of activity for mapped landslides. The selected recurrence times are transformed into probability by the computation of absolute hazard H (N) in a given time span N using the binomial distribution.

2.3.4.2 Obtaining Hazard Maps from Susceptibility and Trigger Analysis

The spatial and temporal probability should be included in order to be able to obtain hazard maps. Therefore, a procedure was followed, in which the hazard (H) was

calculated by multiplication of two probabilities.

$$H=P_f*P_t \quad (26)$$

where:

P_t is the probability of trigger that exceeds a certain threshold

P_f is the probability of failure. The P_f can be formulated as (Eq. 27):

$$P_f=P_s*(P_l|P_t) \quad (27)$$

where;

P_s is the spatial probability

$(P_l|P_t)$ is the conditional probability of having a landslide given that rainfall triggers exceed a certain threshold value for a given time period.

For the computation of $(P_l|P_t)$, a methodology was also developed. In this approach, the logistic regression was computed for modeling the landslide occurrence and rainfall values higher than the critical rainfall value. Then appropriate hazard estimate for the time t for risk analysis takes the following form of joint probability:

$$H= P_t*(P_l|P_t)*Ps \quad (28)$$

2.3.5 Consequence Analysis

2.3.5.1 Literature Review of Consequence Analysis

In quantitative terms, risk is the product of consequence and hazard (Hungr, 2004). The product of the value of an element at risk and its vulnerability is referred to as the consequence of the hazard. Bell and Glade (2004) include the probability of temporal and spatial impact, as well as the probability of seasonal occurrence, in consequence definition in addition to vulnerability as presented in

$$C = Ps\ xPt\ x\ Vp\ xVpe\ x\ Pso; \quad (29)$$

where P is the probability and refers to space (s) or time (t) values and V is the

vulnerability of buildings (p) and people (pe), while Pso is the probability of seasonal occurrence.

The characterization of consequence scenarios might be relatively easier for specific slope situations than regional scale analysis. Because it is more complicated to identify and quantify the elements at risk and the vulnerability of element at risk in regional scale analysis. Hence the definition of elements at risk depends on data requirements and corresponds to the scale of investigation (Bell and Glade, 2004).

2.3.5.1.1 Literature Review of Elements at Risk

The elements at risk can be classified as (AGS, 2000; Düzgün and Lacasse, 2005):

- Property assets, which may be subdivided into portions relative to the hazard, such as furniture, equipment, personnel property, vehicles, machines, cars, trains etc.

- Populations, who either live, work, or spend some time in the area affected by landsliding and who have possibility to be affected by the landslide(s) that may cause losses, in the form of basically fatalities and injuries.

- Structural elements, such as buildings, roads, railway lines, lifeline networks, and communication facilities.
- Services, such as water supply or drainage or electricity supply.

- Natural environment involves flora, fauna, landscape, and environmental quality, for which it is usually difficult to predict losses since they are mostly intangible.

-

The element of population consists of individuals or groups of people who have possibility to be affected by landslides that may cause losses in the form of fatalities and/or injuries. Structural elements comprise buildings, roads, railway lines, and lifeline networks. It is relatively easier to express loss in monetary values for damage in structural elements. Property assets include the content of structural elements, such as furniture, equipment, personnel property, domestic animals, vehicles, machines, cars, trains, etc. Activities refer to any activity interrupted by landslide events, such as commercial, industrial, agricultural activities, etc. Natural environment involves flora, fauna, landscape, and environmental quality, for which it is usually difficult to predict losses since they are mostly intangible. Urban environment is in fact

composed of a combination of some or all of the elements mentioned above, as well as other urban elements such as monuments, recreation areas, historical buildings, and ancient ruins, etc. (Lacasse et al., 2006).

Among these classes, the greatest emphasis is given to buildings, population, and infrastructure. Data collection techniques for a rapid inventory of elements at risk generally use high-resolution images and result in the generation of multipurpose elements at risk databases. Each of the elements at risk has its own characteristics, which can be spatial (the location in relation to the hazard), temporal (such as the population, which will differ in time at a certain location), and thematic characteristics (such as the material type of buildings or the age distribution of the population). The cost of different types of structures can be obtained and represented in maps (Remondo et al., 2005a).

2.3.5.1.2 Literature Review of Vulnerability Assessment

Vulnerability is another fundamental component in the evaluation of landslide risk (Leone et al., 1996). Vulnerability is defined as the level of potential damage, or degree of loss, of a given element or set of elements within the area affected by a hazard (Fell, 1994). It is expressed on a scale of 0 (no loss) to 1 (total loss) (Fell, 1994; Leone et al., 1996; Wong et al., 1997). The understanding of the interaction between a given landslide and the affected elements is fundamental for vulnerability assessment (Dai et al., 2002).

The assessments of vulnerability for landslides in the literature are usually qualitative (Rauthela and Lakhera, 2000) and mostly depend on historical records (Dai et al., 2002; Glade, 2003). For an effective use of QRA in landslides, generalized quantitative models for vulnerability assessment are essential. Reviews of landslide vulnerability are made by Glade (2003) and Lee and Jones (2004).

Vulnerability assessment is much more complex than finding the cost of different types of structures, because vulnerability depends not only on the type of element but also on the type and magnitude of the process (Remondo et al., 2005a).
The major factors would be:

(i) run-out distance; (Finlay, 1996).
(ii) The intensity, the volume, and velocity of sliding;
(iii) The type of landslide mechanism (rock fall, debris flow, slide, etc);
(iiii) the relative location of the vulnerable element in relation to the landslide trajectory or to the position inside the landslide affected area (Cascini et al. 2005).

In the World Vulnerability Report by Zeneb (2003), about 50 different indicators of vulnerability are shown. Thus, vulnerability is complex coactions between natural exposure, physical exposure, social exposure, economic exposure, and political exposure (Taubenböck et al., 2006).

Several procedures are described in the literature for the assessment of vulnerability, among others, Mejia-Navarro et al. (1994), Fell (1994), Leone et al. (1996), Leroi (1996), Glade (2003), Uzelli et al. (2006).

Fell (1994) proposed three different vulnerabilities of the elements of the territory (Chaco et al., 2006). Fell (1994) followed Morgan et al. (1992) to introduce the vulnerability equation as:

$$V = V(S) + V(T) + V(L) \quad (29)$$

V(S) = The spatial vulnerability, which means that an element will be affected by the landslide given that the landslide occurs, and therefore it represents the vulnerability derived from the spatial position of the element at risk.
V(T) = The temporal vulnerability, which expresses a likelihood of the temporal impact, which takes into account temporal changes of the element at risk. A house, for instance, may or may not be occupied, depending on the time of impact.
V(L) = The life vulnerability, which expresses the likelihood of an individual occupant's loss of life in the impacted element, or the proportion of the value of the impacted element which is lost (Chaco et al., 2006).

Romendo et al. 2005 calculates the vulnerability coefficient for each element (or per unit area and/or length) as:

$$V = \text{Damage} / \text{Cost} \quad (30)$$

Vulnerability (0–1) thus obtained expresses the degree of potential monetary loss with respect to the total value of the element.

Düzgün and Lacasse (2005) proposed a 3-dimensional conceptual framework for the assessment of vulnerability. The magnitude (M) of a landslide is the first dimension while scale (S) and elements at risk (E) are the other dimensions (Figure 2.12).

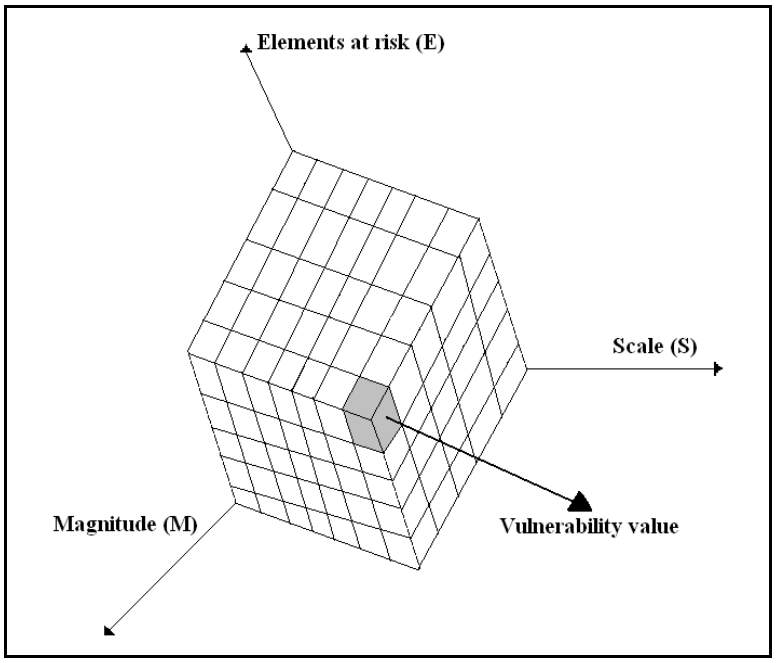

Figure 2.12. Conceptual 3-D vulnerability framework (Düzgün and Lacasse, 2005).

In this approach, the magnitude of a landslide defined by the volume, velocity, depth, run-out and areal extent (Ojeda-Mocayo et al. 2004, Lee and Jones 2004) has an important effect on the vulnerability value of elements at risk. Scale (S) refers to the scale of investigation. It is relatively easier to assess the vulnerability of specific slopes than the assessment on a regional scale analysis. Elements at risk (E), the third dimension, reflect the specific risk, which is assessed from attributes such as property, population, environment, and economy.

The vulnerability of lives and property to land sliding may be different. For instance, a house may have a similar high vulnerability to both slow-moving and rapid landslide, while a person living in it may have a low vulnerability to slow- moving landslide (Fell, 1994; Fell and Hartford,1997).

The vulnerability of a person and/or property to landsliding may be assessed systematically by expert judgment and by the statistics of detailed historical records. As an example of the statistics of historical records, the vulnerability matrix method proposed by Leone et al., 1996 can be given. In this method, the vulnerability of elements at risk depends on the characteristics of the landslide and the technical resistance of the building, such as the type, nature, age, etc (Dai et al., 2002). Following Varnes' (1984) definition of vulnerability, Prina et al. (2004) took account of four factors: physical, social, environmental, and economical vulnerability.

Vulnerability values present several uncertainties due to the empirical nature of the assessment and the completeness, quality and the reliability of brute data on damages. Moreover, many elements which are not present today will exits and be subject to risk in the future. The uncertainties affect the quality of the final risk estimates obtained, as the better the quality of the available data is, the more reliable the results of the assessments become (Remondo et al., 2005a).

2.3.5.2 The Adopted Methodology for Consequence Analysis

The thesis study adopted the 3D procedure of Düzgün and Lacasse (2005) for consequence analysis, which involves scale, elements at risk and magnitude of the devastating event. Depending on this procedure, the consequence may vary at different spatial and temporal dimensions (Figure 2.13). The identification of spatial impact $P(S|H)$ requires the estimation of landslide run-out distances (Finlay et al., 1999; Bertolo and Wieczorek, 2005) which is governed by the volume, velocity and topography of the region (Düzgün, 2008). It may be easier to estimate the parameters for a local slope; however, the estimation of these parameters is not an easy task for multiple landslide locations on a regional scale. Hence simplifying the hypothesis is mostly accepted for spatial impact in regional studies. For local scale analysis, the spatial probability may be estimated by simulating the run-out. In the thesis study, a method was proposed to obtain the spatial probability. In this approach the simulated landslide velocity was associated by the spatial distribution of the element at risk map. This approach was logical because the velocity depends on the topography of the region. Hence, spatial probability increases depending on the velocity level on which the element at risk is located.

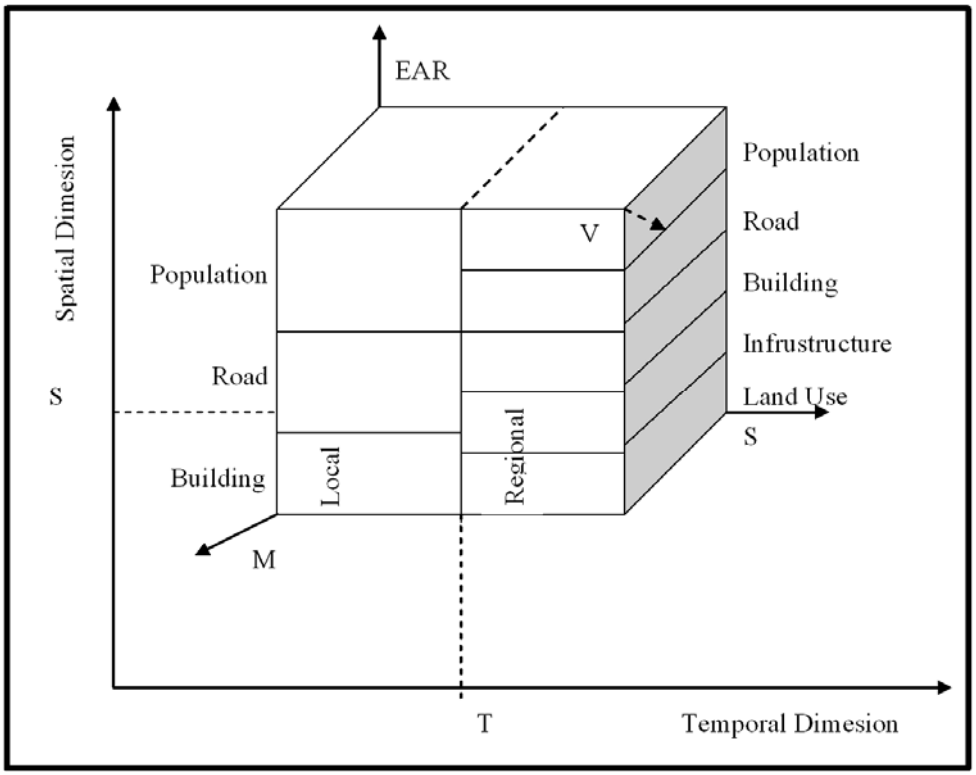

Figure 2.13 The adopted conceptual 3-D vulnerability framework (Adopted from Düzgün and Lacasse, 2005)

The temporal impact should also be considered in the consequence analysis of elements at risk. Because the result damage may vary depending on the temporal occurrence of landslide (a slide at midnight or at low season time can have enormously worse consequences compared to slides in day time or at high season time). The vulnerability of stable elements at risk, such as buildings, land-use, roads, etc. does not vary with time. They are always exposed to threats for all time in all day or all year. Conversely, it is more difficult to estimate the vulnerability for dynamic elements at risk, such as cars, human etc. which exist at run-outs. In the thesis study, in both the local and regional scale analysis, the temporal impact was considered for the residents living in houses. In this context, for regional scale analysis, day and night were considered for occupancy of houses. On the other hand, on local scale it was possible to focus on a more detailed survey to obtain information about occupancy of buildings by people at different times. Hence, in local scale analysis the vulnerability of human was evaluated for day time, night time, high season time, and low season time.

2.3.5.2.1 The Adopted Methodology for Element at Risk

The procedure adopted to obtain the elements at risk varies for local and regional scale analysis. It is difficult to predict run-outs for many landslides, therefore obtaining the elements at risk and quantifying vulnerabilities in large regions is generally a challenging issue. In this thesis study, in large regions the elements at risk were obtained by overlaying the hazard maps with land cover maps and the extracted elements were classified into different categories in order to differentiate the exposure of different types. In addition, the population data was derived from existing census data. The number of inhabitants were then estimated per house by using the population density of Kumluca settlement.

For a single slope, it is easier to focus on a more detailed survey of elements at risk. In addition, the parameters required for the estimation of run-out can be obtained by field surveys. In this thesis study, a high-resolution image was used to extract the elements at risk. The elements were detected by the algorithm developed for risk analysis. The proposed method consists of mainly four steps: first, masking vegetation and shadow areas and obtaining man-made segments, then main road detection, and then filtering thin and long artifacts by Principle Component Analysis (PCA) and eliminating small segments by morphological operations, and finally classifying the result image for building detection, which is masked by vegetation, shadow and road features. For risk to life analysis the number of inhabitants per house was obtained through field surveys by interviews.

As can be presented in the adopted conceptual 3D frame work (Figure 2.13), the buildings, roads, land-use infrastructure and residents living in buildings were considered for regional scale, on the other hand, the buildings, main roads and residents in each building were emphasized for the local scale for consequence analysis.

2.3.5.2.2 The Adopted Methodology for Vulnerability

The adopted vulnerability assessment framework has three dimensions, which involve Magnitude (M), Elements at risk (EAR) and Scale (S) (Figure 2.13). The

magnitude of landslide can be assessed by parameters such as: Volume (x_1), Velocity (x_2), Depth (x_3), Run-out (x_4), and Areal extent (x_5). In the thesis study the magnitude can not be computed due to insufficient information for parameters. Hence it is considered as 1, which means that if a landslide occurs, it may wreak a total destruction.

As indicated previously, the methodology was adopted on two different scales: local and regional, and for each scale, different procedures are adopted for determination of the vulnerability of elements at risk as described.

For local scale analysis, the vulnerability was estimated by adopting a "damage probability matrix"approach (Düzgün, 2008). This approach is used in structural earthquake engineering for evaluating the damage for a given building stock with given earthquake intensity (Ko Ko et al., 2004). In this approach, instead of building blocks, the elements at risk on local scale were considered separately by damage probability matrix.

Conversely, because of lower resolution, it is not an easy task to identify different vulnerability values for different types of element at risk on regional scale. Thus, a generalized assumption was applied and the vulnerability indicator was set to "1" for all EAR on this scale.

2.3.6 Risk Analysis

2.3.6.1 Literature Review of Risk Analysis

Once hazard, value of elements at risk, and vulnerability of elements are obtained, they can be integrated into a risk map (Remondo et al., 2005a). Risk assessment is generally analyzed qualitatively or quantitatively. The assessment of risk depends mostly on both the desired accuracy of the outcome and the nature of the problem, and should be compatible with the quality and quantity of the available data (Dai et al., 2002).

In qualitative risk assessment, the components of the risk, which are basically hazard,

elements at risk, and vulnerability, are expressed verbally and the final result is in terms of ranked or verbal risk levels (IUGS, 1997; Düzgün and Lacasse, 2005). Therefore, qualitative risk maps are based on the experience of experts mostly. In quantitative risk maps, the levels of risk are described in numerical terms, where the prediction results are expressed with probability functions on a continuous scale (Chung and Fabbri, 2003). The risk components are assessed quantitatively, which allows the decision makers to perform an adequate economic cost-benefit analysis for proper land-use planning by quantitatively estimated risk maps. There are a number of risk assessment methods proposed in the literature; however, few of them are published and most of them are not spatially based (Castellanos, 2008). Table 2.11 presents some risk assessment methods defined by different publications.

Table 2.11. Landslide risk assessment methods

Method	Risk formulation	Definition	References
Qualitative	$R(T,I)=D(I)\times H(T,I)$.	$D(I)$= potential worth of losses, at a given intensity	Catani et al., 2005 Arno River (Central Italy)
Qualitative	Rs = f (H, V).	Rs = specific landslide risk , H= landslide hazard, V= vulnerability	Cardinali et al. 2002b Umbria, (Italy)
Review	Rs = H x V Rt = Rs x E = (H x V) x E	Rs: Specific risk, H: Hazard, V: Vulnerability Rt: Total risk, E: Elements at risk	Varnes (1984)
Quantitative	Risk = Hazard x Consequences	Consequences: Potential worth of loss	Einstein (1988)
Quantitative	Rt = Σ(Rs x E) = Σ(H x V x E)	Rt: Total risk, Rs: Specific risk, V: Vulnerability, E: Elements at risk	Fell (1994), Fell et al. 2005
Quantitative	R(prop) = P(L) × P(T:L) × P(S:T) × V(prop:S) × E P(LOL) = P(L) × P(T:L) × P(S:T) × V(D:T)	P(L) = the frequency of the rockfall events of a given magnitude; P(T:L) = the probability of the rockfall reaching the element at risk; P(S:T)= the temporal spatial probability of the element at risk; V(prop:S)= the vulnerability of the element at risk; E= the element at risk V(D:T) = the vulnerability of a person with respect to the rockfall event	Corominas et al., 2005
Quantitative	R(DI) = P(H) x P(S\H) x P(T\S) x V(L\T)	R(DI): Individual risk, P(H): Hazard, P(S\H): Probability of spatial impact, P (T\S): Probability of temporal impact, P (L\T): Probability of loss of life for an individual	Morgan et al. (1992)
Quantitative	R(PD) = P(H) x P(S\H) x V(P\S) x E	R (PD): Specific risk (property), P(H): Hazard, P (S\H): Probability that landslide impacts the property, V(P\S): Vulnerability, E: Value of property	Dai et al. (2002)

Table 2.11. Landslide risk assessment methods (Continued)

Method	Risk formulation	Definition	References
Overview and discussion	R=P x C	R= one event with potential consequences risk P = the probability that this event will occur C = the consequences given the event occurs;	Faber and Stewart (2003)
Quantitative	R = H x C x E	R= The landslide risk H= the probability of the hazardous event or natural hazard and its C= consequences on the elements at risk E.	Bell and Glade (2004) Bildudalur (Iceland)
Quantitative	$R = \sum\left(H\sum\left(VA\right)\right)$	*R* = Risk (€/year); *H* = Hazard (0–1/year) *V* = Physical vulnerability of a particular type of element at risk (0 - 1) *A* = Amount or cost of the particular elements at risk (€). *(VA)* = Consequences for all elements at risk	Leroi (1996) and Lee and Jones (2004)
Quantitative	$R_T = Rs_i + Rs_b + Rs_l$	R_T: Total risk; Rs_i: Specific risk for linear infrastructures; Rs_b: Specific risk for buildings; Rs_l: Specific risk for lands.	Remondo et al. (2005a), Remondo et al. (2008) Bajo Deba area (northern Spain)
Review	Specific risk of a building: $R_s = P(S_{PV}\|T_M) \times P(S_{TV}\|T_M) \times P(R_X\|S_{VT}) \times P(D_B\|S_{VT}) \times C_B$ Specific risk of persons in building: $R_s = P(S_{PV}\|T_M) \times P(S_{TV}\|T_M) \times P(R_X\|S_{VT}) \times P(D_B\|S_{VT}) \times P(I_P\|D_B) \times P(P_H\|S_{VT}) \times N_P$	$P(S_{PV}\|T_M)$= Spatial probability. $P(S_{TV}\|T_M)$ = Temporal probability. $P(R_X\|S_{VT})$= Conditional probability that a runout zone with distance X to the building will be covered. $P(D_B\|S_{VT})$ = Conditional probability of damage to the building of a particular construction type. C_B= Replacement costs of the particular building. $P(I_P\|D_B)$ = Conditional probability of injuries or death for a person present in the house. $P(P_H\|S_{VT})$ = Conditional probability of a person being present in the building. N_P = Number of persons in the building.	van Westen et al. (2005)

The risk equation is similar in terms of the combination of hazard and consequences, but they differ in terms of some abbreviations and details in certain formulations. One of the most widely used definitions of risk, which is presented by Varnes (1984), Fell (1994), and Fell et al. (2005), introduces a distinction between specific (R_S) and total risk (R_t). The specific risk means "the expected degree of loss due to a particular phenomenon". It may be expressed by the product of Hazard (H) times Vulnerability (V). The specific risk would result in a single value of potential losses

for a given probability (van Western et al., 2006). The total risk means ‘‘the expected number of lives lost, persons injured, damage to property and disruption of economic activity due to a particular damaging phenomenon for a given area and reference period’’.It can be clearly seen in the definitions of specific and total risk that in specific risk, only one single element is considered during the calculation of the risk, but because of the variability of the environment, for regional scale analysis, a variety of elements can be under risk. For that reason, all these different elements at risk should be evaluated for the calculation of the risk (Lee and Jones 2004).

In fact, variable types of elements at risk lead to decomposition of total landslide risk into specific risk. For that reason, based on Remondo et al. (2005a) and Remondo et al. (2008), landslide risk mapping should be carried out separately for each type of element (Specific Risk) and then integrated into a total risk map (R_T) by adding all the specific risk maps, as shown in Table 2.11 (Remondo et al. 2005a and Remondo et al. 2008).

Depending on van Western et al. (2005), the estimation of risk turns out to be very complicated when one tries to calculate specific risk for buildings or persons in buildings. The formula should take into account a lot of aspects, which are difficult to evaluate (Figure 2.14).

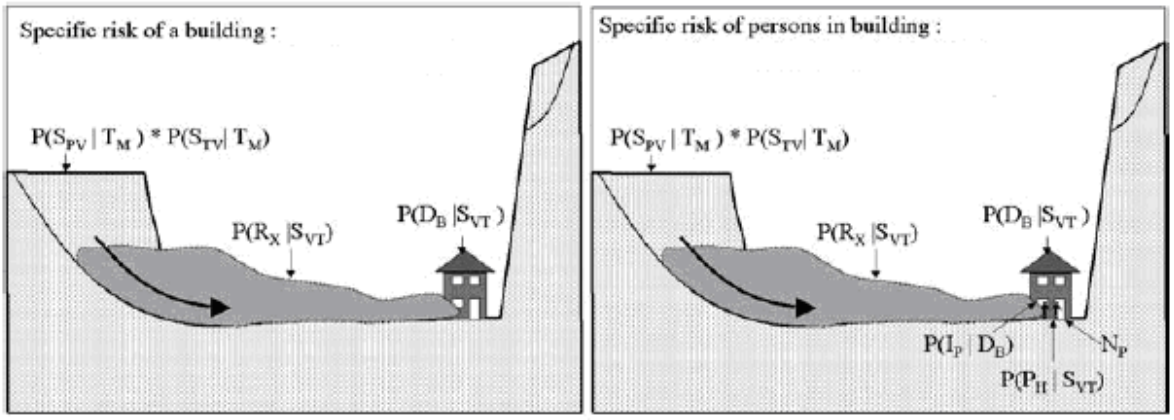

Figure 2.14. Example of possible calculation methods for specific risk to buildings and persons in buildings (van Westen et al., 2005)

In the literature survey, some of the publications define risk as the product of hazard

and vulnerability (Table 2.11). In these studies vulnerability is defined as consequences (Varnes, 1984; Cardinali et al. 2002b; Morgan et al. 1992; Leroi, 1996 and Lee and Jones, 2004). However, Einstein (1988), Faber and Stewart (2003), and Bell and Glade (2004) undertook a parameter of consequences (C) to define the risk. In these studies, landslide risk (R) is defined as a function of the probability of hazardous events or natural hazard (H) and its consequences (C) on elements at risk (E). Catani et al. (2005) define the potential worth of losses (D), which is the combination of vulnerability and exposure at a given intensity (D(I)=V(I)×E) (Table 2.11). The exposure was estimated on the basis of presumed assets and income values of every single object E.

In terms of conditional probability, the probability of spatial and temporal impact is also considered in the risk analysis (Morgan et al.,1992; Dai et al., 2002 and Corominas et al., 2005). Some researchers considered the product of P (S\H) x P (T\S) x V (L\T) in Morgan et al. (1992) or P (S\H) x V (P\S) x E in Dai et al. (2002) as ‘‘consequence’’ (e.g. Wong et al., 1997) or the product of P(H) x P(S\H) as ‘‘hazard’’ (e.g. Leroueil and Locat, 1998).

Although the total risk is defined by the sum of specific risk, in fact it is difficult to evaluate this sum, since the unit of expressing each specific risk is not identical. For example, individual risk has the unit of loss of life/year, while annual property loss has the unit of loss of property/year, in which it is complex and even debatable to convert loss of life into a monetary value (Lacasse et al., 2006).

2.3.6.2 Adopted Methodology for Risk Analysis

The adopted risk procedure involves computation of risk for each element at risk separately. Then all specific risks were added to obtain the total risk. The procedure followed two steps, which involve the creation of risk maps for property and life. For regional and local scale risk map, the procedure follows:

The annual loss of property value, *R(LOP)* and the loss of life probability *R(LOL*) were calculated by the adapted procedure from Dai et al. (2002), which involves multiplication of hazard with the possible consequences as follows:

$$R(LOP) = P(H) * C \quad (31)$$

With R (LOP) is the risk (annual loss of property value); P(H) is the annual probability of landslide event; C is the consequence, and in this study it is considered based on Wong et al. (1997);

Where;

$$C = P(S|H) \text{ x } WOL \quad (32)$$

With P(S|H) is the probability of spatial impact (i.e. of landslide impacting upon the property); WOL is the worth of loss and product of vulnerability and exposure, which is the value of elements at risk adopted from Catani et al.(2005).

Where;

$$WOL = V(P|S) \text{x} EAR \quad (33)$$

With V(P|S) is the vulnerability of the property (proportion of property value lost); EAR is the element at risk (e.g. the value or net present value of the property).
Hence;

$$R(LOP) = P(H) \text{x } P(S|H) \text{x } V(P|S) \text{x} EAR \quad (34)$$

The annual probability that a person may lose his/her life, *R(LOL)* is calculated from

$$R(LOL) = \sum_{i=1}^{2} P(H) \text{x } P(S \mid H) \text{ x } Epe \quad (35)$$

$$C = P(S|H) \text{ x } Epe \quad (36)$$

where R(LOL) is the risk (annual probability of loss of life of an individual); P(H) is the annual probability of landslide event; P(S|H) is the probability of spatial impact given the event; and E_{pe} is the number of people in each building.

Final risk values are highly dependent on the process of each component which involves landslide susceptibility mapping, hazard mapping, and consequence mapping.

The result of the risk maps may vary distinctively depending on the respective susceptibility models. Application of different susceptibility models may result in different landslide susceptibility maps, leading to different hazard and risk maps. There are a variety of susceptibility models applied in the literature, each of which consider different data input and algorithm. For example, application of statistical models versus neural network may provide different spatial probability values at similar mapping units. Hence, the location of high susceptible zone may vary from statistical models to neural network models. The changes of location may also affect the number of threatened properties because of the vulnerabilities of elements at risks.

Another important aspect is that the selection of mapping unit largely influences all the subsequent analyses and modeling the risk. There are various methods that have been proposed to partition the surface into homogeneous regions as discussed in the previous parts. Each method has pros and cons on application level. Each unit is treated as a case or sampling unit in the analysis and a value for each factor is assigned to each mapping unit. Hence the size of the mapping unit influences the value of the factor. The value can be generalized if the size of the mapping unit is far coarser than the factor, or vice versa. As a result, the result of the risk maps may differ depending on the consideration of the generalized factor values.
Another important point for risk mapping is the work scale to be adopted in the analysis. The scale is determined depending on the extent of the study area and data availability. The data acquired from different organizations may be on different scales. Hence, each data should be fetched to the same resolution by upscaling or downscaling. Coarser resolution may decrease the number of pixels in risk mapping, hence the degree of details gets lesser.

Topics like the variation of risk due to different input parameters, process models, risk models, reference units, and data resolution must be considered in the analysis. Actually there are few studies in the literature that considers these topics. In this study, the effect of each component on risk mapping will be discussed and analyzed.

CHAPTER 3

IMPLEMENTATION FOR REGIONAL SCALE RISK ASSESSMENT

In order to demonstrate the implementation of the proposed methodology, Bartın Kumluca watershed in the Western Black Sea Region was selected. The Western Black Sea Region is characterized by a steep topography, and is subjected to heavy precipitation. Due to these adverse effects, the region is prone to extensive and severe landslides (Ercanoğlu and Gökçeoğlu, 2002). Therefore, it needs to be analyzed for landslide risk.

3.1 Description of the Study Area

The Kumluca watershed is located in the south-eastern part of Bartın city and the north-western part of Ulus district in the middle part of the Black Sea Region, Turkey. The area covers 330 km^2 and is located 15 km south-west of Bartın city center (Figure 3.1). The Kumluca watershed includes F28b1, F28b2, F29a1, F29a2, F28b3, F29a4 and F29a3 die plates in 1:25000 scale topographic maps.

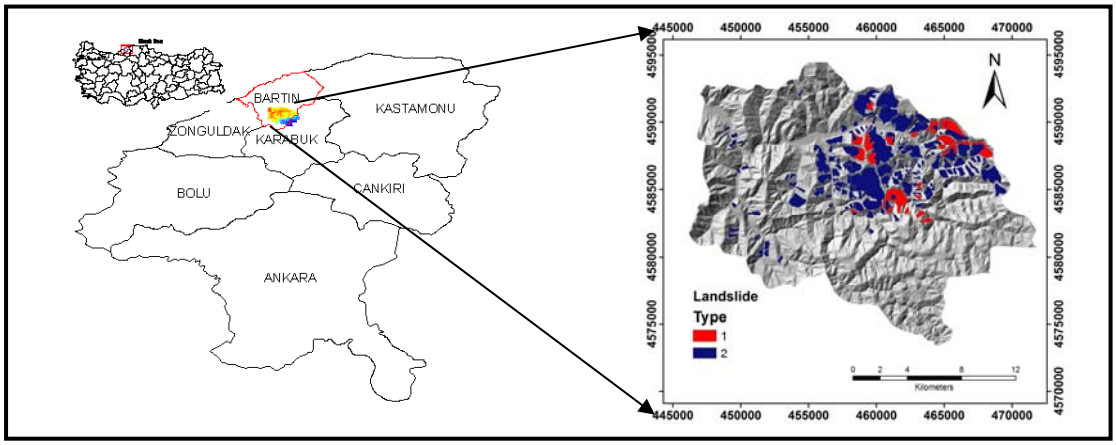

Figure 3.1. Study region, Kumluca watershed, in the south-western part of Bartin city and the map showing the landslide locations with two types of slides, Type 1: Non active and depth >5m, Type 2: Active and depth >5m.

The most common landcover in the area is forest, which is 63% of the whole region. The other parts of the study area are dry farming (36%) and settlement (0.45%). The range of topographical elevation values varies between 80 and 1755 m, while the dominant topographical elevation range is between 350 and 550 m. Although the slope angle values range between 0^0 and 65^0, the majority are between 15^0 and 25^0 degrees. The main stream in the study area is the Kumluca Stream. It has a dendritic drainage pattern and is composed of lower order streams, namely Zafer and Kızıllar (Bartından Haberler, 2009). The largest settlement to the north of the area is Kumluca. In addition, there are approximately 27 villages in the watershed.

The field observations showed that most of the houses are single- to two-storey stone and/or adobe masonry with mud mortar. Based on these observations, the masonry dwellings of rural settlements were found to be the most affected ones by the reactivation of landslides (Figure 3.2a, Figure 3.2b), and some of the buildings which were mainly situated on landslide masses were totally damaged due to the reactivation of landslides (Figure 3.2 c,d). In addition to damages to the houses, some of the road embankments aligning through the toe of landslides were also damaged (Figure 3.3 a and Figure 3.3 b). Furthermore, some parts of the roads which ran parallel to the toe of landslides changed their forms from straight to curve due to the reactivation of landslides (Figure 3.3c, Figure 3.3d).

.

Figure 3.2. The damages observed at the rural settlements during field surveys

Figure 3.3. The damages observed at the road embankments and roads

The reports (Landslide Reports, 1975, 1985, 1987, 1993, 1995, 2005) of the study region showed that the area has both natural and artificial triggers for landslide occurrence. While intense rainfall, rapid snowmelt, and stream erosion of slope toes are the natural triggers, indirect human action such as steeply and improperly cut slopes, poorly controlled surface drainage, uncontrolled settlement, and agricultural activities are the artificial triggers (Akgün and Bulut, 2007).

Most of the study area is covered by Ulus Formation, which is known to be susceptible to landslides in the region (Figure 3.4). Indeed, when the landslide reports obtained from the General Directorate of Disaster Affairs Bartın Division is evaluated for the spatial distribution of slope movements, it is proved that most of the landslides are identified in the Upper Cretaceous Age in Ulus Formation. Ulus formation is composed of mostly thick sandstone levels and sandy, loamy schist, claystone and loamy marl alternations at higher elevations (Landslide Reports, 1985). It is known as a typical flysch sequence and is highly susceptible to weathering (Deveciler, 1986; Demir and Ercan, 1999; Ercanoğlu et al., 2004; Ercanoğlu, 2005).

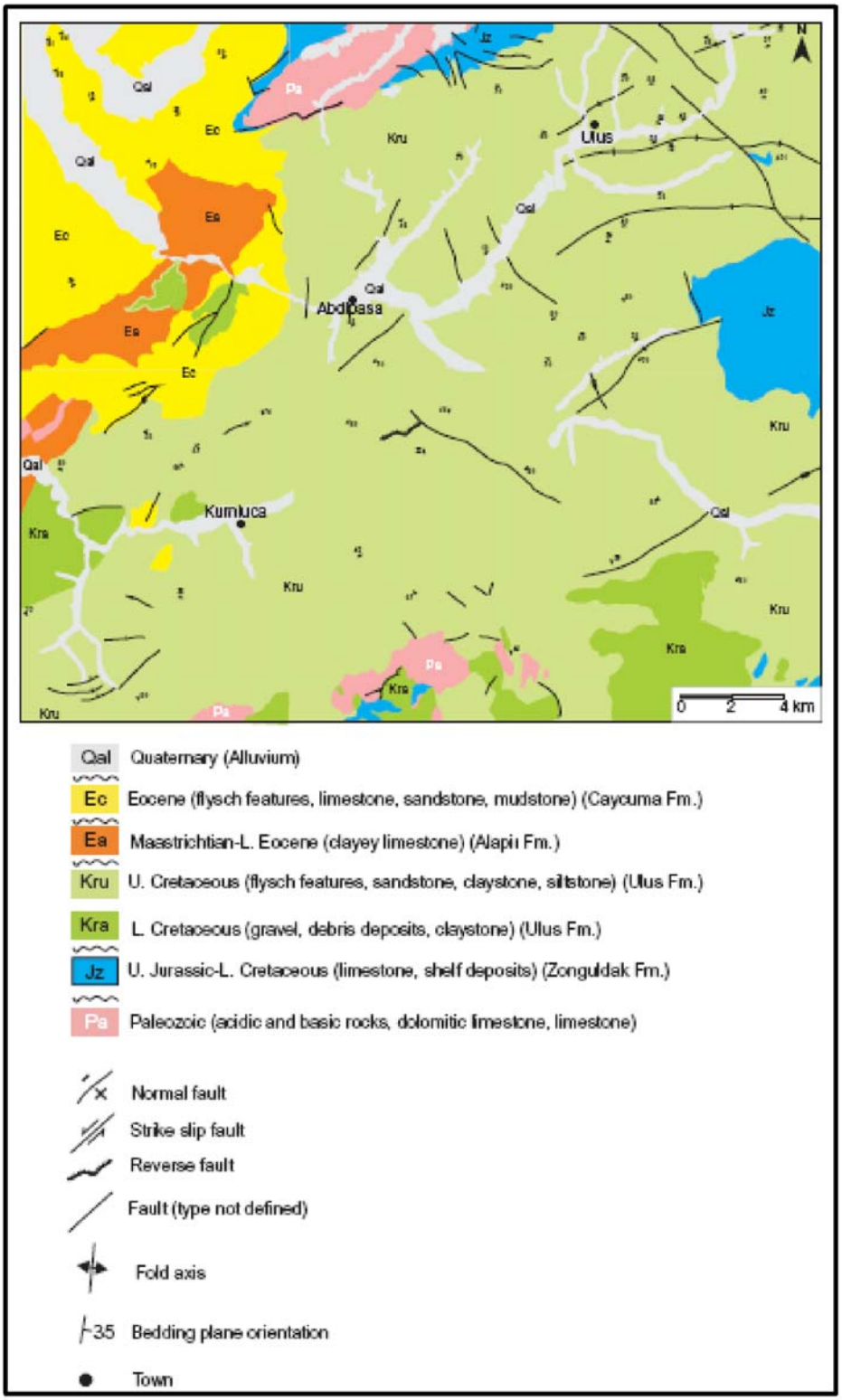

Figure 3.4. Generalized geological map of the study area adopted from Ercanoğlu, 2005 (simplified from Timur et al., 1997).

Long-lasting rainfall periods and slow snowmelt processes are responsible for the rise of the groundwater table, which produces flash floods. Depending on the 30

years of rainfall database from meteorological stations around the study region, the annual mean rainfall was found to be between 900 and 1071 mm. Different years of the analysis of landslide inventory show that 537 houses were moved due to damages that occurred after landslides in the region (Landslide Reports, 1975, 1985, 1987, 1993, 1995, 2005). In the study region, there have been approximately 287 landslides since 1961, which have been recorded by the General Directorate of Disaster Affairs (Landslide Map, 2004). In addition to this, 184 slide regions are mapped by the General Directorate of Mineral Research and Exploration (MTA) on 1:25000 scales as part of the Turkish Landslide Inventory Mapping Project. Most of these reported landslides which have occurred in the study region have frequently been reported in some recent studies (e.g. Temiz, 2000; Ercanoğlu and Gökçeoğlu, 2002; Ercanoğlu, 2003, 2005; Ercanoğlu and Gökçeoğlu, 2004; Ercanoğlu et al., 2004; Duman et al., 2005a).

The field observations showed that a settlement may be vulnerable to different types of disasters such as flooding and landslides (Figure 3.5). As illustrated in Figure 3.5, the area to the south-eastern part of the study region was prone to two different types of slides, in which buildings, roads, bridges, and humans were under risk.

Figure 3.5. A small site in the south-west part of the study region vulnerable to both flooding and landslides with different types (A: mass flow, B: debris flow).

Slides and flows are the two main types of mass movements in the study region. Among the slide types, rotational (Figure 3.6 a, Figure 3.6d) or complex (Figure 3.6 c) landslides are more common. The second most common type of failure is flow, mostly earth and debris flow in highly weathered alteration zones (Figure 3.6 b).

Figure 3.6. Landslides in Bartın Kumluca region: a. rotational slide, b. debris flow, c. shallow complex slide and d. rotational slide.

The relative depth of failure surfaces was classified as shallow (depth<5 m) and deep-seated (depth>5 m) (Gökçeoğlu et al., 2005). All slides in the study area are deep-seated, as presented in Figure 3.1. For simplicity, the activities of mass movements are classified into two groups as active and inactive. In Figure 3.1, type 1 represents inactive slides with a depth greater than 5 m., and type 2 is active slides with a depth greater than 5 m. Active landslides are defined as those currently moving, whereas inactive ones are relict according to WP/WLI (1993). In the study area, both active and inactive slides can be seen, and approximately 86.41% of all landslides are active whereas the rest is composed of non active slides. The morphometric landslide size parameters, such as width, vary from 30 m to several hundred meters, while the length varies from 20 m to several kilometers.

There are totally 184 slide locations including dormant and active slides in the region covering approximately 47.68 km^2 of the study area, and the largest slide area occupies 4.5 km^2.

The main reasons for selecting Kumluca Watershed for implementing the methodology are:

i. The landslides in the region have a wide range of sizes.
ii. The geologic and topographic property of the study region necessitates a landslide susceptibility map.
iii. Depending on the reports of the General Directorate of Disaster Affairs, the most important factor in landslide occurrence is heavy rainfalls and flooding.
iv. Depending on the reports of the General Directorate of Disaster Affairs, 537 buildings have been damaged and the people living in those houses have been moved to safe places because of damages which occurred after landslides.

Depending on the literature surveys, there is yet no study on risk mitigation in the study region. Hence, as the region is highly susceptible to landslides, it provides suitable site characteristics for demonstrating the application of the proposed methodology.

3.2 Data Collection

Data collection is the initial step for risk assessment methodology, which involves obtaining the data required for components of landslide risk assessment, such as susceptibility assessment, hazard analysis, and consequence analysis.

When assessing the susceptibility, the priority was given to the identification of landslide inventory together with the conditions that caused the slope to become unstable.

Depending on the key assumption of susceptibility assessment, which is "the slope failures in the future are more likely to occur under the conditions which led to past and present slope movements" (Varnes, 1984; Carrara et al. 1991; 1995),

determining the areas exposed to landslides provide useful information for identifying future landslide occurrences. Thus, an inventory map which ideally includes individual landslide features, type, style, activity, depth, and the exact date of the slope failure (van Westen, et al. 1999) was required initially. As these inventories are used for the assessment of probability of failure, the accuracy and completeness of these maps are significant.

The information about the past states of landslides was acquired from the MTA on 1:25000 scales. The location of the landslide phenomena was visually surveyed by air photo-interpretation (Figure 3.7) as well as extensive field works. In the field works, a hand GPS (Global Positioning System) receiver with an accuracy of ±5m (at 95% confidence interval) and DGPS were used to check the locations of landslides.

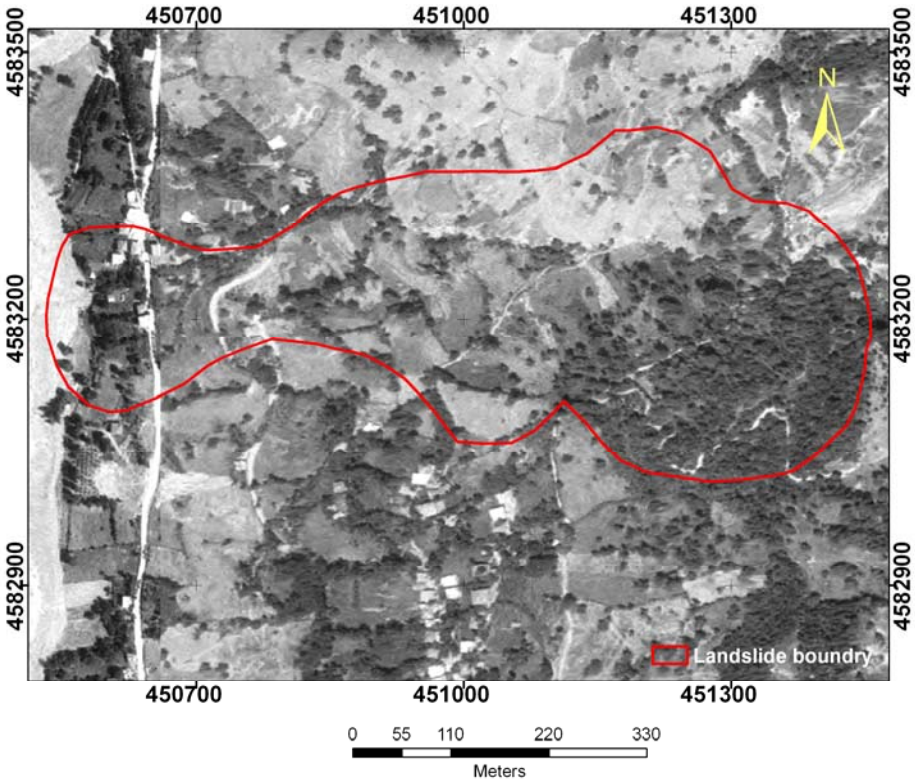

Figure 3.7. Interpretation of landslide boundaries from aerial photo

In the Project of Turkish Landslide Inventory Mapping (Duman et al., 2001), mass movements are classified according to the terminology of Varnes (1978), i.e. slides,

creep, falls, and flows. In the study area, slide type mass movements are dominant and flows are also present. This study separates flows from slide type movements. Hence, the flow deposits present in Kumluca watershed were not included in the landslide inventory map and only the slides were involved in further risk assessment studies.

For landslide susceptibility assessment, several spatial data layers, or landslide influencing parameters, are necessary for evaluation together with the landslide inventory. Therefore, information related to landslide factors were acquired from different organizations. Most of them were on similar scales but with different data formats, projections, and types. Different data formats, projections and types were converted into the same format. Before the production of input data from these raw data, all data set was converted into the same projection system and Universal Transverse Mercator (UTM) projection of ED50 datum was used for all the data set. Then the raw data were used for the production of input data with the same data type. The main data sources are given in Table 3.1 with their properties and scale.

Table 3.1. Characteristics of data for Kumluca basin

Implement Type	Data Source	Data Type	Data Format	Scale	Coordinate System
S*, H*	General Directorate of Mineral Research and Exploration	Landslide Map	ARC/INFO polygon	1:25000	Geographic WGS_84
S	General Directorite of Disaster Affairs	Landslide Map (Landslide Map, 2004)	ARC/INFO Point	1:50000	European Datum 1950
H	General Directorite of Disaster Affairs of Bartın	Landslide reports (Landslide Reports, 1975-1985-1987-1993-1995-2005)	Text		
S	General Command of Mapping	Aerial Photo (14 -26.07.1998)	Tif	1:35000	None
S, R*	General Command of Mapping	Topographic Map (Boundry, topographical elevation, hydrography, Industry, Physography, population, transportation, utilities)	ARC/INFO Vector (Line, point, polygon)	1:25000	UTM Datum: ED_50 Zone 36

Table 3.1 Characteristics of data for Kumluca basin (Continued)

Implement Type	Data Source	Data Type	Data Format	Scale	Coordinate System
S	General Directorate of Mineral Research and Exploration	Geology Map	ARC/INFO Vector (polygon)	1:25000	Geographic WGS_84
S	General Directorate of Village Maintenance	Soil Map	ARC/INFO Vector (polygon)	1:100000	WGS_1984_UTM_Zone_36N
S	NIK	ASTER (Advanced Spaceborne Thermal Emission and Reflection Radiometer) (14 Spectral Band, Level 3A) (22.10.2005)	Raster	VNIR(3): 15m SWIR(6): 30m TIR (5): 90m	WGS_1984_UTM_Zone_36N
R	General Directorate of Highway, General Directorite of Disaster Affairs of Bartın, Soil Yield Production Office	The value of element at risk	Text	2009	
H	Turkish State Meteorological Service	Rainfall Data for Kozcagiz, Ulus, Bartın, Amasra, Kurucaşile and Arıt stations	Excel	1975-2006 daily data	
R	Turkish Statistical Institute (TÜİK)	Population	Excel	2007	

* S =Susceptibility, H=Hazard, R=Risk, C=Consequence

The input data include 1:25,000 scale topographic maps including contour, hydrology and transportation maps; 1:25,000 scale geological maps include fault lines; Aster 3A satellite image includes 14 bands, 1:100,000 scale soil maps include soil depth, erosion, and land-use information; aerial photos containing 17 scenes with a scale of 1:35000 was taken in 1998. From the calculated data, 18 factors (dem, slope, aspect, curvature, plan, profile, wetness index, distance to hydrology network, density of hydrology network, distance to road network, density of road network, geological formations, distance to fault lines, soil type, soil effective thickness, erosion coverage, land cover, and vegetation cover) to be used for landslide susceptibility analysis were extracted. For the further analysis, these created maps relevant to landslide occurrence were constructed in a raster format and a spatial database was created by using the GIS software ARC/INFO and TNT-MIPS for the study region.

The Kumluca region is frequently affected by severe rainfall events. Hence, for the hazard assessment, data for daily rainfall was obtained from different stations distributed around Kumluca Bartın, for a 30-year period. In addition to this, the dates of past landslide events were extracted through landslide technical reports, a systematic review of newspapers, interviews with local witnesses, and inspections of technical and scientific reports and papers. The technical landslide reports were obtained from the General Directorate of Disaster Affairs of Bartın (Landslide Reports, 1975, 1985, 1987, 1993, 1995, 2005). The reports have detailed information about the geology, the reasons of landslide occurrences, the number of affected people, and the name of the villages, but not the spatial location of these slides.

For the consequence analysis, the elements at risk data for property, which include buildings, roads, land–use, and infrastructure, were obtained from digital topographic maps, as well as from the updated land cover map on a scale of 1:25,000. The value of each element at risk was obtained by means of interviews with experts from different organizations and the inspection of technical reports. The exposure of road classes and utility was obtained from the General Directorate of Highways, the building value was obtained from the General Directorate of Disaster Affairs of Bartın and the value of agricultural fields was obtained from the Soil Yield Production Office. For the assessment of risk to life on regional scale, the 2007 population information was used to estimate the number of people living at each building, which was acquired from Turkish Statistical Institute.

3.3 Susceptibility Assessment

Susceptibility assessment involves two main parts (Figure 3.8). The first part of the analysis involves preparation of the data. After obtaining the variables from data preparation part, they are used as an input for susceptibility assessment models.

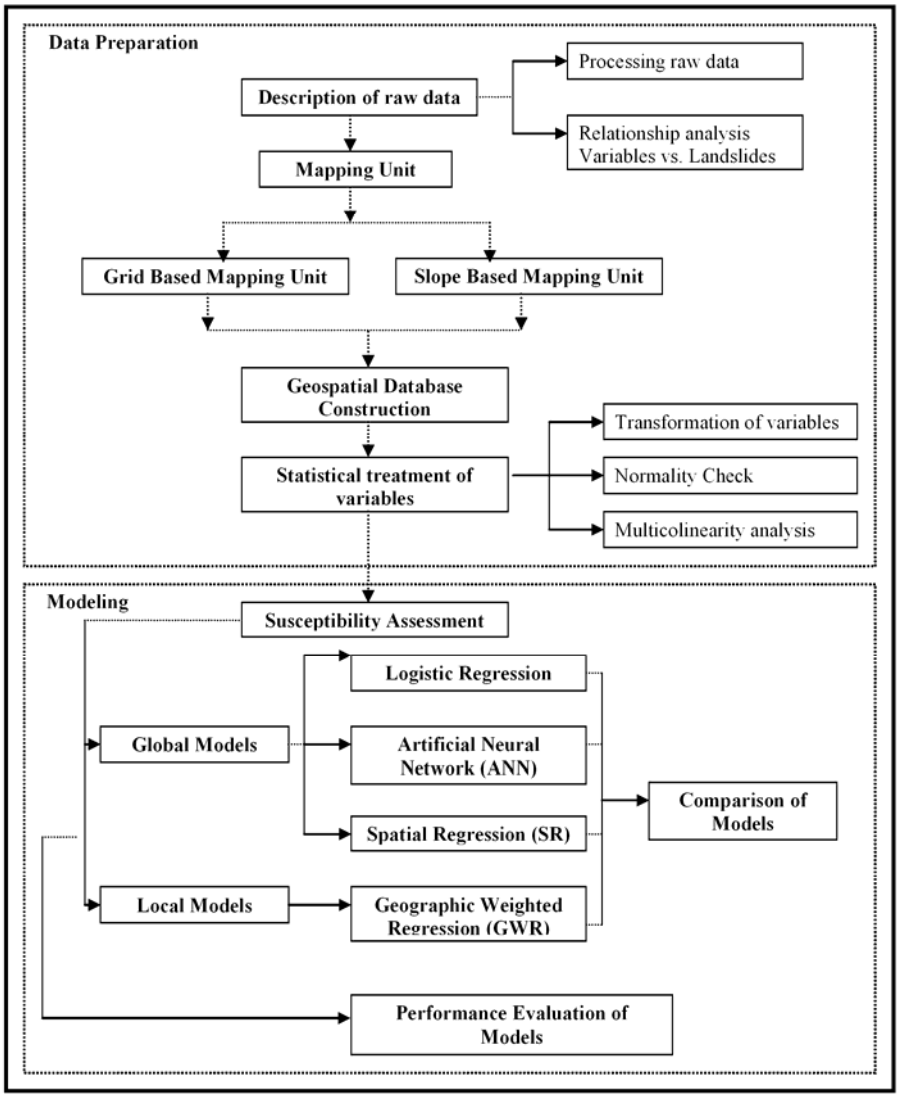

Figure 3.8. The procedure followed for susceptibility assessment methodology

3.3.1 Data Preparation

In order to determine landslide influencing factors for susceptibility assessment, the following stages were followed: (1) description of raw input data set in detail and processing of raw data are presented in Figure 3.9; in addition, analyzing the relationship between each influencing factor and landslide frequency; (2) statistical analysis of the conditioning factors contributing to landslides; (3) construction of the spatial database for further quantitative analysis. The data preparation stage of susceptibility assessment was illustrated in Figure 3.9.

The first stage of data preparation involves description of raw data in detail, which include format, projection, date, where it was obtained, what different sources of data

it contains, etc. After the description of the data, the process to obtain variable maps was described. The raw input data and the processed variable maps were illustrated in Figure 3.9. The relationship between each variable and landslide occurrence was analyzed by using the histograms. For this reason, the continuous variables were first divided up into zones, and then the area of each group and the landslide frequency in percentage was computed.

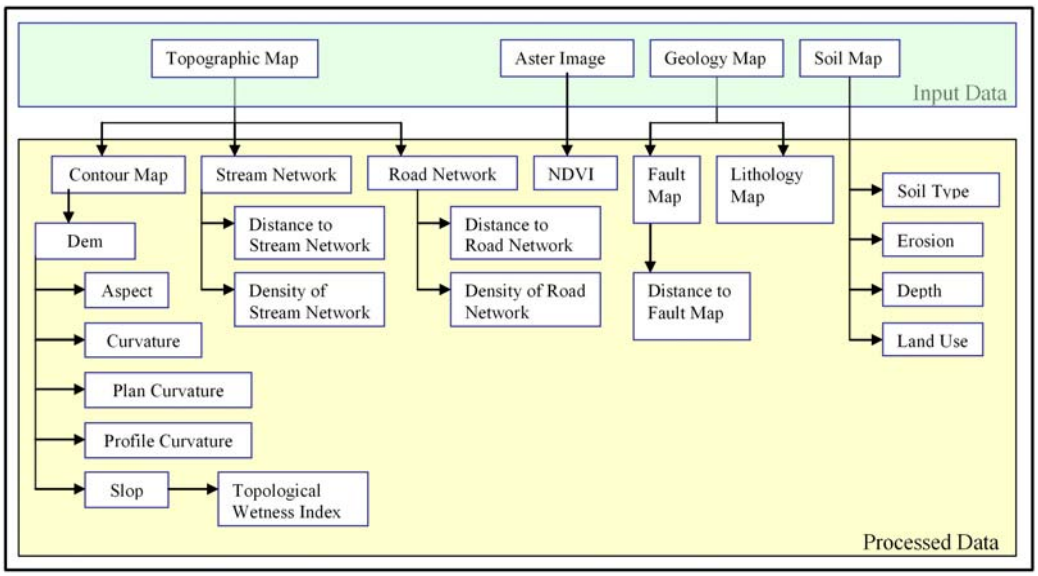

Figure 3.9. The main input data set and processed data to obtain influencing factors

Before the second stage of data preparation, the type of mapping unit was determined. This is defined as the partition of land surface into homogeneous regions. The reason for determining the mapping unit type was that statistical analysis of the variables changes depending on the type of mapping unit. In addition, different geospatial databases should be constructed for each mapping unit to obtain susceptibility maps for each mapping unit. Considering these results, it was determined that the mapping unit to be used in the study would involve grid cells and slope units.

After determining the type of mapping unit, the statistical analysis of the variables for each mapping unit was performed. The statistical analysis involves (i) transformation of qualitative variables; (ii) selection of independent variables by multi colinearity analysis; (iii) testing for normal distribution for each variable.

Following the stage of constructing spatial databases for each mapping unit, landslide susceptibility maps by four different mapping methods were obtained.

3.3.1.1 Processing of Topographical Data

The topographical data was acquired from the General Command of Mapping in digital format. The data set included the contour map, road and stream networks which were in vector coverage format and represented by points, lines, or polygonal features. This discrete form of data was not suitable to be used in landslide susceptibility mapping. For this reason, it was converted into continuous surfaces (Süzen and Doyuran, 2004). As a result, the contour map data were used to generate a DEM. The DEM was then used to describe geomorphologic (slope, aspect, plan curvature, profile curvature) units and topographic wetness index.

In the first stage, to produce the input data, the data format, which was in ARC/INFO E00 format, was transformed into ARC/GIS shape format. The map incorporates 10 m. contour intervals. By using this map, DEM of the study area was generated by using the Triangular Irregular Network (TIN) algorithm (Figure 3.10).

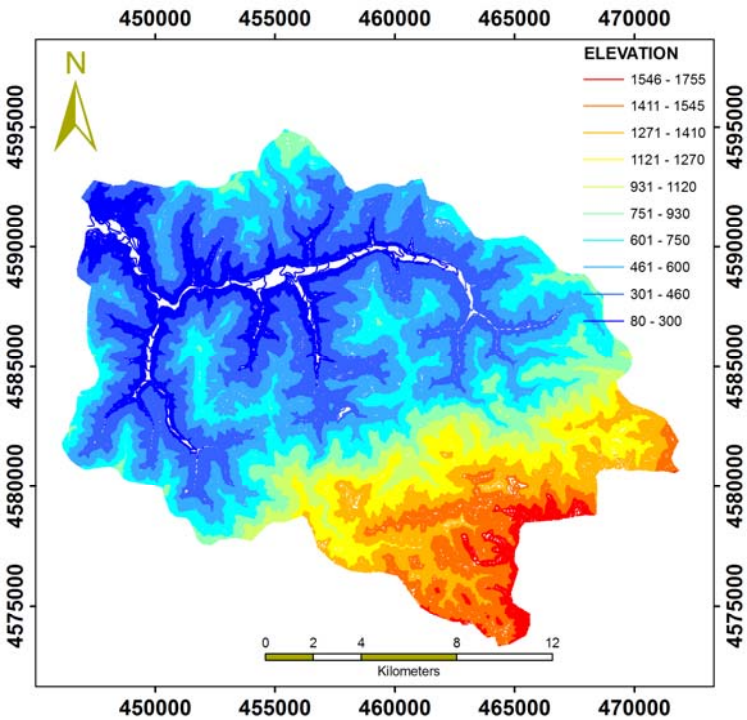

Figure 3.10. The contour map of the study area

After the creation of TIN model, the DEM of the area was produced for 20 m. through interpolation. There are two reasons for selecting 20-m resolution: first, the working scale was selected as 1:25000, and second according to USGS (1993), the positional accuracy needed for 1:25000 scale maps must be ±12.5 m. For this reason, a pixel size of 20 m. was selected for production of DEM. The "linear method", which treats each triangle as a planar surface, was used. By using this method, each output cell was assigned a topographical elevation by finding which triangle, in 2-D space, it fell in and the position of the cell center was evaluated relative to the triangle plane. Accordingly, the total number of pixels for the whole area was 810,005. The DEM generated from the contour map in Figure 3.11 shows that the topographical elevation ranges from 80 to 1755 m in the study area. The mean topographical elevation is 708.99 m. having a standard deviation of 397.66 m. and the maximum concentration of topographical elevation is observed at 200 - 600 meters with a value of about 50%.

The lowest topographical elevations are dominant around the north-western and northern parts of the area, particularly where the landslide occurrences are concentrated. The highest topographical elevations, on the other hand, can be observed around the south-eastern part of the study region.

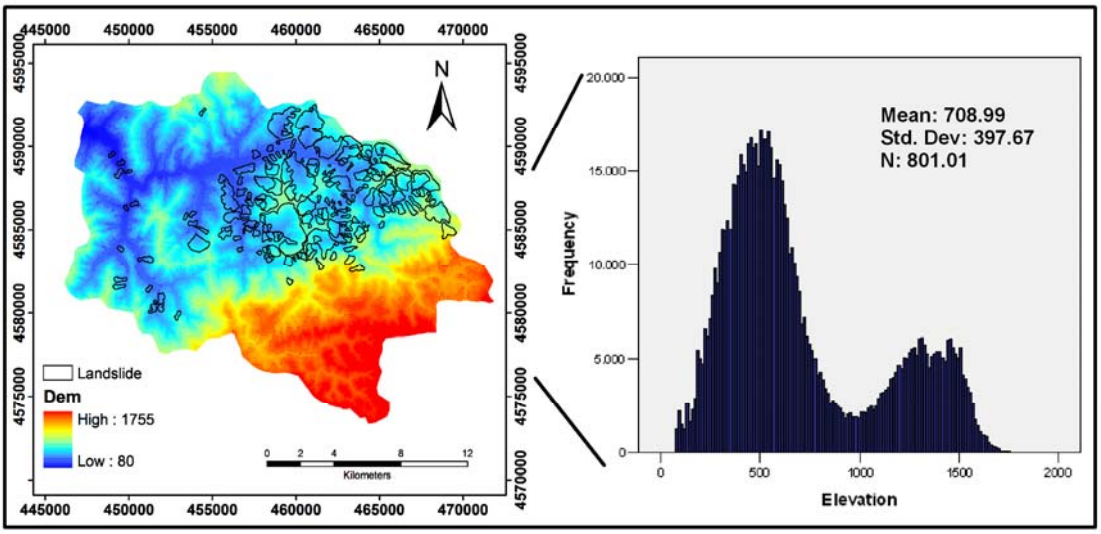

Figure 3.11. DEM of the study region overlaid with the landslide locations and the frequency distribution of values

The relationship between landslide activity and topographical elevation is still

unclear, hence it requires further studies. However, the topographical elevation affects soil characteristics significantly. Gomez and Kavzoglu (2005) refer to Ochoa (1978), arguing that soil texture varies with topographical elevation, as the grain size increases with the altitude.

To analyze the relationship between landslide occurrence and topographical elevation, histograms were constructed (Figure 3.12). The percentage of landslide occurrence is the highest at the 201- 600 m topographical elevation range. Moreover, the area of this zone occupies the largest region (49%). The occurrence of landslide frequency reduces as the topographical elevation increases.

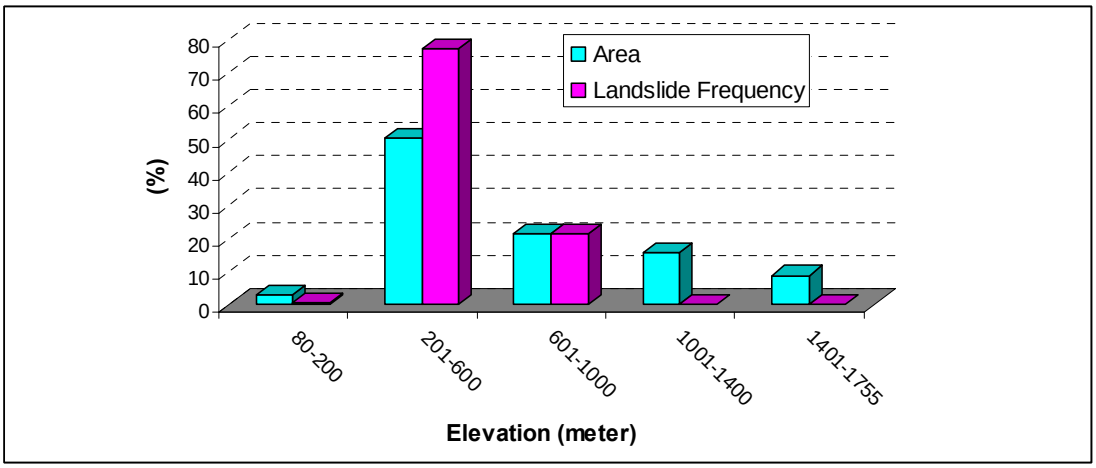

Figure 3.12. Histogram showing the relationship between topographical elevation and landslide frequency.

The construction of an accurate model of the terrain surface is fundamental for landslide susceptibility mapping. In order to test the accuracy of the produced DEM, the principles of DEM accuracy assessment given by USGS were adopted. According to USGS National Mapping Program Technical Instructions, a representative sampling of test points was used to verify the accuracy of any category of the DEM. A minimum number of 28 test points for DEM is required (USGS 2002). The root-mean-square error (RMSE) statistic for topographical elevation was used to describe the vertical accuracy of the DEM.

Vertical RMSE is defined as:

$$\boldsymbol{RMSE}=\sqrt{\frac{\sum\left(z_i - z_t\right)^2}{n}} \qquad (37)$$

Where;

z_i = interpolated DEM topographical elevation of a test point;

z_t=True topographical elevation of a test point and

n = number of test points.

For accuracy assessment, the contour line mid points were extracted and then different sets of 20% of these points were selected randomly as test points for accuracy assessment of the DEM (Table 3.2).

Table 3.2. RMSE of DEM

	Ref. Elev.	DEM Elev.	Diff. Elev.	Diff. Sqr.		Ref. Elev.	DEM Elev.	Diff. Elev.	Diff. Sqr.
1	585	585	0	0	15	635	636.12	1.12	1.2544
2	370	369.19	-0.81	0.6561	16	500	499.42	-0.58	0.3364
3	420	427.6	7.6	57.76	17	825	825	0	0
4	380	382.7	2.7	7.29	18	250	250	0	0
5	530	527.48	-2.52	6.3504	19	425	421.01	-3.99	15.9201
6	550	554.31	4.31	18.5761	20	415	411.22	-3.78	14.2884
7	430	433.77	3.77	14.2129	21	435	434.22	-0.78	0.6084
8	530	530.88	0.88	0.7744	22	635	635	0	0
9	510	514.91	4.91	24.1081	23	460	458.54	-1.46	2.1316
10	80	80.35	0.35	0.1225	24	500	498.1	-1.9	3.61
11	585	582.87	-2.13	4.5369	25	1030	1032	2	4
12	545	549.12	4.12	16.9744	26	370	371.35	1.35	1.8225
13	665	665	0	0	27	390	391	1	1
14	625	628.63	3.63	13.1769	28	130	129.61	-0.39	0.1521
						RMSE= 3.17			

The mean of vertical RMSE was found to be 3.17 m., which is quite admissible within the accuracy requirements of the study (which is much less than the minimum accuracy limit of one-third of the contour interval specified by USGS, 2002).

The produced DEM was used as the topographical elevation input data for topographical elevation attributes of landslides. As the morphometric terrain attributes can be derived directly from the DEM using (local) filter operations or a mathematical formula, initially the slope and aspect, the first derivatives of the DEM, were produced. Subsequently the curvatures, the second derivatives of the DEM, were acquired. Hydrological or flow accumulation-based terrain parameters are typically used to quantify the flow intensity and accumulation potential or erosion potential. Hence the topographic wetness index as the second derivative of the DEM was produced.

Slope angle is an essential component of the landslide influencing factor set, which indicates how steep the ground surface is. The produced and color-coded slope map and its frequency distribution were presented in Figure 3.13a. The slope has a range between 0 and 90, 0 as the flat lying areas and 90 as the vertical ones; any other value is the slope angle measured from horizontal. Hence, in the study area the minimum value of the data is 0 and the maximum is 65.5 degrees. The mean is 20.88^0 with a standard deviation of 8.48^0 (Figure 3.13b). 70% of the region has slope angles between 10^0 and 30^0. The slopes above 50^0 is negligible since their percentages are nearly 0. The higher slopes are dominant mostly in the western and south- eastern parts of the region, where the presence of landslide occurrences is lower.

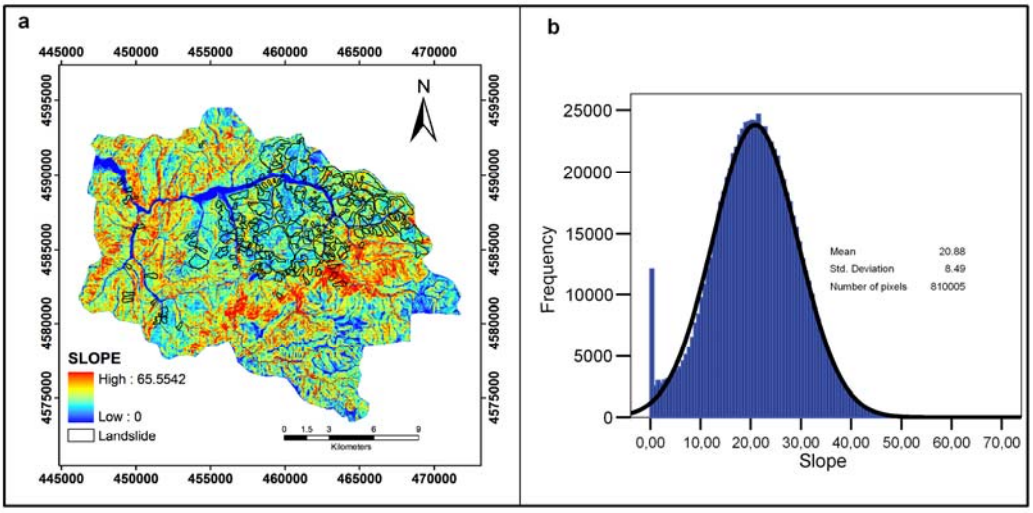

Figure 3.13. Slope map of study region overlaid with landslide locations b. frequency distribution of slope variable

The relationship between landslide frequency and slope angle (Figure 3.14) showed that slope has relevance with landslide occurrences at angle ranges of 11^0- 20^0 rather than the steep slopes. Pachauri and Panta (1992) indicated that the frequency of landslides is higher in steeper slopes (>35^0). However, this was not the case in this study. 55% of the study region has slopes higher than 21^0 and only 35% of the landslides were present in this part. This situation may be related to vegetation or forest cutoff to obtain area for agriculture, or it may be related to accumulation of soil material coming from upper resistant rocks by weathering or erosional processes associated with possible saturation of soil by low groundwater level on gentle slopes (Ercanoğlu, 2005).

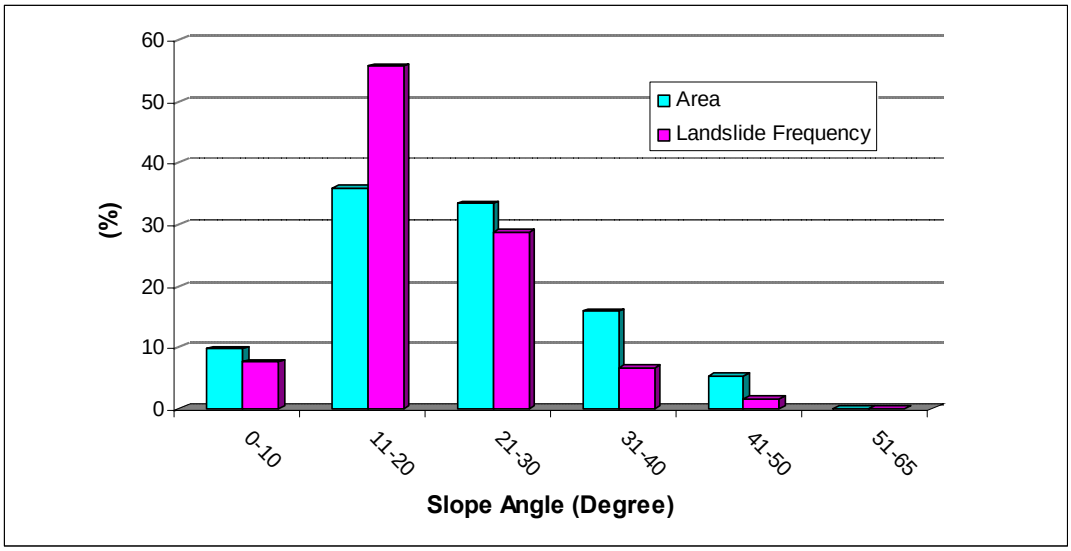

Figure 3.14. Histogram showing the relationship between slope angle and landslide frequency.

Aspect is the orientation of a slope face in degrees (between 0 and 360 degrees). There is yet no general agreement on aspect regarding its relation to landslide occurrence. Some authors (Nagarajan et al., 2000; Fernández et al., 2003; Santacana et al., 2003; Ayalew et al., 2004; Lee, 2004; Melelli and Taramelli, 2004; Süzen and Doyuran, 2004; Gökçeoğlu, 2005; Akgün and Bulut, 2007) took aspect into consideration as a factor controlling landslides while the others (Jose et al., 2000; Van Westen et al., 2003; Ayenew and Barbieri, 2005; Neuhäuser and Terhorst, 2007; Weirich and Blesius, 2007; Wang et al., 2008) did not consider it as a conditioning factor.

Aspect strongly influences potential direct incident radiation and thus temperature. Therefore, the moisture of the soil on the ground may alter. As a result, this parameter was also considered as a conditioning factor for the study area. Flat areas having no downslope direction are given a value of -1; 0 is regarded as the north; any other value is the azimuth measurement from north. The aspect values were preferred to be oriented in 16 principal directions, which are 22.5 degrees apart from each other. The produced and color-coded aspect map was presented in Figure 3.15b. The minimum value is -1^0 and the maximum is 360^0. The aspect has a mean of 184.3^0 with a standard deviation of 110.6^0. The aspect shows a similar frequency distribution in each range (Figure 3.15b).

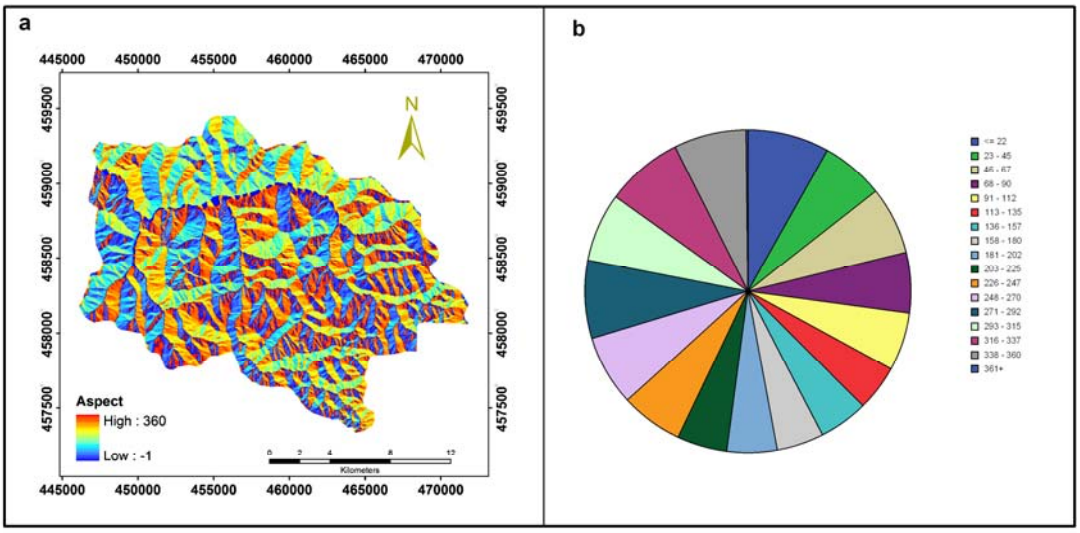

Figure 3.15. a. Aspect map of the study region and b. frequency distribution of values

In untransformed form, aspect is not suitable for quantitative analysis, since 1^0 is adjacent to 360^0. The numbers are very different even though the aspect is roughly the same (McCune and Keon, 2002). For this reason, aspect was transformed for further analysis by using the folded aspect formula, which is proposed by McCune and Keon (2002) (Equation 2). Depending on this approach, aspect is 'folded' about the north-south line, rescaling $0\text{-}360^0$ to $0\text{-}180^0$, such that NE = NW, E = W, etc.:

$$\text{Folded aspect} = 180 - |\text{Aspect} - 180| \qquad (38)$$

The relationship between landslide locations and aspect variable was shown in Figure 3.16. As Figure 3.16 illustrates, landslide occurrences are observed in almost every aspect class, but the slopes facing the north seem to be relatively more susceptible to landslide occurrence.

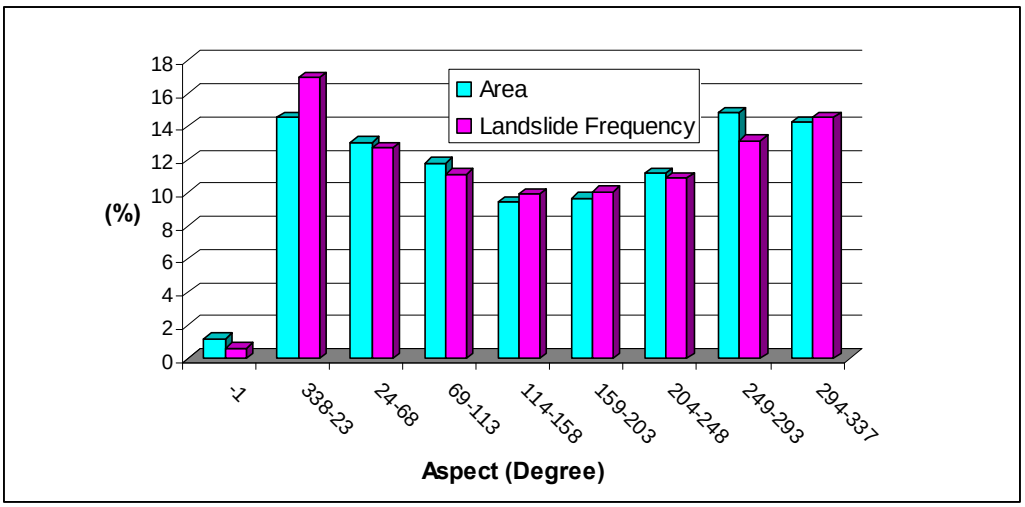

Figure 3.16. Histogram showing the relationship between aspect and landslide frequency.

Curvature values represent the morphology of the landscape. Curvature maps were derived as the second derivative of a DEM. A positive curvature indicates that the surface is convex (Figure 3.17). A negative curvature indicates that the surface is concave (Figure 3.17). A curvature value of zero indicates that the surface is flat.

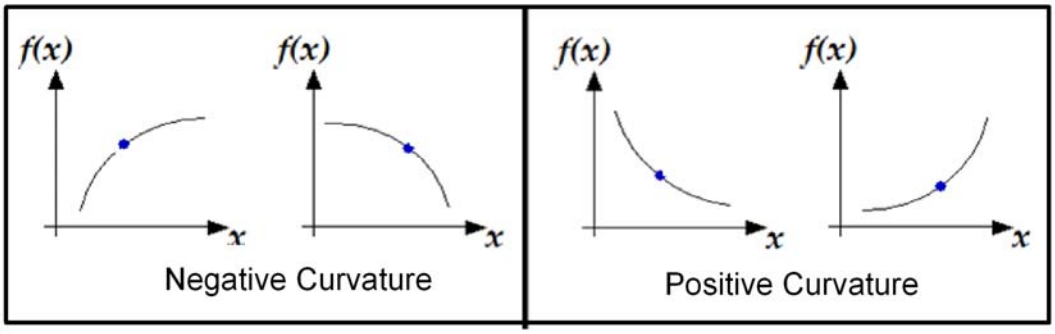

Figure 3.17. The positive and negative curvature

The positive curvature (convex) occupies 45% of the region and the negative curvature (concave) occupies 20% of the region; therefore, they are both dominant in the whole region when compared to the flat areas, which compose 35% of the study region (Figure 3.18). The curvature values have a mean of 0 with standard deviation of 1.05. The maximum and minimum values are -19.08 and 21.35, respectively.

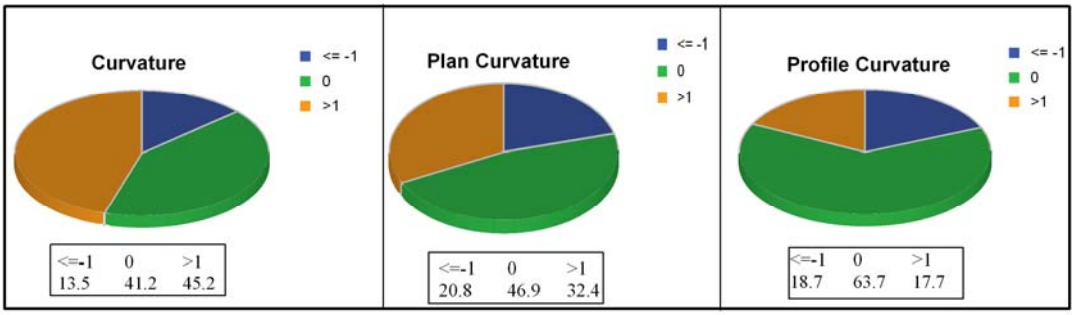

Figure 3.18. Statistics for curvature, plan curvature and profile curvature map (%).

In addition to curvature, plan and profile curvatures were also formed to represent the morphology of the topography. The plan curvature implies that a slope is parallel to the elevation contours, which can be used to help identify divergent or convergent flow areas on the landscape. Convergent flow generally indicates higher erosion and transport potential, while divergent flow indicates lower erosion and transport potential. The profile curvature implies that slope is perpendicular to the elevation contours and indicates whether any particular point on the hill slope profile is in an area of convex or concave curvature. It affects the acceleration and deceleration of the flow, and therefore influences landslide damage potential.

The profile curvature has larger flat areas compared to the plan curvature, they occupy 60% and 45% of the study region respectively (Figure 3.18). The plan curvature values have a mean of 0.13 with a standard deviation of 0.57. The maximum and minimum values are 8.76 and -8.51 respectively and the profile curvature has a mean of 0.13 with a standard deviation of 0.67. The maximum and minimum values are 15.31 and -14.09 respectively.

The relationship between landslide locations and curvature (Figure 3.19) shows that approximately 58% of landslides occur at convex and concave topography whereas 41% occur on flat slope surface.

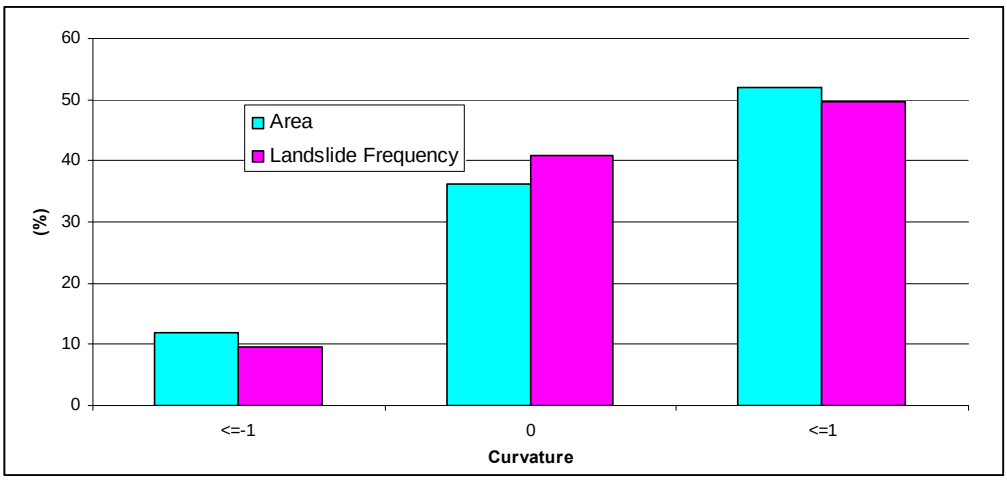

Figure 3.19. Histogram showing the relationship between curvature and landslide frequency

A DEM-based topographic wetness index, (TWI) (Moore et al., 1988), was used to represent the spatial distribution of water flow across the study area. The wetness index represents a theoretical measure of the accumulation of flow at any point within a river basin. The index can be used as a basis for estimating the local soil moisture status and thus areas of landslides which were affected by hydrological conditions due to the topographic effects of surface (Gomez, and Kavzoglu, 2005). The calculation of this index is based on several assumptions (Moore et al., 1991). The flow conditions are assumed to be at a steady state, which means that the water flow is uniform and every calculation unit gets a contribution from its entire upslope contributing area. The rate of groundwater recharge and soil properties is assumed to be uniform over the area. In the computation of the wetness index, a depressionless DEM was calculated to remove the sinks. After multiple flow directions were determined from the resulting DEM image, the flow accumulation area (A_s) and the tangent of slope (tan β) were produced. The topographic wetness index of the study area was then created by using the Eq. (39) as proposed by Moore et al. (1991):

$$TWI = \ln\left(\frac{A_S}{\tan\beta}\right) \tag{39}$$

where, A_s is the specific catchment area , β is the slope gradient.

By employing Eq. (39), the topographic wetness index map was produced in Figure 3.20a. As it can be seen in Figure 3.20a, the topographic wetness index values

are higher around the river bed and the slide area. This might be due to the fact that the index shows the tendency of water to accumulate at any point in the drainage basin and the tendency of the water to move down the slope by gravitational forces. Infiltration of water into slope-forming material results in increased pore water pressure on the material and a decrease in its shear strength (Gökceoglu et al., 2005).

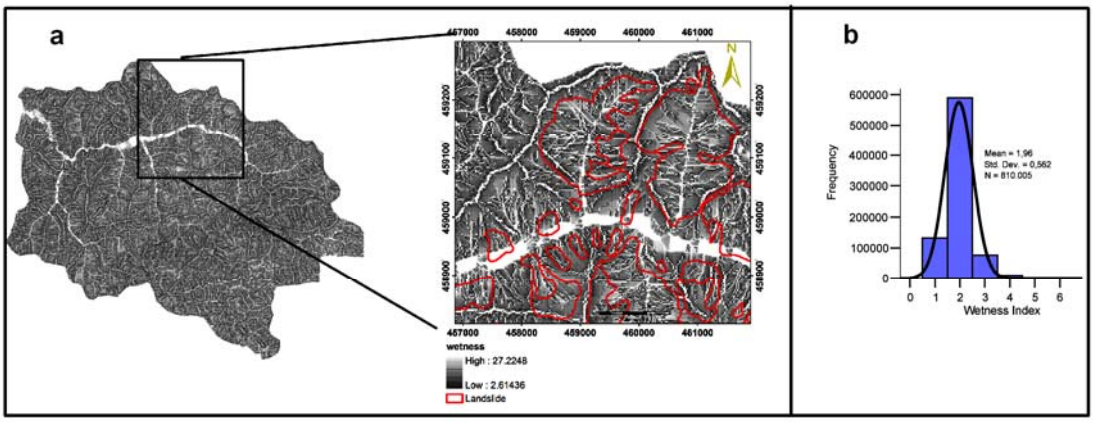

Figure 3.20. Topographic wetness index (TWI) overlaid with landslide locations zoomed in the north-eastern part of study region

The wetness index of the study region has a mean of 196 having a standard deviation of 0,562 (Figure 3.20b). In addition to the statistics, the distribution of the wetness index to the landslide and study region is analyzed as presented in Figure 3.21. It is clear that the percentages of the wetness index distribution is higher for the first two classes (2.6-5 and 5.1-7) from both the study area and landslide region with 70% and 63% frequencies (Figure 3.21). The relationship between TWI and landslide occurrence shows significant relations at the range of 5.1-7 (Figure 3.21) with a value of 37%.

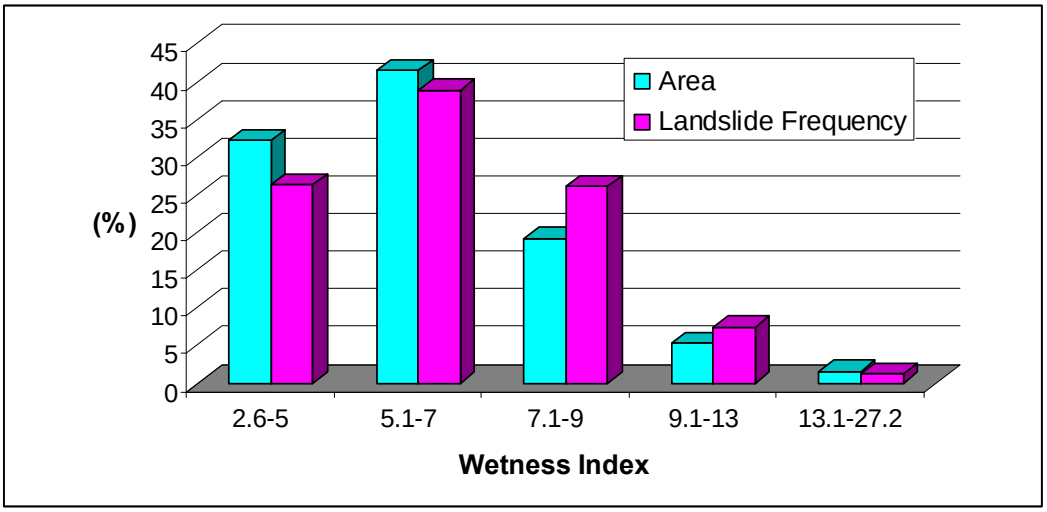

Figure 3.21. Histogram showing the relationship between curvature and landslide frequency

Data acquired from the General Command of Mapping also include the road network map, which shows the main roads and pathways (Figure 3.22a), and the stream network map showing the rivers, dry rivers, and rivers with wide bed in the study region (Figure 3.22b).

The stream network and road network map do not have an elevation value hence a non-interpolative method was implemented to treat such data, where the distance map or the density map was used. A distance map was calculated by computation of the Euclidian distance of each cell to the nearest line in the map and a density map (the number of line/point elements of fixed length in a fixed area) was calculated by using a moving window through calculation of density of the object within a specified area.

A distance map for road lines and stream lines was produced and used in the analysis to consider the effect of each factor on landslide occurrence. For both maps, the distances of each pixel regarding the nearest road line and the nearest drainage-lines (Figure 3.23a, Figure 3.24a) were calculated by using the Euclidian distance. In both maps the minimum distance of pixels was 1 meter and the maximum was 1000 meters. The values of distance to road have a mean of 117.37 m. with a standard deviation of 115.27 m. (Figure 3.23b). The distance to stream lines has a mean of 222.01 m. with a standard deviation of 173.97 m. (Figure 3.24b). The distances to road and stream lines show a similar distribution around the whole region, whereas

the road lines are denser than the stream lines mostly in the north-eastern part of the region (Figure 3.23a).

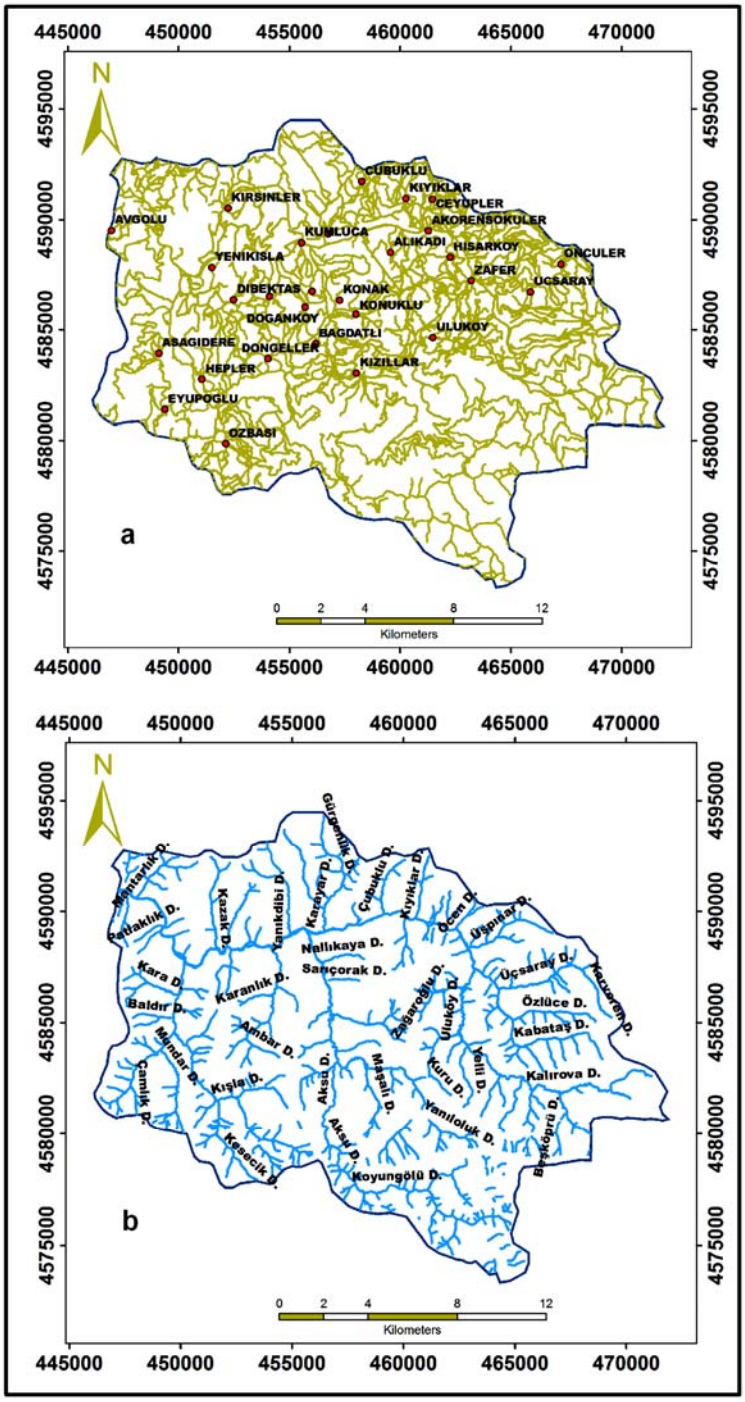

Figure 3.22. a. Road network map overlaid with the villages and b. Stream network map showing the names of rivers

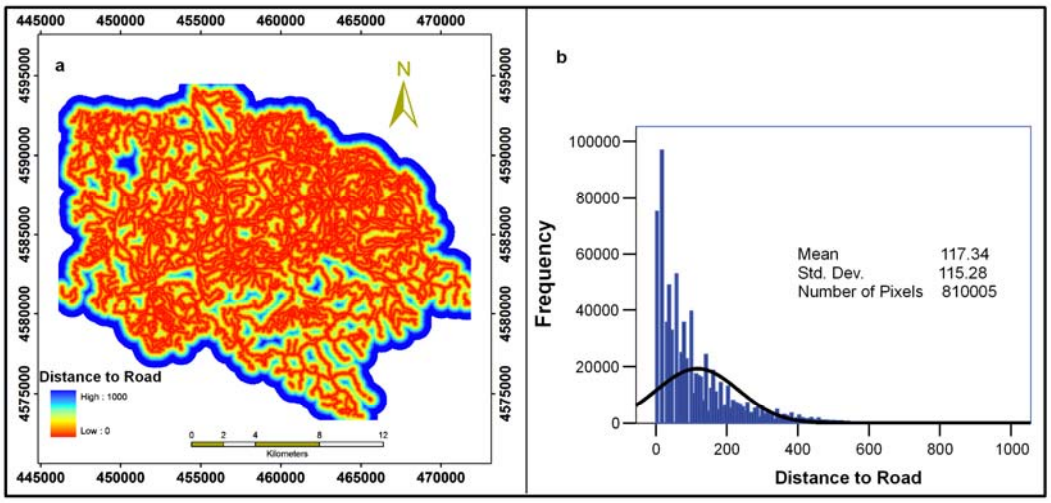

Figure 3.23.a. Distance to road network map and b. Frequency distribution of distance to road network

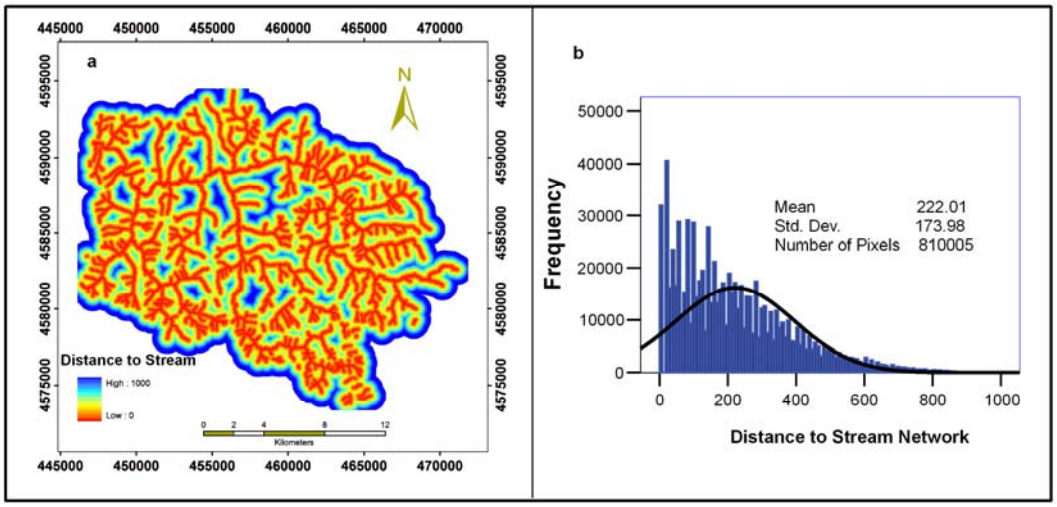

Figure 3.24. a. Distance to stream network map and b. Frequency distribution of distance to stream network

In addition to the distance to road lines and stream lines, the density of road and stream lines were also produced (Figure 3.25a, Figure 3.26a). The density map was computed by the calculation of the ratio of the summation of the number of line/point elements of fixed length to the kernel selected for a fixed area. For the production of the road density map and the stream density map, the road line length and the stream line length were taken into account. For the road density, a 2 km^2 kernel size was selected, which provides density values ranging from 0.27 to 4.33 km/km^2. For the stream density map, a 3 km^2 kernel size was selected, which provides density values ranging from 0.13 to 1.86 km/km^2. The road density values have a mean of 2299.8 m/m^2 with a standard deviation of 893.28 m/m^2 (Figure 3.25b). The stream network

density values have a mean of 1004.46 m/m^2 with a standard deviation of 328.64 m/m^2 (Figure 3.26b). The distance map for road network lines shows higher density in the north-eastern and middle parts of the region (Figure 3.25a), whereas the stream network lines are denser in the northern and north-eastern parts of the region (Figure 3.26a).

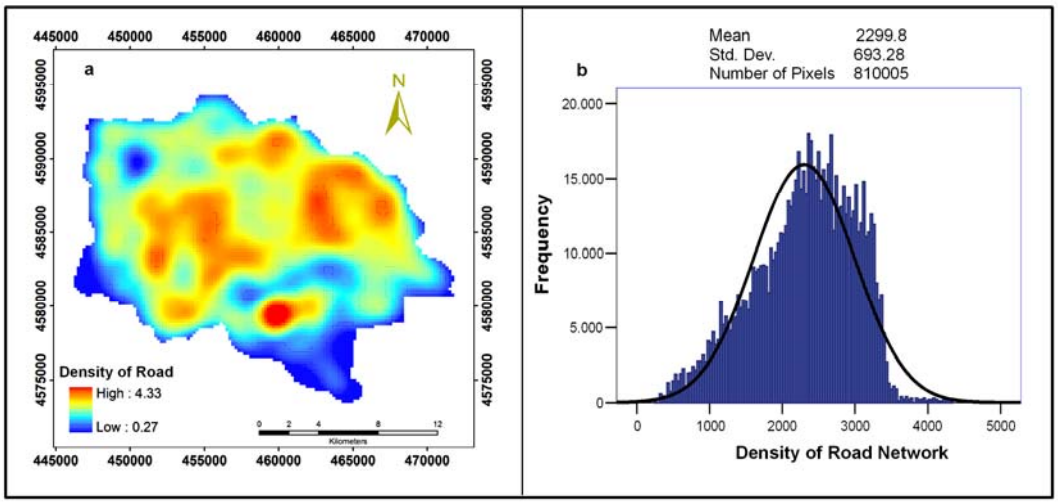

Figure 3.25. a. Density of Road Network map b. Frequency distribution of Road Density

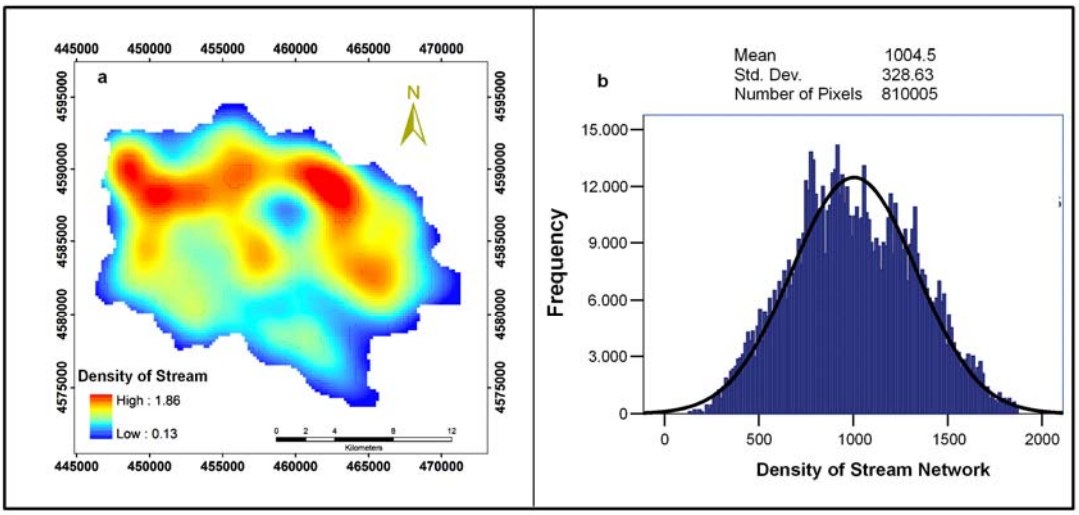

Figure 3.26. a. Density of stream network map b. Frequency distribution of stream density

The relationship between landslide frequency and the distance to road network (Figure 3.27) and the distance to stream network (Figure 3.28) indicates that landslide occurrence increases as the distance to stream network and the distance to

road network decrease. The influence of road distance on landslide occurrence can be explained by the human impact on nature through road cuts. As it can be seen in Figure 3.27, a landslide frequency of 90%is present up to 200 m distance to road network.

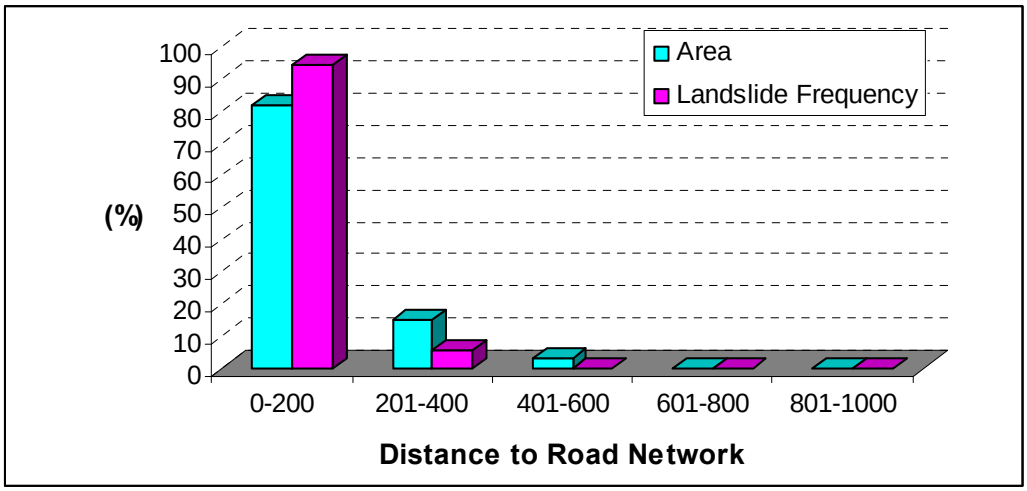

Figure 3.27. Histogram showing the relationship between distance to road network and landslide frequency

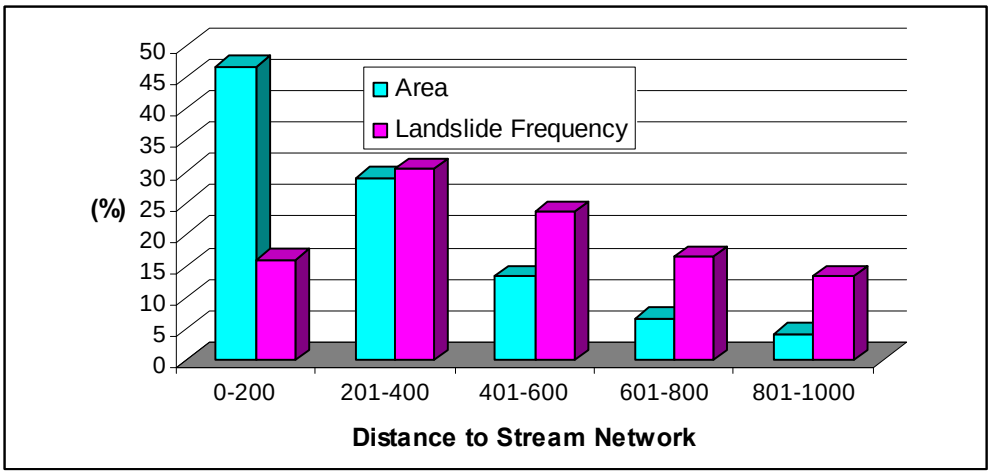

Figure 3.28. Histogram showing the relationship between distance to stream network and landslide frequency

Additionally, the highest correlation between the road density and landslides is observed between 2.17 and 4.33 km/km^2 (95%) (Figure 3.29). In parallel, the highest correlation between landslide occurrence and the drainage network density is in the range from 0.707 to 1.33 km/km^2 (64%) (Figure 3.30).

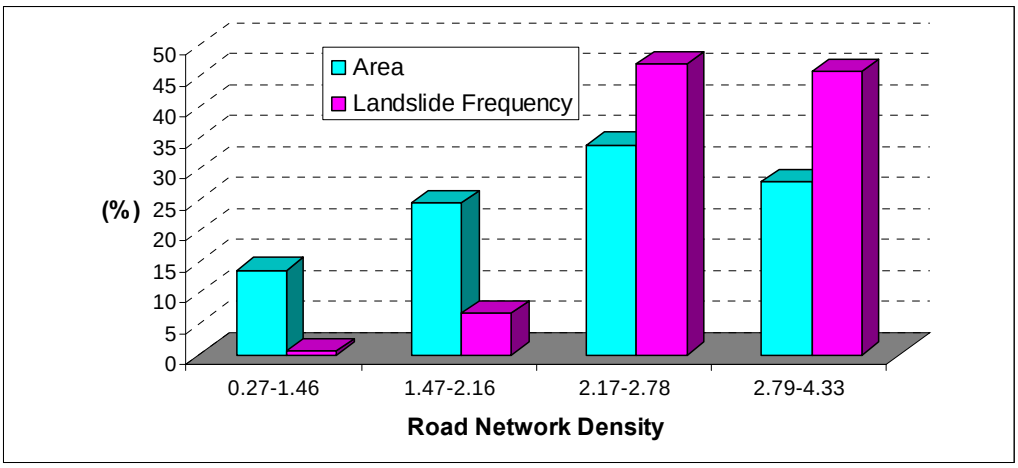

Figure 3.29. Histogram showing the relationship between road density and landslide frequency

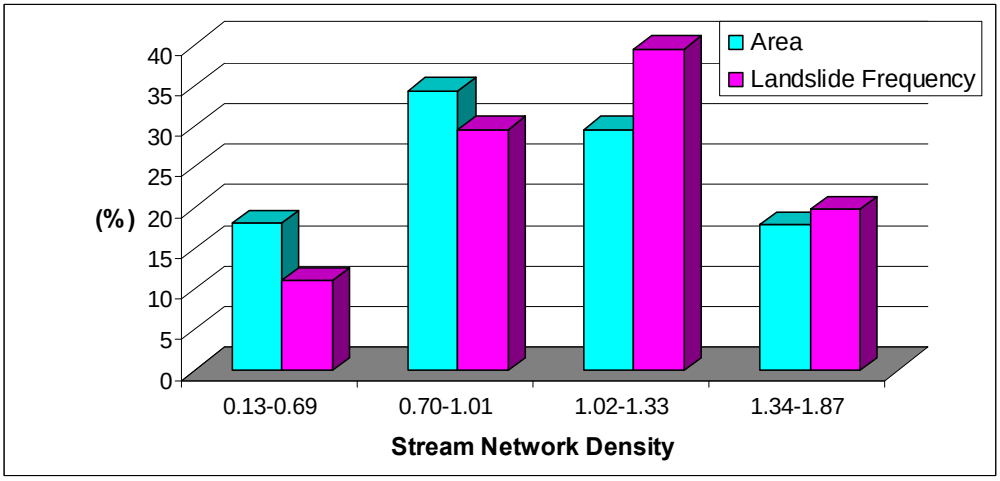

Figure 3.30. Histogram showing the relationship between stream network density and landslide frequency

The vegetation index was produced by using ASTER (Advanced Space borne Thermal Emission and Reflection Radiometer) (14 Spectral Band, Level 3A) satellite imagery acquired on 22.10.2005. The data was projected to WGS84_UTM zone 36 by using 156 GCP geographic coordinates by using PCI 9.1 GCP WORKS. Then it was reprojected to UTM ED50 Zone 36 by using the Focus extension of PCI. After extracting the spectral bands to study the region boundary, the Normalized Difference Vegetative Index (NDVI) was created. NDVI is an index derived from reflectance measurements in the red and near infrared portions of the electromagnetic spectrum, which describes the relative amount of photosynthetically active green biomass present at the time of imagery. It is a measure of the vegetative cover, which is used to determine the density of green areas. The Aster image bands of 3 (NIR) and 2 (R) were used to generate this measure, since these bands best highlight the

chlorophyll absorption and provide good contrast between vegetation and soil. The NDVI was calculated by using NDVI (Figure 3.31a) as given in Equation 40:

$$\text{NDVI} = \frac{NIR - R}{NIR + R} \tag{40}$$

where *NIR*= Near Infrared band; *R*=Red band.

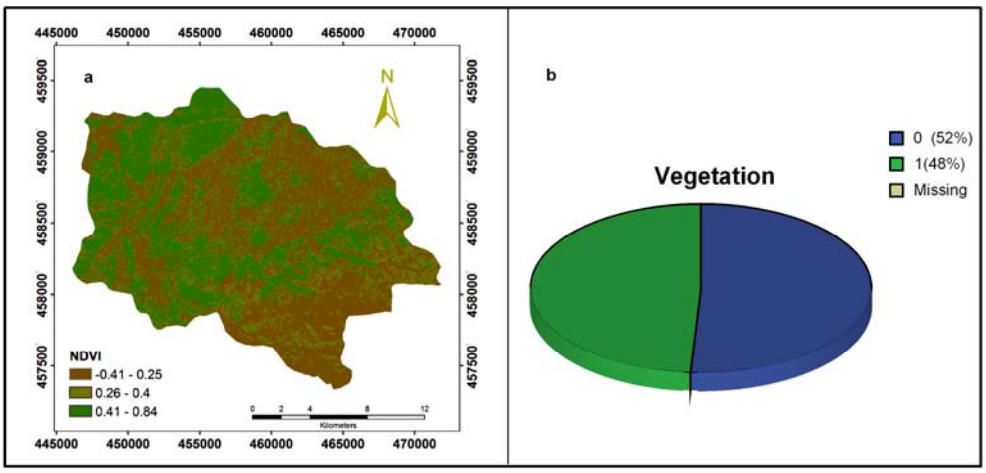

Figure 3.31. a. Vegetation Index Map of the study region calculated from Aster Image b. The percent of vegetation cover after classification of data into 2 classes with threshold 0.3.

NDVI values range between -1 and +1, with dense vegetation having higher values (e.g., 0.4) (USAID, 2009). The index was classified into 2 classes for further analysis and 1 is assigned for vegetated areas and 0 for non-vegetated areas, where 0.3 taken as the threshold. Non-vegetated regions occupy 52% of the whole region while 48% is the vegetated region (Figure 3.31b).

When the relation between the vegetated areas and landslide occurrence was analyzed, it was seen that the vegetation shows a high correlation with landslides. When the area of vegetation class is considered, it can be said that 73.5% of the landslides occurred in non-vegetated areas (Figure 3.32). This indicates that the modification of natural conditions by human activities, such as forest harvesting, has significant affect on landslide occurrence (Gorsevski et al., 2006).

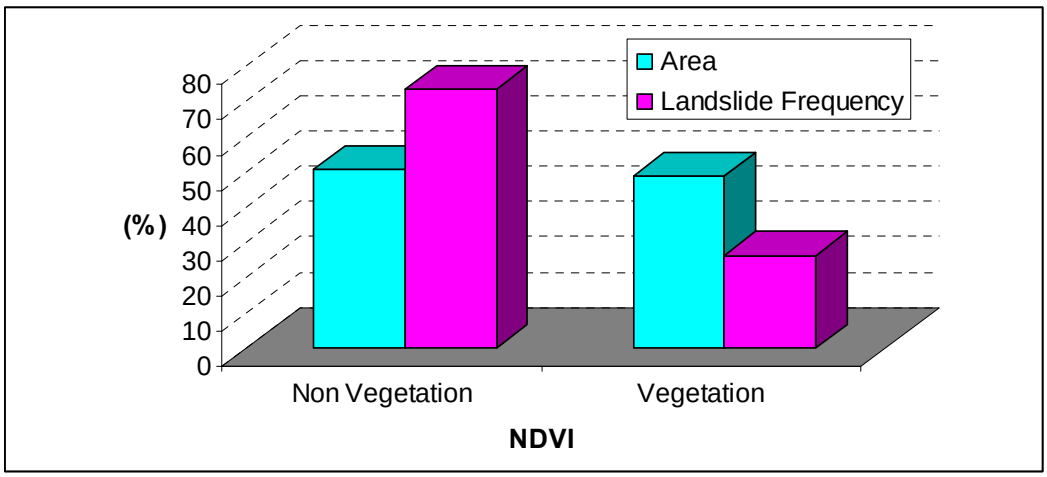

Figure 3.32. Histogram showing the relationship between NDVI and landslide frequency

3.3.1.2 Processing of Geological Data

The geological map of the region was acquired from the General Directorate of Mineral Research & Exploration in digital format on 1:25000 scale. The geology map incorporates the geological units and the faults lines in the area. The geology map has a database concerning the geologic unit names and their ages. The fault map has an attribute of types of faults. The data were originally in .e00 format and were converted into .shp format with the projection transformation from WGS84 geographic coordinate system to National ED50 projection system. In the geological map of the study region, 6 different lithologies exist. Figure 3.33 displays the distribution of geologic units in the region. As shown in Figure 3.34, the major lithological units are represented by Sandstone-Mudstone (70.6%) and Conglomerate (23.7%), which constitutes nearly 95% of the study region. The remaining 4 units cover only 3% of the region.

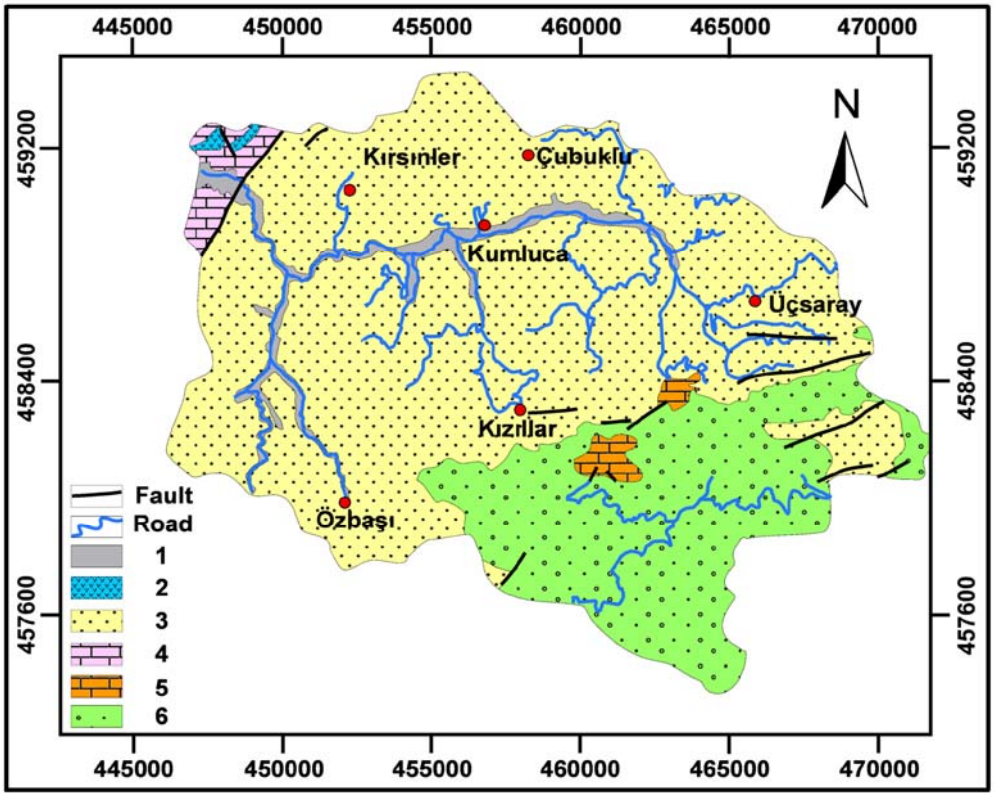

Figure 3.33. Geological map of the study region overlaid with road network and fault lines. The legend refers to 1: Alluvial, 2: Andesite, 3: Sandstone-Mudstone, 4: Marl 5: Limestone, 6: Conglomerate (GDMRE, 2007)

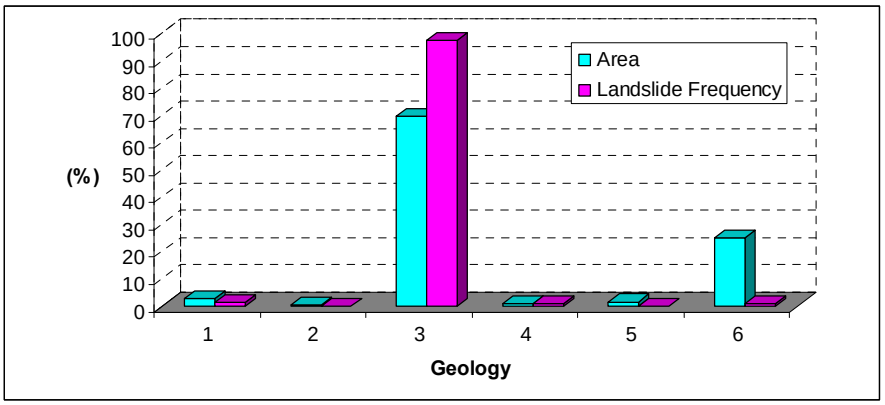

Figure 3.34. Histogram showing the relationship between Geologic units and landslide frequency

The correlation analysis shows a high correlation between landslide occurrence and the Sandstone-Mudstone unit (Figure 3.34) with approximately 91.3%, whereas the rest of the units in the study region do not show a considerable relation to landslide occurrence.

Following the geology map, the fault map of the region was also acquired from the

General Directorate of Mineral Research and Exploration. The fault line map includes 3 different types (types 1, 3, 4) as represented in Figure 3.35. In this study, all the types (fault lines) were included in the analysis. A total of 24.171 kilometer-long fault line was observed in the study area with 39 fault line segments. 52% of the fault line segments occupy a length of 30.1 meters and the average length of fault-lines is 619 meters.

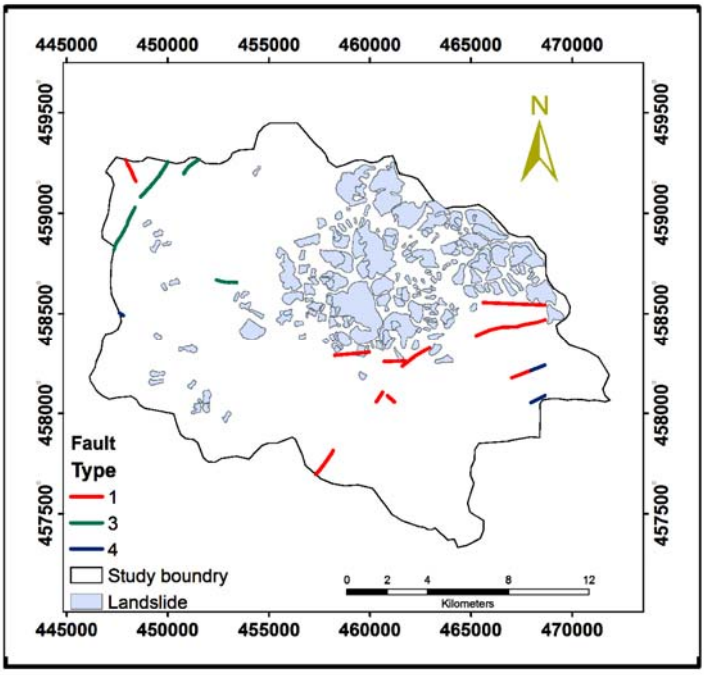

Figure 3.35. Fault line map with three different types where Type 1 represents the active faults, Type 3 and 4 represents half and half approximate fault, overlaid by the landslide map

The fault map was transferred into raster format by using distance analysis. The distance of each pixel to the nearest line was computed and mapped (Figure 3.36a). The maximum distance from the fault line is 8740 m. The distance to fault map shows that the faults are dominant in the north-western and south-eastern parts of the region, where landslide occurrences are not much frequent (Figure 3.36 a). The distance to fault lines map shows a logarithmical distribution, because the frequency decreases while the distance from the fault lines increases (Figure 3.36b). The distribution of fault distance map has a mean of 2625.87 m. with a standard deviation of 1870.46 m. (Figure 3.36 b).

In addition to the lithology, the correlation of the fault distance with landslides was

also analyzed. Figure 3.37 shows that the correlation between the fault line distance and landslide occurrence increases as the distance decreases. The correlation is higher at the distance up to 2000 meters (Figure 3.37).

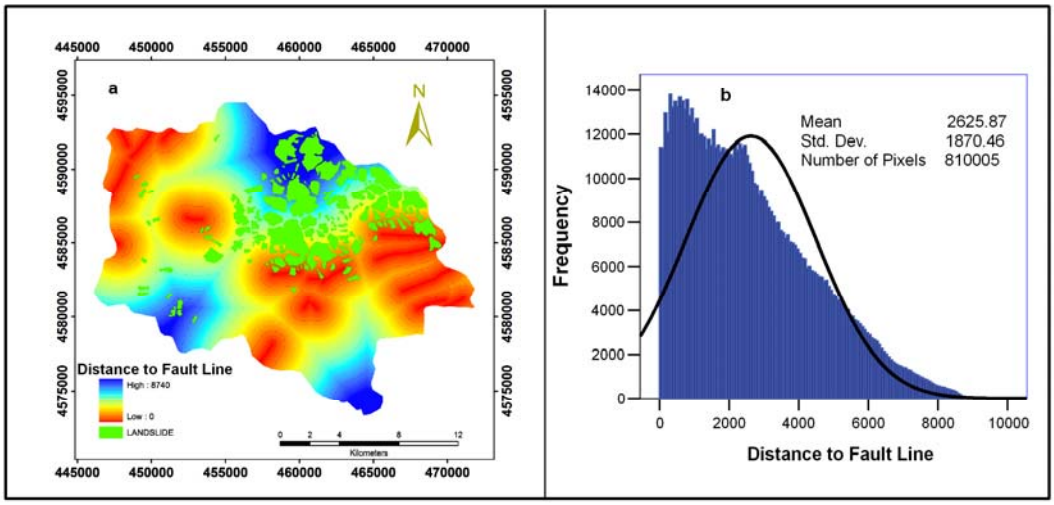

Figure 3.36. a. Distance to fault line map b. Frequency distribution of distance to fault line

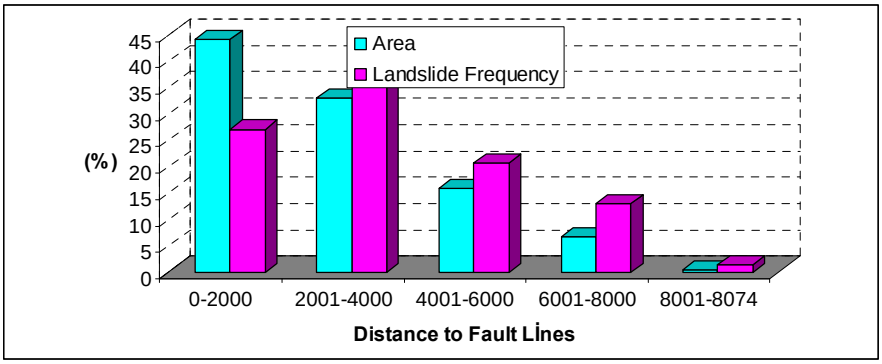

Figure 3.37. Histogram showing the relationship between distance to fault lines and landslide frequency

The soil map of the region was acquired from the General Directorate of Village Maintenance in digital format on 1:100000 scale. The projection of the data was transformed from WGS84 to national projection system (UTM zone 36 ED 50). In the soil map of the area, 5 different soil types exist (Figure 3.38). The most common soil type in the region is brown forest soil (78%) and the second most common is brown forest soil without lime (20%). The remaining 3 units account for only 2% in the region (Figure 3.39). The soil map acquired also includes some additional soil factors that can be used for the analysis as to land-use type, level of erosion, and soil thickness.

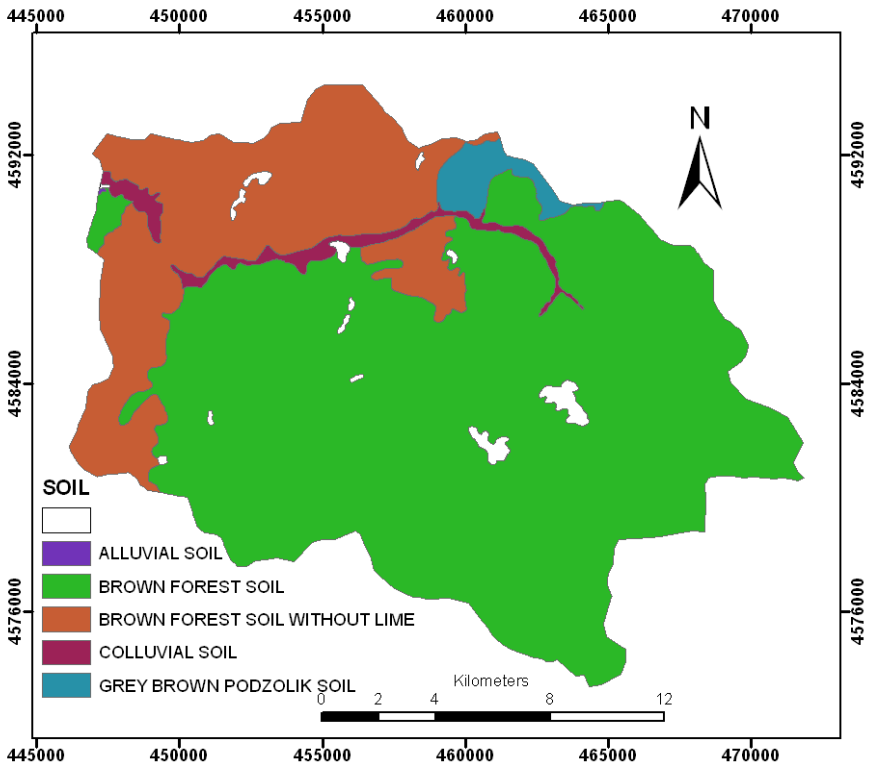

Figure 3.38. Soil Map showing 5 different types in the study region

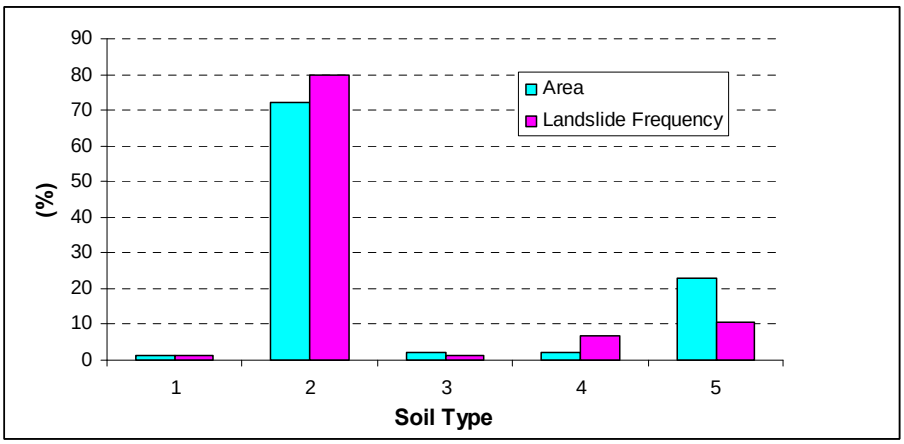

Figure 3.39. Histogram showing the relationship between soil type and landslide frequency where: 1= Alluvial Soil, 2= Brown Forest Soil, 3= Colluvial Soil, 4= Grey Brown Podzol Soil, 5= Brown forest soil without lime

The relationship between landslides and the soil type indicate that 80% of landslides occur in brown forest soil and 10% occur in brown forest soil without lime (Figure 3.39). The high correlation of landslide areas with brown forest soil might be due to the abundance of this soil type in the region (70%).

The land cover map of the region include a total of 5 different types, as seen in

Figure 3.40a. The majority of the area is covered by forests (63%). Dry farming follows forests with a portion of 36% (Figure 3.40b). Many studies have revealed a clear relationship between land cover and slope stability, especially for shallow landslides (Gomez and Kavzoglu, 2005). The analysis of the land cover map of the region confirms that landslide activity increases in the region where the original vegetation cover has been removed or altered. As can be seen in Figure 3.41, the dry farming indicates a clear relationship with landslide occurrence areas. This was confirmed by the reports of Bartın General Directorate of Disaster Affairs (GDDA). As it is reported by the GDDA, landslides mostly occur in dry farming regions, where deforestation takes place.

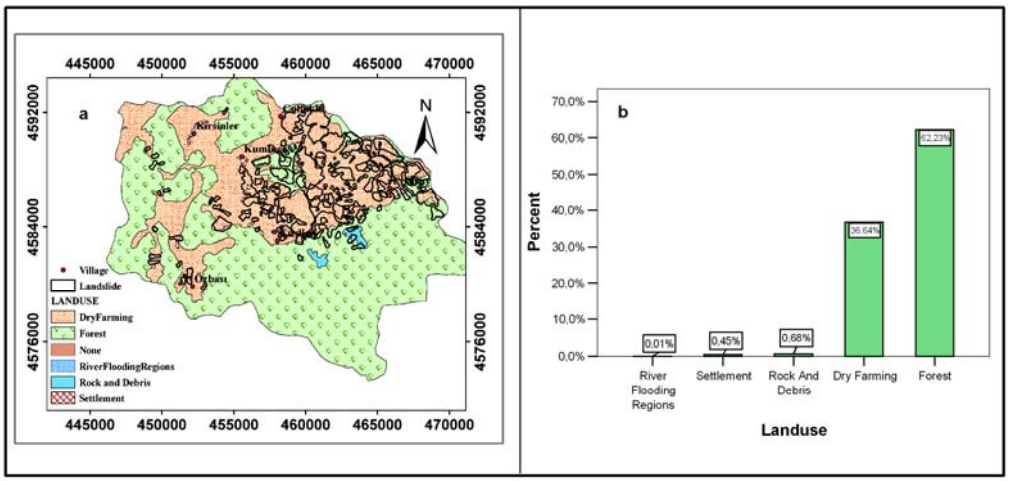

Figure 3.40. a. Land use map of the study region b. The percent frequency of land-use types.

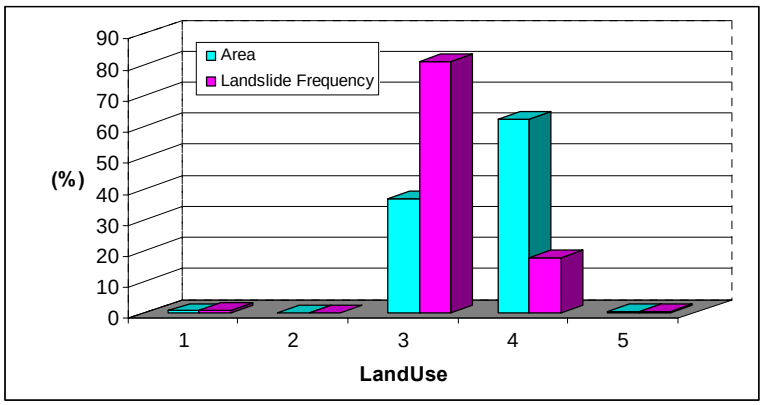

Figure 3.41. Histogram showing the relationship between soil type and landslide frequency where: 1= Rock And Debris, 2= River Flooding Regions, 3= Dry Farming, 4= Forest, 5= Settlement

The depth or thickness of the soil has 4 classes. Very deep soil class has a thickness

of 90 cm and covers a larger area; deep soil class has a thickness between 90 and 50 cm; shallow soil and very shallow soil have a thickness between 50-20 and 20-0 cm. respectively (Figure 3.42). Shallow and very shallow soil class areas occupy 93% of the region. When there is heavy rain, deeper soil has the capability to store more water.

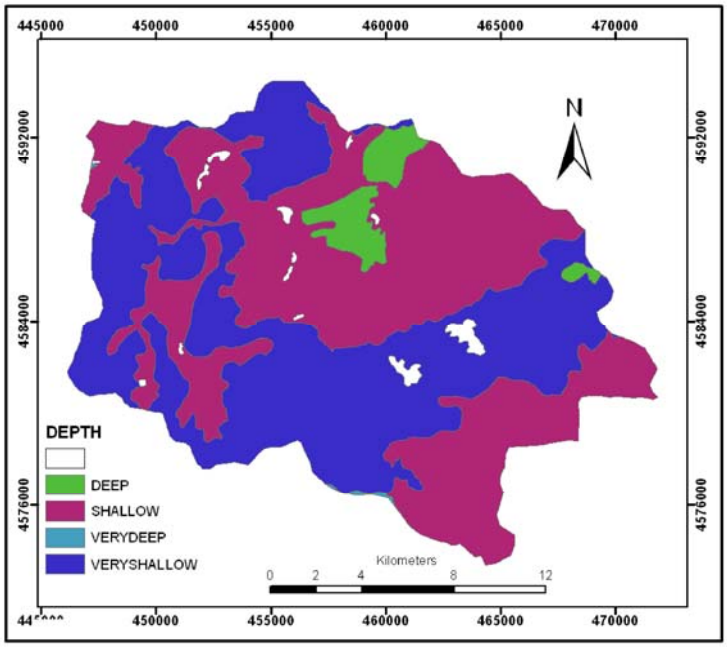

Figure 3.42. Soil depth map showing 4 different classes of thickness

When the relation between landslide occurrence and soil thickness was analyzed, it was observed that 71% of landslide occurrence was in the class of shallow soil thickness (Figure 3.43), as this soil class is abundant (98%) in the region.

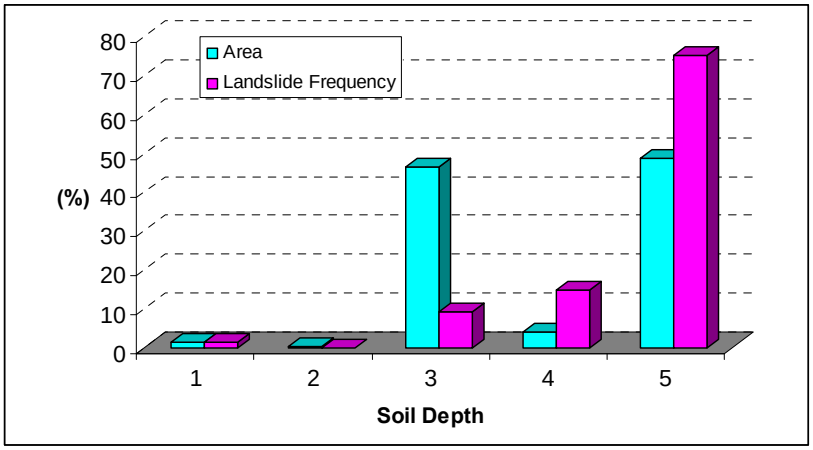

Figure 3.43. Histogram showing the relationship between soil type and landslide frequency where:

1=None, 2=Very Deep, 3=Very Shallow, 4=Deep, 5=Shallow

The last data acquired from the General Directorate of Village Maintenance was the data for erosion level. The attribute table includes the erosion severity of the region. The severity is classified into 4 different levels of erosion (Figure 3.44a). As Figure 3.44b indicates, 92% of the region has severe erosion level.

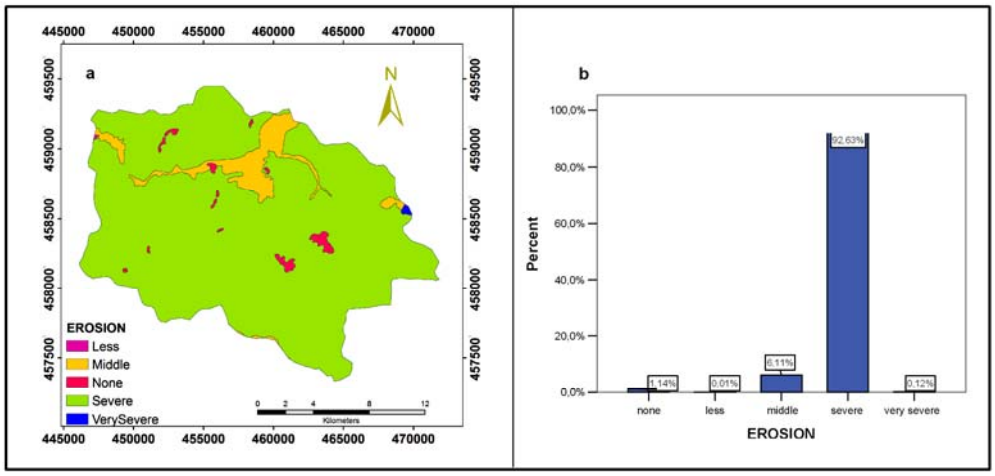

Figure 3.44. Erosion map showing 4 different classes of the erosion b. Percent frequency of each erosion class

The relation between erosion and landslide locations indicates that (Figure 3.45) 81% of landslides occur in the severe erosion area, as a result of the extensiveness of severe erosion class (90%). 12% of landslides occur in the middle erosion class (Figure 3.45).

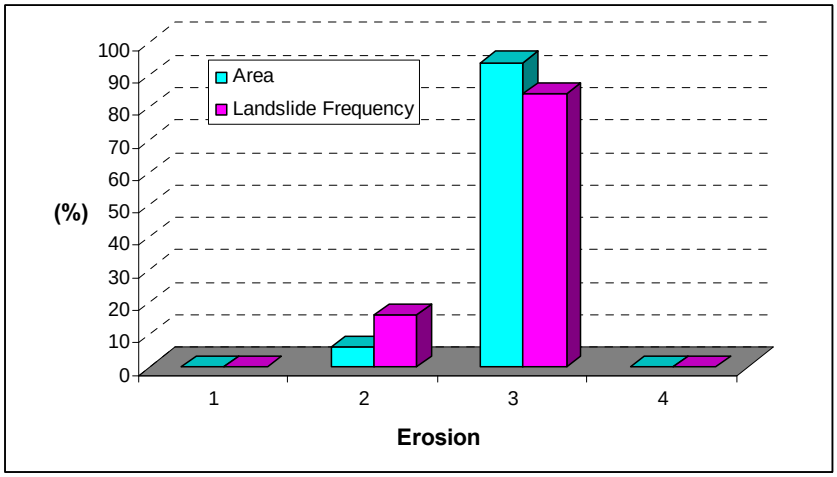

Figure 3.45. Histogram showing the relationship between soil type and landslide frequency where 1=Less, 2=Middle 3=Severe 4= Very Severe

3.3.2 Analyzed Landslide Influencing Factors

The input data in the form of topographic maps, geological maps, soil maps, and Aster 3A satellite image were used to extract the variables that may have an influence on landslide occurrence. The variables extracted for the analysis, the scale of the data, the area and abbreviations are given in Table 3.3. The factors which were considered to have an affect on landslide occurrence were topographical elevation, slope, aspect, curvature, plan curvature, profile curvature, topographic wetness index, NDVI, distance to road, distance to stream network, density of road, density of stream network, geological formations (6 units), distance to fault, soil type (5 units), land use type (5 units), soil depth (4 units), and erosion level (4 units). In total, 37 factors were included into analysis. The variables are in two types with regard to their scale: Continuous and Categorical.

Table 3.3. Variables considered as landslide influencing factors

Variables	Scale of data	# of Categories	Category Type	Area (km^2)	Abreviation
Topographical elevation	Continous	-	-		Elev
Slope	Continous	-	-		Slp
Aspect	Continous	-	-		Asp
Curvature	Continous	-	-		Curv
Plan curvature	Continous	-	-		Plan_Curv
Profile curvature	Continous	-	-		Prof_Curv
Topographic wetness index	Continous	-	-		Wtns
NDVI	Binary	0/1	-	-	Veg
Distance to Road	Continous	-	-		DisttoRoad
Distance to Stream Network	Continous	-	-		DisttoStrm
Density of Road Network	Continous	-	-		DensRoad
Density of Stream Network	Continous	-	-		DensStrm
Distance to Fault	Continous	-			DisttoFault
Geology Formations	Categorical	6	Alluvial	9.04	Geo_ Allv
			Andesite	0.68	Geo_ And
			Sandstone_Mudstone	225.26	Geo_ SM
			Limestone	3.23	Geo_ L
			Marl	5.00	Geo_ M
			Conglomerate	80.74	Geo_ C
Soil Map	Categorical	5	Alluvial Soil	0.03	S_ Allv
			Grey Brown Podzolic Soil	6.27	S_ GBPdz
			Colluvial Soil	6.90	S_ Collv
			Brown Forest Soil	233.31	S_ BFS
			Brown Forest Soil without lime	73.82	S_ BFSWL

Table 3.3. Variables considered as landslide influencing factors (Continued)

Variables	Scale of data	# of Categories	Category Type	Area (km^2)	Abreviation
Land Use	Categorical	5	Rock_And_Debris	2.18	LU_ RD
			RiverfloodingRegions	0.03	LU_ RF
			Dryfarming	118.71	LU_ DF
			Settlement	1.45	LU_S
			Forest	201.64	LU_ F
Soil Depth	Categorical	4	Verydeep	0.38	SD_ VD
			Veryshallow	149.63	SD_ VS
			Deep	12.52	SD_ D
			Shallow	157.80	SD_ S
Erosion	Categorical	4	Less	0.03	E_ L
			Middle	19.78	E_ M
			Severe	300.16	E_ S
			Verysevere	0.37	E_VS

3.3.3 Statistical Analysis of Data for Each Mapping Unit

Before beginning the susceptibility analysis, the statistical analysis of each data set was carried out using the SPSS 13 software. The statistical analysis of the independent variables changes depending on the adopted procedure. Hence, the mapping unit to be used in the study should be determined initially. Mapping unit is the partition of the land surface into homogeneous regions. It is the minimum meaningful spatial unit in the analysis, because each unit is assigned a unique susceptibility value and each unit has a set of ground conditions that are relatively different from its adjacent units. The selection of the mapping unit depends on different considerations such as the type and size of the analysis, the scale of data that is available for the analysis, and the scale of the final model, and several methodological considerations (Beguería and Lorente, 1999).

In this study, two different mapping units were adopted for the analysis. The first one was grid, which is considered to present a continuous variation in space, and the second selected unit was the slope unit, in which space is subdivided into regions based on certain hydrological criteria. Grids are especially adequate to the modeling of continuous variables and can adopt the categorical variables. In slope unit approach, continuous variables can only be treated by their summary statistics (e.g. mean slope, maximum slope, etc.).

After determining the mapping unit types, the following steps for statistical analysis

were carried out for each variable at each mapping unit: (i) transformation of categorical variables into continuous scale; (ii) selection of independent variables by multi colinearity analysis; (iii) normality checks for each variable.

The transformation of categorical variables is essential for further statistical analysis to construct a geospatial database in GIS. It involved conversion of the data in polygon format to a raster format with a 20-m grid spacing, in which each grid cell was assigned a code relevant to the associated variable. The reason for the selection of 20 m. resolution was the working scale, which was selected as 1:25000. According to the USGS (1993), the positional accuracy needed for 1:25000 scale maps must be ±12.5 m., hence the pixel size was selected larger than the accuracy level.

Regression analysis, which is used for susceptibility mapping, requires that variables should be normally distributed. Therefore, after the transformation of categorical variables, normality tests for each variable were applied.

The last step of the statistical analysis involves selection of independent variables by multi colinearity analysis. This is also essential prior to the regression analysis. The main reason is that when a variable A is highly correlated with variable B and both are included in the analysis; A will not contribute to the estimation of the probability of landslide occurrence. Thus, the inclusion of both variables will cause an ill-structured model.

3.3.3.1 Statistical Data Analysis for Grid Mapping Unit

3.3.3.1.1 Assigning the Data Set to Grid-Based Mapping Unit

Grid units have pros and cons. Grid data processing is fast due to its matrix form, but it requires an overwhelming number of grid cells to cover even small areas if the selected cell resolution is high. This mostly leads to unmanageable computer problems and numerical instability when data have to be processed by statistical techniques. Generally speaking, in a grid-based approach, landslide hazard, or the probability of occurrence of a landslide at a point within a given time period, is treated as a continuous variable. This implies that, in theory, the final user of the map

can know exactly the probability of landsliding in a given place. But it is mostly problematic to assign landslide occurrence to many different cells that represent a single movement (Begueria and Lorente, 1999). In this case, the statistical analysis considers that each cell has random independent variables.

It is not an easy task to deal with categorical data in statistical analysis (Baeza and Corominas, 2001). Hence, the landslide factors which are in categorical data format (Land use, Soil, Geology, Soil depth and Erosion) were converted into a discrete data format. The conversion was done by assigning a code in the form of a number, where the numbers are simply labels. For this reason, each category of factor has been physically represented as binary variables, as a function of the presence/absence or 1/0 of a class of slope instability factors in the study region. For instance, the soil map has five different units (Figure 3.46a). Each unit was represented by polygons in GIS environment (Figure 3.46a). These polygons were converted to raster format with 20 m grid spacing (Figure 3.46b). For each category of soilmap, a raster data layer was obtained by the reclassification and then for each layer, each grid was assigned a code representing the soil unit in the center of the cell (Figure 3.46c). Therefore, for each soil unit, a value of either 0 or 1 was assigned in each corresponding column in the database as shown in the Figure 3.46d.

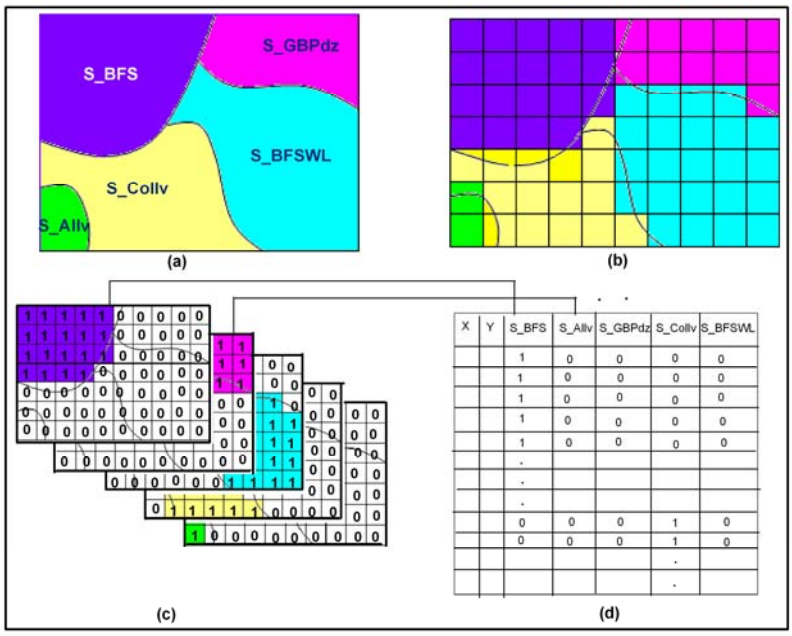

Figure 3.46. Conversion of categorical data to raster format a. The vector layer in the categorical format b. Vector layer converted to raster format c. The raster data is reclassified for each category in the layer and assigned 0 or 1 value d. Each category layer in raster format is assigned to a database

All continuous variables were already in raster format. As a result, the influencing factors include 12 continuous data layers and 25 binary data layers, 37 data layers in total. Hence, all landslide-related factors were converted into a raster map with a resolution of 20 m.

In order to evaluate the landslide characteristics, the landslide inventory map was converted to a Boolean layer using ArcMap with a grid resolution of 20 m. This layer has 810,005 pixels, where 14.7% are in areas of landslides and were reassigned the pixel value of one. All the other pixels were given a value of zero, thereby producing a Boolean layer representing the landslide database to be used in susceptibility mapping.

For further statistical analysis and assessment of susceptibility in the study region, a geospatial database in GIS was constructed. To store the landslide-related information and landslide inventory into a database, mid point of the raster layer was created with 20 m intervals. Then this point mesh was overlaid over all the data layers created for the analysis for the whole study region (Figure 3.47). The attributes of landslides and the previously produced input maps were transferred as separate attribute tables of these points. These tables were then merged to construct a relational database concerning all of the parameters. Each parameter map was treated as a new variable in this database. The database was converted to an ASCII-format file that included the UTM coordinates for the centre of each pixel. The ASCII file was then input to statistical software for modeling.

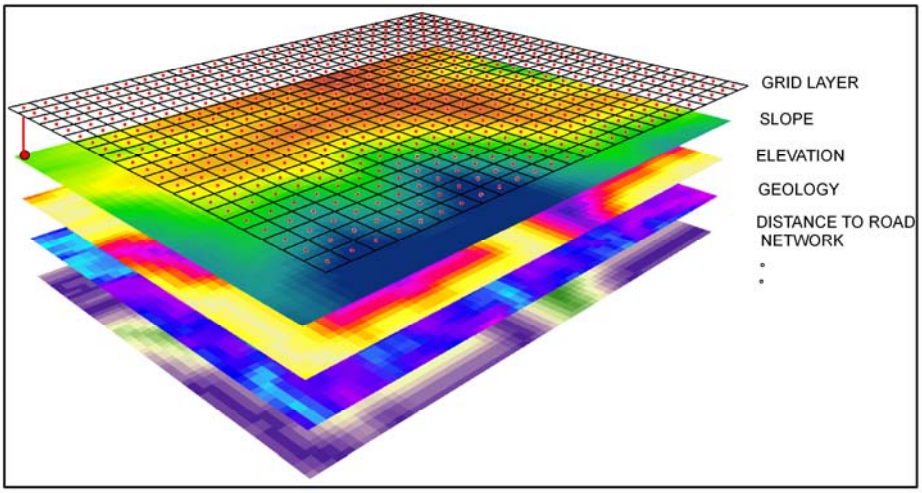

Figure 3.47. Point mesh overlaid with factor layers

3.3.3.1.2 Pre-Analysis of Database

Initially the categorical factors that have regions smaller than 5 km^2 were excluded from the analysis, and the rest of the data was included in the analysis. Although settlement occupies an area of 1.45 km^2, it was included in further analysis as it was thought to have an affect on landslide occurrence. The reason for the exclusion of smaller regions was to reduce the processing time in statistical modeling of the data. As a result, the data excluded from the database were: River Flooding Regions of Land-Use (LU_RF), Rock and Debris Unit of Land-Use (LU_ RD), Very Deep Soil Depth (SD_VD), Less Erosion (E_L), Very Severe Erosion (E_VS), Alluvial Soil (S_Allv), Limestone Unit of Geology (Geo_ L), Marl Unit of Geology (Geo_ M), Andesite Unit of Geology (Geo_ And). Hence, the data layers were reduced to 28 factors.

The presence of a strong correlation between variables may reduce the performance of a regression model. Thus, the strongly correlated variables should be removed before the analysis. The missing data or extreme data was searched initially and then the multicollinearity between factors was analyzed. The data set created for analysis contains nominal and continuous data. For different data formats different procedures were handled in the study. To obtain measures of association for the nominal variables, cross tables were used. The bivariate correlations procedure was useful for studying the pairwise associations for a set of continuous variables. Thus, in the first part of analysis, the co-linearity of continuous dataset was performed by using the correlation matrix. The second part includes the analysis of the co-linearity between nominal factors with cross tabulation analysis. Lastly, the correlation analysis between nominal and continuous data set was performed through regression analysis.

Bivariate correlation analysis involves computing the pairwise associations for a set of variables. It is useful for determining the strength and direction of the association between two scales and ordinal variables. A correlation coefficient is a number between -1 and 1, which measures the degree to which two variables are linearly related. If there is a perfect linear relationship with the positive slope between the two variables, the correlation coefficient is 1. If there is a perfect linear relationship with the negative slope between the two variables, the correlation coefficient is -1. A correlation coefficient of 0 means that there is no linear relationship between

the variables. There are a number of different correlation coefficients that might be appropriate depending on the type of variables being studied. The Pearson correlation coefficient, the Spearman's rho and Kendall's tau-b statistics can be used to measure the association between factors. In this study, Spearman's rho was used as it is a nonparametric measure of correlation. The Table 3.4 presents the Spearman rho coefficients obtained for considered variables.

There is not yet a certain threshold to assign variables as correlated or not. In this study, the coefficients larger than 0.7 were considered as correlated and one of the variables in the correlated pair was excluded for further analysis. The statistical significance of the correlation is also assessed at 95% significance level. The results of correlation matrix demonstrate that Plan Curvature (Plan_Curv) and Profile Curvature (Prof_Curv) are significantly associated with the Curvature (Curv). While the Plan_Curv has a high positive association, the Prof_Curv has a high negative association with the Curv. The density of stream network (DensStrm) also shows a high negative correlation with the topographical elevation (Elev) and the density of road network (DensRoad) shows a positive high association with the DensStrm. For this reason, the Plan_Curv, Prof_Curv, and DensStrm were excluded from the analysis. Therefore, Elev, Curv, and DensRoad were included in the regression models.

For correlation measure of nominal data, cross tabulation of each pair was performed. To test the strength of association in cross tabulation, Phi, Cramer's V and contingency coefficient can be used. Phi coefficient is a measure of correlation coefficient in its interpretation. Cramer's V is a rescaling of phi, so its maximum possible value is always 1. The contingency coefficient takes values between 0 and SQRT[(k-1)/k], where k is the number of smaller rows or smaller columns. In this study, Phi and Contingency coefficients were used to test the correlation between nominal data (Table 3.5).

Table 3.4. Correlation matrix for continuous landslide influenceing factor

	Elev	Curv	Slp	Asp	Plan_Curv	Prof_Curv	DisttoFault	DisttoStrm	DisttoRoad	DensStrm	DensRoad	Wtns
Elev	1	.047	.006	-.079	.017	-.059	-.027	.117	.243	**-.738**	-.473	-.092
Curv	.047	1	.024	.002	**.822**	**-.875**	.001	.118	.024	-.005	-.004	-.364
Slp	.006	.024	1	.029	.019	-.022	-.034	-.054	.078	.021	-.019	-.478
Asp	-.079	.002	.029	1	.004	.001	.031	-.002	-.046	-.002	.013	-.011
Plan_Curv	.017	**.822**	.019	.004	1	-.444	-.003	.072	-.002	.019	.007	-.422
Prof_Curv	-.059	**-.875**	-.022	.001	-.444	1	-.004	-.125	-.040	.024	.012	.213
DisttoFault	-.027	.001	-.034	.031	-.003	-.004	1	.027	.070	-.020	-.008	.006
DisttoStrm	.117	.118	-.054	-.002	.072	-.125	.027	1	.079	-.097	-.052	-.155
DisttoRoad	.243	.024	.078	-.046	-.002	-.040	.070	.079	1	-.136	-.356	-.058
DensStrm	**-.738**	-.005	.021	-.002	.019	.024	-.020	-.097	-.136	1	**.701**	.036
DensRoad	-.473	-.004	-.019	.013	.007	.012	-.008	-.052	-.356	**.701**	1	.018
Wtns	-.092	-.364	-.478	-.011	-.422	.213	.006	-.155	-.058	.036	.018	1

Table 3.5.Correlation between nominal landslide influencing factors

		Veg	LU_S	LU_DF	LU_F	S_GBPdz	S_Collv	S_BFS	S_BFSWL	SD_VS	SD_D	SD_S	ER_M	ER_S	GEO_C	GEO_SM	GEO_Allv
Veg	Phi	1.00	-0.39	-0.37	0.37	-0.05	-0.10	0.03	-0.09	-0.01	-0.27	0.27	-0.06	0.05	0.20	0.02	0.13
	Contingency		0.39	0.35	0.35	0.04	0.10	0.02	0.09	0.01	0.27	0.26	0.06	0.05	0.19	24.00	0.13
LU_S	Phi	-0.39	1.00	-0.05	-0.09	-0.01	-0.01	-0.11	-0.04	-0.02	-0.07	-0.06	-0.02	-0.24	0.37	0.02	0.06
	Contingency	0.39		0.05	0.09	0.01	0.01	0.11	0.04	0.02	0.07	0.06	0.02	0.23	0.04	0.02	0.06
LU_DF	Phi	-0.37	-0.05	1.00	**-0.98**	0.11	0.19	0.02	-0.10	-0.02	**0.71**	**-0.70**	0.14	-0.09	0.42	0.31	0.19
	Contingency	0.35	0.05		**0.70**	0.11	0.19	0.02	0.10	0.02	**0.58**	**0.58**	0.14	0.09	0.39	0.29	0.19
LU_F	Phi	0.37	-0.08	**-0.98**	1.00	-0.11	-0.19	0.02	0.12	0.02	**0.68**	**0.72**	-0.13	0.18	0.42	0.29	0.20
	Contingency	0.35	0.08	**0.70**		0.10	0.19	0.02	0.12	0.02	**0.56**	**0.59**	0.13	0.17	0.39	0.27	0.19
S_GBPdz	Phi	-0.05	-0.01	0.11	-0.11	1.00	-0.02	-0.23	-0.08	-0.05	-0.06	-0.13	0.40	-0.36	0.08	0.09	0.02
	Contingency	0.04	0.01	0.11	0.10		0.02	0.22	0.08	0.05	0.06	0.12	0.37	0.34	0.08	0.09	0.00
S_Collv	Phi	-0.10	-0.01	0.19	-0.19	-0.02	1.00	-0.24	-0.08	-0.01	0.15	-0.14	0.58	-0.52	0.08	0.16	0.01
	Contingency	0.10	0.01	0.19	0.19	0.02		0.23	0.08	0.01	0.15	0.14	0.50	0.52	0.08	0.16	0.01
S_BFS	Phi	0.03	-0.11	0.02	0.02	-0.23	-0.24	1.00	**-0.87**	0.01	0.21	-0.07	-0.37	0.41	0.34	0.21	0.16
	Contingency	0.02	0.11	0.02	0.02	0.22	0.23		**0.66**	0.01	0.21	0.07	0.35	0.38	0.32	0.21	0.16
S_BFSWL	Phi	-0.09	-0.04	-0.10	0.12	-0.08	-0.08	**-0.87**	1.00	-0.02	-0.23	0.19	0.08	-0.04	0.30	0.28	0.08
	Contingency	0.09	0.04	0.10	0.12	0.08	0.08	**0.66**		0.02	0.23	0.18	0.08	0.04	0.29	0.27	0.08
SD_VS	Phi	-0.01	-0.02	-0.02	0.02	-0.05	-0.01	0.01	-0.02	1.00	-0.03	-0.03	0.12	-0.12	0.05	0.05	0.00
	Contingency	0.01	0.02	0.02	0.02	0.05	0.01	0.01	0.02		-0.03	0.03	0.12	0.12	0.05	0.05	0.00
SD_D	Phi	-0.27	-0.07	**0.71**	**0.68**	-0.06	0.15	0.21	-0.23	-0.03	1.00	**-0.90**	-0.07	0.11	0.04	0.02	0.14
	Contingency	0.27	0.07	**0.58**	**0.56**	0.06	0.15	0.21	0.23	0.03		**0.67**	0.07	0.11	0.04	0.02	0.14
SD_S	Phi	0.27	-0.06	**-0.70**	**0.72**	-0.13	-0.14	-0.07	0.19	-0.03	**-0.90**	1.00	-0.24	0.25	0.08	0.01	0.14
	Contingency	0.26	0.06	**0.58**	**0.59**	0.12	0.14	0.07	0.18	0.03	**0.67**		0.23	0.25	0.08	0.01	0.14
ER_M	Phi	-0.06	-0.02	0.14	-0.13	0.40	0.58	-0.37	0.08	0.12	-0.07	-0.24	1.00	**-0.90**	0.13	0.01	0.40
	Contingency	0.06	0.02	0.14	0.13	0.37	0.50	0.35	0.08	0.12	0.07	0.23		**0.67**	0.13	0.01	0.37
ER_S	Phi	0.05	-0.24	-0.09	0.18	-0.36	-0.52	0.41	-0.04	-0.12	0.11	0.25	**-0.90**	1.00	0.13	0.04	0.38
	Contingency	0.05	0.23	0.09	0.17	0.34	0.52	0.38	0.04	0.12	0.11	0.25	**0.67**		0.13	0.04	0.36
GEO_C	Phi	0.20	0.37	0.42	0.42	0.08	0.08	0.34	0.30	0.05	0.04	0.08	0.13	0.13	1.00	**1.00**	**1.00**
	Contingency	0.19	0.04	0.39	0.39	0.08	0.08	0.32	0.29	0.05	0.04	0.08	0.13	0.13		**0.71**	**0.71**
GEO_SM	Phi	0.02	0.02	0.31	0.29	0.09	0.16	0.21	0.28	0.05	0.02	0.01	0.01	0.04	**1.00**	1.00	**1.00**
	Contingency	24.00	0.02	0.29	0.27	0.09	0.16	0.21	0.27	0.05	0.02	0.01	0.01	0.04	**0.71**		**0.71**
GEO_Allv	Phi	0.13	0.06	0.19	0.20	0.02	0.01	0.16	0.08	0.00	0.14	0.14	0.40	0.38	**1.00**	**1.00**	1.00
	Contingency	0.13	0.06	0.19	0.19	0.00	0.01	0.16	0.08	0.00	0.14	0.14	0.37	0.36	**0.71**	**707.00**	

The significance of most of the values is 0.000, indicating a statistical significant relationship. However, the coefficient values are lower than 0.5. Hence, although the relationship is not accidental, it is also not very strong. Thus, as it is presented by bold in Table 3.5, several correlations were observed among landslide influencing factors. First, dry farming unit of land use (LU_DF) is related with forest unit of land use (LU_F), deep soil (SD_D) and shallow soil (SD_S). Second, brown forest soil (S_BFS) is related with brown forest soil without lime (S_ BFSWL). Third, middle erosion (E_M) has an association with severe erosion (E_S). Finally, sandstone-mudstone unit of geology (Geo_ SM) has an association with conglomerate unit of geology (Geo_C) and alluvial unit of geology (Geo_ Allv). All these associations indicate a statistically significant relationship. As a result, while LU_F, SD_ D, SD_S, S_ BFSWL, E_S, Geo_C and Geo_ Allv were excluded, LU_DF, S_BFS, E_M, Geo_SM were included in the analysis.

In the third step, the association between the discrete and continuous pairs was analyzed by using a regression model. In this study, the response variable was considered as the discrete variable which has a binomial distribution. For this reason, a logistic regression was applied (see section 2.3.2.1). In this study, for each discrete variable, all continuous variables were modeled. Table 3.6 represents the logistic regression results for different combinations of factors. The columns represent the independent variables and the rows represent the response variable's coefficients with the significance and coefficient values. It can be seen from Table 3.6 that the topographic wetness index (Wtns) has a low coefficient value and it is insignificant when it is related to settlement (LU_S). Curvature (Curv) and density of road (DensRoad) show insignificance to LU_S, grey brown podzolic soil (S_ GBPdz), SD_VS, and E_M. As a result of this analysis, the Wtns, Curv and DensRoad were excluded from the further analysis while the topographical elevation (Elev), slope (Slp), aspect (Asp), DisttoStrm, DisttoRoad, and DisttoFault were included. The resultant data set used for the further statistical analysis is presented in Figure 3.48. Hence, after multicolinearity analysis 15 variables were selected to be used in susceptibility mapping.

Table 3.6 Logistic regression modelling for correlation analysis between continuous and nominal landslide influencing factors

	LU_S	Sig.	Veg	Sig.	S_Collv	Sig.	S_BFS	Sig.	LU_DF	Sig.	S_GBPdz	Sig.	SD_VS	Sig.	E_M	Sig
Wtns	-.017	**.90**	.065	.01	-.69	.00	.58	.00	-.37	.00	-.27	.00	.53	**.06**	.53	**.06**
Elev	-7.20	.00	1.94	.00	-41.53	.00	10.59	.00	-9.49	.00	-3.71	.00	3.74	.00	3.74	.00
Slp	-6.09	.00	1.69	.00	-9.17	.00	-.79	.00	-4.85	.00	-1.61	.00	-8.59	.00	-8.59	.00
Asp	1.19	.00	-.33	.00	-.33	.00	-1.44	.00	1.41	.00	2.02	.00	-1.83	.00	-1.83	.00
DisttoStrm	4.16	.00	1.14	.00	-.79	.00	-2.35	.00	-.11	.00	2.38	.00	-1.43	.00	-1.43	.00
DisttoRoad	-13.70	.00	1.69	.00	-.85	.00	-2.40	.00	-2.81	.00	-1.56	.00	1.96	.00	1.96	.00
Curv	1.69	**.06**	.35	.00	3.71	.00	-.94	.00	1.47	.00	**-.98**	**.24**	**1.89**	**.22**	**1.89**	**.22**
DisttoFault	1.04	.00	.16	.00	-.57	.00	.64	.00	.14	.00	-12.50	.00	-.58	.00	-.58	.00
DensRoad	-.34	**.15**	-.18	.00	30.99	.00	13.40	.00	14.13	.00	**.19**	**.06**	**-4.10**	**.05**	**-4.10**	**.07**
Constant	-3.71	.00	-1.72	.00	-24.66	.00	-11.80	.00	-9.47	.00	-1.83	.00	-3.76	.00	-3.76	.00

Figure 3.48. The resultant variables considered for grid-based analysis

Dependent Variable	**Scale of data**	**# of Categories**	**Category Type**	**Abreviation**
Landslide	Binary	0/1	Landslide	Landslide
Independent Variables				
Elevation	Continous	-	Elevation	Elev
Slope	Continous	-	Slope	Slp
Aspect	Continous	-	Aspect	Aspp
Distance to Road Network	Continous	-	Distance to Road	DisttoRoad
Distance to Stream Network	Continous	-	Distance to Stream Network	DisttoStrm
Vegetation	Binary	0/1	Vegetation	Veg
Geology Unit	Categorical		Sandstone_Mudstone	Geo_ SM
Soil Type	Categorical	3	Colluvial Soil	S_ Collv
			Brown Forest Soil	S_ BFS
			Grey Brown Podzolic Soil	S_ GBPdz
Distance to Fault	Continous	-	Distance to Fault	DisttoFault
Land use	Categorical	2	Dryfarming	LU_ DF
			Settlement	LU_S
Soil Depth	Categorical	1	VeryShallow	SD_VS
Erosion	Categorical	1	Middle	E_ M

The susceptibility maps were obtained by modeling the relationship between the landslide occurances and the selected variables. Generally, these models require normally distributed random variables. Therefore, the variables selected by multicolinearity analysis to be used for susceptibility mapping, were finally analysed by Q-Q plot. For this purpose, Q-Q plots for each variable is drawn and presented in Appendix A-1. The Q-Q plot is an effective tool to test the normality of each factor considered in the analysis. Q-Q plot is a graphical tool for diagnosing differences in distributions (such as non-normality). The points in the Q-Q plot should lie approximately in a straight line, since the populations being sampled are in fact normal. The purpose of the plot is to check how close the points adhere to the target line. Specific departures indicate skewness, heavy or light tails, and possible extreme values. Different procedures offer different methods to approximate the normal distribution. As a result of the analysis, it is found that topographical elevation (Elev), aspect (Aspt), distance to stream network (DisttoStrm), distance to fault network (DisttoFault) need transformation for better fit to normal distribution (Table A-1 in Appendix A).

3.3.3.2 Statistical Data Analysis for Slope Unit

3.3.3.2.1 Creation of Slope Unit-based Mapping Unit and Assigning the Data Set to Each Mapping Unit

The second mapping unit type selected for the susceptibility mapping analysis was the slope unit, where space is subdivided into regions based on certain hydrological criteria. The slope-unit provides a clear physical relationship between landslide occurrence and the fundamental morphological elements of a hilly or mountainous region, namely drainage and divide lines (Huabin et al., 2005).

Slope unit also has pros and cons. Slope unit considers hazard to be continuous, spatially aggregated, and variable, whereas hazard that is assigned to many different grid cells represents a single movement in the grid. Relatively larger mass movements can be more logically represented by slope unit procedure because they mostly consider the cells that belong to the same landslide (Begueria and Lorente, 1999). The disadvantage of slope unit is that it requires assigning the same probability of landslide occurrence to the entire land unit. Also, it provides no information about which part of the slope is more likely to be affected. The final map is a zonation of the entire area into homogeneous landslide susceptibility units (Huabin et al., 2005).

Physically the slope unit can be considered as the left or right side of a sub-basin of any order into which a watershed can be partitioned. Therefore, slope unit can be identified by the intersection of a ridge line and a valley line. A GIS-based hydrologic analysis and modeling tool, Arc Hydro (Maidment, 2002), was employed to obtain the dividing lines for identifying slope units in this study. The procedure used to extract slope units is as follows (Figure 3.49): In the first step, the DEM and Inverse DEM (InvDEM) are obtained. InvDEM is the reverse DEM, which is obtained by turning the high DEM values into low values, and low DEM values into high values (Xie et al., 2004). In the second step the hydrological model is applied both for the DEM and InvDEM. In the third step, the outline of the watershed polygon both for the DEM (Figure 3.50a) and the InvDEM (Figure 3.50c) is obtained. The watershed boundaries obtained from the DEM are topologically the watershed divides or ridge lines. The watershed boundaries obtained from the

InvDEM are topologically the valley line or drainage line (Figure 3.50b, Figure 3.50c). Then for the fourth step, the watershed boundaries obtained both from the DEM and the InvDEM are combined in the GIS environment to generate slope units (Figure 3.50d).

The catchment model for obtaining watershed boundary can be described as follows (Figure 3.49): The DEM or InvDEM surface is hydrologically connected to obtain watershed boundary. For this reason, the low elevation areas in the DEM or InvDEM, which are surrounded by higher terrain that disrupts the flow path, are filled. The flow direction is calculated by examining the eight neighbors of a cell according to the eight direction method and by determining the neighbor with the direction of the steepest downhill slope with respect to the cell of interest. Then, the associated flow accumulation grid is computed by summing the number of uphill cells that "flow" to any other cell. As a result, each cell-value represents the number of uphill cells flowing to it. In addition, a grid representing a stream network is created by querying the flow-accumulation grid for cell values above a certain threshold. This threshold is defined either as a number of cells or as a drainage area in square kilometers. In general, the recommended size for stream threshold definition is 1% of the maximum flow accumulation (Gopalan et al., 2002). A smaller threshold results in denser stream network and usually in a greater number of delineated catchments. The watershed boundaries are determined for the DEM or InvDEM by following a flow direction grid backward. By this process all of the cells that drain through a given outlet are determined. The created grid carries a value in each cell indicating to which watershed the cell belongs.

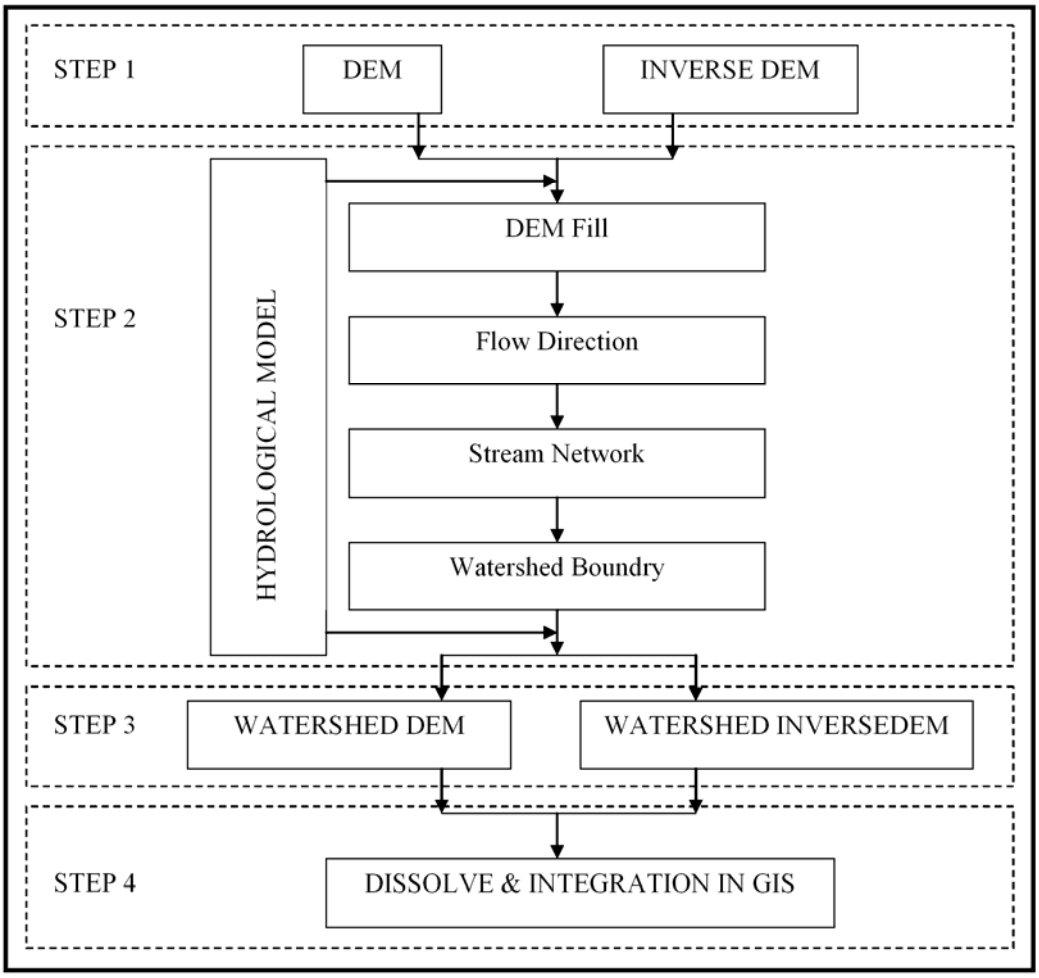

Figure 3.49. Flow chart showing the steps to create slope unit

For the last step of hydrological procedure, these cells were converted to a polygon representing the watershed. More information about the hydrological procedure can be acquired from Chinnayakanahalli et al. (2002) and Gopalan et al. (2002). As a final step, the slope units were obtained by combining the watershed deduced from the DEM and the watershed deduced from the reverse DEM (Figure 3.50d).

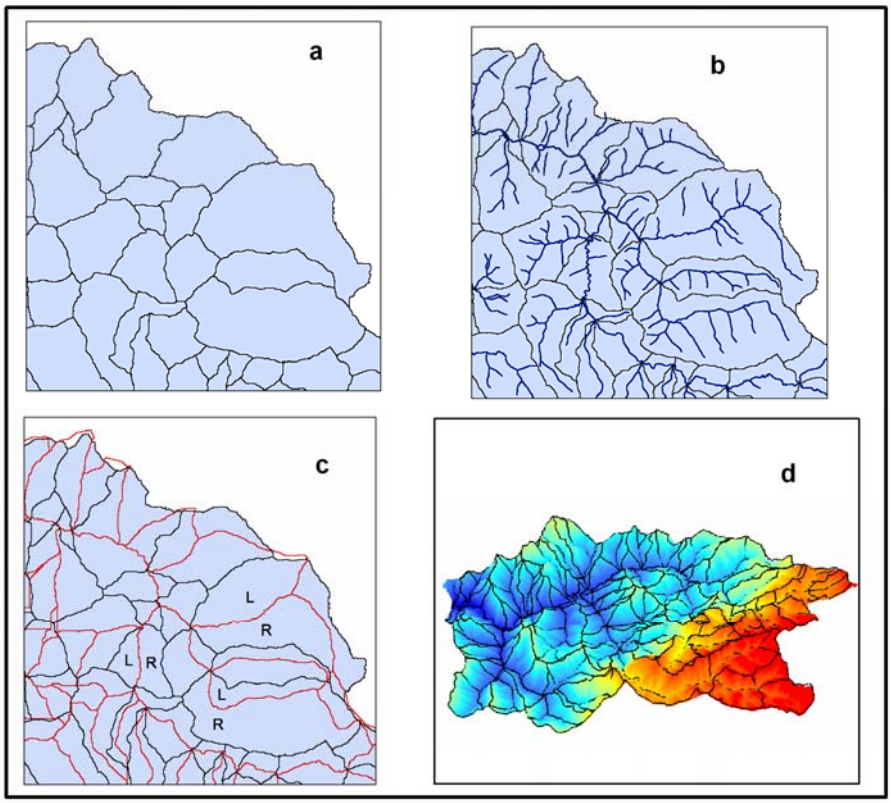

Figure 3.50. a) Watershed boundaries determined using the DEM. b) Drainage line overlaid with watershed of the region c) Watershed boundaries determined using the reverse DEM (shown with red lines) overlaid with watershed boundaries present the left (L) or right (R) side of a sub-basin. d) Slope unit of region obtained in 3D.

The variables that may have an affect to landslide occurrence and that were produced to be input into the analysis were described in Figure 3.48. These variables include topographical elevation (Elev), slope (Slp), aspect (Asp), curvature (Curv), plan curvature (Plan_Curv), profile curvature (Prof_Curv), topographic wetness index (Wtns), NDVI (Veg), distance to road (DisttoRoad), distance to stream network (DisttoStrm), density of road network (DensRoad), density of stream network (DensStrm), geological units (6 units), distance to fault (DisttoFault), soil map (5 units), land use (5 units), soil depth (4 units) and erosion (4 units), which were considered for the slope unit analysis. To adapt the variables so that they were used in the slope unit, each data in raster format was statistically analyzed. Zonal statistical functions were performed on a per-zone basis. As a result, a single output value was computed for each zone.

Depending on the region of the landslide boundaries, most of the landslides were assigned to each corresponding slope unit. However, there may be some important difficulties in assigning landslide occurrence to slope units. Due to the digitization errors of landslide polygons, some of the landslides which occupy large regions seem to be represented not only on one side of the hill, but also on the other side (Figure 3.51a, Figure 3.51b). Therefore, the occurrence of a single slide can be assigned to two different slope units. On the other hand, some landslides have smaller regions; that is why these different slides are assigned to the same slope unit instead of being considered as separate occurrences. The best way to overcome this drawback is to assign each landslide occurrence to a single slope unit.

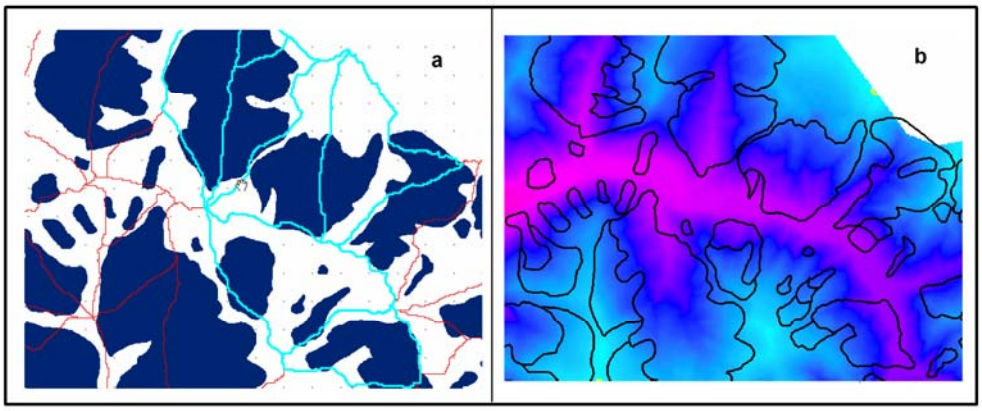

Figure 3.51. a. Landslide boundaries and slope unit boundary b. DEM overlaid with landslide boundaries

Due to the problems described above, to assign the presence or absence of each landslide to the corresponding slope region, a procedure was adopted. In this procedure, an index was determined which shows the percentage of landslide area in each slope unit area. The indexes in each slope unit were evaluated to identify a threshold value, which is defined as 0.6%. If a landslide occupies less than 0.6% of the slope unit, the value of zero was assigned and one was assigned otherwise. Figure 3.52 shows how the presence and absence of a landslide value was assigned to each slope unit. The slope unit was assigned 0 if the landslide boundary only crossed from the corner of that slope unit as presented in slope regions a and b in Figure 3.52. In these slopes, it can be clearly seen that the index value was lower than the threshold. Otherwise, 1 was assigned to that slope unit. As a result, a total of 91

landslide occurrences were assigned to the slope units and there were 138 slope units in the study region with landslide-free zones.

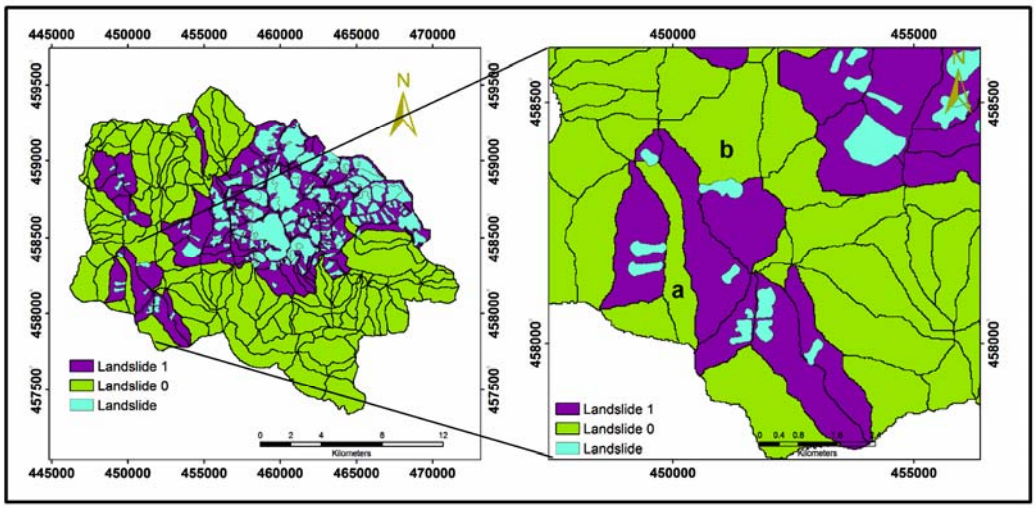

Figure 3.52. Slope Unit map showing landslide and landslide-free regions zooming in the south-western part to show the logic to assign landslide values.

The mean value for each slope unit was calculated and assigned to each slope unit. As an example the slope and fault line was presented in Figure 3.53 and Figure 3.54 respectively. The mean statistics was computed for each slope unit and as a resultant map given in Figure 3.53b was acquired having range of 0^0 to 35^0.

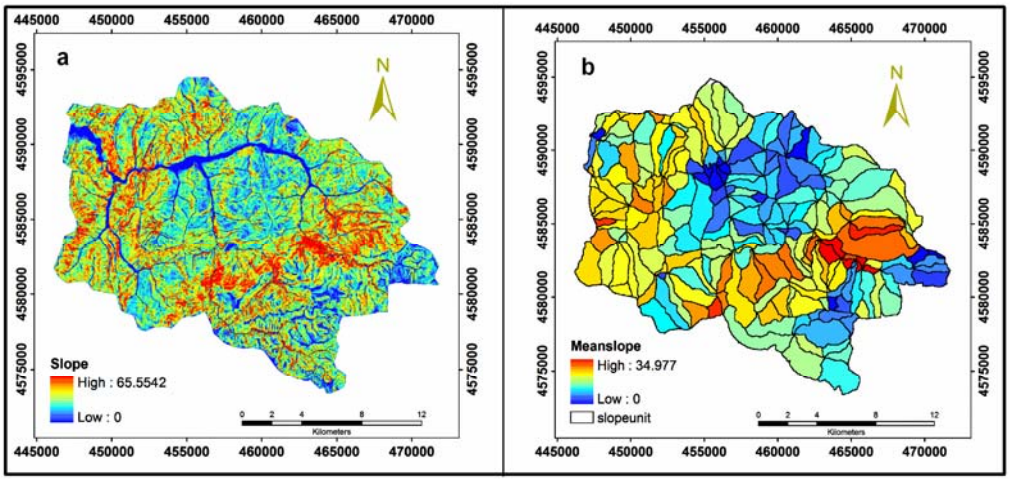

Figure 3.53. a) Slope map of the region ranges between 0 and 65.55 b) Slope unit map showing the mean slope values assigned to each mapping unit

As it can be seen from Figure 3.54a, the distance to the road network ranges between 0 and 1000 m. The closer the road network to each other, the denser the road network on the north-eastern part of the region. The mean computed for all slope units was presented in Figure 3.54b. Figure 3.54b indicates that in the north-eastern part of the region, the road distance is lower. This is due to denser road network present in the north-eastern part of the region; hence, the distance to road line cannot be calculated with higher distances.

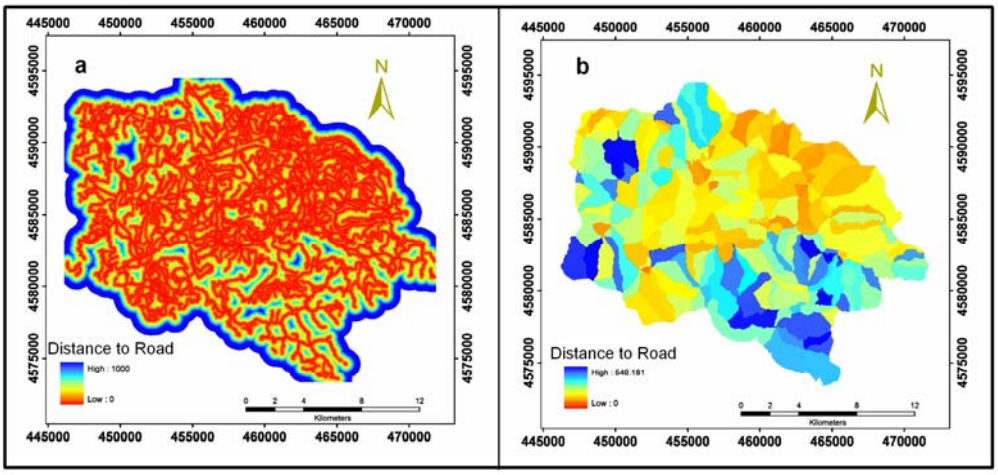

Figure 3.54. a. Road distance computed for each cell unit b. Road distance assigned to each slope unit by computation of mean value.

3.3.3.2.2 Pre-Analysis of Data Set

In the first step, the factors which cover regions smaller than 0.03 km2 were excluded from the analysis as they do not contain much information. The data excluded were: River flooding regions of land use (LU_RF), rock and debris units of land use (LU_ R), very deep soil depth (SD_VD), less erosion (E_L), very severe erosion (E_VS), alluvial soil (S_Allv), limestone unit of geology (Geo_ L), marl unit of geology (Geo_ M), andesite unit of geology (Geo_And). After the exclusion, the data were reduced into 28 variables. These variables were analyzed by using the correlation matrix to assess the multicollinearity between factors. For the analysis of multicollinearity, the spearsman correlation coefficient was used. Table 3.7 shows the highly correlated factors which are considered for slope unit-based mapping unit.

Table 3.7. Correlation between nominal landslide influencing factors

	LU_DF	LU_F	LU_S	SD_VS	SD_D	SD_S	E_S	E_M	Geo_C	Geo_SM	Geo_Allv	S_GBPdz	S_BFS	S_Collv	S_BFWL	Elev	Asp	DistoStrm	Veg	Slp	Distto Road	Distto Fault	Wtns	Curv	Plan_Curv	Prof_Curv	Dens Road	Dens Strm
LU_DF	1.00	**-0.98**	-0.51	-0.05	0.49	0.21	-0.40	0.45	-0.46	0.39	0.43	0.19	-0.26	0.45	0.10	-0.49	0.08	0.00	-0.08	-0.31	-0.55	0.12	0.33	0.23	0.13	0.15	**0.81**	0.43
LU_F	**-0.98**	1	-0.42	0.04	-0.56	-0.19	0.47	-0.44	0.63	-0.35	-0.44	-0.17	0.29	-0.44	-0.08	0.49	-0.06	-0.02	0.08	0.29	0.54	-0.11	-0.32	-0.05	0.23	0.17	-0.49	-0.45
LU_S	0.51	-0.42	1	0.03	-0.25	-0.15	0.22	-0.37	-0.18	0.33	-0.15	0.31	0.42	0.15	0.35	0.19	0.16	-0.24	0.06	0.32	0.32	0.014	0.27	0.02	0.07	0.12	0.41	-0.36
SD_VS	-0.05	0.04	0.03	1	0.02	-0.03	-0.08	0.11	0.1	-0.14	0.02	-0.02	0.06	0.01	-0.02	0.04	-0.06	-0.14	-0.12	-0.04	0.06	-0.07	0.06	-0.07	0.15	0.09	-0.17	-0.1
SD_D	0.49	-0.56	-0.51	0.02	1	-0.04	-0.09	0.18	-0.25	0.14	0.19	0.092	0.08	0.24	-0.16	-0.19	0.13	-0.02	-0.52	-0.52	-0.32	**0.73**	0.35	0.02	0.2	0.12	0.18	0.09
SD_S	0.21	-0.19	-0.15	-0.03	-0.04	1	-0.51	0.56	-0.21	0.12	0.19	0.32	-0.24	0.18	0.22	-0.17	0	0.28	0	-0.29	-0.16	-0.01	0.27	-0.02	0.11	0.13	0.16	-0.01
E_S	-0.4	0.47	0.34	-0.08	-0.09	-0.51	1	**-0.85**	0.31	0.07	-0.61	-0.23	0.58	**-0.72**	-0.24	0.54	0.02	-0.27	0.06	0.21	0.23	-0.01	-0.32	0	0.22	0.19	-0.24	-0.47
E_M	0.45	-0.44	-0.37	0.11	0.18	0.56	**-0.85**	1	-0.38	-0.02	0.68	0.27	-0.51	**0.83**	0.29	-0.59	0	0.22	-0.1	-0.3	-0.24	0.05	0.37	0.03	0.14	0.15	0.27	0.48
Geo_C	-0.46	0.63	-0.18	0.1	-0.25	-0.21	0.31	-0.38	1.00	-0.61	-0.4	-0.14	0.46	-0.35	-0.39	0.51	-0.15	-0.07	-0.2	0.24	.52)	-0.03	-0.23	-0.1	0.18	0.13	-0.38	-0.28
Geo_SM	0.39	-0.35	0.33	-0.14	0.14	0.12	0.07	-0.02	-0.61	1.00	-0.19	0.08	-0.15	-0.11	0.19	-0.21	0.19	0.03	0.27	-0.07	-0.39	0.09	0.05	-0.02	0.22	0.31	0.33	-0.04
Geo_Allv	0.43	-0.44	-0.15	0.02	0.19	0.19	-0.61	0.68	-0.4	-0.19	1	0.15	-0.46	**0.75**	0.28	-0.57	-0.04	0.19	-0.07	-0.22	-0.17	0.1	0.33	0.18	0.26	0.21	0.22	0.6
S_GBPdz	0.19	-0.17	0.31	-0.02	0.092	0.32	-0.23	0.27	-0.14	0.08	0.15	1	-0.21	0.22	-0.06	-0.09	0.2	0.01	-0.15	-0.17	-0.27	-0.19	0.09	0.01	. 19	0.12	0.17	0.07
S_BFS	-0.26	0.29	0.42	0.06	0.08	-0.24	0.58	-0.51	0.46	-0.15	-0.46	-0.21	1.00	-0.52	-0.63	0.58	-0.18	-0.12	-0.23	-0.01	0.11	0.03	-0.09	0.05	0.14	0.18	0.05	-0.22
S_Collv	0.45	-0.44	0.15	0.01	0.24	0.18	**-0.72**	**0.83**	-0.35	-0.11	**0.75**	0.22	-0.52	1.00	0.27	-0.65	-0.03	0.14	-0.14	-0.23	-0.22	0.01	0.31	0.08	0.25	0.21	0.27	**0.84**
S_BFWL	0.10	-0.08	0.35	-0.02	-0.16	0.22	-0.24	0.29	-0.39	0.19	0.28	-0.06	-0.63	0.27	1.00	-0.45	0.2	0.06	0.35	0.06	0.02	0.02	0.02	-0.06	0.15	0.18	-0.22	0
Elev	-0.49	0.49	0.19	0.04	-0.19	-0.17	0.54	-0.59	0.51	-0.21	-0.57	-0.09	0.58	-0.65	-0.45	1	-0.02	-0.07	-0.12	0.15	0.39	-0.04	-0.3	-0.12	0.14	0.15	-0.36	-0.62
Asp	0.08	-0.06	0.16	-0.06	0.13	0	0.02	0	-0.15	0.19	-0.04	0.2	-0.18	-0.03	0.2	-0.02	1	0.03	0.04	0.02	-0.15	0.04	-0.05	0.03	0.02	0.11	-0.04	-0.09
Distto Strm	0.00	-0.02	-0.24	-0.14	-0.02	0.28	-0.27	0.22	-0.07	0.03	0.19	0.01	-0.12	0.14	0.06	-0.07	0.03	1	0.09	-0.26	0.09	0.09	0.37	0.11	0.05	0.1	0.04	0.03
Veg	-0.08	0.08	0.06	-0.12	-0.52	0	0.06	-0.1	-0.2	0.27	-0.07	-0.15	-0.23	-0.14	0.35	-0.12	0.04	0.09	1	0.37	0.15	-0.04	-0.19	0.07	0.12	0.15	-0.03	-0.03
Slp	-0.31	0.29	0.32	-0.04	-0.52	-0.29	0.21	-0.3	0.24	-0.07	-0.22	-0.17	-0.01	-0.23	0.06	0.15	0.02	-0.26	0.37	1	0.32	-0.15	-0.55	-0.1	0.15	0.12	-0.14	-0.01
Distto Road	-0.55	0.54	0.32	0.06	-0.32	-0.16	0.23	-0.24	.52)	-0.39	-0.17	-0.27	0.11	-0.22	0.02	0.39	-0.15	0.09	0.15	0.32	1	0.07	-0.19	-0.07	0.21	0.18	-0.59	-0.27
Distto Fault	0.12	-0.11	0.01	-0.07	**0.73**	-0.01	-0.01	0.05	-0.03	0.09	0.1	-0.19	0.03	0.01	0.02	-0.04	0.04	0.09	-0.04	-0.15	0.07	1	0.18	0.05	0.02	0.05	0.05	0.02
Wtns	0.33	-0.32	0.27	0.06	0.35	0.27	-0.32	0.37	-0.23	0.05	0.33	0.09	-0.09	0.31	0.02	-0.3	-0.05	0.37	-0.19	-55	-0.19	0.18	1.00	0.01	0.15	0.18	0.15	0.16
Curv	0.23	-0.05	0.02	-0.07	0.02	-0.02	0	0.03	-0.1	-0.02	0.18	0.01	0.05	0.08	-0.06	-0.12	0.03	0.11	0.07	-0.1	-0.07	0.05	0.01	1.00	**0.73**	**0.78**	0.16	0.17
Plan_Curv	0.13	0.23	0.07	0.15	0.2	0.11	0.22	0.14	0.18	0.22	0.26	. 19	0.14	0.25	0.15	0.14	0.02	0.05	0.12	0.15	0.21	0.02	0.15	**0.73**	1.00	0.46	0.10	0.70
Prof_Curv	0.15	0.17	0.12	0.09	0.12	0.13	0.19	0.15	0.13	0.31	0.21	0.12	0.18	0.21	0.18	0.15	0.11	0.1	0.15	0.12	0.18	0.05	0.18	**0.78**	0.46	1.00	0.05	0.01
Dens Road	**0.81**	-0.49	0.41	-0.17	0.18	0.16	-0.24	0.27	-0.38	0.33	0.22	0.17	0.05	0.27	-0.22	-0.36	-0.04	0.04	-0.03	-0.14	-0.59	0.05	0.15	0.16	0.10	0.05	1.00	0.47
Dens Strm	0.43	-0.45	-0.36	-0.1	0.09	-0.01	-0.47	0.48	-0.28	-0.04	0.6	0.07	-0.22	**0.84**	0	-0.62	-0.09	0.03	-0.03	-0.01	-0.27	0.02	0.16	0.17	0.70	0.01	0.47	1.00

The same threshold and significance levels for grid cell analysis were used. The severe erosion (E_S) and middle erosion (E_M) show high correlation with colluvial soil (S_Collv). In addition, S_Collv shows a high correlation with the alluvial unit of geology (Geo_Allv). The curvature (Curv) shows high correlation with plan curvature (Plan_Curv) and profile curvature (Profile_Curv). Also, the distance to fault (DisttoFault) shows a high correlation with deep soil depth (SD_D). The density of road network (DensRoad) and density of stream network (DensStrm) show a high correlation with the dryfarming (LU_DF) and colluvial soil (S_Collv), respectively. As a result, the E_S, E_M, S_Collv, Plan_Curv, Prof_Curv, DisttoFault, DensRoad and DensStrm were excluded from the further analysis. Although LU_DF and LU_F show a negative correlation, they were both included into the analysis due to their important correlation with landslide.

After the redundant variables were reduced by multicollinearity analysis the data normality analyses had to be done before regression modeling. As a result of the normality analysis, it was found that dry farming unit of land use (LU_DF), brown forest soil (S_BFS), farming unit of landuse (LU_F), brown forest soil without lime (S_BFSWL), topographical elevation (Elev), aspect (Asp), distance to stream network (DisttoStrm), wetness (Wtns) and curvature (Curv) needed transformation for better fit to normal distribution (Appendix A-2).

As a result of the statistical analysis of the data sets, the data set containing 37 variables were reduced to 15 and 20 variables, for both slope and grid-based mapping units, respectively as given in Figure 3.55. The reduced databases obtained for both mapping unit type were used for further susceptibility modeling for each mapping unit.

Figure 3.55. The resultant influencing parameters after the statistical analysis

Mapping Unit	Morphological Factors	Environmental Factors	Geological Factors
Grid-based Mapping Unit	Elevation, Slope, Aspect	Distance to Road, Distance to Stream Network, NDVI, Dryfarming, Settlement	Sandstone-Mudstone, Distance to Fault, Colluvial Soil, Brown Forest Soil, Grey Brown Podzolic Soil, Very shallow Soil, Middle Erosion
Slope Unit-Based Mapping Unit	Elevation, Slope, Aspect, Curvature	Distance to Road, Distance to Stream Network, NDVI, Forest, Dryfarming, Settlement	Sandstone-Mudstone, Wetness, Conglomerate, Alluvial, Brown Forest Soil, Grey Brown Podzolic Soil, Brown Forest Soil Without Lime, Very Shallow Soil, Shallow Soil, Deep Soil

3.3.4 Quantitative Susceptibility Mapping Models

In this thesis, three global models, namely, logistic regression (LR), spatial regression (SR), artificial neural network (ANN) and a local model, geographically weighted regression (GWR), were constructed for quantitative landslide susceptibility mapping.

3.3.4.1 Logistic Regression (LR)

LR is basically an extension of multiple regressions in situations where the dependent variable is not a continuous one (George and Mallery, 2000). In other words, the dependent variable is sampled as a binary variable (i.e. presence/absence of landslide). The advantage of logistic regression over the multiple regression and discriminant analysis is that logistic regression enables analyzing predictor variables of all types (i.e. continuous, discrete, and dichotomous) and allows one to produce nonlinear models (Mertler and Vannatta, 2002).

In this thesis, at the beginning 15 independent variables were considered for grid-based approach and 20 independent variables were considered in the slope unit-based approach. The forward stepwise procedure was used to obtain LR models for both

grid-based and slope unit-based approaches. The models created for both grid-based and slope unit-based approaches were given in Eq. 41 and 42, respectively. As seen in Eq. 41 and Eq. 42, although approximately similar morphological, environmental and geological factors were included in the analyses, slope unit-based mapping unit results in a more simplified form.

$$f(x) = 0.527Elev + 0.133DisttoFault + 1.251S_BFS + 2.118LU_DF + 2.481LU_S + 3.690E_M + 1.496Geo_SM - 1.340Slp - 0.686Asp - 1.626\ DisttoRoad - 0.146\ DisttoStrm - 0.301Veg - 3.854\ S_Collv - 2.318\ S_GBPdz - 4.849 \quad (41)$$

$$f(x) = 32.871DisttoRoad + 5.264S_BFS + 160.502SD_VS + 30.371Geo_SM + 18.640Geo_C - 52.499LU_F + 10.570 \quad (42)$$

In grid-based mapping unit (Eq.41) factors of slope (Slp), aspect (Asp), distance to road network (DisttoRoad), distance to stream network (DisttoStrm), NDVI (Veg), colluvial soil (S_Collv), grey brown podzolic soil (S_GBPdz) have a reducing affect on landslide occurrence. On the other hand, topographical elevation (Elev), distance to fault (DisttoFault), brown forest soil (S_BFS), dry farming (LU_DF), settlement (LU_S), middle erosion (E_M), sandstone mudstone (Geo_SM) have contribution to landslide occurrence. Among the factors contributing to landslides (Eq. 41), E_M, LU_S and LU_DF have the highest contribution. Conversely, S_Collv and S_GBPdz types have a reducing effect on landsliding in grid-based approach, which is plausible when the spatial distribution of landslides is considered, since very few landslides are observed in these soil types. In addition, the grid-based units does not represent the physical slopes, hence the model reflects this situation with the negative effect of slope parameter on landsliding.

In slope unit-based approach, the regression equation (Eq. 42) involved factors of DisttoRoad, brown forest soil (S_BFS), very shallow soil depth (SD_VS), Geo_SM, conglomerate unit of geology (Geo_C), and forest (LU_F). Among these factors, LU_F has a reducing affect on landsliding while the rest of the factors in Eq.42 have contribution to landsliding. When the coefficients of factors in Eq. 42 were examined, it was found that SD_VS and DisttoRoad had the highest effect on the

occurrence of landslides in the study region. DisttoRoad indicates the role of human effect in the region; hence the analysis shows that human effect has more influence than the other factors.

In order to evaluate the significance of the obtained equations in Eq. 41 and Eq. 42, training sets that were obtained previously were used for performing chi-square Hosmer-Lemeshow test and for evaluating Cox and Snell R^2 and Nagelkerke R^2 values (Table 3.8). The -2 Log-likelihood provides an index of model fit. The lower the value is, the better the model fits the data. The slope unit-based model results indicate that it fits better than grid-based model. The Chi-square value compares the actual values for dependent variable with the predicted values. Cox and Snell R^2 and Nagelkerke R^2 were essentially estimates of R^2 indicating the proportion of variability in the dependent variable which may be accounted for all predictor variables included in the model. Larger pseudo-R^2 statistics indicate that a high amount of variation was explained by the model and it ranges from 0 to 1. As can be seen in Table 3.8, the Cox and Snell R^2 and Nagelkerke R^2 values were higher when the model was constructed by using slope unit-based approach.

Table 3.8. LR Model test results for grid-based and slope unit-based mapping units

Forwardstepwise	Training set No	-2 log likelihood	Cox and Snell R^2	Nagelkerke R^2	Chi-square
Grid-based model	1	132987	0.17	0.33	2867
Slope Unit-based model	2	17.28	0.62	0.87	6.62

Landslide susceptibility maps for both data sets were created after obtaining logistic regression models. The logit of the f(x) function in Eq.43, P (L), which was defined by the logistic function in terms of probability, was calculated for all of the mapping units. As f(x) varies from -∞ to +∞, the probability varies from 0, being no susceptibility, to 1, being complete susceptibility.

$$P(L) = \frac{1}{1 + Exp^{-f(x)}} \tag{43}$$

The calculated probability values of grid-based and slope unit-based approaches were then used to produce thematic landslide susceptibility maps in GIS. Figure 3.56 shows the susceptibility map produced by LR for grid-based mapping unit. Similarly, Figure 3.57 presents the susceptibility map created by logistic regression for slope unit-based mapping unit. The landslide susceptibility maps were produced on a continuous scale, and for comparison purposes, they were rescaled so that the pixel values lie between 0 and 1. 0 indicates the lowest susceptibility and 1 indicates the highest susceptibility to landslides. The LR model prediction map created for landslide susceptibility for grid-based mapping unit (LR_GRD_SUSCP) is illustrated in Figure 3.56 and the LR model prediction map created for landslide susceptibility for slope unit-based mapping unit (LR_SU_SUSCP) is illustrated in Figure 3.57. Looking at the two maps, it can be said that there are places where differences are subtle and there are also areas with dissimilarities. In both of the prediction models, the southern parts of the regions are low susceptible to landslides, compared to the middle and south-eastern parts of the regions which are high susceptible to landslides (Figure 3.56, Figure 3.57). On the other hand, the LR_SU_SUSCP shows the western parts of the region to be medium susceptible to landslides as illustrated in Figure 3.57 by yellow and green colors.

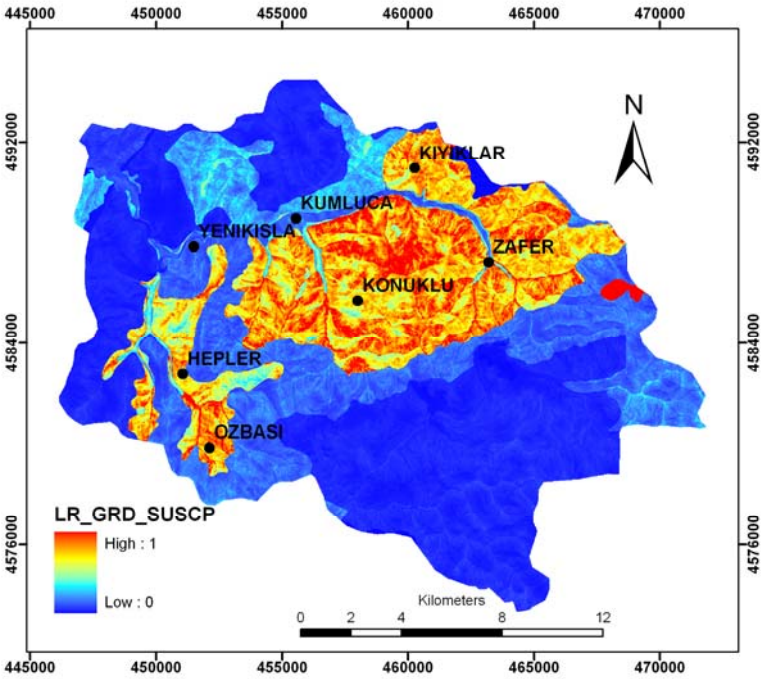

Figure 3.56. LR Model prediction map created for landslide susceptibility for grid-based mapping unit (LR_GRD_SUSCP)

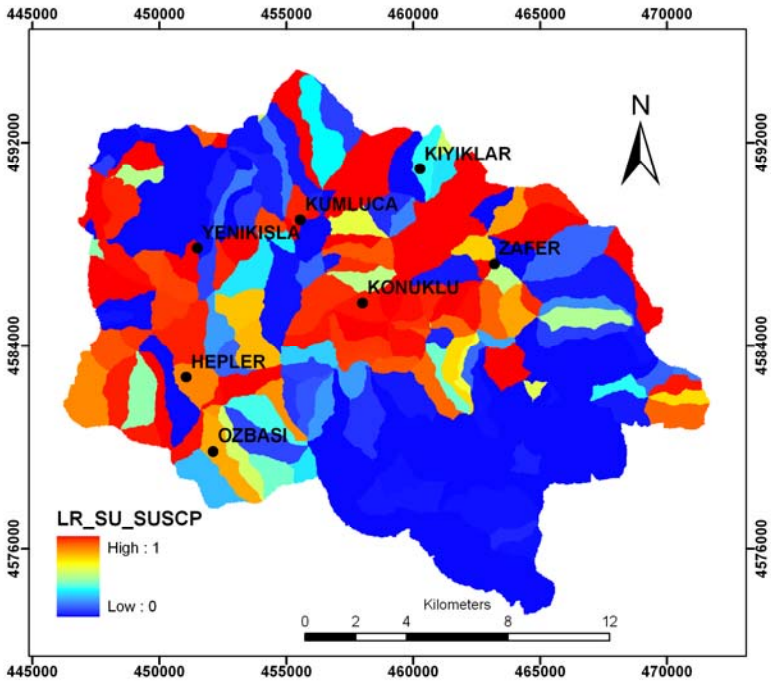

Figure 3.57. LR Model prediction map created for landslide susceptibility for slope unit-based mapping unit (LR_SU_SUSCP)

The prediction models are also compared by the statistical terms. Therefore, the statistics of the original prediction values are computed as presented in Table 3.9. The statistical comparison of prediction maps for grid and slope unit-based mapping unit indicates that the LR_GRD_SUSCP map has a lower mean value than LR_SU_SUSCP (Table 3.9), which means that more areas can be designated as low susceptible by LR_GRD_SUSCP. According to the variation of probability values, LR_SU_SUSCP shows a higher range of probability value representation with 0.43 std. dev. value compared to LR_GRD_SUSCP with 0.23 std. dev. values.

Table 3.9. The statistics of the susceptibility models for different mapping units

Model	Mapping Unit Type	Min	Max	Mean	Std. Dev.
LR	**GRD**	0	0.98	0.25	0.23
	SU	0	1	0.4	0.43
SR	**GRD**	0.07	0.90	0.5	0.18
	SU	0.01	0.99	0.5	0.27
ANN	**GRD**	0.18	0.88	0.33	0.13
	SU	0.01	0.99	0.41	0.37
GWR	**GRD**	0.01	0.8	0.27	0.4
	SU	0	1	0.33	0.32

3.3.4.2 Artificial Neural Networks (ANN)

The attractiveness of ANN was due to its performance in learning and adaptivity, which allows the system to update its internal structure (Jain et al., 1996). Before constracting an ANN model, some initial values such as initial weights, learning rate, and momentum coefficients should be determined. In this thesis, the initial values were determined depending on the heuristics given in 2.3.2.2. The initial weight range was selected as [-1.0; 1.0]. The training rate of an ANN is sensitive to learning rate (η). Small numbers of learning rate may cause the training rate to be slow because of minor changes in the weights. However, selecting large numbers of learning rate may accelerate training and cause oscillates on the error surface and never converges by changing the weight vector (Basheer, Hajmeer, 2000, Sönmez et al., 2006). In this study, by using the grid-based data set, the learning rate range was selected as 0.1. The momentum coefficient is used in weight updating in the back-propagation algorithm. This allows the learning rate to be larger without instability, which speeds the training of network (Heerman and Khazenie, 1992). The momentum coefficient was set to 0.95. As a result, a network structure of 15x4x1 was obtained for grid-based data set. The number of epochs was set to 6000 for the analysis. The root mean square error (RMSE) for the stopping criterion was set to 0.01.

Contrary to the huge data set used in grid-based mapping unit, the data set used in slope unit-based mapping unit is smaller. Consequently, the processes can be carried out in a shorter time in slope unit-based mapping unit. Thus, three different ANN structures were created to select the best one for slope unit-based mapping unit. The selected ANN structures for the analysis are 20x2x1, 20x5x1, and 20x11x1. The ANN was trained with backpropagation algorithm with a learning rate of 0.1. The number of epochs was set to 8000 for the analysis. The root mean square error (RMSE) goal for the stopping criterion was set to 0.01. The relations between the number of training cycles and the RMSE for each combination obtained by ANNES software were given in Figure 3.58.

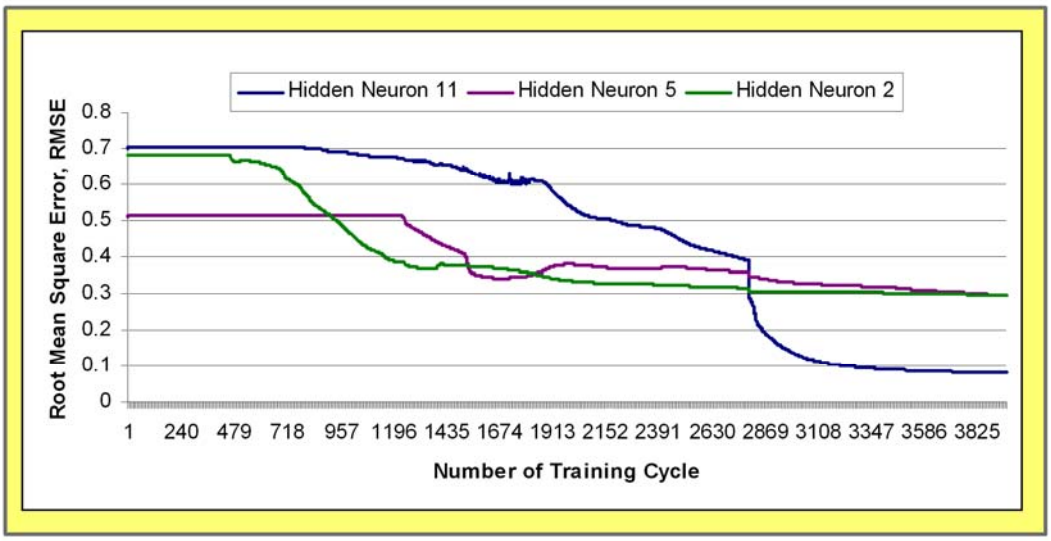

Figure 3.58. The relations between RMSE and number of training cycle for different combinations of hidden neurons

From these trials, a learning rate with a value of 0.1 together with 11 hidden neurons was selected as the best network structure for the data set in the study region, because the RMSE diminishes to a value lower than 0.1 with the use of 11 hidden neurons. For this reason, this combination was used to compute the probabilities for the whole data set in the study. The performance of ANN is computed to be 0.098, which is pretty good. The R^2 is computed as 0.44. After the computation of prediction values for each case in the study region, the susceptibility maps were created, which are given in Figure 3.59 and Figure 3.60, for both grid (ANN_GRD_SUSCP) and slope unit-based (ANN_SU_SUSCP) mapping units, respectively.

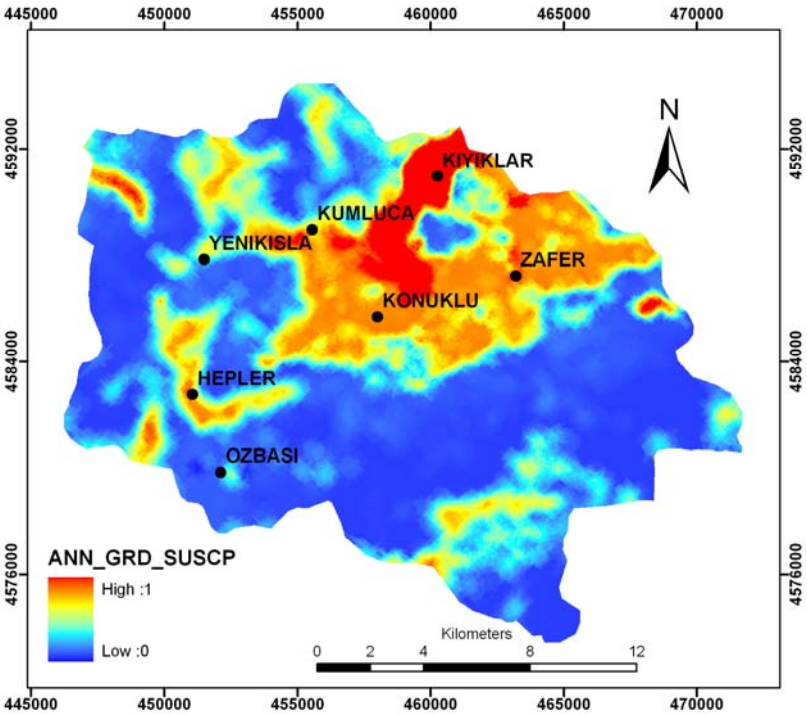

Figure 3.59. ANN prediction map created for landslide susceptibility for grid-based mapping unit (ANN_GRD_SUSCP)

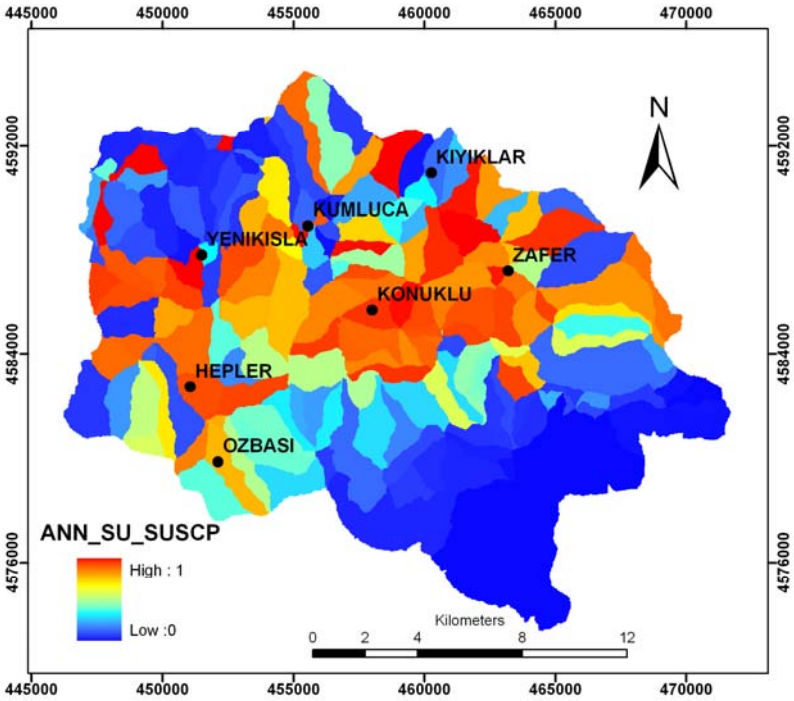

Figure 3.60. ANN prediction map created for landslide susceptibility for slope unit-based mapping unit (ANN_SU_SUSCP)

Visual comparison of both ANN_GRD_SUSCP (Figure 3.59) and ANN_SU_SUSCP (Figure 3.60) maps demonstrate that the southern parts of the region are similar and represent low susceptibility to landslides. On the other hand, the south-eastern part of the region shows medium susceptibility to landslide occurrence and is displayed with green, yellow, and orange colors by ANN_GRD_SUSCP and is represented with high susceptibility by ANN_SU_SUSCP.

The statistical comparison of the prediction maps presented in Table 3.9 for grid and slope unit-based mapping unit displays that the ANN_GRD_SUSCP map and the ANN_SU_SUSCP have similar mean values (Table 3.9), whereas the variation of probability values in ANN_SU_SUSCP (0.27) is larger than ANN_GRD_SUSCP (0.18). This proves that ANN_SU_SUSCP shows a higher range of susceptibility values.

3.3.4.3 Spatial Regression (SR)

There is not yet specialized software available to carry out the SR process. In this thesis, the library of Spatial Econometrics Toolbox in the Matlab environment was adopted for modeling SR (LeSage, 2009). The train data obtained was used for the modeling, which is described in section 3.4. After the application of spatial autoregressive modeling for the dependent variable in grid-based and slope unit-based approaches, the models developed for the study region were presented in Eq. 44 and 45, respectively.

$$f(x) = 0.255LU_DF + 0.112S_BFS + 0.508E_M + 0.01371Geo_SM - 0.304\ Elev - 0.820Slp - 0.297Asp - 0.272DisttoRoad - 0.21Veg - 1.113S_Collv + 0.811326 \quad (44)$$

$$f(x) = 2.45Slp + 7.648Wtns + 0.893DisttoRoad + 3.605S_BFS + 2.980SD_D + 1.71Geo_SM - 2.06Veg - 6.08LU_DF - 7.766LU_F - 1.3411S_VS - 1.638S_S + 0.3420 \quad (45)$$

The developed models for grid-based data set in Eq.44 indicates that factors of dry farming (LU_DF), brown forest soil (S_BFS), middle erosion (E_M), and sandstone-mudstone unit of geology (Geo_SM) have contribution to landsliding while topographical elevation (Elv), slope (Slp), aspect (Asp), distance to road network (DisttoRoad), NDVI (Veg) and colluvial soil (S_C) have a reducing affect on landsliding. When the coefficients of factors in Eq. 44 were examined, it can be seen that LU_DF, E_M provide the highest contribution to landsliding, which are consistent with the observations in the field. On the other hand, Slp and Veg provide the biggest effect on reducing landslides, which is also meaningful.

In slope unit-based approach, regression equation (Eq. 45) involves factors of Slp, topographic wetness index (Wtns), DisttoRoad, S_BFS, deep soil depth (SD_D), conglomerate unit of geology (Geo_C), Veg, LU_DF, forest (LU_F), very shallow soil depth (SD_VS), and shallow soil depth (SD_S). Among these factors, Veg, LU_DF, LU_F, SD_VS, and SD_S have a reducing affect on landsliding while the rest of the factors in Eq.45 have contribution to landsliding. When the coefficients of factors in Eq. 45 were examined, it can be seen that Wtns, S_BFS, and S_D have the biggest effect on landslide occurrence in the study region, which is logical. On the other hand, Veg, LU_DF, and LU_F have the biggest effect on reducing landslides in the study region.

In SR model, the local pseudo R^2 showed that nearly 67% and 87% of the variance in landslide occurrence is explained by the model for grid-based and slope unit-based approaches respectively. The R^2 values of SR models provide considerably higher R^2 values than LR models. The susceptibility maps produced by using Eq. 43 were given in Figure 3.61 and Figure 3.62 for both grid and slope unit-based mapping unit respectively.

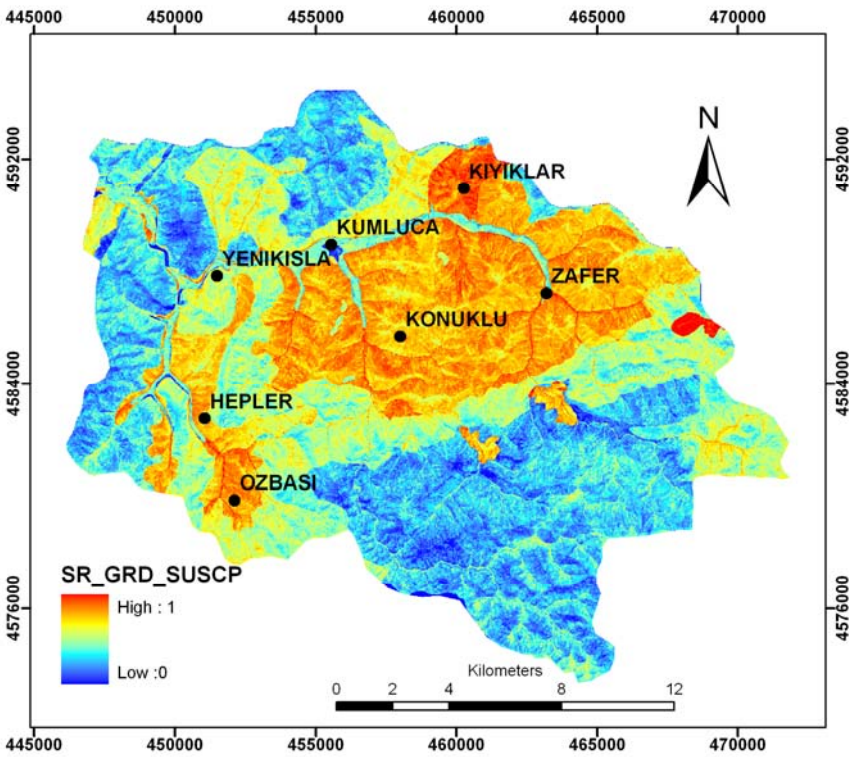

Figure 3.61. SR prediction map created for landslide susceptibility for grid-based mapping unit (SR_GRD_SUSCP)

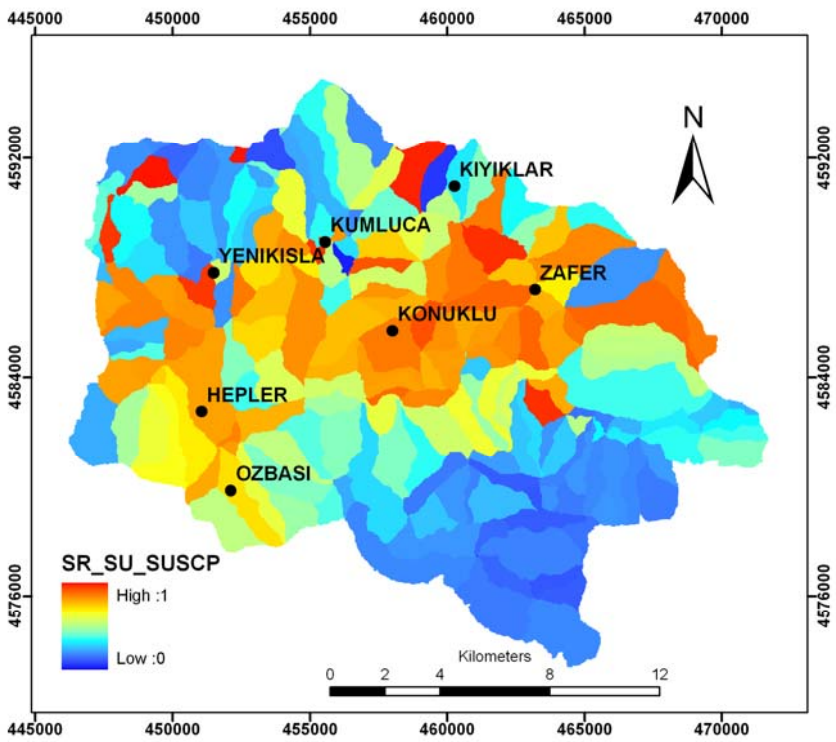

Figure 3.62. SR prediction map created for landslide susceptibility for slope unit-based mapping unit (SR_SU_SUSCP)

Both susceptibility maps based on grid (SR_GRD_SUSCP) (Figure 3.61) and slope unit-based (SR_SU_SUSCP) (Figure 3.62) mapping unit with SR model represent the southern part of the regions to be low susceptible. Similarly, the eastern parts of the regions are illustrated as highly susceptible. However, high susceptibility values are distributed more over the western part of the region by SR_SU_SUSCP than by SR_GRD_SUSCP. Therefore, it can be concluded that SR_SU_SUSCP has much higher susceptibility values than SR_GRD_SUSCP, which might be due to the generalization of variable values of slope unit-based mapping unit.

The mean value of SR_GRD_SUSCP and SR_SU_SUSCP is similar (0.5) and relatively higher compared to the other LR and ANN models (Table 3.9). For this reason, more areas are designated as medium or high susceptible in both maps. The variation of probability values is smaller in SR_GRD_SUSCP (0.13) than in SR_SU_SUSCP (0.37). As a result, it can be said that the SR_SU_SUSCP has a higher range of susceptibility values, which can also be observed in the maps in the western part of the region.

3.3.4.4 Geographically Weighted Regression (GWR)

Up to now, the applied models of SR, ANN, and LR were a global model, which means that one set of result was generated from the analysis and the relationships generated were assumed to be the same for the whole region. However, spatial phenomena have potential variability across space. According to Fortheringham et al. (2000), the relationships might exhibit spatial nonstationary over space due to three main reasons. Firstly, spatial variations exist in relationships due to the random sampling variations. Secondly, the relationships might be intrinsically different across space. Thirdly, it is very difficult to model the reality as some more relevant variables are missed or omitted, or as they are represented by an incorrect functional form. The global analysis lacks information on spatial variation in the relationships being examined (Fortheringham et al., 2000). Recent developments in local spatial analysis provide more accurate and realistic representations of the world being modeled. So the aim of this part of the study was the local modeling of spatial data, where the focus was on testing the presence of “differences” across space rather than

assuming that there is no difference.

Geographically weighted regression (GWR), which is a local modeling technique, is particularly attractive due to its ability to explore local variations in the study region (Paez, 2002). Specialized software, GWR 3.0, was used to undertake the process. Once the variables were selected, the Kernel Type was chosen as 'Fixed' (Gaussian). The kernel bandwidth was determined by cross validation (CV). The dependent variable was binary in GWR model, leading to a logistic GWR modeling. GWR allows exploration of the relation between landslide occurrence and various factors on the cell level. Thus, each cell has unique local regression parameters representing the relationship.

For grid-based and slope-based mapping unit, Local pseudo R^2 from GWR showed that nearly 70% and 87% of the variance in landslide occurrences was explained by the model respectively (Figure 3.63, Figure 3.65). Different from the other global models, the R^2 value ranges between 0.45 and 0.68 (Figure 3.63), and between 0.54 and 0.87 (Figure 3.65) for grid and slope unit-based mapping units respectively. For grid-based mapping unit, the R^2 is the highest in the south-eastern and north-western parts of the region, where the region is free from landslide. In the mean time, for slope unit-based mapping unit, the R^2 is the highest in the south-eastern part of the region, where the region is free from landslide. The prediction values of GWR for grid-based mapping unit also provide a result map similar to LR, SR and ANN presented in Figure 3.64. Furthermore, the prediction values of GWR for slope unit-based mapping unit also provided a result map similar to SR and ANN Figure 3.66.

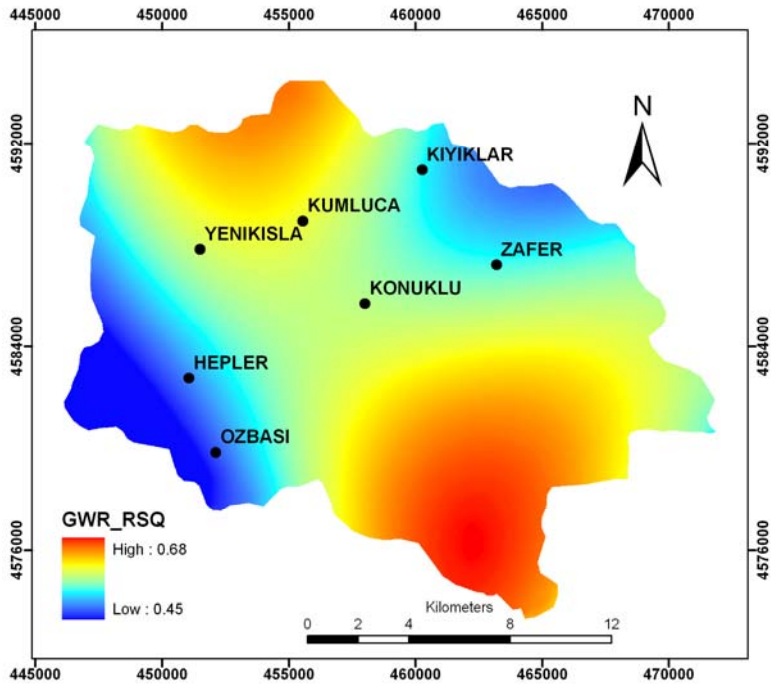

Figure 3.63. The R^2 result map of GWR model for grid-based mapping unit

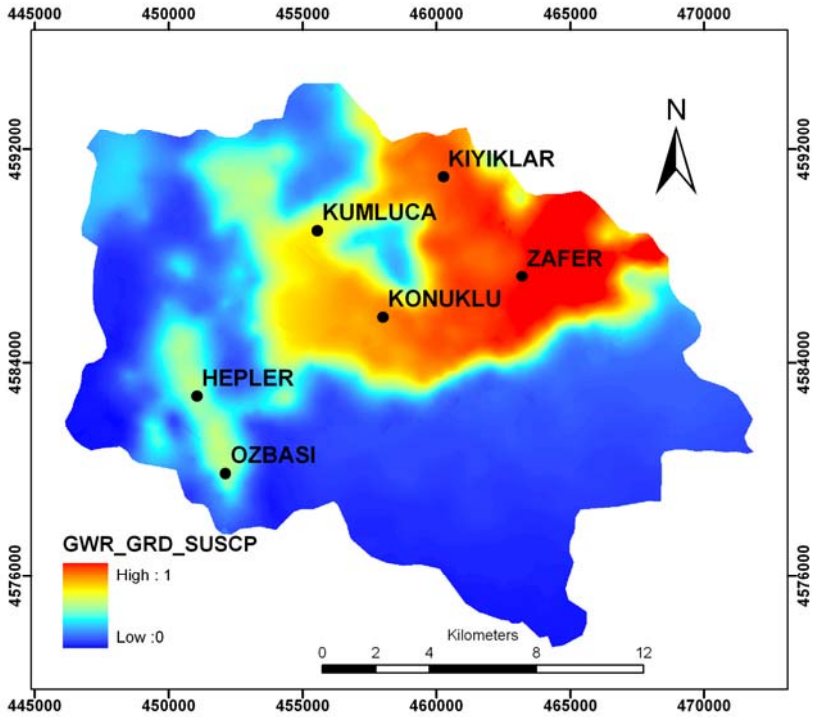

Figure 3.64. The GWR prediction map created for landslide susceptibility for grid-based mapping unit (GWR_GRD_SUSCP)

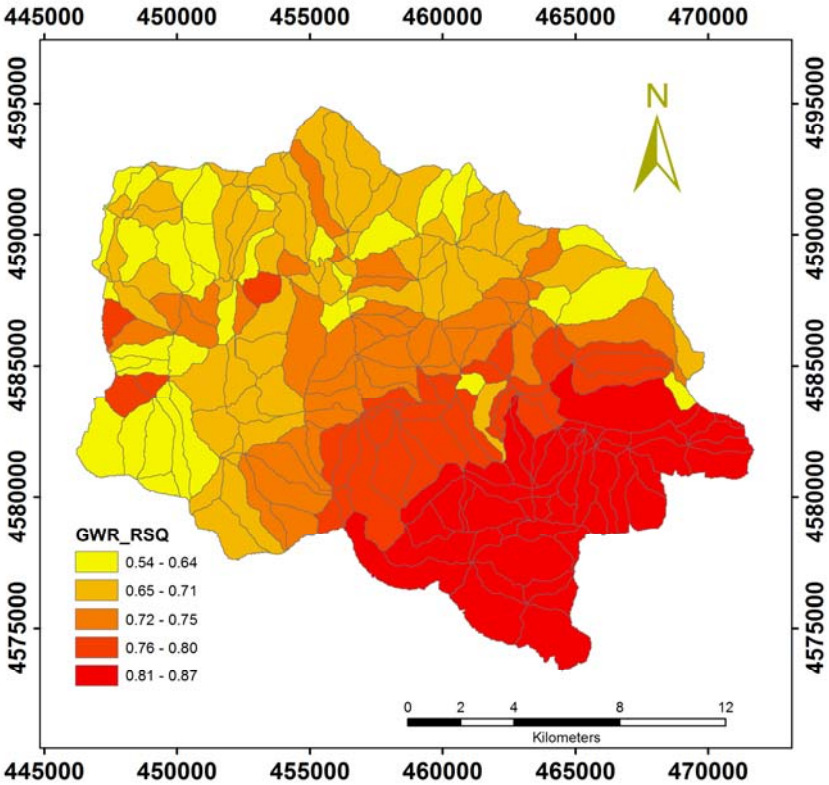

Figure 3.65. The R^2 result map of GWR model for slope unit-based mapping unit

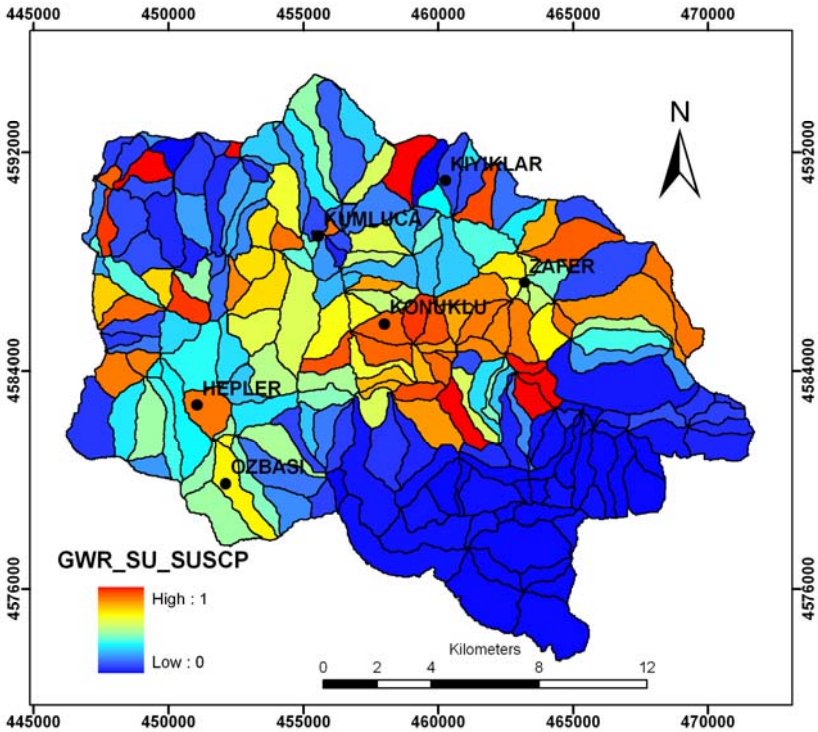

Figure 3.66. GWR prediction map created for landslide susceptibility for slope unit-based mapping unit (GWR_GRD_SUSCP)

When the GWR_GRD_SUSCP and GWR_SU_SUSCP maps are compared, it is evident that both maps provide similar representations of low susceptibility in the southern parts of the region. However, the eastern part of the region does not provide a similar pattern like GWR_GRD_SUSCP and GWR_SU_SUSCP in the sense that the GWR_GRD_SUSCP brings about high susceptibility and the GWR_SU_SUSCP shows medium susceptibility.

The statistical comparison of prediction maps for grid and slope unit-based mapping unit for GWR illustrates that the GWR_GRD_SUSCP map has a lower mean value than GWR_SU_SUSCP (Table 3.9). Thus, more areas can be designated as low susceptible by GWR_GRD_SUSCP. The variation of probability values indicates that LR_GRD_SUSCP shows medium susceptibility with 0.4 Std. Dev. value compared to GWR_SU_SUSCP with 0.33 Std. Dev. values.

As GWR gives different regression parameters for each cell, they can be mapped so that spatial variations of parameters can be examined. The statistics of each variable are illustrated inTable 3.10 andTable 3.11 for grid-based and slope unit-based mapping units respectively.

Table 3.10. Descriptive statistics of GWR parameter estimations for grid-based mapping unit

Factor	Minimum	Maximum	Mean	Std. Deviation
intercept	-7.71	-2.47	-4.19	0.94
Veg	-0.76	-0.10	-0.40	0.10
LU_ DF	1.37	4.77	2.62	0.69
LU_S	0.35	7.42	3.20	1.63
S_ GBPdz	-0.67	4.18	1.93	0.89
S_ BFS	-2.48	2.02	0.95	0.79
Geo_ SM	4.13	7.40	4.64	0.54
Slp	-7.85	0.11	-3.97	1.49
DisttoRoad	-5.01	-0.39	-1.81	1.06
S_ Collv	-26.20	-20.51	-23.32	1.46
SD_VS	-21.27	-16.31	-18.82	1.03
Elev	-14.20	-0.99	-6.63	3.34
Asp	-1.07	0.37	-0.06	0.39
DisttoStrm	-1.05	3.16	0.91	0.95
DisttoFault	-0.95	2.24	0.38	0.70

Table 3.11. Descriptive Statistics of GWR parameter estimations for slope unit-based mapping unit

Factor	Minimum	Maximum	Mean	Std. Deviation
Intercept	-12.01	113.64	22.08	26.54
LU_ DF	-136.06	-2.44	-35.80	31.21
LU_ F	-140.75	-1.87	-37.07	32.68
Geo_ C	-4.42	1.55	-0.79	0.96
Geo_ SM	1.04	8.25	3.43	1.32
S_ GBPdz	6.38	24.11	11.00	3.87
S_ BFS	1.10	17.52	6.91	3.89
S_ BFSWL	-1.45	21.54	6.33	5.33
DisttoStrm	-1.37	5.26	2.49	1.46
Veg	-7.26	4.14	-1.74	2.73
Slp	-5.58	10.23	-0.21	2.98
DisttoRoad	-5.96	6.41	1.44	3.31
Wtns	10.31	37.37	15.60	5.22

It is clear that the magnitude of the relationships between influencing variables and landslide occurrence, as well as the significance of them, vary over space. The variation of GWR parameters across the study area is mapped for each influencing factor. The maps are overlaid by the corresponding maps of t values for each parameter respectively. Then, by evaluating the t values that are higher or lower than the critical values at 0.05 significance level, the maps are obtained for each parameter. These maps present the significant regions, whereas they mask the insignificant regions. Therefore, the maps illustrate the variation of GWR parameters for significant regions. For instance, for grid-based mapping unit, the vegetation (Veg) map of the model indicates a negative propensity to landslide occurrences; however, the contribution of this variable to landslide occurrence is different throughout the study region, where the coefficient values range between -0.01 and -0.77. The negative contribution of Veg means that as the Veg increases, the landslide occurrence decreases, or vice versa. TheVeg values are not significant in the southern and northern parts of the region, for that reason those parts are masked. In the rest of the region, however, they are significant and the variation of Veg is mapped. The negative effect is lower for the eastern parts of the region and it increases across the centre part to the southern part of the region (Figure 3.67).

The LU_DF is insignificant in the eastern and south eastern parts of the region and significant in the rest of the region. It has a positive contribution to landslide occurrence, and the magnitude of the contribution to landslide varies over space (Figure 3.68). LU_DF shows a more positive relationship to the eastern and south-eastern parts of the study area, while the opposite relation occurs in the western and north-western parts of the region. Settlement (LU_S) is significant for the whole region and it shows a strong positive relation to landslide occurence around the center and along a strip running from the north-eastern and south–eastern parts of Kumluca watershed (Figure 3.69).

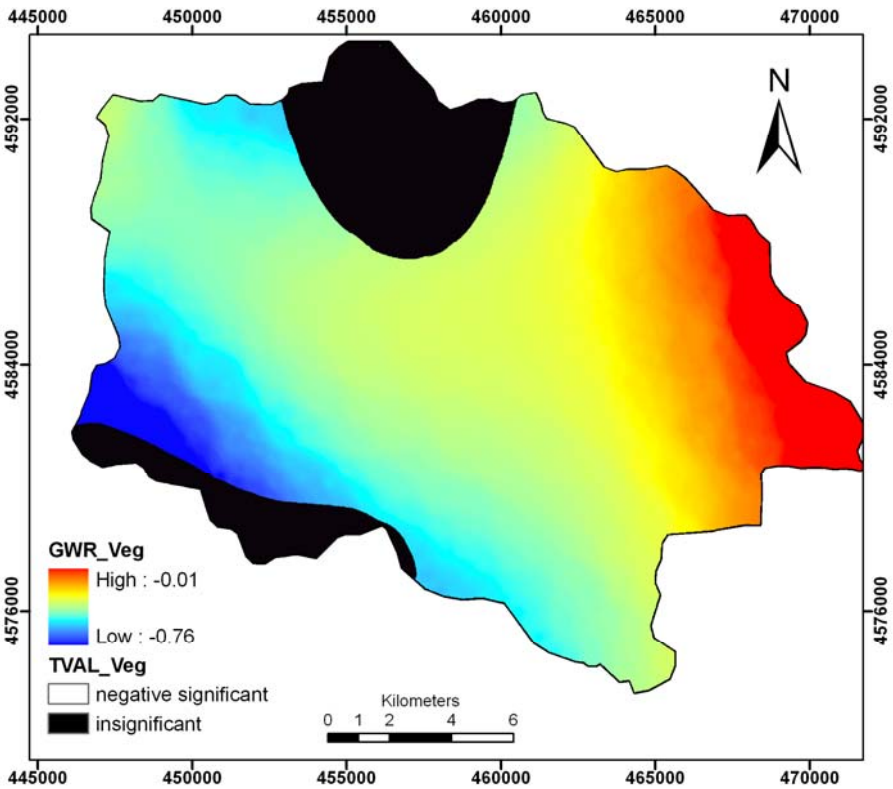

Figure 3.67. GWR parameter variation accross the study area for vegetation (Veg)

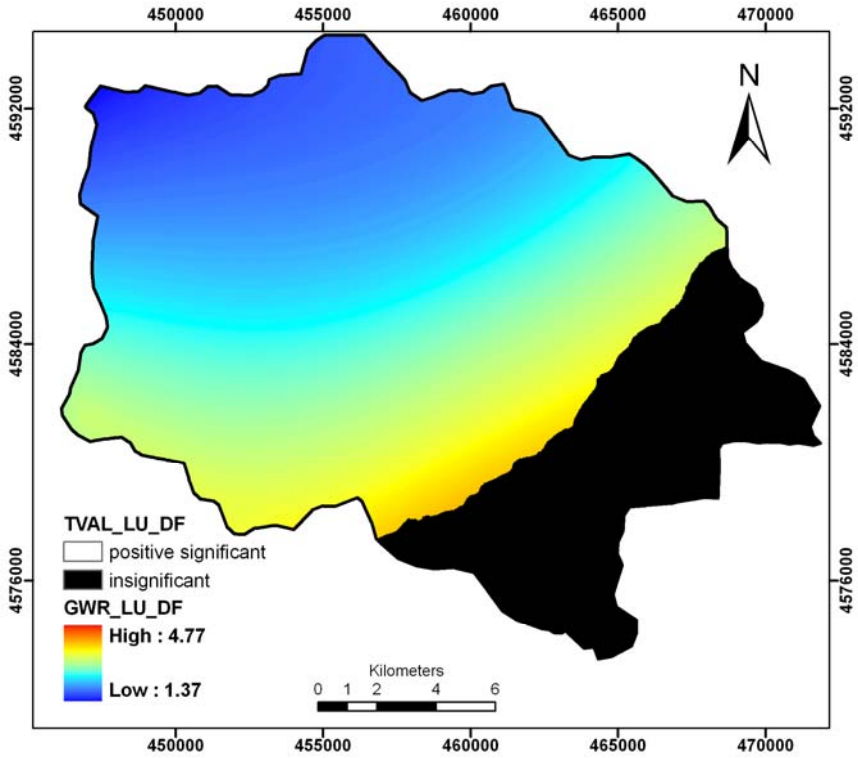

Figure 3.68. GWR parameter variation accross the study area for Land-Use Dry Farming (LU_DF)

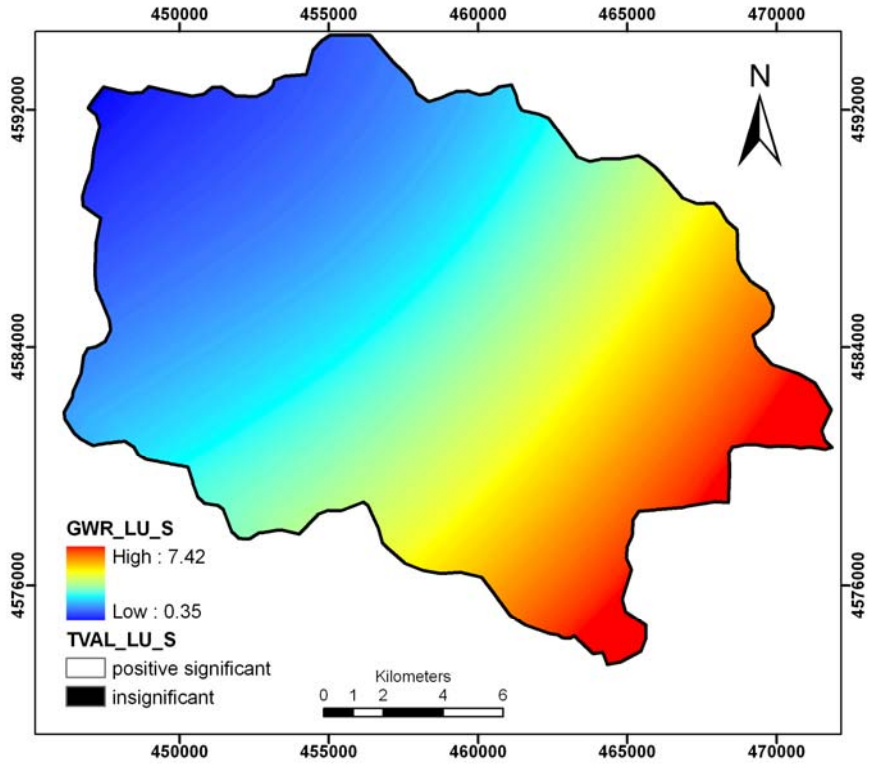

Figure 3.69. GWR parameter variation accross the study area for Land-Use Dry Settlement (LU_S)

Grey Brown Podzolic Soil (S_GBPdz) shows a strong positive relation to landslide occurence along the western part of the region and the magnitude of positive contribution to landslide occurence decreases around the centre. In the mean time, it shows a negative relation to landslide occurrence through the eastern part of the region (Figure B-1 in Appendix B). The parameters of Brown Forest soil (S_BFS) are negatively significant throughout the region and it indicates a positive statistical relationship to landslide occurrence in the western and south-western parts of the region, but a negative relation in the eastern and south-eastern parts of the region (Figure B-2 in Appendix B).

Sandstone-Mudstone unit of Geology (Geo_SM) is insignificant in the western part of the region and shows a strong positive relation to landslide occurrence around the center and the eastern part of the region. The magnitude of positive relation increases throughout the western part of the region (Figure B-3 in Appendix B). This positive affect can also be identified from the relationship evaluation of Geology with landslide occurrence described in section 3.3.1.2. This formation provides the highest correlation with landslide.

Slope (Slp) shows a negative significance throughout most of the study area, with the exception of the eastern part of the region. It has a high negative relationship to the western and north-western parts of the study area and the magnitude of negative significance decreases around the centre (Figure B-4 in Appendix B). Distance to Road (DisttoRoad) shows an insignificance along a strip running from north to south in the western part of the region. The parameters of DisttoRoad indicate a negative relation to landslide occurrence throughout the region. It has a stronger negative relationship to landslide occurrence in the western part; however, the negative relation decreases across the eastern part of the study area (Figure B-5).

Colluvial Soil (S_Colv) is negatively significant throughout the whole region. The parameters of S_Colv are of the greatest magnitude, indicating a stronger negative statistical relationship to landslide occurrence in the eastern part and the magnitude decreases across the western parts (Figure B-6 in Appendix B). Very shallow soil depth (SD_VS) is negatively significant throughout the whole region. It shows a strong negative relation to landslide occurrence across a curve-shaped region in the

northern part of the study area. The magnitude of negative relation decreases from the northern to the southern parts (Figure B-7 in Appendix B).

Topographical elevation (Elev) shows an insignificance around the south-western part of the region and a negative significance to the rest of the region. It has a strong negative relation to landslide occurrence around the eastern part of the region and the negative relation decreases around the center (Figure B-8 in Appendix B). The Aspect is negatively significant throughout the whole region. It shows a negative relation to landslide occurrence around the western and north-western parts of the region. However, it has a positive contribution to landslide occurrence in the eastern parts of the region (Figure B-9 in Appendix B).

The Distance to Stream (DisttoStrm) has a positive significance throughout the whole region. It shows a strong positive relation to landslide occurrence across the northern part of the region and the influence decreases around the centre. Additionally, it has a negative relation to landslide occurrence in the southern part of the study area (Figure B-10 in Appendix B). The Distance to Fault (DisttoFault) parameters are positively significant in most of the region except in the eastern part. It indicates a positive statistical relationship to landslide occurrence across an L-shaped region running from the western to the southeastern part of the study area. However, it has a negative relationship throughout the southern and northern parts (Figure B-11 in Appendix B).

For slope unit-based mapping unit, the Landuse Dry Farming (LU_DF) is insignificant in the eastern and southeastern parts of the region and it is significant in the rest of the region (Figure B-12 in Appendix B). It has a negative contribution to landslide occurrence and the magnitude of the contribution to landslides varies over space. The negative contribution is higher along a strip running to the south of Kumluca. The negative contribution is lower in the northern parts. Forest (LU_F) shows a negative significance throughout most of the study area, with the exception of the eastern part of the region. It has a high negative relationship in the west and north-west of the study area and the magnitude of negative significance decreases around the centre (Figure B-13 in Appendix B).

The Conglomerate unit of Geology (Geo_C) indicates a negative significance

throughout the study area, with the exception of the eastern part of the region. It has a high negative relationship to the south-western part and the magnitude of negative significance decreases around the rest of the region and in the centre (Figure B-14 in Appendix B). The parameters of Sandstone-Mudstone unit of geology (Geo_SM) indicate a positive significance throughout the region. It has a stronger positive relationship to landslide occurrence in the south-eastern part; however, the positive relation decreases from the centre to the western and south-western parts of the study area (Figure B-15 in Appendix B).

The Grey Brown Podzolic Soil (S_GBPdz) indicates a positive significance throughout the study area, with the exception of the south-eastern part of the region. It has a high positive relationship across the cetre and the north-western part of the region (Figure B-16 in Appendix B). The Brown forest soil (S_BFS) shows a positive significance throughout most of the study area, with the exception of the south-eastern part of the region. It has a high positive relationship in the eastern and south-eastern parts of the study area and the magnitude of negative significance decreases in the western and north-western parts of the region (Figure B-17 in Appendix B).

The brown forest soil without lime (S_BFSWL) is negatively significant throughout the whole region except in the L-shaped region running from the north-eastern to the south-eastern part of the study area. It shows little negative relation to landslide occurrence around the western part of the region. However, it has a positive cotribution to landslide occurrence in the eastern parts of the region and in the southern and south-western parts around the centre of Kumluca (Figure B-18 in Appendix B). The distance to stream network (DisttoStrm) is insignificant in the eastern part of the region and significant in the rest of the region. It has a negative relation with landslide occurrence in the eastern part; however, it has a positive contribution to landslide occurrence in the western parts. The positive influence increases from the northern to the southern part (Figure B-19 in Appendix B).

The vegetation (Veg) is insignificant in the south-eastern part of the region and it is significant in the rest of the region. It has a negative relation with landslide occurrence in the southern part; however, it has a positive contribution to landslide

occurrence in the northern parts (Figure B-20 in Appendix B). The parameters of Slope (Slp) are negatively significant throughout the whole region. It indicates a positive statistical relationship to landslide occurrence into the south-eastern part of the region, but a negative relation to landslide occurrence in the western and south-western parts of the region (Figure B-21 in Appendix B).

The distance to road network (DisttoRoad) is insignificant in the south-eastern part of the region and significant in the rest of the region. It has a negative relation with landslide occurrence in the western and southern part; however, it has a positive contribution to landslide occurrence around the centre (Figure B-22). The parameters of topographic wetness index (Wtns) are positively significant throughout the whole region. It indicates a positive statistical relationship to landslide occurrence around the center and along a strip running from east to west in Kumluca. The positive contribution increases in the south-eastern and north-western parts of the region (Figure B-23).

3.3.4.5 Performance Testing and Accuracy Assessment for Susceptibility Assessment Models

After obtaining the prediction maps, the most essential component is to carry out a validation analysis. Without any validation process, the prediction models and the maps obtained are totally useless and have hardly any scientific significance (Chung and Fabbri, 2003). Thus, for validation of the models, the past landslides were partitioned into two subsets. The first subset of data was used for obtaining the prediction maps by using the models; the second subset was used as the test data and compared with the prediction results for validation and to interpret the differences in the performance.

The distribution of past landslides over the entire study area was presented in Figure 3.70. A space-partition technique was used to divide the entire study area into two separated subareas (TEST_LS and TRAIN_LS). For the generation of the first subset, 20% from all dormant landslides was selected randomly. To consider the physical properties of each landslide region, they were not partitioned into grid cells before the selection. The second subset of landslides was composed of active and

inactive landslides and was used for modeling. The spatial distribution of the testing and training data assessment is shown in Figure 3.70.

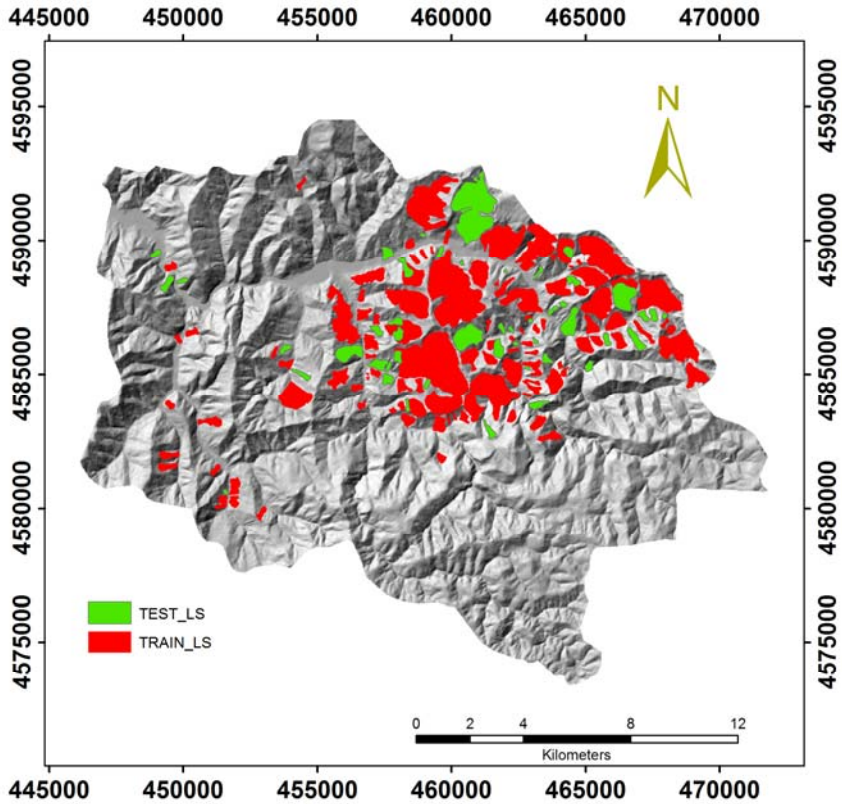

Figure 3.70. Spatial distribution of testing (TEST_LS) and training (TRAIN_LS) landslide inventory data

The relative operating characteristics (ROC) curve was used to compare the predictive abilities of SR, LR, ANN, and GWR models for both grid and slope unit-based mapping units. The first subset of data was used for obtaining the prediction maps and the second subset was used for validating the model results. The second subset of data was compared with LR, SR ANN, and GWR prediction results for accuracy analysis by using the ROC curve. The ROC curves illustrate how well the models predict a landslide. The plot of the curves offers an excellent visual comparison of the models' performances (Yeşilnacar and Topal, 2005). The further the curve lies above the reference line, the more accurate the test becomes. If the ROC value is 1, it indicates a perfect fit, whereas ROC equal to 0.5 shows a random fit. Sensitivity is the probability that a "positive" case is correctly classified, and is plotted on the y-axis in an ROC curve. Specificity is the probability that a "negative"

case is correctly classified. The ROC curves for the developed models are given in Figure 3.71. Based on their distances from the reference line, it can be concluded that all the models display a good performance for predicting landslide occurrences.

For the grid-based mapping unit, the local methods of GWR and SR models show a higher predictive performance than the global models. The LR model provides a higher performance than the ANN. It is very difficult to say that the SR or the GWR model is better than each other. For this reason, it is better to analyze the numerical summary of the area under the curve. Table 3.12 indicates that the asymptomatic significance of each model is less than 0.05, so all are doing better than guessing. From the confidence intervals, it can be seen that GWR model prediction is comparatively higher than all the other models with a value of 0.80. Secondly, the SR shows the highest performance with a value of 0.77. LR and ANN provide the predictive ability value of 0.74 and 0.72 respectively. As a result, we can say that incorporation of spatial correlation in parameters into the analysis increases the performance of the susceptibility mapping.

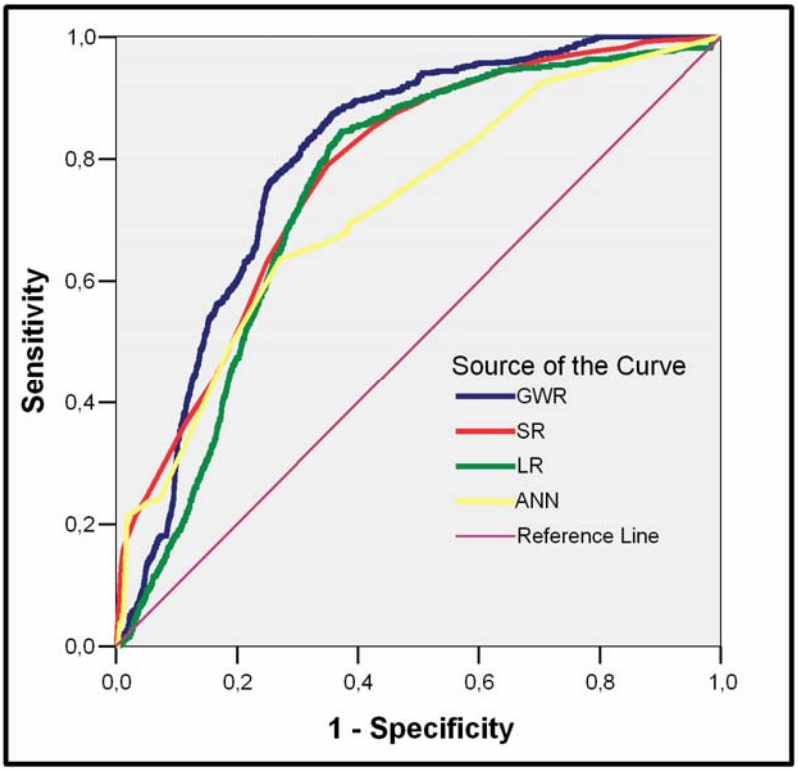

Figure 3.71. Prediction accuracy assessment of models by using ROC curve

Table 3.12. Area under the curve for grid-based mapping unit

Variable(s)	Area	Std. Error(a)	Asymptotic Sig.(b)	Asymptotic 95% Confidence Interval	
				Lower Bound	Upper Bound
GWR	.799	.006	.000	.787	.811
SR	.774	.007	.000	.760	.788
LR	.744	.007	.000	.730	.758
ANN	.718	.009	.000	.700	.736

For slope unit-based mapping unit, by the visual comparison of the models it can be clearly identified that the local model GWR provide a better performance than the global models as SR, LR, and ANN. When the global models are compared, the SR model provides better model performance than the LR model. Also the ANN has a better performance than the LR. The worst prediction performance belongs to the LR model. The asymptotic significance of each model is less than 0.05, so all are doing better than guessing (Figure 3.72).

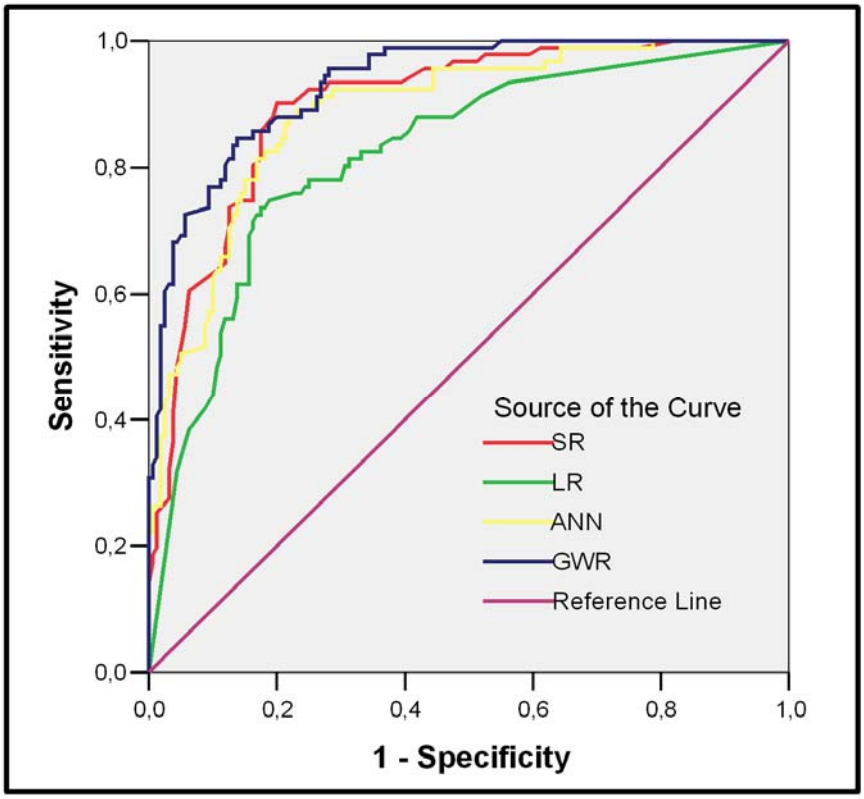

Figure 3.72. Predictive performance of different susceptibility methods for slope unit-based mapping unit

From the confidence intervals, it can be recognized that the LR model predictions are worse than the other (SR, ANN, and GWR) models because the entirety of their intervals lies below the SR, ANN and GWR models. It can be concluded that the models SR (0.90) and GWR (0.93), and ANN (0.89) provide the highest predictive ability compared to the LR (0.82) (Table 3.13). Additionally, the local model (GWR) provides better predictive ability for the study region compared to the global models (LR, SR, and ANN) by obtaining the largest area under the curve.

Table 3.13. Area under the curve for slope-based mapping unit

Test Result Variable(s)	Area	Std. Error(a)	Asymptotic Sig.(b)	Asymptotic 95% Confidence Interval	
				Lower Bound	Upper Bound
SR	.898	.020	.000	.859	.937
LR	.820	.028	.000	.766	.875
GWR	.932	.015	.000	.903	.961
ANN	.888	.021	.000	.846	.929

3.3.4.6 Field Evaluation of Landslide Susceptibility Maps

The landslide susceptibility classes for each method were also evaluated by field surveys. In the study region there exists 28 villages and approximately 18 villages were visited to evaluate the landslide susceptibility, and then the ground truth was compared with the model results. The susceptibility of the slopes was evaluated based on expert opinion. Depending on expert experiments, the evaluated slopes were rated from the first to the third degree, where the first degree indicates highly susceptible slope and the third degree indicates the low susceptible slope. The evaluation considers the observed morphology, the geologic structure, activity, and extends of the landslide. Figure 3.73 is an illustration of a region evaluated with first degree of susceptibility in the field surveys. In this case, some deformations can be observed on the housedue to the movement of the surface. The ground truth data was surveyed by using both the DGPS and Magellan Hand GPS. DGPS has horizontal accuracy lower than dm and Magellan Hand GPS has ±3 m. accuracy. As a result of the field surveys Figure 3.74a illustrates the region which are observed to have high degree of susceptibility, which are displayed with the label “H” on the map.

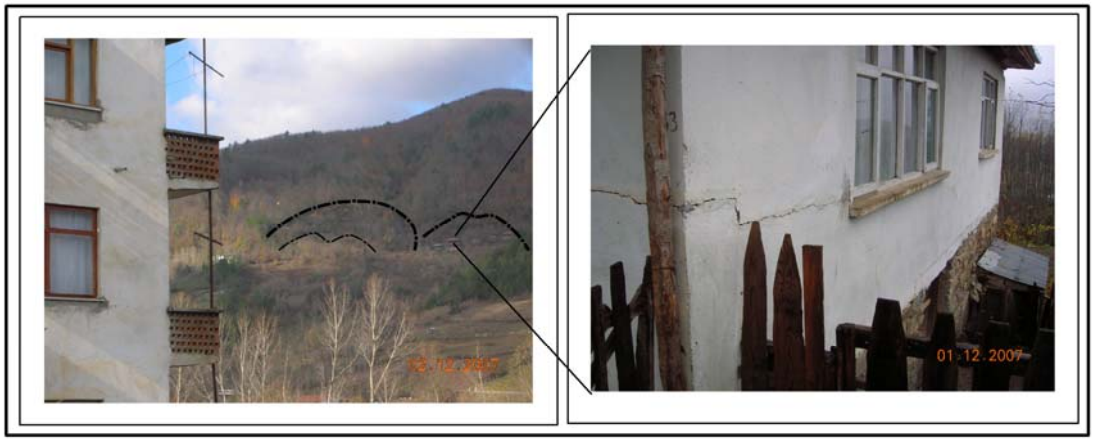

Figure 3.73. Konuklu village showing first degree of risk where the terrain show a clear movement with some indicators as house cracks

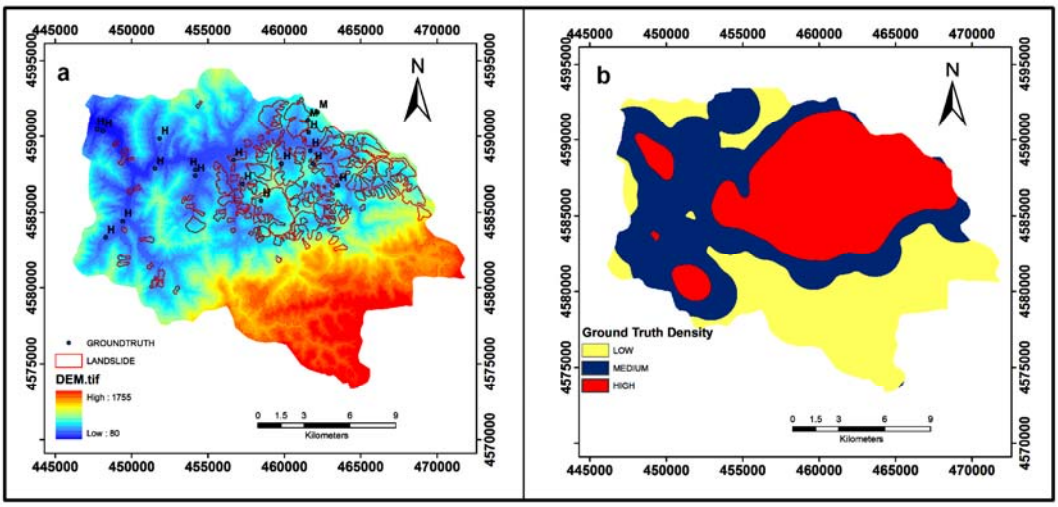

Figure 3.74. a. Ground truth data represented with ”H” was overlaid to the DEM of the study region and existing landslide location b. The density map of the ground truth observed through field surveys with the landslide polygons obtained from MTA.

The ground truth data was overlaid by landslide polygon data, which was acquired from MTA. Figure 3.74a indicates that some slopes in the south-western part of the regions which have high susceptibility were not mapped by MTA. Hence, the slopes which were observed to be highly susceptible through field surveys were merged by the landslide polygon and a database was constructed to be used for the evaluation of model performance. The performance evaluation was done by the computation of

error matrix, which was obtained by the overlay of density map and prediction models. As a result of this error matrix, the obtained overall accuracy and kappa coefficients were evaluated and compared for reliability purposes (Table 3.14).

Table 3.14. Error Matrix resulting from the Model prediction classification

	MODEL		H	M	L	Row Total	Producers Accuracy	Users Accuracy	Overall Accuracy	Kappa
Grid-based Mapping Unit	LR	H	93626	12193	95	105914	0.35	0.88	0.50	0.25
		M	109673	59554	11285	180512	0.21	0.33		
		L	65010	209320	249239	523569	0.96	0.48		
		Column Total	268309	281067	260619	809995				
	SR	H	122829	24082	787	147698	0.46	0.83	0.55	0.33
		M	117987	132893	67864	318744	0.47	0.42		
		L	27493	124092	191968	343553	0.74	0.56		
		Column Total	268309	281067	260619	809995				
	ANN	H	89698	12093	163	101954	0.33	0.88	0.46	0.19
		M	102124	78039	54890	235053	0.28	0.33		
		L	76487	190935	205566	472988	0.79	0.43		
		Column Total	268309	281067	260619	809995				
	GWR	H	169686	17157	753	187596	0.63	0.90	0.61	0.43
		M	65863	88410	20014	174287	0.31	0.51		
		L	32760	175500	239852	448112	0.92	0.54		
		Column Total	268309	281067	260619	809995				
Slope Unit-based Mapping Unit	SR	H	64	36	5	105	0.69	0.61	0.55	0.34
		M	12	20	7	39	0.22	0.51		
		L	17	35	55	107	0.82	0.51		
		Column Total	93	91	67	251				
	LR	H	51	30	10	91	0.55	0.56	0.45	0.20
		M	10	10	4	24	0.11	0.42		
		L	32	51	53	136	0.79	0.39		
		Column Total	93	91	67	251				
	GWR	H	57	25	4	86	0.61	0.66	0.57	0.37
		M	8	26	3	37	0.29	0.70		
		L	28	40	60	128	0.90	0.47		
		Column Total	93	91	67	251				
	ANN	H	60	22	11	93	0.65	0.65	0.53	0.30
		M	18	34	16	68	0.37	0.50		
		L	15	35	40	90	0.60	0.44		
		Column Total	93	91	67	251				

Descriptive measures such as overall accuracy (Eq. 46) were computed by dividing the total number of correctly classified pixels by the total number of reference pixels. The accuracy of individual categories can also be calculated by dividing the number of correctly classified pixels in each category by either the total number of pixels in the corresponding row or column, which is called producers and users accuracy respectively. Overall accuracy does not include the errors of omission and commission (nondiagonal elements) but only include data along the major diagonal. On the other hand, kappa coefficient (Eq. 47) includes both values, which are desirable for computation and analysis.

$$\textbf{Overall Accuracy}=\frac{\sum_{i=1}^{r} x_{ii}}{N} \tag{46}$$

$$\textbf{Kappa=k}=\frac{N\sum_{i=1}^{r} x_{ii} - \sum_{i=1}^{r}(x_{i+} * x_{+i})}{N^2 - \sum_{i=1}^{r}(x_{i+} * x_{+i})} \tag{47}$$

Where;

r=the number of rows in the error matrix

x_{ii}=the number of observations in row i and column i (on the major diagonal)

x_{i+}=the total of observations in row i (shown as marginal total on the right of the matrix)

x_{+i}= the total of observations in column i (shown as marginal total at the bottom of the matrix)

N=the total number of observations included in matrix

The overall accuracy of the LR is 50%; however, the producer's accuracy ranges between 21 and 96 %. Depending on the controls in the study region and depending on the accuracy assessment by kappa and overall accuracy assessment (Figure 3.75), the SR method with grid-based mapping unit shows a better predictive performance compared to the other global prediction models. Furthermore, the local model GWR, provide the highest predictive ability compared to the global models (LR, SR, ANN) for both grid and slope unit-based mapping unit.

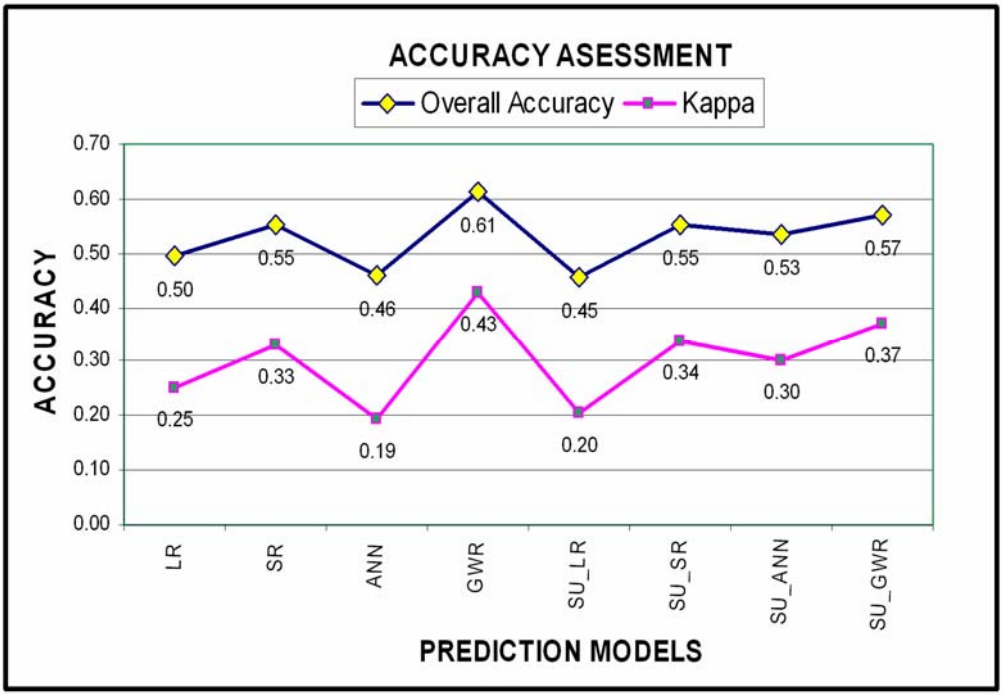

Figure 3.75. Accuracy assessment of the prediction models by kappa and overall accuracy

3.4 Comparison of Susceptibility Maps

The realization of four different models with the help of LR, SR, ANN, and GWR and two different mapping units, grid and slope unit-based mapping units, led to the production of eight different landslide susceptibility maps. The graphical display of each prediction map proved to be rather a useful tool in assessing and portraying the degree of susceptibility to slope instability in a systematic and standardized way (Carrara, 1983). Notwithstanding, each model has a different theoretical basis, which may cause to bring about different prediction values for the same region. Therefore, they should be compared in order to evaluate the susceptibility model and mapping unit differences in the resultant risk maps.

While the models were conducted using different statistical applications, they were mapped in GIS environment by using raster calculations. The landslide susceptibility maps were produced in a continuous scale where the numerical values lie between 0 and 1. For interpretation of maps from the end users for decision purposes and for comparison purposes, it is more suitable to change the susceptibility maps from continuous scale into categorical classes by the defined cutoff values (class

boundaries). If the data is known well, then the classes can be defined manually. However, for comparison purposes it is important to use the same class boundaries or the similar classification scheme for each map in order to avoid misleading results. It is not an easy task to categorize continuous data automatically as there are not any estimated methods. In most studies, authors use their expert opinion to develop class boundaries. In this thesis, four systems of classifiers were taken into consideration for the comparison of susceptibility maps. On the other hand, for the comparison of risk maps, class boundaries are defined by expert opinion. It is because economical values were obtained with monetary terms in risk maps. Hence, the high and low class boundaries can be evaluated and determined, whereas for susceptibility maps, the data is in the range of 0 and 1 and predetermining which features are grouped together is a difficult task. The selection should depend on the characteristics of the histograms showing intervals between numerical values. Hence, for the classification of susceptibility maps, the so-called standard deviations, equal intervals, quantiles, natural breaks, and were considered and the one that best suits the objectives of the study was chosen (Ayalew et al., 2004). Changing the classes can create quite different-looking maps; therefore, it is critical to select the best scheme.

The standard deviation classification scheme shows how much a feature's attribute value varies from the mean. The class breaks are created after calculation of the mean and the standard deviations from the mean values. This scheme may be suitable for visualization but not appropriate for comparison purposes, because class intervals may vary depending on the data set used. The classification scheme that relies on the equal interval divides the range of attribute values into equal-sized sub ranges by allowing the user to specify the number of intervals. This method emphasizes the amount of susceptibility value relative to other values, hence it is not found to be practical for the analysis. In quantile classification, each class contains an equal number of features. This classification may result in putting widely different values into the same class or placing the similar features to adjacent classes. Due to this adverse effect, this method was not used in the analysis. Lastly, the natural break relies on the division of data based on natural groupings inherent in the data. The classification scheme identifies break points by picking the class breaks that best group similar values and maximize the differences between classes (Arcmap 9.1, 2009). Susceptibility maps are mostly multinominal and may show intervals between

numerical values. Therefore, the natural break classification scheme was selected for the division of features into classes. Based on this method, three susceptibility classes were distinguished as low, medium, and high for different models (LR, SR, ANN and GWR) and mapping units (grid and slope unit-based mapping unit).

According to the LR-based susceptibility map for grid-based mapping unit (LR_GRD_SUSCP), 13% of the study region lies in the high susceptibility zone. 22% and 65% of the study region are in the medium and low susceptibility zones respectively (Figure 3.76). For the LR-based susceptibility map for slope unit-based mapping unit (LR_SU_SUSCP), it was found that 36% of the study region lies in the high susceptibility zone. 9% and 55% of the study region are in the medium and low susceptibility zones respectively (Figure 3.77). Therefore, it can be concluded that the slope unit-based susceptibility map has much more susceptible regions than the grid-based susceptibility map. This is mainly due to the higher amount of generalization in slope unit-based mapping unit.

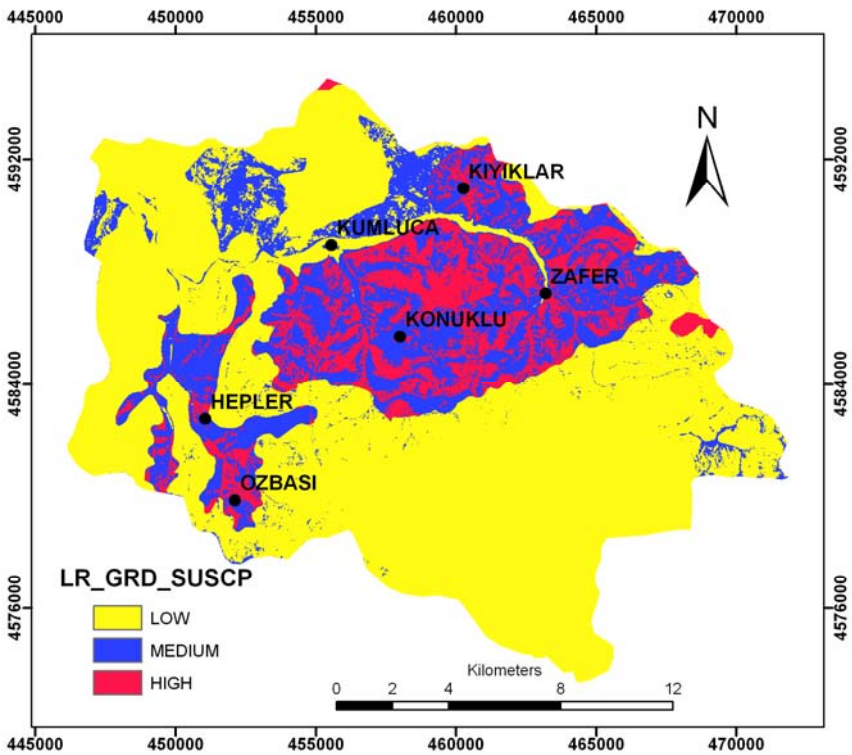

Figure 3.76. The classified LR Model prediction map created for landslide susceptibility for grid-based mapping unit (LR_GRD_SUSCP)

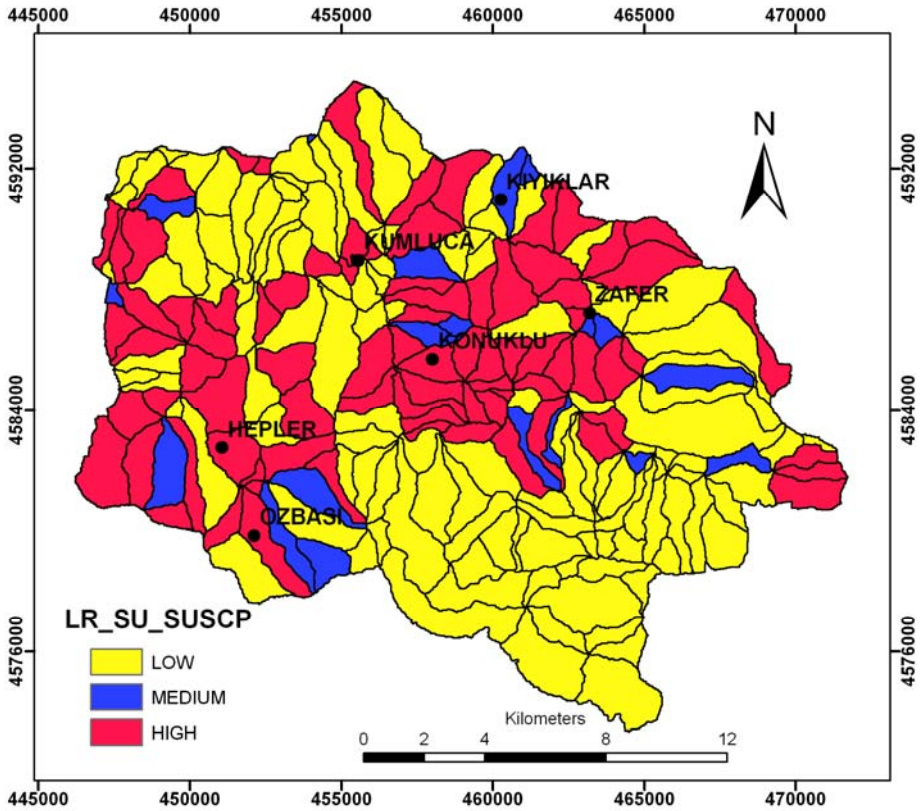

Figure 3.77. The classified LR Model prediction map created for landslide susceptibility for slope unit-based mapping unit (LR_SU_SUSCP)

When the SR model for susceptibility mapping for grid-based mapping unit (SR_GRD_SUSCP) is considered, 18% of the total area is found to be highly susceptible. Low and medium susceptibility zones constitute 42% and 39% of the area respectively (Figure 3.78). Furthermore, the SR-based susceptibility map for slope unit-based mapping unit (SR_SU_SUSCP) illustrates that 40% of the study region lies in the high susceptibility zone and 16% and 44% of the study region are in the medium and low susceptibility zones respectively (Figure 3.79).

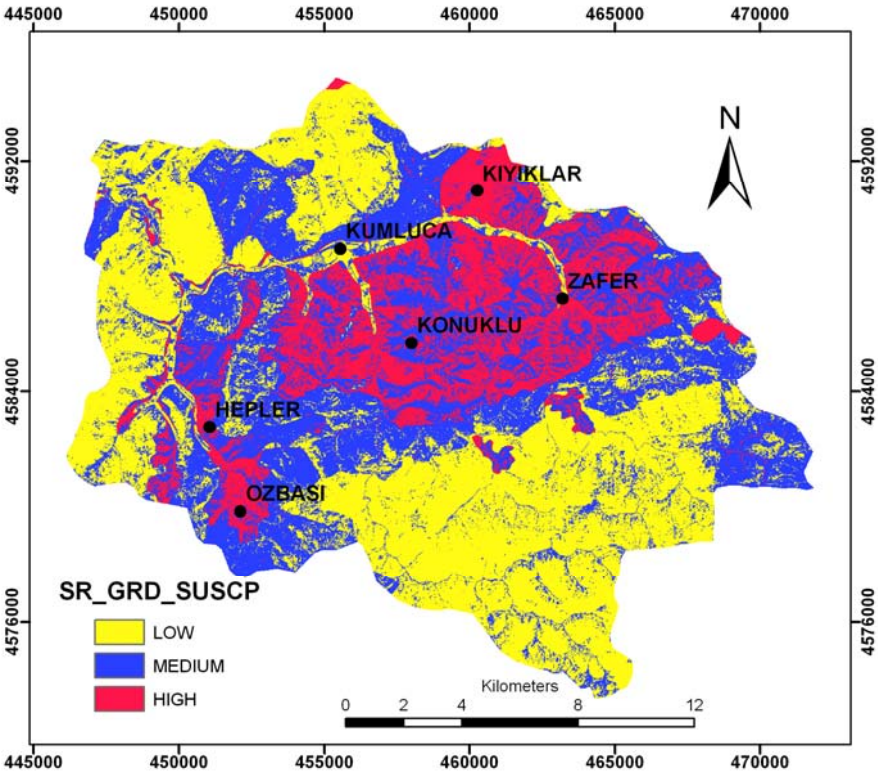

Figure 3.78. The classified SR model prediction map created for landslide susceptibility for grid-based mapping unit SR_GRD_SUSCP)

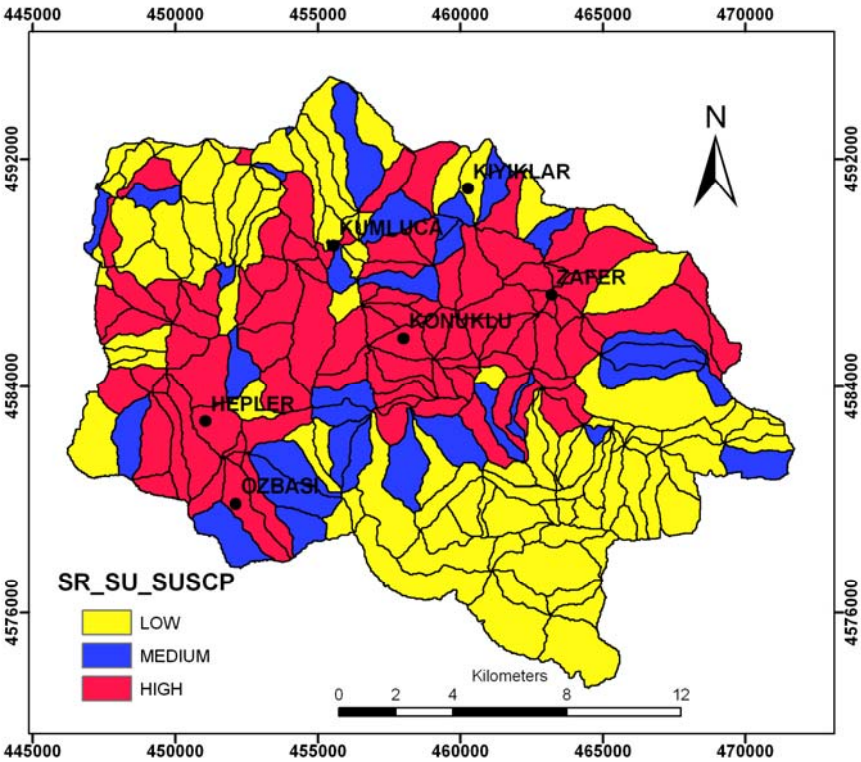

Figure 3.79. The classified SR model prediction map created for landslide susceptibility for slope unit-based mapping unit SR_SU_SUSCP)

The prediction results derived from the ANN-based susceptibility map for grid-based mapping unit (ANN_GRD_SUSCP) (Figure 3.80) and ANN-based susceptibility map for slope unit-based mapping unit (ANN_SU_SUSCP) (Figure 3.81) show that 13% and 37% of the region fall into high susceptibility class respectively, which means that more areas are designated to be in highly susceptible zones by ANN_SU_SUSCP. Additionally, 29% and 24% of the region were classified as medium, and 58% and 39% of the map were classified as low in the ANN_GRD_SUSCP and ANN_SU_SUSCP maps respectively.

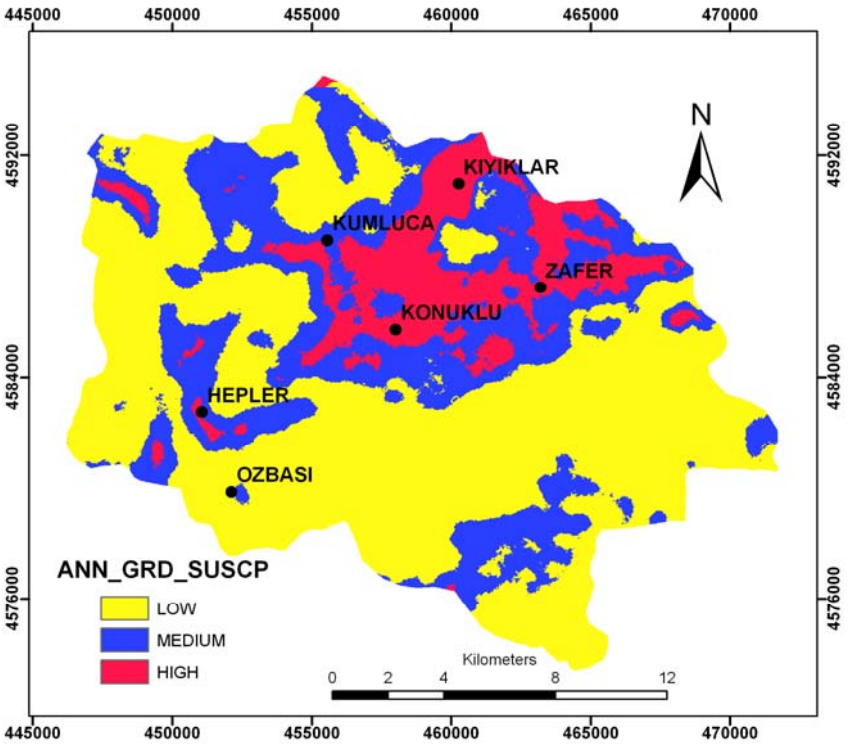

Figure 3.80. The classified ANN model prediction map created for landslide susceptibility for grid-based mapping unit (ANN_GRD_SUSCP)

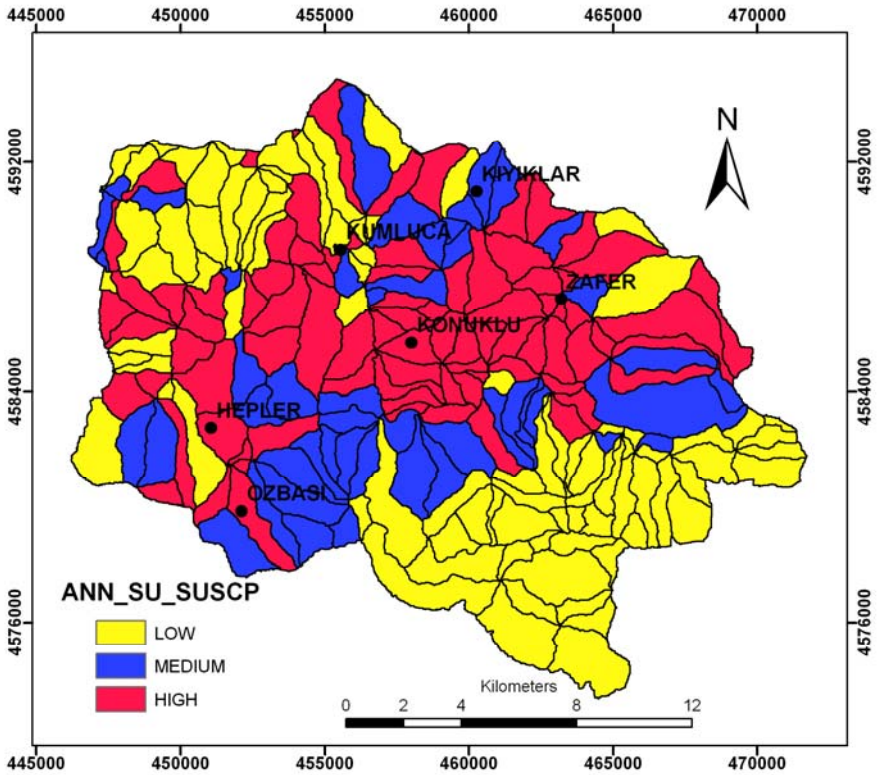

Figure 3.81. The classified ANN model prediction map created for landslide susceptibility for slope unit-based mapping unit (ANN_SU_SUSCP)

Eventually, the GWR model for slope and grid-based mapping unit was categorized. As shown in GWR-based susceptibility map for grid-based mapping unit (GWR_GRD_SUSCP) (Figure 3.82), 23% of the study area was designated to be extremely susceptible. The zones which have low and medium levels of susceptibility make up 22% and 55% of the region respectively. Correspondingly, the GWR-based susceptibility map for slope unit-based mapping unit (GWR_SU_SUSCP) (Figure 3.83) indicates high susceptibility to landslide with 31% of the region and medium and low susceptibility to landslide with 15% and 54% respectively.

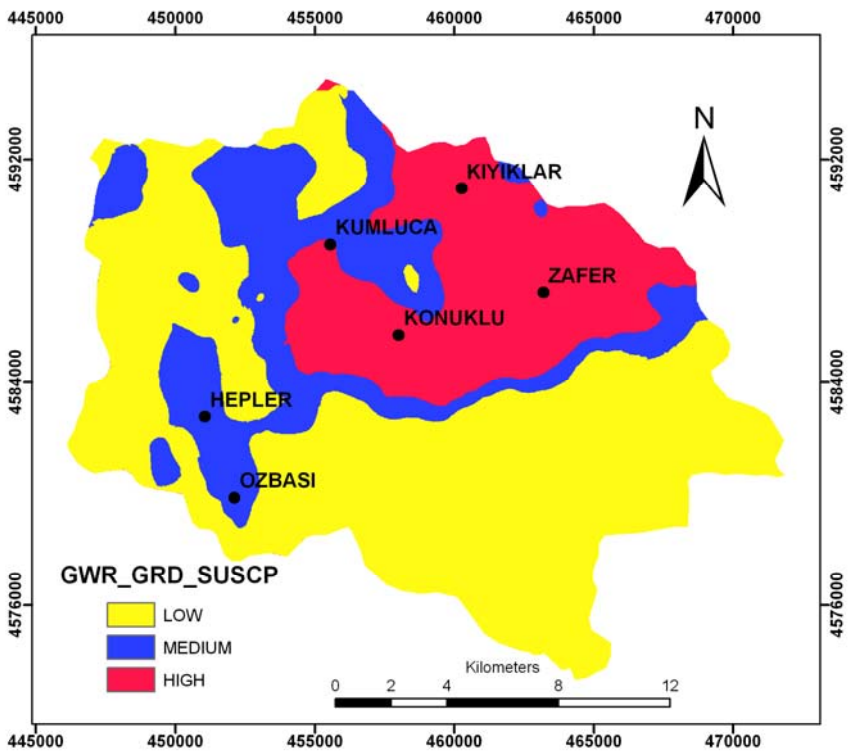

Figure 3.82. The classified GWR model prediction map created for landslide susceptibility for grid-based mapping unit (GWR_GRD_SUSCP)

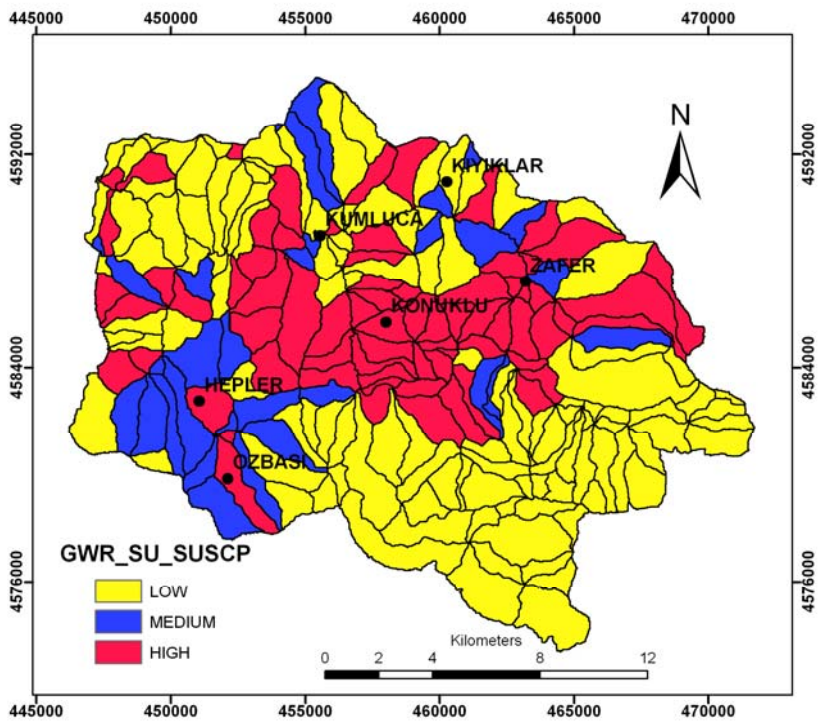

Figure 3.83. The classified GWR model prediction map created for landslide susceptibility for slope unit-based mapping unit (GWR_SU_SUSCP)

The resultant maps are sensitive to the selected susceptibility model and mapping unit. Each map may estimate the susceptibility differently depending on the adopted algorithm. Therefore, in order to see the trends in the estimated values for different categories, the whole picture is illustrated with the help of a bar graphic (Figure 3.84).

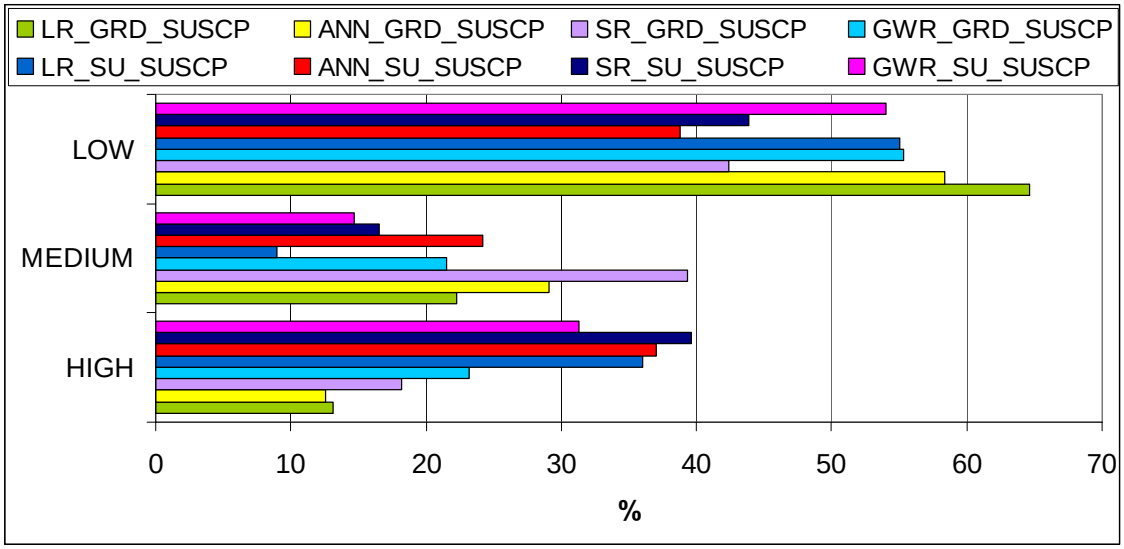

Figure 3.84 Evaluation of grid and slope unit-based models for different classes

When the mapping unit is considered, it can be concluded that the slope unit-based models have a tendency to represent larger percentages of the region which are highly susceptible to landslide when compared to grid-based models. This result is proved by the bar graphic illustrated in Figure 3.85. This might be the result of the adopted procedure to assign the variables to the mapping units. In the grid-based mapping unit, a grid mesh is overlaid for each variable with the selected size. Then the attribute of each variable is assigned to each grid cell. On the other hand, for the slope unit case, each variable is overlaid with the slope unit map and then the variables are assigned to each slope unit by using zonal statistical functions which perform operations on a per-zone basis. Each unit in the slope map contains a variation of data values due to the large extend of the unit. Hence, by using the zonal statistics, the variation of data is reduced to a single value, which may normally cause the smoothing out of the local details and providing a large generalization of the variable values. As a result of this process, the models which have been adopted

for slope-based mapping unit might predict high percentages of high and low susceptibility values.

When the difference of model selection is considered, each model should be assessed individually (Figure 3.85). The models adopted by grid-based mapping unit indicate that the LR, ANN, and SR have an increasing trend from high to low susceptibility. In the mean time, the histogram that belongs to the GWR is negatively skewed, indicating that more areas will fall into the low susceptible zone. The GWR and SR models, in which the spatial autocorrelation among the regression parameters are taken into account, predict higher percentages of high categories compared to the LR and ANN. However, the LR and ANN models predict higher percentages of low categories compared to the SR and GWR.

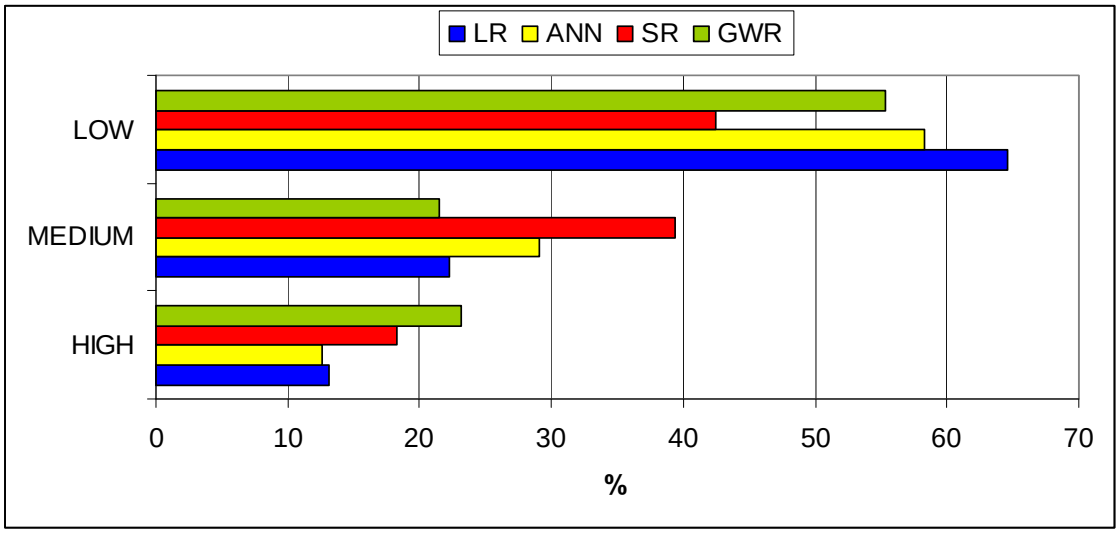

Figure 3.85. Evaluation of grid-based models for different classes

The models adopted by the slope unit-based mapping unit show that all models provide a similar distribution of values where the prediction values decrease in the medium class whereas they increase in the high and low classes. The LR model provides the highest percentages of low estimates like in the grid-based mapping unit. This may indicate the tendency of the LR model to estimate large regions of low susceptibility. Conversely, the SR model has a tendency to estimate large portions of the region at high susceptibility both in grid and slope unit-based mapping unit.

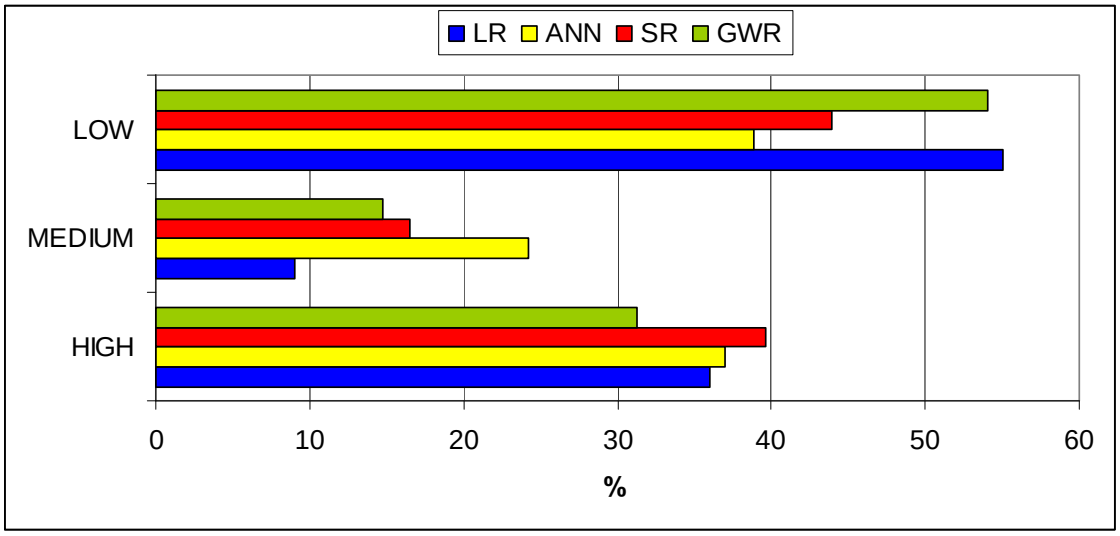

Figure 3.86. Evaluation of slope unit-based models for different classes

The results obtained from the evaluation of Figure 3.84, Figure 3.85 and Figure 3.86, provide a relative comparison of the prediction maps and the inclination of each map for different categories. In order to verify the obtained results and to decide on whether the tendency of each model is right or not, two different comparison approaches were followed. In the first approach, the eight susceptibility maps for all models and for both mapping units were compared by the historical landslide locations respectively. This approach puts forwards a viewpoint towards the evaluation of the quality of each model for the estimation of historical slide locations.

In the second approach, the similarities and dissimilarities of models were analyzed by simply overlaying each map respectively. This provides the ability to compare the maps spatially. By this way, the similarities and dissimilarities can be assessed in the spatial domain.

3.5 Relative Comparison of the Susceptibility Maps with the Landslide Map in terms of Accuracy

In order to verify the practicality of landslide susceptibility maps, each classified susceptibility map was compared with the landslide distribution map. This was done by calculating the landslide density for each class of susceptibility maps in each unit.

This computation was performed in the GIS environment by crossing the various classes of the LR, SR, ANN, and GWR susceptibility maps with the landslide distribution map for grid and slope unit-based mapping units. The results of the entire processes for grid and slope unit-based mappings are presented in the bar graphs in Figure 3.87 and Figure 3.88 respectively. In both histograms, the maps produced by different models follow a negatively skewed distribution where more areas fall into the high susceptible class after their classification into three levels of susceptibility by natural break algorithm.

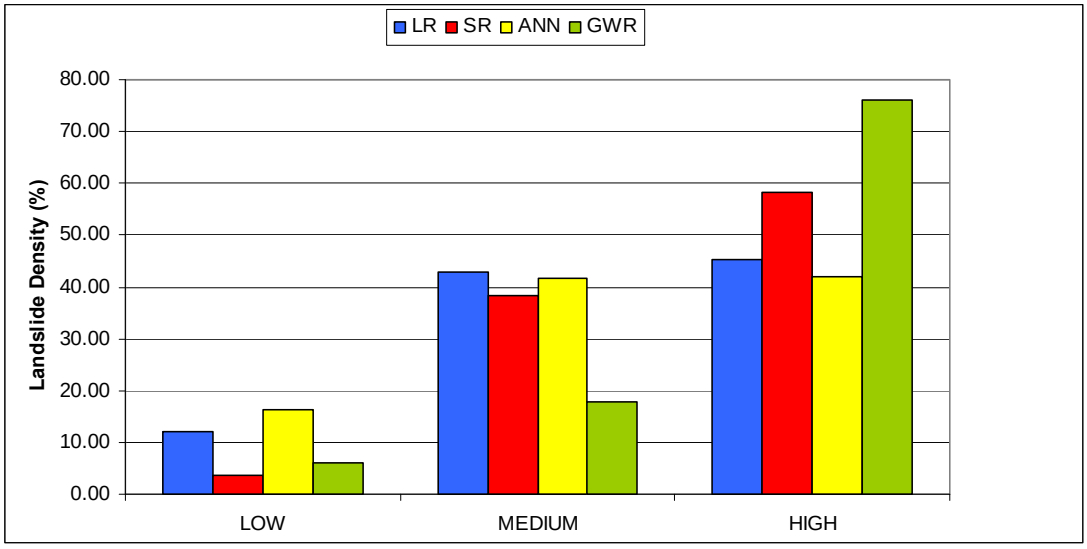

Figure 3.87. Bar graphs showing the relative distribution of landslide densities at various classes of the LR, SR, ANN, GWR susceptibility maps for grid-based mapping unit

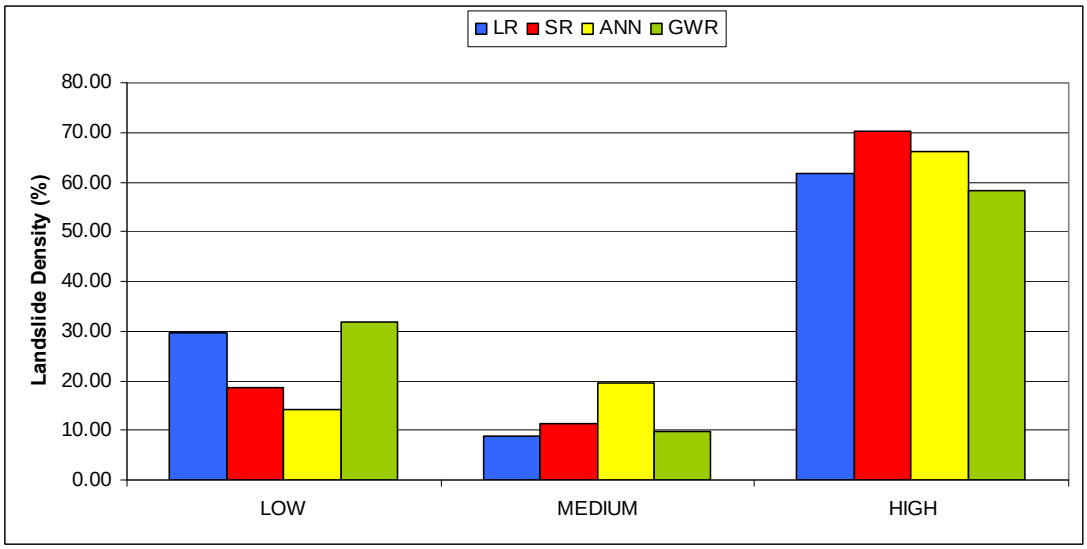

Figure 3.88. Bar graphs showing the relative distribution of landslide densities at each susceptibility level for slope unit-based mapping unit

In slope unit-based mapping unit, most of the landslide distributions fall into high susceptibility class for all maps. On the other hand, in grid-base mapping unit, most of the distributions match with the high and medium susceptibility classes to a large extend. This may indicate the success of prediction models in identifying landslide zones since for all models implemented in both mapping unit types most of the historical landslide locations are present at high and medium classes.

It becomes apparent that the landslide density shows variations on high susceptibility class in Figure 3.87, where the density values are higher in the GWR (76%) and SR (58%) map than in the LR (45%) and ANN (42%) for grid-based mapping unit. However, the landslide density has a similar distribution in the high susceptibility class in Figure 3.88 with LR (61%), SR (70%), ANN (66%) and GWR (59%) mapping methods for slope unit-based mapping unit.

The medium class has different landslide densities for both grid and slope unit-based mapping units. The landslide distribution on medium class for grid-based mapping units shows higher values compared to the slope unit-based mapping units. Contrary to this, the landslide distribution on low class for grid-based mapping unit is lower than the slope-based mapping unit. The total landslide distribution for grid and slope unit-based mapping unit on low class is 39% and 90% respectively.

The SR (3%) and GWR (6%) have the lowest landslide distribution when compared to the LR (12%) and ANN (16%) in the low susceptibility zone of grid-based mapping unit. Additionally, the ANN (14%) and SR (18%) have the lowest landslide distribution when compared to the LR (29%) and GWR (31%) in the low susceptibility zone of slope unit-based mapping unit. In both of the mapping unit types, the SR provides lower landslide distribution on low level of susceptibility classes. This may indicate that the performance of SR is better when compared to other methods for both mapping unit types.

Looking at Figure 3.87, it can be easily concluded that the high and medium susceptibility classes of the SR map together captured the locations of landslide zones (96%) better than the corresponding counterparts of the LR (87%), ANN (84%), and GWR (93%). Additionally, when the Figure 3.88 is evaluated in terms of

landslides, the SR map (82%) shows better estimation values, which is followed by the ANN (86%), than the LR (70%) and the GWR (68%) when both medium and high levels of susceptibility are considered. As a result, it can be concluded that the SR provides a better performance when compared to the other methods for both grid and slope unit-based mapping units. This might be due to the SR approach to take the spatial variations between variables as inputs. However, although the GWR considers the spatial variations between variables as well, it has a better performance in grid-based mapping unit, whereas it has a lower performance in the slope unit-based mapping unit type. This might be due to the fact that a grid-based mapping unit considers a mapping unit as smaller grid cells. In this case, the variation may increase, which may also increase the predictive ability of GWR. In slope unit-based mapping unit, on the other hand, each mapping unit is larger in size when compared to the grid cell. This results in the reduction of the variability in the data set because the value of each slope unit is obtained by generalization of several pixel values, which causes a reduction in the predictive ability of GWR.

3.5.1 Comparison of the Similarity between the Prediction Maps

By the application of different models such as LR, SR, ANN and GWR in different mapping units, a couple of maps were created. In addition to testing the performance of these maps, determining the similarity between these maps in an objective way is also important. However, in most of the analysis, the comparison of maps in an objective way is neglected, which is fundamental (Innovativegis, 2009). Visual comparison is mostly limited and subjective. For that reason in this thesis, the map similarities are analyzed with quantitative techniques.

Looking at the prediction maps which are illustrated in Figure 3.76, Figure 3.77, Figure 3.78, Figure 3.79, Figure 3.80, Figure 3.81, Figure 3.82, and Figure 3.83, it is difficult to identify the similarities or dissimilarities between the displays. To compare the similarities of the created maps, different methods are presented in the literature. One way is comparing the map similarity by the application of non-spatial statistical tests such as T test or F test. Another way is the computation of "differences" between maps for each cell unit or slope unit, which also provide a

viewpoint to determine the spatial distribution of differences.

In the first step, the models are compared quantitatively by statistical tests for each mapping unit to test whether the data are significantly different (Berry, 1999). To compare the maps quantitatively, the data set was prepared for the analysis. For that reason, the maps in GIS were exported to be analyzed in the statistical package. Statistical random sampling, specified administrative zones, or inferred spatial groupings are some kind of the methods that can be used to determine the data for comparison analysis and for the cell unit map analysis. In this study, the random sampling and zoning method were combined to be used for the cell unit map comparisons. 10,000 units are identified randomly from high, medium, and low susceptible zones, whereas, for the slope unit map comparison, all data were used for the analysis.

T test was used in the analysis of map similarity. The Paired-Samples T Test procedure was used to test the hypothesis that there is no difference between two variables. Pairs of models were used for the comparison analysis. The procedure produces the Pearson correlation between each pair and also its significance and a confidence interval for the average difference (95%). The Pearson correlation between the SR_GWR, SR_ANN, LR_SR, LR_GWR, LR_ANN, and ANN_GWR shows that the correlation between pairs of models at cell and slope unit-based models are significant (Table 3.15).

Table 3.15. Paired samples correlations for cell-based and slope unit-based model pairs

	Cell based models		Slope Unit based models	
Model Pairs	Correlation	Sig.	Correlation	Sig.
SR_GWR	.638	.000	.634	.000
SR_LR	.809	.000	.806	.000
SR_ANN	.573	.000	.571	.000
LR_GWR	.663	.000	.668	.000
LR_ANN	.648	.000	.652	.000
ANN_GWR	.714	.000	.718	.000

The paired-samples t test table displays the average difference between all map pairs (Table 3.16). The Std. Dev. column displays the standard deviation of the average difference score. The Std. Error Mean column provides an index of the variability

one can expect in repeated random samples. 95% confidence interval of the difference provides an estimate of the boundaries between which the true mean difference lies in 95% of all possible random samples. The t statistic was obtained by dividing the mean difference by its standard error. The Sig. (2-tailed) column displays the probability of obtaining a t-statistic whose absolute value is equal to or greater than the obtained t-statistic.

The H_0 hypotesis, which indicates "the maps created with different model pairs are similar", is accepted if the p value or significance is greater than 0.05, otherwise it is not accepted. As a result of the t test presented in Table 3.16, it can be concluded that for both cell and slope unit maps the SR_GWR and LR_ANN pairs are similar. This may be due to the fact that the SR model considers the spatial correlation between parameters as in GWR. Therefore, SR resembles local models more compared to the other global models of LR and ANN. On the other hand, LR and ANN, which do not include the spatial variation of parameters, resemble each other more.

Table 3.16. Paired samples test

Model Pairs				**95% Confidence Interval of the Difference**				
Cell Unit	**Mean**	**Std. Deviation**	**Std. Error Mean**	**Lower**	**Upper**	**t**	**df**	**Sig. (2-tailed)**
SR_GWR	-.040	.741	.074	-.188	.107	-.542	98	.589
SR _LR	.242	.517	.052	.139	.346	4.667	98	.000
SR_ANN	.162	.765	.077	.009	.314	2.101	98	.038
LR_GWR	.283	.715	.072	.140	.425	3.937	98	.000
LR_ANN	-.081	.695	.070	-.219	.058	-1.157	98	.250
ANN_GWR	.202	.654	.066	.072	.333	3.072	98	.003
Slope Unit								
SR_ GWR	-.030	.745	.074	-.178	.118	-.403	99	.688
SR_LR	.250	.520	.052	.147	.353	4.809	99	.000
SR_ANN	.170	.766	.077	.018	.322	2.219	99	.029
LR_GWR	.280	.712	.071	.139	.421	3.934	99	.000
LR_ANN	-.080	.692	.069	-.217	.057	-1.157	99	.250
ANN_ GWR	.200	.651	.065	.071	.329	3.071	99	.003

The result of the t tests compares the entire area and does not depict the geographical differences between the maps. To analyze the map differences spatially, the differences between the maps were computed for the study region. The difference

maps between each grid-based and slope unit-based mapping unit were analyzed separately. For each mapping unit, six map differences were created, where four different methods were compared. The difference maps that illustrate the SR_GWR, SR_LR, SR_ANN, LR_ANN, LR_GWR, and GWR_ANN for both grid-based and slope unit-based mapping units are shown from Figure C-1 to Figure C-12 in Appendix C. These maps illustrate the similar or dissimilar regions in a spatial domain. Additionally, similarly and dissimilarly estimated regions were computed in percentages for grid and slope units shown in Figure 3.89 and Figure 3.90 respectively. The second map was subtracted from the first map; so if the difference is negative, then it indicates that the second map is overestimated (O) at that location. If the difference is positive, the second map is underestimated (U). Finally, if the difference is 0, then the maps are similar (S) in those regions.

As a result of difference maps, when both grid and slope unit-based model pairs are evaluated, it is seen that the similarity is high within the SR_GWR pair (Figure C-1 and Figure C-8 in Appendix C). This result is also displayed quantitatively in Figure 3.89 and Figure 3.90. For example, the spatial distribution of the difference computed for SR_GWR grid-based models indicates that the pair maps are fairly similar in the north-eastern part and the southern part of the region, where the landslide distribution is frequent and less respectively. However, the GWR is underestimated in the eastern part of the region and overestimated in the northern part. The similar regions at SR_GWR given in Figure 3.89 show that 245 km^2 of region on both maps are similar, which occupies 75% of all regions and the dissimilarity is approximately 24%.

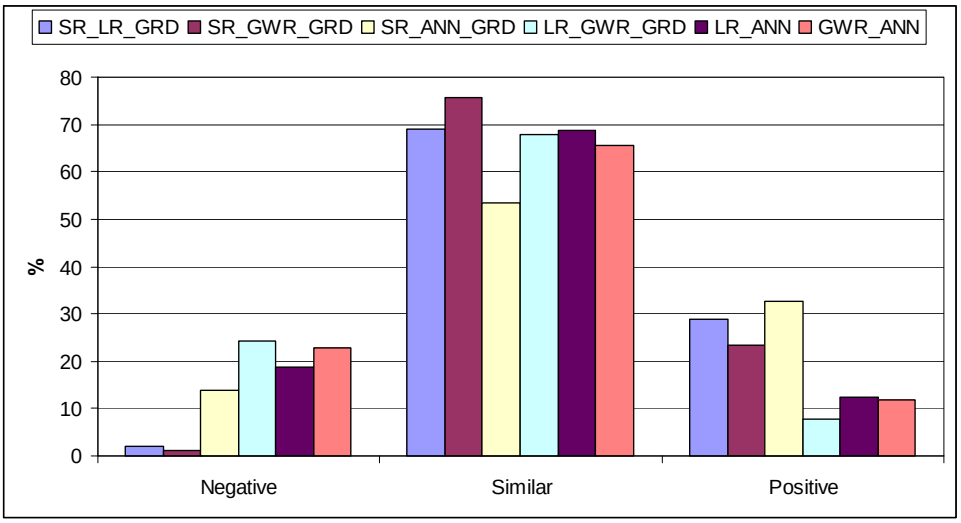

Figure 3.89. The area and percentage of different and similar regions between the pair of maps for cell-based mapping unit.

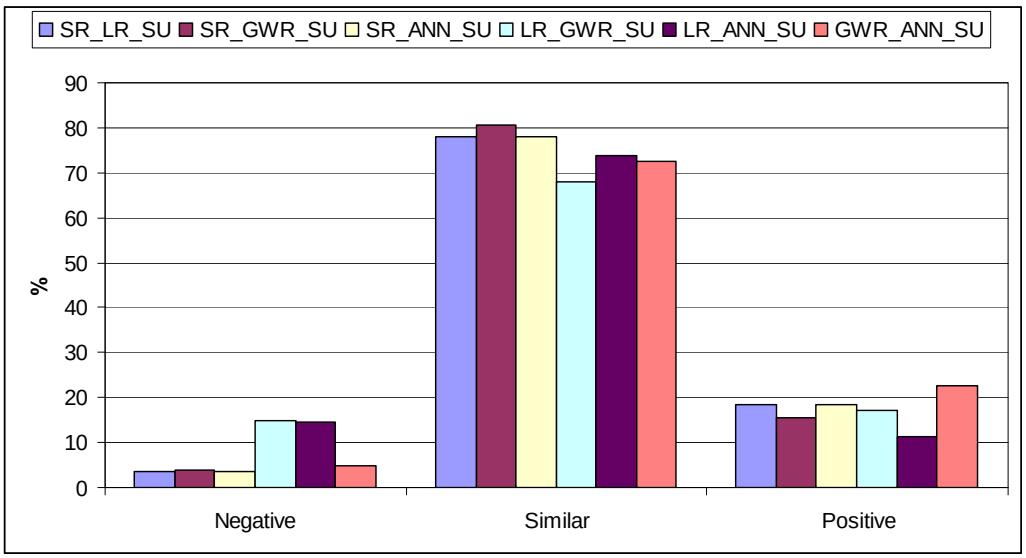

Figure 3.90. The area and percentage of different and similar regions between the pair of maps for slope unit-based mapping unit.

For grid-based mapping unit, the total dissimilarity is higher for SR_ANN (47%) and GWR_ANN (34%), correspondingly for slope unit-based mapping unit the dissimilarity is higher for LR_GWR (32%) and GWR_ANN (27%). The similarity declines from 78% to 53% for SR_ANN maps for grid and slope unit-based mapping units respectively. As a result, it can be concluded that the slope unit-based mapping unit provides relatively higher percentages of similarities for each mapping unit type when compared to the grid-based mapping unit. The relative comparisons of each model in Figure 3.89and Figure 3.90 are the evidence of this result.

3.6 Analysis of Triggers

Landslide hazard calculation requires determining the spatial and temporal probability of occurrence of damaging events (Bell and Glade, 2004). The overall objective of studying the spatial and temporal pattern of landslides is to make a more precise prediction of future landslide occurrence. Depending on the literature surveys, it can be seen that there has been no study on risk mitigation in the study region. However, as the region is highly susceptible to landslides and floods, the identification of regional thresholds is an important issue for developing early warning systems for civil protection authorities and the population. For this reason, in this study, the temporal occurrence of landslides was aimed to be defined, so that the susceptibility maps created in the first part can be combined with the probability of critical rainfall thresholds to obtain hazard maps. The focus of this part of the study is related to the time-varying aspects of landslide hazard on rainfall-induced landslides, because precipitation triggers the majority of landslides in the study region. The methodology adopted for hazard assessment is presented in Figure 3.91.

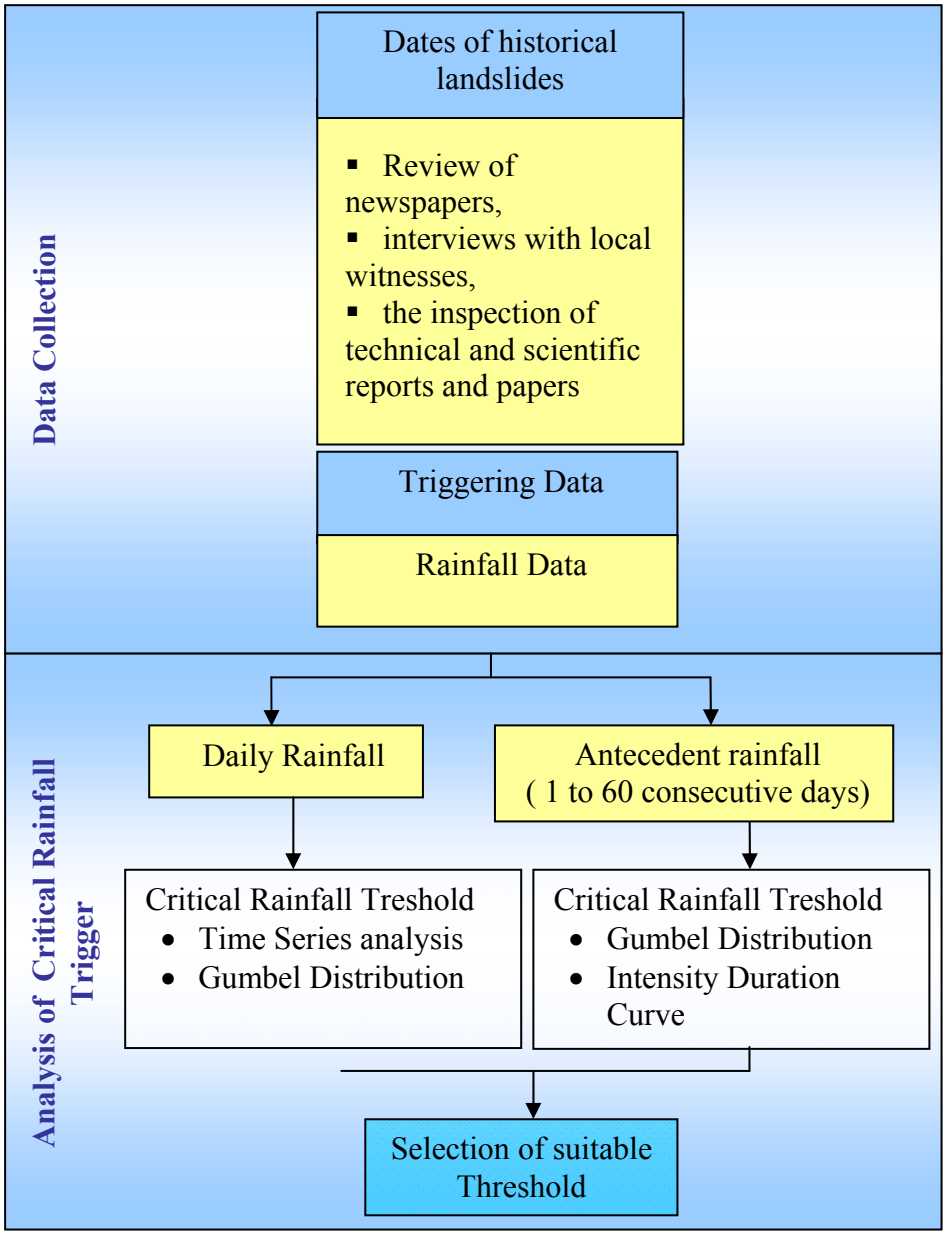

Figure 3.91. The methodology adopted for analysis of triggers

The first part of the methodology involves collection of mainly two types of data, triggering event data and dates of landslide occurrences. The second part of the methodology is the analysis part, which involves the estimation of critical rainfall thresholds based on rainfall records coupled with the documented times of landslide events. In this part, the critical rainfall thresholds were estimated for daily and antecedent rainfalls by using different methods. The most suitable triggering threshold for the purpose of the study was selected for the further analysis.

3.6.1 Analysis of Data Used for Triggering Analysis

The Kumluca region is frequently affected by severe meteorological events. Hence, for the hazard assessment, triggering data was obtained daily from different stations distributed around the Kumluca basin for a 30-year period. In addition to this, the dates of past landslide events were reconstructed through technical landslide reports, systematic review of newspapers, and interviews with local witnesses. Technical landslide reports were obtained from the General Directorate of Disaster Affairs of Bartın (Landslide Reports, 1975, 1987, 1993, 1995, 2005). The reports have detailed information about the geology, the reasons for landslide occurrences, the number of affected people, and the name of the village, but not the exact spatial location of these slides.

The reports provided by the Disaster Affairs provide information about the movement of the inhabitants due to landslides between 1975 and 2005 for each village in the study region. The reports also include the number of conveyed homes, the number of people who died, the geological properties of the region, the reasons for landslide occurrences, the number of houses and the number of people in each village. In the period between 1975 and 2005, approximately 537 houses are reported to be conveyed to safer regions. The houses moved in each village and the year of the movement are presented in Figure 3.92 a and b. The direct or indirect damage was not ascertained in the reports.

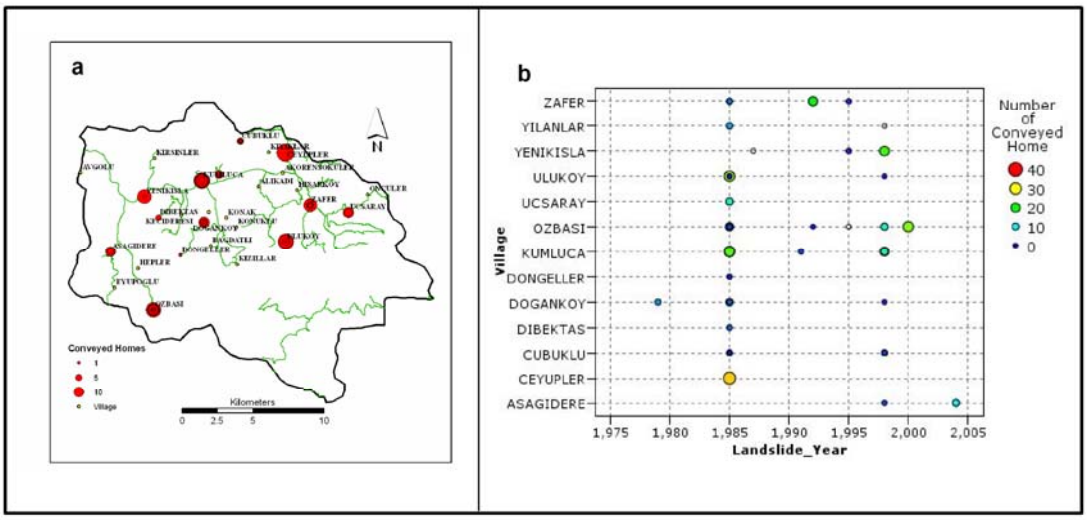

Figure 3.92.a. Spatial distribution of the conveyed house frequency after devastating landslide events b. Showing the year and the frequency of each devastating landslide event

The reports rarely include the exact date of the slides. Depending on the preparation date of the report, the year of the slide is known but the exact month and day is not. Through systematic review of newspapers, interviews with local witnesses, and inspection of technical and scientific reports and the papers, it was found that significant slides due to flooding, which are exactly known, occurred on 1st May 1975, 1st July 1988, 13rd-14th December 1994, 20th-21st-22nd May 1998, and 17th of August 2004. The reported slides in addition to flooding days are 15th February 1985 and 3rd April 1985.

The historical reports reflect only the minimum number of events that actually occurred. For this reason, another category is also possible in the analysis as ‘‘probably induced landslides”, which means it cannot be assumed that landsliding did not occur on these days (Glade et al., 2000). This latter category is obtained by analyzing the similar or larger landslide-triggering rainfall amounts on the preceding and following days of the hazard. Depending on the reports of 1991 and 1985, it is known that landslides occurred in those years; nevertheless, the exact days are not provided in the reports. Hence, the most probable days were determined based on the previous landslide days. In this approach, the maximum rainfall value was found from the meteorological data corresponding to the prior data of the reports depending on the known landslide days, and then the maximum rainfall value was compared with the daily rainfall of all days in the probable landslide year. The probable days for landslides were obtained by determining the rainfall values higher than the maximum rainfall value. As a result, six more probable slide days were added to the database. In total, there were sixteen landslide events to be used in the further analysis (Figure 3.93). In the following calculation, both days with landslides and days of probable landslides were treated as landslide events providing a binary variable corresponding to the presence or absence of a landslide event.

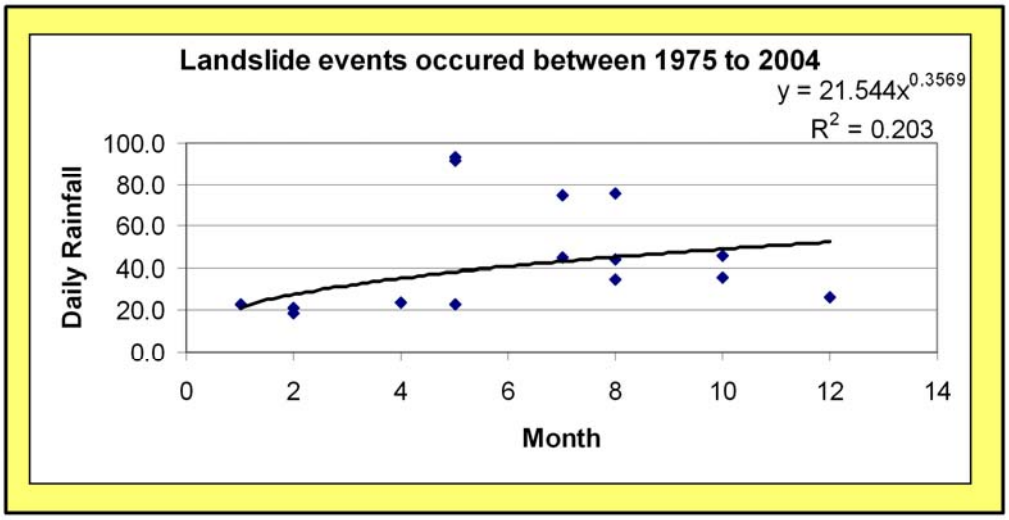

Figure 3.93. The landslide events distribution over months and daily rainfalls on each event day.

It is extremely important to identify the most suitable rainguage that is associated to a slide. Even the closer rainguages can provide different precipitation values depending on factors such as topographical elevation, aspect, and even prevailing wind direction in the area. The meteorological data acquired from the General Directorate of Meteorological Affairs are mostly distributed around the study region. In other words, there are no meteorological stations located spatially inside the watershed that represents the rainfall characteristics of the region (Figure 3.94). As presented in Figure 3.94 most of the stations are closed or do not provide accurate measurements. For this reason, only the available station measurements were acquired. These stations, which are distributed to the northern part of the study region, are: Kozcagiz, Ulus, Bartın, Amasra, Kurucaşile and Arıt (Figure 3.94). The characteristics of the available stations for the analysis are given in Table 3.17.

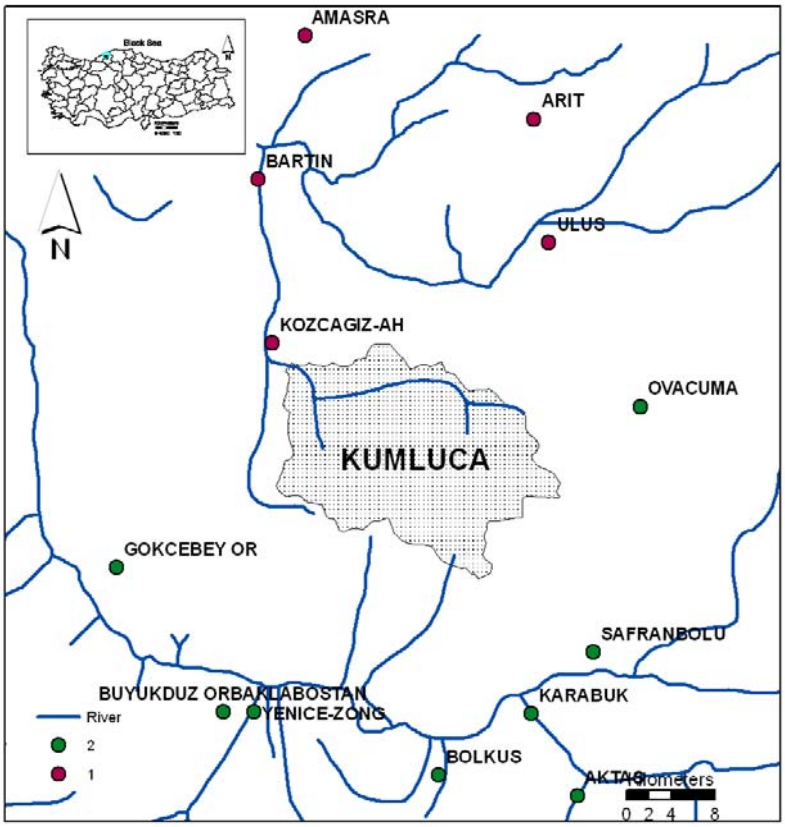

Figure 3.94. Meteorological stations distributed around the study region. See Table 3.17 for station characteristics. Legend 1 indicates that the meteorological station measurements are available for analysis. 2 indicate the station measurements are not present or the station is closed.

Table 3.17. Characteristics of meteorological stations which are available for analysis.

Meteorological Station	Record interval	Elevation (m)	Distance to study region (km)
Kozcagiz	1996-2006	75	16
Ulus	1975-2006	157	25
Bartın	1975-2006	35	27
Amasra	1975-2006	13	39
Kurucaşile	1989-1990	432	48
Arıt	1985-1991	365	33

The median elevation of the study region corresponds to 50% of the area, which is acquired from the hypsometric (area-evelation) curve (Usul, 2005). A hypsometric curve is an empirical cumulative distribution function of elevations in a catchment. The curve shows the percentages of areas above certain elevations (Figure 3.95). From the presented curve, the median elevation value corresponds to approximately 700 m.

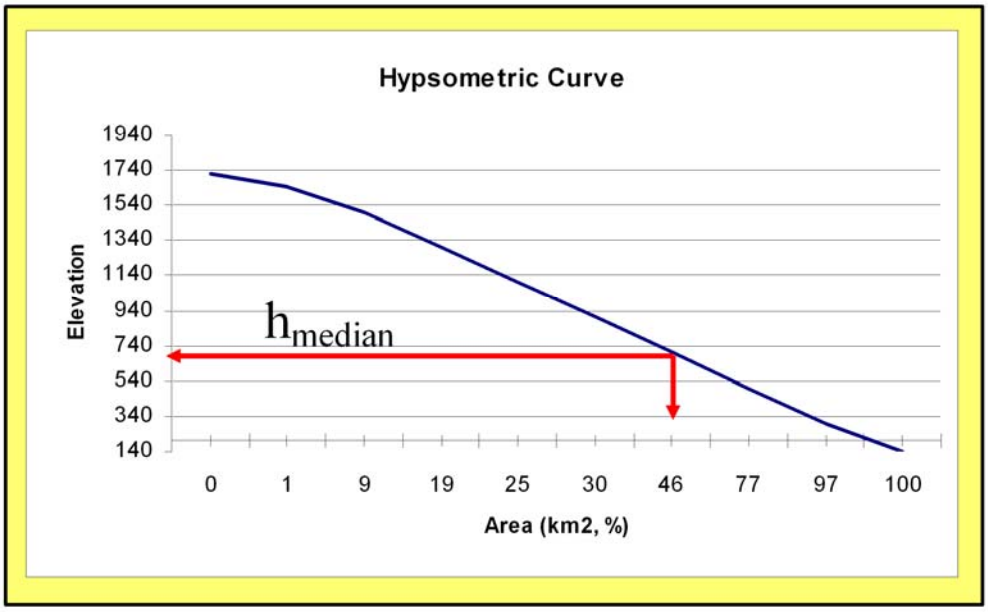

Figure 3.95. Hypsometric Curve of Bartın Kumluca watershed

There are no meteorological stations at the median elevation of the study region. Additionally, the measurements obtained from all stations can not be transformed to 700 m. height because there is not a good relation depending on the elevation and temporal scale of annual precipitation measurements of the stations. In general, a station may be ideal for a landslide triggering analysis if the dates of rainfall periods overlap with the dates of landslide occurrences, if the station is on median elevation, and finally if it is spatially closer to the study region. The landslide occurrence information in our study ranges between 1975 and 2004. However, the stations with the heighest elevation (Kurucaşile, Arıt) or spatially the closest stations (Kozcağız) (Table 3.17) have rainfall measurements which are not obtained in an adequately long period to represent the rainfall values recorded during the past landslides. In this respect, these stations are not suitable for the aims of the study.

In addition to the above analysis, to determine the rainguage that best represents the rainfall characteristics of the region, the correlation analysis between the stations was evaluated. In this approach to measure the correlation between the station measurements, one of the most devastating event measurements was used, which is the 1998 rainfall event. The daily rainfall measurement of May 1998 was plotted for each station. The non-measured days in the stations were presented with the cuts on

the graph. The plot in Figure 3.96 indicates that the stations (Kozcağız, Ulus, Bartın, Amasra) show a similar trend for the May 1998 rainfall. In addition to the daily rainfall graphic, the Pearson correlation was computed to evaluate the correlation between the stations relatively. The result of the Pearson correlation for each pair of stations also indicate the high correlation between stations (Figure 3.97).

As can be seen from Figure 3.97, the Kumluca basin has the highest correlation with Bartın station records and it has the most complete rainfall data series, particularly the longest (30 years) daily precipitation measurements, hence it was selected as the reference station. The reference meteorological station is assumed to be the representative of the Kumluca watershed concerning rainfall regime (Figure 3.97).

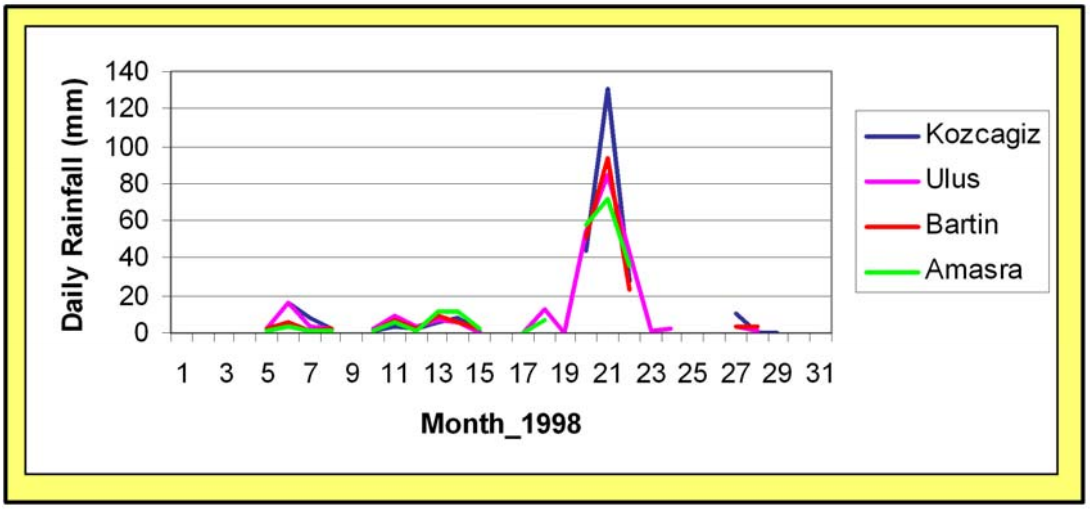

Figure 3.96. The daily rainfall pattern of each station in 1998 May

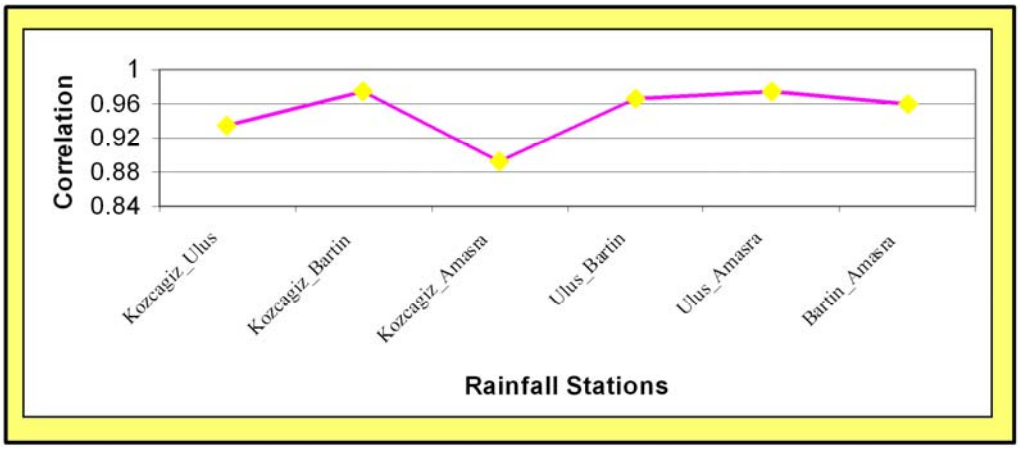

Figure 3.97. The graph showing the correlation between the meteorological stations for 1998 May.

After obtaining the station that best represents the rainfall characteristics of the region, the rainfall values were transformed into height of the study region depending on the median elevation of the study region.

Rainfall analysis was carried out using 31 years (1975–2006) of daily precipitation records registered in the reference meteorological station of Bartın. The mean annual precipitation (MAP) at Bartın station is (for this period) 1008.206 mm. A preliminary analysis of the rainfall regime shows variability on inter-seasonal scale. Rainfall exceeds the mean monthly average rainfall between the first and the second month and the eighth and the twelfth month (Figure 3.98). All the dated events reveal that they are mainly concentrated between these ranges of months (59%) when extreme rainfall occurs, which is the wettest period of the year (Figure 3.93). During the rest of the year, landslides occur under low precipitation.

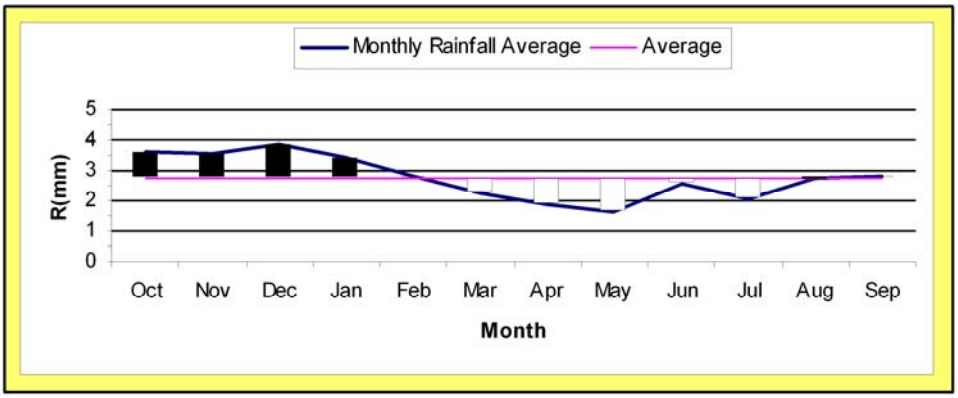

Figure 3.98. The lowest and the highest monthly rainfall average from mean

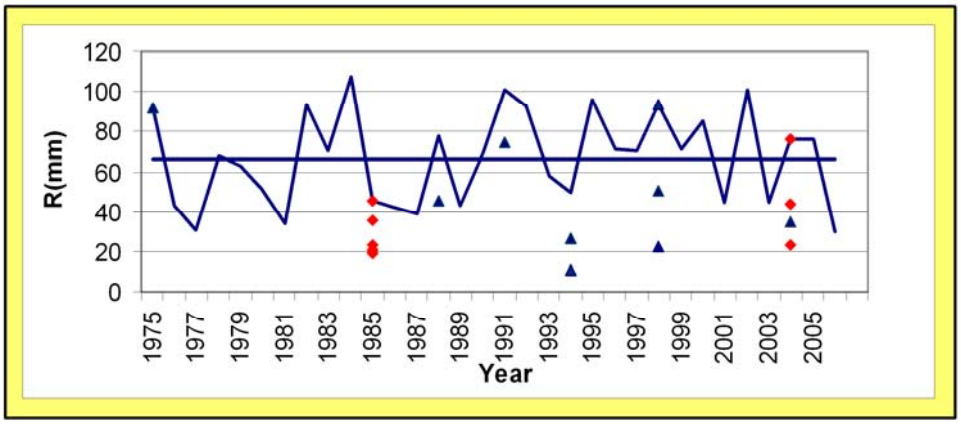

Figure 3.99. The annual maximum precipitation in Bartın (reference meteorological station) from 1975 to 2006. The horizontal line indicates the mean annual maximum precipitation (MAMP) Legend: triangles indicate landslide events triggered with flood; squares indicate potential landslide events

The annual maximum precipitation and the landslide occurrences at Bartın station shown in Figure 3.99 indicate that 76% of the slides occur in lower precipitation compared to mean annual maximum precipitation.

3.6.1.1 Determination of Critical Rainfall Thresholds

It is aimed to define thresholds based on the statistical analysis of the relationship between rainfall and occurrence of mass movements. The threshold curves define the lowest level of rainfall above which one or more than one landslide can be triggered. The rainfall data obtained daily was evaluated first with landslide occurrence days by time series analysis. Secondly, the daily data set was tested for suitable probability distribution of the data set. After determining that the data set follows the Gumbel Distribution, also known as Fisher–Tippett type I Extreme Value distribution, the Gumbel extreme value diagram was used to plot data for probability distribution and to obtain triggering rainfall values for different return periods.

In addition to the evaluation of daily rainfall data, depending on the interviews with the local people and information related to technical documents, it is seen that antecedent rainfall influences the groundwater level and soil moisture in the study region, which may cause devastating landslides. The 1998 landslide was an example of such an event. The landslide occurred three days after the intense rainfall in May 1998. Thus, the antecedent rainfall data are computed from daily data for different time periods. After testing and selecting the right number of antecedent days, they were used to obtain the critical rainfall threshold for landslides for different time periods. The antecedent rainfall was analyzed first by the Gumbel theoretical distribution. Then the intensity duration analysis was performed.

As a result of these critical rainfall analyses, different thresholds were obtained. These thresholds were compared to select the most suitable one for the further hazard analysis.

3.6.1.2 Time Series Analysis of Rainfall Pattern with ARIMA Model Fitting

The daily rainfall values of Bartın reference station was analyzed with time series model. The aim of building a time series model was to forecast the outliers with the

fitted model and then analyze if the outliers predicted by the model overlapped with the landslide data. Afterwards, to define a critical threshold, Box-Jerkins ARIMA model was fit to daily data from a 31–year period.

The ARIMA procedure has three steps as identification, estimation, and diagnosis. In the identification step, the order of the ARIMA model was identified by determining the three integers as *p*, *d*, and *q*. Before building a tentative model, the nature of the data was examined by plotting the daily rainfall over each day. The plot indicates no hint of seasonal variations and trends in the data. The values seem to fluctuate with a constant variation around a constant mean. Therefore, it was reasonable to believe that the time series was stationary (Figure 3.100).

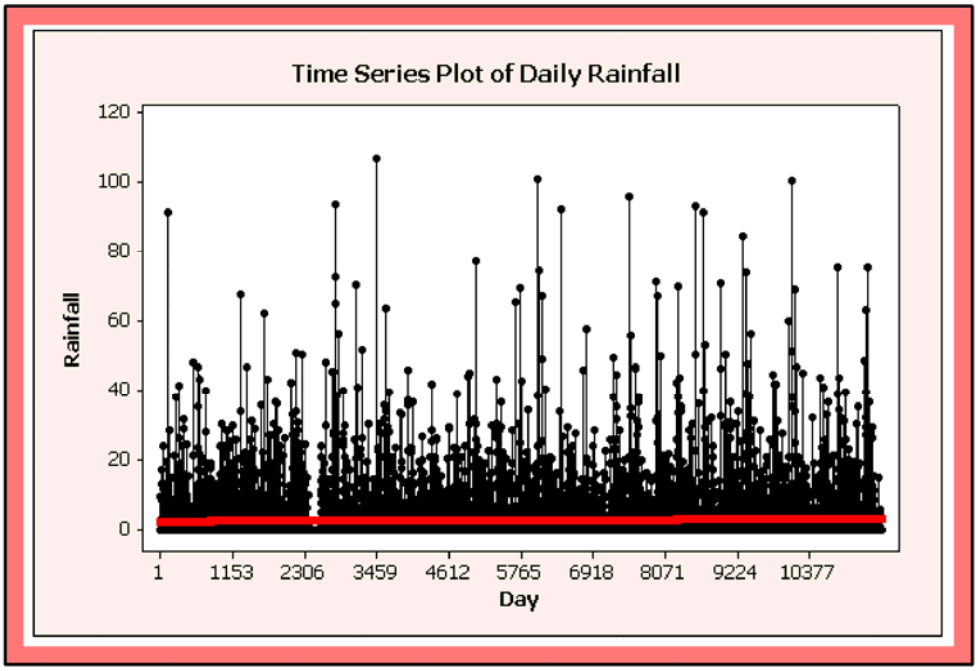

Figure 3.100. The time series plot of daily rainfall of Bartın station

To evaluate the stationary of the data, there are more sophisticated methods (Table 3.18). One way is to apply the unit root tests. The null hypothesis is that the process is not stationary. When the Rho value is larger than 0.05, the null hypothesis is accepted. If a series is not stationary, the data set should be transformed until it becomes stationary. The most common transformation is differencing, which replaces each value in the series by the difference between that value and the preceding value. Differencing is necessary when the mean is not stationary.

Logarithmic and square-root transformations are useful when the variance is not stationary, such as when there is more short-term variation with large series values than with small series values. According to the test result (Table 3.18), the H_0 is rejected in favor of H_1, on 5% significance level, which indicates that the process is stationary.

Table 3.18. Stationary analysis of data

Ty pe	Lags	Pr < Rho
Zero Mean	0	0.0001
	1	0.0001
Single Mean	0	0.0001
	1	0.0001
Trend	0	0.0001
	1	0.0001

Once a stationary series is obtained, the next step is to identify the *p* and *q* values, which are the orders of autoregression (AR) and moving-average (MA). Pure autoregressive and moving-average processes have characteristic signatures in the autocorrelation and partial autocorrelation functions. Therefore, the autocorrelation function (ACF) and partial autocorrelation function (PACF) are plotted to determine the decision levels.

1. An ACF with large spikes at initial lags that decay to zero or a PACF with a large spike at the first and possibly at the second lag indicates an autoregressive process.

2. An ACF with a large spike at the first and possibly at the second lag and a PACF with large spikes at initial lags that decay to zero indicate a moving average process.

3. The ACF and the PACF both exhibiting large spikes that gradually die out indicate that both autoregressive and moving average processes are present.

As seen obviously, the lags are significant when the lag values pass the red line (Figure 3.101, Figure 3.102). Red line indicates the %5 significance level of autocorrelations. The ACF plot indicates that the spikes are at the first lag, so this signifies an autoregressive process. Another and more informative evidence is on autocorrelation values. As indicated in Table 3.19, the first lag shows autocorrelation, and it dies out in the further lags.

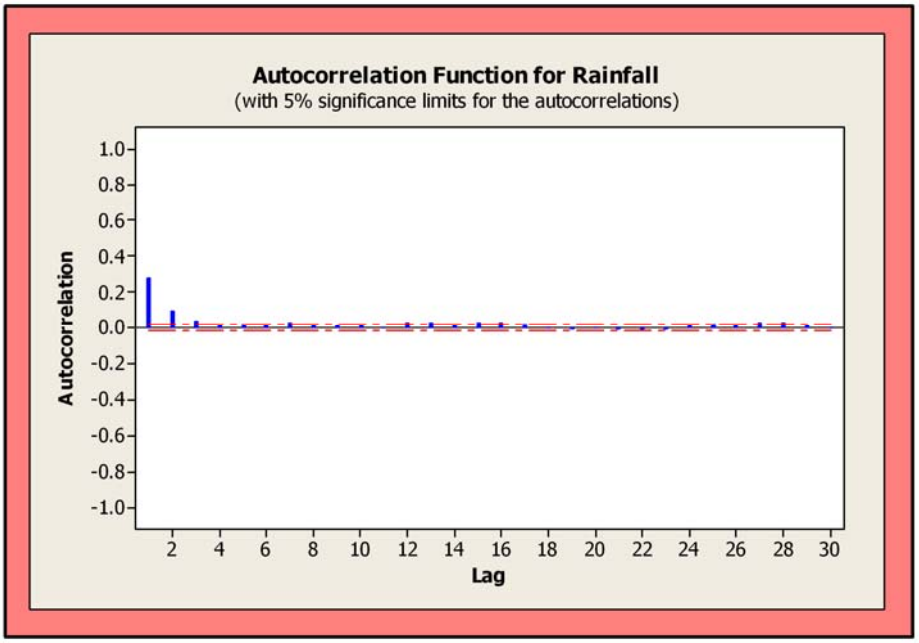

Figure 3.101. Autocorrelation plot of daily rainfall

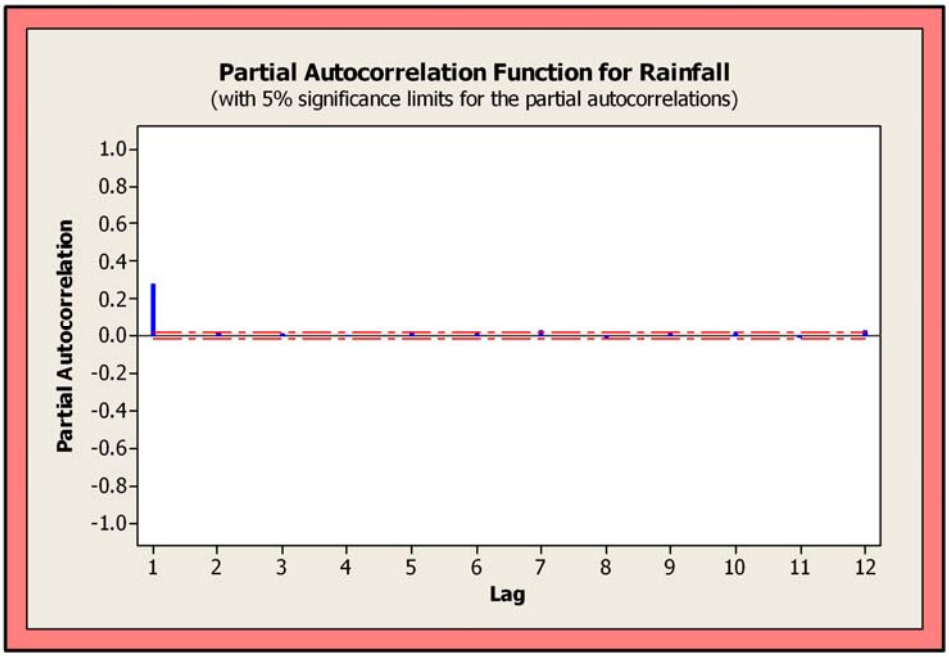

Figure 3.102. Partial autocorrelation plot of daily rainfall

Table 3.19. Auto correlation values of daily rainfall

Lag	Covariance	Correlation	-1 9 8 7 6 5 4 3 2 1 0 1 2 3 4 5 6 7 8 9 1	Std Error
0	54.45583	1	|********** |	0
1	15.09268	0.27715	|****** |	0.009315
2	4.973635	0.09133	|** |	0.010004
3	1.903785	0.03496	|* |	0.010077
4	0.794854	0.0146	| |	0.010087
5	1.123563	0.02063	| |	0.010089
6	0.848131	0.01557	| |	0.010093
7	1.467678	0.02695	|* |	0.010095
8	0.540696	0.00993	| |	0.010101
9	0.552005	0.01014	| |	0.010102
10	0.96001	0.01763	| |	0.010103
11	-0.01823	-0.00033	| |	0.010105
12	1.218949	0.02238	| |	0.010105
13	1.196695	0.02198	| |	0.01011
14	0.79369	0.01457	| |	0.010114
15	1.253197	0.02301	| |	0.010116
16	1.147122	0.02107	| |	0.01012
17	0.754119	0.01385	| |	0.010124
18	0.068086	0.00125	| |	0.010126
19	-0.57908	-0.01063	| |	0.010126
20	-0.07646	-0.0014	| |	0.010127
21	-0.28373	-0.00521	| |	0.010127
22	-0.40666	-0.00747	| |	0.010127
23	-0.49369	-0.00907	| |	0.010127
24	0.278758	0.00512	| |	0.010128
25	1.018968	0.01871	| |	0.010128
26	0.301703	0.00554	| |	0.010131
27	1.403869	0.02578	|* |	0.010131
28	1.385011	0.02543	|* |	0.010137
29	0.347609	0.00638	| |	0.010143
30	0.159672	0.00293	| |	0.010143

After the identification of likely models, the ARIMA procedure was applied. In the ARIMA procedure, different combinations of AR and MA levels are evaluated to get the best results. The probability value in the maximum likelyhood estimation is an indicator to detect the statistical significance of the model. If the probability value is smaller than 0.05, the parameter is significant on 95% significance level. When the parameter is significant, it should be involved in the model. Another issue to be considered in the significance of the model is the standard squared (SS) error. The lower the ss value is, the higher the accuracy of the model is.

In Table 3.20, the parameter estimate, error, t value, p values and ss values are indicated. In all the levels, residuals and sum of square values have a slight difference, which does not indicate an improvement between trials. In the Arima (1,0,0) and Arima (0,0,1) situations, all p values are smaller than 0.05. Therefore, these two models fit data quite sufficiently as all the probability values are smaller than 0.05. To identify the better suitable model for the data set, the Acaice Information Coefficient (AIC) parameters are compared. The lower the AIC value is, the better the model is. As a result, with the lowest AIC value, the Arima (1, 0, 0) is suitable and selected for the analysis.

Table 3.20. Maximum Likelihood Estimation

Parameter	Estimate	Error	t Value	Pr > |t|	Lag	ss	AIC
Arima(1,0,1)						579294	77865.15
MU	2.76415	0.09298	29.73	<.0001	0		
MA1,1	0.05911	0.03356	1.76	0.0782	1		
AR1,1	0.33167	0.03171	10.46	<.0001	1		
Arima(1,0,0)						579443	77866.13
MU	2.76416	0.09137	30.25	<.0001	0		
AR1,1	0.27714	0.00895	30.96	<.0001	1		
Arima(0,0,1)						583670	77949.9
MU	2.76416	0.08317	33.23	<.0001	0		
MA1,1	-0.2547	0.009011	-28.27	<.0001	1		

The autocorrelogram in Figure 3.103 and partial autocorrelogram in Figure 3.104 have no spikes, which is also an indication for the evidence of the sufficiency of the Arima(1,0,0) model and there is no need to improve the model.

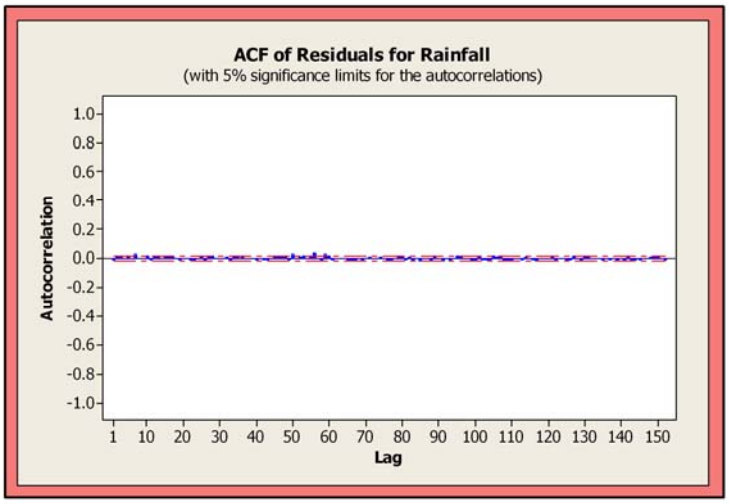

Figure 3.103. Autocorrelogram of residuals of ARIMA(1,0,0)

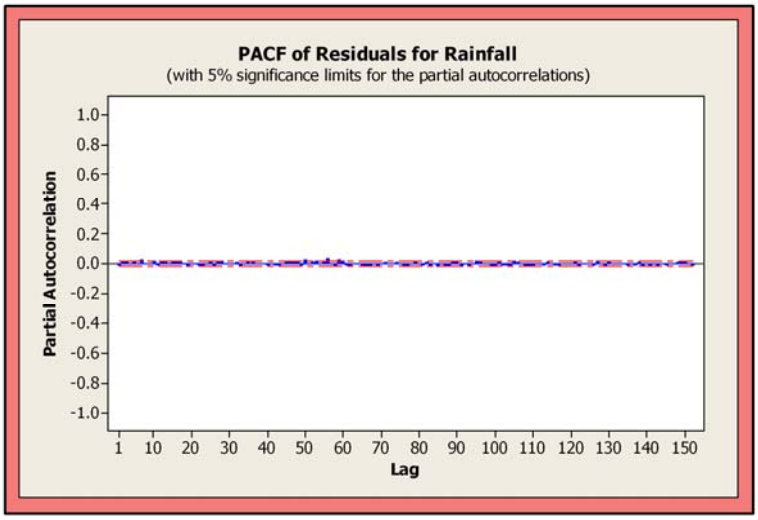

Figure 3.104. Partial Autocorrelogram of residuals of ARIMA(1,0,0)

After the determination of the suitable model, it was run to predict the outliers. The estimated outliers were compared with the rainfall values obtained in a 40-day period (20 days before and 20 days after the landslide) when landslides occurred to find out whether there were any similar values within this period. The "landslide occurance" column in Table 3.21 indicates the range of time when the estimated outliers and the recorded rainfall values were relatively closer. Table 3.21 presents that the outliers can detect 8 of the 16 landslide occurrences with an approximation of 1 to 20 days. Therefore, the resultant outliers of ARIMA(1,0,0) model indicate a reasonable result.

Table 3.21. The outliers detected for the model ARIMA(1,0,0)

Obs Day	Estimate	Chi- Square	Prob	Landslide occurrence
3450	101.20	1244.2	<.0001	--
10088	96.10	1122.18	<.0001	--
6035	94.99	1096.28	<.0001	10 days later (7.7.1991)
6404	90.71	999.74	<.0001	--
7502	89.17	966.12	<.0001	--
122	86.937	918.11	<.0001	The same day (1.5.1975)
8686	78.726	752.88	<.0001	--
5042	76.05	702.68	<.0001	20 days prior
9306	75.65	695.39	<.0001	--
8559	73.04	648.20	.0001	The same day, one day prior, one day later (20-22. 05.1998)
6045	**71.68**	**624.25**	**<.0001**	**The same day (7.7.1991)**
7925	70.15	597.98	<.0001	----
8963	69.65	589.49	<.0001	---
11306	69.07	579.73	<.0001	---
3132	68.481	569.77	<.0001	----
10839	82.07	546.53	<.0001	The same day (12.8.2004)

The outlier values which estimate eight of the landslide are ranked and the minimum rainfall value which triggers a landslide is found to be approximately 71.7 mm by the model. Therefore, we can assume a threshold value of 71.7 for triggering of landslide occurrences.

3.6.1.3 Critical Rainfall Analysis with Gumble Distribution Approach

The estimation of return period is usually accomplished by standard statistical approaches. These approaches include different types of distributions. The Gumbel (Type I Extreme Value distribution) is commonly preferred for the extreme value analysis (Usul, 2005; Marques et al., 2007). Therefore, in this study Gumbel extreme value diagram was used to plot the data for probability distribution. The plotting position of the probability values were computed depending on the Weibull definition given by following Eq. 48:

$$q = \frac{m}{n+1} \tag{48}$$

Where n is the recorded number of years of and m is the rank of the event (smaller to larger). The daily precipitation of landslide events were ranked from the smallest to the largest and then the plotting position (pp) were calculated (Usul, 2005) as shown in Table 3.22. The plotting position defines the probability of nonoccurrence and was taken in percentages.

Table 3.22. Calculated Plot positions (pp) for daily precipitation of landslides

	1	2	3	4	5	6	7	8	9	10	11	12	13	14	15	16
R(mm)	10.9	19.0	20.8	22.6	23.5	26.1	34.8	35.9	43.8	45.3	45.8	50.5	74.8	75.8	91.8	93.2
pp(%)	5.88	11.76	17.65	23.53	29.41	35.29	41.18	47.06	52.94	58.82	64.71	70.59	76.47	82.35	88.24	94.12

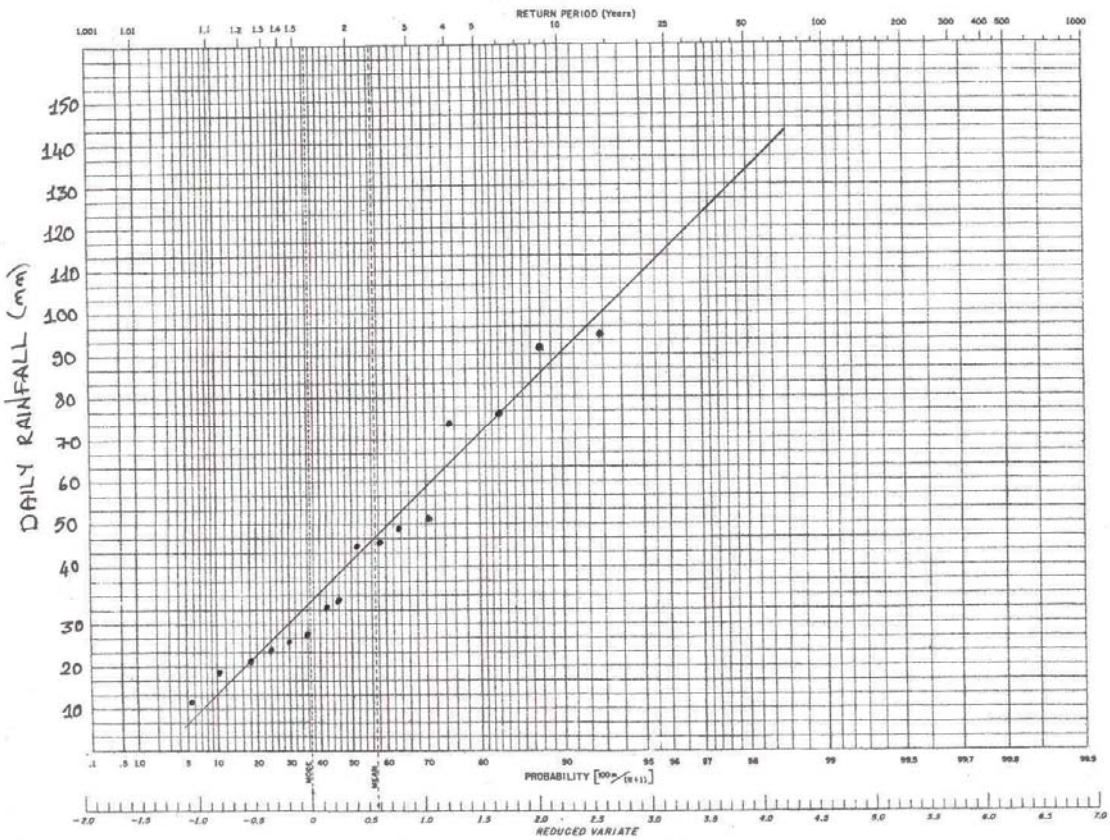

Figure 3.105. Gumble distribution diagram for estimation of rainfall with 50 years return period

The magnitudes of daily precipitations R (mm) of landslides were plotted against the plotting position on Gumbel probability papers shown in Figure 3.105. The coefficient of determination referred to as R^2 is equal to 97%. The coefficient of the correlation was computed with the following formulation of Eq.49.

$$R^2 = \frac{\sum (y-\bar{y})^2 - \sum (y-y_s)^2}{\sum (y-\bar{y})^2} \tag{49}$$

where;

y = daily rainfall that is observed

$\bar{y}$ = mean of the observed daily rainfalls

y_s = simulated daily rainfalls

Data from at least n = 30 years should be included to give an acceptable estimation of values related to a 50-year return period. The data set includes landslide occurences between 1975 and 2006. The rainfall corresponding to 50-year return

period was read from the corresponding line, which is approximately 133 mm for rainfall with the probability of occurence of 0.02. For different return periods, the rainfall values are presented in Table 3.23.

Table 3.23. Rainfall values estimated from the Gumbel distribution diagram for different return periods for daily data

Return period	Rainfall (mm)	Probability (P_s)
50	133	0.02
10	90	0.1
5	72	0.2

3.6.1.4 Antecedent Rainfall Model Construction and the Threshold Approach

The literature studies indicate that the antecedent moisture content of the soil is of vital importance to threshold values of rainfall because antecedent precipitation influences the groundwater levels and soil moisture (Wieczorek, 1987; Aloetti, 2004; Guzzetti et al., 2007). Less water is required for slide initiation if the antecedent moisture content is high. Antecedent precipitation was used in this study to determine when landslides are likely to occur. Antecedent Rainfall Model is represented by two factors: rainfall which occurs over a given period preceding a given day and the rainfall total on the given day.The Antecedent Rainfall model employed by Crozier and Eyles (1980) uses the antecedent rainfall index (Bruce and Clark, 1966) calculated as follows:

$$X_n = kP_1 + k^2 P_2 + \cdots k^n Pn \qquad (50)$$

where X is the antecedent rainfall for day X; P_1 is the daily precipitation for the day before X; P_n is the daily precipitation for the *nth* day before day X. k is the constant.

Crozier and Eyles (1980), following Bruce and Clark (1966), used *k* as 0.84, which comes from Ottawa (United States) streamflow data (Glade et al. 2000). In the literature, the k values typically range between 0.8 and 0.9 depending on the draining capacity and the hydrological characteristics of the area (Capecchi and Focardi,

1988, Marques et al. 2007). In this study, k is considered as 0.9, where the analysis consists of the computation of the cumulative absolute rainfall. The antecedent rainfall was computed for time periods of 1, 2, 3, 5, 10, 15, 20, 30, 45, and 60 days.

To identify the importance selecting the right number of antecedent days, some of the selected antecedent rainfalls accumulated over a different number of days were compared with the daily rainfall. For a reliable comparison, both the antecedent and daily rainfall values were normalized before presenting the graphs (Terlien, 1998). The normalized values were compared with the landslide event days exceeding 0.6. A comparison of the plots reveals that the considering the antecedent days are important for identification of landslide events. The accumulated antecedent rainfall of 15 and 20 days proved to give the best distinction between days with landslides and days without landslides (see Figure 3.106) for those landslides triggered by high daily rainfall amounts. The normalized accumulated plots of antecedent days of 3 (Figure 3.106a), 5 (Figure 3.106b), 10 (Figure 3.106c), 15 (Figure 3.106d), and 20 (Figure 3.106e) days provide 31.2, 37.5, 32.2, 62.5, and 68.7% of landslide days. Thus, for further analysis, results from antecedent 5 and 20 days were considered for modeling the hazard.

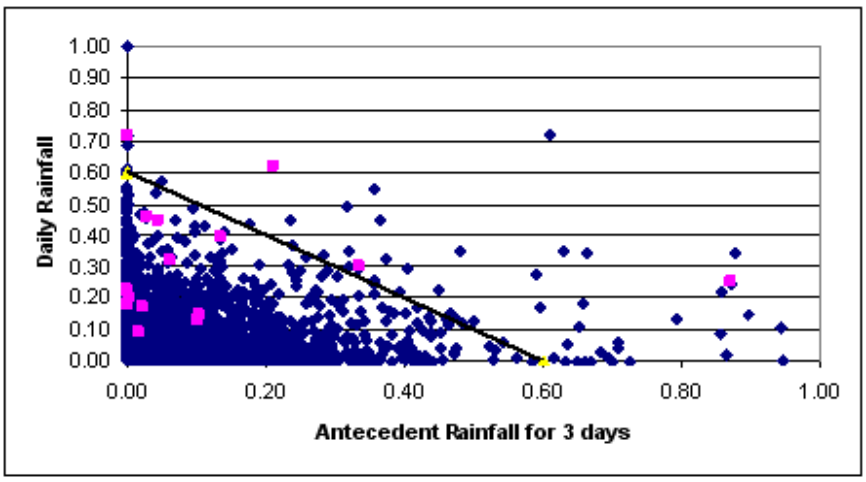

(a)

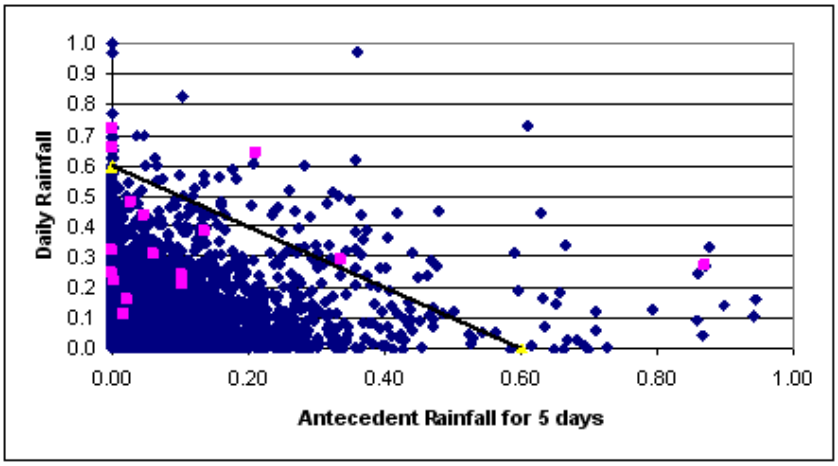
Daily Rainfall
1.0
0.9
0.8
0.7
0.6
0.5
0.4
0.3
0.2
0.1
0.0
0.00
0.20
0.40
0.60
0.80
1.00
Antecedent Rainfall for 5 days

(b)

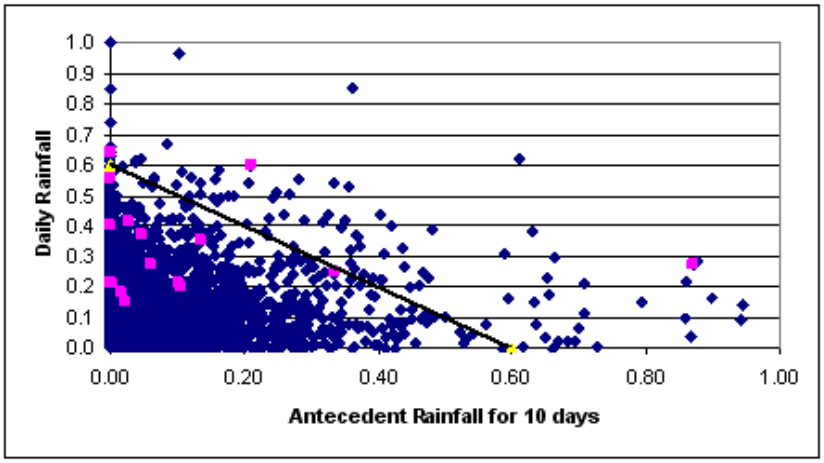
Daily Rainfall
1.0
0.9
0.8
0.7
0.6
0.5
0.4
0.3
0.2
0.1
0.0
0.00
0.20
0.40
0.60
0.80
1.00
Antecedent Rainfall for 10 days

(c)

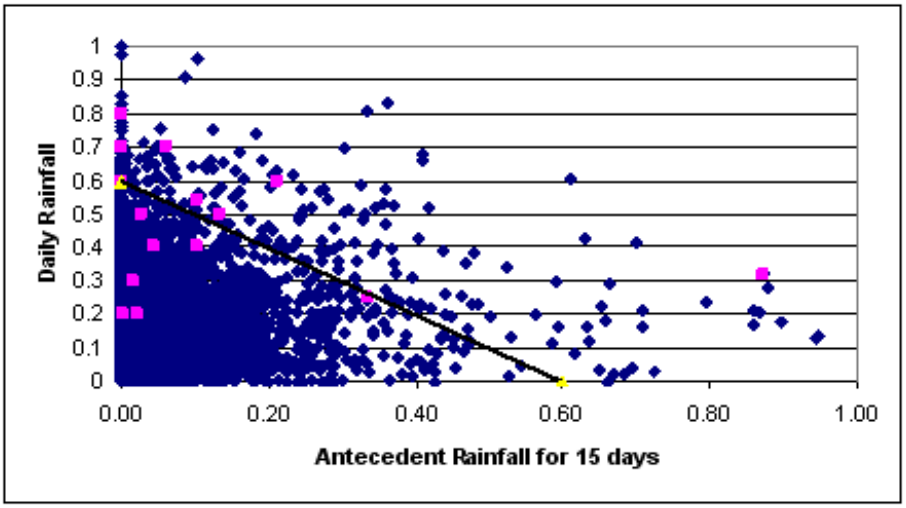
Daily Rainfall
1
0.9
0.8
0.7
0.6
0.5
0.4
0.3
0.2
0.1
0
0.00
0.20
0.40
0.60
0.80
1.00
Antecedent Rainfall for 15 days

(d)

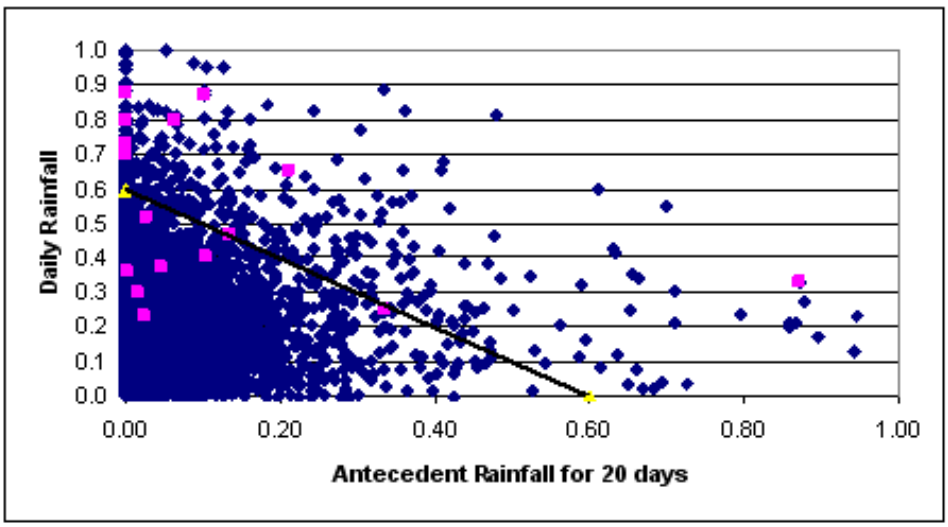

(e)

Figure 3.106. Plots of normalized accumulated rainfall versus normalized daily rainfall for landslide events shown with pink square and non-landslide events labeled with blue point: a for 3 days; b for 5 days; c for 10 days; d for 15 days ; e for 20 days

3.6.1.4.1 Critical Rainfall Threshold for Antecedent Days by Gumbel Distribution Approach

The return period of each rainfall amount and duration combination was computed using the Gumbel theoretical distribution. The Gumbel theoretical distribution considers the distribution of the largest or the smallest values observed in repeated samples. In this extreme distribution, the probability (p) of the occurrence of a magnitude which is equal to or greater than any value of the observations (x) and the theory of extremes was applied by using the Equation below:

$$q = 1 - e^{-e^{-y}} \tag{51}$$

where y= reduced variate and computed with the equation below as:

$$y=a(x_i-x_0) \tag{52}$$

where a=dispersion parameter (a scale parameter), x_0 is the location parameter of the distribution.

$$a = \frac{\sigma_n}{\sigma_x} \tag{53}$$

$$x_0 = \bar{x} - y_n(a) \tag{54}$$

Where $\bar{x}$ and σ_x are the mean and the standard deviation of the observations respectively and they are found by equations as follows:

$$\bar{x} = \frac{\sum x}{n} \tag{55}$$

$$\sigma_x = \sqrt{\frac{\sum (x - \bar{x})^2}{n - 1}} \tag{56}$$

Since the record length is longer than 30 years (1975 to 2006), the values y_n and σ_n are constants and the values are equal to 0.45 and 1.28255 respectively. For each antecedent day of each landslide day, the standard deviation, mean, scale parameter, and location parameter were computed. Then, by using these parameters for each antecedent day, the critical rainfall value was computed for different return periods by the eq. (52) and given in the following Table 3.24 . Table 3.24. indicates that in a 50-year period, if it rains 112.64 mm on one single day, a landslide may occur. Or in a 50-year period, if it rains for five days with a daily amount of 41.79 mm, a slide may occur.

Table 3.24. The rainfall values for different Return Periods, RP (year)

	Rainfall(mm) Antecedent			**Rainfall(mm) for 1 Day**		
Antecedent Day	RP 50, $p_s(0.02)$	RP 10, $p_s(0.1)$	RP 5, $p_s(0.2)$	RP 50, $p_s(0.02)$	RP 10, $p_s(0.1)$	RP 5, $p_s(0.2)$
1	112.64	78.87	69.00	112.64	78.87	69.00
5	208.94	140.80	109.84	41.79	28.16	21.97
20	266.85	231.87	204.15	13.34	11.59	10.21

3.6.1.4.2 Estimation of Threshold Values by Using Intensity-Duration Curves

The antecedent precipitation values were used to create an intensity duration curve. Critical pairs of rainfall amount-duration were defined as proposed by D'Ecclesiis et

al. (1991) with reference to the applied studies of Zezere et al. (2004) and Marques et al. (2007), depending on the assumption that the critical pair is the combination with higher return period. The applied assumption is not physically based; however, it provides discrimination between rainfall periods characterized by landslide activities and rainfall periods. After determination of higher return period for each event, the corresponding antecedent day was determined to compute the intensity (Table 3.25) with the given formula:

$$I = P_r/X \quad (57)$$

where;

I= Intensity

Pr= Absolute antecedent precipitation for the day with higher return period,

X=Antecedent day of the higher return period

The results obtained are presented in Table 3.25 and critical amount durations are highlighted in bold.

After the computation of critical pairs of rainfall amount–duration for the reported landslide events, intensity values corresponding to duration is plotted (Figure 3.107) and the regression line that relates Intensity duration is also plotted by using Eq. 57:

$$y=68.527x^{-0.6243} \quad (58)$$

where y=intensity, x=duration

Table 3.25. Absolute antecedent rainfall from 1 to 60 days and corresponding return periods for 16 landslide events

	day1	day2	day3	day4	day5	day10	day15	day20	day30	day45	day60	Critical day	I (mm/year)
1/5/1975	**91.80**	102.60	106.00	111.50	111.50	118.30	141.20	150.90	151.10	204.90	219.20	1	91.80
R.P	**18.37**	8.86	5.99	5.51	5.18	3.24	2.56	2.21	1.78	2.22	1.92		
15/02/1985	19.00	21.90	21.90	21.90	21.90	60.30	77.90	87.40	115.10	**178.00**	178.00	45	3.96
R.P	1.16	1.26	1.20	1.21	1.18	1.36	1.27	1.24	1.38	**1.78**	1.46		
19/02/1985	20.80	24.10	34.10	35.80	54.80	61.70	102.20	115.70	142.80	**193.40**	213.80	45	4.30
R.P	1.20	1.29	1.38	1.41	1.75	1.38	1.58	1.54	1.67	**2.01**	1.84		
3/4/1985	23.50	34.60	38.60	39.00	39.00	43.40	59.60	66.50	66.50	102.70	**219.40**	60	3.66
R.P	1.26	1.53	1.47	1.46	1.41	1.17	1.13	1.11	1.10	1.15	**1.92**		
12/10/1985	**45.80**	0.30	0.30	0.30	0.30	2.30	2.30	2.30	12.00	21.80	35.90	1	45.80
R.P	**2.43**	1.04	1.04	1.06	1.04	1.01	1.00	1.00	1.01	1.00	1.01		
13/10/1985	**35.90**	23.20	23.20	23.20	23.20	23.20	25.20	25.20	34.20	44.70	58.80	1	35.90
R.P	**1.73**	1.28	1.22	1.23	1.19	1.05	1.02	1.01	1.03	1.02	1.02		
1/7/1988	**45.30**	45.30	45.30	45.60	45.60	58.50	62.00	106.10	116.90	146.20	178.10	1	45.30
R.P	**2.38**	1.89	1.63	1.60	1.53	1.33	1.14	1.42	1.39	1.42	1.46		
7/7/1991	**74.80**	75.10	75.10	75.10	75.10	94.00	195.20	233.90	263.20	329.40	378.50	1	74.80
R.P	**8.29**	3.99	2.90	2.62	2.47	2.13	5.88	6.63	5.45	7.99	8.02		
13/12/1994	26.10	29.90	29.90	30.00	35.70	94.20	156.70	254.20	352.20	381.10	**455.30**	60	7.59
R.P	1.33	1.41	1.31	1.31	1.35	2.14	3.21	8.92	15.53	14.44	**17.65**		
14/02/1994	10.90	37.00	40.80	40.80	40.90	69.40	166.80	257.40	350.50	392.00	**464.00**	60	7.73
R.P	1.06	1.60	1.52	1.50	1.44	1.50	3.74	9.36	15.21	16.39	**19.33**		
20/05/1998	50.50	**143.70**	143.70	150.50	150.80	169.60	180.70	189.10	216.90	228.60	268.90	2	71.85
R.P	2.90	**31.66**	15.74	13.32	12.60	9.01	4.65	3.55	3.29	2.76	2.85		
21/05/1998	93.20	115.80	**166.30**	166.30	173.10	190.40	202.70	211.70	236.70	251.20	288.70	3	55.43
R.P	19.63	13.25	**28.66**	19.26	21.27	14.01	6.65	4.83	4.06	3.45	3.39		
22/05/1998	22.60	22.60	115.80	**166.30**	166.30	181.30	199.90	211.70	225.10	251.20	284.40	4	41.58
R.P	1.24	1.27	7.65	**19.26**	18.11	11.54	6.35	4.83	3.59	3.45	3.26		
12/8/2004	**75.80**	90.10	90.10	90.10	90.10	136.20	137.20	137.20	141.70	141.70	158.40	1	75.80
R.P	**8.68**	6.11	4.08	3.51	3.31	4.56	2.42	1.90	1.65	1.39	1.32		
17/08/2004	34.80	52.50	52.50	52.50	66.90	**157.00**	203.10	204.10	204.10	208.60	225.30	10	15.70
R.P	1.67	2.23	1.84	1.77	2.14	**6.93**	6.70	4.35	2.89	2.30	2.00		
25/08/2004	43.80	51.00	51.00	51.00	53.10	130.00	**234.50**	234.50	281.60	286.10	288.10	15	15.63
R.P	2.26	2.15	1.80	1.73	1.71	4.05	**11.41**	6.69	6.72	4.96	3.37		

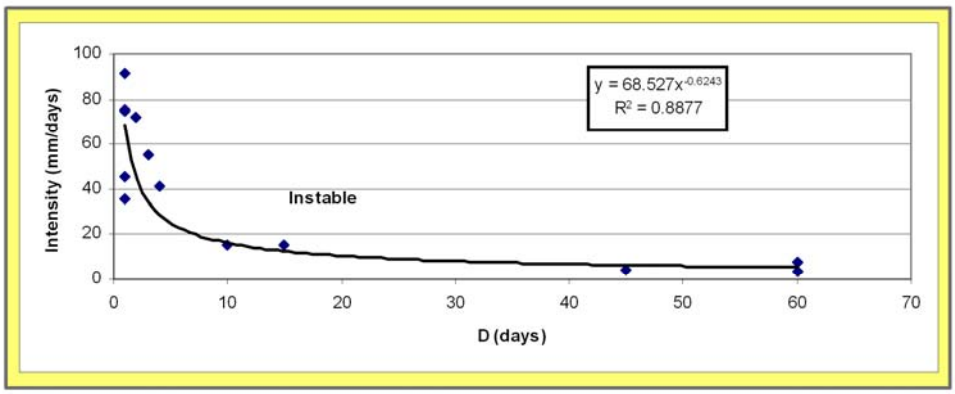

Figure 3.107. Intensity Duration plot of 16 reported landslide events

The threshold indicates that the sustained intensities of 68.53 mm for 1 day, 44.46 mm for 2 days, 34.51 mm for 3 days, and 25.09 mm for 5 days are sufficient to trigger landslides in the study region (Figure 3.107).

3.6.1.5 Evaluation Rainfall Thresholds Obtained from Various Methods

Calculation of temporal probability of landslide is necessary for landslide hazard mapping. The initial step to obtain temporal probability is to estimate the critical rainfall thresholds. In this study two different approaches were adopted for daily and antecedent rainfall data to relate landslide occurrence to rainfall data. As a result of this analysis, different critical rainfall thresholds were estimated. The sensitivity of the analysis results was analyzed by comparison of critical thresholds obtained from different methods. For comparison, the thresholds obtained for three different antecedent days and for a 5-year return period were tabulated (Table 3.26). 5-year return period was selected due to the common return period for determination of critical rainfall thresholds for the methods.

Table 3.26 indicates that all methods provide similar results for daily rainfall threshold which has 71 mm, 72 mm, 68.53 mm and 69 mm for time series, gumbel approach for daily data, intensity duration and gumbel approach for antecedent rainfall data respectively. Additionally, the rainfall thresholds obtained as a result of Intensity Duration (ID) and Gumbel distribution methods resemble for 5 and 20 antecedent days, namely 125.44 and 109.84, and 211.18 and 204.15 respectively. As a result, we can confirm that the rainfall triggering thresholds obtained from either method can be used for further hazard analysis. Therefore, by considering that landslides are influenced by antecedent rainfalls in the study region, the thresholds obtained as a result of antecedent rainfall analysis can be selected. Gumbel distribution approach was preferred for further analysis due to the probability of obtaining critical rainfall thresholds for three different return periods (5, 10, and 50) as illustrated in Table 3.24.

Table 3.26. The critical rainfall thresholds obtained from Gumbel analitical process and Intensity Duration Curves.

	Daily Data Analysis		Antecedent Data Analysis	
Day	**Time Series**	**Gumble Approach**	**Intensity Duration (ID)**	**Gumble Approach**
1	71	72	68.527	69
5	-	-	125.44	109.84
20	-	-	211.18	204.15

3.7 Hazard Assessment

After the computation of rainfall triggering threshold value, the hazard map was created based on a developed hazard assessment procedure, which was described in section 2.3.4.2. As described in this section, the hazard assessment procedure requires determination of $(P_l|P_t)$ and P_t in addition to the P_s, which was created in susceptibility part.

The folowing approaches were developed to estimate the $(P_l|P_t)$ value. $(P_l|P_t)$ value is the conditional probability of having a landslide given that rainfall triggers exceed a certain threshold value for a given time period, which is necessary for hazard analysis. The proposed approach involves modeling landslide occurrence and rainfall values higher than the critical rainfall value by logistic regression. For each critical threshold value which was obtained by Gumbel approach, the $(P_l|P_t)$ was computed with logistic regression respectively. In this approach, the antecedent rainfall values greater or lower than the corresponding critical antecedent rainfall threshold were assigned a value of 1 or 0 respectively. In this approach, it was assumed that rainfall values that exceed critical threshold may cause a landslide. For instance, critical rainfall threshold for five antecedent days is 125.44 mm. Therefore, depending on the assumption, the rainfall data set of five antecedent days was transformed to dichotomous data type by assigning 1 to rainfalls greater than the threshold and 0 to the rest. Relatively, the landslide events were assigned 1 if any occurred on that rainfall day, or else 0 was assigned. Then logistic regression was computed. It was computed based on the equation:

$$f(x)=\text{logit}((P_l|P_t))= \ln((P_l|P_t) /(1- (P_l|P_t))= \beta_0 + \beta_1\times \text{Rainfall} \quad (59)$$

The result of logistic regression was then evaluated using a chi-square of Hosmer-Lemeshow test, Cox and Snell R^2 and Nagelkerke R^2 (Table 3.27). The -2 Log likelihood provides an index of model fit. The lower the value is, the better the model fits the data. Chi-square value is also similar to the Godness of fit, which compares the actual values for cases on dependent variable with the predicted values on the dependent variable. Cox and Snell R^2 and Nagelkerke R^2 are essential estimates of R^2 indicating the proportion of variability in the dependent variable that may be accounted for by all predictor variables included in the equation. Larger pseudo r-square statistics indicate that more of the variation is explained by the model from a minimum of 0 to a maximum of 1.

Table 3.27. Model summary of logistic regression for rainfall values greater than the tresholds

Step	-2 Log likelihood	Cox & Snell R Square	Nagelkerke R Square	Chie-square
Daily (69),5 RP	188.65	0.005	0.11	24.112
Day5 (140.8) ,10 RP	212.7	0.002	0.09	20.96
Day20 (266.85),50 RP	200.85	.004	0.173	41.628

The models created after the regression was presented with Eq. 60-62 for daily, 5-day threshold and 20-day threshold respectively.

$$Ln((P_l|P_t) /(1- (P_l|P_t)) = -5.889 + 4.057 \times Rainfall_{daily} \quad (60)$$

$$Ln((P_l|P_t) /(1- (P_l|P_t)) = -6.581+ 3.56 \times Rainfall_{5day\ accum} \quad (61)$$

$$Ln((P_l|P_t) /(1- (P_l|P_t)) = -7.142+ 4.292 \times Rainfall_{20dayaccum} \quad (62)$$

The logit of the f(x) function, P (L), which is defined by the logistic function in terms of probability, was calculated for all of the pixels of the study region by using Eq.43. The $(P_l|P_t)$ values are obtained by analyzing the probability values where rainfall values exceed the critical rainfall value.

After obtaining the $(P_l|P_t)$ values, the P_t value, which is the probability of trigger that exceeds a certain threshold, was obtained. For computations of P_t value, Gumbel distribution was used. The estimated $(P_l|P_t)$ and P_t values are presented in Table 3.28.

Table 3.28. Parameters required for the creation of probabilistic Hazard Maps

Rainfall Treshold	Return Period (year)	$(P_l \| P_t)$	Gumble, P(t)
Daily (63)	5	0.16	0.2
Day5 (140.8)	10	0.14	0.1
Day20 (266.85)	50	0.06	0.02

The triggering scenarios are combined with conditional probability to obtain an ultimate probability of trigger that exceeds a certain threshold for annual hazard. The ultimate probability of trigger was computed by Eq. 63.

$$P_t = \sum_{i=1}^{n} P_{ti}\left(P_l \middle| P_{ti}\right) \tag{63}$$

Where; P_t is the ultimate probability of trigger, n is the number of scenarios.

By taking into account the ultimate probability of trigger and information of spatial probability, the yearly hazard probability can be estimated based on Eq 64. The result maps are probabilistic landslide hazard maps of Kumluca watershed of Bartın site for different mapping model and mapping units.

$$H = P_S x P_t \tag{64}$$

Figure 3.108 shows hazard maps produced by the LR, SR, and ANN methods for grid-based mapping unit. Similarly, Figure 3.109 presents hazard maps created by the LR, SR, and ANN methods for slope unit-based mapping unit. Looking at the maps which are obtained by using three different methods in both mapping units, it can be seen that the differences are subtle and there are also areas with obvious dissimilarities. In LR and ANN maps at both mapping units, the south-eastern and north-western parts of the regions have low hazard compared to the spatial regression counterpart. This means that more areas can be classified as low susceptible if the hazard map is produced by LR or ANN. In contrast, the map from the SR shows medium hazard illustrated with yellow, green and light blue for the south-eastern and north-western parts of the regions.

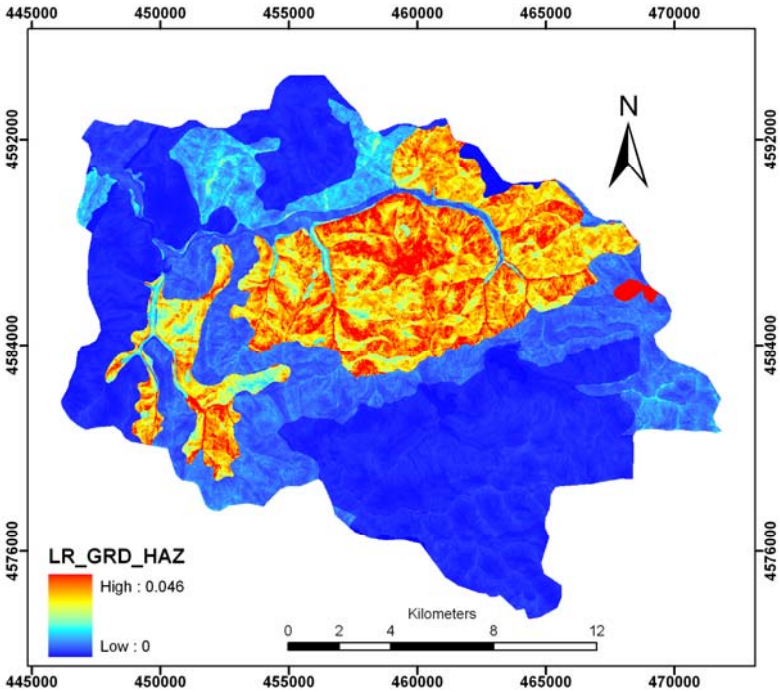
445000
450000
455000
460000
465000
470000
4592000
4584000
4576000
N
LR_GRD_HAZ
High : 0.046
Low : 0
Kilometers
0 2 4 8 12

(a)

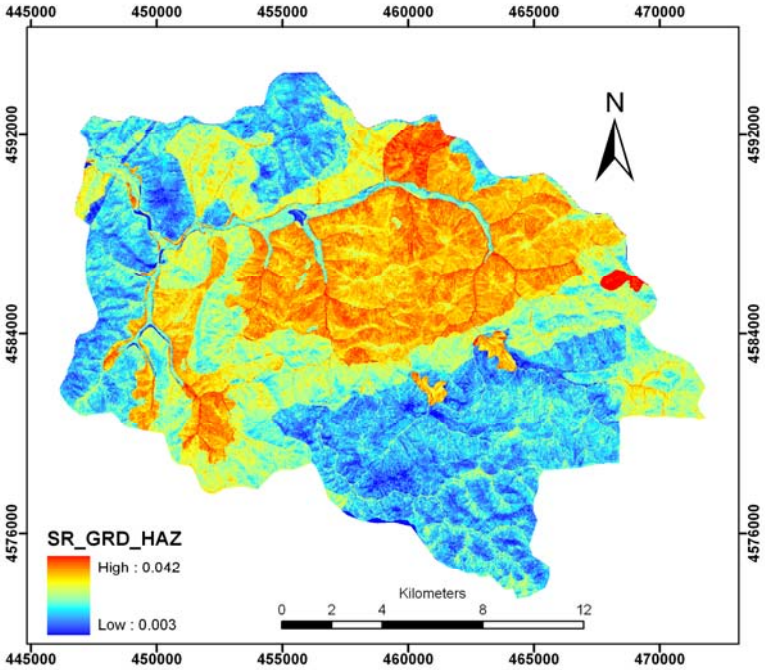
445000
450000
455000
460000
465000
470000
4592000
4584000
4576000
N
SR_GRD_HAZ
High : 0.042
Low : 0.003
Kilometers
0 2 4 8 12

(b)

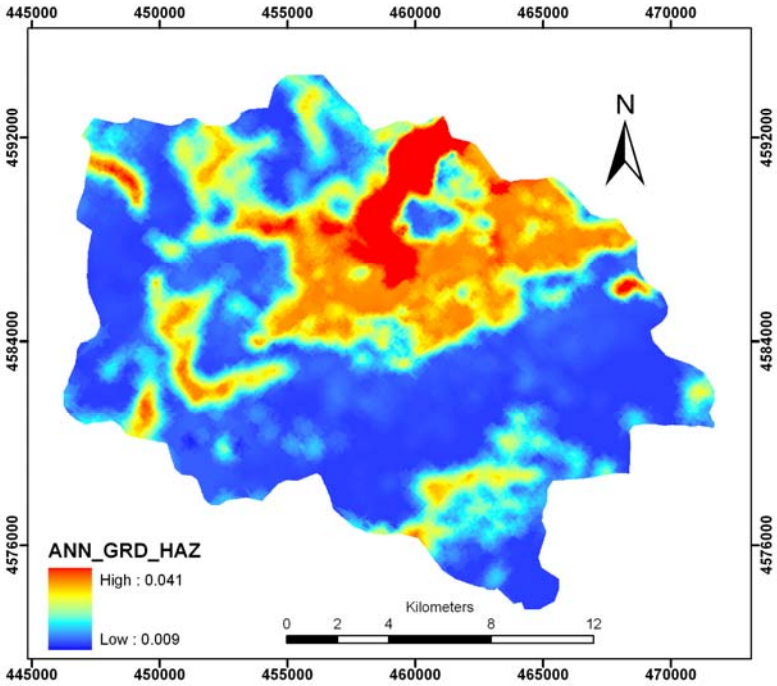

(c)

Figure 3.108. Landslide hazard map of Bartın Kumluca region obtained annually for different mapping methods where a. LR, b. SR and c. ANN, expressed as annual probability of landslide occurrence probability for each pixel

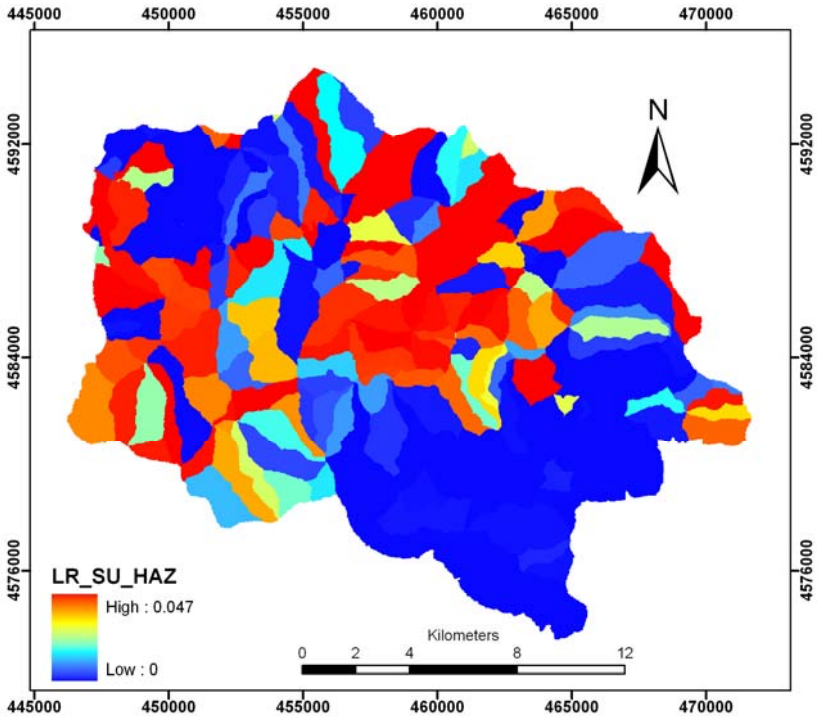

(a)

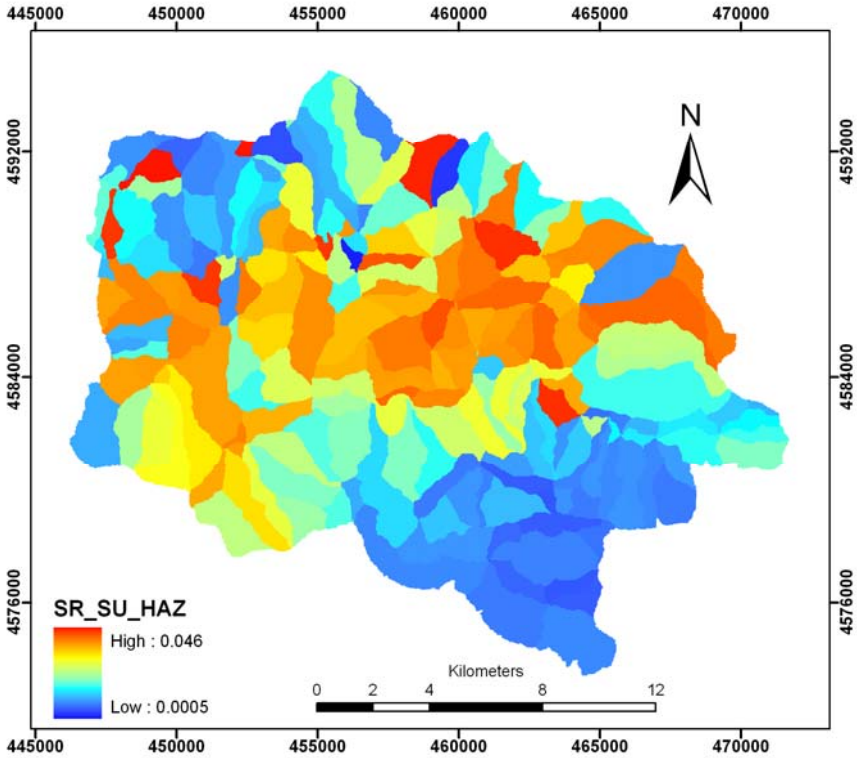

(b)

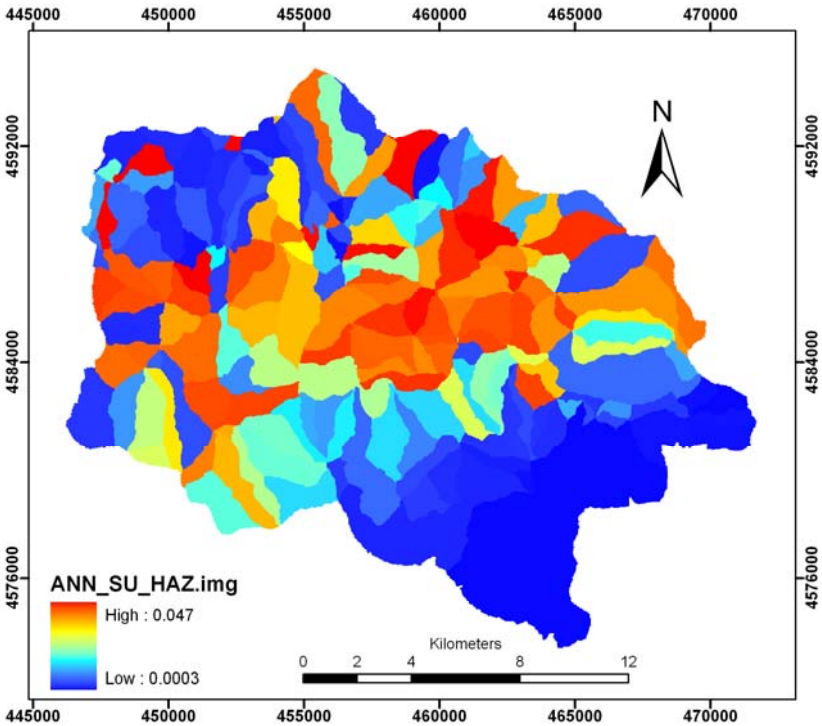

(c)

Figure 3.109. Landslide hazard map of Bartın Kumluca region obtained annually for different mapping methods where a. LR, b. SR and c. ANN, expressed as annual probability of landslide occurrence probability for each pixel

The areas which are low hazard at the LR and ANN can then be designated as medium hazard by the SR. This situation can also be confirmed by the statistics of hazard maps presented in Table 3.29. The mean value of hazard map obtained by the SR with grid-based mapping unit (SR_GRD_HAZ) is higher compared to the other methods, and the standard deviation of the hazard map obtained by SR with slope unit-based mapping unit (SR_SU_HAZ) is the lowest, which indicates that the variation of susceptibility is low.

Table 3.29. The statistics obtained from the hazard maps

	Min	Max	Mean	Std. Dev
LR_GRD_HAZ	0	0.05	0.01	0.01
SR_GRD_HAZ	0	0.04	0.03	0
ANN_GRD_HAZ	0.01	0.04	0.02	0.01
LR_SU_HAZ	0	0.05	0.02	0.02
SR_SU_HAZ	0	0.05	0.02	0.01
ANN_SU_HAZ	0	0.05	0.02	0.02

3.8 Consequence Analysis

Depending on the definitions of AGS (Australian Geomechanics Society), consequence is the outcomes or potential outcomes arising from the occurrence of a landslide expressed qualitatively or quantitatively, in terms of loss, disadvantage or gain, damage, injury or loss of life (AGS, 2000). The characterization of consequence scenarios is based on elements at risk, vulnerability of elements at risk and determination of the probabilities of spatial impact and temporal impact (Bell and Glade, 2004).

3.8.1 Probability of Spatial Impact

Hazard analysis must necessarily take the run-out distances into account, which is the maximum distance that the landslide mass is able to travel in its downslope movement (Corominas et al., 2003). Landslide run-out distances need to be estimated to calculate the probability of spatial impact P (S|H), which can be input to risk studies (Finlay et al., 1999; Bertolo and Wieczorek, 2005). Analytical techniques for determining the travel distance may be categorized either as empirical or dynamic in

nature (Fannin and Wise, 2001). For regional studies, the input parameters cannot be measured easily, therefore simplifying assumptions are often made. In this study, the run-out was not estimated. Therefore, a simplifying hypothesis was accepted. This hypothesis assumes that susceptibility values at least partially reflect the effects of run-out. Because for the majority of the mapped phenomena (slow moving landslides), which are used in susceptibility assessment, the deposition area was mapped together with the detachment zone (Catani et al., 2005).

3.8.2 Probability of Temporal Impact

The probability of temporal impact should also be considered in the risk analysis. The properties (such as buildings, infrastructure, etc.) are always exposed to threats for all the time. For this reason, the probability of temporal impact for properties is 100% whereas for humans the temporal probability may change depending on the occupancy of buildings (e.g. between night and day, week days and weekends; summer and winter). Hence, it is necessary to make allowance for the probability that persons (or a particular number of persons) will be in the area affected by the landslide (AGS, 2000).

Therefore, the duration of people's stay in their houses or their working in a factory, or even pupils' attending in schools needs to be determined. For varying occupancy, it is simply a calculation of the proportion of a day (0 to 1.0) when a certain number of people occupy the building (Catani et al., 2005). In this study, the day and night are considered for occupancy of houses. In the daytime, people are considered to work at farms, and at night, they are thought to be in their houses.

3.8.3 Vulnerability Analysis

Vulnerability (V) is one of the fundamental components in the assessment of risk (Leone et al., 1996). It is defined as the degree of loss of a given element or set of elements at risk within the landslide-affected area (Varnes and IAEG 1984; Fell 1994; Leone et al., 1996; Wong et al., 1997). The vulnerability value is generally

expressed on a scale of 0 (no damage) to 1 (total loss).

Vulnerability to a property and to an individual differs (Dai et. al., 2002). Generally, to derive a qualitative index for vulnerability of a property, many different cases should be evaluated. Physically the run-out distance, the volume, and the velocity of sliding, the elements at risk for property (buildings and other structures), and their nature, such as the technical resistance of the building (type, nature, age, and the like.), and their proximity to the slide should be determined (Finlay, 1996; Dai et al., 2002). In addition the social, economic, and environmental factors should also be combined for an accurate assessment of vulnerability indicator. Hence, it is not feasible to derive a vulnerability index for small scale studies. Most of the vulnerability assessment publications are related to large-scale studies or on a site-investigation scale (Leone et al. 1996; Ragozin and Tikhvinsky 2000; Barbat 2003); there are relatively few studies on a small-scale risk assessment.

Due to lower resolution on regional scale, it is not an easy task to identify different vulnerability values for different types of elements at risk. Thus, in this scale the vulnerability indicator is set equal to "1" for all elements at risk (E) and the number of persons per building (E_{pe}). It is assumed that if a landslide occurs, it may provide a total destruction, which means that a complete loss will occur wherever the event happens. Vulnerability and exposure were summarized by the definition of potential worth of losses. The worth of loss (WOL) is the representation of the amount of elements at risk when the vulnerability is considered as 1.

3.8.4 Elements at Risk

One of the essential data for landslide risk assessment is elements at risk. The definition of elements at risk is limited due to data constraints and it corresponds to the scale of investigation (Bell and Glade, 2004).

The elements at risk can be classified as (AGS, 2000; Düzgün, 2008):

- Property assets, which may be subdivided into portions relative to the hazard being considered such as furniture, equipment, personal property, vehicles, machines, cars, trains etc.

- Humans, who either live, work, or may spend some time in the area affected by landsliding and have possibility to be affected from the landslide(s) that may cause losses of basically fatality and injury

- Structural elements, such as buildings, roads, railway lines, lifeline networks, communication facilities.

- Services, such as water supply or drainage or electricity supply.

- Natural environment involves flora, fauna, landscape, environmental quality, which is usually difficult to predict losses since they are mostly intangible.

Element at Risk for loss of Property

In this study, among the elements at risk classes described above, the emphasis was mostly given to buildings, roads, land-use and infrastructure. For the extraction of elements at risk, the relevant information was selected from digital topographic maps, as well as from the updated land cover map at a scale of 1:25,000. Sets of thematic data were constructed and the information stored in ARC/INFO coverages (vector data) is presented in Table 3.30.

A simple classification approach was adopted in which transport, buildings, infrastructures and other land uses were divided into subclasses. Using a raster-based method, specific vector data layers of elements at risk were transformed into raster data with 20 m x 20 m size grid cells.

The element at risk for property (road network, building damage and utility, etc.) was represented in monetary terms by first attributing the exposure of each element at risk to respective pixels and then overlaying the value of each property on pixel basis (Figure 3.114). When more than one type of element at risk was present within the same unit area (or pixel), then the sum of the object value it contained was considered for a pixel value.

Table 3.30. Classification of economic value with loss estimation of the principal elements at risk in TL/pixel

Main	Subclasses	Data format and unit	Element at Risk	Cost of EAR (TL) per unit	Loss (TL/ pixel)
Road	Provincial Highway (12 m wide)	Line_km	29.62	844723	16894
	Provincial Road (10 m. wide)	Line_km	140.61	751100	15022
	Local Road (8 m.)	Line_km	4.30	659200	13184
	Pathway	Line_km	1044.42	50000	1000
	Bridge and Cross	Line_km	1.28	25000	500
Building	House	Point_Number	4694	23600	23600
	Official Building	Point_Number	160	-	-
Infrastructures	PowerNetwork (Above Ground)	Line_km	97.29	50.00	1000
	Telephone Network	Line_km	65.78	62.00	1240
Landuse	Agriculture	Polygon_hectare	118	800	320

The Kumluca watershed has twenty-eight settlements and a total of 4,854 houses inside the study boundary. The houses are predominantly wooden and brick and mostly built on two floors, where the first floor is generally barn and the second floor is the dwelling. The houses are generally aligned through the margin of stream or constructed on the slopes. Hence, many of the houses are vulnerable to inundation or landslides. As shown in Figure 3.110, the building typology is subdivided into public houses and official buildings, where official buildings involve hospitals, educational, religious and communication buildings.

The identification of the value or the exposure of each element at risk is a difficult task. The value of each class was obtained through interviews with experts in different organizations in 2009 as presented in Table 3.30. The cost of buildings was obtained from the General Directorate of Disaster Affairs of Bartın. Considering the interviews, the cost was assigned to each individual building of house category. No cost was defined formally for official buildings; hence they were excluded from the data base. At this scale, each house is represented with a point label, where one pixel corresponds to an individual house. Thus, the attribute of cost is a unit value and assigned to each house as presented in the loss column in Table 3.30.

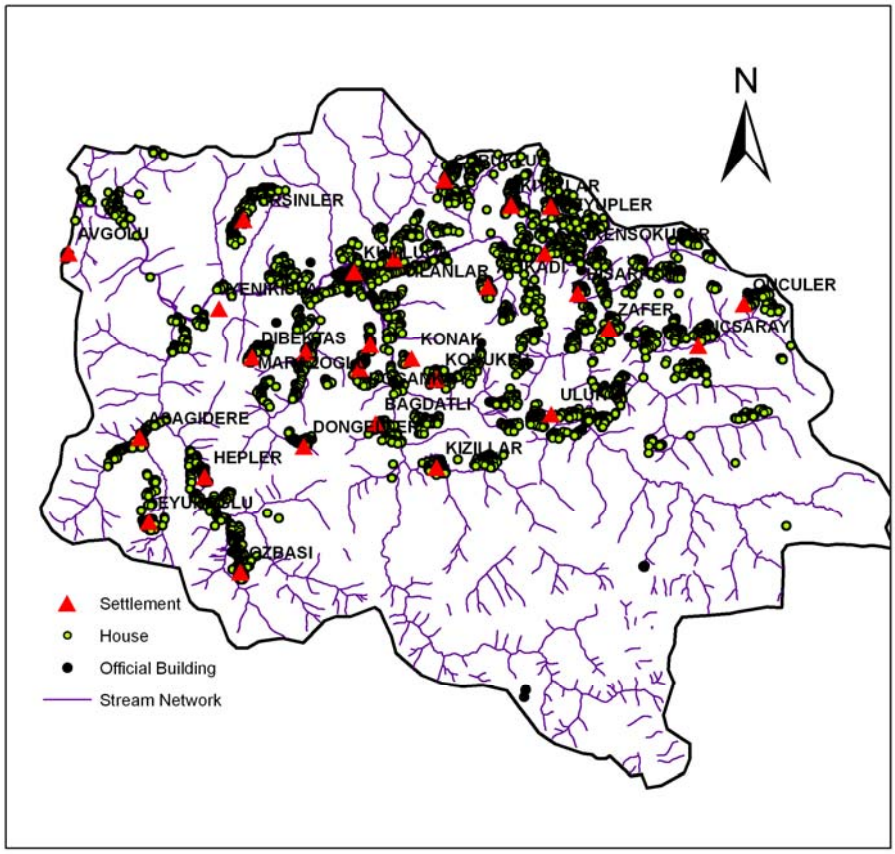

Figure 3.110. Category of the buildings and their spatial distribution over the stream network

The road network has five different categories (Figure 3.111). The first type is the Provincial highway transmitted through the southern part of the study region which is 12 m in width and 29.62 km in lenght. The second type is the Provincial road, which connects the Provincial highway to the villages. The local road is 10 m. wide and 140.61 km long. The local road is the road inside the district with 8-m width and 4.3-km lenght. The pathways connect small villages and are distributed throughout the mountainous topography with a length of 1044.42 km. The last category is the bridges. They cross and involve 1.28 km of the road network.

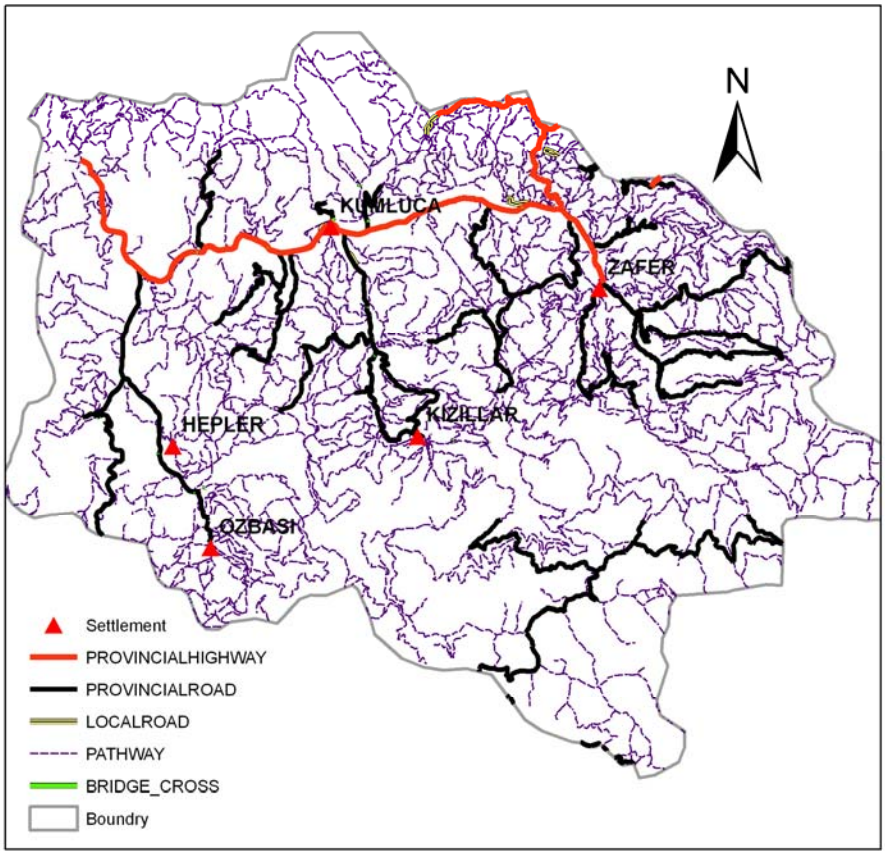

Figure 3.111. The road network categories

The infrastructures have two different types (Figure 3.112). The first type is the power network, which supplies power to the district with a length of 97.29 km, and the second type is the telephone network with a length of 65.78 km. The economic value of the road network and the infrastructure per km is supplied by the General Directorate of Transportation.

The categorization of cost for road network depends on engineering design and materials used for construction. In general terms, the road has better resistance to disasters if it has a higher cost. The cost of power and telephone network was determined depending on the quality of fiber and/or telephone pole used. An average cost was computed by considering the average required for quality, type, and length necessities.

To assign the cost value to each pixel, the value for road and infrastructures was produced by the conversion of cost per km to cost per pixel by considering 20 m

pixel resolution. The value produced after computation is presented in the Loss column in Table 3.30.

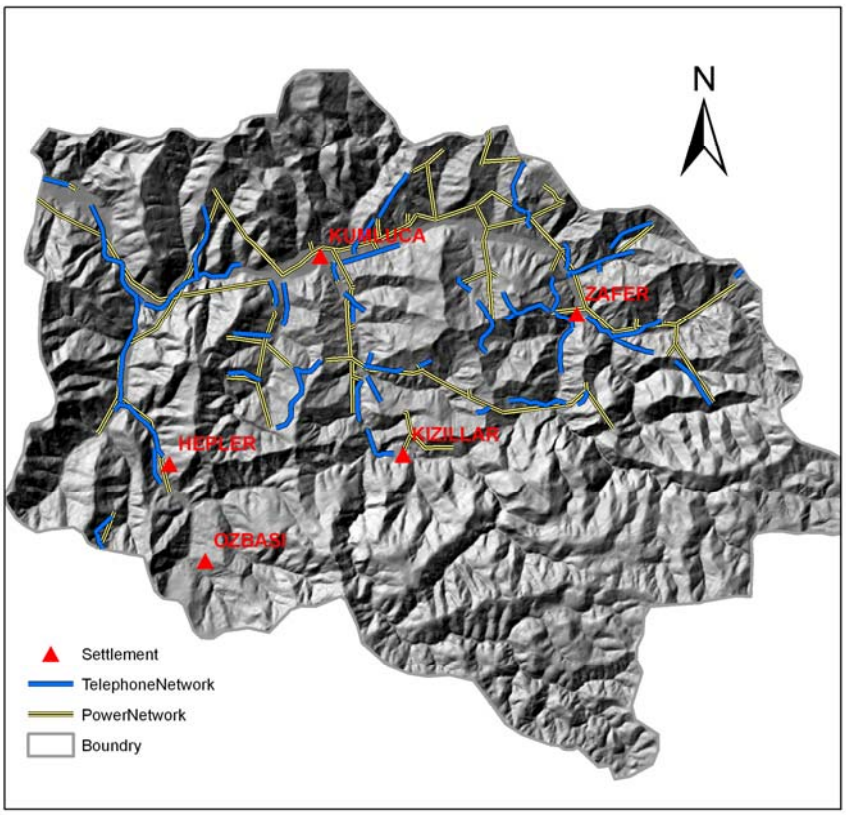

Figure 3.112. The power and road network overlaid on to hillshade of study region

The land cover map obtained from the General Command of Mapping presents that 36% of the region is covered by agricultural fields (Figure 3.113). These fields are mostly covered by a variety of harvest yield, such as wheat, corn, chestnut, nut, and apple. (Kumluca ve Çevresinden Bilgiler, 2009). However, it is not possible to map and collect information on different types of fields at this scale. Depending on the interviews from the Soil Yield Government Department (TMO, 2009), wheat and corn fields are the dominant types of fields; hence they were concerned for the analysis. An average economic value per hectare was estimated both for wheat and corn fields as presented in Cost of EAR (TL) per unit column of Table 3.30. Then for the further risk assessments, the cost per hectare for land-use was converted into cost per square meters (20 m x 20 m) as presented in Table 3.30.

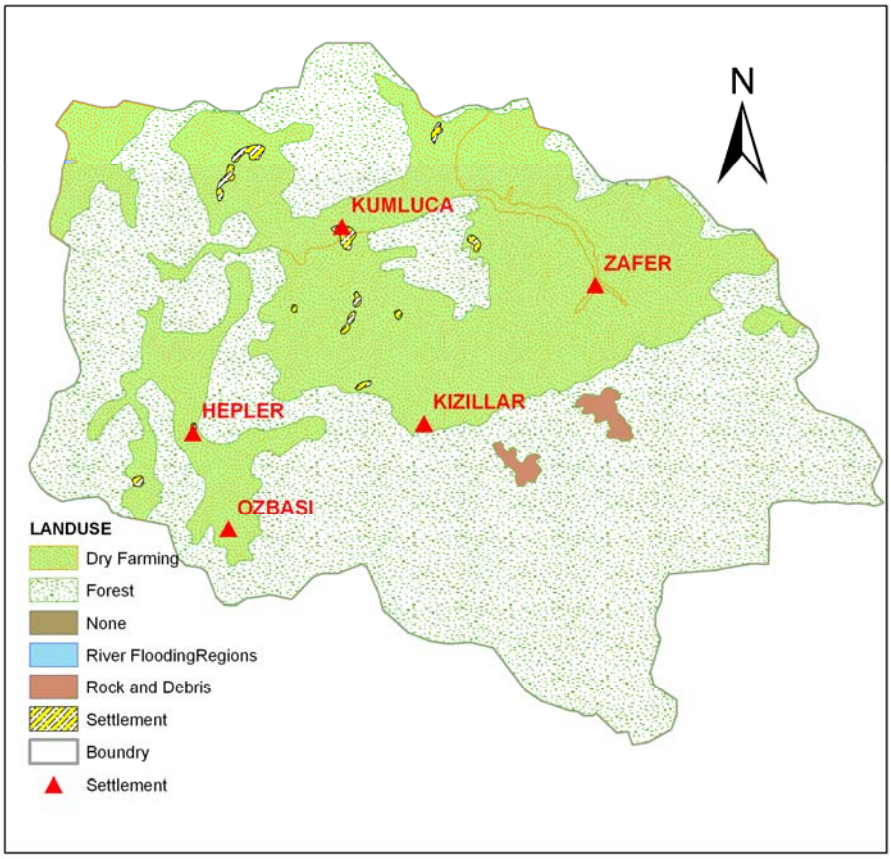

Figure 3.113. Land Use map of the study region

Once all the economic costs for buildings, roads, infrastructures, and agricultural regions per pixel are prepared, they are added in order to obtain the total cost of elements at risk as presented in Figure 3.114. The raster-based elements at risk map is a general map created to be used for further risk analysis for different models and mapping unit results.

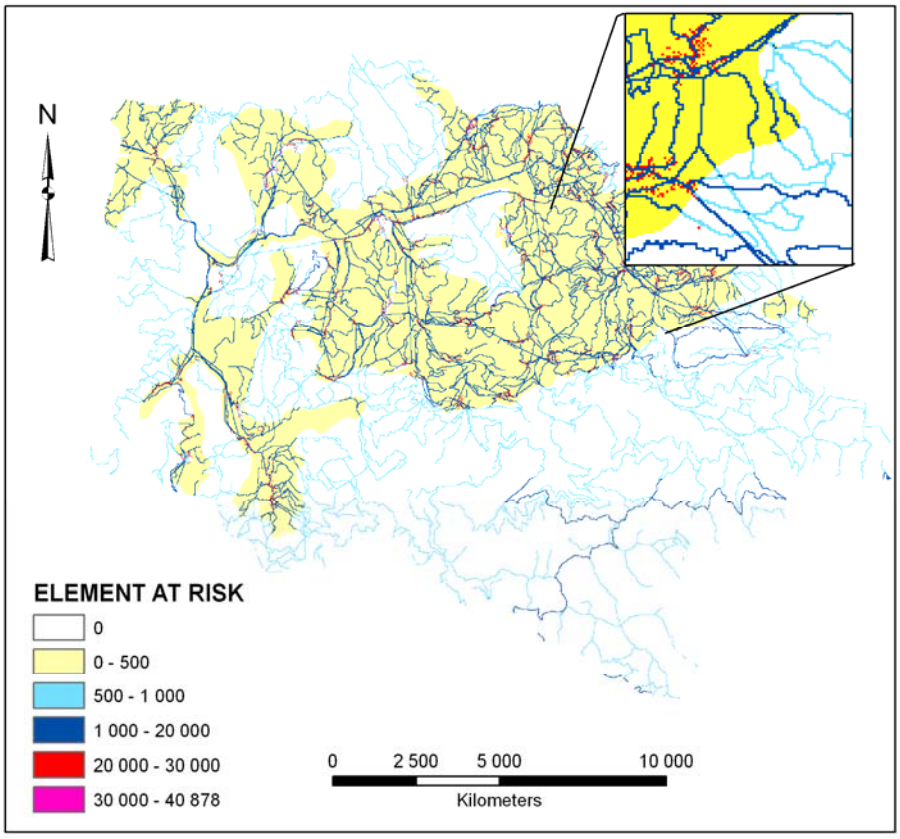

Figure 3.114. Elements at risk map generated with monetary terms at pixel basis (TL/per pixel)

Elements at Risk for Loss of Life

It is not an easy task to map the number of inhabitants in each house on regional scale. However, by reliable assumptions and stepwise estimation on population, risk assessment was also carried out for loss of life. The elements at risk for loss of life were computed by considering the occupancy of inhabitants in the buildings. Thus, the number of inhabitants living in each house was required for the assessment of risk to life. For this reason, ARC/INFO coverages of buildings at 1:25000 scale and the total population of the settlement was used. As the total population of villages and the number of existing houses in each village was known, the number of individuals in each house was estimated. For the estimation and assignment of the population information for each building, all houses except the houses in boundaries of Kumluca town were considered as detached house in the study region. Thus, the houses in Kumluca town were excluded by overlaying the boundaries of Kumluca town with the building layers.

The total number of the buildings in the study region is 4,857, where 5 buildings are health centres, 55 buildings are schools, 70 buildings are mosques, and the rest are private houses. By the assumption that public facilities have a better construction than private houses, these buildings and the houses in the city centre are excluded from the building database. Finally, there were 4,707 buildings left with detached houses. The total population for the villages is 123,343 for 2007.

In Bartın, there are 202 villages. Hence, assuming that the population is uniformly distributed throughout the villages, for each village approximately 610 people can be assigned. In Kumluca, there are 28 villages; hence, a population of 17,097 can be assigned to all the villages of Kumluca. The number of total detached houses is 4,707; hence, approximately 4 inhabitants were estimated to be living in each building.

Building data layers are transformed into raster data, attributing the number of residents in each building to respective grid cells. 4 residents were assigned to each building for the risk analysis. Hence, a data layer was created representing the spatial pattern of residents, which are points on the map (Figure 3.115).

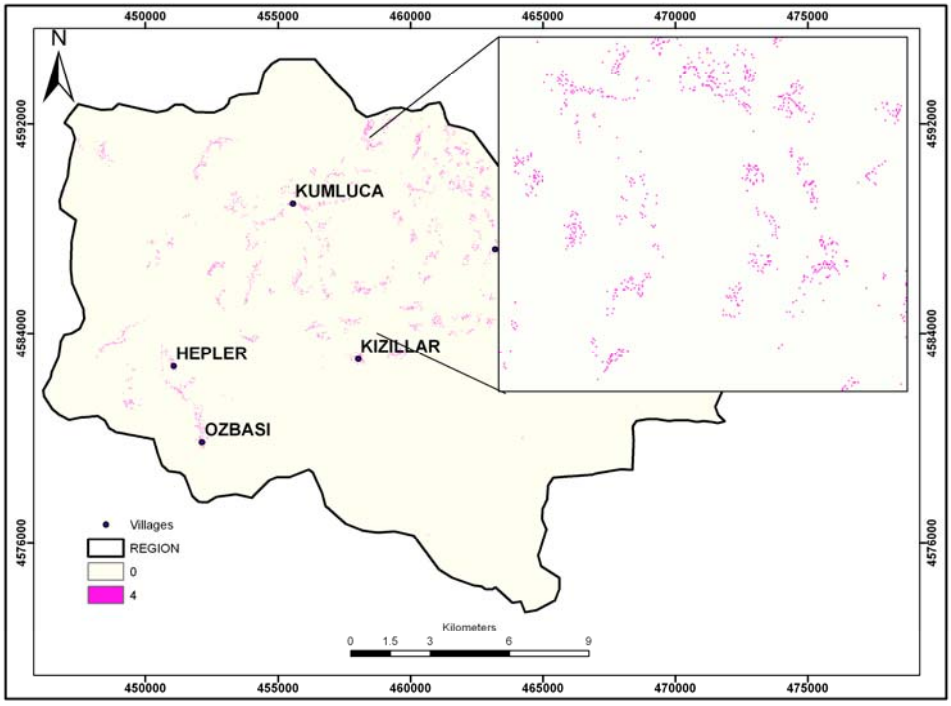

Figure 3.115. The spatial pattern of residents that are points on the map

3.9 Risk Assessment

To create risk maps for property and loss of life, two steps are followed. In the first step, the consequence map is produced. In the second step, the result of consequence layer is multiplied by each hazard probability value for each hazard map.

3.9.1 Risk Analysis for Property

The quantitative analysis of total risk was expressed as expected economic losses on a pixel basis, for each pixel. The risk value was assessed on the basis of the product of hazard, and consequence parameters as given in Eq. 65;

$$R(_{PROP}) = P(H) x\ P(S|H) x\ V(P|S) x E \quad (65)$$

or

$$R(_{PROP}) = P(H) x\ C \quad (66)$$

As discussed previously, the P(H) is the hazard probability obtained from the previous part of the study annually; P(S|H) and V(P|S) were set to 1, considering that the event is devastating in the probability of its occurrence. The amount of elements at risk is given in Table 3.30. As a result, the quantitative risk for properties is expressed as TL/pixel annually, where each pixel has a single risk value.

Quantitative risk maps were created for Kumluca region considering the landslide risk for roads, houses, infrastructures, and agriculture. The computation of risk is illustrated for LR method and grid and slope unit-based mapping unit in Table 3.31. Since it was not possible to illustrate the continous scale hazard values in this display, the mean value of hazard was considered.

To create risk maps for property, two steps were followed. In the first step, the consequence map was produced by multiplication of P(S|H), V(P|S) and Loss value of element at risk for property. In the second step, the resultant consequence layer was multiplied by each hazard probability in each hazard map in sequence to calculate the risk according to Eq. 66.

Table 3.31. Risk calculation for property. Hazard values are mean value and loss value according to Table 3.30.

Hazard Method	Element At Risk	E (TL/Pixel)	P(H) (mean)	P(S|H)	V(P|S)	$R_{(PROP)}$
LR_GRD_HAZ	Provincal Highway	16894	0.01	1	1	168.94
	Provincal Road	15022	0.01	1	1	150.22
	Local Road	13184	0.01	1	1	131.84
	Pathway	1000	0.01	1	1	10
	Bridge and Cross	500	0.01	1	1	5
	House	23600	0.01	1	1	236
	Official Building	None	0.01	1	1	None
	Power Network	1000	0.01	1	1	10
	Telephone Network	1240	0.01	1	1	12.4
	Agriculture	320	0.01	1	1	3.2
LR_SU_HAZ	Provincal Highway	16894	0.02	1	1	337.88
	Provincal Road	15022	0.02	1	1	300.44
	Local Road	13184	0.02	1	1	263.68
	Pathway	1000	0.02	1	1	20
	Bridge and Cross	500	0.02	1	1	10
	House	23600	0.02	1	1	472
	Official Building	None	0.02	1	1	None
	Power Network	1000	0.02	1	1	20
	Telephone Network	1240	0.02	1	1	24.8
	Agriculture	320	0.02	1	1	6.4

The illustration of risk maps on a continous scale provides a representation of the variation of risk values in the spatial domain. Figure 3.116 illustrates the spatial variation of risk values for property in grid–based mapping unit for three different methods. The risk maps for property obtained by LR (LR_GRD_RISK_PROP) (Figure 3.116a), SR (SR_GRD_RISK_PROP) (Figure 3.116b), and ANN (ANN_GRD_RISK_PROP) (Figure 3.116c) indicate that the pattern of risk values are similar, whereas the minimum and maximum values range from 1069.25 to 1575.44. The highest risk is observed in the provincal highway and the provincial road. Compared to the SR_GRD_RISK_PROP and ANN_GRD_RISK_PROP, the LR_GRD_RISK_PROP highlights the risk to power network on the medium level.

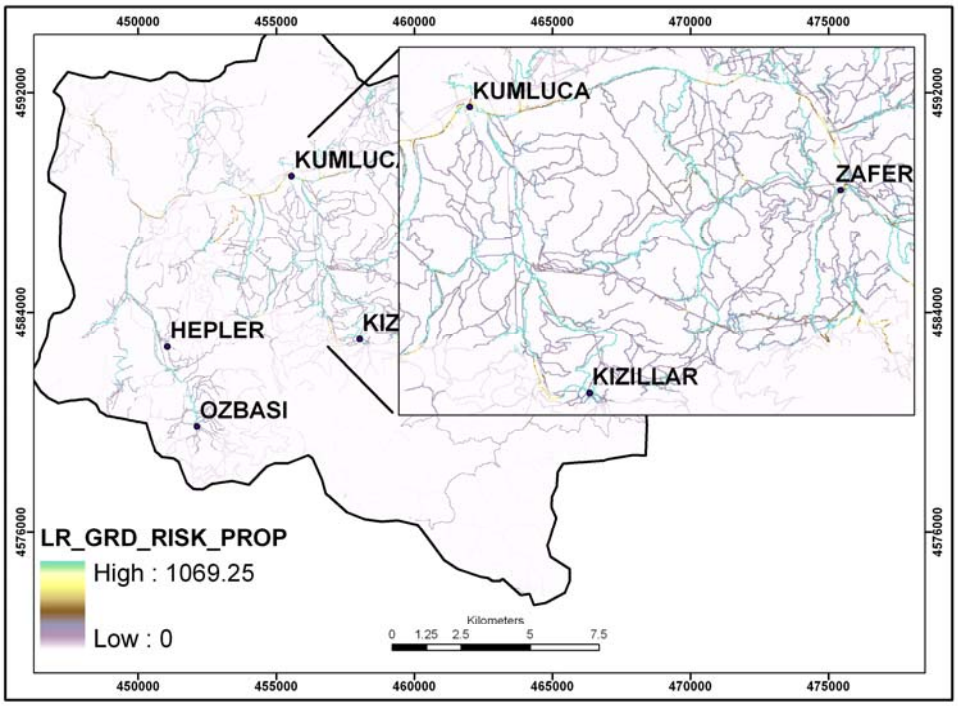
450000
455000
460000
465000
470000
475000
4592000
4584000
4576000
KUMLUCA
KUMLUC
ZAFER
HEPLER
KIZ
KIZILLAR
OZBASI
LR_GRD_RISK_PROP
High : 1069.25
Low : 0
Kilometers
0 1.25 2.5 5 7.5

(a)

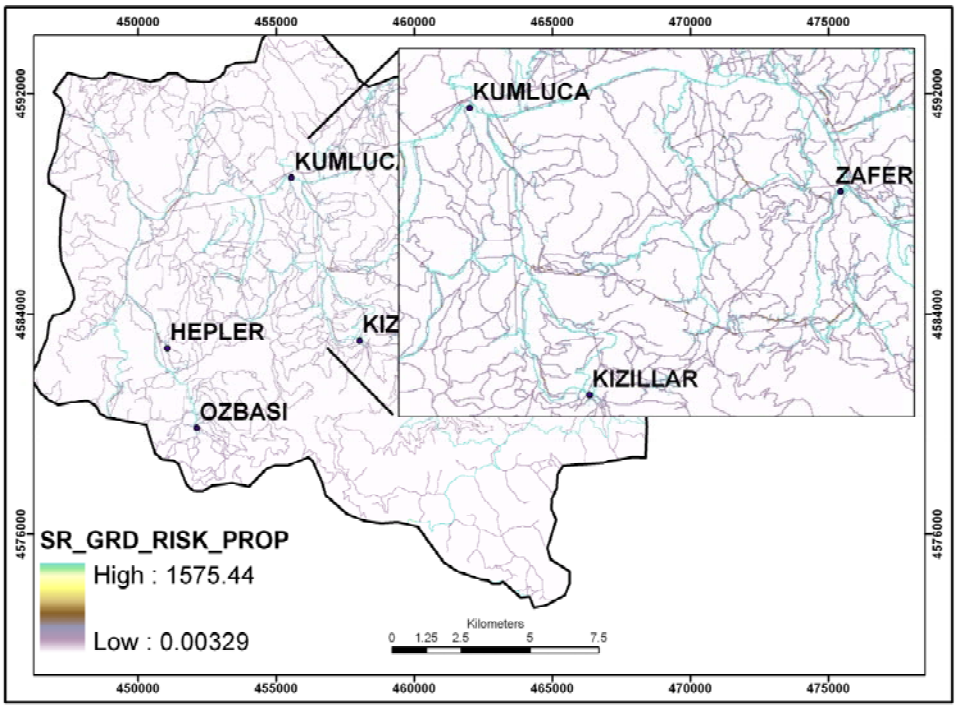
450000
455000
460000
465000
470000
475000
4592000
4584000
4576000
KUMLUCA
KUMLUC
ZAFER
HEPLER
KIZ
KIZILLAR
OZBASI
SR_GRD_RISK_PROP
High : 1575.44
Low : 0.00329
Kilometers
0 1.25 2.5 5 7.5

(b)

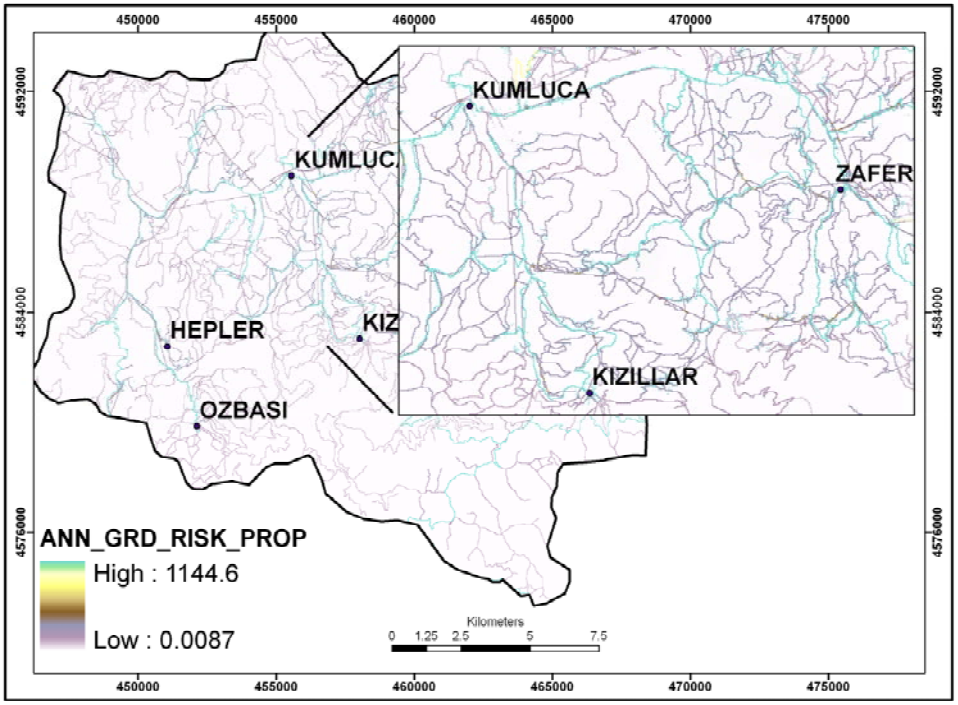

(c)

Figure 3.116. The risk to property for grid-based mapping unit for different methods, a. LR, b. SR and c. ANN

Figure 3.117 illustrates the spatial variation of risk values for risk to property in slope unit–based mapping unit for three different methods. The risk maps for property obtained by LR (LR_SU_RISK_PROP) (Figure 3.117a), SR (SR_SU_RISK_PROP) (Figure 3.117b), and ANN (ANN_SU_RISK_PROP) (Figure 3.117c) indicate that the pattern of risk values are similar to each other as in the grid-based maps (Figure 3.117a, b, c), whereas the minimum and maximum values range from 1827.81 to 1903.97. The SR_SU_RISK_PROP and ANN_SU_RISK_PROP illustrate the highest risk in the provincal highway and the provincial road; however, LR_SU_RISK_PROP illustrates the highest risk in the provincial road only.

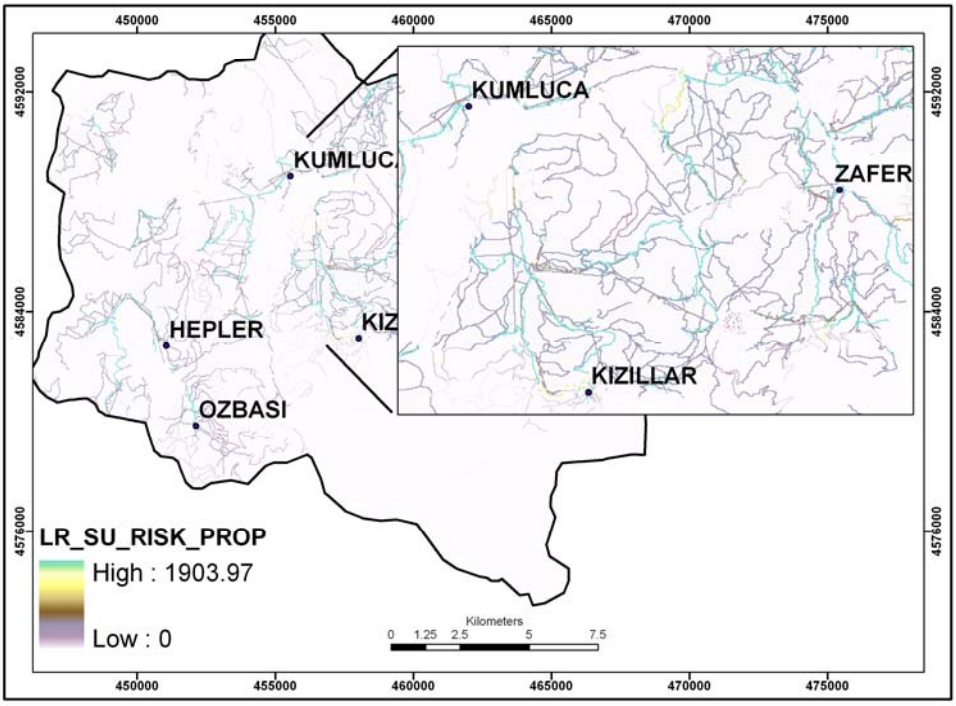
450000
455000
460000
465000
470000
475000
4592000
4584000
4576000
KUMLUCA
KUMLUC
ZAFER
HEPLER
KIZ
KIZILLAR
OZBASI
LR_SU_RISK_PROP
High : 1903.97
Low : 0
Kilometers
0 1.25 2.5 5 7.5

(a)

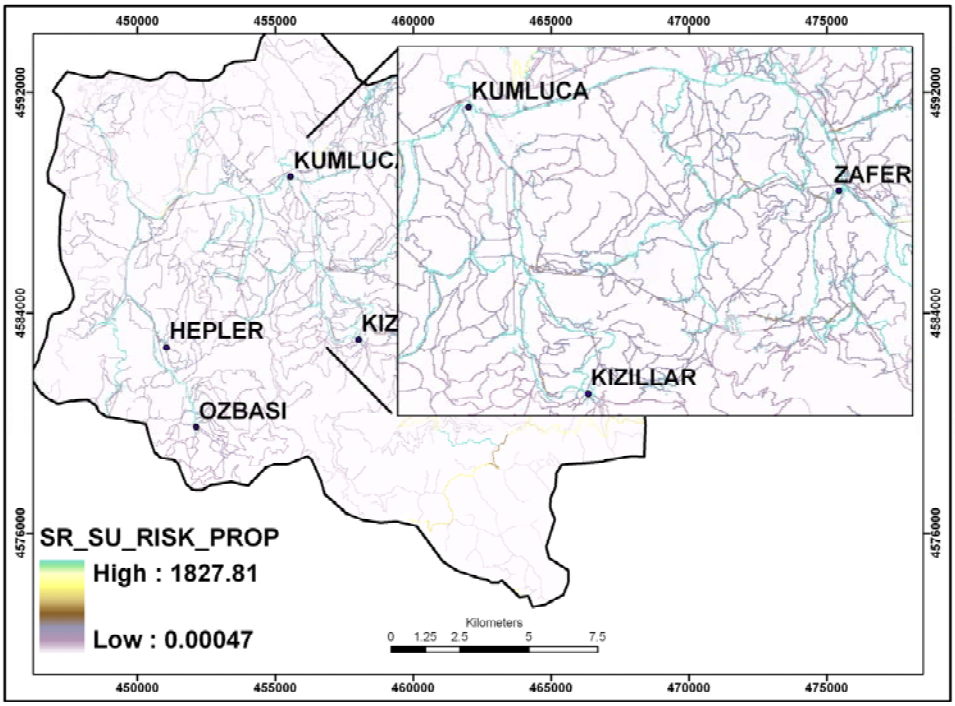
450000
455000
460000
465000
470000
475000
4592000
4584000
4576000
KUMLUCA
KUMLUC
ZAFER
HEPLER
KIZ
KIZILLAR
OZBASI
SR_SU_RISK_PROP
High : 1827.81
Low : 0.00047
Kilometers
0 1.25 2.5 5 7.5

(b)

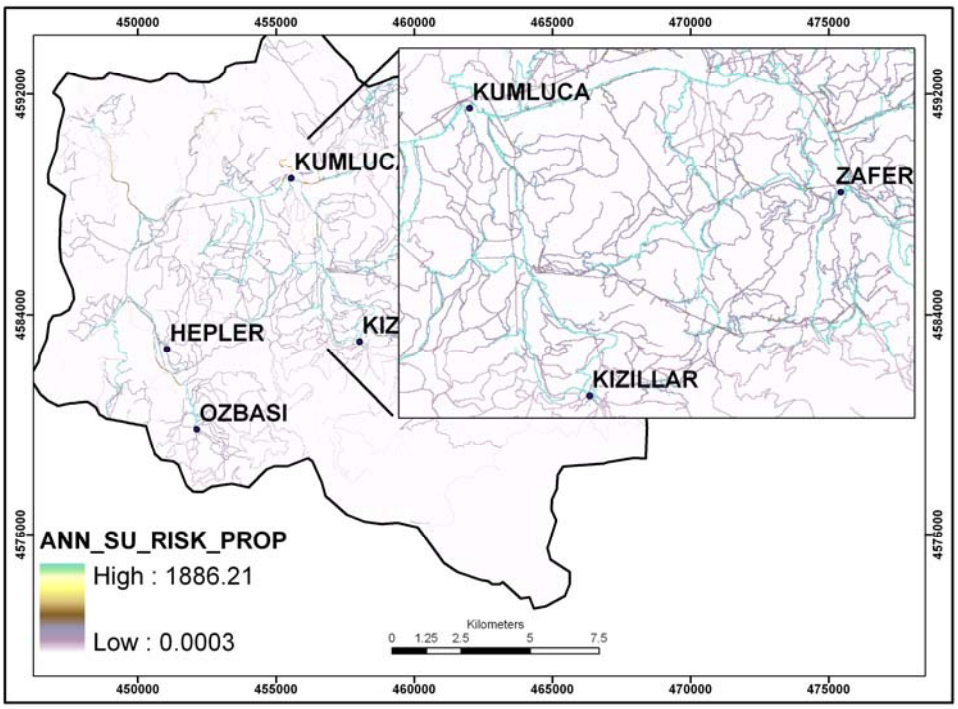

(c)

Figure 3.117 The risk to property for slope unit-based mapping unit for different methods, a. LR, b. SR and c. ANN (TL/per pixel)

The risk to property maps obtained by using grid-based and slope unit-based mapping unit for different methods were also evaluated by the computation of statistics for each map. The statistics obtained from risk maps indicated that the maximum values range between 1069.25 and 1903.97, and the mean value ranges between 4.36 and 14.31 (Table 3.32). The risk map obtained from the LR model with grid-based mapping unit (LR_GRD_RISK) provides the smallest maximum, standard deviation and mean value. On the other hand, the largest mean value is obtained from the risk map created from SR model with grid-based mapping unit (SR_GRD_RISK) with the largest standart deviation. In general, the LR_GRD_RISK and the risk map obtained from the ANN model with grid-based mapping unit (ANN_GRD_RISK) have smaller maximum, mean, and std.dev values than SR_GRD_RISK, the risk map obtained from the LR model with slope unit-based mapping unit (LR_SU_RISK), the risk map obtained from the SR model with slope unit-based mapping unit (SR_SU_RISK), and the risk map obtained from the ANN model with slope unit-based mapping unit (ANN_SU_RISK) maps.

Table 3.32. The statistics of the property risk maps for different methods and mapping units (TL/per pixel)

	Min	Max	Mean	Std. Dev.
LR_GRD_RISK	0	1069.25	4.36	32.94
SR_GRD_RISK	0	1575.44	14.31	84.35
ANN_GRD_RISK	0.01	1144.6	8.34	52.79
LR_SU_RISK	0	1903.97	10.46	81.9
SR_SU_RISK	0	1827.81	12.23	79.57
ANN_SU_RISK	0	1886.21	11.42	82.26

The risk values vary spatially depending on the hazard values because the element at risk values used for risk computation is stable for different prediction maps. Therefore, the range of risk values dependes on the variation on the predicted probabilities of hazard maps. For example, the hazard value of a method A and B is *a* and *b* respectively and the element at risk value is *t,* then the computed risk value will depend on the hazard value. If *a* is larger than *b*, then the risk value computed by *a* will be larger than the risk value computed by *b*.

3.9.2 Risk analysis for Loss of Life

The quantitative map for risk to life for Kumluca was created by considering the occupancy of buildings by people. For the estimation and assignment of population information for each building, the detached houses were considered and the houses at the boundaries of Kumluca town and the official buildings were excluded as discussed in the previous part.

The results calculated for risk to life are different from the results of the property risk with all ”risk cells“, and the risk was computed for day and night for humans where;

$$R(\mathrm{LOL}) = \sum_{i=1}^{2} \mathrm{P(H)x\ P(S\,|\,H)\ x\ Epe} \qquad (67)$$

$$R(\mathrm{LOL}) = 0.5 * (\mathrm{P(H)x\ P(S\,|\,H)\ x\ Epe})_{\mathrm{day}} + 0.5 * (\mathrm{P(H)x\ P(S\,|\,H)\ x\ Epe})_{\mathrm{night}} \qquad (68)$$

$$\mathrm{C= P(S|H)\ x\ E_{pe}} \qquad (69)$$

During the day, it is assumed that the inhabitants may be out of home and at least one inhabitant may be at home and at night all inhabitants are mostly at home. For that reason, for night computations, the number of inhabitants at home was considered as four, whereas during the day it was considered as one.

As discussed earlier, the P (H) is the hazard map produced in the previous part of the study obtained annually; P (S|H) is set to 1 considering that the event is devastating in the probability of its occurrence. Table 3.33 illustrates the computation of risk to life for different mapping methods and mapping units. Owing to continuous scale of hazard, the mean value was used to illustrate the risk computation. The final risk map to life was obtained with two steps. In the first step, the consequence map was produced by multiplication of P (S|H) by the number of residents in each building. In the second step, the result consequence map was multiplied by each probability of each hazard map in sequence.

Table 3.33. Risk calculation for life. Hazard values are mean value obtained from Table 3.30

METHOD	P(H) (mean)	P(S|H)	E_{day}	E_{night}	R(LOL)
LR_GRD	0.01	1	4	1	0.025
SR_GRD	0.03	1	4	1	0.075
ANN_GRD	0.02	1	4	1	0.05
LR_SU	0.02	1	4	1	0.05
SR_SU	0.02	1	4	1	0.05
ANN_SU	0.02	1	4	1	0.05

Figure 3.118 illustrates the spatial variation of risk values for risk to life in grid–based mapping unit for three different methods. The risk maps for loss of life obtained by LR (LR_GRD_RISK_POP) (Figure 3.118a), SR (SR_GRD_RISK_POP) (Figure 3.118b) and ANN (ANN_GRD_RISK_POP) (Figure 3.118c) indicate that the pattern of risk values varies for different mapping methods for grid-based maps (Figure 3.118a, b, c). The maximum risk value is similar for SR_GRD_RISK_POP and ANN_GRD_RISK_POP, which is 0.164 and 0.162 respectively and higher in the LR_GRD_RISK_POP with 0.181 risk value, whereas the variation of values varies much for each method. For instance, the SR_GRD_RISK_POP illustrates the buildings as high risk regions, and the region surrounded by Kumluca, Kızıllar, and Zafer has medium risk. The southern parts of the region are illustrated with a

combination of medium and low risk. On the other hand, ANN_GRD_RISK_POP and LR_GRD_RISK_POP illustrate the southern parts of the region with low levels of risk.

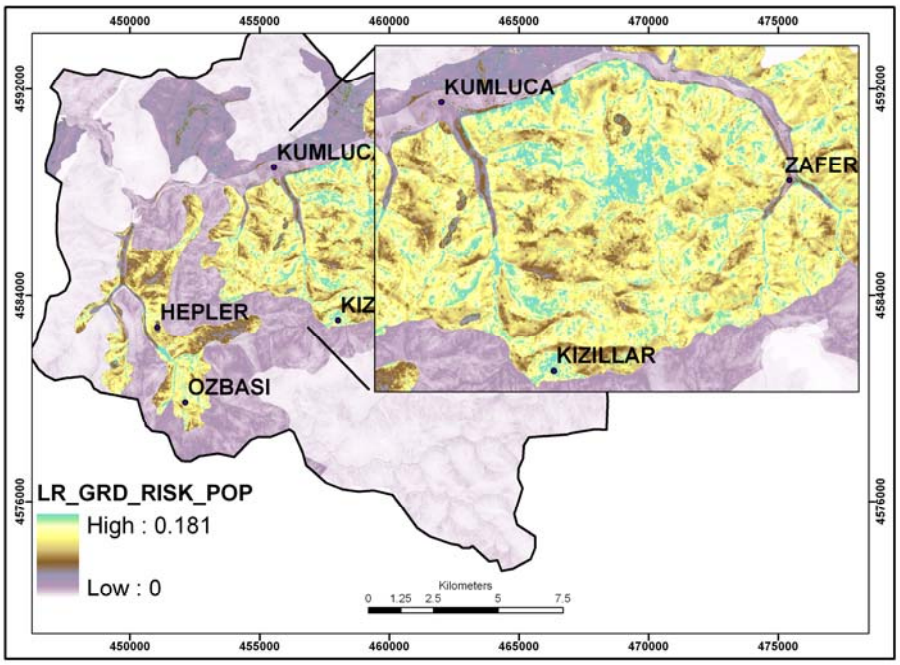

(a)

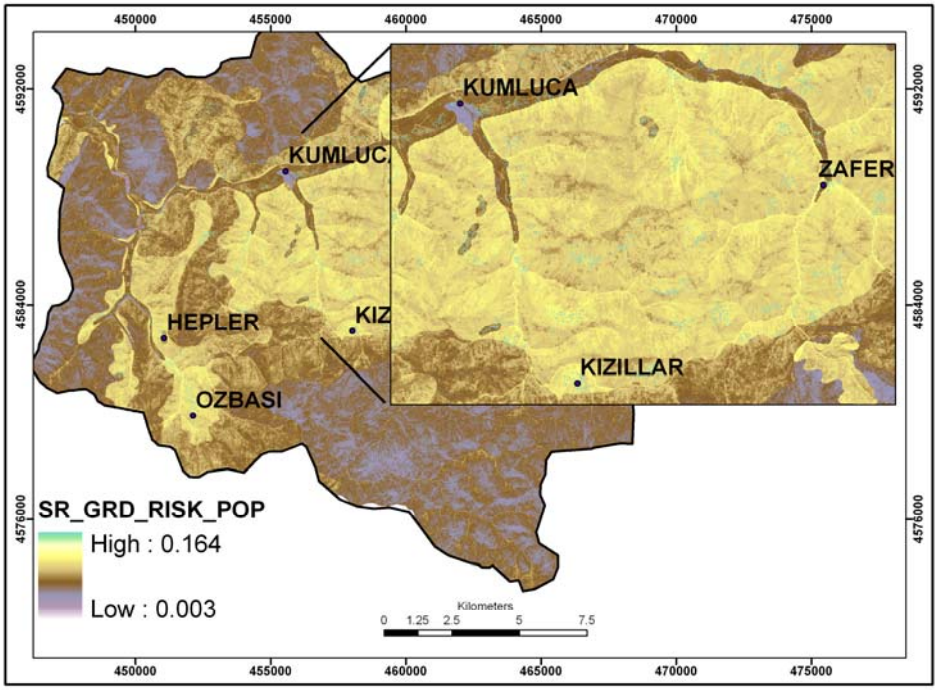

(b)

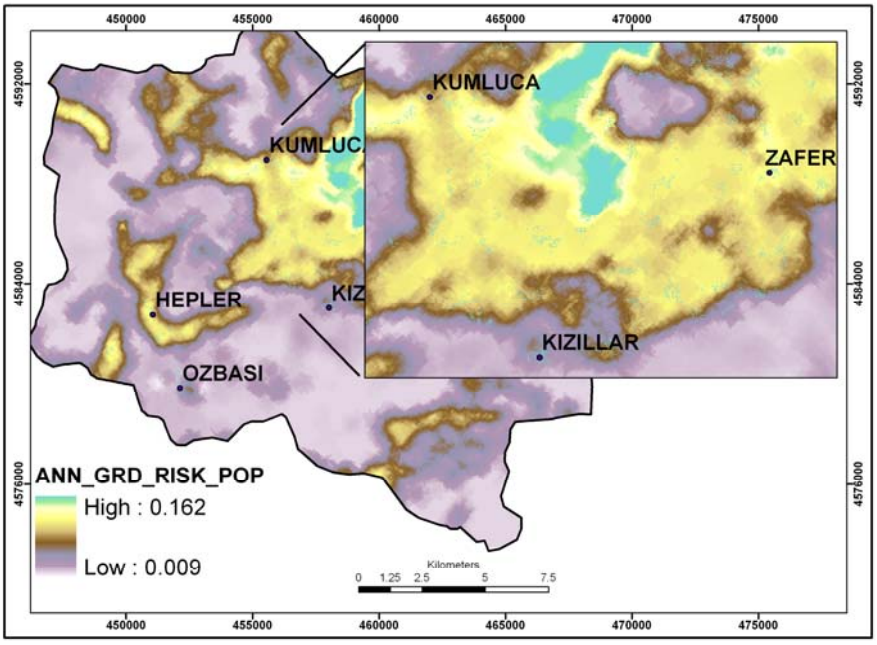

(c)

Figure 3.118. The risk to population for grid-based mapping unit for different methods, a. LR, b. SR and c. ANN (Loss of Life/per pixel)

The ANN_GRD_RISK_POP illustrates the region surrounded by Kumluca, Kızıllar, and Zafer with medium risk and high risk regions are mostly the buildings and a S-shaped region in the south-eastern parts The LR_GRD_RISK_POP illustrates the region surrounded by Kumluca, Kızıllar, and Zafer with medium risk and high risk values.

For slope unit-based mapping unit, Figure 3.119 illustrates the spatial variation of risk values for risk to life for three different methods. The risk maps for loss of life obtained by LR (LR_SU_RISK_POP) (Figure 3.119a), SR (SR_SU_RISK_POP) (Figure 3.119b), and ANN (ANN_SU_RISK_POP) (Figure 3.119c) provide a similar pattern of risk values for different mapping methods for slope unit-based maps (Figure 3.119a, b, c). The ANN_SU_RISK_POP and LR_SU_RISK_POP obtained lower risk levels, which are close to 0 in the southern parts of the region when compared to SR_SU_RISK_POP. The maximum risk value is similar for all mapping methods, which is 0.188, 0.184, and 0.187 for LR_SU_RISK_POP, SR_SU_RISK_POP, and ANN_SU_RISK_POP respectively. The highest risk values are obtained for the inhabitants living in each building for each method.

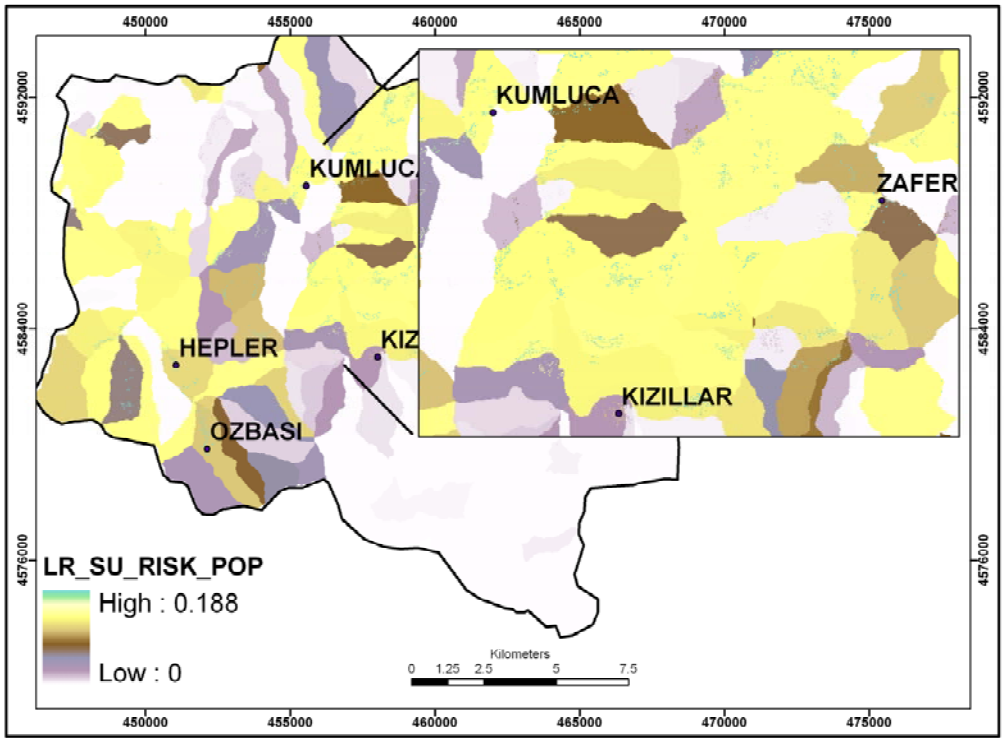
450000
455000
460000
465000
470000
475000
4592000
4584000
4576000
KUMLUCA
KUMLUC
ZAFER
HEPLER
KIZ
KIZILLAR
OZBASI
LR_SU_RISK_POP
High : 0.188
Low : 0
Kilometers
0 1.25 2.5 5 7.5

(a)

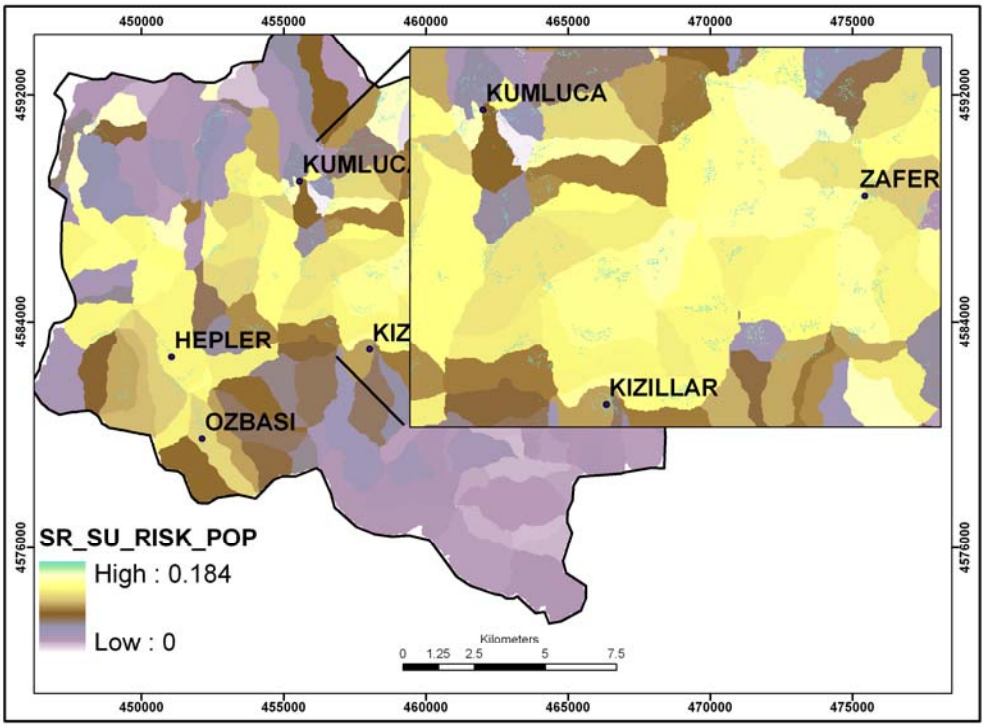
450000
455000
460000
465000
470000
475000
4592000
4584000
4576000
KUMLUCA
KUMLUC
ZAFER
HEPLER
KIZ
KIZILLAR
OZBASI
SR_SU_RISK_POP
High : 0.184
Low : 0
Kilometers
0 1.25 2.5 5 7.5

(b)

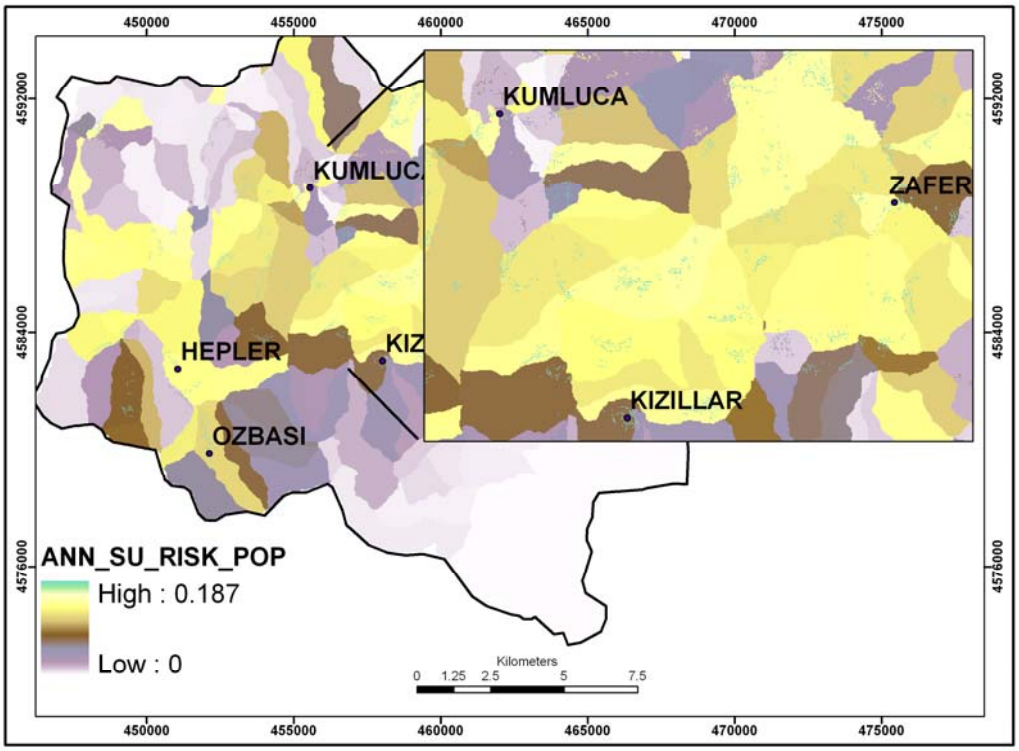

(c)

Figure 3.119. The risk to population for slope unit-based mapping unit for different methods, a. LR, b. SR and c. ANN (Loss of Life/per pixel)

When the statistics of risk maps are compared for grid and slope unit-based mapping unit for all methods, it is evident that the ANN_GRD_RISK, LR_SU_RISK, SR_SU_RISK, and ANN_SU_RISK have similar mean values (Table 3.34). LR_GRD_RISK has the smallest mean and SR_GRD_RISK has the largest mean value, which can also be observed in the statistics of hazard (Table 3.34). The risk maps to life obtained by grid-based mapping unit provide a lower variation of risk values than the risk to life obtained by slope unit-based mapping unit.

Table 3.34. The statistics of the risk maps of life for different methods and mapping units (Loss of Life/per pixel)

	Min	Max	Mean	Std. Dev.
LR_GRD_RISK	0	0.18	0.01	0.01
SR_GRD_RISK	0	0.16	0.03	0.01
ANN_GRD_RISK	0.01	0.16	0.02	0.01
LR_SU_RISK	0	0.19	0.02	0.02
SR_SU_RISK	0	0.18	0.02	0.02
ANN_SU_RISK	0	0.19	0.02	0.02

3.10 Comparison of Risk Maps for regional scale

The realization of the elements at risk and hazard probabilities for LR, SR, ANN models and for grid and slope-based mapping units led to the production of six different landslide risk maps for both property and life on local and regional scales. The risk maps for property and life portray the expected losses in TL per pixel and probability of life loss per pixel respectively. Numerically, for each pixel (20 m^2), a single value of *R* (*LOP*) and *R(LOL)* was computed. The maps for risk to property and risk to life portray the annual economic loss of property and annual probability of loss of life respectively. The development, evaluation, and comparison of these risk maps were performed within the GIS environment by carrying out some raster calculations.

For comparison purposes, six risk maps for both property and life on regional scale were rescaled so that the pixel values lie between 0 and 1. Then they were classified into three similar class ranges. The class ranges were defined by examining the cutoff values at each map. As a result, the risk maps were classified into three different levels of risk, putting the pixel ranges of 0 to 0.38 into low, 0.39 to 0.60 into medium, and 0.61 to 1 into high risk zones for property and life.

Two different approaches were adopted to compare the risk maps for regional scale analyses. In the first approach, the categorized risk values were quantified relatively by using bar graphs. Therefore, the number of pixels at low, medium, and high range classes was computed. The comparison of maps based on the histogram bar graphs provides quantitative comparison of the models; however, it does not yield spatial differences. Thus, in the second approach the risk maps were overlaid in sequence and the differences were computed. By overlaying the risk maps, it is easily possible to make a quantitative comparison of the models for similar and dissimilar regions in spatial domain. The differences are computed by subtracting the second map from the first map. Hence, any negative differences indicate that the second map overestimate (O) at that location compared to the first map. The positive difference shows that the second map underestimate (U) else if the difference is zero; then the maps are similar (S) on those regions. Six different difference maps were created for three different models and for two different mapping units. The differences

were analyzed for property and life risks individually. In addition to the illustrations of similarities in spatial domain, the percentage of pixels at each similarity was computed to make a quantitative comparison of risk maps.

The risk maps created after the classification process are illustrated to display the variation of risk values spatially in the study region for risk to property (Figure 3.120 and Figure D-1 to Figure D-5 in Appendix D) and for risk to life (Figure 3.121 and Figure D-6 to Figure D-10 in Appendix D). SR_GRD, ANN_GRD, LR_SU and SR_SU illustrate the risk to road or infrastructures in addition to houses when the spatial distribution of risk values is displayed in Figure D-1, Figure D-2, Figure D-3, Figure D-4 respectively when both mapping units are evaluated.

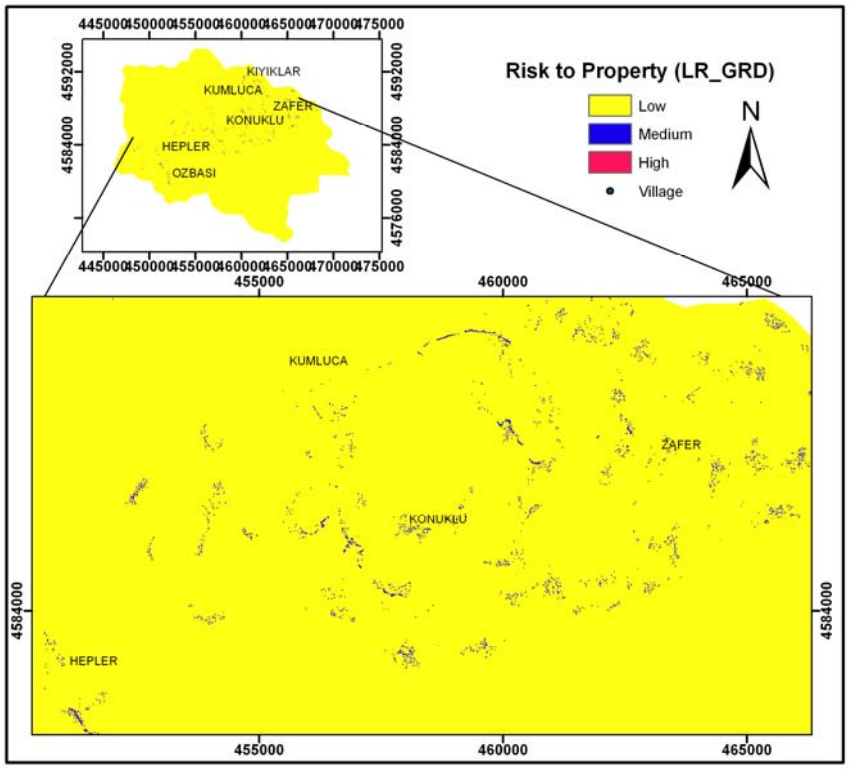

Figure 3.120. Risk to property for LR model and grid-based mapping unit (LR_GRD) (TL/per pixel)

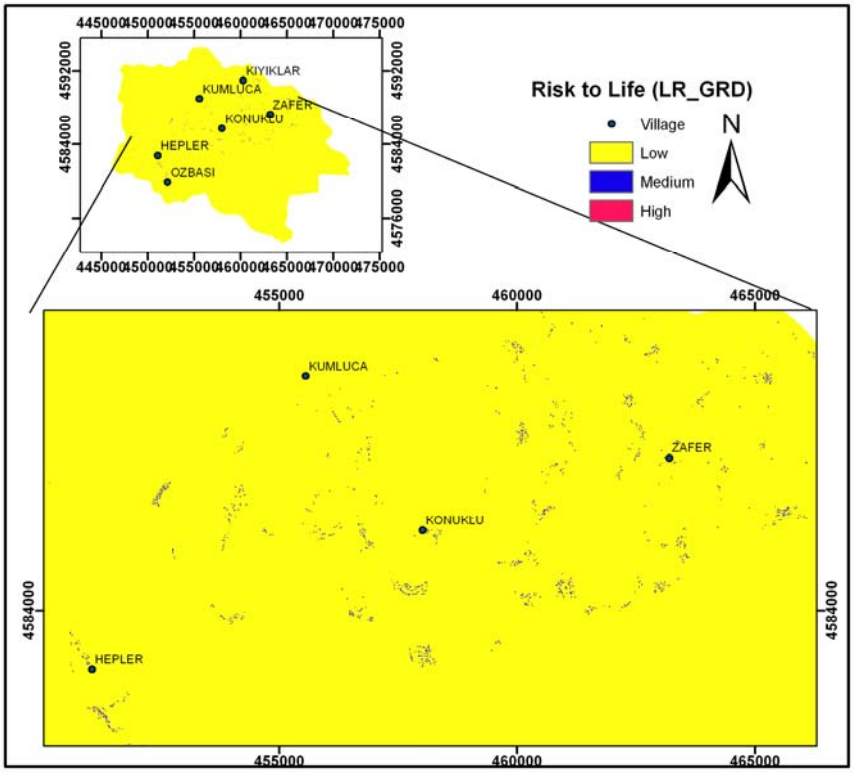

Figure 3.121. Risk to life for LR model and grid-based mapping unit (LR_GRD) (Loss of Life/per pixel)

However, LR_GRD and ANN_SU mostly display the risk values at the buildings in Figure 3.121 and Figure D-5 respectively.The categorized risk values were quantified by using the bar graphs as shown in Figure 3.122 and Figure 3.123.

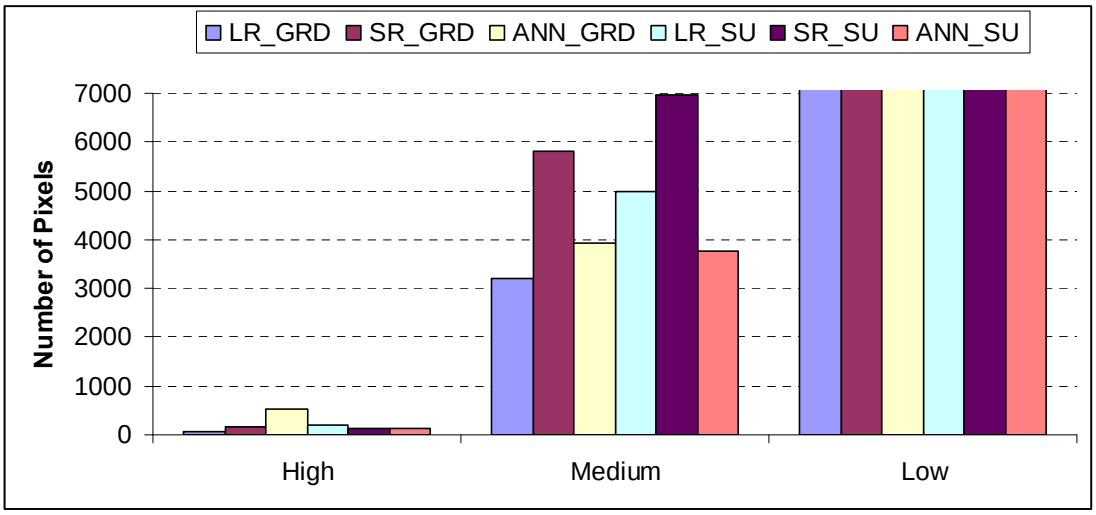

Figure 3.122. Bar graphs showing the relative distribution of risk levels for property for different class ranges

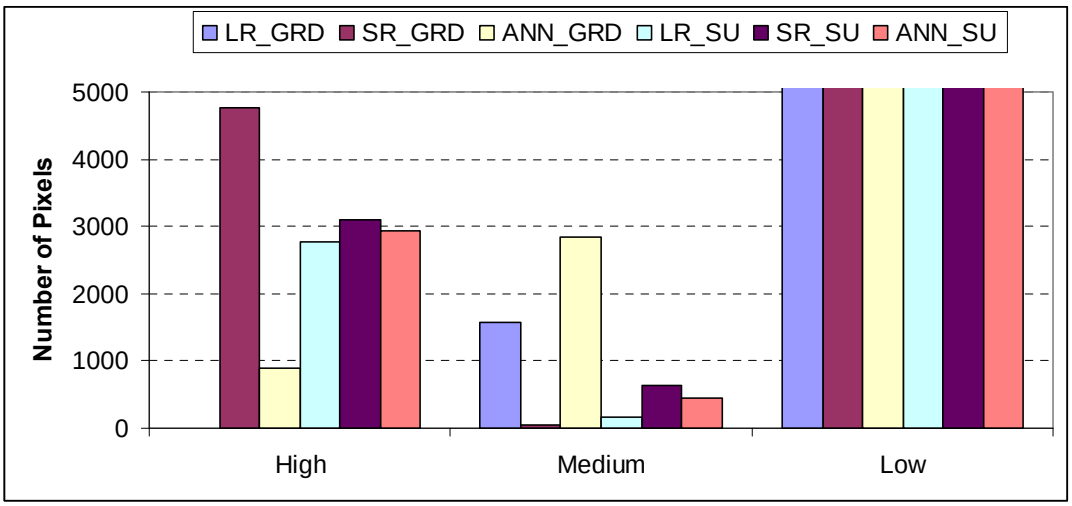

Figure 3.123. Bar graphs showing the relative distribution of risk levels for life for different class ranges

Therefore, the number of pixels at each class range was computed. The study region except from elements at risk has low risk values, which cover 99% of the region. Therefore, the number of pixels at low class is very high. In general, all risk maps were skewed to right, where the high risk class has the lowest number of pixels and the low risk class has the highest number of pixels. ANN_GRD (Figure D-2) has the highest number of risk values at high class and LR_SU (Figure D-3) follows in the second order. SR_SU (Figure D-4) represents most of the elements at risk classes at medium class, then SR_GRD (Figure D-1), and LR_SU (Figure D-3) follow.

Contrary to risk to property, the risk to life provides a distribution where the pixels at high risk class are higher. The SR_GRD has the highest number of risk values at the high risk class whereas the LR_GRD does not have any high risk values. The ANN_GRD provides the highest medium, then the LR_GRD comes. However, the SR_GRD has the lowest number of pixels in the medium class.

By overlaying the risk maps, a quantitative comparison of the models for similar and dissimilar regions at spatial domain is applied. The differences were computed for each slope and grid-based mapping unit separately by subtracting the second map from the first map, where the differences were represented at the top of Figure 3.124 and Figure 3.125 in the legend. For each mapping unit, 6 different difference maps were created for three different models and for two different mapping units. In

addition to the illustrations of similarities in spatial domain, the percentage of pixels at each similarity was computed to make a quantitative comparison of risk maps (Figure 3.124 and Figure 3.125).

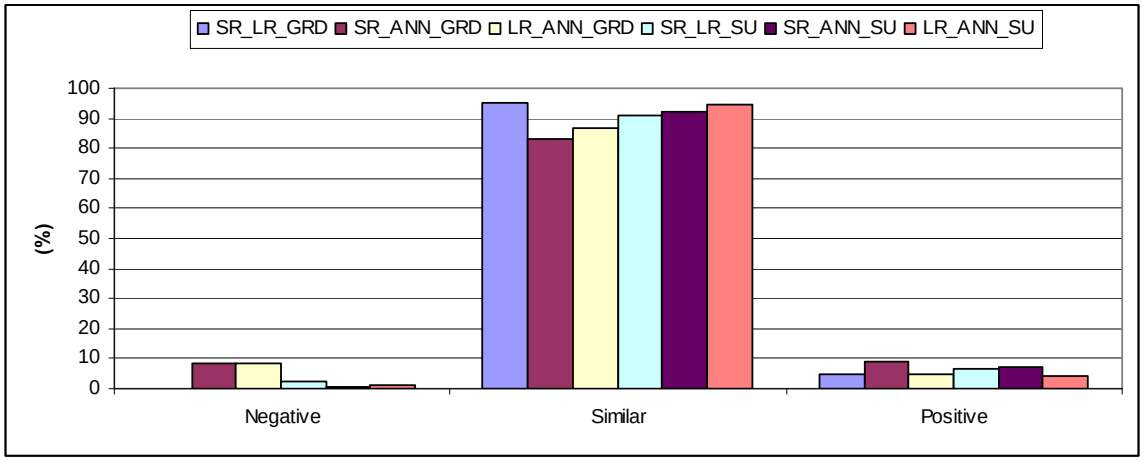

Figure 3.124. Bar graphs showing the percentage difference of risk levels based on different models and mapping units for property

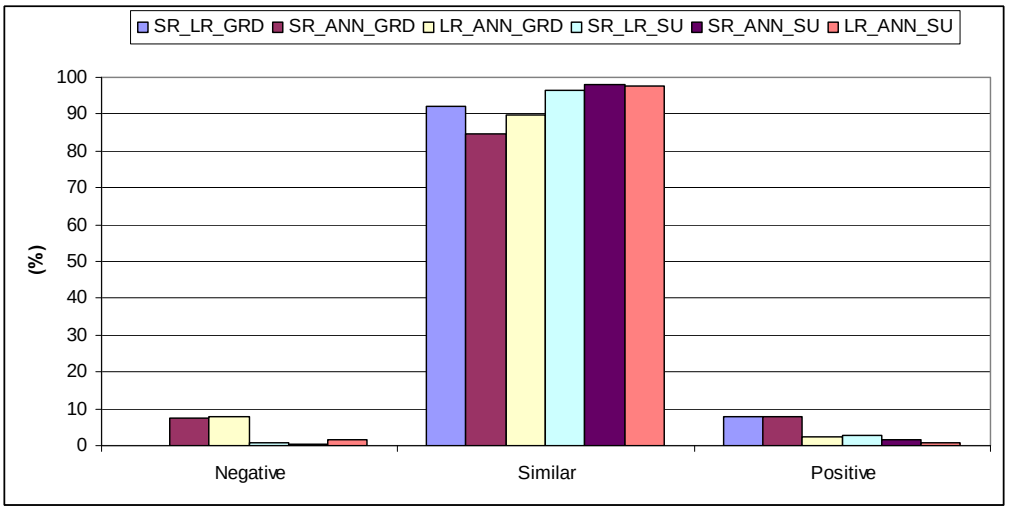

Figure 3.125.Bar graphs showing the percentage difference of risk levels based on different models and mapping units for life

The similarity values were higher for each model and mapping unit. As described before, it is due to the extension of the study region. The southern part of the region was at low risk for all risk maps as presented in (Figure 3.120, Figure D-1, Figure D-2, Figure D-3, Figure D-4, Figure D-5, Figure D-6, Figure D-7, Figure D-8, Figure

D-9, Figure D-10 and Figure 3.121) for risk to property and to life. Therefore, the number of low risk values was high at each risk map. To compare the similarities, it is important to identify the variation of histograms. Thus, the 750,000 pixel values were subtracted from all similarity values for both property and population risk values. Negative and positive values were fairly lower than the similarity values. Therefore, they are kept as the original. Afterwards, the percentage of pixels at each similarity class was computed to identify the similarities between risk maps.

As illustrated in Figure 3.124 the SR_LR_GRD shows the highest similarity, then LR_ANN_SU, SR_ANN_SU, SR_LR_SU, LR_ANN_GRD and SR_ANN_GRD follows the order. Therefore it is evident that while the SR_LR_GRD is more similar, SR_ANN_GRD is more dissimilar. This conclusion is also proved by the evaluation of negative and positive dissimilarities. SR_ANN_GRD provides the highest dissimilarities at both negative and positive classes.

When risk similarities for life are analyzed, it is seen that the LR_ANN_SU, SR_ANN_SU, and SR_LR_SU provide the highest similarities (Figure 3.125). This can also clearly indicate that the risk maps obtained by slope unit-based mapping unit provide higher similarities between LR, SR, and ANN compared to the models obtained by grid-based mapping unit. This can be proved by the evaluation of negative and positive risk values. The SR_ANN_GRD and LR_ANN_GRD illustrate the highest dissimilarities at negative and positive classes.

CHAPTER 4

IMPLEMENTATION FOR LOCAL SCALE RISK ASSESSMENT

4.1 Determination of High Hazard Zone

The hazard maps produced for regional scale were used for selection of the site for local scale risk analysis. Hepler district was identified as one of the high risk zones from the risk maps created after modeling the LR, SR, and ANN maps for grid and slope-based units. Hepler village was zoomed in to identify the local risk in the study region as presented in Figure 4.1-Figure 4.6.

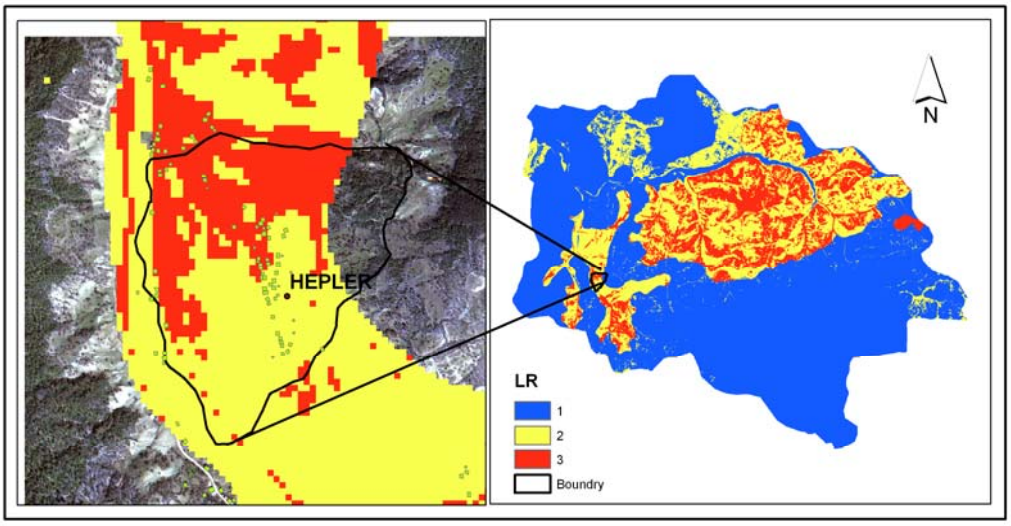

Figure 4.1. The grid-based LR hazard map levels for Hepler district

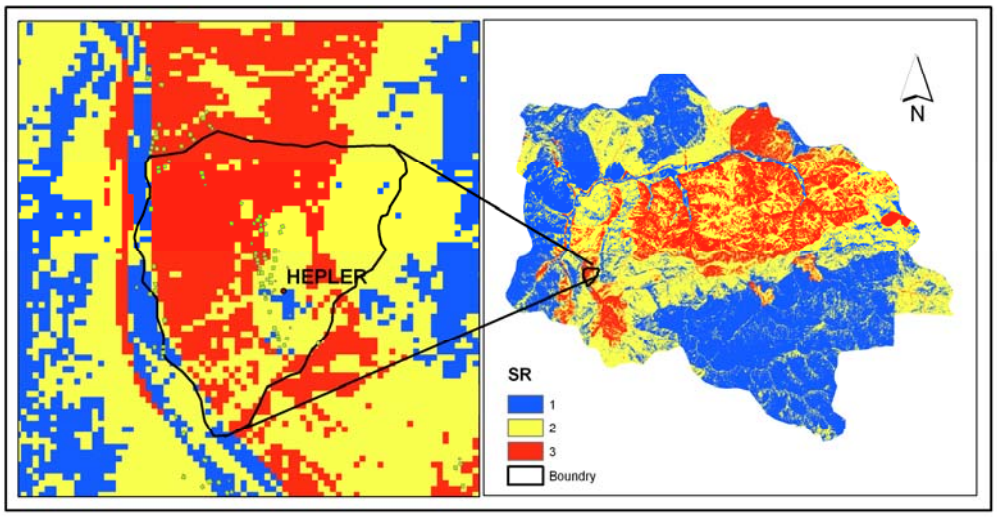

Figure 4.2. The grid-based SR hazard map levels for Hepler district

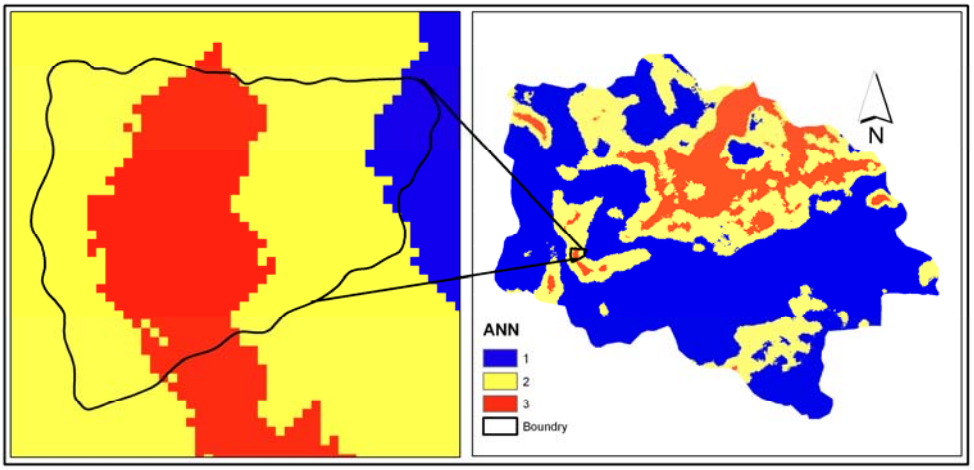

Figure 4.3. The grid-based ANN hazard map levels for Hepler district

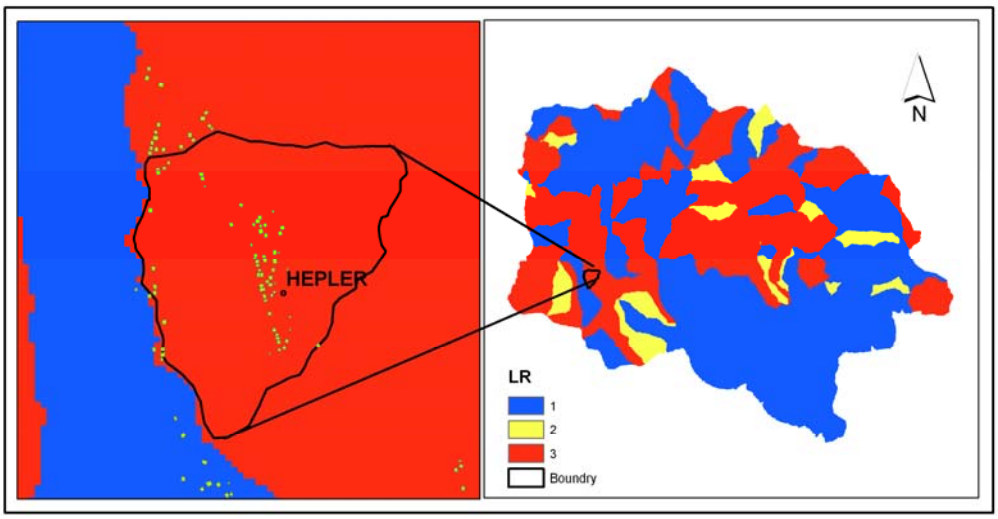

Figure 4.4. The slope unit-based LR hazard map levels for Hepler district

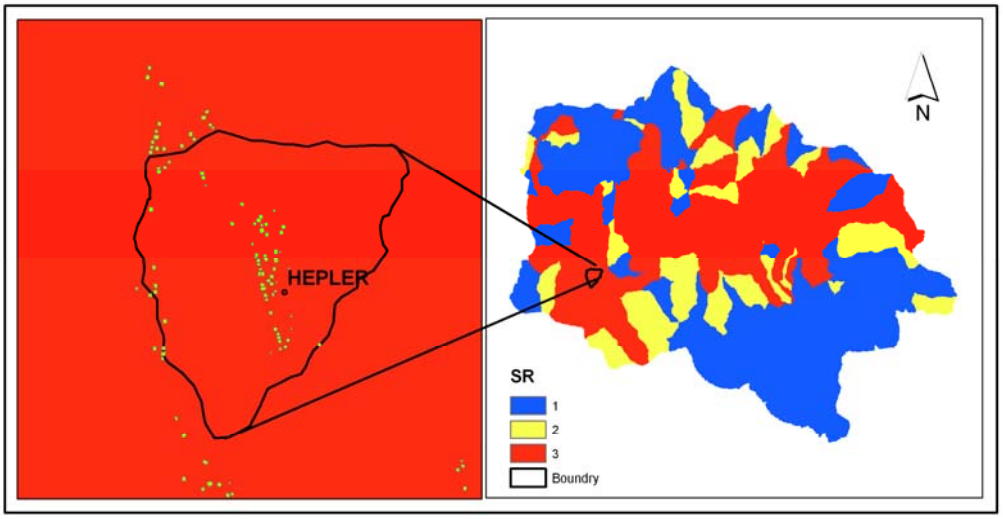

Figure 4.5. The slope unit-based SR hazard map levels for Hepler district

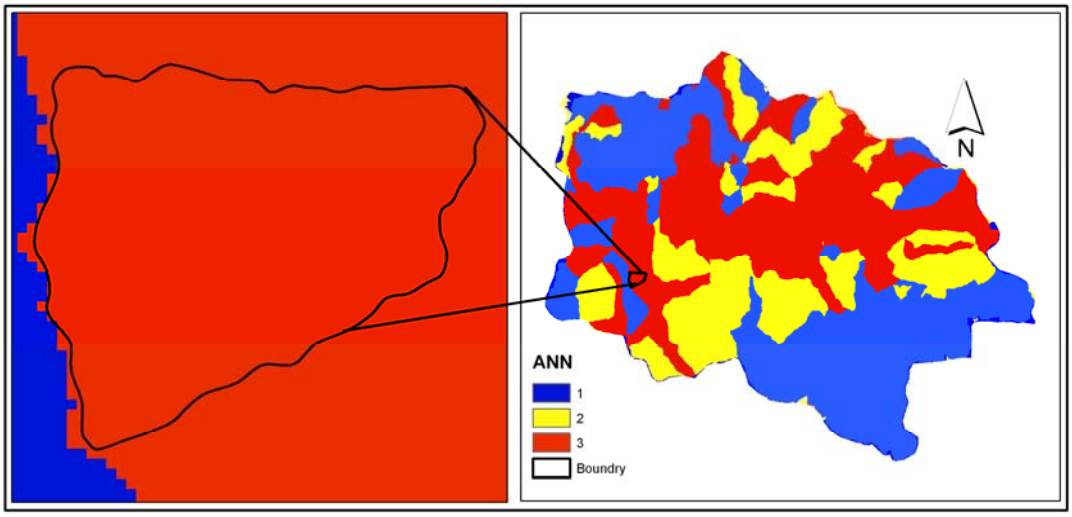

Figure 4.6. The slope unit-based ANN hazard map levels for Hepler district

These figures are also the evidence of model performances in the local region. It can be clearly seen from the figures that the local slope boundary is represented in the middle and/or high risk zone in all of the model results. The slope unit-based LR, SR, and ANN maps provide a generalization and they represent the region at high risk zone as presented in Figure 4.4, Figure 4.5 and Figure 4.6 respectively. However, in the LR, SR, and ANN grid-based mapping units, the spatial distribution of high, medium, and low classes differs at the slope boundary and the slope mass is represented with high and medium classes dominantly.

4.2 Characteristics of the Study Area: Hepler Village

Hepler is a small district located on a hillside. The Hepler region exhibits mountainous topographical features, and is frequently subject to heavy precipitation. Due to these adverse effects, the region is prone to extensive and severe landslides (Ercanoğlu and Gökceoğlu, 2002). There are approximately 45 buildings, many of which are constructed on the slope with one and two stories. The population in Hepler district is approximately 250, which may change during summer or winter. The region covers 0.5 km^2 and is located approximately 8 km SW of Kumluca city. The 3D view of the study region is given in Figure 4.7. Topographical elevation varies from 241 to 527 m above sea level. The predominant slope angle is approximately 24^0 with slope angles ranging from 0^0 to 65^0. The vegetation cover and land-use mainly consist of woodlands, grass pastures, and rice plantations. Depending on the reports of the General Directorates of Disaster Affairs of Bartın, the region is settled down on an old landslide mass. Landslide mass is identified in lithologic units of Upper Cretaceous age Flysch, which is named as the Ulus formation. The Flysch formation is comprised mostly of thick sandstones in the lower parts, then sandy, clay schist, clay marl and claystone units on the upper parts. On average, the soil varies between 30 and 40 cm in thickness. The Flysch formation is saturated due to extreme snowmelt in the winter and rainy season in the spring. It is reported that it rains above average during seasonal rains and it snows more than 1.5 m high. The snow melts slowly and as a result the terrain covered with clay absorbs the whole water and become slippery ground. As the terrain becomes saturated with water, landslide and mud flows occur.

In 1967, 1985 March, 1998 May, and 2000 June, devastating landslide events occurred in Hepler village. 1985 and 1998 slides were reported to be a flow type slide. There is no information about the others. 10, 25, and 12 houses were moved due to 1985, 1998, and 2000 landslides respectively.

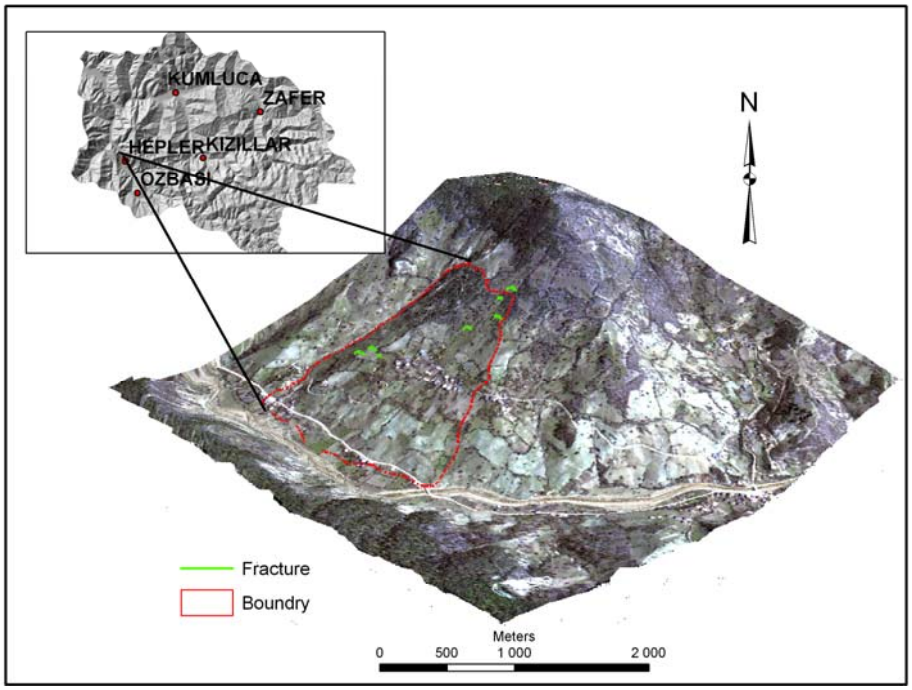

Figure 4.7. Location of the study region in 3D View

4.3 Data Acquisition and Preparation

The data sets utilized in this study are from various types of sources and consist of mainly fieldwork, documentations, and remotely sensed imagery. As it was not possible to collect detailed data, such as slope geometry, strength parameters, and geology required for geotechnical models for slope stability analysis, the hazard prediction values were obtained from the regional scale hazard maps. The data collection for local scale focuses on obtaining rainfall data (Table 4.1) and X, Y, Z data for simulation of the run-out, additionally, extensive field works and an analysis of remote sensing images for consequence analysis (Table 4.1).

Table 4.1. Characteristics of data for local slope analysis

Implement Type	Data Source	Data Type	Data Format	Data	Coordinate System
R*	NIK	Quickbird (10.04.2003)	Raster	R, G, B, NIR : 4 m Pan : 1 m	WGS_1984_UTM_Zone_36N
C*	Turkish State Meteorological Service	Rainfall Data for Bartın station	Excel	1998, May 17-23 hourly data	

*R=Risk, C=Consequence

Assuming that the same rainfall situation that produced slides in the past will produce the same effects in the future, an event like the one in 1998 was simulated. The simulation aimed to estimate the velocity of the debris to be input for estimation of vulnerability. To start a simulation with FLO-2D, there are two important steps, which involve developing the hydrology from hourly rainfalls and obtaining the topographic database. In order to develop a hydrograph, the 7-day (1998, May 17-23) hourly data was acquired from Bartın station.

In order to determine a detailed topography of the slope and assess the properties of the landslide, extensive field work was carried out. The Ashtech Kinematic GPS (Global Positioning System) was used to collect the X, Y, and Z coordinates of the surface topography with an accuracy of ±0.5m (at 95% confidence interval). When terrain conditions were not suitable to collect data point with GPS because of the dense vegetation cover or steep slopes, TruPulse 200 Laser Range Finder was used. Laser works by sending a laser pulse in a narrow beam towards the object and then measuring how long it takes for the pulse to bounce off the target and return to the sender. The measurement range of the range finder is up to 3280 ft (1000 m) in distance and +/- 90 degrees as inclination. It has an accuracy of +/- 1 ft (+/- 30 cm) in distance and +/- 0.25 degrees as inclination. The data points were collected homogenously from the whole slope and as a result, the DEM was constructed at 1 m grid size with ArcGIS 9.1 software, using triangular irregular network (TIN) approach.

In addition to the collection of data points for the topography of slope, field observations also focused on the identification of the activity of the slope and the vulnerability information of the buildings in the study region. The observed cracks and scarps through the field survey were mapped onto the remote sensing image of the study region (Figure 4.8).

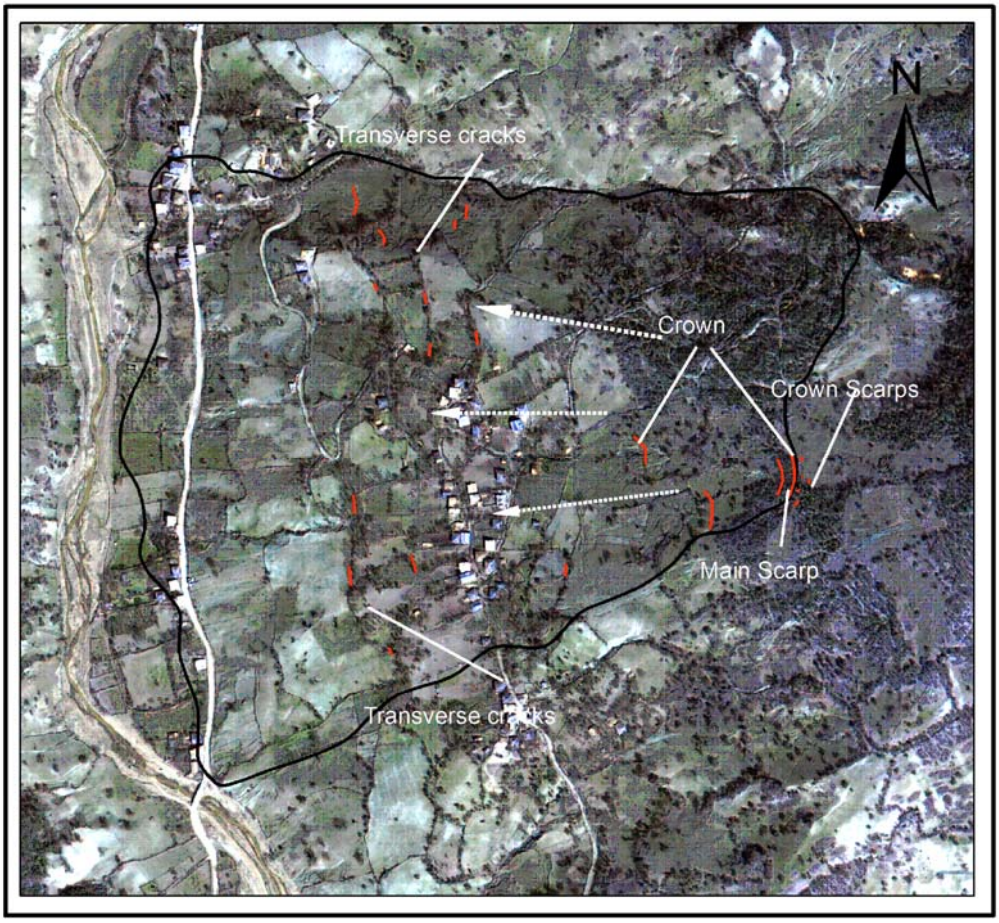

Figure 4.8. The cracks and scarps observed and mapped through field survey at 6-7 June 2009

As presented in Figure 4.8, in the southern part of the region, transverse cracks were observed. Moreover, the main scarp boundary and crowns were observed at the top of the slope. Some of these cracks are shown in Figure 4.9b,Figure 4.9c,Figure 4.9d, Figure 4.10a, and Figure 4.11a. The crowns observed through the study region are mostly 30-40 cm deep and depending on the interviews with the local people, these artifacts occurred between 2008 and 2009. Thus, these fractures indicate that the slope mass is still active and slowly moving, which has a potential to damage the houses. The upper scarp of the slide is displayed in Figure 4.11b and Figure 4.11c. The scarp is approximately 1.8 m in height and approximately 20 m in width.

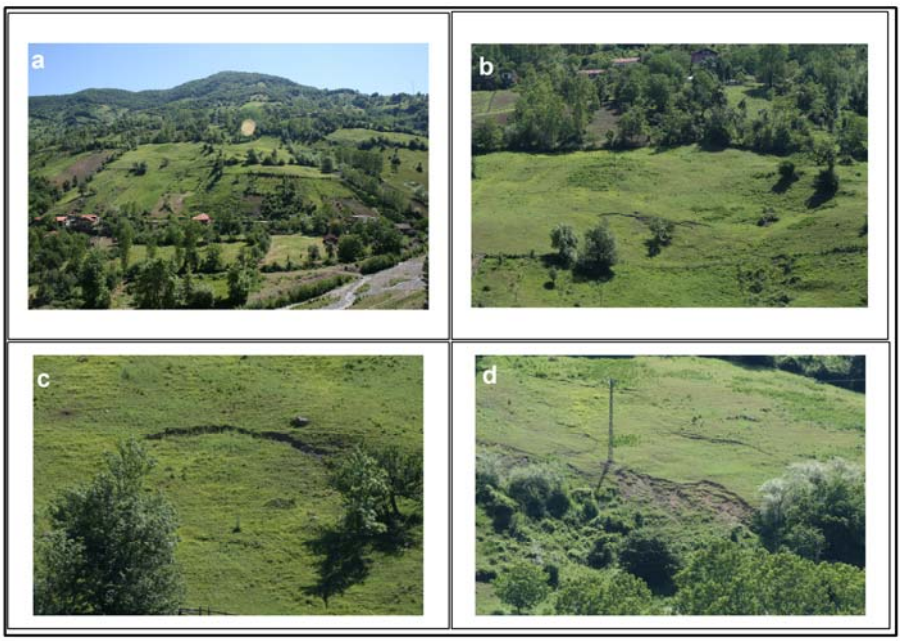

Figure 4.9. The photos of the terrain with scarps and crowns

Figure 4.10. The anomalies investigated through the field surveys, the photos are overlaid to the remote sensing image of the region a. A fracture representation of the region b. The protection wall of a house in the region c. The cracks inside the house

Figure 4.11. Some photos from the field survey a. The crack on the terrain, b. The toe of the upper scarp c. The main scarp and head of the upper scarp d. The deformation observed at the column of the building e. The cracks observed outside the building

The cracks inside and outside the walls of houses (Figure 4.10c, and Figure 4.11e respectively) and some deformations on buildings (Figure 4.11d) were observed during the field work. As presented in Figure 4.11d, the column of the house was bent on and the stairs were separated (Figure 4.11e) from the main body of the house. Local people indicate that these kinds of deformations frequently occur in the houses; hence, some houses were even evacuated.

During the field surveys, the population living in the houses is also collected. Depending on the interviews with the local people, it can be said that the population of each house increases in summer and decreases in winter. Hence, the range of the population for most of the houses were collected and added as additional information to the database to be used for further risk assessment study.

In the study region, the buildings and the main road were extracted from the remote sensing data by the developed algorithm for element at risk studies. Quickbird image of the study area, which was acquired on April 10, 2003, was used. The image was

acquired with four bands for the study region, where the R, G, B, NIR bands are in 4 m. spatial resolution and the Pan band is in 1 m spatial resolution at the WGS84 datum UTM projection 36 North hemispehere zone. The former image has 2656x3402 pixels and the latter image has 10624x13608 pixels with 16-bit spectral resolution.

4.4 Consequence Analysis

This study focuses on the quantitative assessment of risk to property and risk to life on local scale. The methodology of the study followed the same procedure with some differences in the application of regional risk assessment methodology. The risk analysis consists of the following steps: hazard assessment, consequence analysis, and risk calculation. To calculate the landslide risk of Hepler village, the spatial and temporal probability of occurrence of potential damaging events were adopted from regional maps created by different models and mapping units. Therefore, the methodology followed the consequence analysis after data collection for further risk analysis.

Consequence study involves determination of spatial impact, vulnerability and elements at risk for property and life. On local scale, the effect of run-out distance was considered for probability of spatial impact. Hence, a physical process model Flo 2D was used for modeling the run-out. The vulnerabilities were estimated depending on the output of run-out velocity for each building. The distribution of the elements at risk in space and time was extracted from the Quickbird image for the consequence analysis.

4.4.1 Probability of Spatial Impact

This part of the study aims at determining the affected areas using a model to predict landslide prone areas. To define the flow depositions produced from the landslides, a two–dimensional Flo2D model (O'Brein et al., 1993) was applied in the study. The main aim of running the simulation with Flo-2D was to obtain the velocity of the debris flow so that the vulnerability of the buildings could be predicted depending on their exposure to slide velocity. In this approach, the spatial vulnerability of

building and also the vulnerability of people living on that house may be estimated based on these velocity outputs. Flo 2D is a two dimensional finite difference model that simulates clear water, flood hazards, mud flows, and debris flows. The objective of this model is to estimate the probable range of flow properties in terms of velocity and depth to predict a reasonable area of inundation (O'Brein et. al., 1993).

The FLO-2D model developed by O'Brien (Obrien et. al., 1993; O'Brien, 1999) can be applied to simulate hyperconcentrated sediment flows such as mudflows and the transition from water flows to fully developed mud and debris flows (Bello et. al., 2003). Hyperconcentrated sediment flows are defined as flood events with sediment concentrations that exceed 20% by volume (O'Brien, 1999).

It was aimed to simulate the event occurred in 1998 due to torrential rainfalls observed in the Hepler district. During the first two weeks of May 1998, intermittent rainfall during a wet rainy season saturated the steep slopes of the Hepler district. As it is presented in Figure 4.12, the rainfall data indicates that a low intensity but continuous rainfall occurred between May 1 and May 19, with a total amount of 45.4 mm in the study region. Rainfall intensity increased between the days May 20-22. The Bartın station reported that during these three days a total precipitation of 166.3 mm. occurred. Then, torrential rainfalls over a three-day period (May 20-22) spawned landslides throughout the upper slopes of the terrain. Slide surges destroyed most of the houses and also killed animals in Hepler. According to local reports, 25 houses moved after the devastating event.

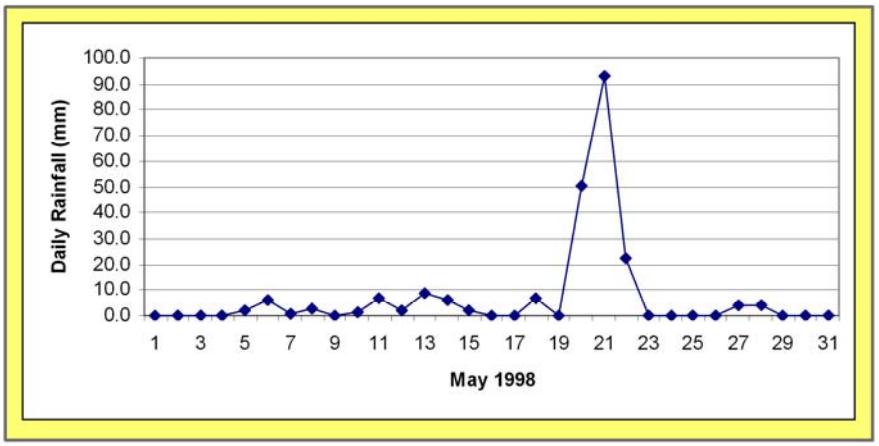

Figure 4.12. The daily rainfall pattern of Bartın station in 1998 May

Hence, to simulate the run-out of local slopes in 1998, the 7-day (May 17-23) hourly rainfall data was acquired from the Bartın station. In order to create a storm distribution, the relative accumulation was computed by using the hourly records of 7-day precipitation (Figure 4.13). This data was then used to be input to compute the hydrograph, which would then be used as input for simulation. In other words, the storm distribution was used to compute the discharge (Q m^3/s) in each cell in the selected region.

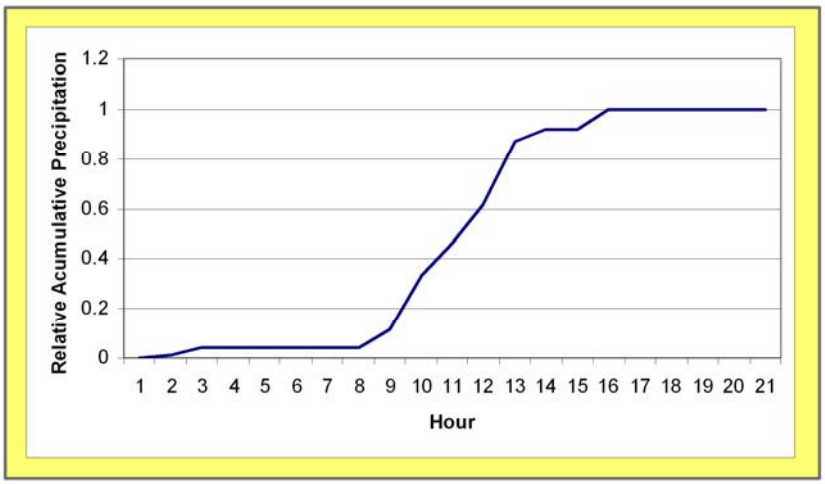

Figure 4.13. Rainfall distribution at Bartın Station May 17-23, 1998.

Two-dimensional governing equations include the continuity equation and the equation of motion. For the application of equations, a finite difference model was used. More details about the algorithm and the implementation can be found in Flo 2D user manual 2003. There are two important steps to start a simulation with FLO-2D. The first step is obtaining the digital terrain model and second step is developing the inflow flood hydrology of rainfall. In addition to these, data channel geometry, study region limits (coordinates), land-use shape files and tables and floodplain roughness of Manning's Roughness (n-value) are required (GDS help file). Hence, to simulate the flow, after division of the topography into uniform square grids, each grid is assigned the following information: location, topographical elevation, roughness factor, and area and flow width reduction factors.

By using the flow depth, the discharge flow was routed through the grid system. For each grid element and time step, the discharge across each of the four boundaries was computed and summed. The resultant volume change is uniformly distributed over

the available flow area in the element (O'Brein et al., 1993). For both the water and mudflow sediment volumes, mass conservation was obtained as the flow hydrograph was routed over the grid system. At each time step, the model computes the change in water and sediment volumes and the sediment concentration.
In this study, the mudflow behavior as a function of sediment concentration was considered as a landslide property, which is a block sliding failure with internal deformation during the slide.

The FLO-2D software package includes a Grid Developer System (GDS) program that overlays a grid system on a set of random digital terrain model (DTM) points and that interpolates and assigns elevations to grid elements. The GDS reformats the topographic data into a file that identifies contiguous grid elements. To create a FLO-2D grid system and model, the following steps were completed for the analysis. The DTM data (terrain data) with 1-m resolution was exported to Ascii grid file to be input for the GDS and a 10-m square grid system was prepared (Bertolo and Wieczorek, 2005). The channel geometry was estimated through the data collected from the fieldwork, visual inspection of remote sensing images and also the slope unit model. Then, the shape file slide boundary was imported to the system and the simulation area (computational domain) for the FLO-2D model was determined based on this boundary. The elevation data was interpolated and FLO-2D grid element elevations were assigned to each grid cells. The Manning's roughness (n-value) was not present for the study region, hence some general assumptions provided by O'Brien 1999 were used as presented in Table E-1 in Appendix E. By the field surveys, the region was observed to have dense grass and vegetation; therefore, the overland flow manning's n roughness value was considered as 0.32 depending on the physical surface type in Table E-1 in Appendix E.

After the determination of outflow nodes, the FLO-2D simulated the flooding by routing the flood hydrograph. The flow depths and velocities were predicted for every grid element in eight potential flow directions for a time step in the order of seconds (Garcia et al., 2004).

The FLO-2D results include depth and velocity files that can be imported to the MAPPER post-processor program, which graphically displays the output such as

maximum flow depth and velocity contours to assist in the interpretation of the results.

For each cell of the analysed data, FLO-2D returns volume concentration, velocity, discharge and depth during all times in the simulation. The velocity map of the simulated slide changes with the volume concentration and ranges between 0.01 and 1.55 m/s (Figure 4.14). The spatial variation of velocity values over the study region and the distribution of houses are also illustrated in Figure 4.15. The velocity map was used for further vulnerability estimation.

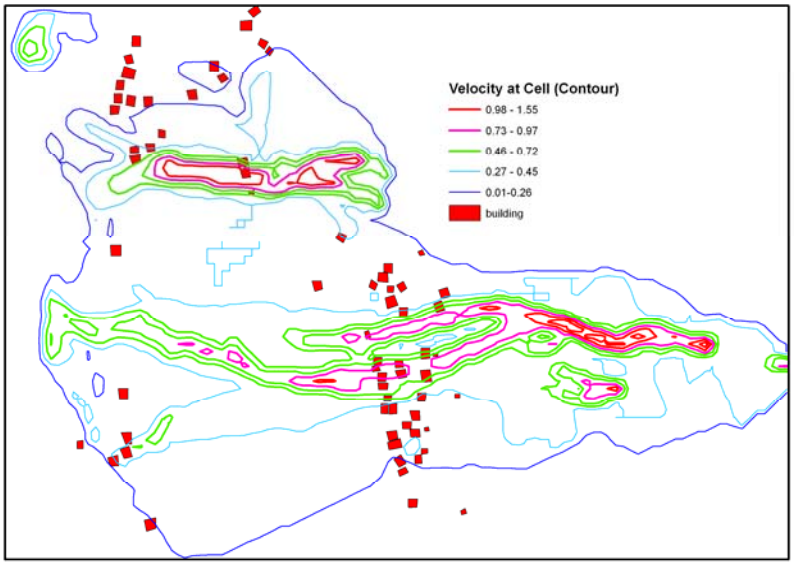

Figure 4.14. The velocity map of the simulation result (m/s)

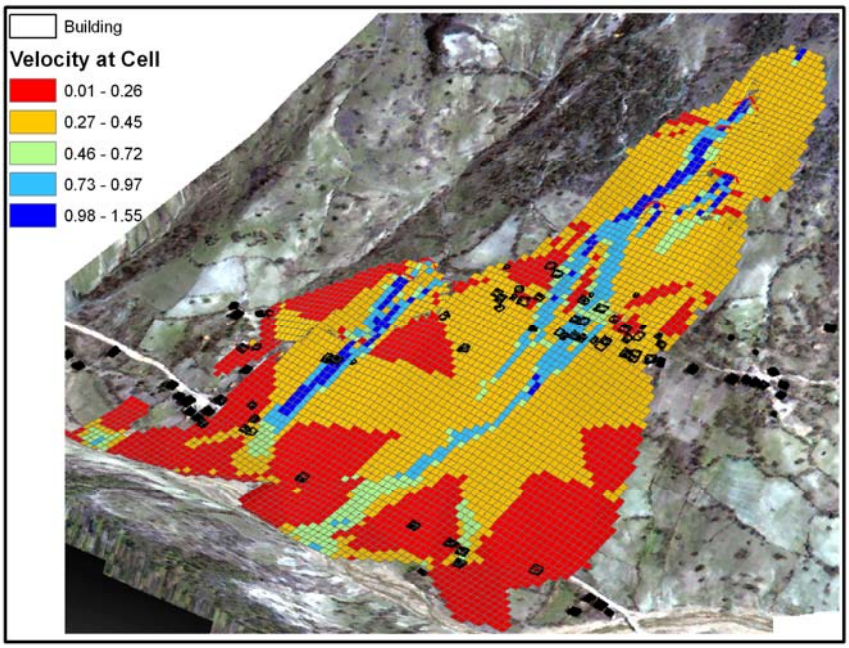

Figure 4.15. The spatial distribution of velocity values over the 3D image of the study region

4.4.2 Identification of Elements at Risk by Remote Sensing

On local scale, it was possible to focus on a more detailed survey of the buildings, condition of them, the number of inhabitants per house, and seasonal or daily movement of the population. Hence, during the fieldwork, information in as much detail as possible was collected for buildings, the condition of buildings, population, and roads. The building features and main local road was also detected by the developed algorithm for risk analysis. Since limited information could be surveyed about the type and cost of agriculture, it was not considered for vulnerability analysis. Most of the houses are one or two-storey buildings and are found in the mid part of the landslide. Buildings are predominantly concrete and a few are wooden buildings. In Figure 4.11d, a typical house in the district is presented. Additionally, the distribution of houses is illustrated in Figure 4.15. In this study, a generic algorithm was developed with the collaboration by Computer Vision and Intelligent Systems Research Laboratory in Department of Electrical and Electronics Engineering, METU to gain an automated way to extract buildings from high resolution satellite image. The proposed method consists of mainly four steps: first, masking the vegetation and shadow areas and obtaining man-made segments, then the main road detection, and then filtering thin and long artifacts by PCA and eliminating small segments by morphological operations, and finally classifying the resultant image, which is masked by vegetation, shadow and road features. The main steps of the methodology are given in Figure 4.16. The algorithm was applied to four different subregions as presented in Figure 4.17.

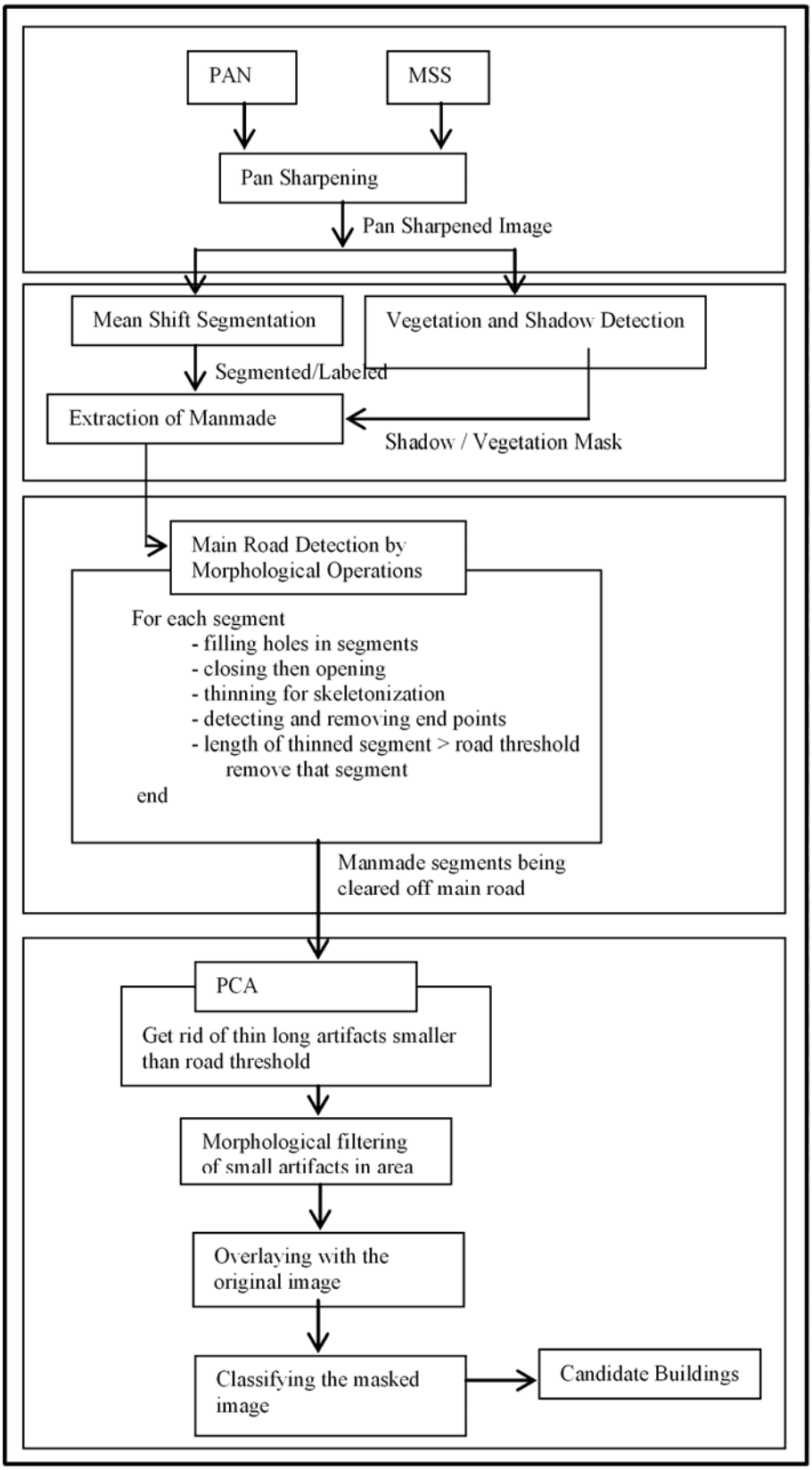

Figure 4.16. Flowchart of the Methodology

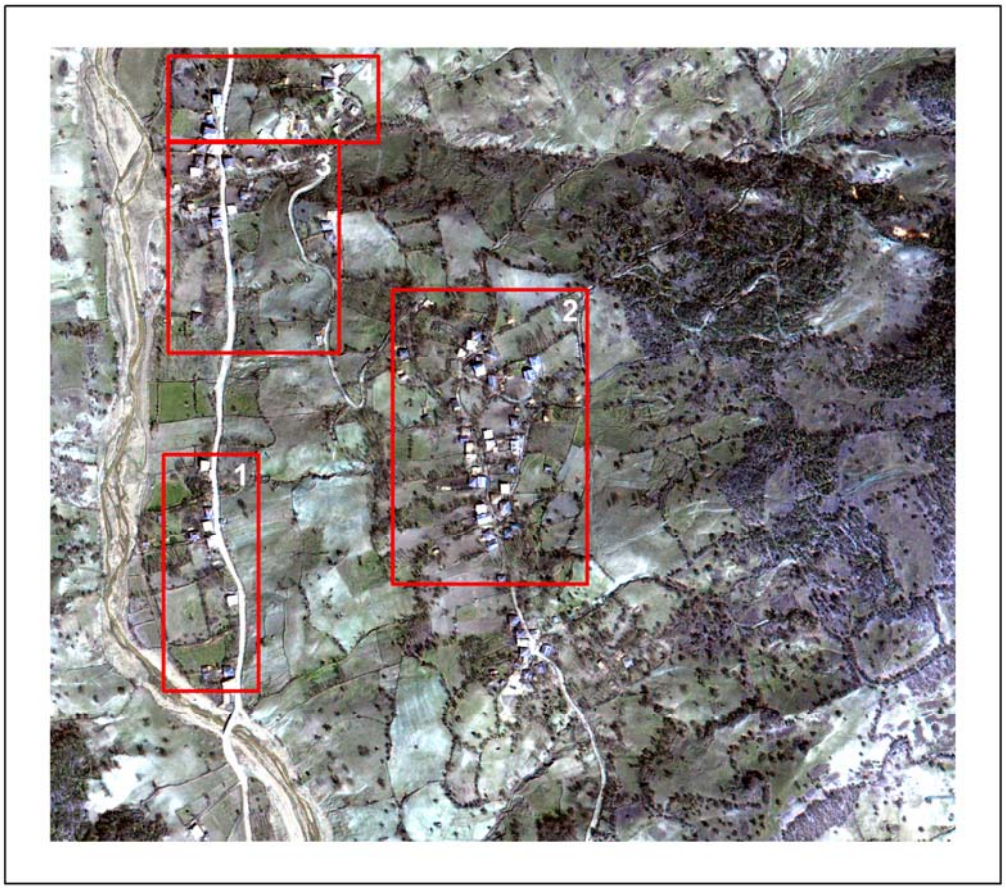

Figure 4.17. The subregions used for the building detection algorithm

Initially low-resolution multi-spectral imagery (MSS) and high-resolution panchromatic imagery (PAN) of Quickbird data were fused by using PANSHARP algorithm (Zhang, 2002) of PCI Geomatica. NDVI was calculated by using the near infrared (NIR) and Red (R) bands of pan-sharpened image as described previously. High index values indicate vegetation regions whereas low values represent man-made regions. Since the histogram of the index image would have two classes, a suitable threshold was determined according to Otsu's method (Otsu, 1979), which relies on maximizing between class scattering and at the same time minimizing within class scattering. To remove the shadow regions, ratio of chromaticity to intensity was used and the best performance was obtained in YIQ color space (Tsai, 2006). RGB space was converted to YIQ space. The shadow regions will have higher ratio of Q to I. A suitable threshold was determined by using Otsu's method. The performance of shadow detection method is illustrated in Figure 4.18_4c, where the building shadows are clearly identified. At this point, vegetation (Figure 4.18_1b, Figure 4.18_2b, Figure 4.18_3b Figure 4.18_4b) and shadow areas (Figure 4.18_1c, Figure 4.18_2c, Figure 4.18_3c, Figure 4.18_4c) were masked out, leaving man-

made structures to be segmented Figure 4.18). After masking out vegetation and shadow regions, the image was then segmented by mean shift segmentation algorithm (Comaniciu and Meer, 2002). This algorithm is based on computing mean shift vector, which is proportional to the normalized density gradient estimate computed with a kernel. The iterative calculation of mean shift vectors converges to a stationary point of density, which corresponds to the modes of the image, i.e. homogenous structures in general.

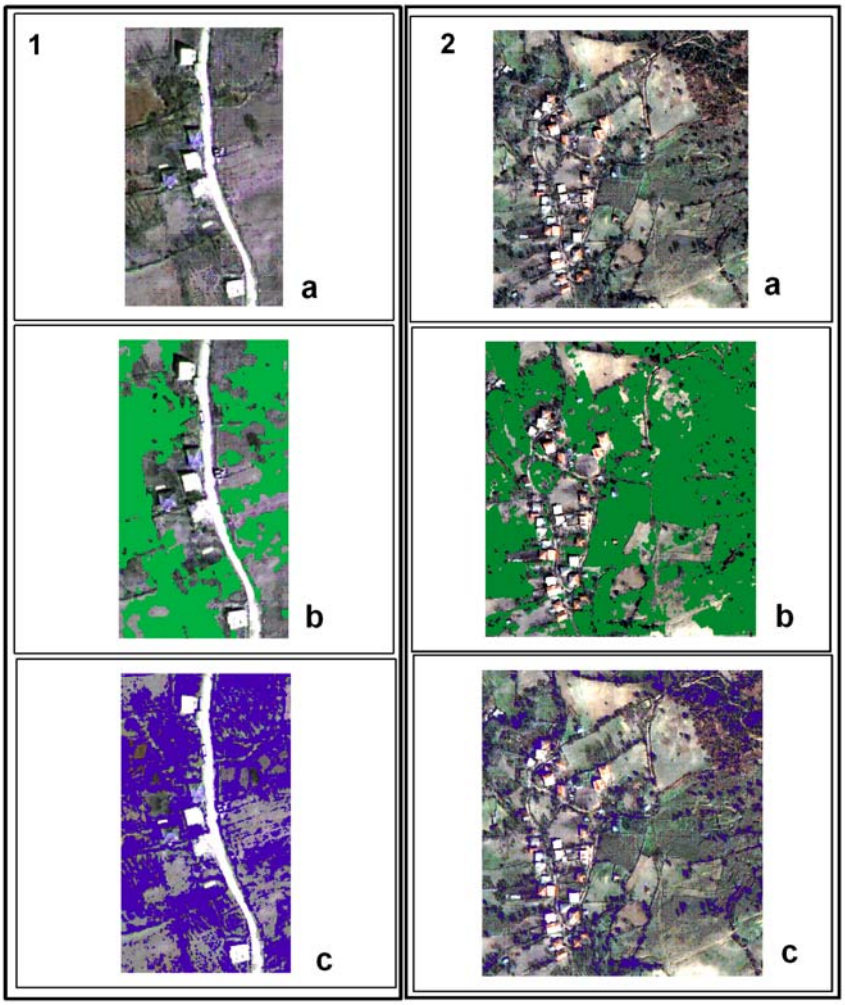

(a)

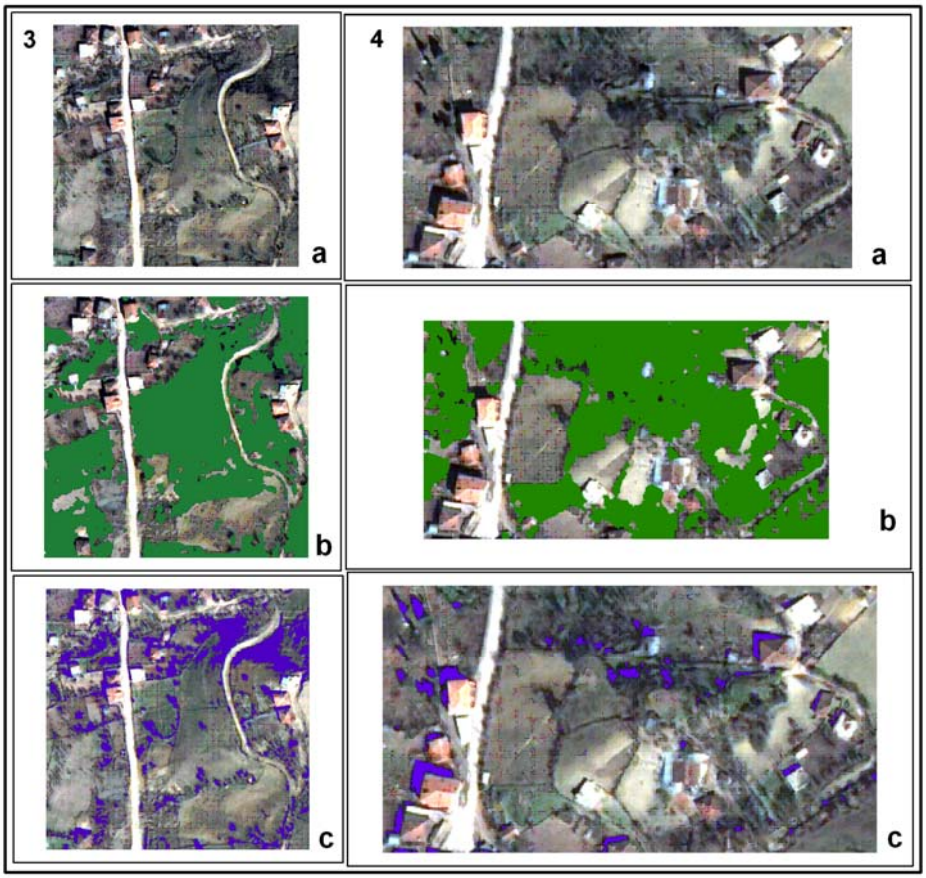

(b)

Figure 4.18. Vegetation mask and shadow mask are summed and overlaid onto the original image a. Subregions 1 and 2 b. Subregions 3 and 4.

The pixel points converging to the same mode, i.e. the basins of attractions of convergent points, are closer to each other in terms of spatial extend and color bandwidth. These pixels were segmented and labeled as the same cluster (Figure 4.19). In fact, mean shift vectors are aligned towards the similarity of colors incorporating spatial information as well. Then, the resultant image obtained by mean shift segmentation includes only the building rooftops along with some irrelevant segments generated by side effects of the previous masking processes.

For example, in Figure 4.19_1, Figure 4.19_3 and Figure 4.19_4 the road is highly correlated with rooftops, and likewise in Figure 4.19_2 bared soil regions are highly correlated with rooftops. In order to obtain the main road segments, a methodology was proposed based on the hypothesis that road segments were longer and thinner than buildings.

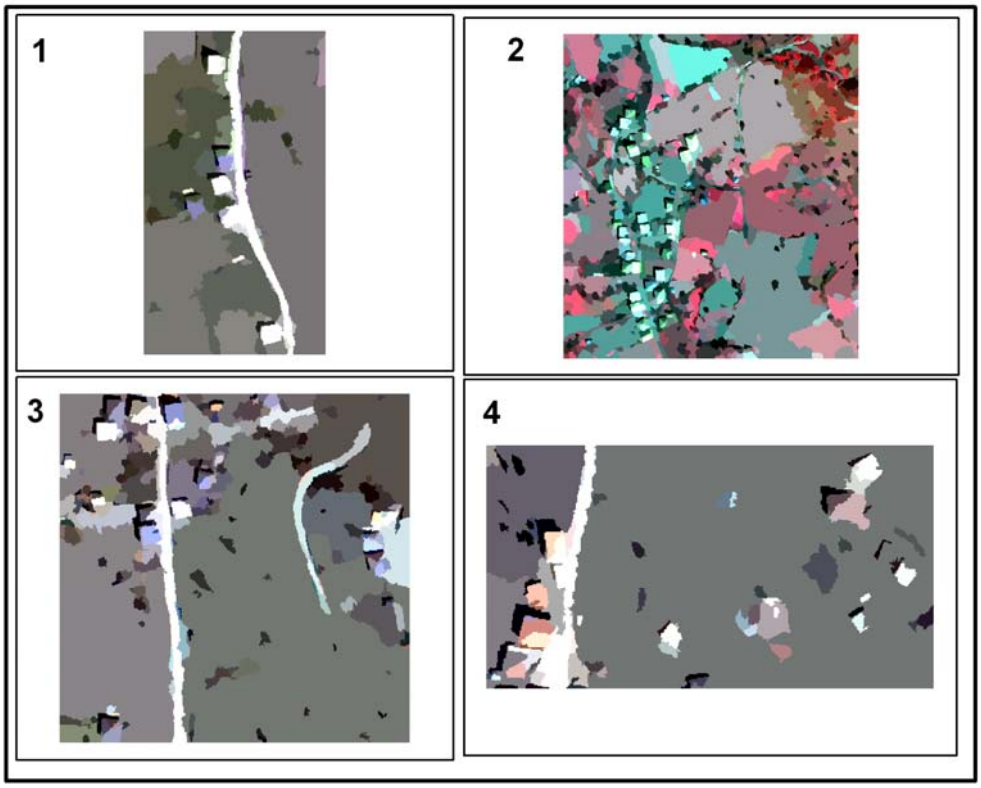

Figure 4.19 The segmentation result of the original image

Ideally, it is expected that road segments are different from building structures in length and width as being longer and thinner with undefined branches. With this motivation, all the segments were processed one by one to assess the shape characteristics of segments in terms of length as a measure. As a first step, each segment was filled to cover the holes that may come from small objects. Consequently, closing and opening morphological operations were applied. After these pre-processing operations, in order to obtain representative one-pixel wide skeletons of the segments, the thinning algorithm described by Lam et al. (1992) was applied, which generates skeletons of the segment. Skeletons may contain erroneous protrusions outgoing from the main body due to the boundary imperfections of segments. Thus, to mitigate the effect of undesirable protrusions, end points of the skeletons were removed. Finally, the algorithm ends up with a single-pixel wide skeleton of the corresponding segment. The length of the skeleton of each segment is equal to the number of pixels on the skeleton. The distribution of the length of the segments may be regarded as the evaluation criteria of being road or building segments. A threshold was applied to eliminate the main road segments, where the

threshold is automatically estimated from the distribution of segment lengths. The obtained main road segments for each sub region are shown in Figure 4.20.

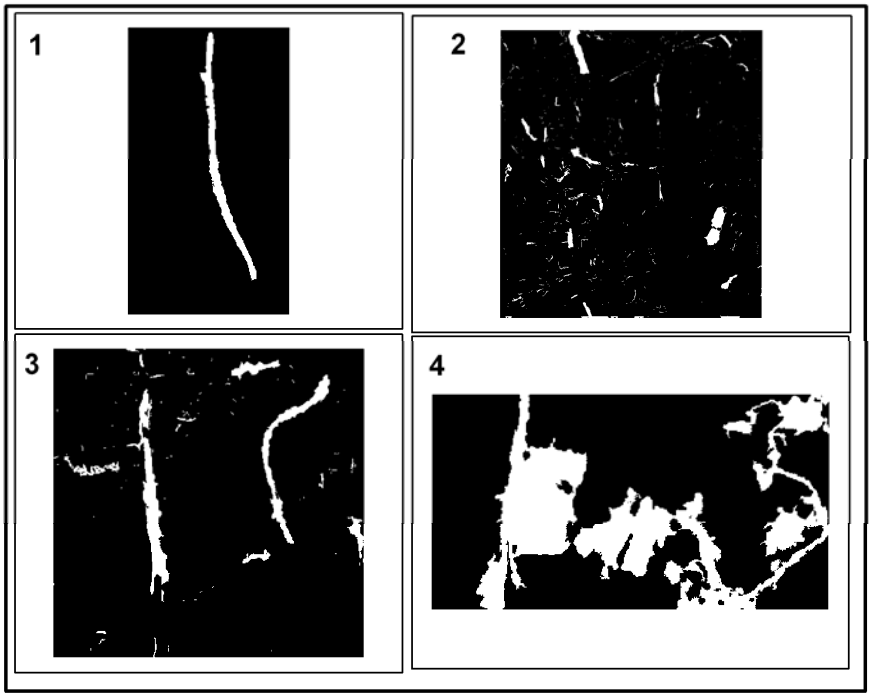

Figure 4.20. Linear Features extracted by the algorithm

After this elimination step, there still occur artifacts of road segments, lengths of which are smaller than the determined threshold and comparable to the lengths of the buildings. In addition, some artifacts of small sizes compared to the area of buildings exist. In the following step, these two types of artifacts are handled.

There are two types of artifacts. One of them is unreasonably small in the area and the other one is unreasonably thin but shorter in length than the road threshold defined in the previous section. In order to decide on whether a given segment is an artifact or not, the principle component analysis (PCA) was applied to each segment in order to compute the extend of the segment in terms of principle components. Considering thin artifacts, they show large variances along the first principle component but a small variance along the second principle component. Therefore, the ratio of the corresponding eigen values provides the variances along the corresponding eigenvectors and offers a measure of how thin the segment is. Higher ratios represent

thin segments. Then, this ratio was threshold in order to detect the artifact segments where the threshold value was automatically estimated from the distribution of the ratios.

The second type of artifacts, which are small in area but are not thin enough, was eliminated by comparing their area to a threshold which is an empirical evidence of not being a building. Figure 4.21_1, Figure 4.21_2, Figure 4.21_3 and Figure 4.21_4 show the delineated candidate buildings detected for each subregion with the proposed algorithm and overlaid over the manually labeled ground truth.

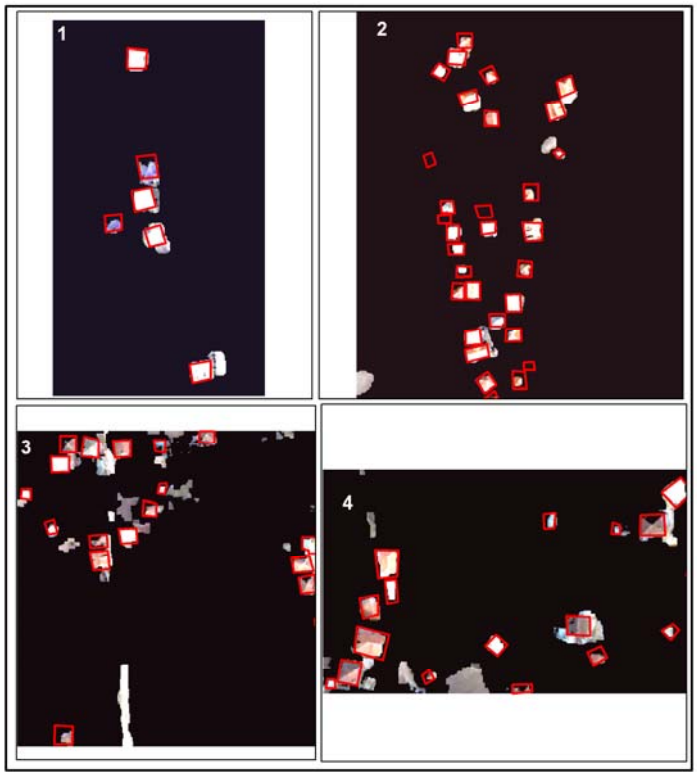

Figure 4.21. The candidate buildings extracted at the end of the algorithm overlaid on the ground truth

Road objects are significant infrastructures for the risk analysis. Thus, the roads were also considered in the thesis study for the vulnerability analysis and extracted automatically by the developed algorithm from the high resolution remote sensing image.

In the study region, there are two kinds of roads. One is the Provincial Road and the

other is pathways. Figure 4.22 shows the Provincial Road. Pathways link the houses to the main road and it is narrower than the Provincial Road. The pathway network is not clearly identified from the remote sensing images. Thus, it is aimed to detect the Provincial Road from the remote sensing image. The Provincial Road is approximately 2 km long and 10 m wide.

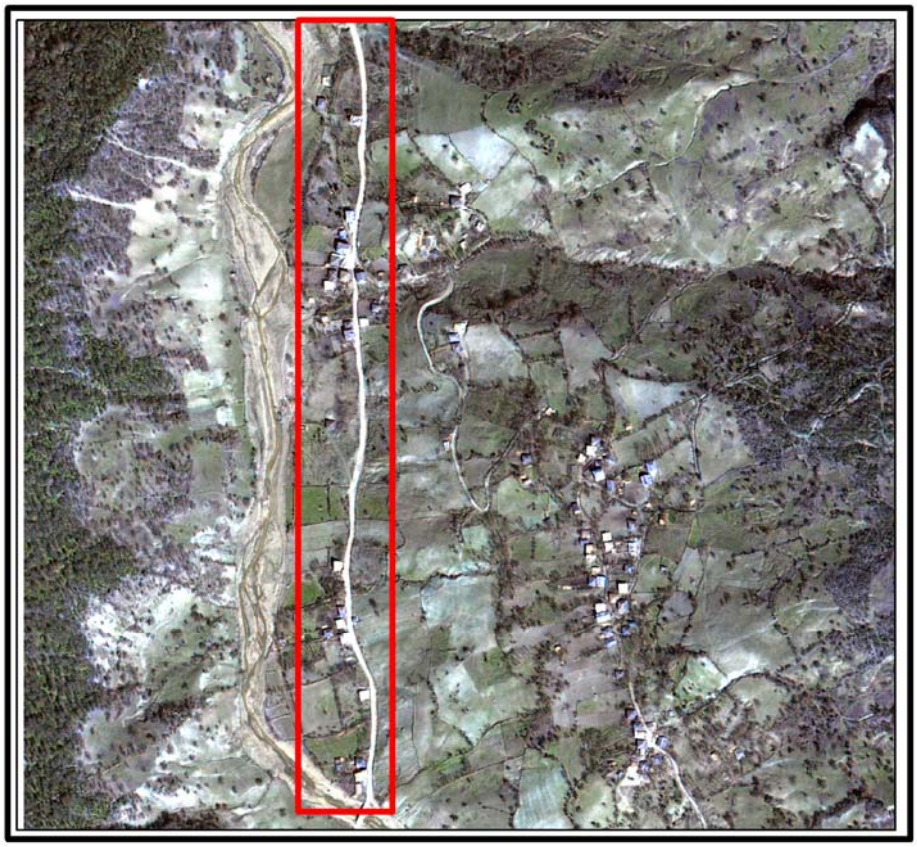

Figure 4.22. The local main road in the study region

The developed algorithm, which was described previously in the building extraction part, was used to detect the road. However, in this part the mask obtained from the linear feature detection algorithm together with the PCA algorithm was used to define the road feature. In other words, the algorithm was run until the fourth step. In the building part the PCA was used to define the thin, long artifacts. However, in this part these artifacts may be a part of the road feature; hence they are used to complement the missing features in linear feature detection algorithm. The results of each step are presented in Figure 4.23. As can be seen in the Figure 4.23, the linear feature (Figure 4.23_2) and the PCA (Figure 4.23_3) complement each other to define the road feature (Figure 4.23_4). Hence, both resultant maps are overlaid to

obtain the road feature. Then morphological processes are implemented to clarify the feature (Figure 4.23_5). As a result, the Provincial Road is obtained automatically from the developed algorithm as shown in step 6 of Figure 4.23, which is overlaid to the image.

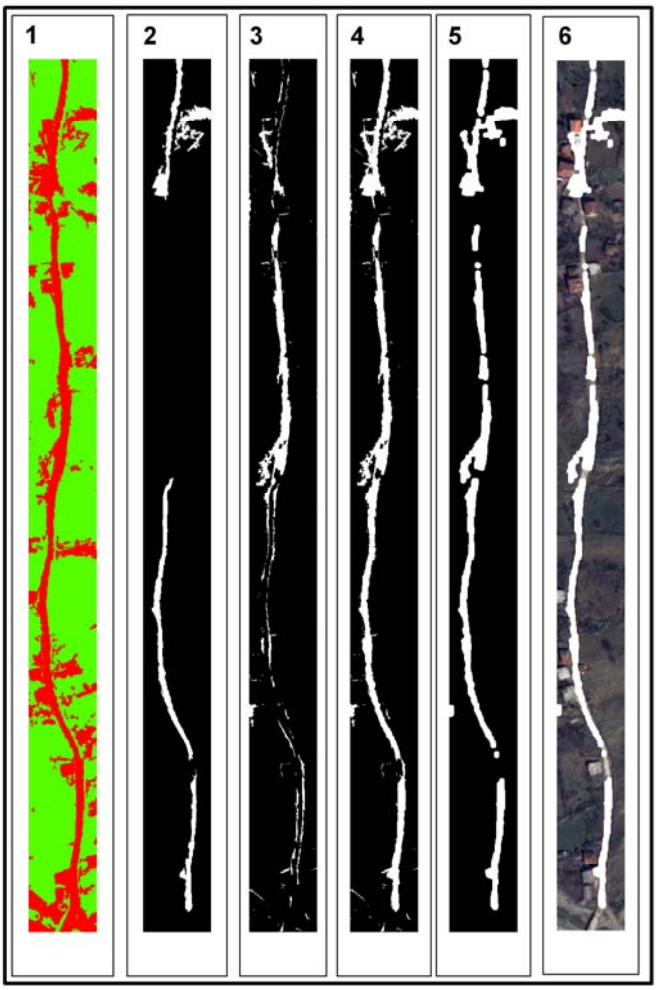

Figure 4.23. The road detection outputs in sequence where 1: The vegetation and shadow mask; green is the vegetation and shadow mask, red is the man-made features (road and buildings) 2: The result map obtained from the linear feature detection algorithm. 3: The result map after PCA algorithm. 4: The result map of both linear feature detection and PCA is overlaid to obtain the road feature 5: The morphological processes (imfill imopen, erode, close) implemented to road feature 6: The road feature overlaid to the remote sensing image

In order to assess the accuracy of the proposed methodology, the original image was labeled in the GIS environment (i.e. building pixels are labeled) to obtain a ground truth data. The ground truth data, which involves the boundaries of each building and the road line, was compared with the resultant image obtained by the methodology respectively. Three different regions used for building detection were combined into one region. The building features and the road feature were evaluated separately for

accuracy assessment. The accuracy assessment involves computation of True Positive (TP), True Negative (TN), False Positive (FP), and False Negative (FN) components by the comparison of ground truth and the resultant image. TP refers to the regions determined as a feature (building or road) both in the ground truth and in the result image. TN refers to the regions that are not determined as a feature in the ground truth and in the result image respectively. FP refers to the features that cannot be determined and FN refers to the regions which are determined as features although they are not in the ground truth (Shufelt et al., 1997). In addition to these components, the split factor (SF) (FP/TP), missing factor (MF) (FN/TP), percent of feature determination (PBD)(100*TP/(TP+FN)), and quality percent (QP)(100* TP/(TP+FP+FN)) are computed.

The results of the accuracy assessment show that the algorithm provides 95.85% and 74.28% of PBD for buildings and roads respectively. The QP is calculated as 90.53% and 54.73% for buildings and roads respectively. In Table 4.2, it can be concluded that the algorithm provides better performance for building extraction compared to road detection. This brings about more erroneous detection performance for roads compared to buildings.

Table 4.2. Accuracy Components

Accuracy Assessment of the Proposed Methodology							
	Number of Pixels			%			
	TP	TN	FP	SF	MF	PBD	QP
BUILDING	215960	176653	13241	0.06	0.04	95.85	90.53
ROAD	15634	77523	7516	0.48	0.35	74.28	54.73

Masking areas which are not man-made structures may cause twofold mistakes as either removing the true buildings or roads or not efficiently masking the regions out of interest (see Figure 4.18). In this study, the success of masking is evaluated empirically. As a further study, the evaluation can be performed by quantitative indexes.

4.4.3 Vulnerability Assessment

Elements at risk (buildings and provincial road) determined from high resolution RS image should be quantified for further risk assessment studies. The damage to buildings and road (vulnerability) can be estimated by adopting a damage probability matrix (Yücemen, 2002; Düzgün, 2008). This approach was used in structural earthquake engineering for evaluating the damage for a given building stock at a given earthquake intensity (Ko Ko et al., 2004). In this approach, instead of building blocks, the buildings and the road were considered separately by damage probability matrix. Damage to the buildings and the road was categorized into four groups based on the level of damage. Damage state (DS) was considered in four levels, changing from none to destruction, in which none and destruction stands for no and complete damage. RDR is the range of damage ratio for each damage percentage. RDR is defined as 0, 0-10, 20-40 and 50-100 (Table 4.3) (Düzgün, 2008). Central Damage Ratio (CDR) is defined as the mean value of RDR. SPD is the probability of observing damage state for the given temporal condition (season in a year and time in a day). The properties (such as buildings, roads, etc.) are always exposed to threats for all the time. Hence the temporal probability is not considered for the vulnerability analysis of properties. SPD is computed by considering the spatial vulnerability of buildings, which is determined by modeling the landslide velocity using Flo 2D.

The velocity ranges between 0.01 and 1.55 as obtained from the simulation. Hence, in the first step the velocity was normalized to 0 and 1. In the second step, the velocity map was classified into four different classes depending on the natural break method. Finally, the percentage area of each property on each level of landslide velocity was computed by the overlay of velocity map with buildings and roads respectively. The SDP is the percentage ratio of each feature computed for buildings and roads on each velocity level (Table 4.3, Table 4.4).

Table 4.3. Damage Probability Matrix for Building

DS	RDR (%)	CDR (%)	SPD
None	0	0	0.23
Light	0-10	0.05	0.52
Moderate	20-40	0.3	0.12
Destruction	50-100	0.75	0.11
Mdr (%)			15.00

Table 4.4. Damage Probability Matrix for Road

DS	RDR (%)	CDR (%)	SDP
None	0	0	0.71
Light	0-10	0.05	0.11
Moderate	20-40	0.3	0.19
Destruction	50-100	0.75	0.00
Mdr (%)			6.08

The MDR is computed for each damage state by sum of the multiplication of CDR and SPD values as presented in Eq. 70

$$MDR = \sum_{j=1}^{4} CDR_j x SPD_j \tag{70}$$

Where j is the level of damage state that ranges between 1 and 4, in which 1=None, 2=Light, 3=Moderate and 4= Destruction

The quantitative risk map to loss of life for Kumluca was created by damage probability matrix for landslide. The damage probability matrix was created by considering the occupancy of people in the building. In contrast to the property, human exposure to the landslide occurrence may vary depend on the temporal impact. The day and night and also the summer and winter should be considered for

the assessment of consequences.

The study region is a small village where the local people mostly maintain their life's by farming. The occupancy of buildings during the day time, night time, in high season time and low season time changes. The local people mostly move to different cities for mining works in the low season and turn back for farming in the high season. In addition their relatives are coming to spend their summer holiday in the high season. Hence, depending on the interviews with the local people, the occupancy of each building changes between 3 and 10 people for low and high season time, respectively.

Hence, the time which involves 7 months of the year (October, November, December, January, February, March, April) may be considered as the low season (LS) and the other 5 months may be considered as the high season (HS) (Düzgün, 2008). The probability of landslide occurrences in low (PLS) and high seasons (PHS) can be given as 0.58 (7/12) and 0.42 (5/12) respectively.

During daytime (DT), people were considered to work in the field, and at night (NT), they were thought to be in their homes. Hence, a landslide at night may have more damage to the life than daytime. As a result, time component of both daily and seasonal changes should be considered. In addition to time component, the spatial vulnerability of each house should also be considered. Depending on the simulated velocity of landslide, the vulnerability of each house was determined.

The probability of observing damage state for a given temporal condition (season in a year and time in a day) is expressed by SPD. The SPD was computed by considering the time and also the spatial vulnerability of buildings. The assumptions are as described below for the SPD computation:

In the high season, it was considered that the number of people in each house is 10 and in low season it becomes 4. In daytime during the high season, 80% of the people were considered to be studying in fields and 20% were at home. In the high season at night, all people were considered to be at home but only one person might be outside. In the low season in daytime, three of the one person were considered to be at home and three of the two people to be outside. At night, 90% were at home

and the rest might be outside. In addition to the occupancy of buildings, the spatial vulnerability of buildings was also considered. The velocity map was classified into four levels, where 1 is the lowest velocity and 4 is the highest velocity. The number of buildings on each level was computed. Then it was assumed that if the building was on level 4, then it might cause fatality when a landslide occured. If the building was on level 1, then nothing would happen, and if it was on level 2 or 3, then some injures might happen.

By considering these assumptions, a SPD was computed for the damage probability matrix. Depending on the simulated landslide velocities and the survey data, a quantitative SPD was defined. SPD values are consistent with each other, where MDR for HSNT has the highest value, while MDR for LSDT has the lowest one (Table 4.5). Damage state (DS) was considered in three levels which involve none, injury, and fatal. The range of damage ratio (RDR) for each damage percentage was defined as 0, 10-80 and 80-100 by adopting the assumption of Düzgün, (2008).

Table 4.5. Damage Probability Matrix for Loss of Life

DS	RDR (%)	CDR (%)	HSDT	HSNT	LSDT	LSNT
None	0	0.00	0.44	0.22	0.41	0.34
Injury	10-80	45.00	0.53	0.27	0.49	0.41
Fatality	80-100	90.00	0.10	0.51	0.03	0.25
Mdr (%)			32.87	57.64	24.74	40.95

4.4.4 Risk Asessment

4.4.4.1 Risk Assessment for Property

Risk to property was obtained for Hepler by considering the roads and buildings on local scale. It is better to define a replacement cost for each building, which can be estimated by experts in field surveys by taking into account the building material, condition, age, topology, size vs. for each house. However, it is quite difficult to assess economic values for each building in the study region and there is not a

national regulation to define the cost of each house. Hence, the cost of buildings, which is determined from the General Directorate of Disaster Affairs of Bartın, was used to assign the economical value, which is 23,600 TL/Pixel. The cost of roads was obtained from the General Directorate of Transportation for provincial type, which is 751,100 for one km and computed as 15,022 TL for per pixel.

The risk was computed for each property (building and road) separately. Then the results were overlaid. The risk computation involves multiplication of each property value with MDR values and then multiplication by hazard value. The hazard values were interpreted from the hazard maps produced in the regional part.

$$Risk_{Porp} = R_{Building} + R_{Road} \quad (71)$$

$$Risk_{Porp} = H \times (MDR_{Building} \times 23600) + H \times (MDR_{Road} \times 15022)$$

As a result, for the assumed damage probability matrix in Table 4.3,Table 4.4, the annual risk to Hepler was estimated for TL/pixel cost of damage for grid and slope-unit based mapping units and for different mapping methods. Figure 4.24 illustrates the spatial variation of risk values for risk to property for three different methods for grid-based mapping unit. The risk maps for loss of property obtained by LR (LR_GRD_RISK_PROP) (Figure 4.24a), SR (SR_GRD_RISK_PROP) (Figure 4.24b) and ANN (ANN_GRD_RISK_PROP) (Figure 4.24c) provide a similar pattern of risk values for road (Figure 4.24a, b, c); however, the risk values vary for houses. The ANN_GRD_RISK_PROP illustrates mostly high risk for houses, whereas the SR_GRD_RISK_PROP and LR_GRD_RISK_PROP provide medium and high levels of risk for houses. The maximum risk value ranges from 138.09 to 70.27 and it is the highest in SR_GRD_RISK_PROP.

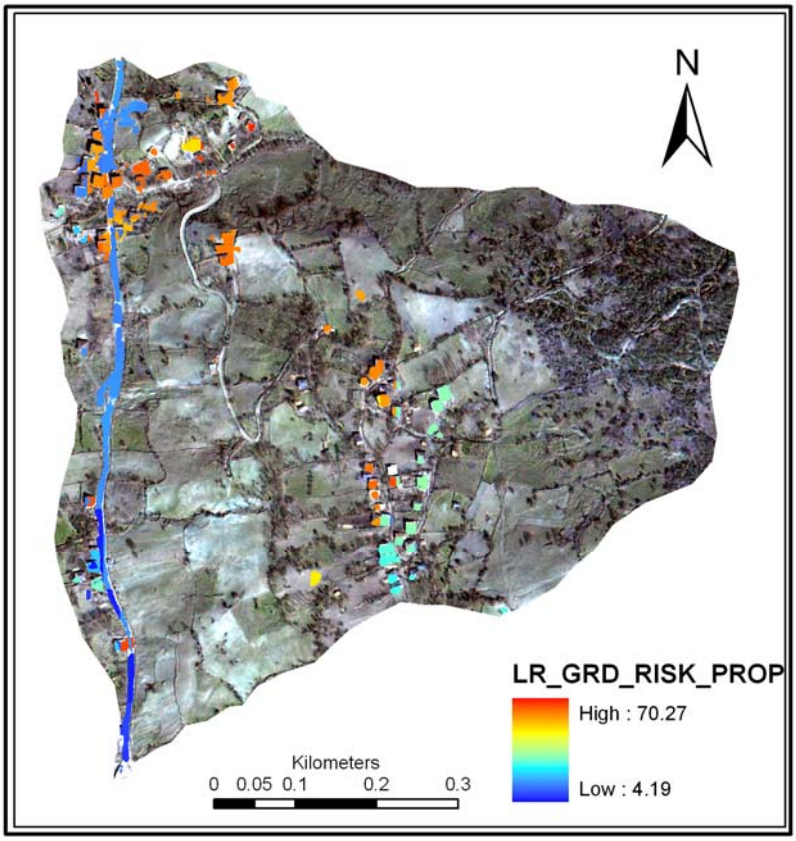
N
LR_GRD_RISK_PROP
High : 70.27
Low : 4.19
Kilometers
0 0.05 0.1 0.2 0.3

(a)

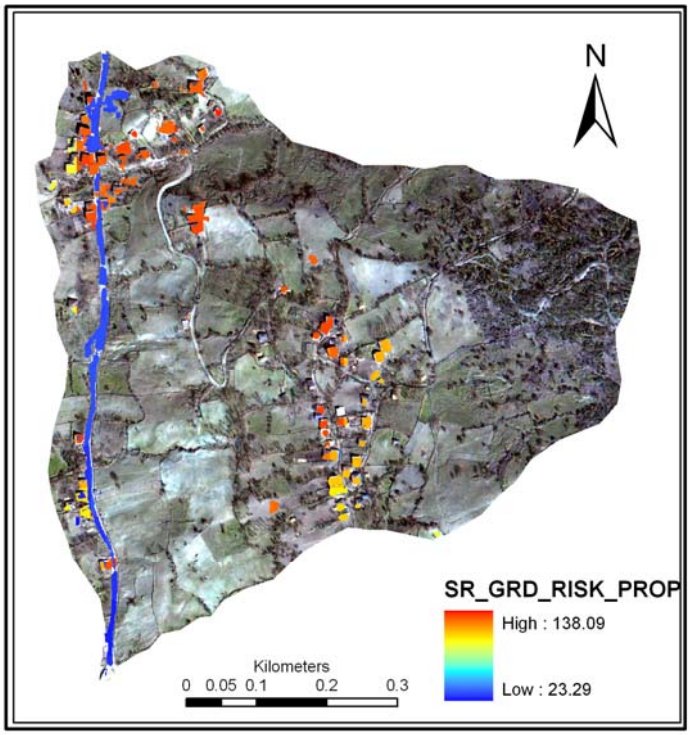
N
SR_GRD_RISK_PROP
High : 138.09
Low : 23.29
Kilometers
0 0.05 0.1 0.2 0.3

(b)

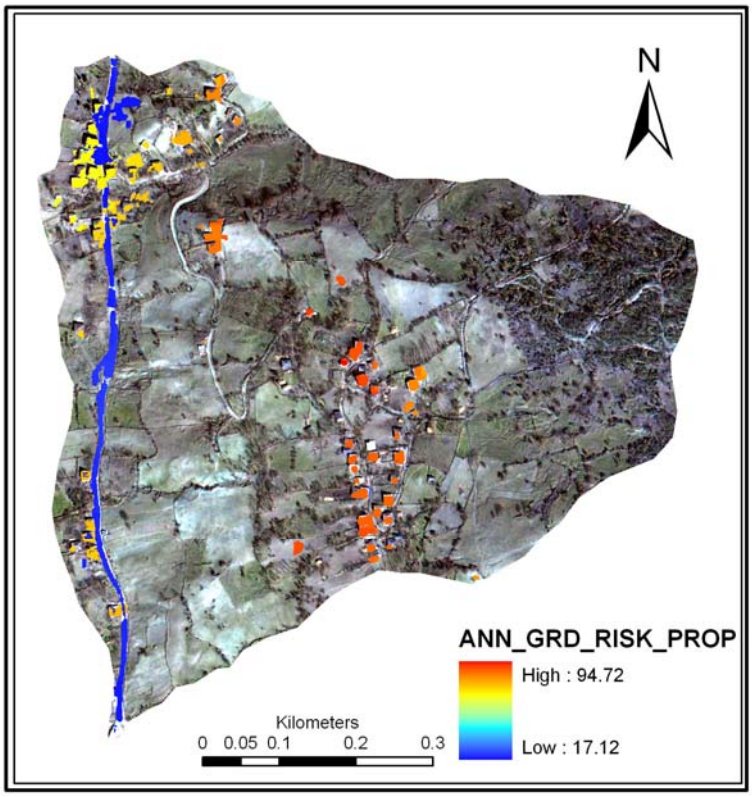

(c)

Figure 4.24. Risk to property for grid-based mapping unit for different methods, a. LR, b. SR and c. ANN (TL/Pixel)

The risk to property for slope unit-based mapping unit is presented in Figure 4.25 for LR (LR_SU_RISK_PROP) (Figure 4.25a), SR (SR_SU_RISK_PROP) (Figure 4.25b), and ANN (ANN_SU_RISK_PROP) (Figure 4.25c). SR_SU_RISK_PROP and ANN_SU_RISK_PROP provide a similar pattern of risk values for both house and road features, where the houses are illustrated by high risk values and road is presented by low risk values. Moreover, similar to the other two methods, LR_SU_RISK_PROP provides low risk values for road, but the risk values vary from medium to high for houses. The maximum risk value is the highest in the LR_SU_RISK_PROP, which ranges between 163.27 and 133.10.

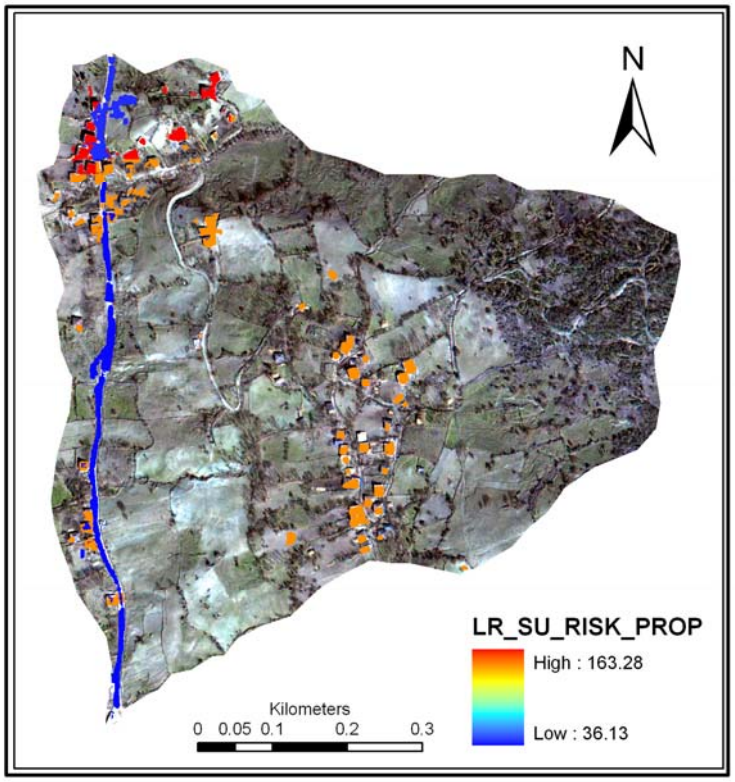
N
LR_SU_RISK_PROP
High : 163.28
Low : 36.13
Kilometers
0 0.05 0.1 0.2 0.3

(a)

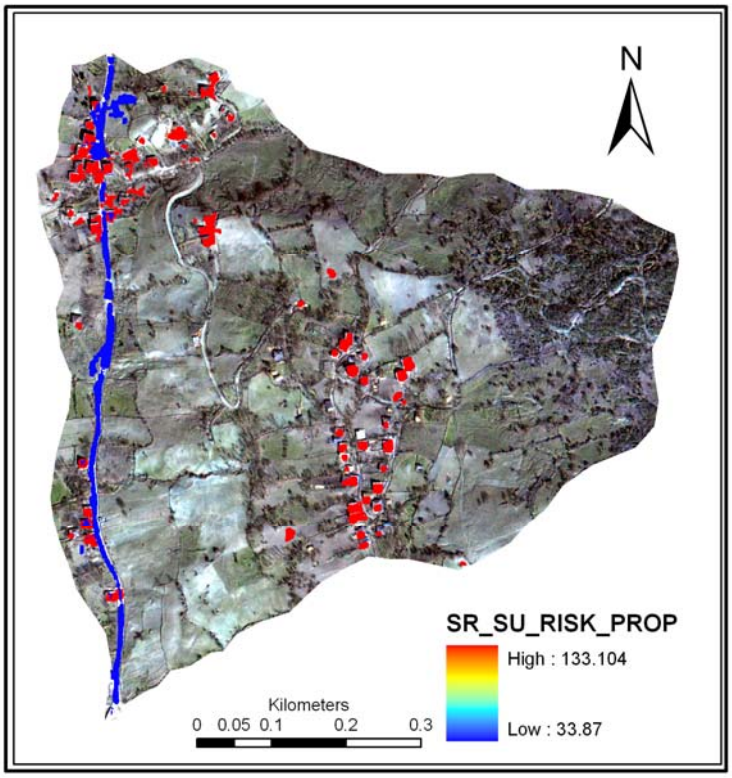
N
SR_SU_RISK_PROP
High : 133.104
Low : 33.87
Kilometers
0 0.05 0.1 0.2 0.3

(b)

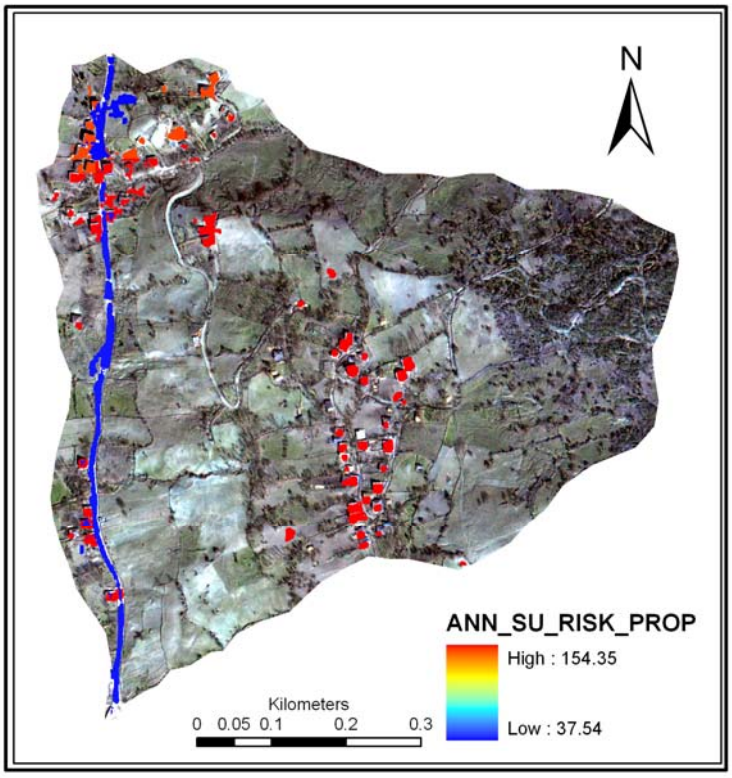

(c)

Figure 4.25. Risk to property for slope unit-based mapping unit for different methods, a. LR, b. SR and c. ANN (TL/Pixel)

When the statistics of risk maps are compared (Table 4.6) for grid and slope unit-based mapping units for all methods, it is evident that the LR_SU_RISK_PROP has the largest maximum value with the largest std.dev. and mean value following the ANN_SU_RISK_PROP.

Table 4.6. The statistics of the risk maps of loss of property for different methods and mapping units (TL/Pixel)

	Min	Max	Mean	Std. Dev.
LR_GRD_RISK_PROP	4.19	70.27	33.54	21.26
SR_GRD_RISK_PROP	23.29	138.1	81.59	45.27
ANN_GRD_RISK_PROP	17.12	94.72	52.87	30.50
LR_SU_RISK_PROP	36.13	163.28	98.16	54.49
SR_SU_RISK_PROP	33.88	133.1	89.05	49.3
ANN_SU_RISK_PROP	37.55	154.35	102.24	56.73

The methods obtained by the slope unit-based mapping unit have more variation of risk values compared to the methods by grid-based mapping unit. Furthermore, the methods obtained by the slope unit-based mapping unit have the largest mean,

minimum, and maximum risk values compared to the methods obtained by grid-based mapping.

4.4.4.2 Risk Assessment for Loss of Life

The landslide risk of loss of life can be computed by the sum of the multiplication of H and MDR values for damage states for loss of life as given in Eq (72):

$$R_{LOL} = H\left[P_{HS}\left(MDR_{HSDT} + MDR_{HSNT}\right) + P_{LS}\left(MDR_{LSDT} + MDR_{LSNT}\right)\right] \qquad (72)$$

For each mapping unit and mapping method, different hazard values were obtained from the region-based hazard maps. As a result, different annual risk maps for loss of life were estimated, which is illustrated in Figure 4.26. The risk of loss of life for grid-based mapping unit is presented in Figure 4.26 for LR (LR_GRD_RISK_POP) (Figure 4.26a), SR (SR_GRD_RISK_POP) (Figure 4.26b) and ANN (ANN_GRD_RISK_POP) (Figure 4.26c). LR_GRD_RISK_POP and SR_GRD_RISK_POP provide a similar pattern of risk values for loss of life, where the maximum value of risk varies from 0.0153 to 0.03004 respectively. LR_GRD_RISK_POP and SR_GRD_RISK_POP illustrate the houses located in the eastern part of the slope with low risk; however, these houses are presented by medium to high risk values by ANN_GRD_RISK_POP. Furthermore, the houses located in the northern part of the region parallel to main road are illustrated with medium to low risk values by LR_GRD_RISK_POP and SR_GRD_RISK_POP, which are seen as low to medium risk values by ANN_GRD_RISK_POP.

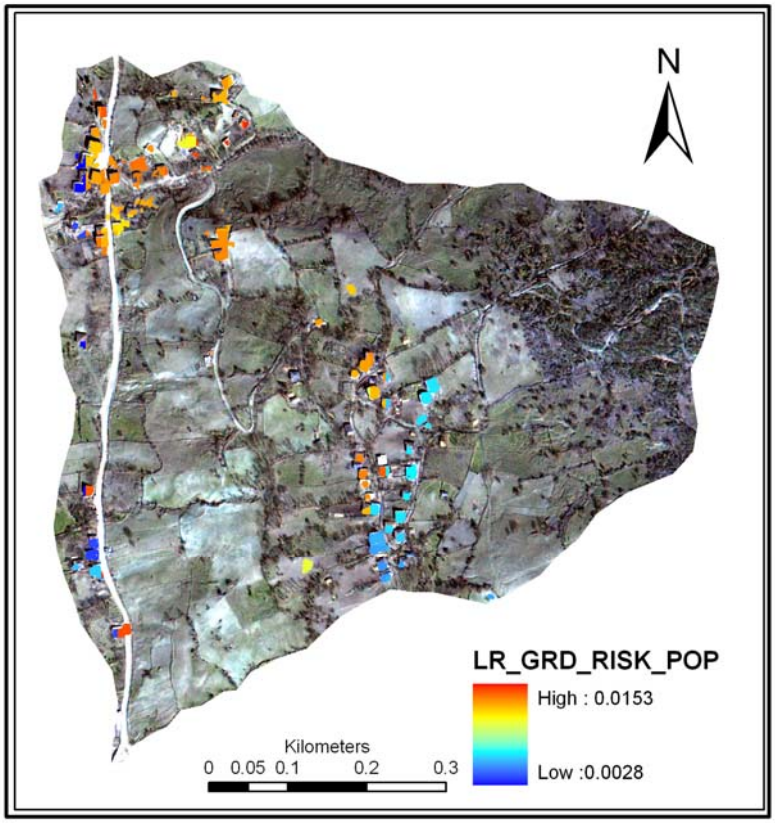
N
LR_GRD_RISK_POP
High : 0.0153
Low :0.0028
Kilometers
0 0.05 0.1 0.2 0.3

(a)

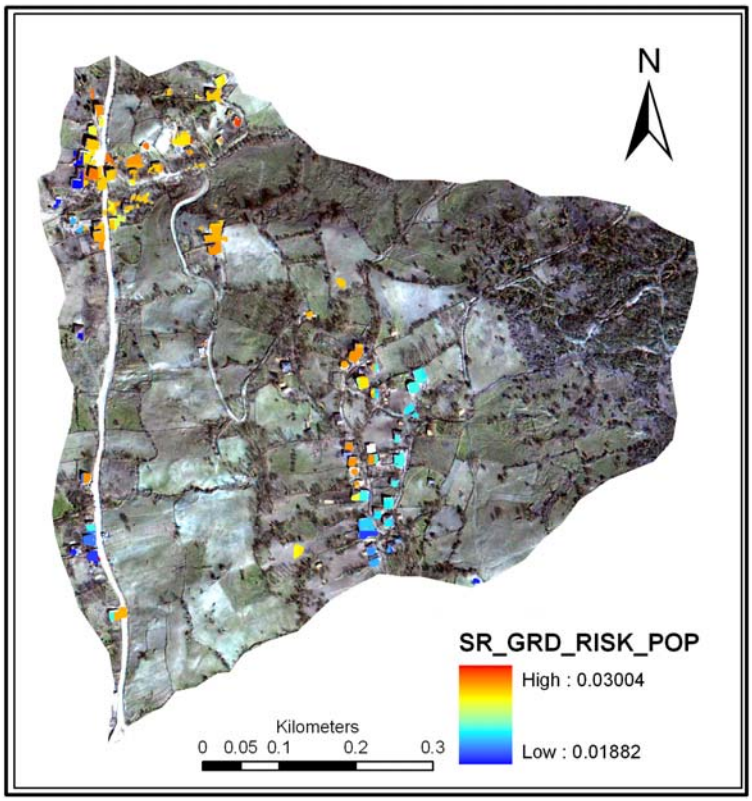
N
SR_GRD_RISK_POP
High : 0.03004
Low : 0.01882
Kilometers
0 0.05 0.1 0.2 0.3

(b)

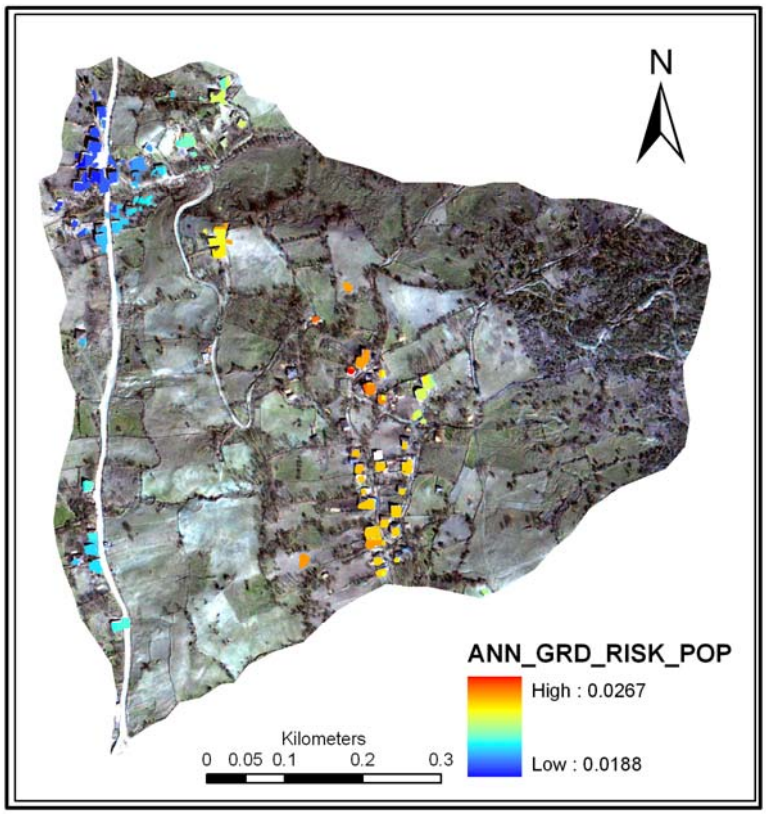

(c)

Figure 4.26. Risk of loss of life for grid-based mapping unit for different methods, a. LR, b. SR and c. ANN (Loss of Life/Pixel)

The risk to property for slope unit-based mapping unit is presented in Figure 4.27 for LR (LR_SU_RISK_POP) (Figure 4.27a), SR (SR_SU_RISK_POP) (Figure 4.27b), and ANN (ANN_SU_RISK_POP) (Figure 4.27c). The SR_SU_RISK_PROP provides risk values which are the same for all the houses in the region. The LR_SU_RISK_POP and ANN_SU_RISK_POP provide reverse risk values for risk to life. For example, the houses in the northern part of the region aligning along the road are illustrated with low risk values by LR_SU_RISK_POP (Figure 4.27a), whereas these houses are represented by high risk values by ANN_SU_RISK_POP (Figure 4.27c). Furthermore, the houses in the eastern part display low risk in LR_SU_RISK_POP, which display high risk in ANN_SU_RISK_PROP.

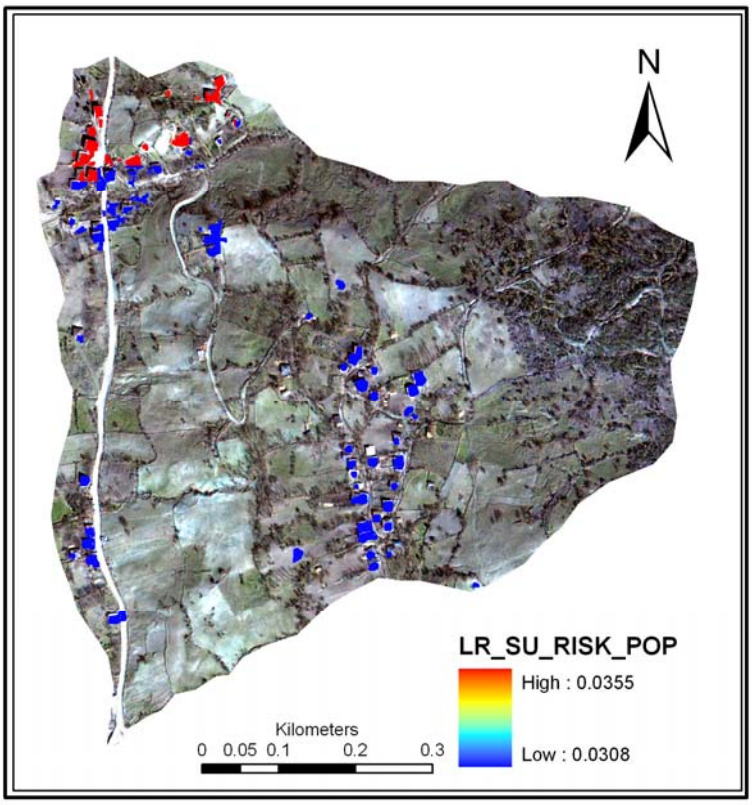
N
LR_SU_RISK_POP
High : 0.0355
Low : 0.0308
Kilometers
0 0.05 0.1 0.2 0.3

(a)

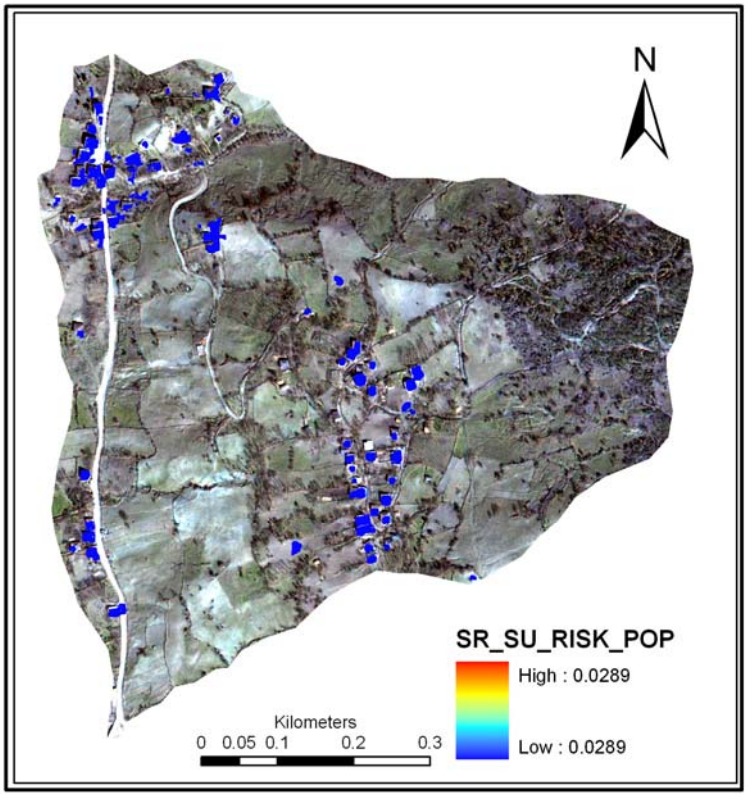
N
SR_SU_RISK_POP
High : 0.0289
Low : 0.0289
Kilometers
0 0.05 0.1 0.2 0.3

(b)

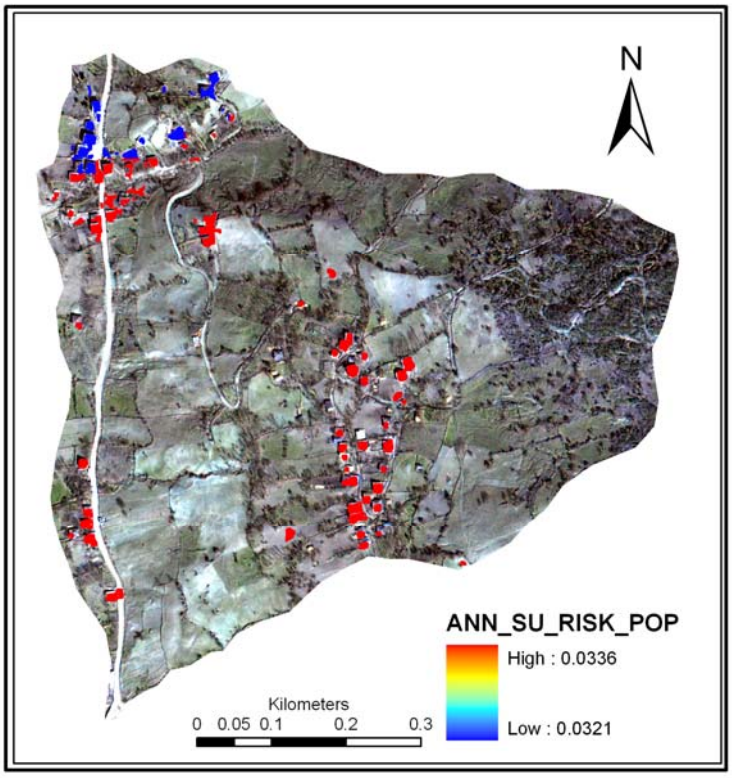

(c)

Figure 4.27. Risk of loss of life for slope unit-based mapping unit for different methods, a. LR, b. SR and c. ANN (Loss of Life/Pixel)

The values for risk of loss of life are meaningful when at least the first four digits are considered (e.g. values between 0.0336 and 0.0321 in Figure 4.27) because when compared to the cost values of property, which is relatively much higher, the number of inhabitants considered for risk computations for loss of life is quite low. This cause the probability value of risk to loss of life to be relatively lower than the probability value of risk to loss of property. Therefore, the first four digits of risk values are evaluated to assess the statistics of risk maps. When the statistics of risk maps are compared (Table 4.7) for grid and slope unit-based mapping units for all methods, it is evident that there is no variation of risk values because all methods have zero standart deviation in both mapping units. The largest maximum value of risk of loss of life is computed by LR_SU_RISK_POP and the smallest maximum value is obtained by LR_GRD_RISK_POP. The mean values of risk to life range from 0.01 to 003 and the minimum mean in the risk map is obtained by LR_GRD_RISK_POP.

Table 4.7 The statistics of the risk maps of loss of life for different methods and mapping units (Loss of Life/Pixel)

	Min	Max	Mean	Std. Dev.
LR_GRD_RISK_POP	0.0028	0.0153	0.01	3.47×10^{-3}
SR_GRD_RISK_POP	0.0188	0.03004	0.03	2.44×10^{-3}
ANN_GRD_RISK_POP	0.0188	0.0267	0.02	2.14×10^{-3}
LR_SU_RISK_POP	0.0308	0.0355	0.03	1.94×10^{-3}
SR_SU_RISK_POP	0.0289	0.0289	0.03	0
ANN_SU_RISK_POP	0.0336	0.0321	0.03	0.62×10^{-3}

4.5 Comparison of Risk Maps on Local Scale

The realization of damage probability matrix and hazard values from the result of LR, SR, and ANN models for grid and slope based mapping units led to the production of six different landslide risk maps for both property and life. The risk maps obtained as a result of the analysis mostly depend on the selected models and the mapping unit. The risk map is the product of hazard times consequences. The consequences and the hazard are a single value; hence, the risk maps depend on the variation of probability values. These changes of probability values depend on the selected model and the mapping unit. Hence, the distribution of risk levels varies depending on the theoretical basis of different models and the selected mapping unit.

The classification procedure for comparison purposes is described in section 3.10. Depending on this procedure, the risk maps in local scale are classified into three different levels of risk similar to regional scale, putting the 0 to 0.38 range of pixels into low, 0.39 to 0.60 into medium, and 0.61 to 1 ranges of pixels into high risk zones for property and life.

The classification results of risk maps based on grid-based mapping unit for property are illustrated in Figure 4.28 and Figure E-1 and Figure E-2 in Appendix E. Furthermore, the classification results of risk maps based on slope unit-based mapping units for property are illustrated in Figure 4.29 and Figure E-3 and Figure E-4 in Appendix E. The risk to property maps for grid and slope unit based mapping units are presented quantitatively in Figure 4.30. There are more low risk classes produced by the LR_GRD model (Figure 4.28), which means most properties can be classified as low annual economic loss, when compared to the other models. In

contrast, ANN_SU (Figure E-4 in Appendix E) shows a lower risk class. This has been confirmed by the corresponding histogram (Figure 4.30) generated on the basis of the defined intervals. SR_GRD (Figure E-1), ANN_GRD (Figure E-2) and SR_SU (Figure E-3) do not represent any classes in the medium class. Except for the LR_GRD (Figure 4.28) model-based risk map, the rest of the maps were designed to represent equal levels of high risk class. This might be due to the fact that the higher economical loss value belongs to the road and the road overlaid by the hazard values provides the higher class. The threshold selected for the classification of risk maps then might provide the same number of higher risk class, which involves the road feature.

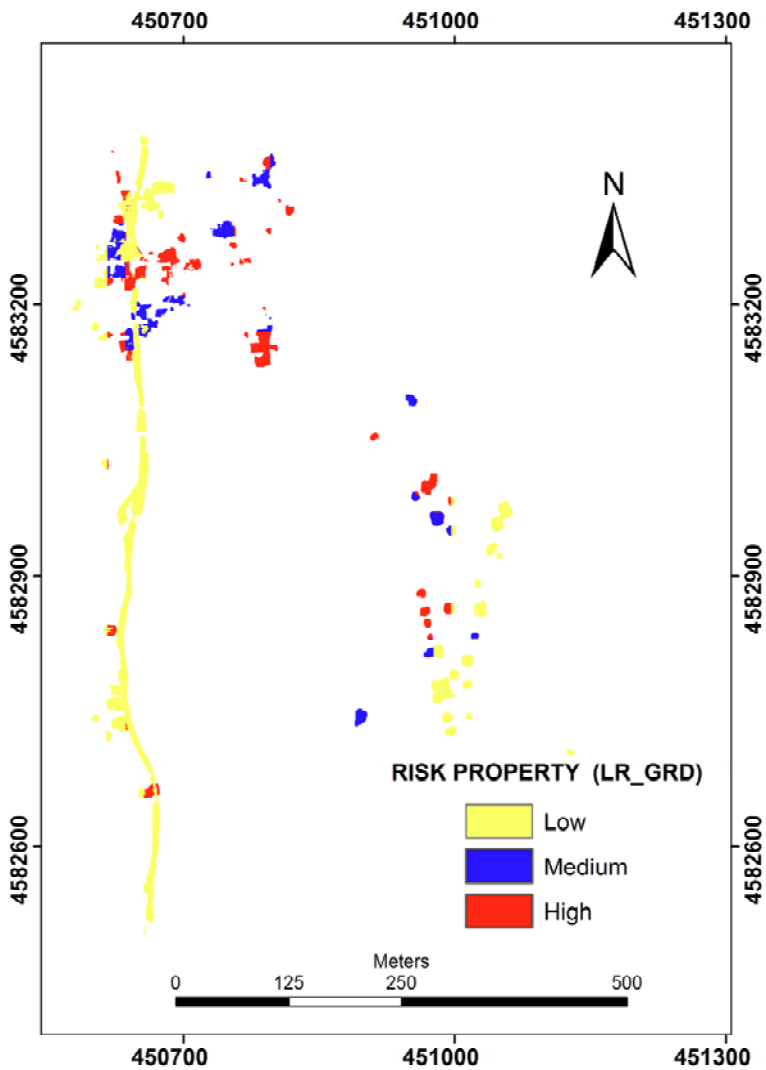

Figure 4.28. Risk to property map created based on the LR model at grid-based mapping unit (LR_GRD) (TL/Pixel)

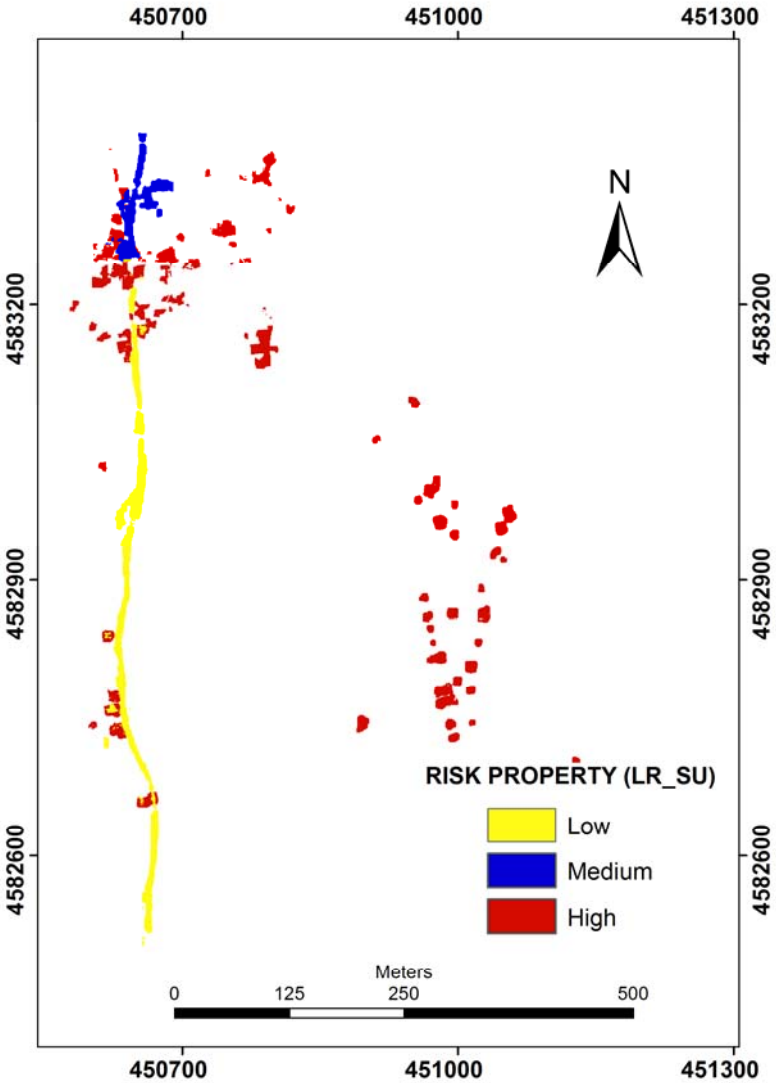

Figure 4.29. Risk to property map created based on the LR model at slope unit-based mapping unit (LR_SU) (TL/Pixel)

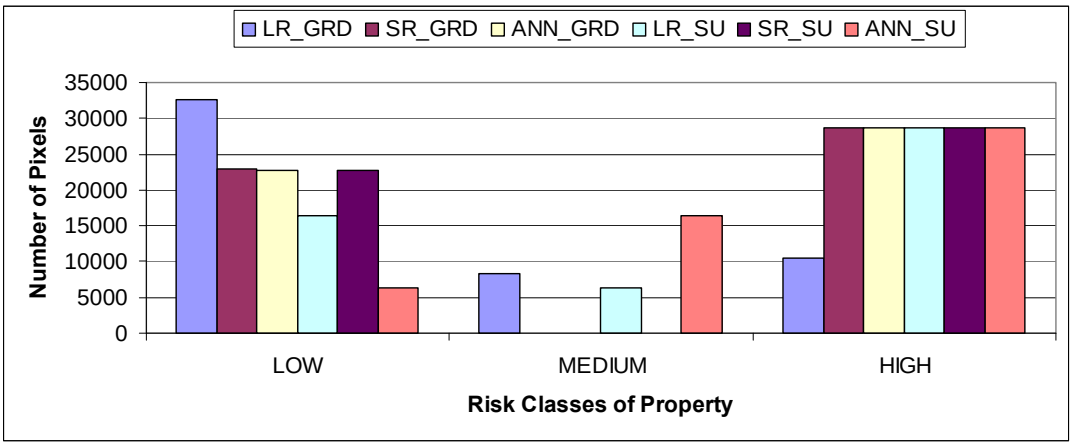

Figure 4.30. Bar graphs showing the relative distribution of risk levels for property

To analyze the map differences spatially, 6 different difference maps were created, among which 3 different methods are compared for each cell-based and slope unit-based maps. As shown in Figure 4.31 and Figure E-5 and Figure E-6 in Appendix E the difference maps created are SR_LR, SR_ANN, and LR_ANN for grid-based mapping unit respectively. Moreover, as presented in Figure 4.32 and Figure E-7 and Figure E-8 in Appendix E the difference maps created are SR_LR, SR_ANN, and LR_ANN for slope unit-based mapping units, respectively. Furthermore, the similar overestimated and underestimated regions are computed quantitatively to analyze the map similarity where the area and percentages are shown in Figure 4.36.

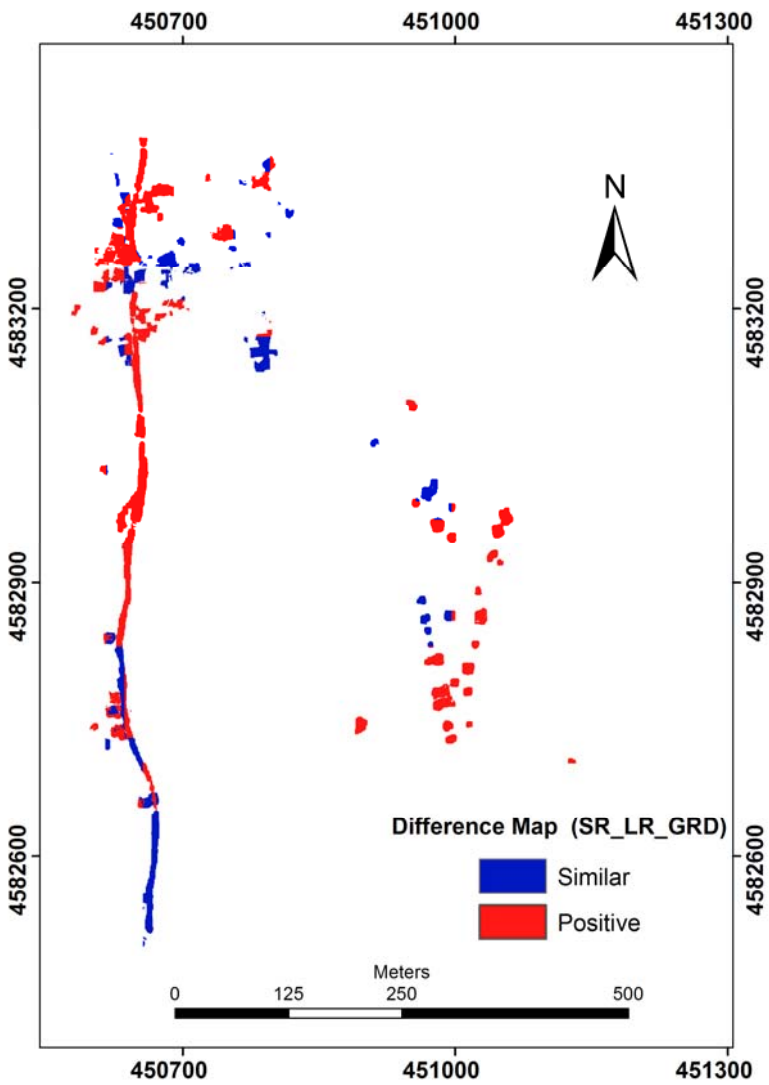

Figure 4.31. Difference of risk to property maps between SR and LR models at grid-based mapping unit (SR_LR_GRD)

A large proportion of road feature is predicted as low risk level and most of the buildings are estimated as high risk level for both LR (Figure 4.29) and SR (Figure E-3 in Appendix E) models for slope-based mapping units (88%); a smaller degree of disagreement exists between models SR and LR for slope-based mapping units (SR_LR_SU) (Figure 4.36) for the southern part of the road feature and few buildings (12.4 %) as presented in the spatial domain in Figure 4.32.

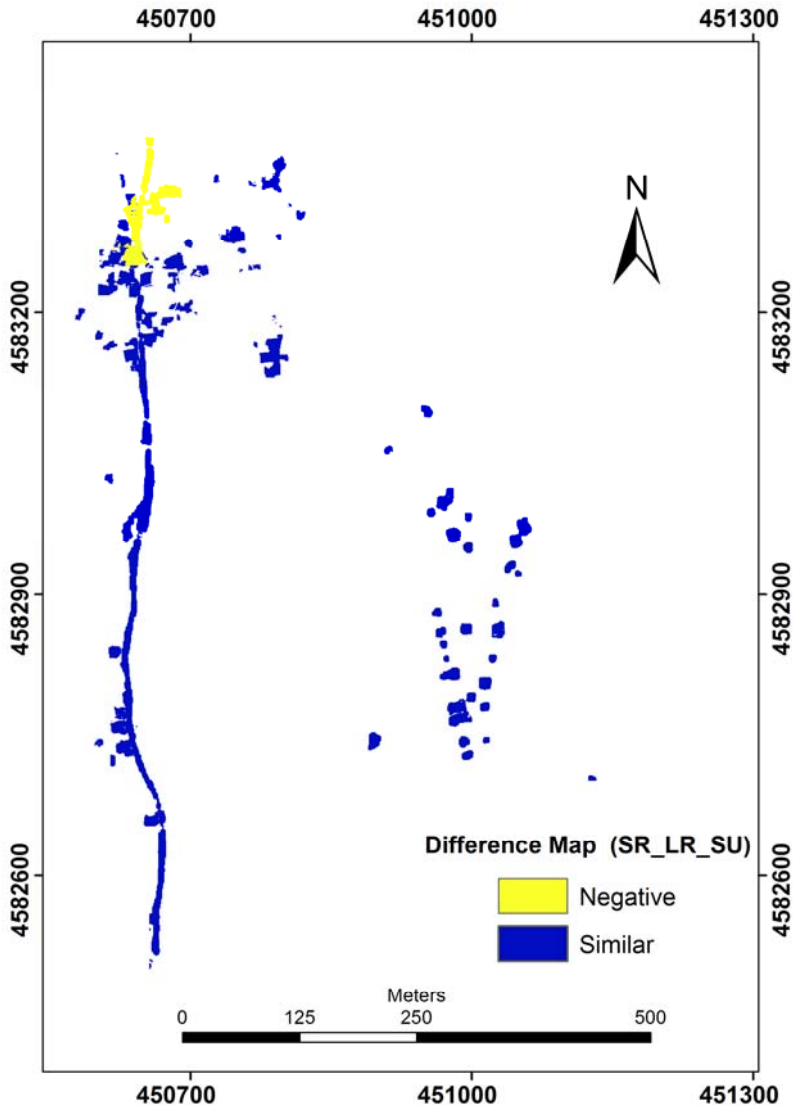

Figure 4.32. Difference of risk to property maps between SR and LR models at slope unit-based mapping unit (SR_LR_SU)

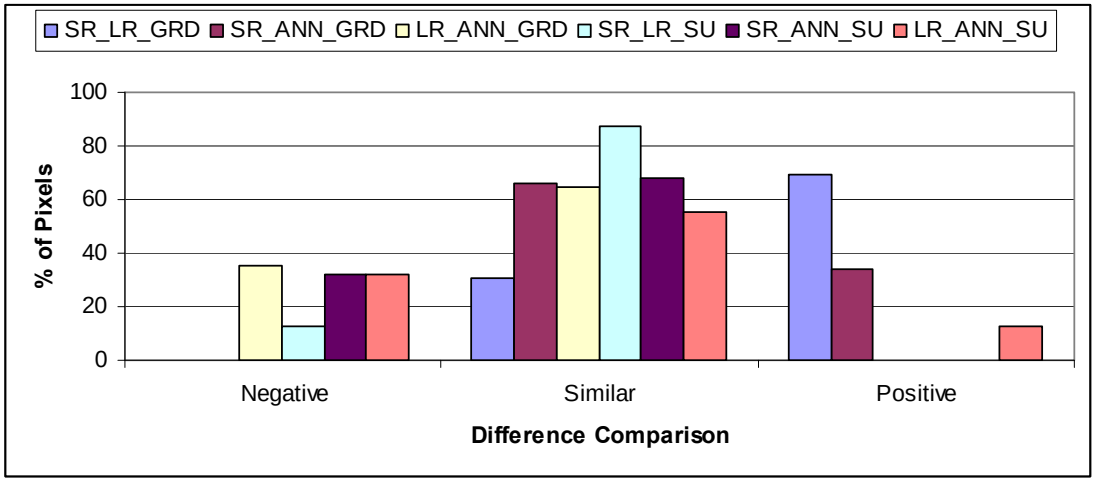

Figure 4.33. Bar graphs showing the percentage difference of risk levels based on different models and mapping units for property

SR_ANN_GRD (66%) (Figure E-5 in Appendix E), LR_ANN_GRD (65%) (Figure E-6 in Appendix E), SR_ANN_SU (68%) (Figure E-7 in Appendix E), and LR_ANN_SU (56%) (Figure E-8 in Appendix E) difference maps provide nearly similar percentages of features in the same class, whereas the risk difference maps based on the SR and LR models at grid-based mapping unit (SR_LR_GRD) (Figure 4.31) provide the lowest similar regions (31%) (Figure 4.36). SR_LR_GRD risk difference maps provide the dissimilarity (69%) at most of the road features in the northern parts of the region and in most of the buildings in the southern part of the region (Figure 4.31). There is a positive dissimilarity, which means that the LR-based risk map overestimates the risk compared to the SR-based risk models for grid-based mapping unit (Figure 4.31).

The ANN-based risk maps provide a positive mismatch (34%) compared to the SR-based risk map at grid-based mapping unit (Figure 4.36) (Figure E-5 in Appendix E), conversely the ANN-based risk map provides a negative disagreement (35%) compared to the LR-based risk map in grid-based mapping unit (Figure 4.36) (Figure E-6 in Appendix E),. The ANN-based risk maps provide a similar level of dissimilarity (32%) compared to the SR (Figure 4.36) (Figure E-7 in Appendix E) and LR (Figure 4.36) (Figure E-8 in Appendix E) risk maps in slope-based mapping unit, additionally the ANN-based risk maps provide a smaller degree of disagreement (12%) for the LR-based risk map.

The risk maps to life created based on the SR, LR, and ANN models and slope and grid-based mapping units are also compared spatially. Therefore, the risk maps created for risk to loss of life were initially reclassified into three different risk classess as described in in section 3.10. The risk maps to loss of life classified are presented in Figure 4.34 and Figure E-9 and Figure E-10 in Appendix E for grid-based mapping unit and Figure 4.35 and Figure E-11 and Figure E-12 in Appendix E for slope unit-based mapping unit. In addition spatial distribution of to risk maps to loss of life, the risk levels are analyzed quantitatively (Figure 4.36). In the resultant maps of risk to life, the higher levels of low risk zone are represented in the SR_SU model-based risk map (Figure 4.36). The rest of the models provide fewer numbers of pixels on low risk levels of risk to life. The risk maps obtained from the slope-based mapping unit does not determine medium level risk. This might be due to the, physical properties of the mapping unit type. The slope-based units divide the terrain depending on the natural boundaries in terms of hydrological lines. The slope units that crossed the buildings at Hepler village correspond to a single or two different slope units. Hence, the probability of susceptibility values does not show variability compared to grid-based mapping unit. As a result, the risk to life values may get one or maximum two different values which correspond to higher or lower values of risk on these maps. LR_GRD (Figure 4.34), SR_GRD (Figure E-9 in Appendix E), LR_SU (Figure 4.35), and ANN_SU (Figure E-12 in Appendix E) show similar numbers of risk to life on a high level, whereas the ANN_GRD (Figure E-10) has lower number of pixels on the high level of risk. SR_SU (Figure E-11) does not have a high risk level, which means all features on SR_SU risk map are classified as low annual probability of loss of life.

A large proportion of risk to life units in the north-eastern part of the buildings which were predicted as high risk level by the SR-based risk maps (SR_GRD) (Figure E-9 in Appendix E) are also classified as high risk by the LR based risk model (LR_GRD)(82%) (Figure 4.34) in grid-based mapping unit.

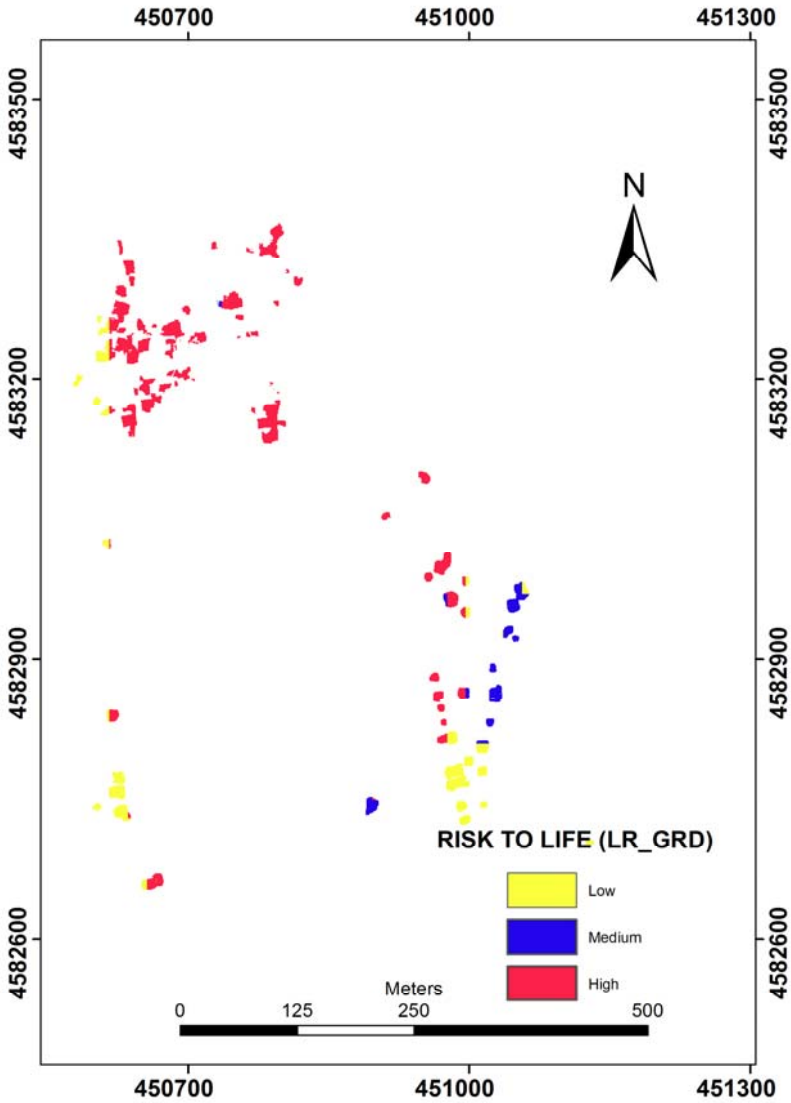

Figure 4.34. Risk to life map created based on the LR model at grid-based mapping unit (LR_GRD) (Loss of Life/Pixel)

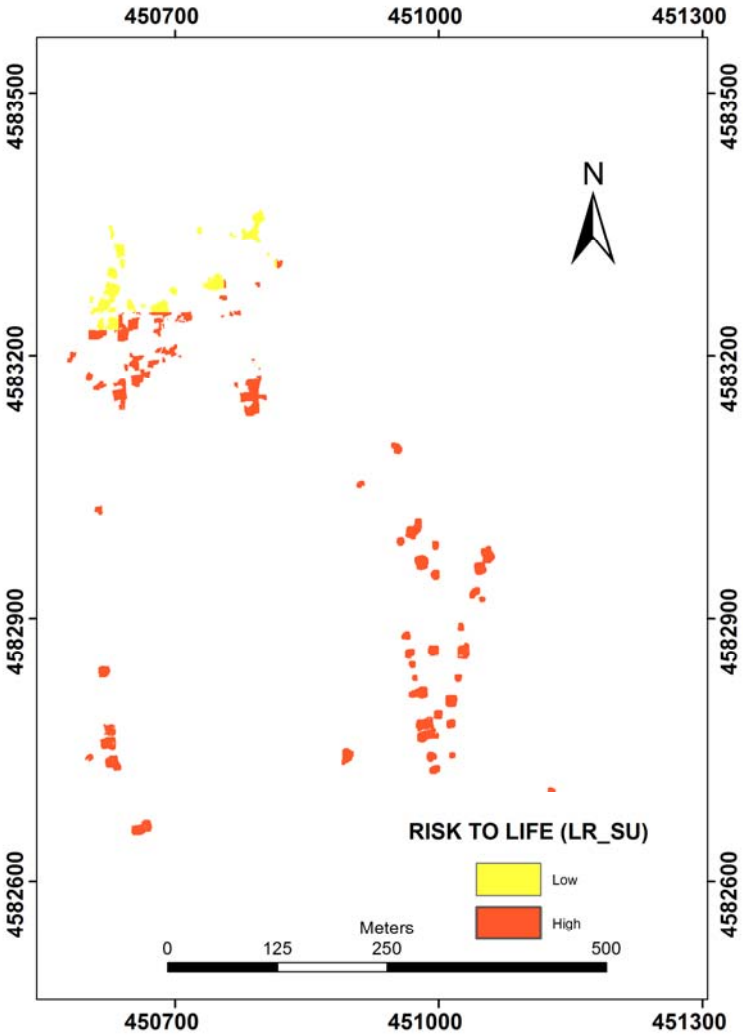

Figure 4.35. Risk to life map created based on the LR model at slope unit-based mapping unit (LR_SU) (Loss of Life/Pixel)

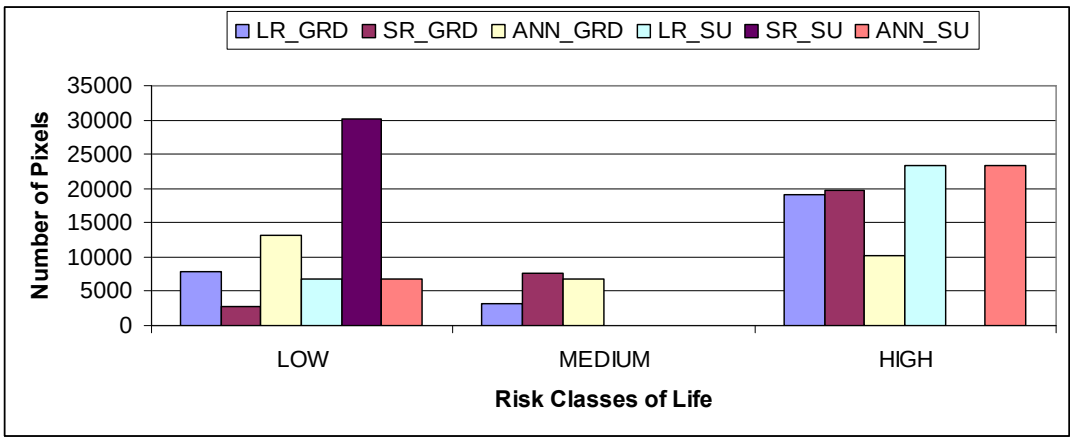

Figure 4.36. Bar graphs showing the relative distribution of risk levels for life

The difference maps are obtained for risk to loss of life as presented in Figure 4.37 and Figure E-13 and Figure E-14 for SR_LR_GRD, SR_ANN_GRD and LR_ANN_GRD, respectively for grid-based mapping unit and Figure 4.38 and Figure E-15 and Figure E-16 in Appendix E for SR_LR_SU, SR_ANN_SU and LR_ANN_SU, respectively for slope unit-based mapping unit. In addition to the spatial distribution illustration of the difference maps it is also presented quantitatively in **Figure 4.39**.

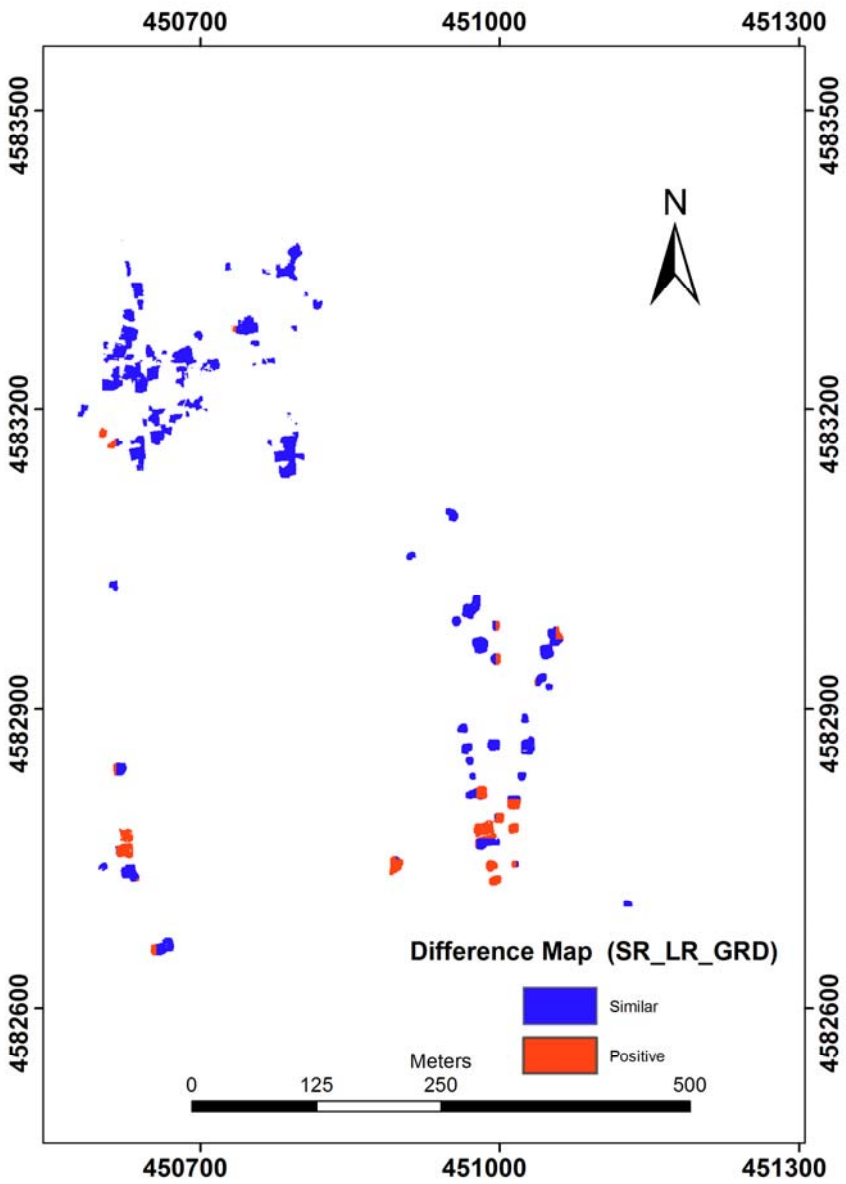

Figure 4.37. Difference of risk to life maps between SR and LR models at grid-based mapping unit (SR_LR_GRD)

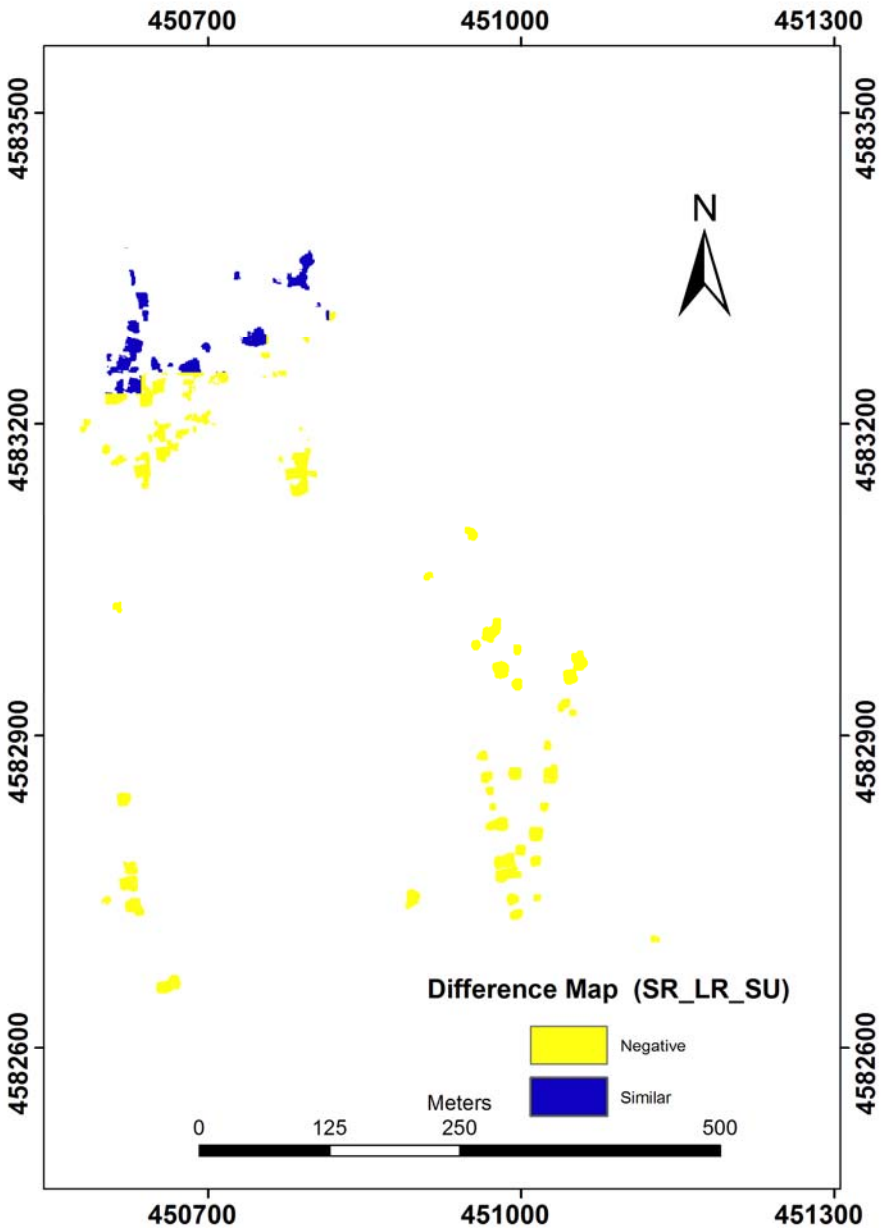

Figure 4.38. Difference of risk to life maps between SR and LR models at slope unit-based mapping unit (SR_LR_SU)

The similarities between the risk maps indicate that a smaller degree of agreement exists between SR_LR_SU (Figure 4.38), SR_ANN_SU (Figure E-15 in Appendix E), and LR_ANN_SU (Figure E-16 in Appendix E) with 22.6% and SR_ANN_GRD (Figure E-13 in Appendix E) and LR_ANN_GRD (Figure E-14 in Appendix E) difference maps with 30.6% (Figure 4.39). The SR-based risk maps (Figure E-11 in Appendix E) estimate all buildings as low risk to life for slope-based mapping unit, whereas LR-based (Figure 4.35) and ANN-based (Figure E-12 in Appendix E) risk maps predicted the buildings in the southern part of the region to display with high

and medium level risk respectively. Hence, the SR _LR_SU (Figure 4.38) and SR_ANN_SU (Figure E-15 in Appendix E) difference maps has 77% negative dissimilarity, which means that the SR-based risk model was underestimated at these buildings. In grid-based mapping unit, the SR (Figure E-9 in Appendix E) and LR (Figure 4.34) risk maps have lower levels of negative dissimilarities with 17% and 20% but higher percentages of dissimilarities on positive level with 52.5% and 42% respectively (Figure 4.39). The LR (Figure 4.35) and ANN (Figure E-12 in Appendix E) based risk maps provide higher positive dissimilarities (78%) in the slope-based mapping unit. This is due to the fact that the LR-based risk map estimates the southern part of the buildings to display high risk to life and the same regions are predicted as medium on the ANN-based risk maps.

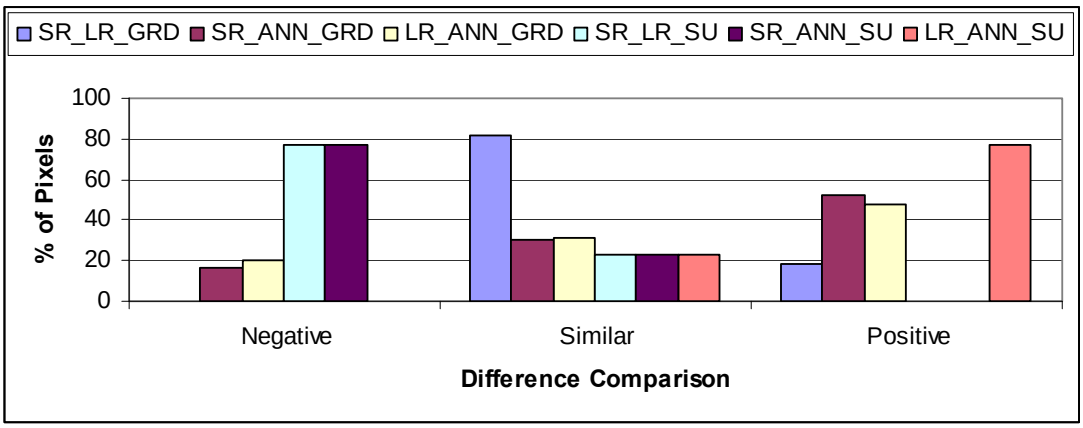

Figure 4.39. Bar graphs showing the percentage difference of risk levels based on different models and mapping units for life

CHAPTER 5

CONCLUSION

5.1. Overview of the Results

The main objective of this thesis, which is the development of a comprehensive landslide risk assessment methodology for landslides, is successfully achieved for Bartın Kumluca region. In addition to the main objective of developing the methodology, several sub objectives, which are described in section 1.3, are also evaluated at the end of the implementation of the methodology.

This thesis presents comparative studies on different modeling approaches and different mapping units to create risk maps for landslides. It is not easy to recommend a single approach of mapping method or mapping unit as the most suitable one. Indeed, the selection of the approach or mapping unit to be adopted depends on the study area and economic concerns.

The risk assessment is carried out for two different scales, local and regional, considering the specific characteristics of Bartın related to data availability for each stage of risk. The methodology involves quantitative assessment of risk for both scales based on GIS and RS techniques. Each component of risk, i.e. hazard assessment, vulnerability and consequence analysis, was quantitatively assessed for each scale. Each component of risk assessment procedure requires the incorporation of diverse disciplines due to its multidisciplinary structure. It requires highly advanced statistical background

as well as background on geology, economics and hydrology. To begin with, the spatial information or data in catalogs required for each component of risk differs depending on the types of data and the methods for obtaining them. The data acquired from different sources and organizations may have different scales, data formats, projections and types as every organization has its own rules, formats and standards in data production. In order to achieve reliable risk maps, the consistency of data format is crucial for the analysis.

While both landslide inventory and influencing factors are necessary to obtain susceptibility maps, triggers are the required data for hazard assessment of temporal probability and a list of elements at risk are required to create a consequence map. Data may be acquired by field mapping or measurements, existing maps or laboratory analysis. In the last decade, the remote sensing imagery has proven to be a very important tool for capturing, displaying, and determining the relevant data such as landslide inventories, digital elevation models, elements at risk and land-use maps, which may be required at different stages of the risk assessment procedure. Additionally, GIS is an important tool to be used to store, monitor, evaluate, compile, manipulate, and manage data in each step of quantitative risk assessment. Moreover, the mapping and the visualization of the spatial distribution of the maps, and the evaluation of simple statistics of the data were done in GIS environment in an objective way compared to laborious and time-consuming hand-made products. In order to create reliable risk maps, it is crucial to obtain data as complete as possible in spatial and temporal domain in order to reduce uncertainty. Quantitative risk maps provide opportunity for decision makers to perform cost-benefit analyses quantitatively for proper land-use planning. In addition, it is useful when the authorities would like to provide information about the landslide risk. Therefore, it is very important to identify the potential landslide occurrence areas and risk to property and life.

The main component of risk assessment procedure requires obtaining the spatial probability for landslide occurrence. The resultant risk maps change depending on the

adopted mapping method, the mapping unit, and the scale of susceptibility assessment. It is therefore important to test the effects of several susceptibility methods and mapping units on the resultant risk maps on different scales. Much of the landslide susceptibility and hazard work is based on the assumption that "the past is key to the future". Therefore, based on this assumption, influencing factors are evaluated with historical landslide locations to predict the spatial probability of future landslides. Data collection is directly related to the scale. Therefore, for regional scale, hazard and risk assessment data in the form of maps are obtained, whereas for local scale data is compiled based on extensive field surveys and risk assessment procedures are adopted. Before the susceptibility analysis, the analysis of data set prior to constructing the database for further analysis is crucial, which may involve the transformation of qualitative variables into continuous scale, testing the multicolinearity etc.. The construction of database may vary depending on the adopted mapping unit; therefore, it is crucial to identify the mapping unit type, which can be basically grid cells, slope units, terrain units, topographic units, or unique conditions units. The adoption of different mapping unit types may cause the creation of different susceptibility maps with similar susceptibility methods. This might be the result of the adopted procedure to assign the variables to the mapping units. The adopted procedure initially creates the mapping unit with the selected size. The selection of the size of each mapping unit is intrinsically subjective or depends on the algorithm adopted for the creation of mapping unit. This may result in a cumbersome computational process with a small-size unit or the reduction of information with a large-size unit. By overlying the mapping unit onto variables, each unit that is assigned a value for each factor is taken into consideration and each unit is treated as a case or a sampling unit in the analysis. The value assigned to each mapping unit may change depending on the adopted mapping unit type. In the grid-based mapping unit approach, by considering the mapping scale, each cell may be assigned the exact value of each variable. For instance, for a 1:25000 scale, 20 m. grid cell is the minimum size to obtain variables. Therefore, each grid has a unique value of that variable. However, each slope or the other type of mapping unit may vary in size and each unit holds a variation of values. Generally, zonal statistical functions are used,

which perform operations on a per-zone basis to assign the variable values to each unit. By using the zonal statistics, the variation of data is reduced to a single value, which may normally cause the smoothing out of the local details and providing a large generalization of the variable values. This may also result in the generalization of the maps obtained by smoothed local details in each mapping unit.

In addition to the mapping unit, the selected mapping method also influences the result of susceptibility maps, and ultimately that of risk maps. Notwithstanding, depending on the adopted algorithm, each model has different theoretical basics which may enable us to provide different prediction values for the same region and for the same mapping unit type. Although there are various methods of obtaining susceptibility maps, the efficiency and performance of each method should be evaluated. Global models like LR and ANN ignore spatial dependence of data between the observations in susceptibility assessment. However, to assess the probability of landslide, it is important to understand the spatial correlation between landslide occurrences and influencing factors. By including these relations, the predictive ability of the developed model increases. In this study innovative SR and GWR techniques were adopted and applied for landslide risk assessment on different scales.

Compared to various other methods and models applied in other countries, these models consider spatial variability in the parameters and provide better representations of landslide susceptibility for different mapping unit types. Unlike SR, where regression coefficients for each independent variable and the intercept are obtained for the whole study region, in GWR the regression coefficients as well as the significance of the relationships between the influencing variables and the landslide occurrence are computed for each spatial zone. Therefore, the regression coefficients can be mapped for each spatial zone by GWR, which results in the mapping and visualization of local details.

In order to assess the accuracy and to evaluate the performance of SR, LR, ANN, and GWR models for both grid- and slope unit-based mapping units, the relative operating characteristics (ROC) curve was evaluated in addition to field surveys. In the ROC curve evaluation it is seen that for both grid- and slope unit-based mapping units, the models considering spatial correlation, GWR and SR show a higher predictive performance with values of 0.80 and 0.77 (Figure 3.105) and 0.93 and 0.90 (Figure 3.107), respectively than the conventional models of LR and ANN. This result is also supported by field surveys, where the model results are compared with the ground truth data.

In addition to the accuracy assessment, the obtained susceptibility results are also evaluated in terms of two different comparison approaches. In the first approach, four susceptibility maps obtained from LR, SR, ANN, and GWR for both grid- and slope unit-based mapping units were compared with historical landslide locations. This approach provides insight into the evaluation of the quality of each model for the estimation of historical slide locations. In the second approach, the similarities and dissimilarities of models were analyzed by simply overlaying each map. This provides ability to compare the maps spatially.

In slope unit-based mapping unit, many of the landslide distributions fall into the high susceptibility class for all mapping types. On the other hand, in grid-based mapping unit, many of the distributions match with the high and medium susceptibility classes to a large extend. This may indicate the success of prediction models for identification of landslide zones since for both mapping unit types and for all models, most of the historical landslide locations are present in high and medium classes (Figure 3.123 and Figure 3.124)

SR provides a better performance when compared to the other methods for both grid (96%) and slope unit-based (82%) mapping units for the estimation of landslide occurrences in high and medium susceptibility classes. This might be due to the

approach of SR to take spatial variations between variables as inputs. However, GWR also considers the spatial variations between variables on a local scale. It has a better performance in grid-based mapping unit when compared to slope unit-based mapping unit type. This might be due to the fact that a grid-based mapping unit considers the mapping unit as smaller grid cells where the variation may increase, which may also increase the predictive ability of GWR. In slope unit-based mapping unit, each mapping unit is larger in size when compared to grid cell, where parameters are obtained by generalization of information at smaller grid cells overlain by the corresponding slope unit (3.193).

In the second approach: To analyze the similarity between susceptibility maps, difference maps were analyzed. As a result of the difference maps for both cell and slope unit-based model pairs, it is seen that the similarity is high between the SR and GWR (Figure 3.129 and Figure 3.136 in spatial domain and Figure 3.127 and Figure 3.128 quantitatively). This may be the result of characteristics of both models which depend on the consideration of the spatial correlation of parameters between variables.

When mapping units are compared in terms of similarity, it is seen that the slope unit-based mapping unit provides relatively higher percentages of similarities for each mapping method compared to the grid-based mapping unit (Figure 3.127 and Figure 3.128). This might be due to the larger unit size and the generalization of variable values of slope unit-based mapping unit.

As a result of the whole susceptibility assessment methodology, it can be concluded that the landslide susceptibility mapping performance is enhanced by using spatial regression and geographic weighted regression.

In order to obtain temporal probability, the relation between triggering events (rainfall or earthquakes) and landslide occurrence dates is required. Therefore, an extensive landslide inventory data, in which the landslides are dated, are required in addition to

triggering measurements. If the considered trigger is rainfall, it is extremely important to identify the most suitable rain gauge that is associated with a slide. The rainfall intensities or antecedent rainfall can be assessed to estimate the rainfall thresholds by using different methods. In this thesis study, as the landslides in Kumluca Basin is mostly triggered by rainfalls, the relation between landslides and rainfall intensity is analyzed. To estimate the temporal probability the initial step is to obtain the rainfall trigger. The critical rainfall thresholds were estimated by using daily and antecedent rainfalls and landslide occurrence dates based on three different approaches: Time Series, Gumble Distribution and Intensity Duration Curves. The first approach was to investigate the appropriate time series model for daily rainfall data and then use the model to determine a threshold for landslide triggering rain. The second approach was to investigate the Gumbel distribution graphically and analytically to determine thresholds for daily and antecedent rainfalls, respectively. Lastly the third approach was the creation of rainfall intensity–duration relationships for antecedent rainfall events that caused landslides.

In addition to triggering threshold, it is necessary to obtain the conditional probability of having a landslide given that rainfall triggers exceed a certain threshold value for a given time period for hazard analysis. In this respect, a new approach is proposed, which involves modeling landslide occurrence and rainfall values higher than the critical rainfall value by using logistic regression. This approach is successfully implemented in Bartın region to obtain temporal probability. The temporal probability of landside is combined with spatial probability to obtain hazard maps by the proposed methodology.

Consequence analysis, which involves elements at risk and vulnerability, is crucial for risk mapping. The elements at risk values and vulnerability values depend very much on the scale of the investigation. Thus, the changes in consequence in different scales should be considered to assess changes in the resultant maps. On regional scale, more general data is used where generalizations are adopted. On the other hand, on local scale the data used is more detailed and uncertainty in the results is diminished.

For regional scale analysis, the element at risk is mostly derived from existing cadastral databases as it is very expensive and sometimes unaffordable to create data for the numerous run-outs of slopes. In addition, population data may be derived from existing census data. Therefore, the element at risk used in the analysis, mostly depends on the availability of digital databases and the accuracy also depends on the existing database. In the thesis, the elements at risk were obtained from existing digital databases and the inhabitants were estimated per house basis in rural areas using the population density of Kumluca settlement, which shows a possible solution for obtaining elements at risk for risk studies over large areas. This technique could be used to estimate population per house whenever buildings in digital format and population information of that city are present. For local scale analysis, it is possible to do a detailed survey of elements at risk and to obtain population information for each building in the field. The elements at risk can also be obtained by high resolution remote sensing images by the developed algorithms in an automatic or semiautomatic way. However, the accuracy of the extraction of each element depends on the algorithm. As a result of the algorithm, the features obtained may not be the real features or the features on the ground truth may not be detected by the algorithm. In addition to the performance of algorithm in the extraction of elements at risk, the size of each element may also be crucial while obtaining vulnerabilities. The elements at risk may change depending on the extent of each element covered by the run-out. Here it is also important to indicate the accuracy of the run-out model that is used.

Due to the unavailability of data related with the exposure (physical, natural, economic, social and the like) of each element at risk, the estimation of vulnerability value is limited. The generalization is adopted in the thesis study for vulnerability because it is not possible to estimate the run–outs, the technical resistance of buildings (type, nature, age, and so on), and their proximity to the slide, additionally, the social, economic and environmental factors for an accurate assessment of vulnerability indicator for landslide locations on regional scale. Hence, it is not feasible to derive a vulnerability index for

small scale studies. On the other hand for local scale analysis, the vulnerability was estimated by adopting a “damage probability matrix“approach. As a result the quantitative risk maps were obtained for both local and regional scale by thedeveloped methodology for risk assessment through combination of hazard maps with the consequence maps.

To assess the effect of susceptibility mapping unit and mapping method on the risk maps, the risk values were categorized since it was not possible to evaluate the differences on a continuous scale. Therefore, the adoption of a classification procedure has an utmost importance in the visualization and comparison of different maps. The change in cutoff values may cause a change in class ranges, which may result in different evaluations of each class. In this thesis, similar cutoff values were adopted for both local and regional scale risk maps by analyzing the most proper cutoff values in each map. The conclusions derived from the comparison of risk maps are as follows: The realization of elements at risk and hazard probabilities for LR, SR, ANN models and for grid and slope-based mapping units led to the production of six different landslide risk maps for both property and life on local and regional scale. On regional scale, risk values for property are higher in the risk map which is created based on the ANN model in the grid-based mapping unit (ANN_GRD) (Figure 3.202) and then in the risk map based on the LR model in slope unit-based mapping unit (LR_SU) (Figure 3.202). The properties which are in the higher risk class at ANN_GRD (Figure 3.191) are the buildings around the Kıyıklar village. For the LR_SU (Figure 3.192), the properties in higher classes are the buildings distributed around Kumluca, Konuklu and Zafer. In the medium class, the highest risk values belong to the risk maps which are based on the SR model for both slope (SR_SU) and grid-based mapping units (SR_GRD) (Figure 3.202). The properties which belong to this medium class for SR_SU (Figure 3.193) are the provincial highway, provincial road, and also the buildings distributed around the central and eastern parts of the region. Additionally, for SR_GRD (Figure 3.202) the buildings distributed around the eastern, western, and central parts of the region are in the medium class. The SR_GRD and LR_GRD provide the highest

similar risk values for property (Figure 3.203). In addition to this, the comparison of different methods for both grid and slope unit-based mapping units also reveal a high degree of similarities. Here it is important to indicate that the similarities are high due to the large number of low risk values around the region. Contrary to risk to property, in risk to life, the risk map based on the SR model for grid-based mapping unit (SR_GRD) has the highest number of risk values in the high risk class. Additionally, the ANN model in grid-based mapping unit (ANN_GRD) provides the highest medium risk class (Figure 3.202). The risk to life values are represented for each building in the region. The similarity of risk to life values for slope unit-based mapping unit is higher when compared to grid-based mapping unit for SR, LR, and ANN values (Figure 3.204).

On local scale, the risk values for property show similar values to high risk values for SR and ANN for grid-based mapping unit and SR, ANN, and LR for slope unit-based mapping unit (Figure 4.37). Low risk values are larger in the grid-based mapping unit based on the LR model. The risk to property does not provide medium class risk values with the selected range for SR_GRD, ANN_GRD, and SR_SU. The similarity between risk values is higher in the LR and SR-based risk maps in slope unit-based mapping unit, whereas the dissimilarity is higher in the grid-based mapping units for SR and LR.

For risk to life, the SR model provides a larger number of pixels in the low risk class for slope unit-based mapping unit. Depending on the mapping unit, the slope of Hepler may get varying hazard values for grid-based mapping unit, however, one or two hazard values for slope unit-based mapping unit. Therefore, risk to life values do not provide any medium class for slope unit-based mapping units for the SR, LR, and ANN models (Figure 4.42). The similarity between maps is prominent in the grid-based mapping unit for the SR and LR models (Figure 4.43).

5.2. Conclusions

The conclusions and also the contribution of this thesis to literature derived from the development of the methodology and from the implementation of the methodology are as follows:

Landslide risk assessment is still in its developing stage, and most countries do not have a standardized landslide risk assessment programme. In Turkey, there are even no studies for risk mapping for landslides. Therefore, this study contributes to the literature by designing a quantitative systematic risk assessment methodology.

As quantitative risk assessment methodology requires allaborative data collection, the thesis contributes in providing a schematic overview of the main data sets required for the components of landslide risk assessment.

In the literature, there are very few studies dealing with the comparison of different susceptibility assessment methods and none describe its effect on the resultant risk maps. However, any change in the landslide susceptibility map implies high degree of dissimilarity in hazard and ultimately in risk maps especially when different statistical methods and mapping units are used on different scales. Therefore, this research is contributes by investigating the effect of different susceptibility assessment models, mapping units, and scales on the resultant risk maps.

In addition to the existing methods, a new approach to enhance the performance of susceptibility assessment method, which considers the spatial correlation structure of the parameters, was proposed. These, innovative techniques SR and GWR were adapted and proposed for landslide susceptibility assessment on different scales. As a result of these models it is observed that the predictive ability of the susceptibility maps are increased considering the spatial variability. Moreover, the conventional LR and ANN models are also adopted in this study. As a result the influence of four different susceptibility

mapping methods on the resultant risk maps was investigated by using two different mapping units, namely slope unit-based and grid-based mapping units in local and regional scale.

The critical rainfall thresholds were estimated by using three different approaches namely Time Series, Gumble Distribution and IntensityDuration Curves. Time series model is a new approach proposed in the syudy to obtain the rainfall trigger when the landslide days and daily rainfall is present. As a result of the comparison of different methods to obtain triggering threshold, they provide similar results when they are compared on the same return period level.

To obtain temporal probability, a new approach is proposed in this thesis, which involves modeling landslide occurrence and rainfall values higher than the critical rainfall value by logistic regression. The conversion from susceptibility to hazard involves the combination of temporal probability of landside with spatial probability by the proposed methodology. The proposed methodology also contributes in transforming spatial occurrence probabilities obtained from susceptibility mapping into temporal occurrences probabilities (hazard maps).
In this thesis study, a loss estimation approach due to landslides was developed for regional and local scales. The thesis study adapted the 3D procedure of Düzgün and Lacasse (2005) for consequence analysis, which involves scale, elements at risk and magnitude of the devastating event. For regional scale analysis, the elements at risk were obtained from existing digital cadastral databases in GIS environment. On the other hand, on local scale the elements at risk are obtained by high resolution remote sensing images. The elements at risk on local scale were obtained in an automatic way by the new developed algorithm which is another contribution of the thesis.

In the thesis, the use of run-out modeling opens a new possibility to assess the vulnerability values quantitatively on local scale. The velocity values were evaluated with the number of inhabitants per house to evaluate the vulnerabilities. Furthermore,

the vulnerability of buildings and road were estimated by adopting the damage probability matrix approach. On the other hand, for regional scale analysis, a generalization approach was adopted for vulnerability values and each element at risk was evaluated in monetary terms in the thesis.

The risk maps were obtained by the evaluation of hazard and consequence maps for each element at risk. A combined landslide risk map was obtained by adding risk for each element at risk. As a result, quantitative risk maps were produced on a continuous scale where numerical values indicate the distribution of risk including the annual probability of expected loses in TL per pixel and the annual probability of life loss per pixel for property and life, respectively.

The effect of susceptibility mapping unit and mapping method on the risk maps on regional and local scale was assessed which is another contribution to the related literature. Here it can be concluded that in all cases different levels of risk values may be obtained for different reasons which may be given as: The replacement of cost values of properties may vary for different features. It is high for road and building and low for infrastructures and land-use features per unit. Therefore, low values of risk may be obtained for different maps since low replacement cost values may correspond to low hazard values. Additionally, high risk values may be obtained by corresponding to high replacement cost features with high hazard values. The relative distribution of elements at risk is also important for the variability of obtaining different risk classes. The low density of elements at risk in high hazard may provide low risk values. Furthermore, risk values for regional and local scale vary depending on the susceptibility assessment method and the mapping unit used. The risk map comparison illustrates this concept markedly. Any change in the landslide susceptibility map implies a high degree of dissimilarity in hazard and ultimately in risk maps, especially when different statistical methods and mapping units are used on different scales. The reason is that, in its simplest form risk is defined by multiplication of hazard and consequences, where hazard is the product of susceptibility and trigger. The hazard, elements at risk and

vulnerability values are similar for all of the risk maps, whereas spatial probabilities vary depending on the model and mapping unit for susceptibility assessment. The spatial probability values of a method may vary depending on the adoption of different mapping units, likewise in a unique mapping unit different methods provide different probability values for each pixel due to model differences. Therefore, any change in spatial probability causes a change in hazard and hence in risk maps. As a result, the selection of the mapping unit and also the susceptibility model influence the resultant risk map to a great extent.

5.3. Future Work and Recommendations

The influencing factors considered in the analysis are limited to the availability of the data and economical conditions. It is possible to obtain various data sets relevant with the characteristics of landslides. Obtaining a large set of data may be cumbersome in further computer processing for modeling of susceptibility. For instance, when a small size of mapping unit is used for a large area where each unit keeps relevant information for each influencing factor, a bulk of data is acquired, which may not be easy to handle. Therefore, it is crucial to select the appropriate size of mapping unit. In addition, the consideration of relevant influencing factors is also important; therefore, the irrelevant influencing factors should be reduced by measuring the correlations between factors to obtain a smaller but a more efficient data set. Hence, it is recommended to adopt a preliminary analysis for indicators for susceptibility assessment.

GIS is efficiently used for different stages of risk mapping but is insufficient for modeling susceptibility. The data set created for modeling susceptibility is transmitted into other software apart from GIS for statistical treatment of data, which may take time. Therefore, for future studies certain modeling approaches may also be adopted by the GIS environment and risk assessment processes may be automated in a single environment.

For obtaining the elements at risk for local scale, the data is mostly acquired by field surveys, which are very expensive. The developed algorithm to obtain features from high resolution remote sensing images provides an automatic way for obtaining these features. The cost of these images is comparatively lower for a small region than field observations when considering transportation and individual expenses in addition to expenses for equipments. However, for the future work, this algorithm can be improved to reduce errors by adapting new image processing methods suitable for rural areas.

The assessment of vulnerability differs for different scales and there is not a common method of vulnerability assessment in landslide risk mapping. In this thesis, for local and regional scales appropriate vulnerability indicators were designed and applied. The vulnerability approach designed for local scale is based on damage probability matrix and run-out velocity, which may bring a new possibility to assess the vulnerability values quantitatively. The use of the velocity value of run-out is new for vulnerability assessment and several issues such as rheology computation and model calibration are needed to be incorporated into the analysis. In addition to temporal impact, which is considered in the vulnerability approach, the probability of being in run-out zone for elements at risk, the construction type, the replacement cost of particular buildings etc. may also be considered for further vulnerability assessment studies.

For comparison and visualization purposes, it is crucial to identify cutoff values for classification of quantitative risk maps. It is not an easy task to evaluate the maps on a continuous scale and the selection of different methods for the visualization of different maps may be misleading for end users, who will provide decisions based on the interpretation of these maps. There are yet no internationally accepted classification procedures for visualization or comparison of risk mapping. However, for a true evaluation and comparison of maps, a common standard would be highly valuable.

For future studies, Interferometric Synthetic Aperture Radar (InSAR) can be used for measuring surface displacements by using the technique of Persistent Scatter Interferometry (PSI), which uses a large number of radar images and works as a time

series analysis for a number of fixed points in the terrain with stable phase behavior over time, such as rocks or buildings. As a result of these analyses, the vulnerabilities of buildings can be estimated for regional scale analysis. Additionally, stable GPS measurements can be surveyed for different time periods to model the movement on a local slope.

REFERENCES

Adams, J., 1980. Contemporary uplift and erosion of the Southern Alps, New Zealand: *Geological Society of America, Bulletin*, Vol. 91, No. 1, part 1, pp. 2–4 and part 2, pp. 1–114.

AGS, 2000. Landslide risk management concepts and guidelines, *Australian Geomechanics Society (AGS),* Sub-committee on landslide risk management.

Akgün, A. and Bulut, F., 2007. GIS-based landslide susceptibility for Arsin-Yomra (Trabzon, North Turkey) region. *Environ Geol*., Vol. 51, pp. 1377–1387.

Aleotti, P. and Chowdhury, R., 1999. Landslide hazard assessment: summary review and new perspectives. *Bull Eng Geol Env.,* Vol. 58, pp. 21–44.

Aleotti, P., 2004. A warning system for rainfall-induced shallow failures *Engineering Geology,* Vol. 73, pp. 247–265.

Alexander, E.D., 1989. Urban landslides. *Progress in Physical Geography*, Vol. 13, pp. 157–191.

Amadesi, E., Vianello, G., 1978. Nuova guida alla realizzazione di una carta di stabilita dei versanti. *Memorie Societa Geologica Italiana,* Vol. 19, pp. 53–60, in Italian.

Anagnosti. P. and Lesevic, Z., 1991, Probabilistic versus deterministic approach in hazard assessment of landslides along man made reservoirs. *Landslides,* Vol.2, pp. 1221-1227

Anbalagan, R., 1992, Landslide hazard evaluation and zonation mapping in mountainous terrain. *Engineering Geology*, Vol. 32, pp. 269– 277.

Anselin, L. 1995. Local Indicators of Spatial Association-; LISA. *Geographical Analysis*, Vol. 27, pp. 93-115.

Arcmap 9.1, 2009. Tutorial Document of ArcMap 9.1.

Ardizzone, F., Cardinali, M., Carrara, A., Guzzetti, F., Reichenbach, P., 2002. Uncertainty and errors in landslide mapping and landslide hazard assessment. *Natural Hazards and Earth System Science,* Vol. 2 (1–2), pp. 3 – 14.

Ardizzone, F., Cardinali, M., Galli, M., Guzzetti, F., Reichenbach, P., 2005. Validation of a landslide inventory map and of landslide risk assessments using event inventory maps. *Geophysical Research Abstracts*, Vol. 7, pp. 05198, 2005.

Atkinson, P.M., Massari, R., 1998. Generalized linear modelling of susceptibility to landsliding in the central Appennines, Italy. *Comput Geosci*, Vol. 24(4), pp. 373–385.

Ayalew, L., Yamagishi, H., Ugawa N., 2004. Landslide susceptibility mapping using GIS-based weighted linear combination, the case in Tsugawa area of Agano River, Niigata Prefecture. Japan. *Landslides*, Vol. 1, pp. 73–81.

Ayala-Carcedof, J., Cubillo-Nielsen, S., Alvarez, A., Dominguez, M.J., Lain, L., Lain, R. and Ortiz, G., 2003, Large Scale Rockfall Reach Susceptibility Maps in La Cabrera Sierra (Madrid) performed with GIS and Dynamic Analysis at 1:5,000. *Natural Hazard,* Vol. 30, pp. 325–340.

Ayalew, L., Yamagishi, H., Marui, H. and Kanno, T., 2005. Landslides in Sado Island of Japan: part II. GIS-based susceptibility mapping with comparisons of results from two methods and verifications. *Engineering Geology*, Vol. 81, pp. 432–445.

Ayalew, L. and Yamagishi, H., 2005. The application of GIS-based logistic regression for susceptibility mapping in the Kakuda-Yahiko Mountains Central Japan. *Geomorphology*, Vol. 65(1-2), pp. 15-31.

Ayenew, T. and Barbieri, G., 2005. Inventory of landslides and susceptibility mapping in the Dessie area, northern Ethiopia. *Engineering Geology*, Vol. 77, pp. 1– 15

Baeza, C.,1994. Evaluación de las condiciones de rotura y la movilidad de los deslizamientos superficiales mediante el uso de técnicas de análisis multivariante, Tesis Univ. Pol. Catalunya.

Baeza, C. and Corominas, J., 1996. Assessment of shallow landslide susceptibility by means of statistical techniques. *In: Proceedings of the Seventh International Symposium on Landslides*, pp 147–152

Baeza, C. and Corominas, J., 2001. Assessment of Shallow Landslide Susceptibility By Means of Multivariate Statistical Techniques. Earth Surface Processes and Landforms Earth Surf. Process. *Landforms*, Vol. 26, pp. 1251–1263.

Bailey, T.A.,1994. A review of statistical spatial analysis in geographical information systems. *In: Fotheringham S. and Rogerson P. (Editors) Spatial Analysis and GIS. Taylor & Francis*, *London*, pp. 13-44.

Barbat, A.H., 2003. Vulnerability and disaster risk indices from engineering perspective and holistic approach to consider hard and soft variables at urban level. Information and indicators program for disaster risk management. *Universidad Nacional de Colombia, Manizales, Colombia*, pp 19.

Barnard, P.L., Owen, L.A., Sharma, M.C. and Finkel, R.C., 2001. Natural and human-induced landsliding in the Garhwal Himalaya of Northern India. *Geomorphology,* Vol. 40, pp. 21–35.

Basheer, I. and Hajmeer M., 2000. Artificial neural networks: Fundamentals, computing, design, and applications. Journal of Microbiological Methods, Vol. 43, pp.3–31.

Bartından Haberler, 2009. http://site.mynet.com/bartin_kumluca/kumluca/id1.htm. Last accessed December 29, 2009.

Begueria, S. and Lorente, A. 1999. Hazard mapping by multivariate statistics: comparison of methods and case study in the Spanish Pyrenees. Debris fall assessment in mountain catchments for local end-users. *Instituto Pirenaico de Ecología, CSIC*, 202, 50080- Zaragoza, Spain.

Bell, R. and Glade T., 2004. Quantitative risk analysis for landslides – Examples from Bildudalur, NW-Iceland. *Natural Hazards and Earth System Sciences*, Vol. 4, pp. 117–131.

Bello, B.C., Hirth, F., Gould, A.P., 2003,. A pulse of the Drosophila Hox protein Abdominal-A schedules the end of neural proliferation via neuroblast apoptosis. *Neuron*, Vol. 37 (2), pp. 209-219.

Benda, L, Zhang, W., 1990. Accounting for the stochastic occurrences of landslides when predicting sediment yields. *Proc Fiji Symp, IAHS-AISH Publ*, Vol. 192, pp. 115-127.

Bernknopf, R.L., Cambell, R.H., Brookshire, D.S., Shapiro, C.D., 1988. A probabilistic approach to landslide hazard mapping in Cincinnati, Ohio, with applications for economic evaluation. *Bulletin of the International Association of Engineering Geology*, Vol. 25, pp. 39–56.

Berry, 1999. Use Statistics to Compare Map Surfaces, Beyond Mapping column. *GEOWorld*, October issue, pp. 23-24.

Bertolo, P. and Wieczorek, G. F., 2005. Calibration of numerical models for small debris flows in Yosemite Valley, California. *USA.Natural Hazards and Erath System Sciences*, Vol. 5, pp. 993-1001.

Bianchi F., Catani F., 2002. Landscape dynamics risk management in Northern Apennines (Italy). In: Brebbia CA, Zannetti P (eds) Development and application of computer techniques to environmental studies. *WIT*, Southampton, UK, Vol. 1, pp. 319–328.

Binaghi, E., Boschetti, M., Brivio, P.A., Gallo, I., Pergalani, F., Rampini, A., 2004. Prediction of displacements in unstable areas using a neural model. Nat Hazards, Vol. 32, pp. 135–154.

Bowerman B.L., O'Connell, R.T., 1993. Inc. ISBN 0-534-93251-7, 1993

Blake, T.F., Hollingsworth, R.A., Stewart, J.P., D'Antonio, R., Earnest, J., Gharib, F., Horsman L., Hsu, D., Kupferman, S., Masuda, R., Pradel, D., Real, C., Reeder, W., Sathialingam, N., Simantob, E., 2002. Recommended procedures for implementation of DMG special publication 117 guidelines for analyzing and mitigating landslide hazards in California. *Southern California Earthquake Center*, Los Angeles, California, pp. 110.

Blanc, R.P., Cleveland, G.B., 1968. Natural slope stability as related to geology, San Clemente Area, Orange and San Diego Counties, California. *California Division of Mines and Geology Special Report,* Vol. 98, pp. 19.

Bonham-Carter, G.F., 1994. Geographic Information Systems for geoscientists: modelling with GIS. Ottawa: Pergamon.

Borga, M., Dalla Fontana, G., Da Ros, D. and Marchi, L.,1998. Shallow landslide hazard assessment using a physically based model and digital elevation data, *Environmental Geology*, Vol. 35, pp. 81–88.

Boverman, and O'Connell, 1993. Forecasting and Time Series: An Applied Approach, Wadsworth

Brabb, E.E., Pampeyan, E.H., Bonilla, M.G.,1972. Landslide susceptibility in San Mateo County, California. Misc Field Studies Map MF360. *US Geological Survey*, Reston, Va.

Brabb, E.E., 1976. The Landslide Hazard in the San Francisco Bay Region. *Water, Air, and Soil Pollution*, Vol. 7, pp. 23 7-238.

Brabb, E.E., 1984. Innovative approaches to landslide hazard and risk mapping. Proc., Fourth International Symposium on Landslides. *Canadian Geotechnical Society*, Toronto, Canada, Vol. 1, pp. 307–324.

Brand, E.W., Premchitt, J., Phillipson, H.B., 1984. Relationship between rainfall and landslides. *Proc. 4th International Symposium on Landslides*, Toronto, BiTech Publishers, Vancouver, Canada, Vol. 1, pp. 377– 384.

Brand, E.W., 1988. Special lecture: landslide risk assessment in Hong Kong. *In Proceedings of 5th International Symposium on Landslides*, Rotterdam: Balkema, pp.1059–74.

Bruce, R.H. and Clark, 1966. Introduction to Hydrometeorology, *Pergamon Press*, pp.320.

Brunsdon, C., Fotheringham, A.S., Charlton, M., 1998. Spatial nonstationarity and autoregressive models. *Environment and Planning*, Vol. 30, pp. 957–973.

Caine N., 1980. The rainfall intensity-duration control of shallow landslides and debris flows. *Geogr. Ann.*, Vol. 62 A, pp. 23-27.

Campbell, R.H. and Bernknopf, R.L., 1993. Time-dependent landslide probability mapping: American Society of Civil Engineers, *Proceedings of the 1993 Conference*, *Hydraulic Engineering* '93; San Francisco, pp. 1902-1907.

Can, T., Nefeslioglu, H.A., Gökçeoğlu, C., Sönmez H., Duman T.Y., 2005. Susceptibility assessments of shallow earth flows triggered by heavy rainfall at three catchments by logistic regression analyses. *Geomorphology* , Vol. 72, pp. 250–271.

Cancelli, A., Nova, R.,1985. Landslides in soil debris cover triggered by rainstorms in Valtellina (central Alps, Italy) In: Sassa K (ed) Proceedings of 4th International Conference on Landslides, Tokyo, *The Japanese Landslide Soc*, Tokyo, pp. 267–272.

Cannon, S.,H.,, Ellen, S.D,. 1988. Rainfall that resulted in abundant debris-flow activity during the storm. In Landslides, Floods, and Marine Effects of the Storm of January 3–5, 1982, in the San Francisco Bay Region, California, Ellen SD, Wieczorek GF (eds). *US Geological Survey Professional Paper* Vol. 1434, pp. 27–34.

Capecchi, F., Focardi, P., 1988. Rainfall and landslides: research into a critical precipitation coefficient in an area of Italy. In: *Proceedings of the V International Symposium on Landslides*, Lausanne, July Vol. 10–15, pp. 1131–1136.

Cardinali, M., Carrara, A., Guzzetti, F., Reichenbach, P., 2002a. Landslide hazard map for the Upper Tiber River basin. *CNR GNDCI,* Publication No. 2116, map at 1: 100,000 scale.

Cardinali M., Reichenbach P., Guzzetti F., Adrizzone F., Antonini G., Galli M., Cacciano M., Castellani M. and Salvati P., 2002b. A geomorphological approach to estimate landslide hazards and risk in urban and rural areas in Umbria, Central Italy. *Natural Hazards and Earth System Sciences*, Vol. 2, pp. 57-72.

Cardinali, M., Galli, M., Guzzetti, F., Ardizzone, F., Reichenbach P. and Bartoccini P.,2006. Rainfall induced landslides in December 2004 in South-Western Umbria, Central Italy, *Natural Hazards and Earth System Sciences*, Vol. 6, pp. 237–260.

Carmassi, F., Liberati, G., Ricciardi, C., Sciotti, M., 1992. Stability evaluation for unified power plant siting in geothermal areas. *In: Proc VI Int Symp on Landslides*, Christchurch.

Carrara, A., Merenda, L., 1976. Landslide inventory in northern Calabria, southern Italy. *Geol Soc Am Bull*, Vol. 87, Vol. 1153–1162.

Carrara, A., Catalano, E., Sorriso-Valvo, M., Reali, C., Ossi, I., 1978. Digital Terrain Analysis for land evaluation. *Geologia Applicata e Idrogeologia*, Vol. 13, pp. 69–127.

Carrara A, 1983. Multivariate methods for landslide hazard evaluation. *Mathematical Geol*, Vol. 15, pp. 403–426

Carrara, A., 1988. Drainage and divide networks derived from high-fidelity digital terrain models. In: C.F. Chung et al. (eds.), Quantitative analysis of mineral and energy resources, *NATO-ASI Series*, pp. 581-597, D.Reidel Pub. Co., Dordrecht.

Carrara, A. et al., 1989. Landslide hazard mapping by statistical methods: a ‘‘black-box’’ model approach. In: Siccardi, F., Brass, R. Eds. , *International Workshop on Natural Disasters in European–Mediterranean Countries*, Perugia, CNR-US NFS, pp. 427–445.

Carrara, A., Cardinali, M., Detti, R., Guzzetti, F., Pasqui, V. and Reichenbach, P., 1990. Geographical information systems and multivariate models in landslide hazard evaluation. In: A. Cancelli, Editor, *Proceedings of the 6th International Conference and Field Workshop on Landslides: Alps'90, Milan*, pp. 17–28.

Carrara, A., Cardinali, M., Detti, R., Guzzetti, F., Pasqui, V., Reichenbach, P., 1991. GIS Techniques and statistical models in evaluating landslide hazard. *Earth Surface Processes and Landform,* Vol. 16, pp. 427–445.

Carrara, A., Cardinali, M., Guzzetti, F., 1992. Uncertainty in assessing landslide hazard and risk. *ITC Journal* Vol. 2, pp. 172– 183.

Carrara, A., Cardinali, M., Guzzetti, F., Reichenbach, P., 1995. GIS technology in mapping landslide hazard. In: Carrara A, Guzzetti F (eds) Geographical information systems in assessing natural hazards, advances in natural and technological hazards research. *Kluwer Academic Publishers*, Dordrecht, The Netherlands, pp.135–176.

Carrara, A., Guzzetti, F., Cardinali, M. and Reichenbach, P., 1999. Use of GIS Technology in the Prediction and Monitoring of Landslide Hazard. *Natural Hazards*, Vol. 20, pp. 117–135.

Carrara, A., Cardinali, A., Guzzetti, F., Reichenbach, P., 2001. GIS-based techniques for mapping landslide hazard. *Research Centre for Informatics and Telecommunication Systems*, National Research Council.

Carrara, A., Crosta, G. and Frattini, P., 2003. Geomorphological and historical data in assessing landslide hazard, *Earth Surface Processes and Landforms*, Vol. 28, pp. 1125–1142.

Carrasco, R.M., Pedraza, J., Martin-Duque, J.F., Matter, M., Sanz, M.A. and Bodoque, J.M., 2003. Hazard Zoning for Landslides Connected to Torrential Floods in the Jerte Valley (Spain) by using GIS Techniques Natural Hazards Vol.30, pp.361–381, 2003.

Cascini, L. and Versace, P., 1988. Relationship between rainfall and landslide in a gnesis cover. *Proc. 5th Int. Symp. On Landslides*, Vol. 1, pp. 565-570.

Cascini, L., Bonnard, Ch., Corominas, J., Jibson, R., Montero-Olarte, J., 2005. Landslide hazard and risk zoning for urban planning and development. Landslide Risk Management-Hungry, Fell, *Couture and Eberhardt(eds)*, *Taylor &Francis Group, London*, ISBN 04 1538 043 X.

Castellanos, A.E.A., 2008. Multi-scale landslide risk assessment in Cuba. *University of Utrecht Phd Thesis. ITC .Printing Department.*

Catani, F., Casagli, N., Ermini, L., Righini, G., Menduni, G., 2005. Landslide hazard and riskmapping at catchment scale in the Arno River basin, *Landslides,* Vol. 2, pp. 329–342

Chacon, J., Irigaray, C., Fernandez, T., El Hamdouni, R., 2006. Engineering geology maps: landslides and geographical information systems, *Bull Eng Geol Environ,* Vol. 6, pp. 341–411.

Chen, Z. and Wang, J., 2006. Landslide hazard mapping using logistic regression model in Mackenzie Valley, Canada. *Nat Hazards*. DOI 10.1007/s11069-006-9061-6.

Chen, Z. and Wang, J., 2007. Landslide hazard mapping using logistic regression model in Mackenzie Valley, Canada. *Nat Hazards,* Vol. 42, pp: 75-89.

Chinnayakanahalli, K., Tarboton, D.G., and Pack, R.T., 2002. An Objective Method for the Intercomparison of Terrain Stability Models. *Eos Trans. AGU 84 (47) Fall Meet.Suppl., Abstract H31C-0480*.

Chowdhury R.N. and Flentje, P.N., 2002. Uncertainties in rainfall- induced landslide hazard. *Quarterly Journal of Engineering Geology and Hydrogeology*, Vol.35, pp. 61-70.

Chowdhury R.N., 1984. Recent developments in landslide studies: probabilistic methods – state-of-art-report. *In: Proc of the IV Int Symp on Landslides*, Toronto, Vol. 1, pp. 209–228.

Chung, C. F. and Fabbri, A. G.: 1993. The representation of geoscience information for data integration. *Nonrenewable Resources*, Vol. 2(2), pp. 122–139.

Chung, C.F., Fabbri, A.G. and Van Westen, C.J., 1995. Multivariate regression analysis for landslide hazard zonation. In: A. Carrara and F. Guzetti, Editors, *Geographical Information Systems in Assessing Natural Hazards*, Kluwer, Dordrecht, pp. 107–133.

Chung, C.J.F., and Fabbri, A.G., 1999. Probabilistic Models for landslide Hazard Mapping. *Photogrammetric Engineering & Remote Sensing*, Vol. 65, pp.1389-1399.

Chung, C.J.F. and Fabbri, A., 2003. Validation of spatial prediction models for landslide hazard mapping. *Natural Hazards*, Vol. 30, pp. 451–472.

Chung, C.J.F. and Fabbri A., 2005. Systematic procedures of landslide-hazard mapping for risk assessment using spatial prediction models. In: T. Glade, M.G. Anderson and M.J. Crozier, Editors, *Landslide Hazard and Risk, John Wiley & Sons*, New York, pp. 139–174.

Clerici, A., Perego, S., Tellini, C., and Vescovi, P., 2002. A procedure for landslide susceptibility 10 zonation by the conditional analysis method. *Geomorphology*, Vol. 48, pp. 349–364.

COE, 1997. Technical engineering and design Guide, No:19

Coe, J.A., Michael, J.A., Crovelli, R.A., Savage, W.Z., 2000. Preliminary map showing landslide densities, mean recurrence intervals, and exceedance probabilities as determined from historic records, Seattle, Washington. *US Geological Survey Open-File Report 00-303*.

Comaniciu, D. and Meer, P., 2002. Mean shift: A robust approach toward feature space analysis. *IEEE Trans. Pattern Anal. Machine Intell*., Vol. 24, pp. 603–619.

Copons, R. and Vilaplana, J. M. 2008. Rockfall susceptibility zoning at a large scale: From geomorphological inventory to preliminary land use planning. *Engineering Geology*, Vol. 102 (3-4), pp. 142-151.

Corominas J. and Moya J., 1999. Reconstructing recent landslide activity in relation to rainfall in the Llobregat River basin, Eastern Pyrenees, Spain. Geomorphology, Vol. 30 (1-2), pp. 79-93.

Corominas, J., 2000. Landslides and climate. In: Bromhead E, Dixon N, Ibsen ML (eds). *Keynote lecture of Proceedings of the 8th International Symposium on Landslides*, A.A. Balkema, Cardiff, Wales, Vol. 4, pp. 1–33.

Corsini, A., Pasuto, A. and Soldati, M., 2000. Landslides and climate change in the Alps since the Late-glacial: evidence of case studies in the Dolomites (Italy). In: E. Bromhead, N. Nixon and M.-L. Ibsen, Editors, *Landslides in Research, Theory and Practice, Thomas Telford Publishing*, London, pp. 329–334.

Corominas, J., Copons, R., Vilaplana, J. M., Altimir, J., Amigo, J., 2003. Integrated landslide susceptibility analysis and hazard assesment in the Principality of Andorra. *Natural Hazards*, Vol. 30, pp. 421-435.

Corominas, J., Ayala, F.J., Cendrero, A., Chacón, J., Díaz de Terán, J.R., Gonzáles, A., Moja, J., Vilaplana, J.M., 2005. Impacts on natural hazard of climatic origin. In: ECCE Final Report: A Preliminary Assessment of the Impacts in Spain due to the Effects of Climate Change. Ministerio de Medio Ambiente.

Cotecchia, V., 1978. Systematic reconnaissance mapping and registration of slope movements. *Bulletin International Association Engineering Geology*, Vol. 17, pp.5–37.

Crosta, G., 1998. Regionalization of rainfall thresholds: an aid to landslide hazard evaluation. *Environmental Geology,* Vol.35 (2–3), pp. 131–145.

Crosta, G.B., 2004. Introduction to the special issue on rainfall-triggered landslides and debris flows. *Engineering Geology*, Vol. 73, pp. 191–192.

Crovelli, R.A., 2000. Analytic resource assessment method for continuous (unconventional) oil and gas accumulations—the “ACCESS” method, US Geological Survey Open-File Report, No: 00-044, pp.34.

Crozier, M.J. and Eyles, R.J., 1980. Assessing the probability of rapid mass movement. In The New Zealand Institution of Engineers—Proceedings of Technical Groups (ed.), Proc. Third Australia–New Zealand Conference on Geomechanics, Wellington, pp. 2.47–2.51.

Crozier, M.J. 1986: Landslides: causes, consequences and environment. London: Croom Helm.

Crozier, M.J. and Glade, T., 1999. Frequency and magnitude of landsliding: fundamental research issues. Zeitschrift für Geomorphologie N.F. Vol. 15, pp. 141–155.

Cruden, D. M., 1997. Estimating the risks from landslides using historical data. In: D. M. Cruden, and R. Fell (eds.), Landslide risk assessment. Balkema Publisher, Rotterdam, pp. 177–184.

Cruden D.M. and Fell R., 1997. Landslide Risk Assessment. *Proceedings International Workshop on Landslide Risk Assessment, Honolulu*, Balkema, Rotterdam, pp.371.

Çan, T., Nefeslioglu, H.A., Gökçeoglu, C., Sönmez, H. and Duman, T.Y., 2005. Susceptibility assessments of shallow earthflows triggered by heavy rainfall at three subcatchments by logistic regression analyses. *Geomorphology*, Vol. 72(1-4), pp. 250-271.

Dai, F.C., Lee, C.F., Zhang, X.H., 2001. GIS-based geo-environmental evaluation for urban land-use planning: a case study. *Engineering Geology*, Vol. 61 (4), pp. 257–271.

Dai, F.C. and Lee, C.F., 2001. Terrain-based mapping of landslide susceptibility using a geographical information system: a case Study. *Can. Geotech. J.,* Vol. 38, pp. 911–923

Dai, F.C., Lee, C.F., Ngai, Y.Y., 2002. Landslide risk assessment and management: an overview, *Engineering Geology,* Vol.64, pp. 65–87.

Dai, F.C. and Lee, C.F., 2002. Landslide characteristics and slope instability modeling using GIS, Lantau Island, Hong Kong. *Geomorphology*, Vol. 42, pp. 213-228.

Dai, F.C, Lee, C.F., 2003. A spatiotemporal probabilistic modelling of storm-induced shallow landsliding using aerial photographs and logistic regression. *Earth Surface Processes and Landforms*, Vol. 28 (5), pp. 527–545.

David, M., Dagbert, M, Beaucheimin, Y. 1977. Statistical analysis in geology: Correspondence analysis method. *Quarterly Journal of the Colorado School of Mines*, Vol. 72, pp. 1–45.

D'Ecclesiis, G., Grassi, D., Merenda, L., Polemio, M. and Sdao, F., 1991. Evoluzione geomorfologica di un'area suburbana di Castronuovo S. Andrea (PZ) ed incidenza delle piogge su alcuni movimenti di massa. *Geol. Appl. Idrogeol. XXVI*, pp. 141–163.

Degraff, J. V. and Romersburg, H. C., 1980. Regional landslide-susceptibility for wildland management: A matrix approach*, in Coates and Vitek (eds.),* pp. 410–414.

Demek, J., 1972. Manual of Detailed geomorphologic mapping, Academia, Prague.

Demek, J. and Embleton, C., 1978. Guide to medium-scale geomorphological mapping, IGU Commission on Geomorphological Survey and Mapping. *E. Schweizerbart'sche Verlagsbuchhandlung, Stuttgart, Germany*, pp. 348.

Derbyshire, E., 2001. Geological hazards in loess terrain, with particular reference to the loess regions of China, *Earth-Science Reviews*, Vol. 54, pp. 231–260.

Deveciler, E., 1986. Alapli–Bartin–Cide (B. Karadeniz) jeoloji raporu (in Turkish). MTA yayinlari, Derleme no. 7938, pp. 58.

Dhakal, A.S., Amada, T., Aniya, M., 1999. Landslide hazard mapping and the application of GIS in the Kulekhani watershed, Nepal. *Mountain Research and Development,* Vol. 19, pp. 3–16.

Dikau, R. and Schrott, L., 1999. The temporal stability and activity of landslides in Europe with respect to climatic change (TESLEC): main objectives and results. *Geomorphology,* Vol. 30, pp. 1–12.

Dillon, W.R., Goldstein, M., 1986. Multivariate Analysis. *Methods and Applications. John Wiley:* Chichester, pp. 324-425.

Dixon, N. and Ibsen, M.L., 2000. Editors, Landslide in Research, Theory and Practice vol. 3, Thomas Telford, London (2000), pp. 961–968.

Dobson, A. J. (1990) An Introduction to Generalised Linear Models*. Chapman and Hall, London,* pp. 192

Donati, L., Turrini, M.C., 2002. An objective method to rank the importance of the factors redisposing to landslides with the GIS methodology: application to an

area of the Apennines (Valnerina; Perugia, Italy). Engineering Geology, Vol. 63, pp. 277– 289.

Dubin, R.A., 1992. Spatial Autocorrelation and Neighborhood Quality. Reg. Sci. Urban Econ., Vol. 22, pp. 433–452.

Duman, T. Y., Emre, O., Can, T., Ates, S., Kecer, M., Erkal, T., Durmaz, S., Dogan, A., Corekcioglu, E., Goktepe, A., Cicioglu, E., and Karakaya, F., 2001. Turkish Landslide Inventory Mapping Project: Methodology and results on Zonguldak quadrangle (1/500000), *Working in progress 25 on the Geology of Turkey and its surroundings, In: Abstract Book of the 4th Int. Turkish Geology Symp*., Vol. 24–28, pp. 392, 2001.

Duman, T.Y., Can, T., Emre, Ö., Kecer, M. , Doğan, A., Ateş, S., Durmaz, S., 2005a. Landslide inventory of northwestern Anatolia, Turkey, *Engineering Geology*, Vol. 77, pp. 99– 114.

Duman, T. Y., Can, T., Gökçeoğlu, C., and Nefeslioglu, H.A., 2005b. Landslide susceptibility mapping of Cekmece area (Istanbul, Turkey) by conditional probability. *Hydrol. Earth Syst. Sci. Discuss*., Vol. 2, pp. 155–208.

Duman, T.Y., Can, T., Gökçeoğlu, C., Nefeslioglu, H.A., Sönmez, H., 2006. Application of logistic regression for landslide susceptibility zoning of Cekmece Area, Istanbul, Turkey. *Environmental Geology*, Vol. 51, pp. 241-256.

Düzgün, H.S.B. and Lacasse, S., 2005. Vulnerability and Acceptable Risk in Integrated Risk Assessment Framework, *Proc. of International Conference on Landslide Risk Management and 18th Vancouver Geotechnical Society Symposium*, May 31 - June 4, Vancouver, Canada.

Düzgün, H.S.B.and Karpuz, C., 2006, GIS-Based Landslide Risk Assessment for Bandirma Harbor Evaluacion de RiesgoDeslizamiento Basado en SIG para el Puerto de Bandirma.

Düzgün, H. S. B. and Özdemir, A., 2006. Landslide risk assessment and management by decision analytical procedure for Dereköy, Konya, Turkey. *Nat Hazards,* Vol. 39, pp. 245–263.

Düzgün, H.S.B. and Grimstad, S., 2007. Reliability-based stability analysis and risk assessment for rock slides in Ramnefjell. *Proc. Of Applications and Statistics and Probability in Civil Engineering*, ICASP10, Tokyo, Japan, pp. 189-198.

Düzgün H.S.B., 2008. A Quantitative Risk Assessment Framework for Rock Slides. *Proc. Of 42nd US Rock Mechanics Symposium*, June 29-July 2. San Francisco, USA.

Düzgün, H.S.B., 2008. A Quantitative Risk Assessment Framework for Rock Slides. *The 42nd US Rock Mechanics Symposium and 2nd U.S. Canada Rock Mechanics Symposium, San Francisco*, June 29-July 2, 2008. ARMA, pp. 08-279.

Düzgün, H.S.B. and Bhasin, R.K. 2009."Probabilistic Stability Evaluation of Oppstadhornet Rock Slope Norway". Rock Mechanics and Rock Engineering, Vol. , pp.

Düzgün, H.S.B., 2009. Rock Slide Risk Assessment: A semiquantitative Approach, *Geophisical Research Abstracts*, Vol. 11, EGU 2009-0.

Eastman, R., 1999. Multi-criteria evaluation and GIS. Chap.35 In:Longley PA, Goodchild MF, Maguire DJ, Rhind DW (eds) *Geographical information systems*, Wiley, New York, pp 493–502.

Einstein, H.H.,1988. Special lecture: Landslide risk assessment procedure, *Proc. 5th Int. Symp. on Landslides, Lausanne*, Switzerland, 2: 1075-1090.

Emami, S.M.R., Iwao, Y., Harada, T., 1998. Performance of Artificial Network system in prediction issues of earthquake engineering. Proc. of 8th Int. IAEG Congress, pp. 733– 738. *Eng. Geol*., Vol. 71, pp. 303–321.

Ercanoğlu, M., Gökçeoğlu, C., 2002. Assessment of landslide susceptibility for a landslide-prone area (North of Yenice, NW Turkey) by fuzzy approach. *Environmental Geology,* Vol. 41, pp. 720– 730.

Ercanoğlu, M., Gökçeoğlu, C. and Van Asch Th.,W.J., 2004. Landslide susceptibility zoning north of Yenice (NW Turkey) by multivariate statistical techniques, *Natural Hazards*, Vol. 32, pp. 1–23.

Ercanoğlu, M. and Gökçeoğlu, C., 2004. Use of fuzzy relations to produce landslide susceptibility map of a landslide prone area (West Black Sea Region, Turkey), *Engineering Geology,* Vol. 75, pp. 229–250.

Ercanoğlu, M., 2005. Landslide susceptibility assessment of SE Bartin (West Black Sea region, Turkey) by artificial neural networks. *Nat Hazards Earth Syst Sci*. Vol. 5, pp. 979–992.

Ercanoğlu, M., 2003. Bulanık mantik ve istatistiksel yöntemlerle heyelan duyarlılık haritalarının üretilmesi: Bati Karadeniz Bölgesi (Kumluca Guneyi-Yenice Kuzeyi). *H.U. Fen Bil. Enst. Doktora Tezi*, Ankara, pp. 202 (in Turkish).

Erener, A. and Düzgün, H.S.B., 2006. Comparison of Statistical Landslide Hazard Assessment Methods at Regional Scale. *International Disaster Reduction Conference (IDRC), Davos, Switzerland*, Vol: 3, pp.164.

Erener, A. and Lacasse, S., 2007. Landslide Susceptibility Mapping Using GIS, *28th Asian Conference on Remote Sensing ACRS2007*, Kuala Lumpur, Malesia, 12 – 16 November.

Erener, A., Lacasse, S., Kaynia, A. M., 2007. Hazard Mapping in quick clay area using GIS, Joint CIG / ISPRS Conference. Geomatics for Disaster and Risk Management, Toronto, Canada Assessment Framework. *Proc. of International Conference on Landslide Risk Management*.

Erener, A. and Düzgün, H.S.B., 2008. Analysis of Landslide Hazard Mapping Methods: Regression Models Versus Weight Rating. *XXIst ISPRS Congress* 3-11 July. Beijing, China. Commission VIII papers, Vol. 37, Part B8,ISSN 1682-1750.

Erener, A. and Düzgün, H.S.B., 2009. Prediction of Population in Urban Areas by Using High Resolution Satellite Images. *4th international conferance on Recent Advances in Space Technologies (RAST 2009).* Space for the Developing World. 11-13 June 2009, İstanbul, Turkey.

Ermini, L., Catani, F., Casagli, N., 2005. Artificial neural networks applied to landslide susceptibility assessment. *Geomorphology*, Vol. 66, pp.327–343

Evans, N.C., Huang, S.W., King, J.P., 1997. The natural terrain landslide study phases I and II. Special Project Report, SPR 5/97. *Planning Division, Geotechnical Engineering Office, Civil Engineering Department, Hong Kong*, pp.119.

Evans, N.C. and King, J.P., 1998. Natural Terrain Landslide Study Debris Avalanches Susceptibility. Technical Note TN 1/98, *Geotechnical Engineering Office*, Hong Kong, pp. 96.

Faber, M.H. and Stewart, M.G., 2003. Risk assessment for civil engineering facilities: critical overview and discussion. *Reliability Engineering and System Safety*, Vol. 80, pp. 173–184.

Fall, M. and Azzam, R., 2001. An example of multi-disciplinary approach to landslide assessment in coastal area. International conference on landslide. *Proceedings International Conference on Landslides: Causes Impacts and Countermeasures*, Davos, Switzerland.

Fall, M., Azzam, R., Noubactep, C., 2006. A multi-method approach to study the stability of natural slopes and landslide susceptibility mapping. *Engineering Geology,* Vol. 82, pp. 241– 263.

Fannin, R.J. and Wise, M.P., 2001. An empirical-statistical model for debris flow travel distance. *Canadian Geotechnical Journal*, Vol.38, No.5, pp.982-994.

Fell, R., Chapman, T.G. and Maguire, P.K., 1991. A model for prediction of piezometric levels in landslides. In: R.J. Chandler, Editor, *Slope Stability Engineering*, Thomas Telford, London, pp. 73–82.

Fell, R. 1994: Landslide risk assessment and acceptable risk. *Canadian Geotechnical Journal,* Vol. 31, pp. 261-272.

Fell, R. and Hartford, D., 1997. Landslide risk management, in: Landslide risk assessment, *Proceedings of the Workshop on Landslide Risk Assessment, Honolulu, Hawaii*, USA, 19–21 February, edited by: Cruden, D. M. and Fell, R., A. A. Balkema, Rotterdam, 51–109.

Fell, R., Ho K.K.S., Lacasse, S., Leroi, E., 2005. A framework for landslide risk assessment and management. *Taylor &Francis Group, London*, ISBN 04 1538 043 X.

Fenti, V., Silvano, S., Spagna, V., 1979. Methodological proposal for an engineering geomorphological map. Forecasting rockfalls in the Alps. *Bull of the Int Assoc Eng Geol* Vol. 19, pp. 134–138.

Fernández, T., Irigaray, C., El Hamdouni, R., Chacón, J., 2003. Methodology for landslide susceptibility mapping by means of a GIS. Application to the contraviesa area (Granada, Spain), *Nat Hazards,* Vol. 30(3), pp. 297–308.

Fiener, Y.A.O., Haji, A.F., 1999. Application of hazard and risk maps for highway slopes management and maintenance. In: Yagi, N., Yamagami, T., Jiang, J.C. (Eds.), *Slope Stability Engineering*, Vol. 2. Balkema, Rotterdam, pp. 1287–1290.

Finlay, P.J., 1996. The risk assessment of slopes. *PhD Thesis*, School of Civil Engineering, University of New South Wales.

Finlay, P.J., Mostyn, G.R. and Fell, R., 1999. Landslide risk assessment: prediction of travel distance, *Can. Geotech. J.*, Vol. 36, pp. 556–562.

Flentje, P.N., Chowdhury, R.N. 1999. Quantitative landslide hazard assessment in an urban area. *In: Proc of 8th Australia –New Zealand Conf*

Foster, D.R., Knight, D.H. and Franklin, J.F., 1998. Landscape patterns and legacies resulting from large, infrequent disturbances. *Ecosystems*, Vol. 1, pp. 497-510.

Fotheringham, A.S., Charlton, M., Brunsdo, C., 1996. The geography of parameter space: An investigation of spatial nonstationarity. *International Journal of Geographical Information Systems,* Vol.10(5), pp.605–627.

Fotheringham, A.S.,1997. Trends in quantitative methods I: stressing the local. Progress in Human Geography, Vol.21, Vol.88- 96.

Fotheringham, A.S., Brunsdon, C. and Charlton, M., 2000. Quantitative Geography Perspectives on Spatial Data Analysis, *Sage publications*, pp. 15- 46.

Fourniadis, I.G., Liu, J.G., Mason, P.J., 2007. Landslide hazard assessment in the Three Gorges area, China, using ASTER imagery: Wushan–Badong. Geomorphology Vol.84, pp. 126–144

Fourniadis, I.G., Liu, J.G., Mason, P.J., 2007. Landslide hazard assessment in the Three Gorges area, China, using ASTER imagery: Wushan–Badong. Geomorphology 84 (2007) 126–144

Gamerman, D. and Moreira, A.R.B., 2004. Multivariate Spatial Regression Models, Journal of Multivariate Analysis,Vol. 91, pp. 262-281.

Garcia, R., Rodríguez, J.J., and O'Brien, J. S., 2004. Hazard Zone Delineation for Urbanized Alluvial Fans. ASCE publications. pp. 1-10, (doi10.1061/40737(2004)11)

Gens, A., Hutchison, J. N., and Cavounidis, S., (1988). Three-dimensional analysis of slices in cohesive soils, *Geotechnique,* Vol.38, pp. 1–23.

George, D. and Mallery, P., 2000. SPSS for Windows step-bystep: a simple guide and reference (2nd ed.) Boston: Allyn and Bacon

Glade, T., 1998. Establishing the frequency and magnitude of landslide-triggering rainstorm events in New Zealand. *Environmental Geology* Vol. 35, pp.2–3.

Glade, T., 2000. Modelling landslide-triggering rainfalls in different regions of New Zealand—the soil water status model. Zeitschrift für Geomorphologie N.E.Vol. 122, pp. 63–84

Glade, T. Crozier M. and Smith, P., 2000. Applying probability determination to refine landslide-triggering rainfall threshold using an empirical Antecedent Daily Rainfall Model, *Pure and Applied Geophysics* Vol.157, pp. 1059–1079.

Glade, T., 2003. Landslide occurrence as a response to land use change: a review of evidence from New Zealand, Catena Vol. 51, pp. 297–314.

Glade, T., Dikau, R. and Bell, R., 2003. National Landslıde Susceptibility Map For Germany. *Geophysical Research Abstracts*, Vol. 5, pp.12692, 2003

Glassey, P., Barrell, B., Forsyth, J., Macleod, R., 2003. The geology of Dunedin, New Zealand, and the management of geological hazards. Quaternary Int Vol.103(1), pp.23–40

Gomez, H, Kavzoglu, T., 2005. Assessment of shallow landslide susceptibility using artificial neural networks in Jabanosa River basin, Venezuela. Eng Geol Vol.78, pp.11–27

Gopalan, H., Whiteaker, T. and Maidment, D., 2002. Determining Watershed Parameters Using Arc Hydro (2002). web http://gis.esri.com/library/userconf/proc03/p0805.pdf last revisited at 24.11.2008

Gorsevski, P.V., Gessler P.E., Foltz R.B., Elliot W.J., 2006. Spatial prediction of landslide hazard using logistic regression and ROC analysis. Trans GIS Vol.10(3), pp.395–415

Gorsevski, P.V., Gessler, P., Foltz, R.B., 2000. Spatial prediction of landslide hazard using logistic regression and GIS. 4th Int. Conference on Integrating GIS and Environmental Modelling, Alberta, Canada., pp.9

Gökçeoğlu, C. and Aksoy, H., 1996, Landslide susceptibility mapping of the slopes in the residual soils of the Mengen region (Turkey) by deterministic stability analyses and image processing techniques. *Engineering Geology*, Vol.44, pp.147-161.

Gökçeoğlu, C., Sönmez, H. and Ercanoğlu, M. 2000: Discontinuity controlled probabilistic slope failure risk maps of the Altindag (settlement) region in Turkey. Engineering Geology Vol.55, pp.277–96.

Gökçeoğlu, C., Sönmez, H., Nefeslioglu, H. A., Duman, T.Y. , Can, T., 2005. The 17 March 2005 Kuzulu landslide (Sivas, Turkey) and landslide-susceptibility map of its near vicinity. Engineering Geology Vol.81, pp. 65–83

Greco R., Sorriso-Valvo M., Catalano E, 2007. Logistic Regression analysis in the evaluation of mass movements susceptibility: The Aspromonte case study, Calabria, Italy. Engineering Geology Vol.89 (2007) pp.47–66

Gritzner, M.L., Marcus, W.A., Aspinall, R., Custer, S.G., 2001. Assessing landslide potential using GIS, soil wetness modeling and topographic attributes, Payette River, Idaho. Geomorphology Vol.37, pp.149–165.

Grunert, J. and Hardenbicker, U., 1997. The frequency of landsliding in the north Rhine area and possible climatic implications. In: Matthews, J.A., Brunsden, D., Frenzel, B., Gläser, B. and Weiß, M.M., Editors, 1997. Rapid Mass Movement as a Source of Climatic Evidence for the Holocene Palaeoclimate Research vol. 19, Gustav Fischer, Stuttgart, pp. 17–31.

Gupta, R.P., Joshi, B.C., 1990. Landslide hazard zoning using the GIS approach—a case study from the Ramganga catchment, Himalayas. Engineering Geology Vol. 28, pp.119–131.

Guzzetti, F., Cardinali, M. and Reichenbach, P. 1994: The AVI Project: a bibliographical and archive inventory of landslides and floods in Italy. Environmental Management Vol. 18, pp.623–33.

Guzzetti, F., Carrara, A., Cardinali, M., Peichenbach, P.,1999. Landslide hazard evaluation: a review of current techniques and their application in a multi-scale study, Central Italy. *Geomorphology* Vol.31, pp.181–216

Guzzetti, F., Cardinali, M., Reichenbach, P., Carrara, A., 2000. Comparing landslide maps: a case study in the Upper Tiber River Basin, Central Italy. Environmental Management Vol.25, pp.247– 263.

Guzzetti, F., Reichenbach, P., Cardinali, M., Galli, M, Ardizzone, F., 2005. Landslide hazard assessment in the Staffora basin, northern Italian Apennines. *Geomorphology*, Vol.72, pp.272–299.

Guzetti, F., Reichenbach, P. Ardizzone, F. Cardinali M. and Galli, M. 2006. Estimating the quality of landslide susceptibility models, Geomorphology Vol.81, pp. 166–184.

Guzetti, F., Peruccacci, S., Rossi, M., and Stark, C. P., 2007. Rainfall thresholds for the initiation of landslides in central and southern Europe, Meteorol. Atmos. Phys., Vol.98, pp.239–267, 2007.

Gömez, H. and Kavzoğlu, T., 2005. Assessment of Shallow Landslide Susceptibility Using Artificial Neural Networks in Jabonosa River Basin, Venezuela, *Engineering Geology*, Vol.78, pp.11-27 (2005).

Haneberg,W.C., 1991. Pore pressure diffusion and the hydrologic response of nearly saturated, thin landslide deposits to rainfall, *J. Geol.*,Vol.99, pp.886–892.

Hansen, A., 1984. Landslide hazard analysis. In: Brundsen D, and Prior DB (eds) ”Slope Instability“, Wiley, New York, pp 523–602

Hansen, A., Brimicombe, A., Franks, C., Kirk, P. and Tung, F., 1995. Application of GIS to hazard assessment, with particular reference to landslide in Hong Kong. In: Carrara, A., Guzzetti, F. (Eds.), Geographical Information Systems in Assessing Natural Hazards. Kluwer Academic Publishers, The Netherlands, pp. 273– 298.

Hartlen, J. and Viberg, L. 1988: Evaluation of landslide hazard. In Proceedings of 5th International Symposium on Landslides, Rotterdam: Balkema, 1037–58.

Hearn, G.J. and Griffiths, J.S. 2001: Landslide hazard mapping and risk assessment. Geological Society Special Publication Vol.18, pp.43–52.

Heerman, P.D. and Khazenie, N., 1992. Classification of Multispectral remote sensing data using a back- propagation neural network. IEEE Transaction on geoscience and remote sensing, Vol. 30, No:1.

Hinojosa J.A., Leon, C.O., 1978. Unstable soil mapping in Spain. In: Proceedings of 3rd International Cong. IAEG, Madrid, section I, (I), pp. 217–227

Ho et al., 2000. K. Ho, E. Leroi and B. Roberts , Keynote lecture: quantitative risk assessment—application, myths and future direction. In: Proceedings of the International Conference on Geotechnical and Geological Engineering, GEOENG 2000, Melbourne, Australia vol. 1, Technomic, Lancaster (2000), pp. 236–312.

Hollingsworth, R., Kovacs, G.S., 1981. Soil slumps and debris flows: prediction and protection. Bulletin American Association of Engineering Geologists Vol.18-1, pp.17–28.

Hosmer, D.W., Lomeshow, S., 2000 Applied logistic regression, 2nd edn. Wiley, New York, pp 373

Huabin, W., Gangjun, L., Weiya, X. and Gonghui, W., 2005, GIS-based landslide hazard assessment:an overview, Progress in Physical Geography Vol.29-4, pp. 548–567

Hung, J.J., 2000. Chie-Chie Earthquake Induced Landslides in Thaiwan. Earthquake Engineering and Engineering Seismology, Vol. 2, No: 2, pp. 25-33

Hungr, O., 2004. Landslide Hazards in BC-Achieving balance in risk assessment. Innovation, Journal of the Association of Professional Engineers and Geoscientists of BC: April issue, pp. 12-15.

Hungr, O., 1994, A general limit equilibrium model for three-dimensional slope stability analysis: Discussion, Canadian Geotechnical Journal Vol.31, pp.791–795.

Hutchinson, J.N., 1986. A sliding-consolidation model for flow slides. Canadian Geotechnical Journal Vol.23, pp.115– 126.

Hutchinson, J.N. 1988. General report: morphological and geotechnical parameters in relation to geology and hydrogeology. In Proceedings of the 5th International Symposium on Landslides, 10–15 July 1988, Lausanne, Switzerland. Edited by C. Bonnard. A.A. Balkema, Rotterdam. Vol. 1, pp. 3–35.

Hutchinson, J.N., Bromhead, E.N. and Chandler, M.P. 1991: Investigations of the landslides at St Catherine's Point, Isle of Wight. In Chandler, R., editor, Slope stability engineering–developments and applications, London: Thomas Telford, pp.169–79.

Hutchinson, J.N.: 1995, Keynote paper: Landslide hazard assessment, In: Landslides-Glissements de Terrain, VI International Symposium on Landslides, Vol. 3, Christchurch, New Zealand, 1992. Balkema, Rotterdam, pp. 1805–1841.

Hylland, M.D., Lowe, M., 1997. Regional landslide-hazard evaluation using landslide slopes, Western Wasatch County, Utah. Environmental and Engineering Geoscience Vol.3, pp.31–43.

Ibsen, M. and Brunsden, D.,1996. The nature, use and problems of historical archives for the temporal occurrence of landslides, with specific reference to the south coast of Britain, Ventnor, Isle of Wight. Geomorphology Vol.15, pp.241–258

Ildir, B.: 1995, Turkiyede heyelanlarin dagilimi ve afetler yasasi ile ilgili uygulamalar, In: Proc. Of 2nd National Landslide Symposium of Turkey, Sakarya University, pp. 1–9 (in Turkish).

Innovativegis, 2009. Quantitative Methods for Analyzing Map Similarity and Zoning. http://www.innovativegis.com/basis/present/GIS02_similarity/GIS02_similarity.htm. Last accessed December 29, 2009.

Irigaray, C., 1995. Movimientos de ladera: inventario, análisis y cartografáa de susceptibilidad mediante un Sistema de Información Geográfica. Aplicación a las zonas de Colmenar (Ma), Rute (Co) y Montefrío (Gr), Tesis Doctoral, University Granada.

Iverson, R.M., 2000. Landslide triggering by rain infiltration. Water Resources Research Vol.36(7): pp.1897-1910

Ives, J.D. and Messerli, B.,1981. Mountain Hazard Mapping in Nepal: Introduction to an Applied Mountain Research Project. Mountain Research And Development,Vol. 1 : pp.223–230.

Ives, J.D.and Messerli, B.,1981. Mountain Hazard Mapping in Nepal: Introduction to an Applied Mountain Research Project. Mountain Research And Development, Vol.1, pp 223–230

Jaboyedoff, M., Baillifard, F., Philippossian F. and Rouiller, J.D., 2004. Assessing fracture occurrence using "weighted fracturing density" a step towards estimating rock instability hazard, *Natural Hazards and Earth System Sciences*, Vol.4 (2004), pp. 83–93.

Jade, S. and Sarkar, S., 1993. Statistical models for slope stability classification. *Engineering Geology*, Vol.36, pp. 91–98.

Jager, S., Wieczorek, G.F., 1994. Landslide susceptibility in the Tully Valley Area, Finger Lakes Region. U.S. *Geological Survey Open-File Report*, pp.94– 615.

Jain, A.K., Mao, J., Mohiuddin, K.M., 1996. Artificial neural networks: a tutorial. Comput. IEEE March, pp.31–44.

Jakob, M.,2000. The impacts of logging on landslide activity at Clayoquot Sound, British Columbia. Catena Vol.38, pp.79–300

Janbu, N., 1973, Slope stability computations, Embankment-Dam Engineering, Casagrande Volume, Wiley, New York, pp. 47–86.

Jiang, H., Eastman, J.R., 2000. Application of fuzzy measures in multicriteria evaluation in GIS. Int J Geog Inf Sci Vol.14, pp.173–184

Jibson, R.W., Harp, E.L. and Michael, J.A., 1998. A method for producing digital probabilistic seismic landslide hazard maps: An example from the Los Angeles California area. US Geol. Surv. Open-File Rep. 98-113 17 pp.

Jose, I.B., Annetty, B., Javier, H. and Cees, J. van Westen, 2000. Comparing heuristic landslide hazard assessment techniques using GIS in the Tirajana basin, Gran Canaria Island, Spain. JAGVol. 2, Issue 1

JTC,2008. Joint Technical Committee on Landslides and Engineered Slopes (Jtc-1), 2008.

Keaton, J.R., Anderson L.R. and Mathewson C.C., 1988 Assessing debris flow hazards on alluvial fans in Davis County, Utah. In: R.J. Fragaszy, Editor, Proceedings 24th Annual Symposium on Engineering Geology and Soil Engineering, Washington State University, Pullman (1988), pp. 89–108.

Keefer, D.K., 1999. Earthquake-Induced Landslides and Their Effects on Alluvial Fans. *Journal of Sedimentary Research*, Vol. 69, No. 1, pp. 84–104

Kienholz, H., 1978. Maps of geomorphology and natural hazard of Grindewald, Switzerland, scale 1:10,000. *Arctic Alpine Res*. Vol. 10(2), pp.169–184

Kim, S.K., Hong, W.P. and Kim, Y.M., 1991. Prediction of rainfall-triggered landslides in Korea. In: Bell, D.H., Editor, 1991. *Landslides*, Balkema, Rotterdam, pp. 989–994.

Ko Ko, C., Flentje, P., Chowdhury, R. 2004 Interpretation of Probability of Landsliding Triggered by Rainfall.Landslides, Vol. 1, pp. 263-275

Kobashi, S., Suzuki, M., 1988. Hazard index for the judgement of slope stability in the Rokko Mountain region. Proc., Interpraevent, 1988, Graz, Austria, Vol. 1, pp. 223–233.

Koirala, N.P., Watkins, A.T.,1988. Bulk appraisal of slopes in Hong Kong. In: Bonnard C (ed) Proc 5th International Symposium on Landslides. A A Balkema, Lausanne, pp 905–909

Kumluca ve Çevresinden Bilgiler, 2009. http://www.kumluca74.com/index2.htm. Last accessed December 29, 2009.

Lacasse, S., Eidsvig, U.M.K. and Düzgün, H.S.B., 2006. "An integrated framework for risk assessment of slopes", Porc. Of 59th Canadian Geotechnical Conference and 7th Joint CGS/IAH Grandwater Spatiality Conference, Vancouver, Canada., pp.426-433.

Lam, L., Lee S.W., and Wuen C. Y. 1992. Thinning Methodologies-A Comprehensive Survey. IEEE TrPAMI, Vol. 14, No.9, pp. 869-885.

Landslide Map, 2004. General Directorate of Disaster Affairs, Ankara.

Landslide Reports, 1985. The Ministry of Public Works and Settlement, General Directorate of Disaster Affairs, The Geologic Etude and Investigation Directory of Bartın.

Landslide Reports, 1987. The Ministry of Public Works and Settlement, General Directorate of Disaster Affairs, The Geologic Etude and Investigation Directory of Bartın.

Landslide Reports, 1993. The Ministry of Public Works and Settlement, General Directorate of Disaster Affairs, The Geologic Etude and Investigation Directory of Bartın.

Landslide Reports, 1995 The Ministry of Public Works and Settlement, General Directorate of Disaster Affairs, The Geologic Etude and Investigation Directory of Bartın.

Landslide Reports, 2000. The Ministry of Public Works and Settlement, General Directorate of Disaster Affairs, The Geologic Etude and Investigation Directory of Bartın.

Lang et al., 1999. A. Lang, J. Moya, J. Corominas, L. Schrott and R. Dikau , Classic and new dating methods for assessing the temporal occurrence of mass movements. *Geomorphology*, Vol.30 (1999), pp. 33–52.

Lang, A. Moya, J. Corominas, J. Schrott L. and Dikau , R. , 1999. Classic and new dating methods for assessing the temporal occurrence of mass movements. Geomorphology Vol.30 (1999), pp. 33–52.

Larsen, M. C., Simon, A., 1993. A Rainfall intensity-duration threshold for landslides in a humid-tropical environment, Puerto Rico: Geographica Annaler, vol.75-A. No. 1-2, pp. 13-23.

Lateltin O., 1997. Berücksichtigung der Massenbewegungsgefahren bei raumwirksamen Tätigkeiten. Empfehlungen 1997. Swiss Federal Office for Water and Geology (FOWG).

Lebart, L., Morineau A., Fenelan J.P., 1982. Traitement des don´ees statistiques. Dunad: Paris.

Lee, S., Chwae U. and Min, K., 2002. Landslide susceptibility mapping by correlation between topography and geological structure: the Janghung area, Korea. Geomorphology Vol.46, pp. 149–162.

Lee, S. and Min, K., 2001. Statistical analysis of landslide susceptibility at Yongin, Korea. Environmental, Geology, Vol.40, pp.1095–1113

Lee, J., Angelier, J., Chu, H.T., Hu, J.C. and Jeng, F.S, 2001.Continuous monitoring of an active fault in a plate-suture zone: A creepmeter study of the Chihshang active fault, eastern Taiwan, Tectonophysics, Vol.33, pp.219– 240.

Lee, S., Ryu, J.H., Min, K., Won, J.S.,2003a. Landslide susceptibility analysis using GIS and artificial neural networks. Earth Surf Processes Landforms Vol.28(12),pp.1361–1376

Lee, S., Ryu, J.H., Lee, M.J., Won, J.S., 2003b. Use of an artificial neural network for analysis of susceptibility to landslides at Boun, Korea. Environmental Geology Vol.34 (1), pp.59–69.

Lee S., 2004. Application of Likelihood Ratio and Logistic Regression Models to Landslide Susceptibility Mapping Using GIS. Environmental Management Vol. 34, No. 2, pp. 223–232

Lee, E.M., Jones, D.K.C., 2004. Landslide risk assessment. Thomas Telford, London, pp 454

Lee, S., Choi, J. and Min, K., 2004. Probabilistic landslide hazard mapping using GIS and remote sensing data at Boun, Korea. Int. J. Remote Sensing, 10 June, 2004,Vol 25, No. 11, pp.2037–2052

Lee, S.,2005. Application of logistic regression model and its validation for landslide susceptibility mapping using GIS and remote sensing data. Int J Remote Sensing. Vol. 26, pp.1477–1491

Lee, S, Tu Dan N. 2005, Probabilistic landslide susceptibility mapping in the Lai Chau province of Vietnam:Focus on the relationship between tectonic fractures and landslides, Environ Geol. Vol.48,pp. 778-787.

Lee, S. and Pradhan, B., 2006. Probabilistic landslide hazards and risk mapping on Penang Island, Malaysia, J. Earth Syst. Sci. Vol.115, No. 6, pp. 661–672

Lees, B.G., 1996. Neural networks applications in the geosciences: an introduction, Computer and Geosciences Vol.22 (1996), pp. 955–957.

Leiba, M., Baynes, M., Scott F.G. and Granger, K. 2003. Regional landslide risk to the Cairns community. Natural Hazards, Vol.30, pp.233-249.

Leone, F., Aste, J.P., Leroi, E.,1996. Vulnerability assessment of elements exposed to mass-movement: working toward a better risk perception. A.A. Balkema In: Senneset K (ed) Landslides, Vol. 1., pp.263–269

Leroi, E.,1996. Landslide hazard-Risk maps at different scales: Objectives, tools and developments. In: Senneset K (ed) Landslides-Glissements de terrain. VII International Symposium on Landslides. Trondheim, Norway. Balkema, Rotterdam, pp 35–51

Leroueil S.and Locat, J. 1998. Slope movements geotechnical characterization, risk assessment and mitigation. In: B. Maric, L. Lisac and A. Szavits-Nossan, Editors, Geotechnical Hazards, Balkema, Rotterdam (1998), pp. 95–106

LeSage, 2009. Econometrics Toolbox: by James P. LeSage. Support from National Science Foundation BCS-0136229 and generous contributors of code . http://www.spatial-econometrics.com/. last revisited 1/2009

Leshchinsky, D. and Huang Ching-Chang: 1992, Generalized three dimensional slope stability analysis, Journal of Geotechnical Engineering Vol.118(11), pp.1748–1763.

Lsao, A., 1996. Designs of medium scale hazard maps of mountain slopes in Japan. GeoJournal Vol.38(3), pp. 365-372.

Lu, P, Rosenbaum M.S.,2003. Artificial neural networks and grey systems for the prediction of slope stability. *Nat Hazards*, Vol. 30(3), pp.383–398

Lu, D., Weng Q. and Li G., 2006. Residential population estimation using a remote sensing derived impervious surface approach. *International Journal of Remote Sensing,* Vol. 27, No. 16, 20 August, pp.3553–3570

Lumb, P., 1975. Slope failures in Hong Kong. Quarterly Journal of Engineering Geology Vol.8, pp. 31–65

Luzi, L., Pergalani, F., 1996. Application of statistical and GIS techniques to slope instability zonation (1:50000 Fabriano geological map sheet). Soil Dynamics and Earthquake Engineering Vol.15, pp.83-94.

Luzi, L. and Pergalani, F. 1999. Slope instability in static and dynamic conditions for urban planning: the 'Oltre Po Pavese' case history, Natural Hazards Vol.20 (1999), pp. 57–82.

Luzi, L., Pergalani, F. and Terlien, M.T.J., 2000: Slope vulnerability to earthquakes at subregional scale, using probabilistic techniques and geographic information systems. Engineering Geology Vol.58, pp.313–36.

Maharaj R (1993) Landslide processes and landslide susceptibility analysis from an upland watershed: a case study from St. Andrew, Jamaica, West Indies. Eng Geol Vol.34, pp.53–79

Maharaj, R., 1993. Landslide processes and landslide susceptibility analysis from an upland watershed: a case study from St. Andrew, Jamaica,West Indies. Engineering Geology Vol.34, pp.53– 79.

Mahiny, A.S. and Turner, B.J., 2003. Modeling past vegetation change through remote sensing and GIS: a comparison of neural networks and logistic regression methods. Proceedings of the 7th International Conference on Geocomputation. University of Southampton, United Kingdom.

Mahr T., Malgot J.,1978. Zoning maps for regional and urban development based on slope stability. In: Proceedings of the IIIrd I.A.E.G. Congress I, Spain Vol.1:14.pp.124–137

Maidment, R.D., 2002. ArcHydro GIS for Water resources. ESRI Press, 380 New York Street, Redlands, California. ISBN-13:978-1-58948-034-6

Manel, S., Dias, J.M. and Ormerod, S.J., 1999. Comparing discriminant analysis, neural networks and logistic regression for predicting species distributions: a case study with Himalayan river bird. Ecological Modelling, Vol. 120, pp. 337–347.

Marquinez, J. Lastra J. and Garcia, P. 2003. Estimation models for precipitation in mountainous regions: the use of GIS and multivariate analysis, *J. Hydrol.*Vol. 270 (2003) (1–2), pp. 1–11.

Marques R., Zezere J., Trigo R., Gaspari J.and Trigo I., 2007. Rainfall patterns and critical values associated with landslides in Povoaçao County (Sao Miguel Island, Azores): relationships with the North Atlantic Oscillation. *Hydrol. Process.*Vol. 22, pp. 478–494 (2008)

Matlab 7.1, 2008. Matlab 7.1 help documants

McCune, B. and Keon D., 2002. Equations for potential annual direct incident radiation and heat load, Journal of Vegetation Science , Vol.13, pp. 603-606.

Mertler, C. A. and Vannatta R. A., 2002. Advanced and Multivariate Statistical Methods. Practical Applications and interpretations (2nd ed.) Pyrczak Publishing.

Meijerink, A.M.J. 1988: Data acquisition and data capture through terrain mapping unit. *InternationalComputer Journal*, Vol.1, pp. 23–44.

Mejia-Navarro, M., Wohl, E.E., Oaks, S.D., 1994. Geological ´ hazards, vulnerability and risk assessment using GIS: model for Glenwood Springs, Colorado. *Geomorphology*, Vol.10, pp.331– 354.

Melelli, L. and Taramelli, A., 2004. An example of debris-flows hazard modeling using GIS. *Natural Hazards and Earth System Sciences* . Vol. 4, pp.347–358

Menard, S.,1995. Applied logistic regression analysis. Sage university paper series on quantitative applications in social sciences, Thousand Oaks, California, Vol. 106, pp 98

Miles, S.B. and Ho, C.L. 1999.Rigorous landslide hazard zonation using Newmark's method and stochastic ground motion simulation, *Soil Dynamics and Earthquake Engineering* ,Vol.18, pp. 305–323.

Montgomery, D.R., Wright, R.H., Booth, T., 1991. Debris flow hazard mitigation for colluvium-filled swales. *Bulletin Association of Engineering Geologists* Vol.28-3, pp.303–323.

Montgomery, D.R. and Dietrich, W.E., 1994. A physically based model for the topographic control of shallow landsliding. *Water Resources Research* Vol.30-4, pp. 1153–1171.

Moon, A.T. Olds, R.J. Wilson R.A. and Burman, B.C.,1992. Debris flow zoning at Montrose, Victoria, Landslides, Proc. Sixth Int Symp. on landslides, Christchurch, Balkema, Rotterdam (1992), pp. 1015–1022.

Moore, I.D., Grayson, R.B., Ladson, A.R., 1991. Digital terrain modeling: a review of hydrological, geomorphological, and biological applications. Hydrological Processes Vol.5, pp. 3– 30.

Moreiras, S.M., 2005. Landslide susceptibility zonation in the Rio Mendoza Valley, Argentina. *Geomorphology*, Vol.66, pp.345–357.

Morgan, G.C., Rawlings G.E. andSobkowicz , J.C. , 1992. Evaluating total risk to communities from large debris flows. In: Proceedings of 1st Canadian Symposium on Geotechnique and Natural Hazards, BiTech Publishers, Vancouver, BC, Canada (1992), pp. 225–236.

Morton, T.A. and Yuan, F.,2008. Analysis of population dynamics using satellite remote sensing and US census data". *Geocarto International* 2008, pp.1–20.

Mostyn G.R. and Fell R., 1997. Quantitative and semiquantitative estimation of the probability of landsliding. In: D. Cruden and R. Fell, Editors, Landslide Risk Assessment, Balkema, Rotterdam (1997), pp. 297–315.

Mulder, H.F. 1991: Assessment of landslide hazard. Profschrift ter Verkrijging van Graad van Doctor an de Rijkuniversiteit te Utrecht, University of Utrecht, 150 pp.

Nagarajan, R., Roy, A., Vinod Kumar, R., Mukhetjess, A., Khire, M.V., 2000. Landslide hazard susceptibility mapping based on terrain and climatic factors for tropical monsoon regions. Bulletin of Engineering *Geology and the Environment*, Vol. 58 (4), pp.275– 287.

Nash, D., 1987. A comparative review of limit equilibrium methods of slope stability analysis. In: Anderson, M.G., Richards, K.J. (Eds.), Slope Stability. Wiley, New York, pp. 11– 75.

Neaupane K.M. and Piantanakulchai, M.,2006. Analytic network process model for landslide hazard zonation, Engineering Geology Vol.85 (2006), pp. 281–294.

Neeley, M.K., Rice, R.M., 1990. Estimating risk of debris slides after timber harvest in northwestern California. Bulletin American Association of Engineering Geologists Vol.27-3, pp.281–289.

Negnevitsky, M., 2002. Artificial Intelligence – A Guide to Intelligent Systems, Addison – Wesley Co., Great Britain, 394, 2002.

Neuhäuser B. and Terhorst B., 2007. Landslide susceptibility assessment using "weights-of-evidence" applied to a study area at the Jurassic escarpment (SW-Germany). *Geomorphology* Vol. 86, Issues 1-2, 15 April 2007, pp.12-24

Neuland, H., 1976. A prediction model of landslips, Catena Vol.3, pp.215–230.

Nguyen V.V. and Chowdhury R.N., 1984. Probabilistic analysis of mining special piles – Two techniques compared. *Int J Rock Mechanics and Min Science*, Vol.21, pp.303–312

Nguyen V.V. and Chowdhury R.N.,1985. Risk analysis with correlated variables. Geotechnique, Vol.35, pp.47–59

Nguyen, Q.P. and Bui, H.B. 2004. Landslide hazard mapping using Bayesian approach in GIS: case study in YangSan area, Korea, GIS-IDEAS (GeoInformatics for Spatial-Infrastructure Development in Earth & Allied Sciences) Symposium 2004, Hanoi, Vietnam (2004), pp. 125–130.

Nieto, A.S., 1989. Mechanical models and geological observations: closing the prediction gap. In: Siccardi, F., Brass, R. Eds. , International Workshop on Natural Disasters in European Mediterranean Countries, Perugia, 27 June–1 July 1989. CNR-US NFS, pp. 145–164.

Nilsen, T.H. and Brabb, E.E., 1977. Slope stability studies in the San Francisco Bay region, California. Geological Society of America, Reviews in Engineering Geology Vol.3, pp.235–243.

Nilsen, T.H., Brabb, E.E., 1977. Slope stability studies in the San Francisco Bay region, California. Geological Society of America, Reviews in Engineering Geology Vol.3, pp.235–243.

O'Brien, L., 1992. Introducing Quantitative Geography. Measurement, Methods and Generalised Linear Models. Routledge, London, pp. 365.

O'Brien, J.S.,1999. Flo2D Users Manual Tetra Tech ISG, Nutrioso, AZ.

O'Brien, J.S., Julien, P.Y. and Fullerton, W.T. 1993. Two-dimensional water flood and mudflow simulation. Journal of Hydraulic Engineering Vol.119 (2),pp.244-261.

Ochoa, 1978 G. Ochoa, La influencia de la altitud sobre algunas propiedades físico-químicas de los suelos de los Andes venezolanos, Revista Geográfica XVI–XIX (1978), pp. 56–72.

OFDA/CRED, 2007. EM-DAT International Disaster Database- Universite Catholique de Louvain, Brussels, Belgium.

Ohlmacher, G.C., Davis, C.J., 2003. Using multiple logistic regression and GIS technology to predict landslide hazard in northeast Kansas, USA. Engineering Geology, Vol.69, pp.331–343

Ojeda-Moncayo, J., Locat, J., Couture, R. and Leroueil, S. 2004. The magnitude of landslides: An overview. In Landslides: Evaluation and Stabilization, Lacerda, Ehrlich, Fontoura, Satao (eds), pp.379-384.

Okunushi K. and Okumura T., 1987. Groundwater models for mountain slopes. In: Anderson M.J. and Richards D., Eds, Slope Stability – Wiley & Sons, London, pp.265-285.

Olshansky, R., 1990. Landslide hazard in the United States. Case studies in planning and policy development. Garland Publishing, New York, pp.178

Otsu, N., 1979. A threshold selection method from graylevel histograms," IEEE Trans. Sys. Man Cyber., Vol. 9, No. 1, pp. 62–66.

Ottenbacher, K.J., Smith, P.M., Illig, S.B., Linn, R.T., Fiedler, R.C., Granger, C.V., 2001. Comparison of logistic regression and neural networks to predict rehospitalization in patients with stroke. Journal of Clinical Epidemiology Vol.54, pp.1159– 1165.

Öztürk K., 2002. Heyelanlar ve Türkiye'ye Etkileri, G.Ü. Gazi Eğitim Fakültesi Dergisi Cilt 22, Sayı 2, pp. 35-50

Pace K.,1997. Performing Large Spatial Regressions and Autoregressions. Econ. Lett., pp. 283–291.

Pace K., Barry R., Clapp J.M. and Rodriguez M.,1998. Spatiotemporal Autoregressive Models of Neighborhood Effects. J. Real Estate Finance Econ., pp. 15–34.

Pachauri, A.K. and Pant, M., 1992. Landslide hazard mapping based on geological attributes. *Engineering Geology*, Vol.32, pp.81– 100.

Pachauri, A.K., Gupta, P.V., Chander, R., 1998. Landslide zoning in a part of the Garhwal Himalayas. *Environmental Geology*, Vol.36, pp.325–334.

Paez, A., 2002. Spatially weighted regression:space and non-stationarity in multiple contexts. Ontario, Canada

Page M.J., Trustrum N. A., and DeRose R.C. 1994. A high resolution record of storm induced erosion from Lake sediments, New Zealand. *Journal of Paleolimnology* Vol.1, pp.333-348

Parise, M.,2001. Landslide mapping techniques and their use in the assessment of the landslide hazard. *Phys Chem Earth C*, Vol. 26(9), pp.697–703

Pike, R.J.,1988. The geometric signature: quantifying landslide terrain types from digital elevation models. Mathematical Geology , Vol.20, pp. 491–511.

Pistocchi, A., Luzi, L., Napolitano, P.,2002.i The use of predictive modeling techniques for optimal exploitation of spatial databases: a case study in landslide hazard mapping with expert system-like methods. Environ Geol, Vol.41, pp.765–775

Pomeroy, J.S., 1974. Landslide susceptibility and processes in the Maryland Coastal Plain. Schultz AP, Southworth CS (eds) Landslides of eastern North America. US Geological Survey Circular 1008, Chap. 2, pp 5–9

Premchitt, J., Brand, E.W., Chen, P.Y.M.,1994. Rain-induced landslides in Hong Kong. Asia Eng Vol.6, pp.43–51

Preston, N.J.and Crozier, M.J., 1999. Resistance to shallow landslide failure through root-derived cohesion in East Coast Hill Country soils, North Island, New Zealand, Earth Surface Processes and Landforms Vol.24, pp. 665–675.

Prina, E., Bonnard, Ch., Vulliet, L., 2004. Vulnerability and risk assessment of a mountain road crossing landslides. Rivista Italiana Geotecnica Vol. XXXVIII(2), pp. 67–79

Radbruch, D.H., Colton, R.B., Davies, W.E., Lucchitta I., Skipp B.A., Varnes D.J., 1982. Landslide overview map of the conterminous United States. US Geological Survey Miscellaneous Field Studies Map MF-771, 1 sheet, scale 1:7,500,000. Washington Division of Geology and Earth Resources, USA

Ragozin, A.L. and Tikhvinsky I.O., 2000. Landslide hazard, vulnerability and risk assessment, 8th International symposium on landslides. Thomas Telford, Cardiff, Wales

Rautela, P. and Lakhera, .RC., 2000. Landslide risk analysis between Giri and Tons rivers in Himachal Himalaya (India). IAG Vol.2(3/4), pp.153–160

Reger, J.P., 1979. Discriminant analysis as a possible tool in landslide investigations. *Earth Surface Processes and Landforms* Vol.4, pp.267– 273.

Remondo, J., Gonzalez-Diez, A., De Teran, J.R.D. and Cendrero, A., 2003. Landslide susceptibility models utilizing spatial data analysis techniques. A case study from the Lower Deba Valley, Guipuzcoa (Spain), *Natural Hazards* Vol.30 (2003), pp. 267–279.

Remondo, J., Bonachea, J., Cendrero, A., 2005a. A statistical approach to landslide risk modelling at basin scale; from landslide susceptibility to quantitative risk assessment. Landslides Vol.2, 321–328.

Remondo J., Soto J., González-Díez A., Díaz de Terán J.R., Cendrero A., 2005b. Human impact on geomorphic processes and hazards in mountain areas in northern Spain. *Geomorphology* Vol.66(1–4), pp.69–84

Remondo, J., Bonachea, J., Cendrero, A., 2008. Quantitative landslide risk assessment and mapping on the basis of recent occurrences. *Geomorphology*, Vol. 94, pp.496–507

Richard, D. and Lothar, S., 1999. The temporal stability and activity of landslides in Europe with respect to climatic change (TESLEC): main objectives and results . Geomorphology Vol.30, Issues 1-2, pp. 1-12

Rodriguez, Ortiz J.M., Prieto, C., Hinojosa, J.A.,1978. Regional studies on mass movements in Spain. In: Proceedings of the IIIrd I.A.E.G. Congress I, Vo1.29, pp.267–278

Rouiller, J.D. and Marro, Ch., 1997. Application de la méthodologie “MATTEROCK” à l’evaluation du danger lié aux falaises, Eclogae Geologicae Helveticae Vol.90 (1997), pp. 393–399.

Rouiller, J.D. Jaboyedoff, M. Marro, Ch. Philippossian F. and Mamin, M. 1998. Pentes instables dans le Pennique valaisan, Rapport final du Programme National de Recherche PNR 31/CREALP vol. 98

Rowbotham, D.and Dudycha, D.N., 1998. GIS modelling of slope stability in Phewa Tal watershed, Nepal. *Geomorphology*, Vol.26, pp.151– 170.

Rumelhart, D.E., Hinton, G.E. and Williams, R.J. 1986. Learning representations by back-propagating errors. Nature Vol.323, pp.533–36

Rupke, J., Cammeraat, E., Seijmonsbergen, A.C., van Westen, C.J., 1988. Engineering geomorphology of Widentobel Catchment, Appenzell and Sankt Gallen, Switzerland: a geomorphological inventory system applied to geotechnical appraisal of slope stability. *Engineering Geology*, Vol. 26, pp.33–68.

Saaty, L.T.,1994. Fundamentals of decision making and priority theory with analytic hierarchy process, RWS publications, Pittsburgh, pp.527

Saaty, L.T.,1988. The analytic hierarchy process: planning, priority setting, resource allocation, RWS publications, Pittsburgh, pp.287

Saaty L.T., Vargas L.G.,2001. Models, methods, concepts, and applications of the analytic hierarchy process. Kluwer Academic, Boston, pp .333

Sakellariou,M.G., Ferentinou,M.D.,2001. GIS-based estimation of slope stability *Nat. Hazard Rev*. Vol.2, pp.12-21

Salvucci,G.D., Entekabi, D.,1994."Explicit expressions for Green-Ampt (Delta function diffusivity) infiltration rate and cumulative storage" Water Resour Res Vol.30, pp.2661-2663

Santacana, N., Baeza, B., Corominas, J., De Paz, A., Marturia´, J., 2003. A GIS-based multivariate statistical analysis for shallow landslide susceptibility mapping in La Pobla de Lillet Area (Eastern Pyrenees, Spain). *Natural Hazards* Vol.30 (3), pp.281– 295.

Sarkar, S., Kanungo, D.P., 2004. An integrated approach for landslide susceptibility mapping using remote sensing and GIS. Photogrammetric Engineering and Remote Sensing Vol.70, pp.617–625.

Sarma, S. K.: 1973, Stability analysis of embankments and slopes, *Geotechnique* Vol.23(3), pp.423–433.

Schädel, K. and Stober, I., 1988. Rezente Großrutschungen an der Schwäbischen Alb, Jahreshefte des Geologischen Landesamtes Baden-Württemberg Vol. 30 (1988), pp. 413–439

Scheidegger, A., 1973. On the prediction of the reach and velocity of catastrophic landslides. Rock Mechanics Vol.5, pp.231– 236.

Schumacher, M., Robner, R., Vach, W., 1996. Neural networks and logistic regression: Part I. Computational Statistics & Data Analysis 21, 661–682.

Schuster, R.L. and Fleming, R.W., 1986. Economic losses and fatalities due to landslides. Bulletin of the Association of Engineering Geologists Vol.23 (1), 11–28.

Schuster, R.L., 1995a. Socioeconomic significance of landslides. In: Turner, A.K., Schuster, R.L. Eds. , Landslides, Investigation and Mitigation. Transportation Research Board Special Report 247. National Academy Press, WA, pp. 12–35.

Scott G.R.,1972. Map showing landslides and areas susceptible to landslides in the Morrison Quadrangle, Jefferson County, Colorado. US Geological Survey. Map I-790-B. USA

Shufelt, A. A.and Mckeown, D. M., 1993 "Fusion of Monocular Cues to Detect Man-Made Structures in Aerial Imagery", CVGIP: Image Understanding, Vol.57 (3), pp.307-330.

Soeters, R., Van Westen, C.J., 1996. Slope stability: recognition, analysis and zonation. In: Turner AK, Shuster RL (eds) "Landslides: investigation and mitigation". Transportation Research Board – National Research Council, Special Report 247, pp 129–177 Sorriso-Valvo

Sönmez, H., Gökçeoğlu C., Nefeslioglu H.A., Kayabasi A, 2006. Estimation of rock modulus: For intact rocks with an artificial neural network and for rock masses with a new empirical equation, International Journal of Rock Mechanics & Mining Sciences 43: 224–235

Süzen, M.L. and Doyuran, V, 2004. A comparison of the GIS based landslide susceptibility assessment methods: multivariate versus bivariate, *Environmental Geology*, Vol. 45, pp.665–679, 2004a.

Süzen M. L. and Doyuran V. 2004. Data driven bivariate landslide susceptibility assessment using geographical information systems: a method and application to Asarsuyu catchment, Turkey. *Engineering Geology,* Vol.71 (2004), pp. 303–321

Süzen M.L.,2002. Data driven landslide hazard assessment using geographical information systems and remote sensing. PhD Thesis, Middle East Technical University, Turkey

Swanston, D.N., Schuster, R.L., 1989. Long-term landslide hazard mitigation programs: structure and experience from other countries. *Bulletin American Association of Engineering Geologists* Vol.26-1, pp.109–113.

Taubenböck, H., Esch, T.and Roth, A., 2006. An urban classification approach based on an object-oriented analysis of high resolution satellite imagery for a spatial structuring within urban areas. First Workshop of the EARSeL Special Interest Group on Urban Remote Sensing "Challenges and Solutions".

Terhors, B., 1997. Formenschatz, Alter und Ursachenkomplexe von Massenverlagerungen an der schwäbischen Juraschichtstufe unter besonderer Berücksichtigung von Boden- und Deckschichtenentwicklung, Tübinger Geowissenschaftliche Arbeiten. Reihe D,Vol. 2 (1997), pp. 1–212.

Terhorst, B.,2001. Mass movements of various ages on the Swabian Jurassic escarpment: geomorphologic processes and their causes, Zeitschrift für Geomorphologie N.F. Supplementband Vol.125 (2001), pp. 65–87.

Terlien, M.T.J., van Westen, C.J. and van Asch, Th.W.J., 1995. Deterministic modelling in GIS-based landslide hazard assessment. In: Carrara, A. and Guzzetti, F. Editors, 1995. Geographical Information Systems in Assessing Natural Hazards Kluwer Academic Publisher, Dordrecht, The Netherlands, pp. 57–77.

Terlien, M.T.J.,1996. Modelling spatial and temporal variations in rainfall-triggered landslides. ITC publication 32. ITC, Enschede, The Netherlands

Terlien, M.T.J. 1998, The determination of statistical and deterministic hydrological landslide-triggering thresholds, Environmental Geology Vol.35 , pp. 124–130.

Thein, S., 2000. Massenverlagerungen an der Schwäbischen Alb: Statistische Vorhersagemodelle und regionale Gefährdungskarten unter Anwendung eines Geographischen Informationssystems, Tübinger Geowissenschaftliche Arbeiten. Reihe D, Vol. 6, pp. 83–104.

Thomas, G., Michael, J.C., 2004. A review of scale dependency in landslide hazard and risk analysis. Landslide hazard and risk, 2004 - John Wiley&Sons, Ltd

Thurston, N. and Degg M., 2000. Transferability and terrain reconstruction within a GIS landslide hazard mapping model: Derbyshire Peak District. In: A.E. Bromhead, N. Dixon and M.L. Ibsen, Editors, Landslide in Research, Theory and Practice, Thomas Telford, London (2000), Vol. 3, pp. 961–968.

TMO, 2009. Toprak Mahsulleri Ofisi. http://www.tmo.gov.tr/tr/index.php. Last accessed December 29, 2009.

Topraksu Genel Müdürlüğü, 1978. Konya Kapalı Havzası Toprakları. Toprak Etüdleri ve Haritalama Dairesi Topak Etüdleri Fen Heyeti Md., Ankara. Yayın No: 288.

Tsai, 2006. "A comparative study on shadow compensation of color aerial images in invariant color models", IEEE Transactions On Geoscience And Remote Sensing, Vol. 44, No. 6, June.

Tu, J.V., 1996. Advantages and disadvantages of using artificial neural networks versus logistic regression for predicting medical outcomes. Journal of Clinical Epidemiology Vol.49 (11), 1225– 1231.

Tunusluoglu, M.C., Gökçeoğlu, C.,Nefeslioglu, H.A. and Sönmez H., 2008. Extraction of potential debris source areas by logistic regression technique: a case study from Barla, Besparmak and Kapi mountains (NW Taurids, Turkey). *Environmental Geology*, Vol. 54(1), pp.9-22.

Turrini, M.C. and Visintainer, P. 1998: Proposal of a method to define areas of landslide hazard and application to an area of the Dolomites, Italy. Engineering Geology 50, 255–65.

Turrini, M.C., Visintainer, P., 1998. Proposal of a method to define areas of landslide hazard and application to an area of the Dolomites, Italy. Engineering Geology 50, 255–265.

Upton, G.J.G. and Fingleton, B.,1989. Spatial Data Analysis by Example. Volume 2 Categorical and Directional Data. John Wiley & Sons, Chichester.

Uromeihy A. and Mahdavifar M.R., 2000. Landslide hazard zonation of the Khorshrostam area, Iran. *Bull Eng Geol Env*, Vol. 58, pp.207–213

USAID, 2009. Agro-Climatic Monitoring. http://www.fews.net/pages/imageryhome.aspx?pageID=Ndvi, Last accessed December 29, 2009

Usul, N., 2005. Engineering Hydrology, Metu Press, Ankara, ISBN:975-7064-43-2.

Uzielli, M., Düzgün, H.S.B. and Vangelsten, B.V., (2006), "A first –Order Second-Moment Framework for probabilistic estimation of vulnerability to landslides", ECI Conference: Geohazards - Technical, Economical and Social Risk Evaluation 18 - 21 June 2006, Lillehammer, Norway.

Van Den Eeckhaut, M., Poesen, J., Verstraeten, G., Vanacker, V., Nyssen, J., Moeyersons, J., van Beek, L.P.H., Vandekerckhove, L. , 2007. Use of LIDAR-derived images for mapping old landslides under forest, *Earth Surface Processes and Landforms* ,Vol. 32, Issue 5, 30 April 2007, pp. 754-769

Van Westen, C.J., Van Duren I., Kruse H.M.G., Terlien M.T.J.,1993. GISSIZ: training package for geographic information systems in slope instability zonation. Enschede, The Netherlands ITC publ no. 15, vol. 1 and 2. ITC,

Van Westen, C.J. 1993: Application of Geographical Information System to landslide hazard zonation. Enschede: ITC Publication Vol.15, pp.245

Van Westen, C.J. 1994: GIS in landslide hazard zonation: a review with examples from the Colombian Andes. In Price, M.F. and Heywood, D.I., editors, Mountain environments and Geographic Information Systems, London: Taylor and Francis, 135–65.

Van Westen, C.J. and Terlien, T.J. 1996: An approach towards deterministic landslide hazard analysis in GIS: a case study from Manizales Colombia. Earth Surface Processes and Landforms Vol.21, pp.853–68.

van Westen, C.J., Rengers, N., Terlien, M.T.J. and Soeters, R. 1997: Prediction of the occurrence of slope instability phenomena through GIS-based hazard zonation. Geologische Rundschau Vol.86, pp. 404–14.

Van Westen, C.J., 1997. Statistical landslide hazard analysis. ILWIS 2.1 for Windows application guide. ITC Publication, Enschede: pp.73–84

Van Westen C., Rengers N. and Soeters R., 2003. Use of geomorphological information in indirect landslide susceptibility assessment, *Natural Hazards* Vol.30, pp. 399–419.

Van Westen. C.J., 2004. Geo-information tools for landslide risk assessment: an overview of recent developments. In: Lacerda WA, Ehrlich M, Fontoura SAB, Sayao ASF (eds) Landslides: evaluation and stabilization, vol 1. Balkema, London, pp 39–56

Van Westen, C.J., Van Asch, T.W.J. and Soeters, R., 2005. Landslide hazard and risk zonation; why is it still so difficult?, Bulletin of Engineering geology and the Environment Vol.65 (2), pp. 167–184.

Van Westen, C.J., van Asch, T.W.J., Soeters, R., 2006. Landslide hazard and risk zonation—why is it still so difficult?, *Bull Eng Geol Env*, Vol. 65, pp.167–184

van Westen C. J., Castellanos E. and Kuriakose S.L., 2008. Spatial data for landslide susceptibility, hazard, and vulnerability assessment: An overview . Engineering Geology, Vol.102(3-4), pp. 112-131

Vanacker, V., Vanderschaeghe, M., Govers, G., Willems, E., Poesen, J., Deckers, ., De Bievere, B., 2003. Linking hydrological, infinite slope stability and land-use change models through GIS for assessing the impact of deforestation on slope stability in high Andean watersheds. *Geomorphology*. Vol.52, pp. 299–315.

Varnes, D.J., 1978. Landslides Types and Processes. In: Landslides and Engineering Practice. E.B. Eckel, (ed.), Highway Research Board Special Report, 29, 20-47.

Varnes, D.J. and IAEG Commission on Landslides and Other Mass-Movements: 1984, Landslide Hazard Zonation: A Review of Principles and Practice, UNESCO Press, Paris. pp. 63.

Van Zuidam, R.A.,1986. Terrain classification, ITC-textbook, ITC, Enschede, The Netherlands.

Wachal, D.J. and Hudak, P.F., 2000. Mapping landslide susceptibility in Travis County, Texas, USA. *GeoJournal,* Vol. 51, pp. 245–253.

Wang, F.X., 1990. The biology of Cathaya argyrophylla. Science Press, Beijing.

Wang, S.Q. and Unwin, D.J., 1992. Modelling landslide distribution on loess soils in China: an investigation. *International Journal of Geographical Information Systems* Vol.6, pp.391–405

Wang, W.D., Xie, C.M., and Du, X.G., 2008. Landslides susceptibility mapping based on geographical information system, GuiZhou, south-west China. *Environ Geology*, Vol 58, pp. 33-44.

Ward, T.J., Li R.M. and Simons, D.B., 1981. Use of a mathematical model for estimating potential landslide sites in steep forested drainage basins. IAHS Publ Vol.132 : pp.21-41

Ward, T.J., Li, R.M. and Simons, D.B.,1982. Mapping landslides in forested watersheds. *J Geotech Eng Div* Vol.8, pp.319-324

Wegmann, K.W.,2002. Landslide Inventory Mapping Between Kelso and Woodland, Cowlitz County, Washington State, Cordilleran Section - 98th Annual Meeting (May 13–15, 2002). Session No. 45, Booth15. Engineering Geology Case Histories of Landslides (Posters)

Weirich, F. and Blesius, L., 2007. Comparison of satellite and air photo based landslide susceptibility maps. *Geomorphology,* Vol. 87, Issue 4, pp. 352-364

Wieczorek, G.F., 1987. Effect of rainfall intensity and duration on debris flows in central Santa Cruz Mountains, California. In: Costa, J.E. and Wieczorek, G.F.,

Editors, 1987. Debris Flows/Avalanches: Process, Recognition and MitigationReviews in Engineering Geology Geological Society of America, Boulder, CO, vol. VII, pp. 93–104.

Wieczorek, G.F., and Jager, S., 1996, Triggering mechanisms and depositional rates of postglacial slope-movement processes in the Yosemite Valley, California: Geomorphology, Vol.. 15, pp. 17–31.

Wieczorek, G.F., 1996. Landslide triggering mechanisms. In: Landslide: Investigation and MitigationSpec. Rep. Transp. Res. Board, Nat. Acad. of Sciences vol. 247, pp. 76–90 Washington

Wieczorek, G.F., Gori, P.L., Jager, S., Kappel, W.M., Negussey, D., 1996. Assessment and management of landslide hazards near Tully Valley Landslide, Syracuse, New York, USA. Proc. 7th Int. Symposium on Landslides, Trondheim. Balkema, Rotterdam, pp. 411– 416.

Wieczorek, G.F., Mandrone, G. and DeColla, L., 1997. The influence of hill-slope shape on debris-flow initiation. In: C.L. Chen, Editor, Debris Flow Hazards Mitigation: Mechanics, Prediction, and Assessment, American Society of Civil Engineers, New York (1997), pp. 21–31.

Wieczorek, G.F. and Snyder, 1999. J.B.,Rock falls from Glacier Point above Camp Curry, Yosemite National Park, California, U.S. Geological Survey Open-file Report Vol. 13 pp.99–385, http://greenwood. cr.usgs.gov/pub/open-file-reports/ofr-99-0385/, 1999.

Wieczorek, G.F. and Guzzetti, F., 1999. A review of rainfall thresholds for triggering landslides. In: Proc. of the EGS Plinius Conference, Maratea, Italy October 1999, pp. 407–414.

Wieczorek, G.F. and Glade, T. 2005.Climatic factors influencing occurrence of debris flows. 978-3-540-20726-9 (Print) 978-3-540-27129-1 (Online), Springer Berlin Heidelberg . pp.325-362

Wieczorek,G.F. and Glade,T., 2005. "Climatic factors influencing occurrence of debris flows" In: Jakob, M, Hungr, O eds. , Debris flow hazards and related phenomena, Berlin Heidelberg, Springer, pp 325-362

Wilson, R.C.and Wieczorek, G.F., 1995. Rainfall thresholds for initiation of debris flows at La Honda, California. *Environ Eng Geosci* Vol.1,pp.11–27

Wong, H.N., Ho, K.K.S., Chan, Y.C., 1997. Assessment of consequence of landslides. In: Cruden, R., Fell, R. (Eds.), Landslide Risk Assessment. Balkema, Rotterdam, pp. 111 – 149.

Wrigley, N.,1985. Categorical Data Analysis for Geographers and Environmental Scientists. Longman, Harlow.

Wu, W., and Sidle R.C., 1995. A distributed slope stability model for steep forested hillslopes, *Water Resources Research*, Vol.31(8), pp.2097-2110.

Wu, T.H. and Abdel-Latif, M.A. 2000: Prediction and mapping of landslide hazard. *Canadian Geotechnical Journal*, Vol. 37, pp.781–95.

Xie, M., Esaki, T. and Zhou, G., 2004. GIS-Based Probabilistic Mapping of Landslide Hazard Using a Three-Dimensional Deterministic Model. *Natural Hazards* Vol.33, pp.265–282

Yeşilnacar, E.and Topal, T., 2005. Landslide susceptibility mapping: A comparison of logistic regression and neural networks methods in a medium scale study, Hendek region (Turkey). *Engineering Geology* ,Vol.79, pp. 251–266.

Yin, K.L.and Yan, T.Z., 1988. Statistical prediction model for slope instability of metamorphosed rocks. In: Bonnard, C. (Ed.), Proc., Fifth International Symposium in Landslides, Lausanne, A.A. Balkema, Rotterdam, Netherlands, Vol. 2., pp.1269– 1272.

Yong, R.N., Alonso, E., Tabba, M.M., Fransham, P.B., 1977. Application of risk analysis to the prediction of slope instability. Canadian Geotechnical Journal Vol.14-3, pp.540–543.

Yücemen, M.S., 2002. Prediction of Potential Seismic Damage to Reinforced Concrete Buildings Based on Damage Probability Matrices, In Proceedings of 6th International Conference on Concrete Technology for Developing Countries, Amman, October: Vol.3, pp.951-960.

Zhang, Y., 2002. A new automatic approach for effectively fusing Landsat 7 as well as IKONOS images. IEEE/IGARSS'02, Toronto, Canada, June 24-28.

Zhang, B.G., 2003. Application of Remote Sensing Echnology to Population Estimation. *Chinese Geographical Science*, Volume 13, Number 3, pp. 267-271, 2003 Science Press, Beijing, China 1, pp.893–898

Zanutta, A., Baldi, P., Bitelli, G., Cardinali, M., and Carrara, A.,2006. Qualitative and quantitative photogrammetric techniques for multi-temporal landslide analysis. *Annals of Geophysics*, Vol. 49, No. 4/5, August/October 2006

Zeneb, 2002. Zentrum für Naturrisiken und Entwicklung (2002): Materialsammlung

zum deutschen Beitrag für den World Vulnerability Report des United Nations Development Programme.

Zezere, J.L., Ferreira, A.B., Rodrigues, M.L., 1999. Landslides in the north of Lisbon Region (Portugal): conditioning and triggering factors. Physical and Chemical Earth (A) 24, Vol.10, pp.925– 934.

Zezere J. L., Reis E., Garcia R., Oliveira S., Rodrigues M. L., Vieira G., and Ferreira A. B., (2004). Integration of spatial and temporal data for the definition of different landslide hazard scenarios in the area north of Lisbon (Portugal), *Natural Hazards and Earth System Sciences* Vol.4, pp. 133–146

Zhang, Y., A new automatic approach for effectively fusing Landsat 7 as well as IKONOS images. IEEE/IGARSS'02, Toronto, Canada, June 24-28, 2002.

Zhou, G., Esaki, T., Mitani, Y., Xie, M., and Mori, J., 2003, Spatial probabilistic modeling of slope failure using an integrated GIS Monte Carlo simulation approach, *International Journal of Engineering Geology*, Vol. 68, pp 373–386.

Zhu, L., Huang, J., 2006. GIS-based logistic regression method for landslide susceptibility mapping in regional scale, Journal of Zhejiang University Science A, Vol.7 (12), pp. 2007-2017

APPENDIX A

Q-Q PLOTS

Table A-1. The Q-Q plot for factors considered in grid-based mapping unit

Factors	Normal QQ Plot	Detruded Normal QQ Plot
Slp	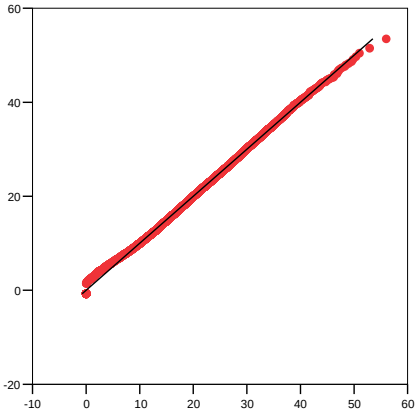	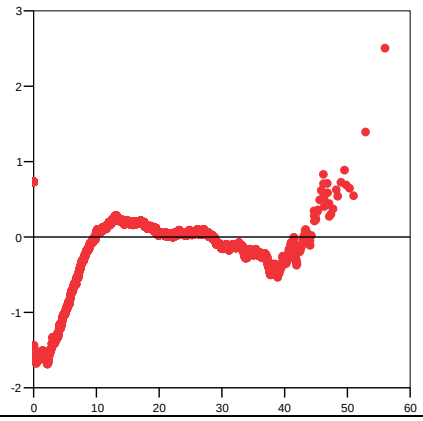
Elev	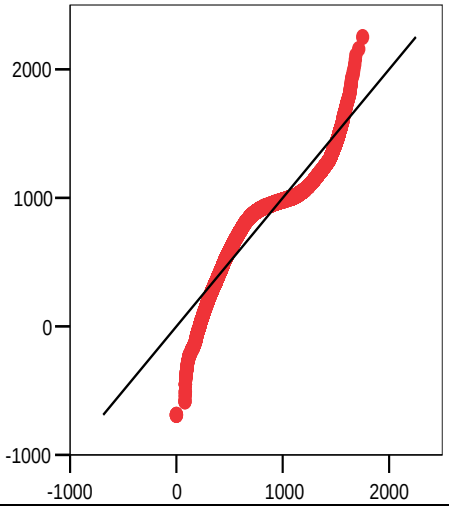	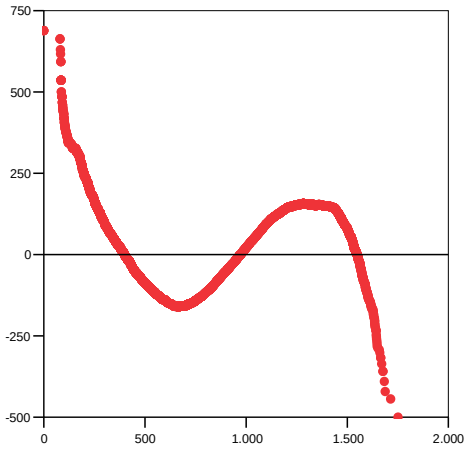

Asp	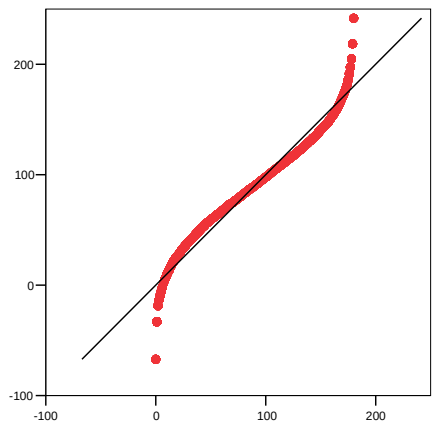	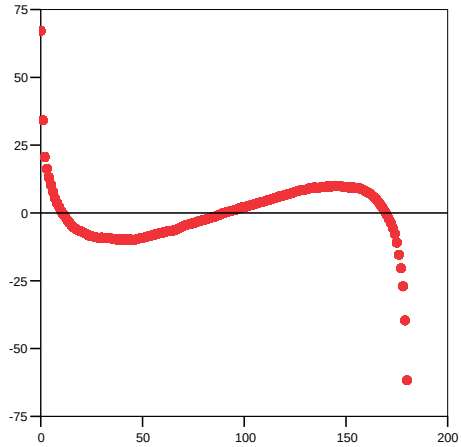
DisttoStrm	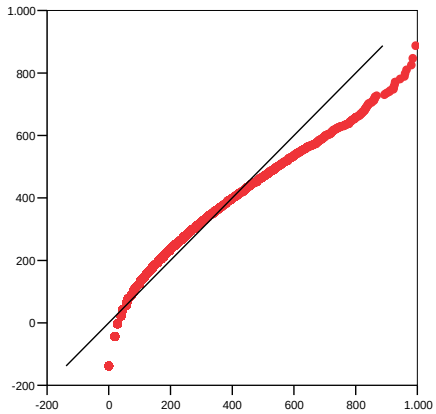	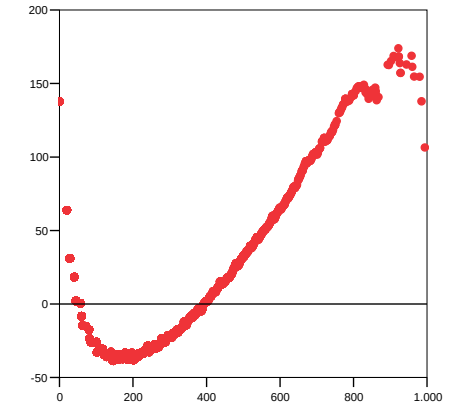
DisttoRoad	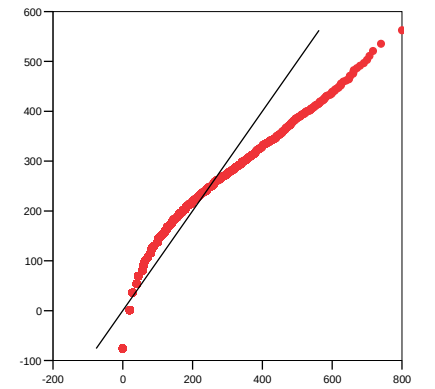	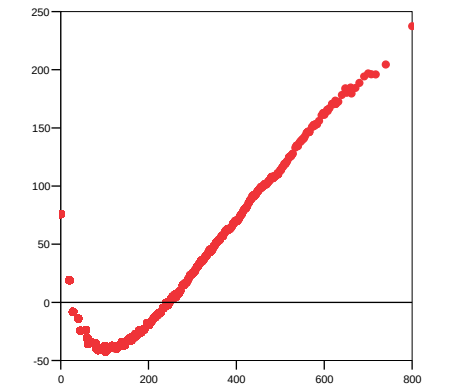
DisttoFault	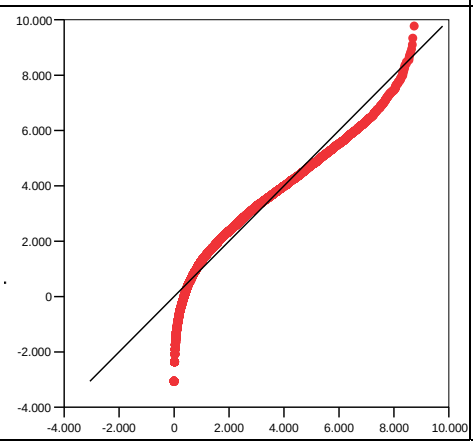	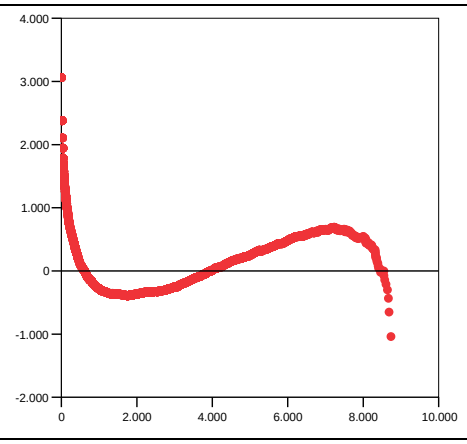

Table A-2. The Q-Q plot for factors considered in slope unit-based mapping unit

	Normal QQ Plot	Detruded Normal QQ Plot
SD_S	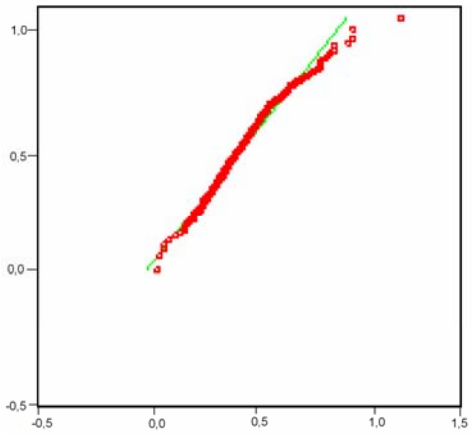	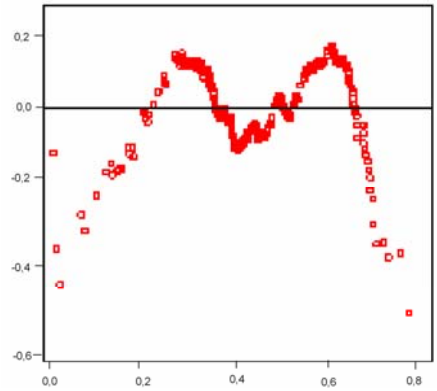
LU_DF	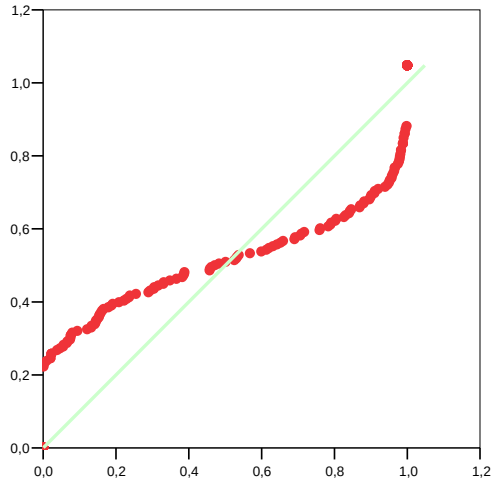	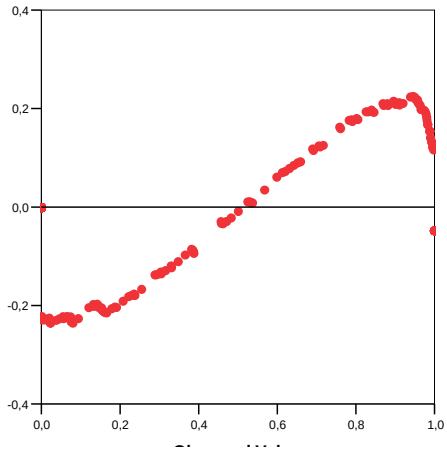
S_BFS	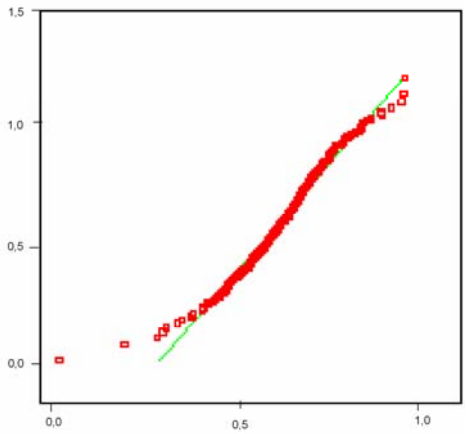	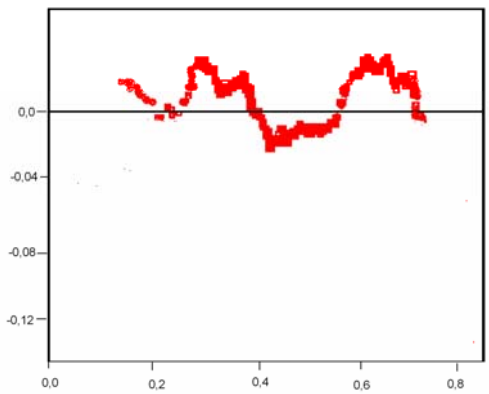

LU_F	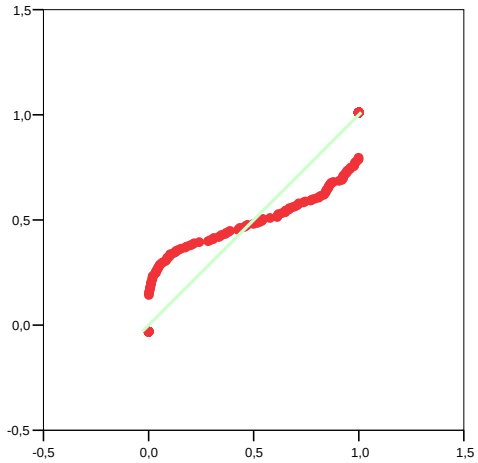	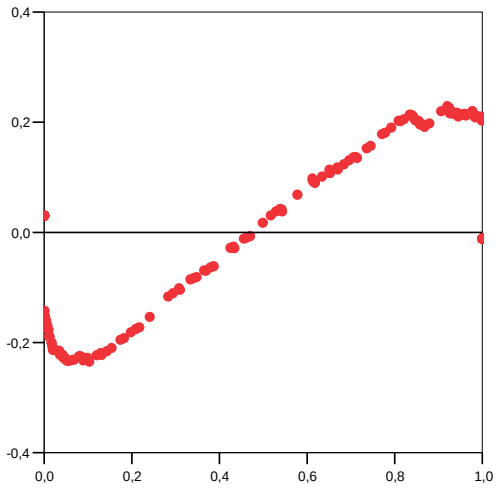
Geo_SM	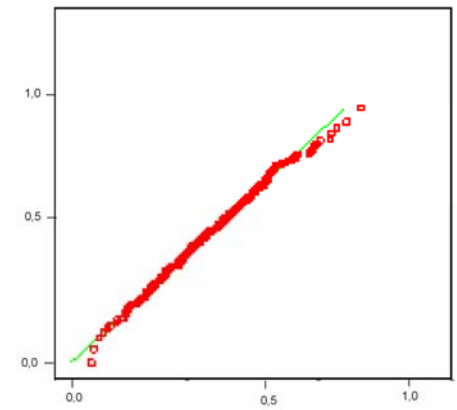	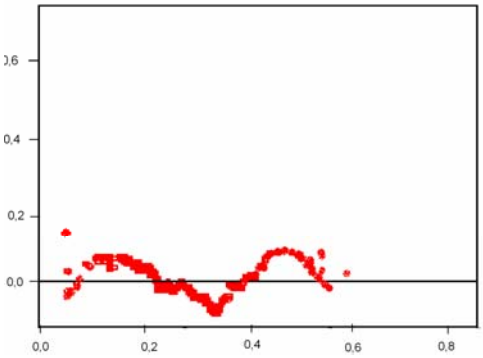
SD_D	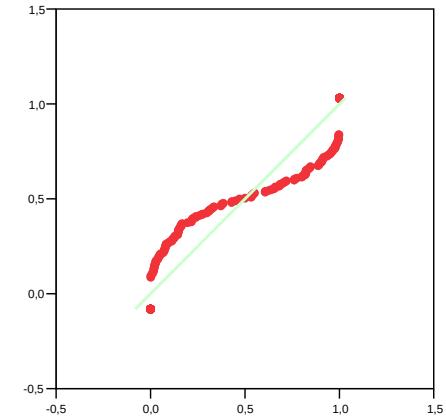	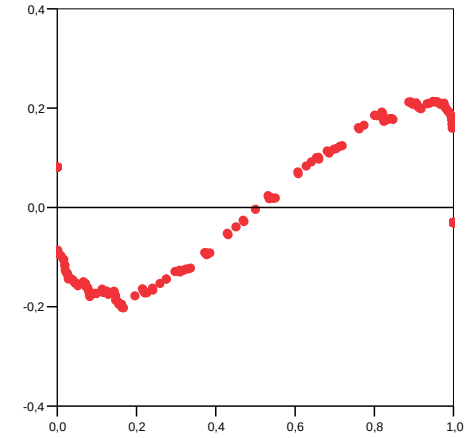
Geo_Allv	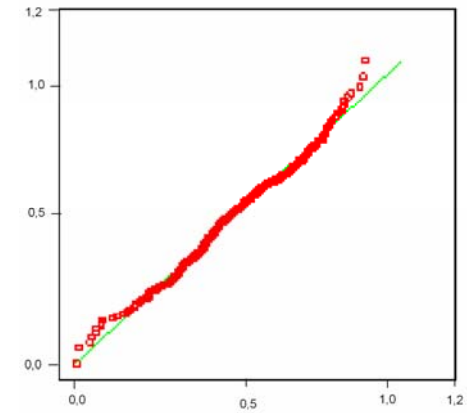	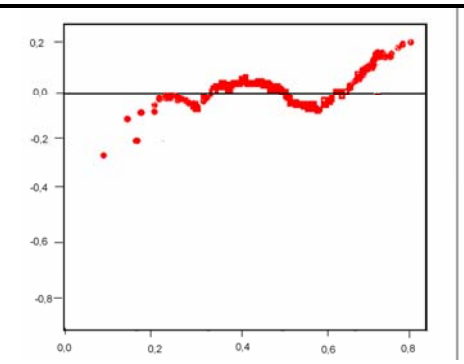

Veg	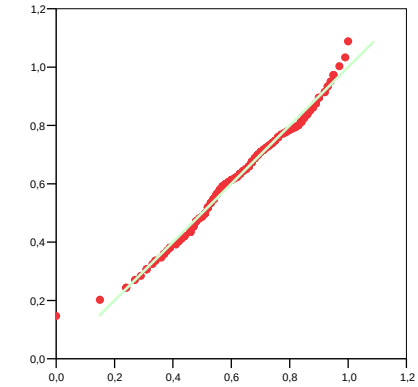	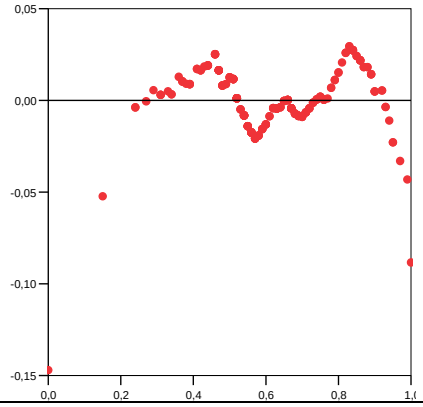
Geo_C	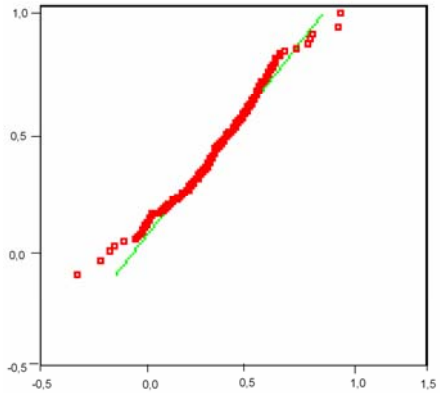	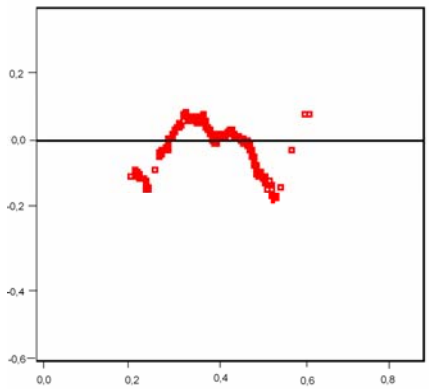
S_BFSWL	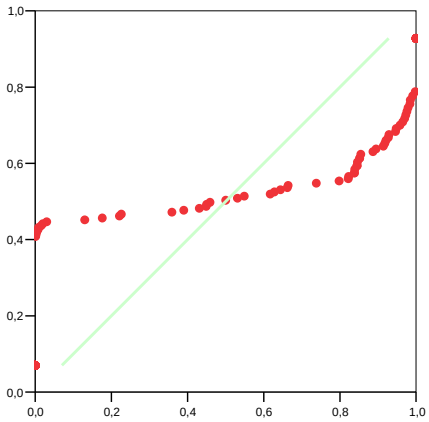	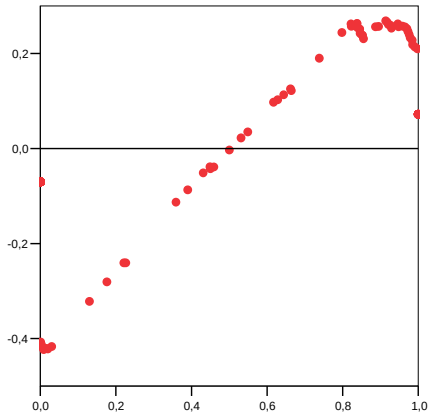
Elev	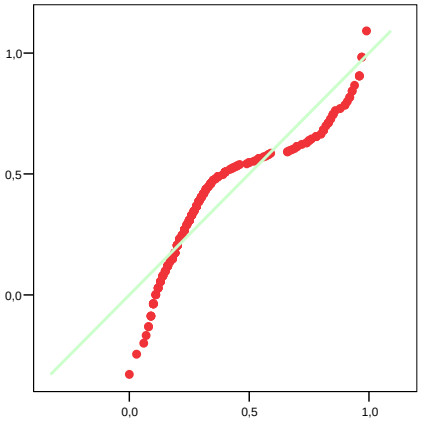	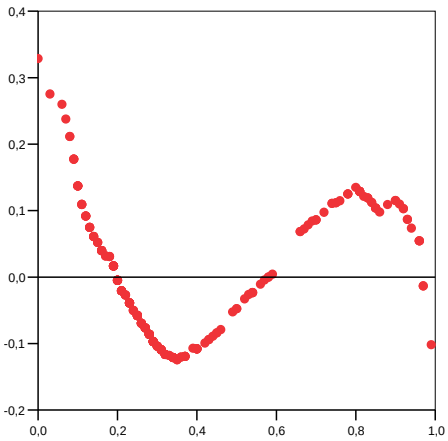

Asp	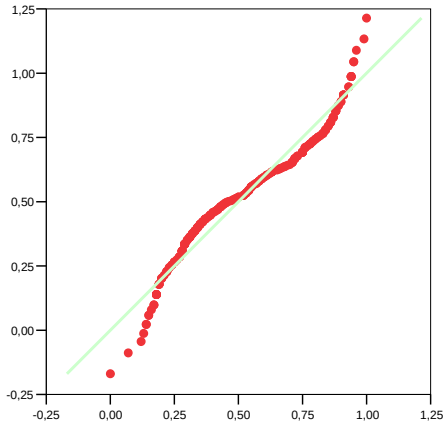	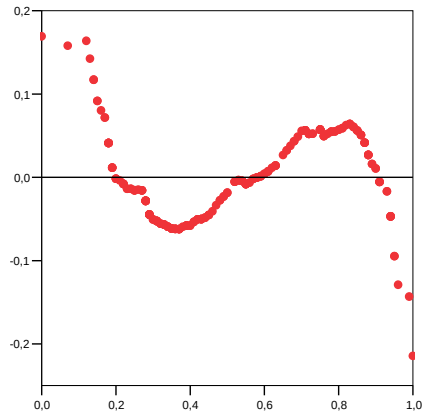
DisttoStrm	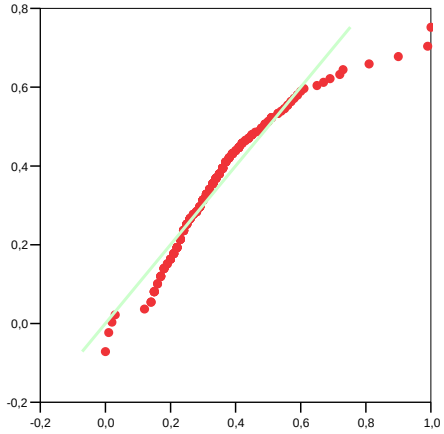	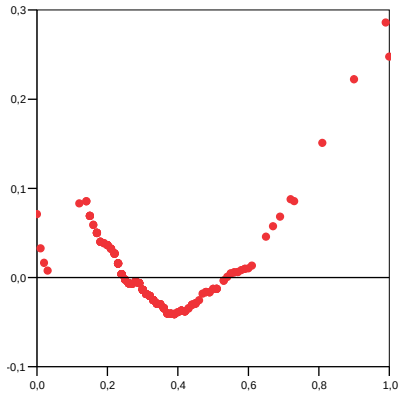
Slp	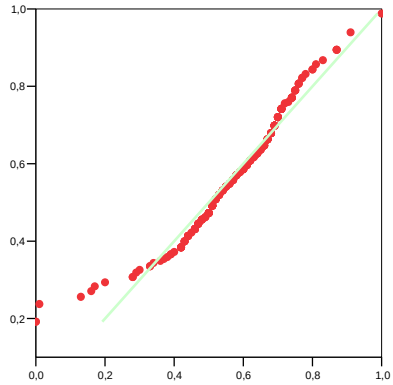	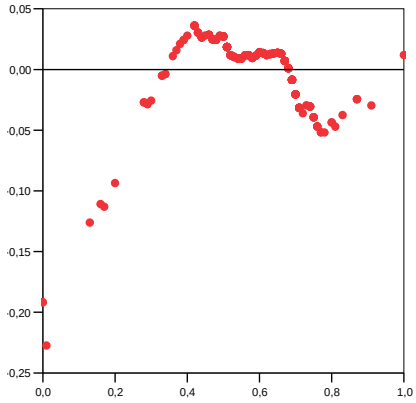
DisttoRoad	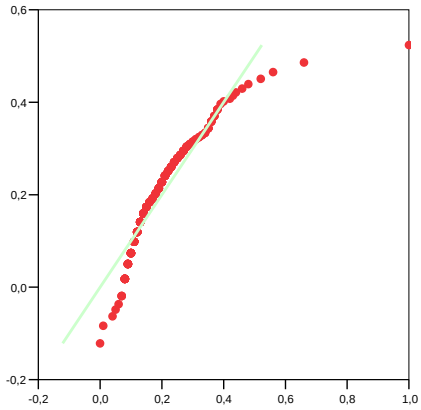	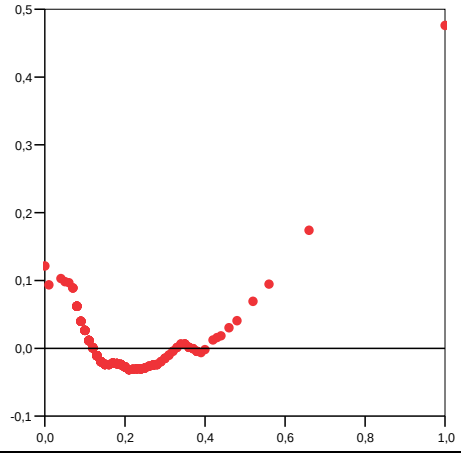

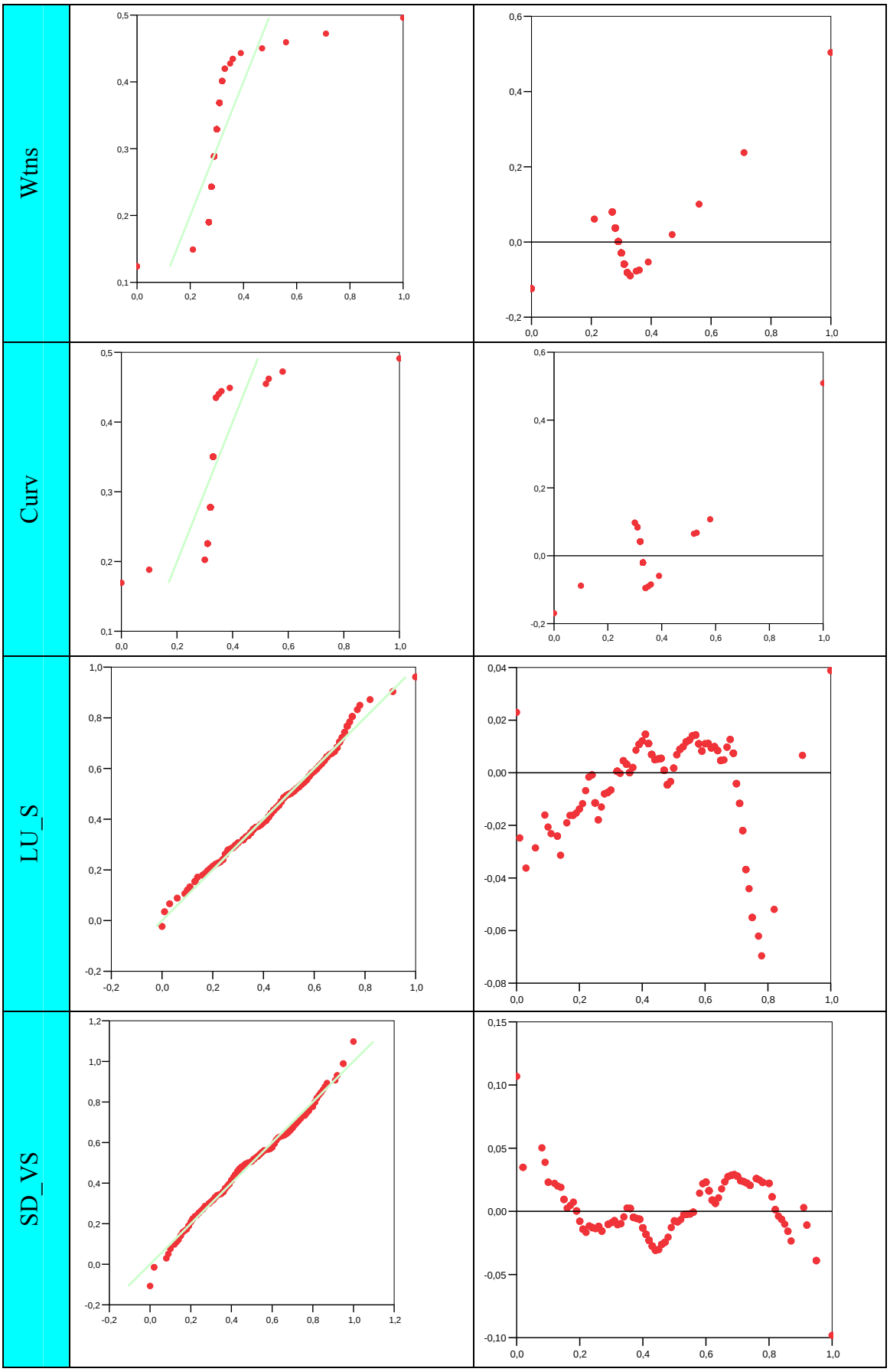
Wtns
Curv
LU_S
SD_VS

APPENDIX B

MAP of GWR PARAMETER DISTRIBUTION

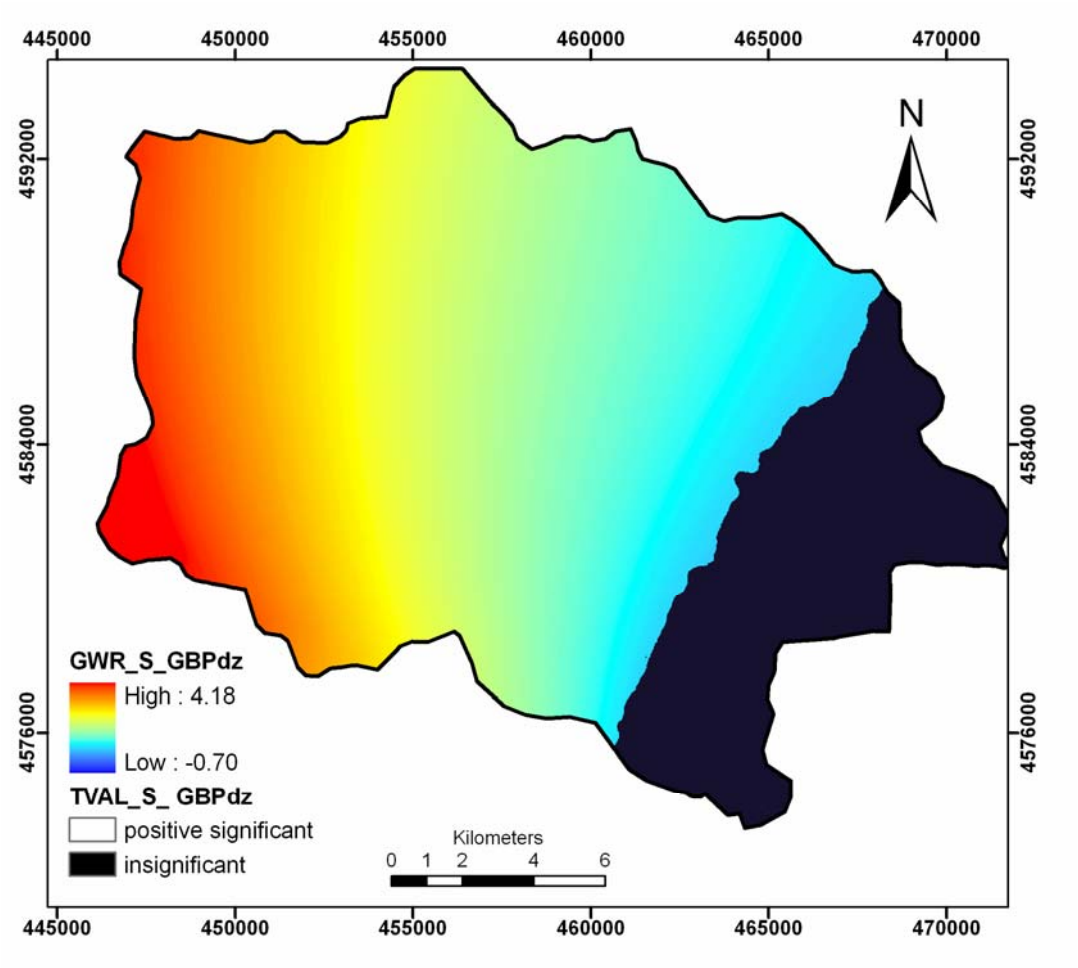

Figure B-1. GWR parameter variation across the study area for Greybrown Podzolic Soil (S_GBPdz) for grid-based mapping unit

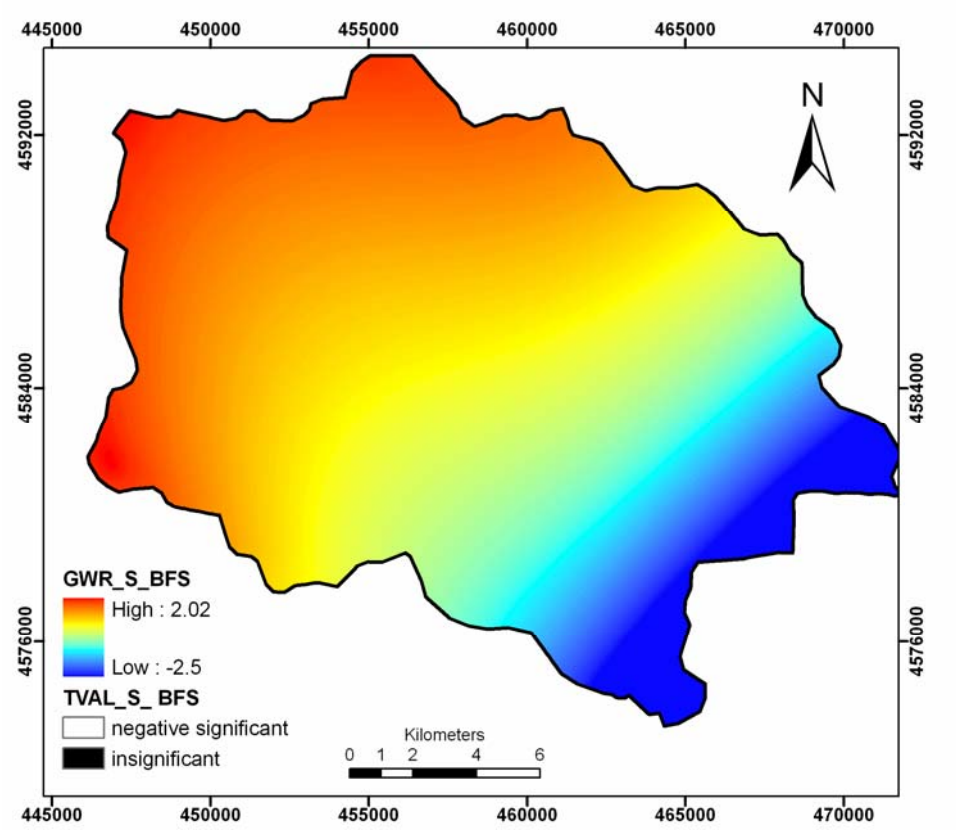

Figure B-2. GWR parameter variation across the study area for Brown Forest Soil (S_BFS) for grid-based mapping unit

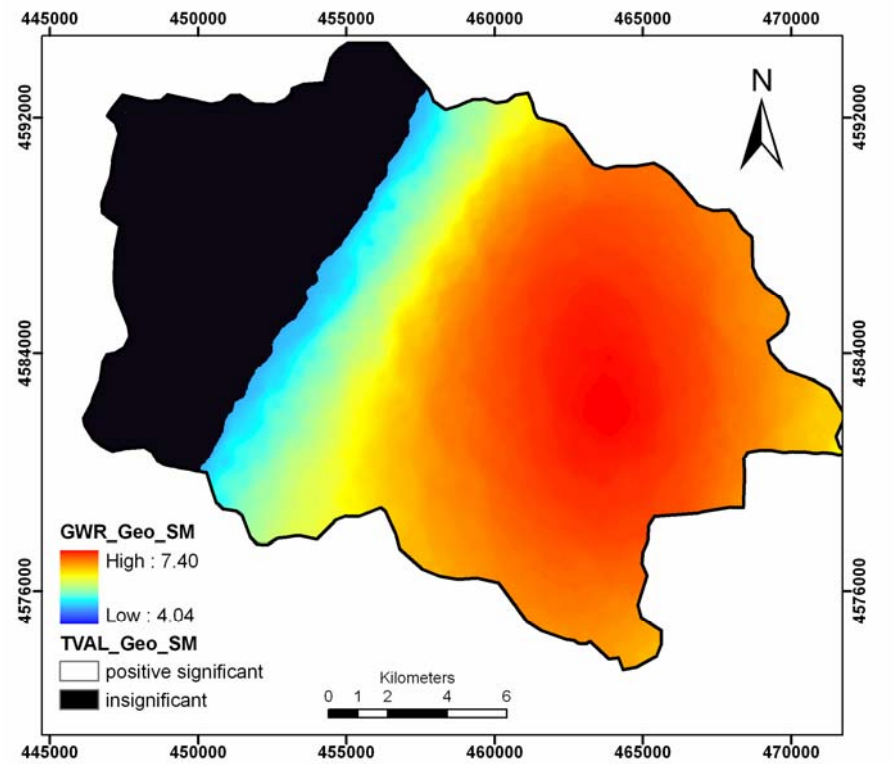

Figure B-3. GWR parameter variation across the study area for Sandstone-Mudstone unit of Geology (Geo_SM) for grid-based mapping unit

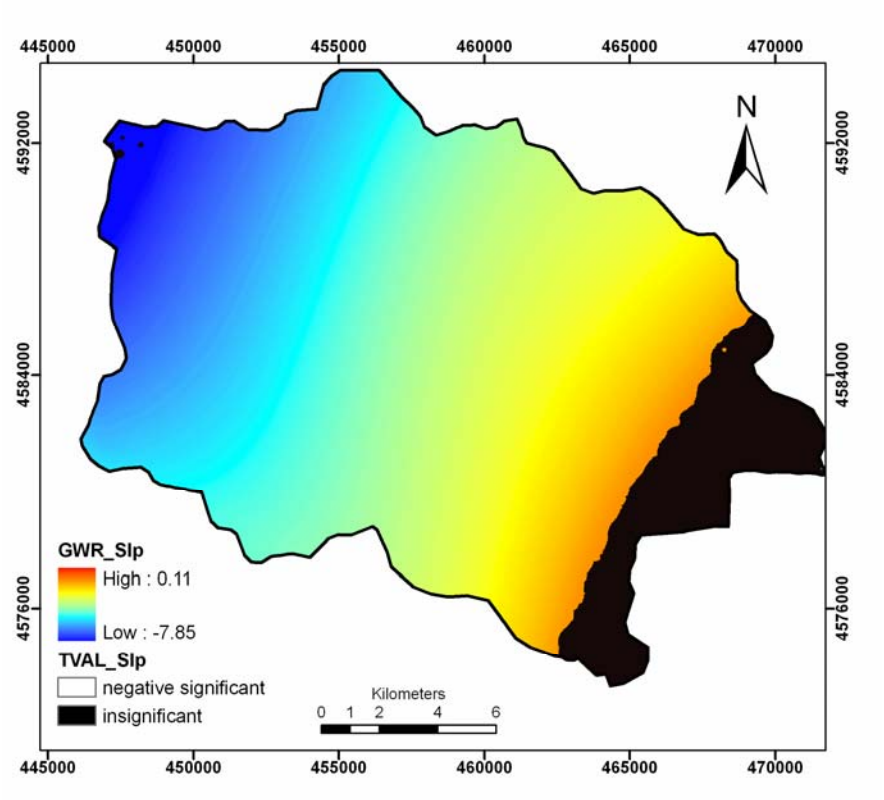

Figure B-4. GWR parameter variation across the study area for Slope (Slp) for grid-based mapping unit

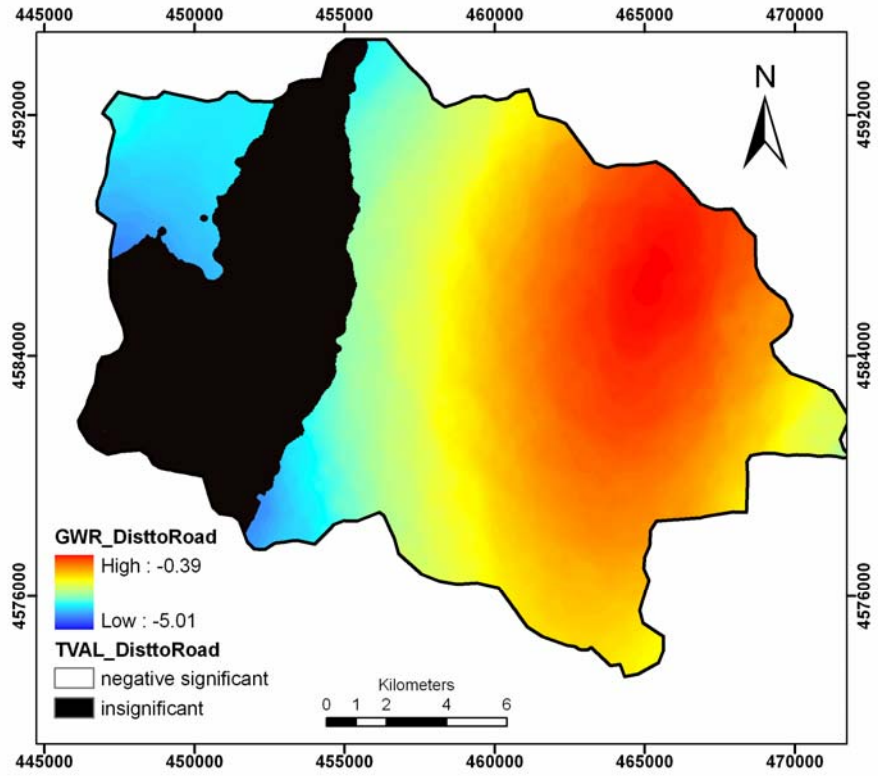

Figure B-5. GWR parameter variation across the study area for Distance to Road (DisttoRoad) for grid-based mapping unit

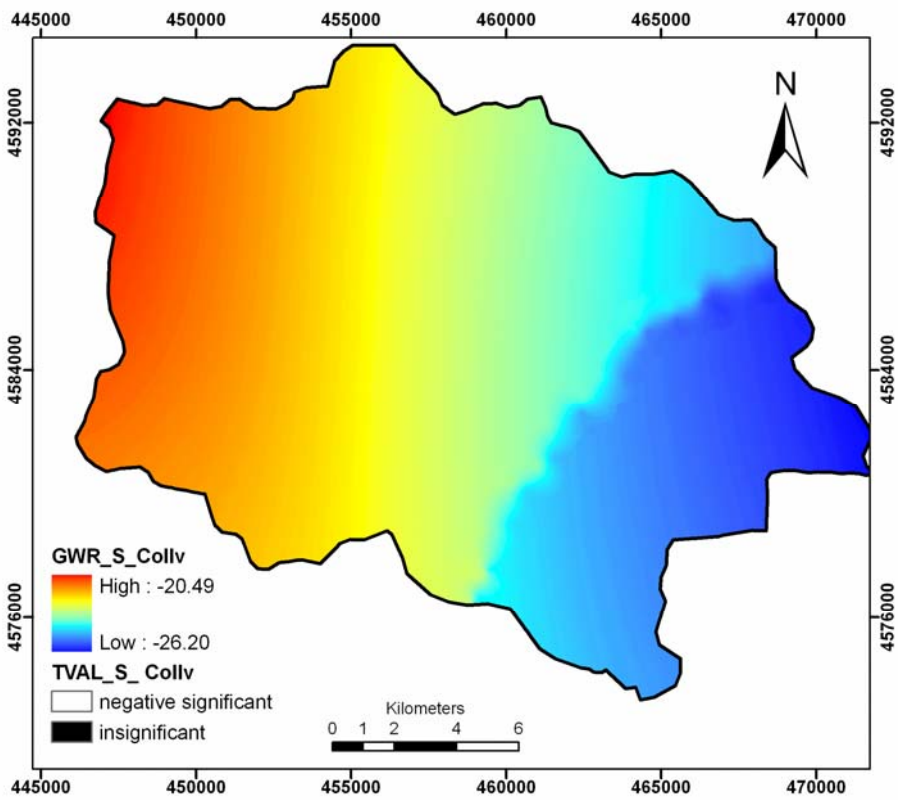

Figure B-6. GWR parameter variation across the study area for Colluvial Soil (S_Colv) for grid-based mapping unit

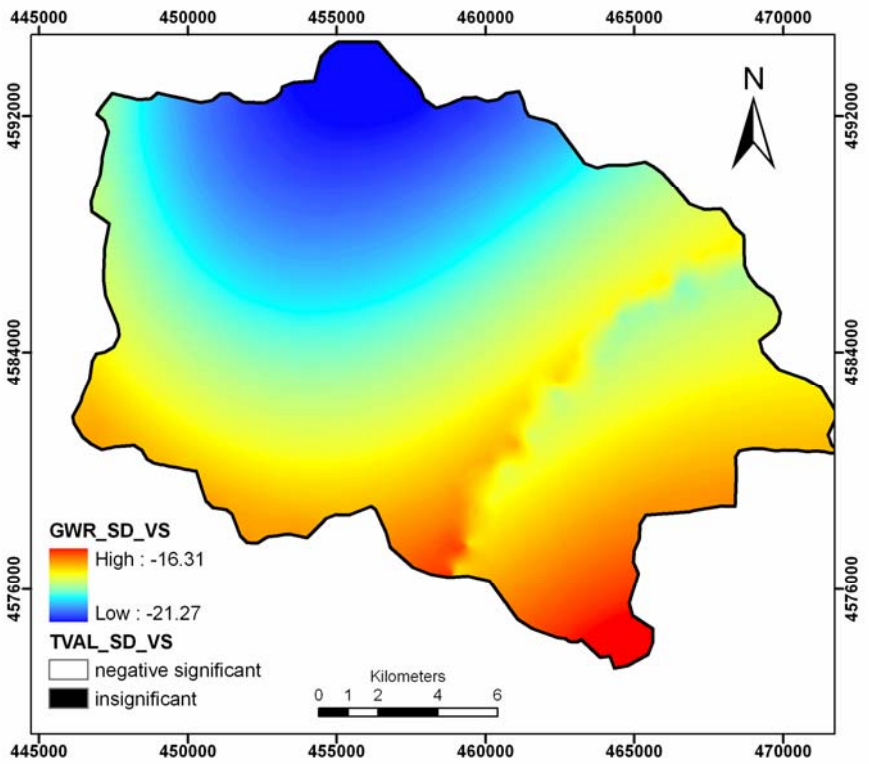

Figure B-7. GWR parameter variation across the study area for very shallow soil depth (SD_VS) for grid-based mapping unit

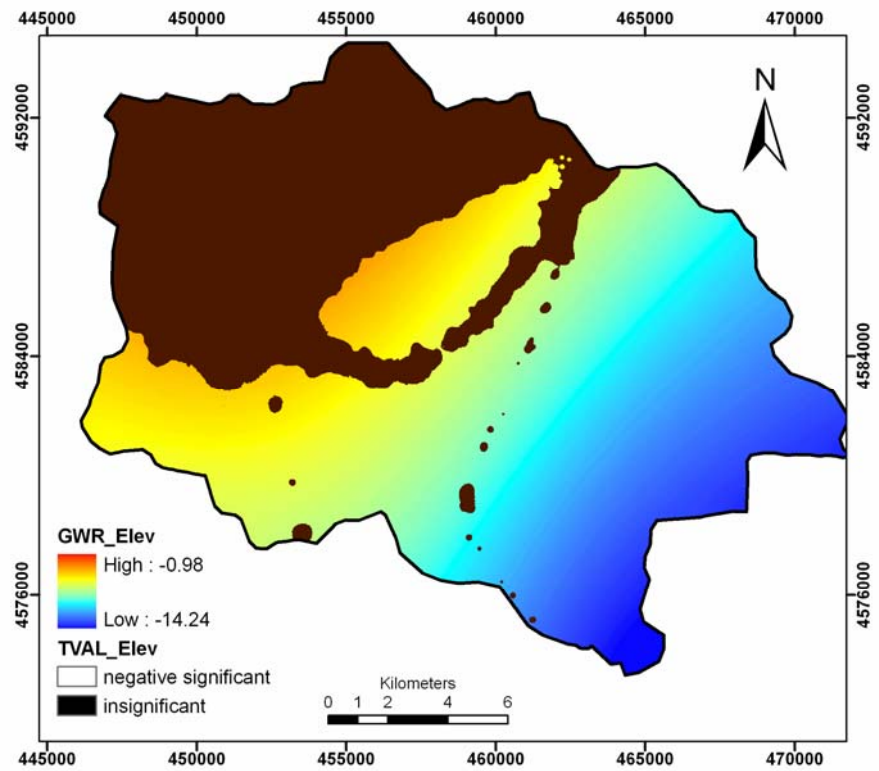

Figure B-8. GWR parameter variation across the study area for Elevation (Elev) for grid-based mapping unit

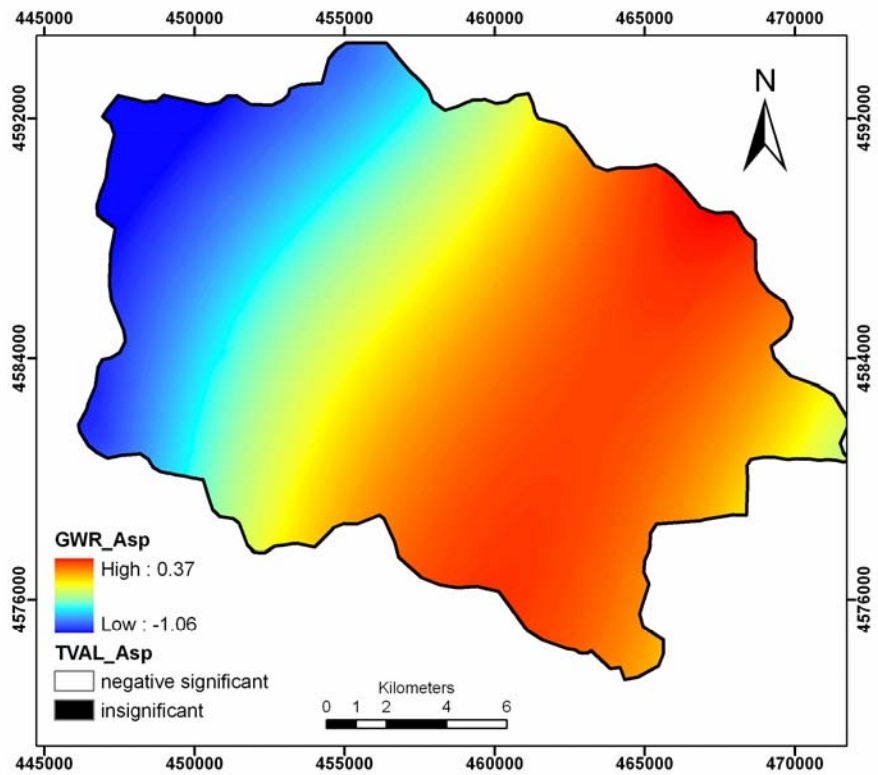

Figure B-9. GWR parameter variation across the study area for Aspect (Asp) for grid-based mapping unit

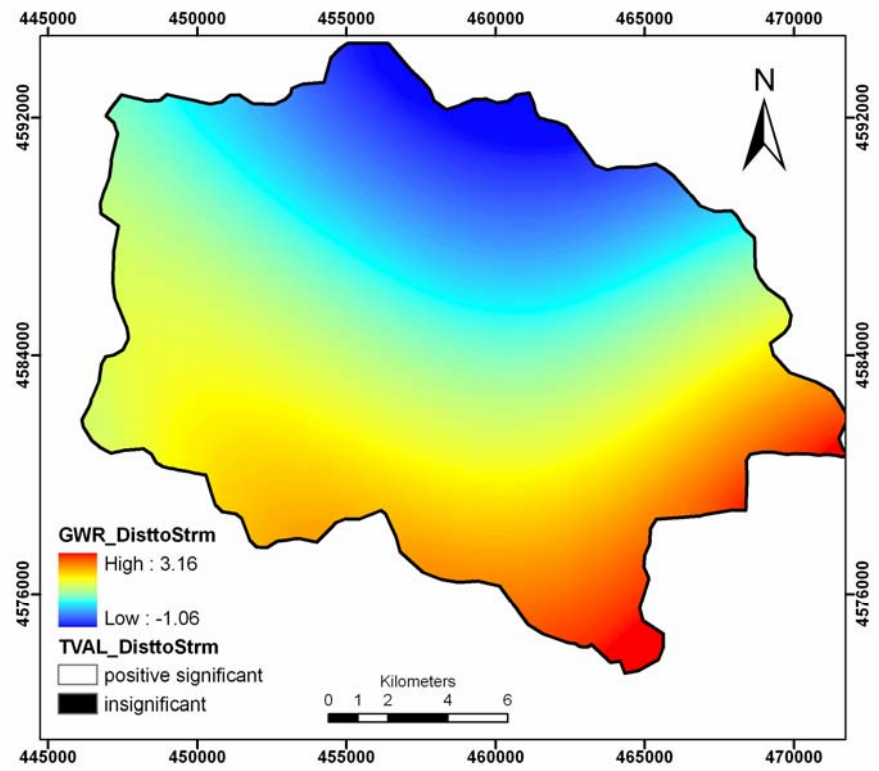

Figure B-10. GWR parameter variation across the study area for Distance to Stream (DisttoStrm) for grid-based mapping unit

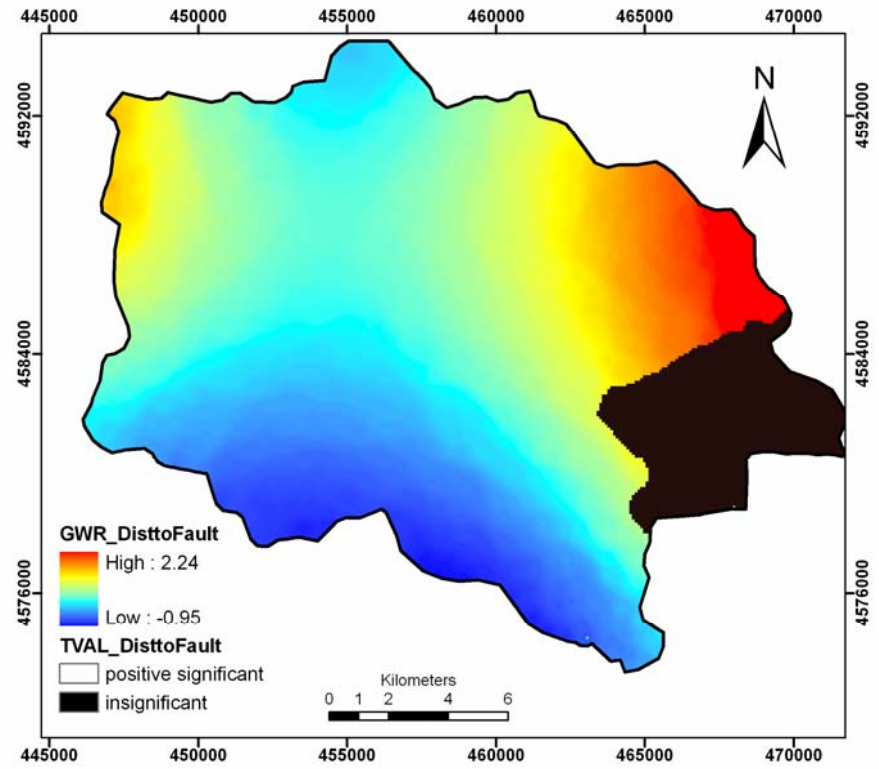

Figure B-11. GWR parameter variation across the study area for Distance to Fault (DisttoFault) for grid-based mapping unit

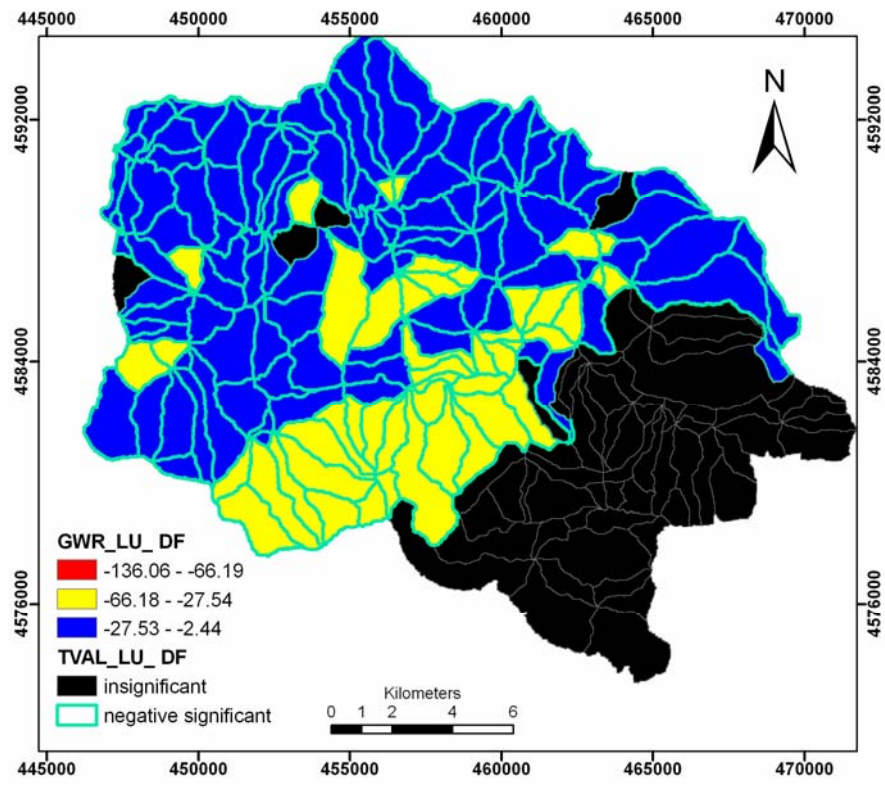

Figure B-12. GWR parameter variation across the study area for Land use Dry Farming (LU_DF) for slope unit-based mapping unit

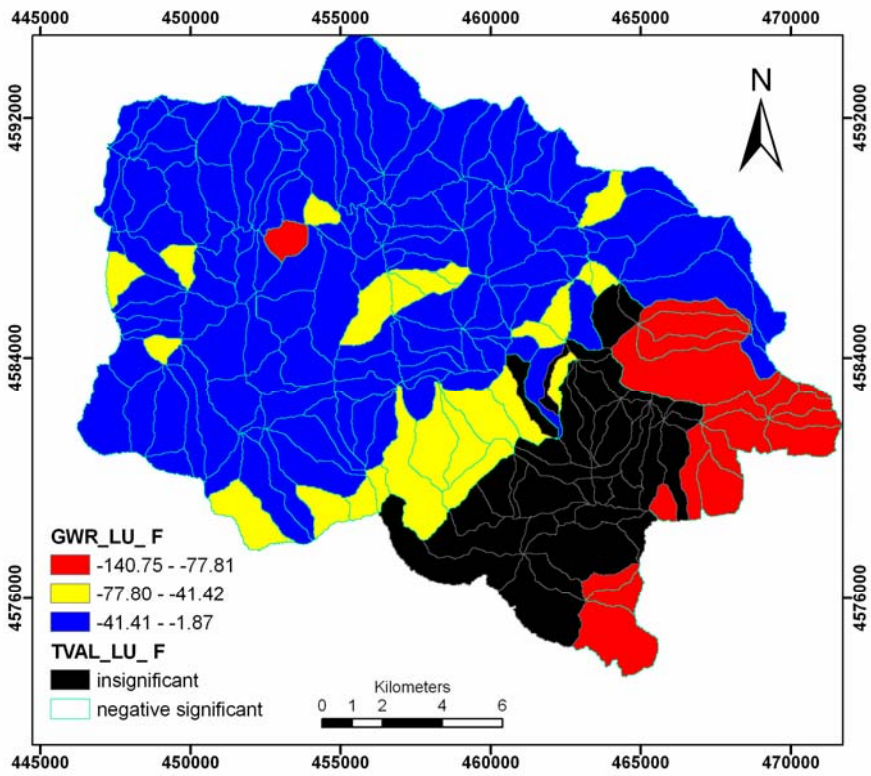

Figure B-13. GWR parameter variation across the study area for Forest (LU_F) for slope unit-based mapping unit

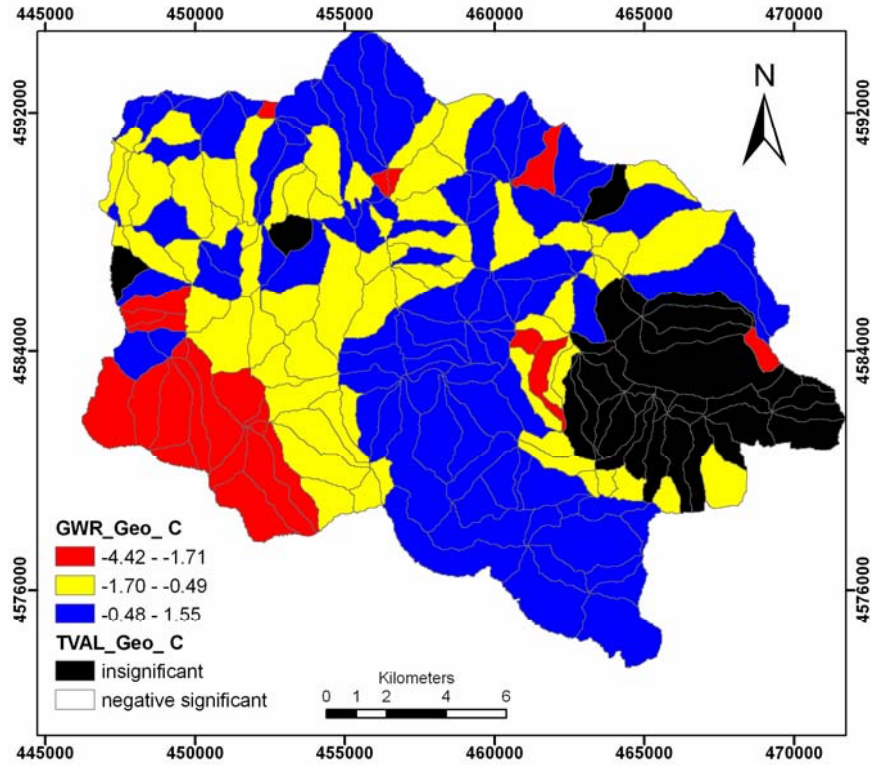

Figure B-14. GWR parameter variation across the study area for the Conglomerate unit of Geology (Geo_C) for slope unit-based mapping unit

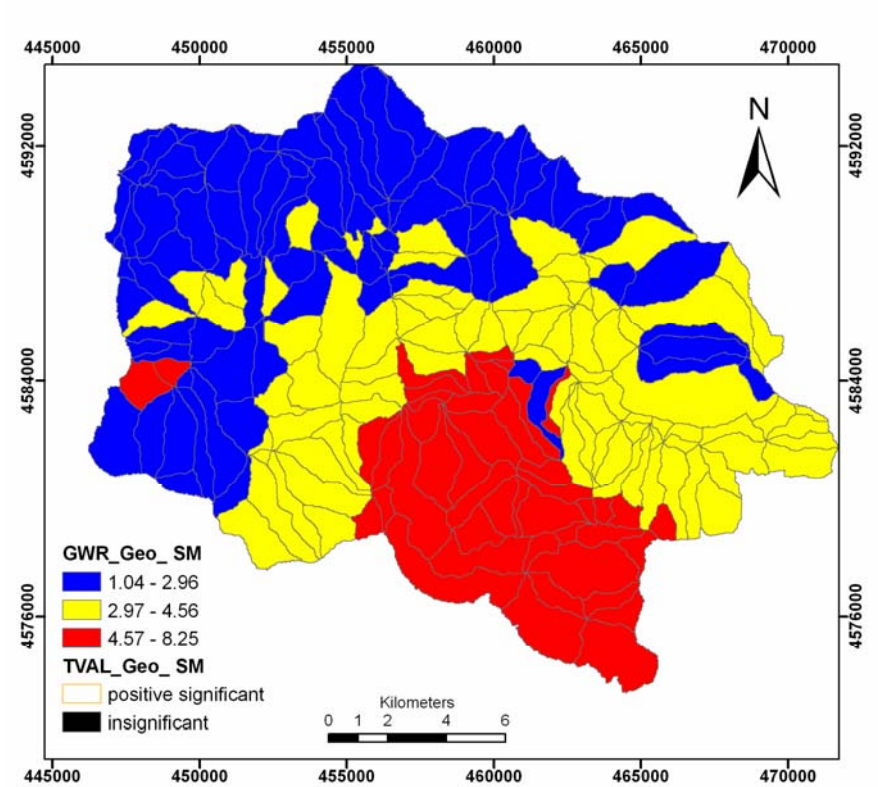

Figure B-15. GWR parameter variation across the study area for the Sandstone Mudstone unit of geology (Geo_SM) for slope unit-based mapping unit

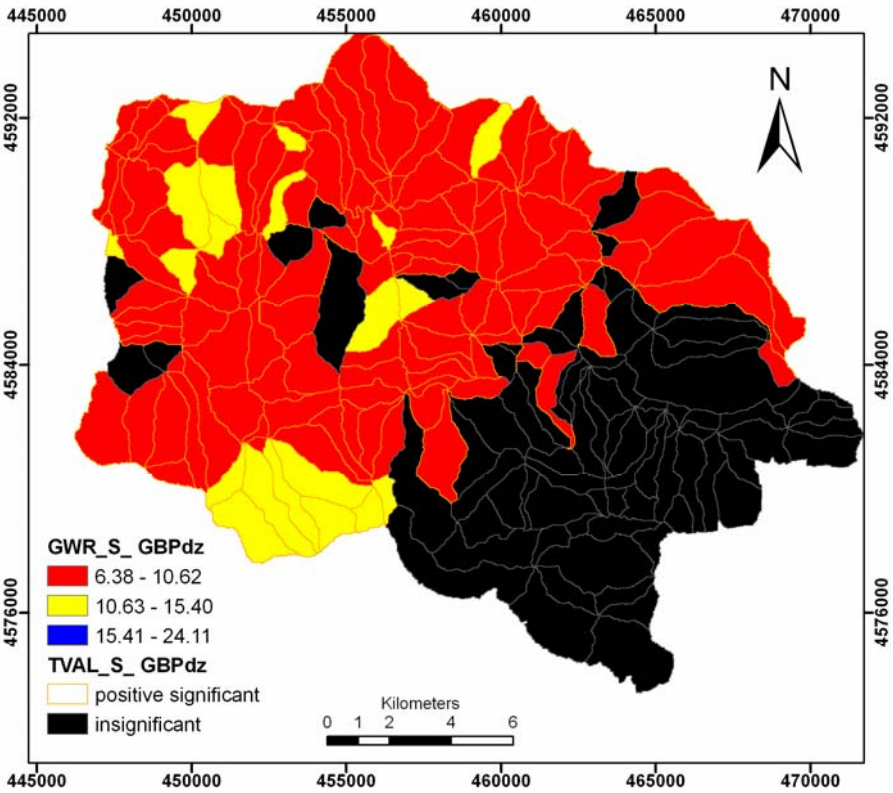

Figure B-16. GWR parameter variation across the study area for the Grey brown podzolic soil (S_GBPdz) for slope unit-based mapping unit

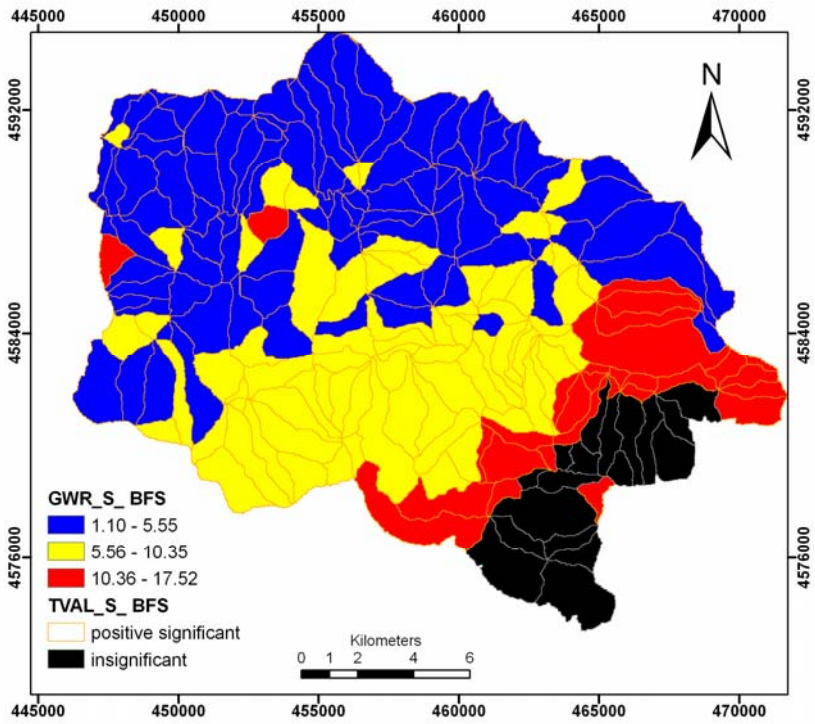

Figure B-17. GWR parameter variation across the study area for the brown forest soil (S_BFS) for slope unit-based mapping unit

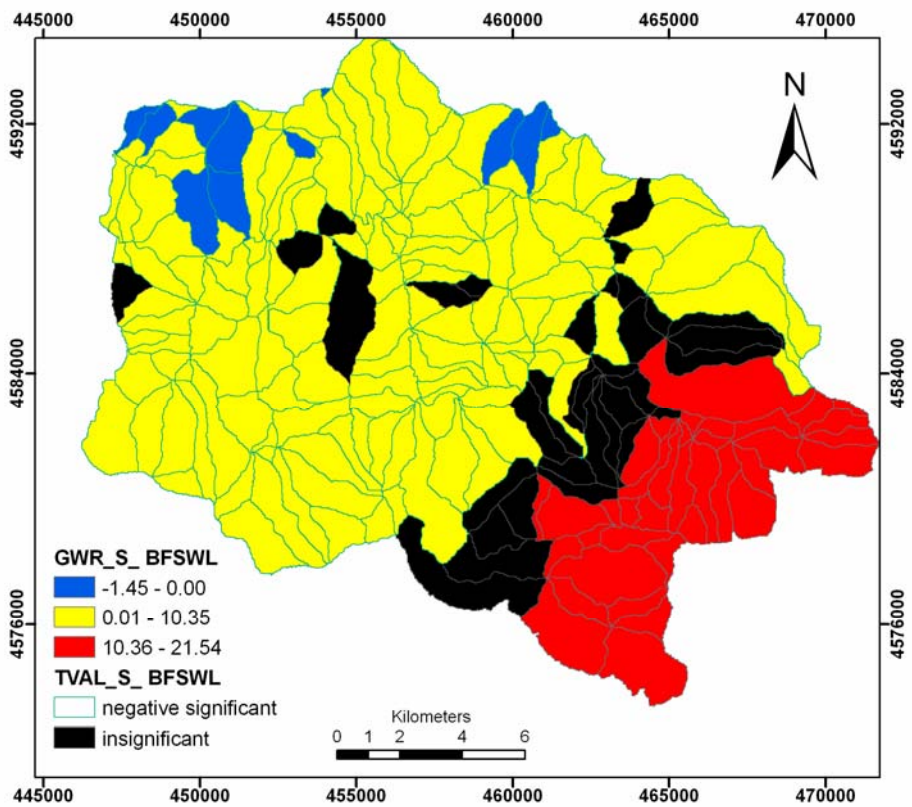

Figure B-18. GWR parameter variation across the study area for the brown forest soil without lime (S_BFSWL) for slope unit-based mapping unit

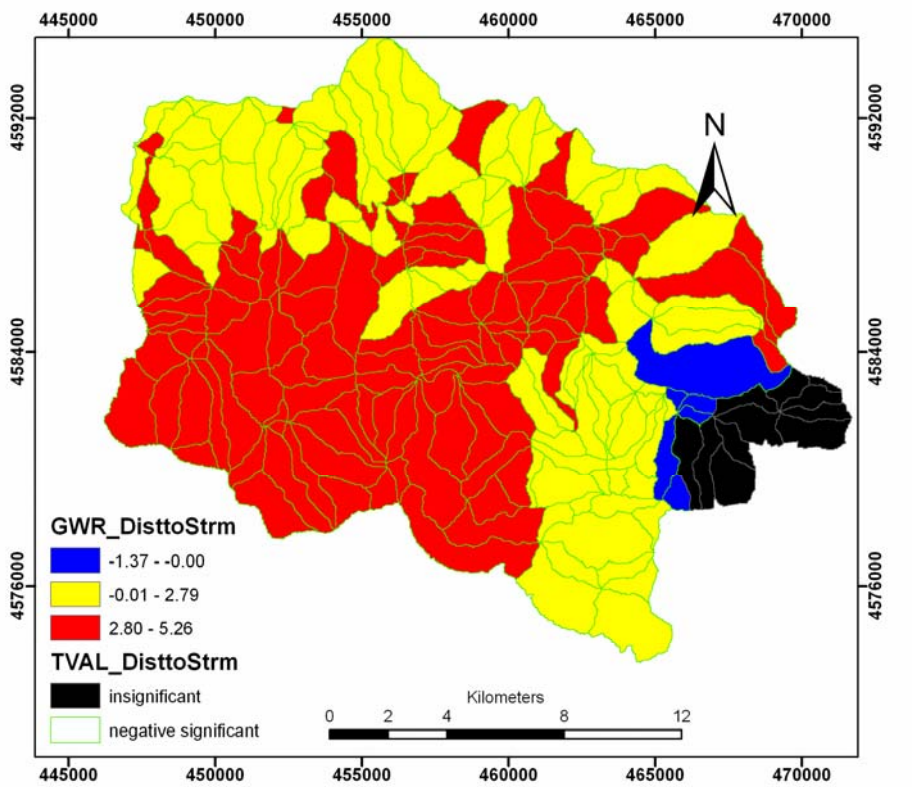

Figure B-19. GWR parameter variation across the study area for the distance to stream network (DisttoStrm) for slope unit-based mapping unit

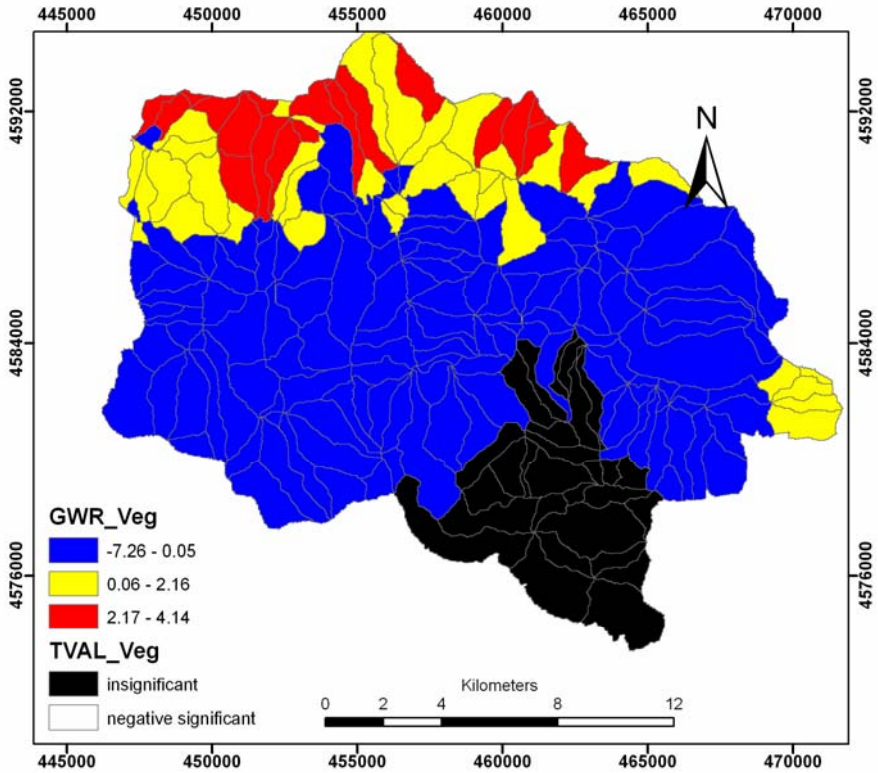

Figure B-20. GWR parameter variation across the study area for the distance to vegetation (Veg) for slope unit-based mapping unit

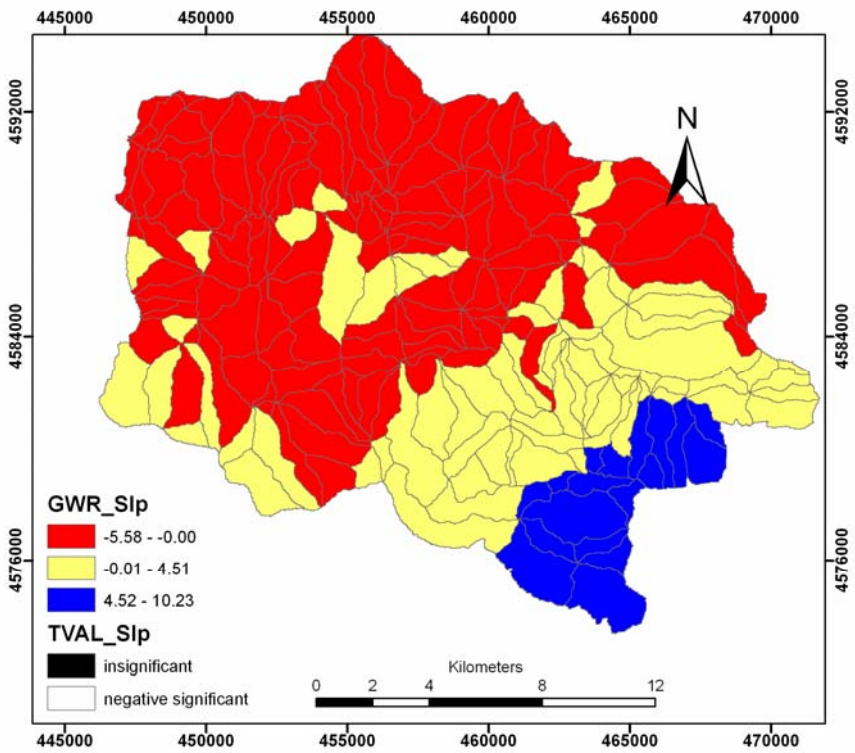

Figure B-21. GWR parameter variation across the study area for the distance to Slope (Slp) for slope unit-based mapping unit

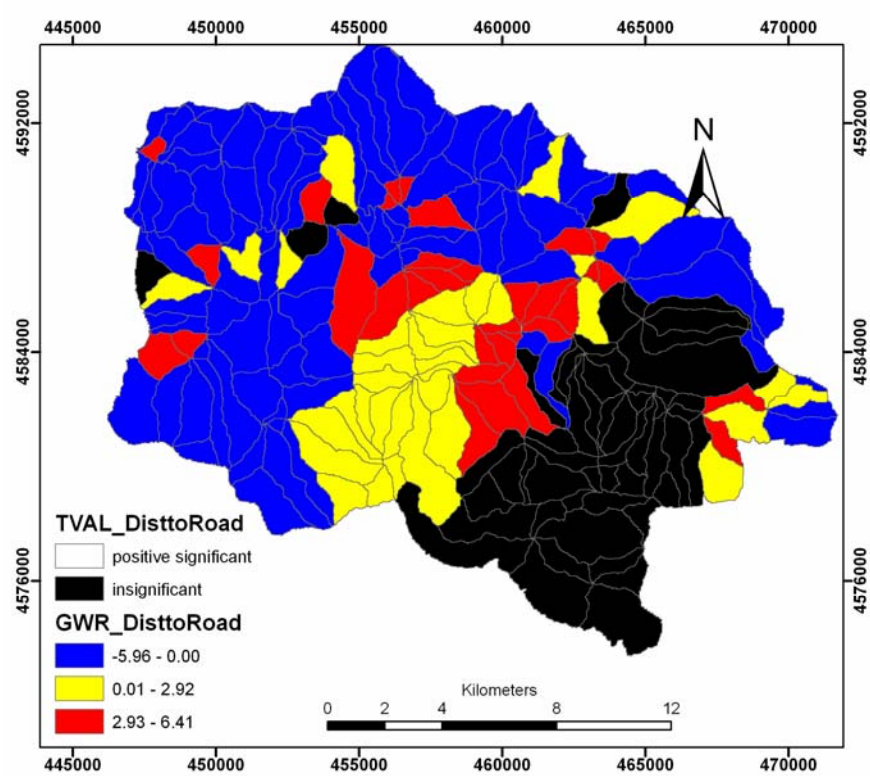

Figure B-22. GWR parameter variation across the study area for the distance to distance to road network (DisttoRoad) for slope unit-based mapping unit

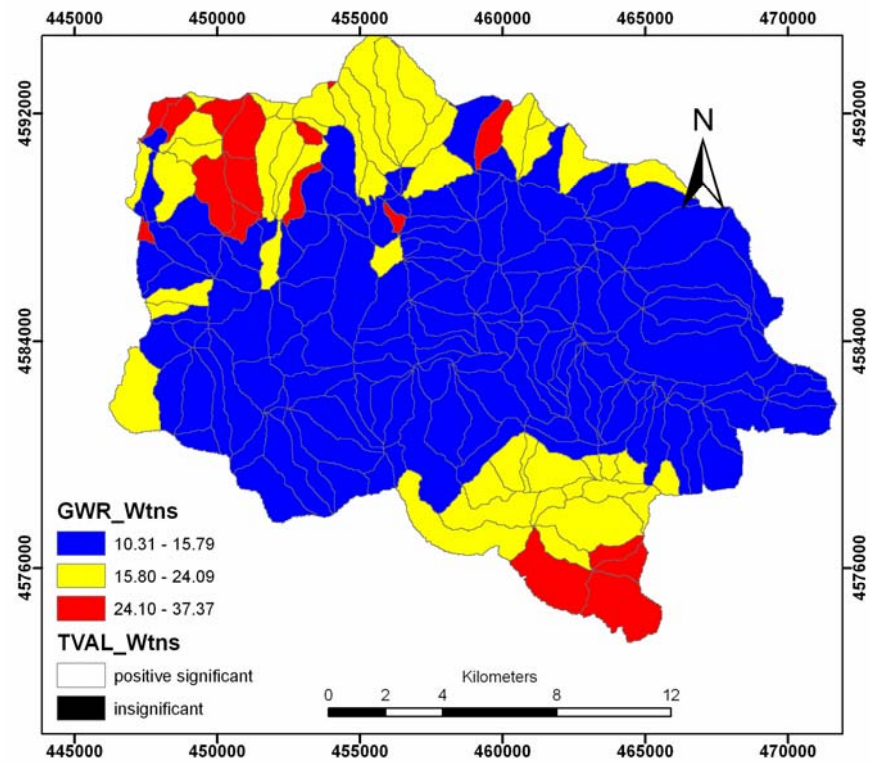

Figure B-23. GWR parameter variation across the study area for the distance to topographic wetness index (Wtns) for slope unit-based mapping unit

APPENDIX C

THE SPATIAL DISTRIBUTION OF SIMILARITY AND DISSIMILARITY BETWEEN SUSCEPTIBILITY MAPS

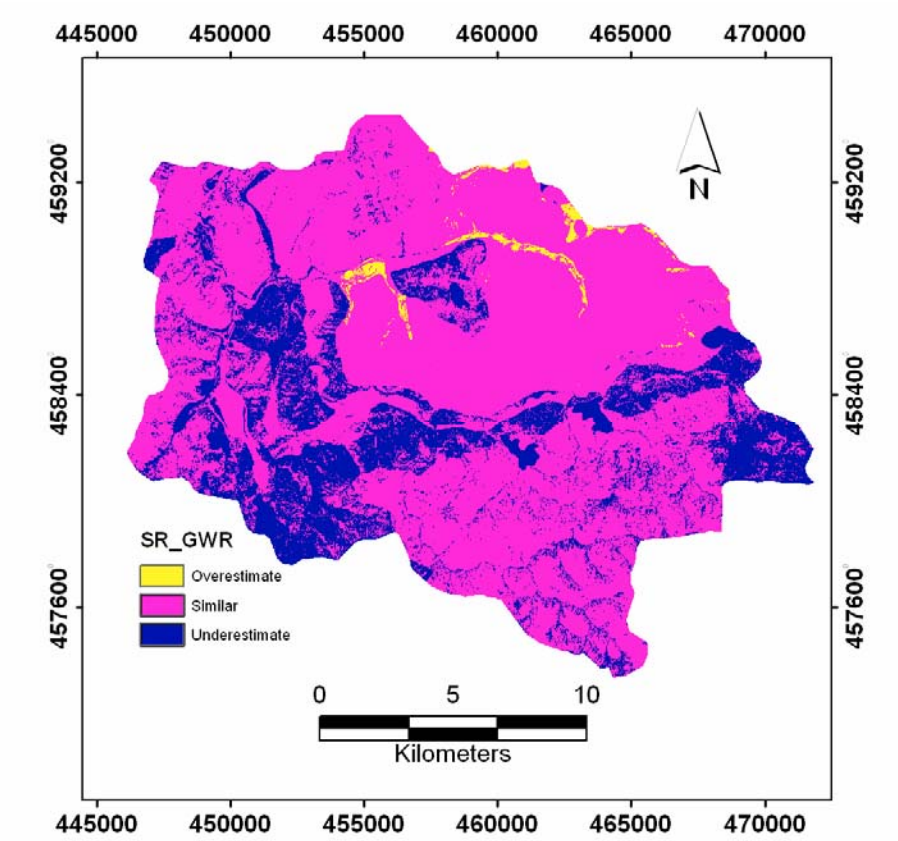

Figure C-1. Map similarity computed for SR_GWR for grid-based mapping unit

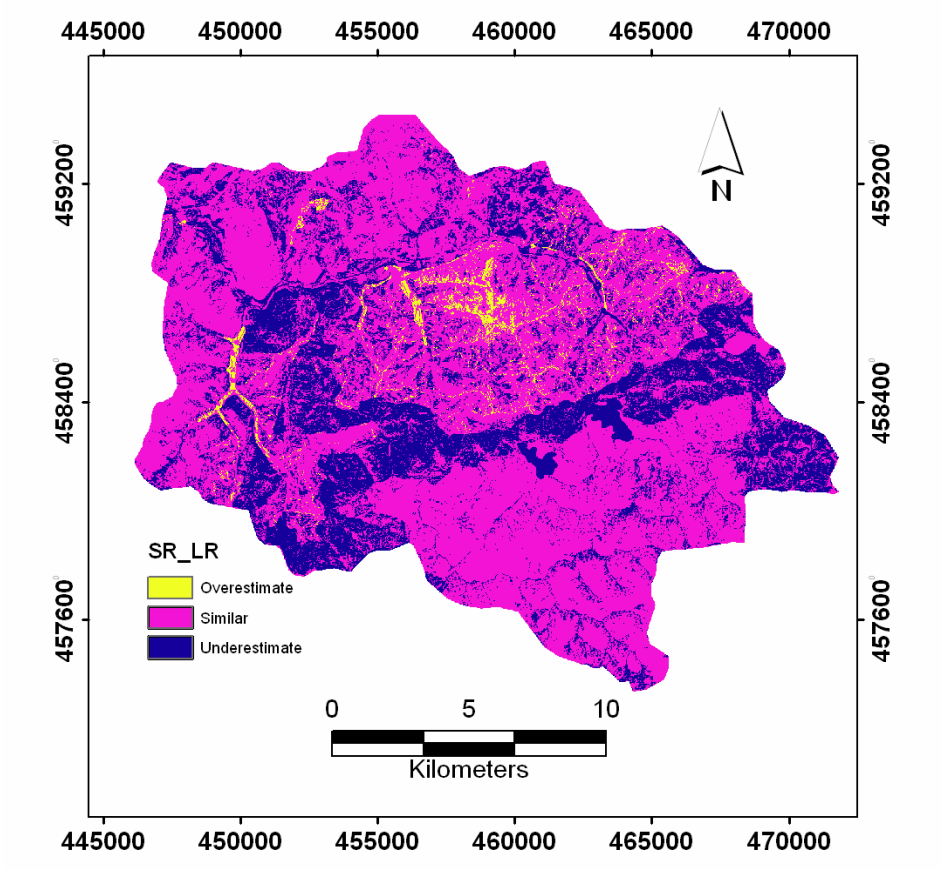

Figure C-2. Map similarity computed for SR_LR for grid-based mapping unit

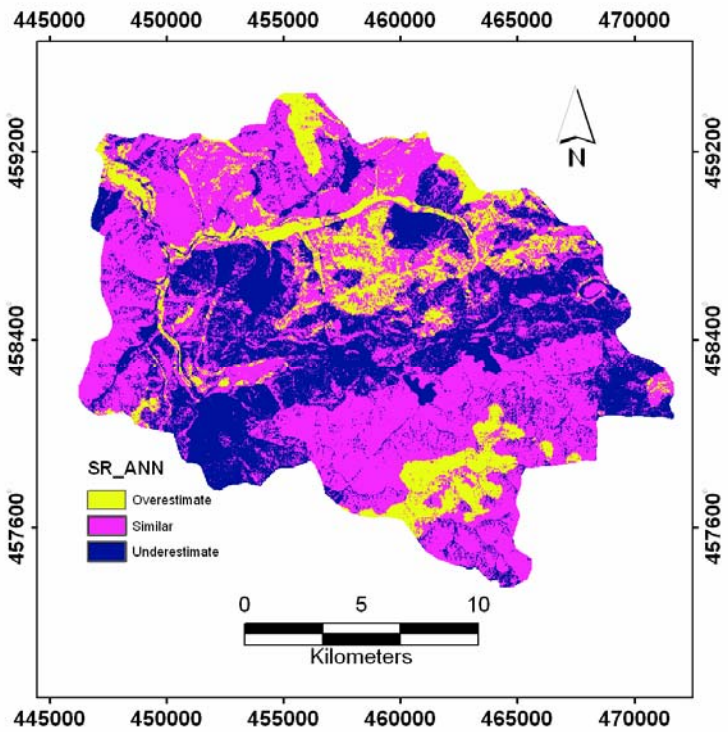

Figure C-3. Map similarity computed for SR_ANN for grid-based mapping unit

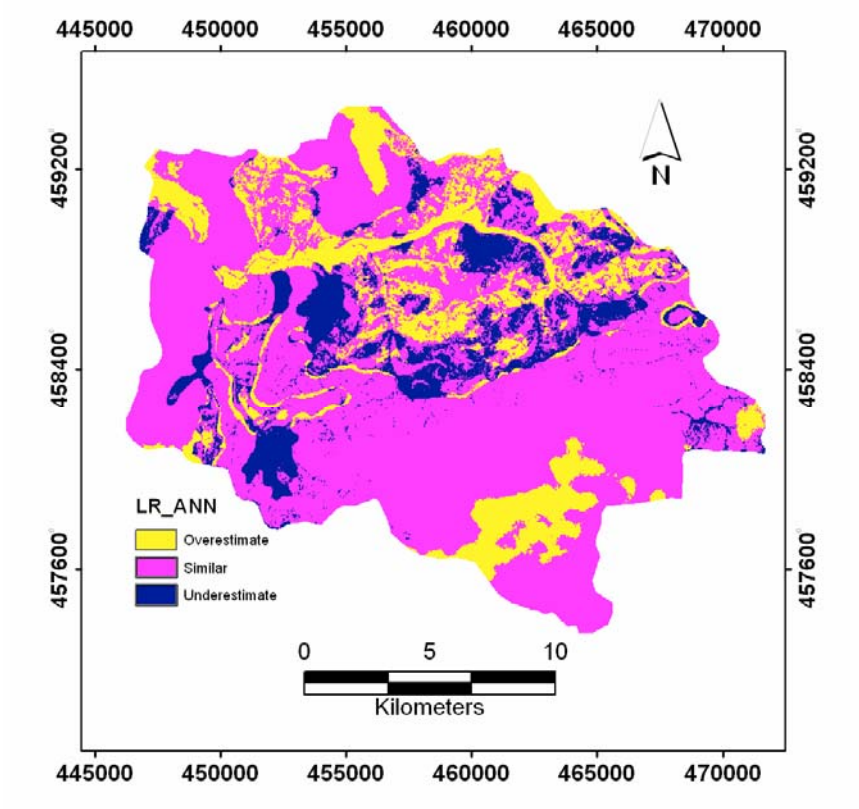

Figure C-4. Map similarity computed for LR_ANN for grid-based mapping unit

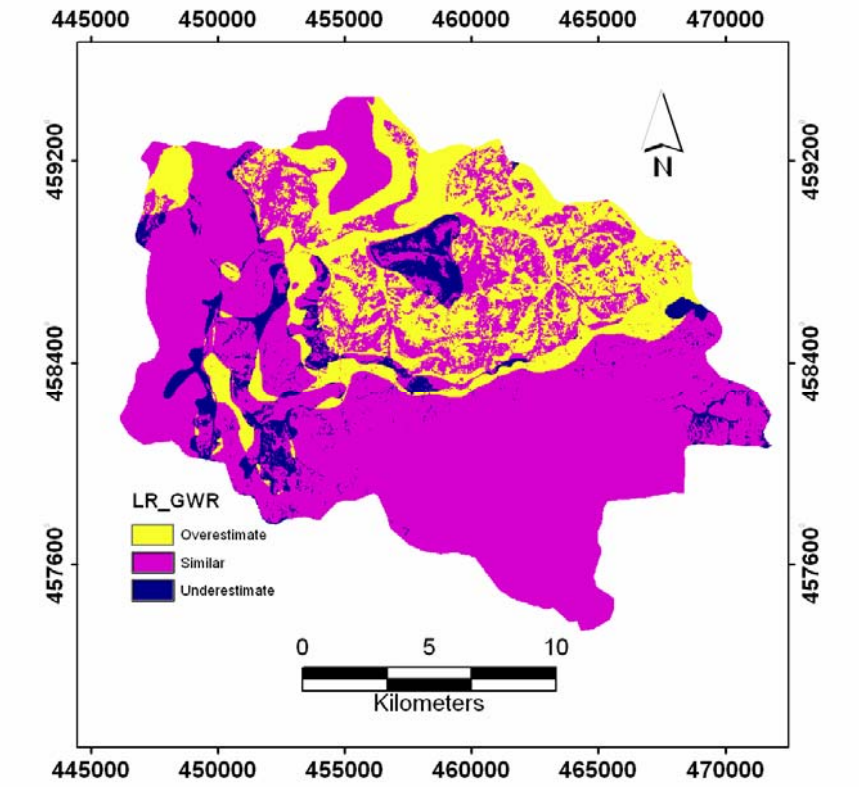

Figure C-5. Map similarity computed for LR_GWR for grid-based mapping unit

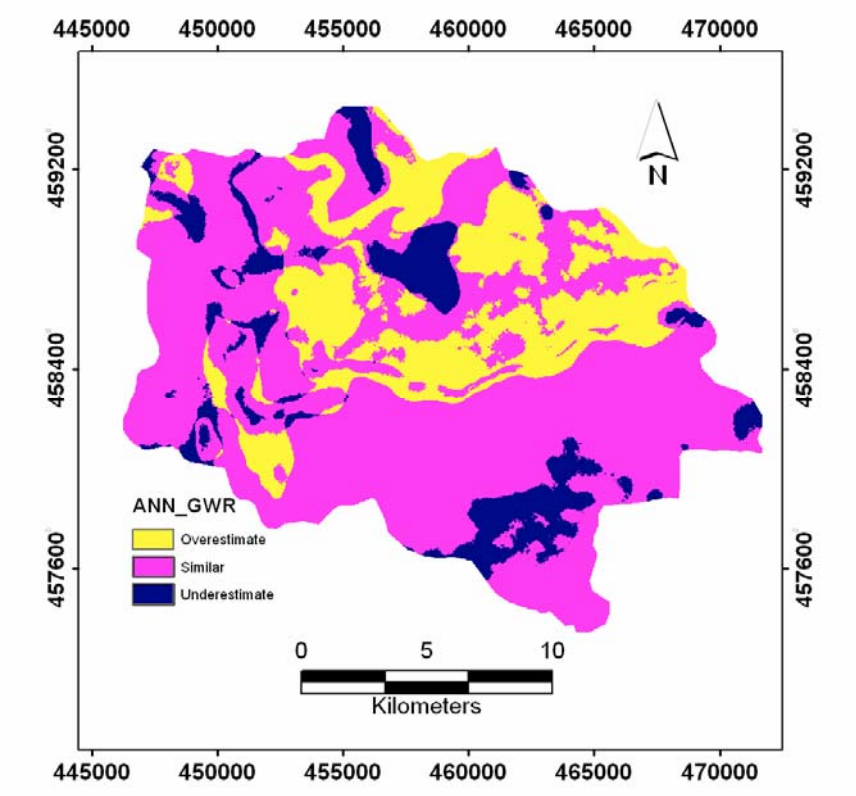

Figure C-6. Map similarity computed for ANN_GWR for grid-based mapping unit

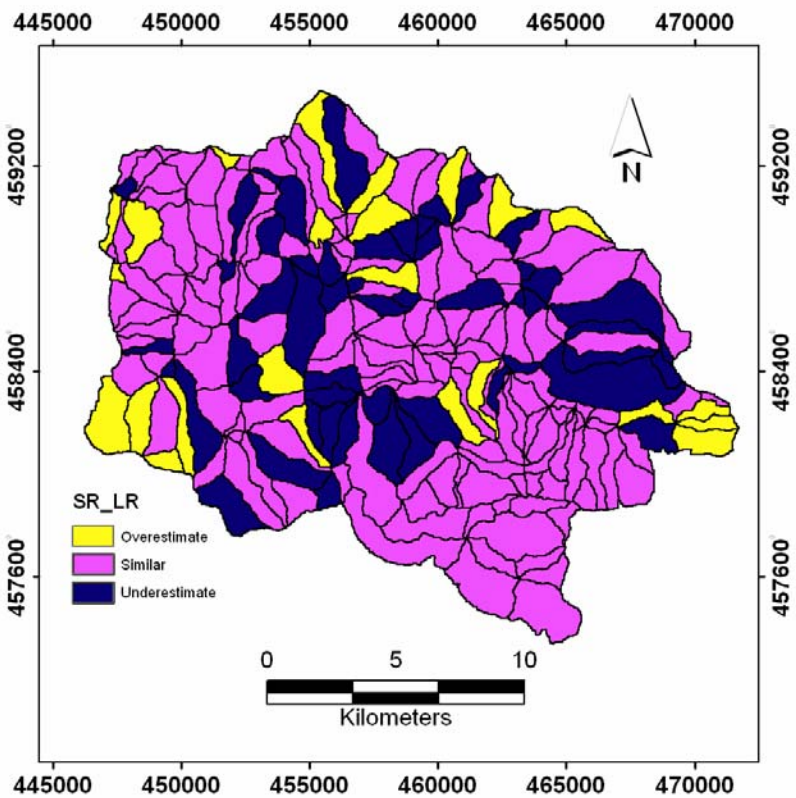

Figure C-7. Map similarity computed for SR_LR slope unit-based mapping unit.

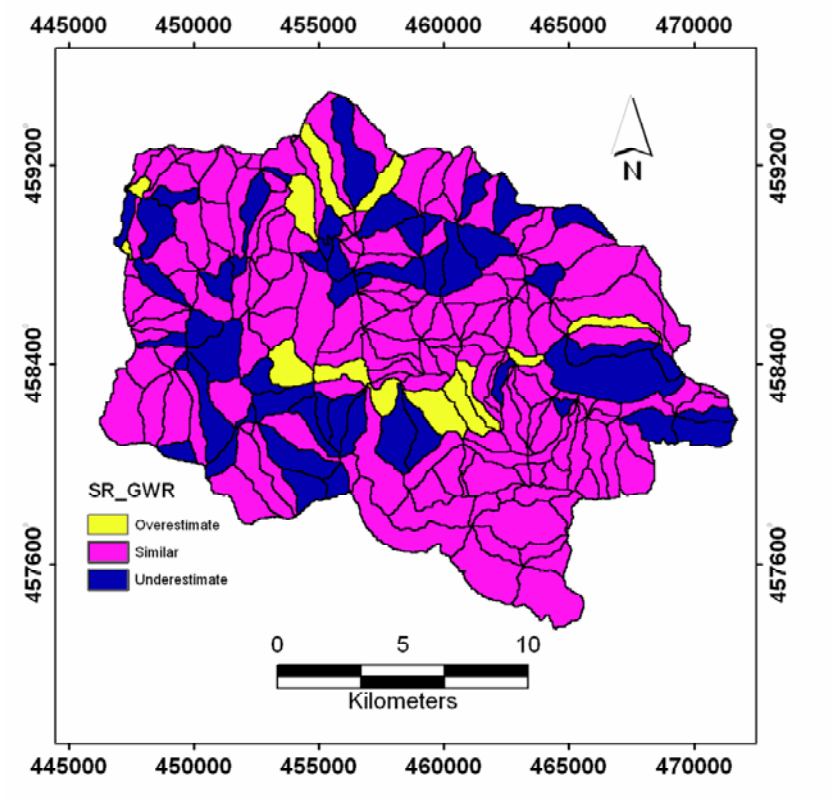

Figure C-8. Map similarity computed for SR_GWR slope unit-based mapping unit.

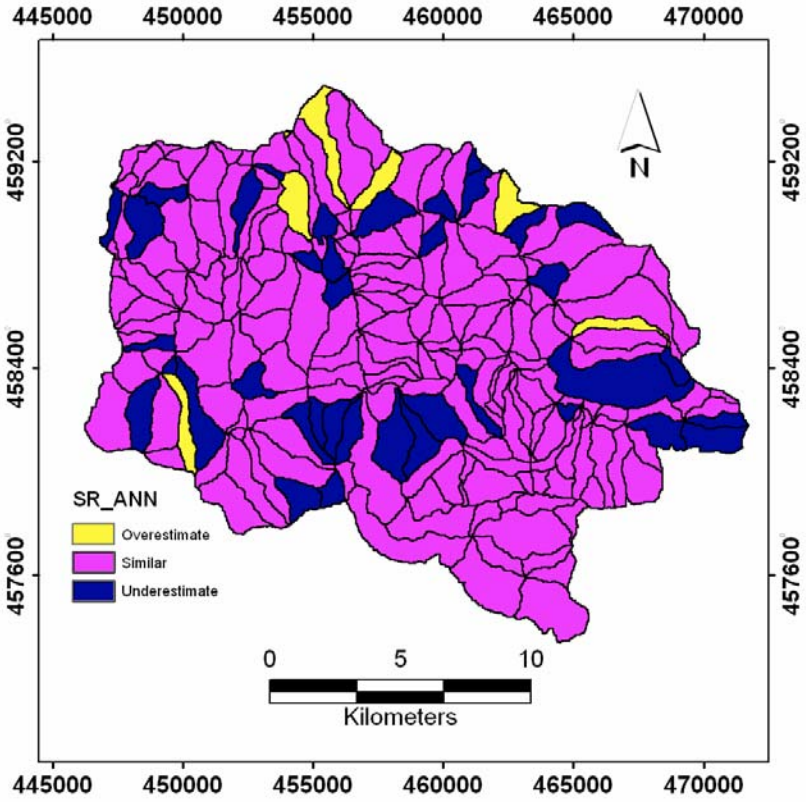

Figure C-9. Map similarity computed for SR_ANN slope unit-based mapping unit.

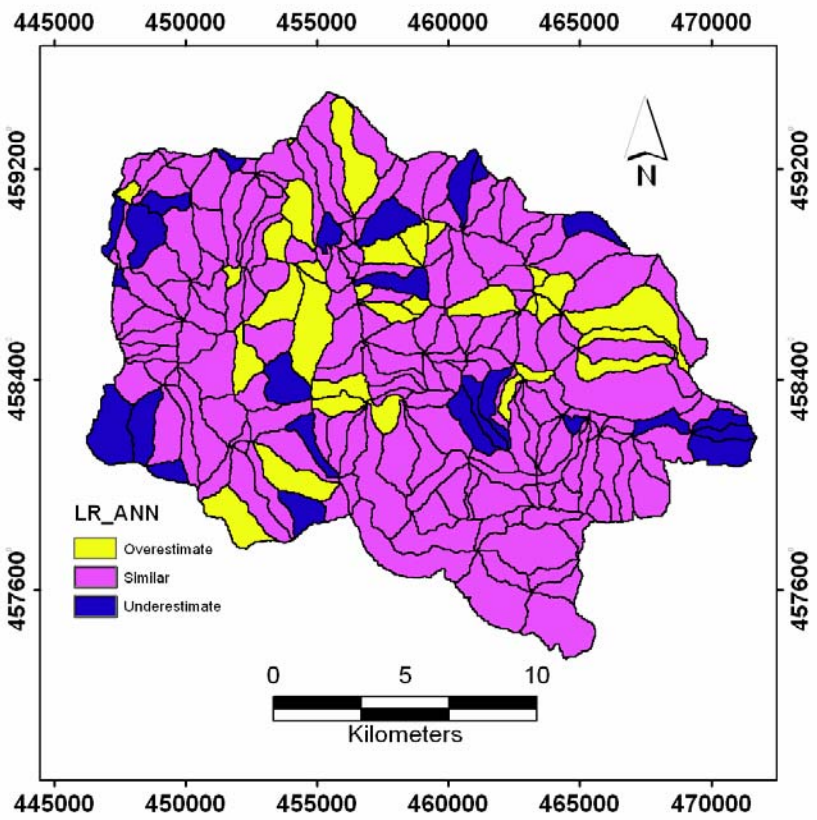

Figure C-10. Map similarity computed for LR_ANN slope unit-based mapping unit.

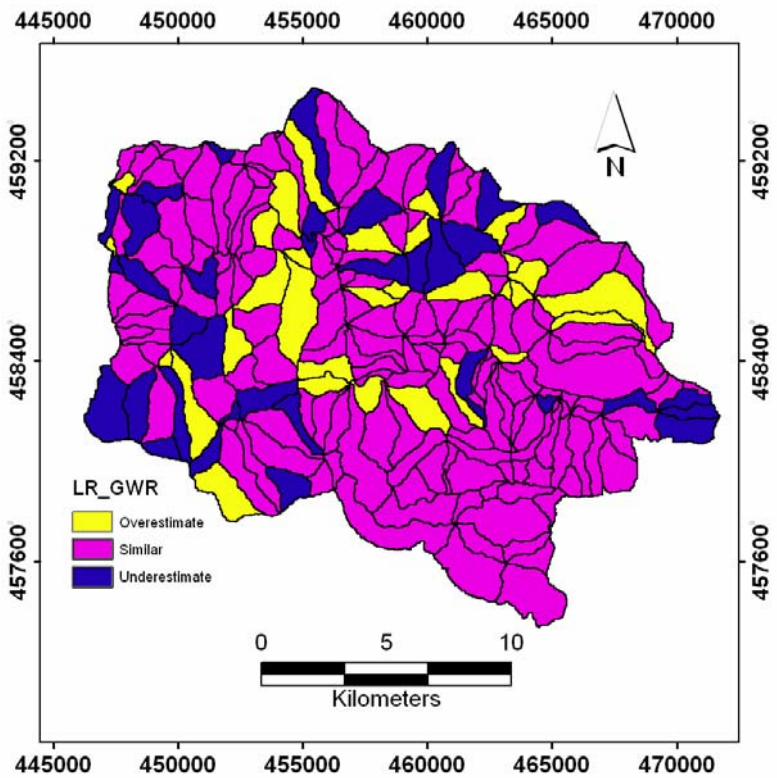

Figure C-11. Map similarity computed for LR_GWR slope unit-based mapping unit.

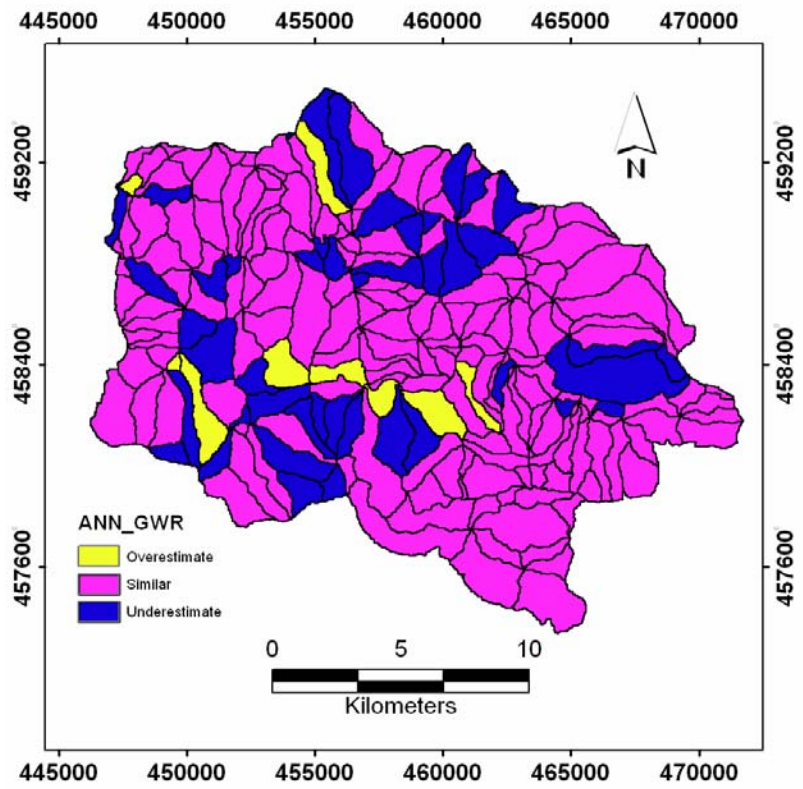

Figure C-12. Map similarity computed for ANN_GWR slope unit-based mapping unit.

APPENDIX D

RISK MAPS CREATED FOR REGIONAL SCALE

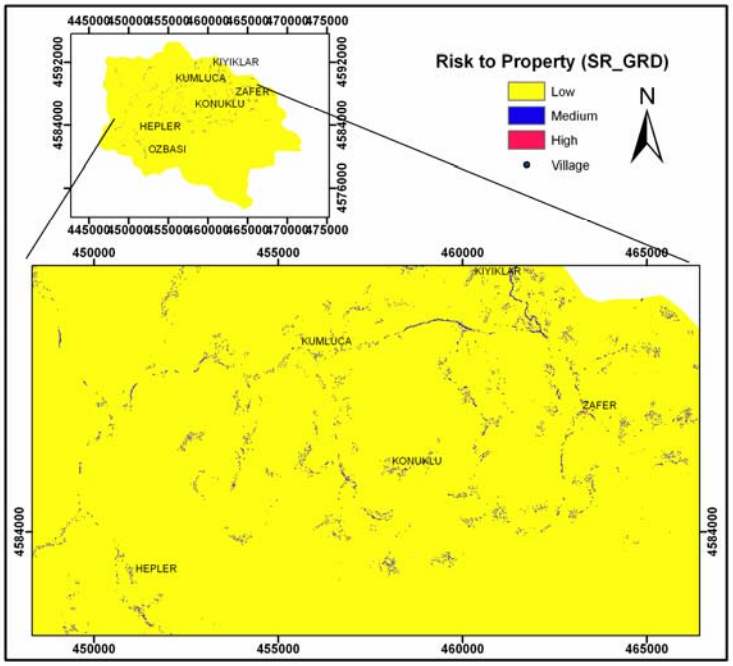

Figure D-1. Risk to property for SR model and grid-based mapping unit (SR_GRD)

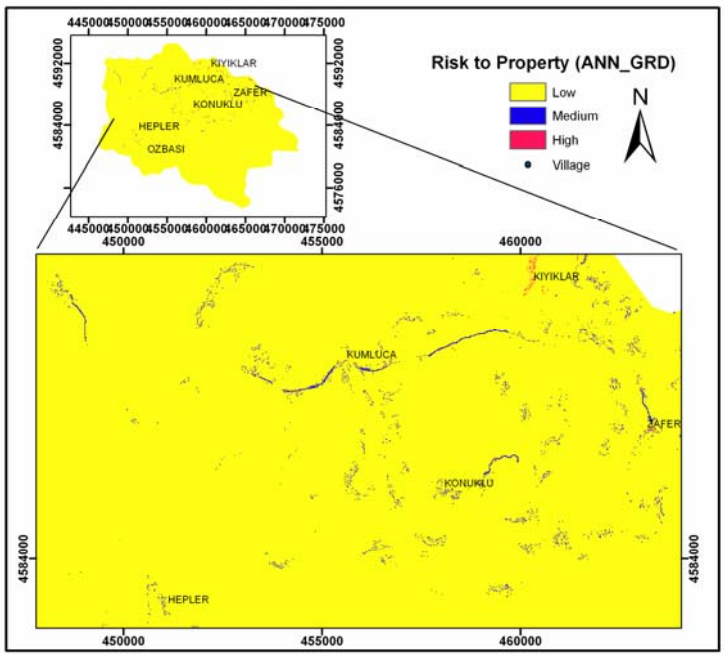

Figure D-2. Risk to property for ANN model and grid-based mapping unit (ANN_GRD)

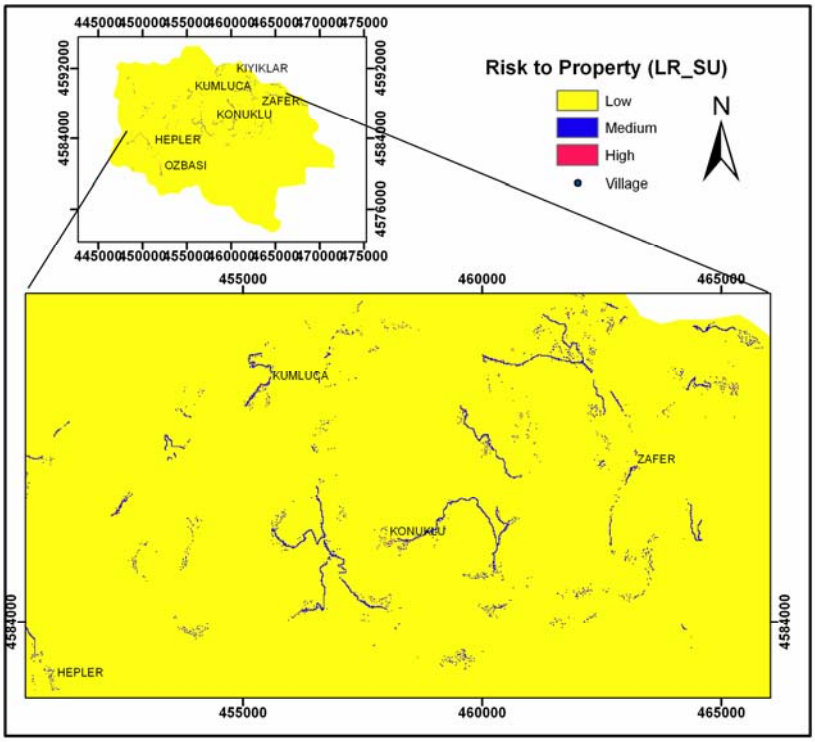

Figure D-3. Risk to property for LR model and slope unit-based mapping unit (LR_SU)

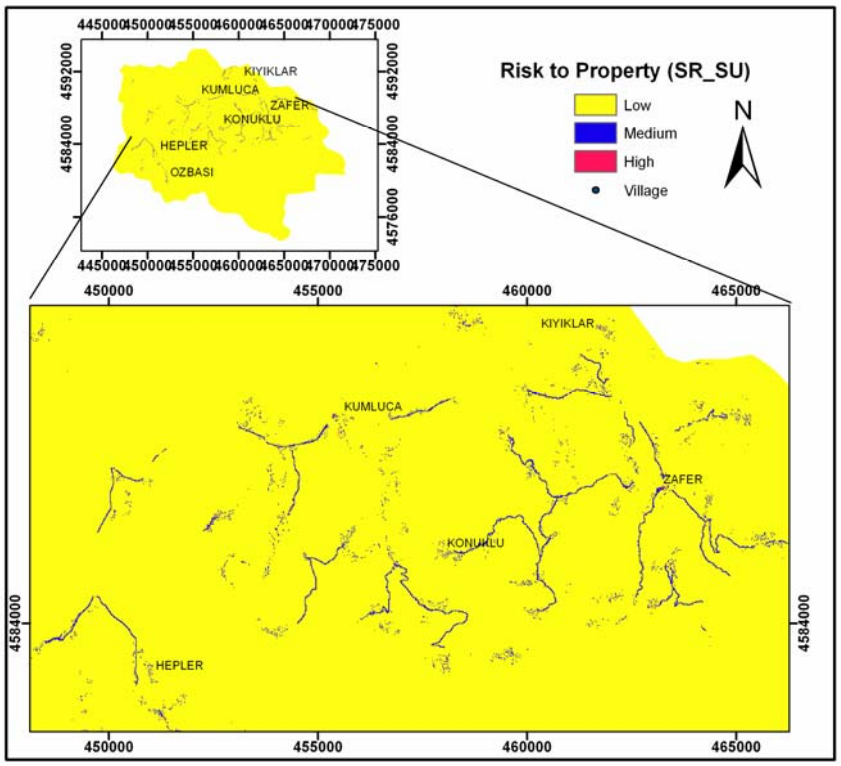

Figure D-4. Risk to property for SR model and slope unit-based mapping unit (SR_SU)

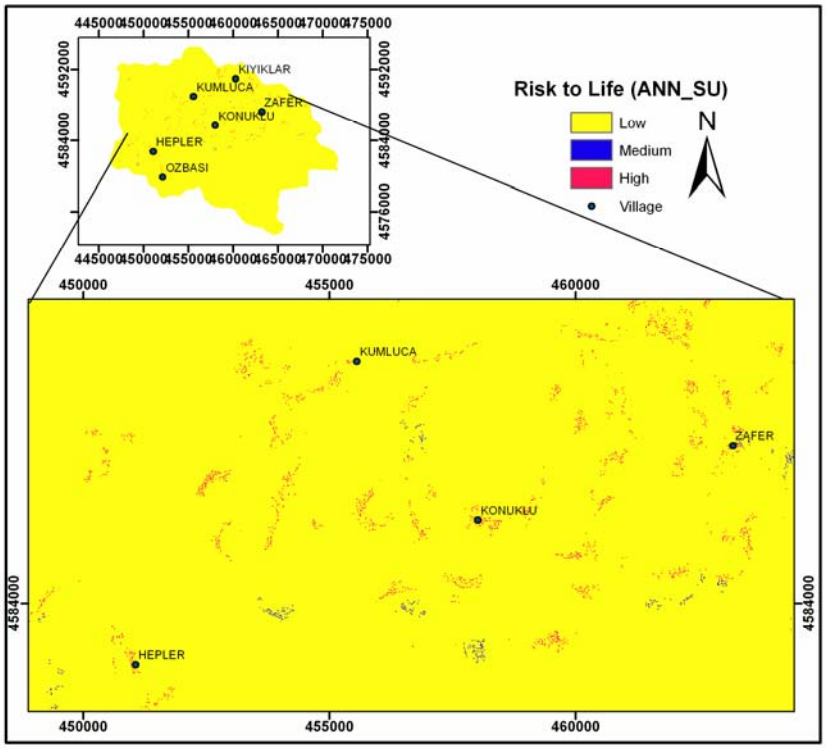

Figure D-5. Risk to property for ANN model and slope unit-based mapping unit (ANN_SU)

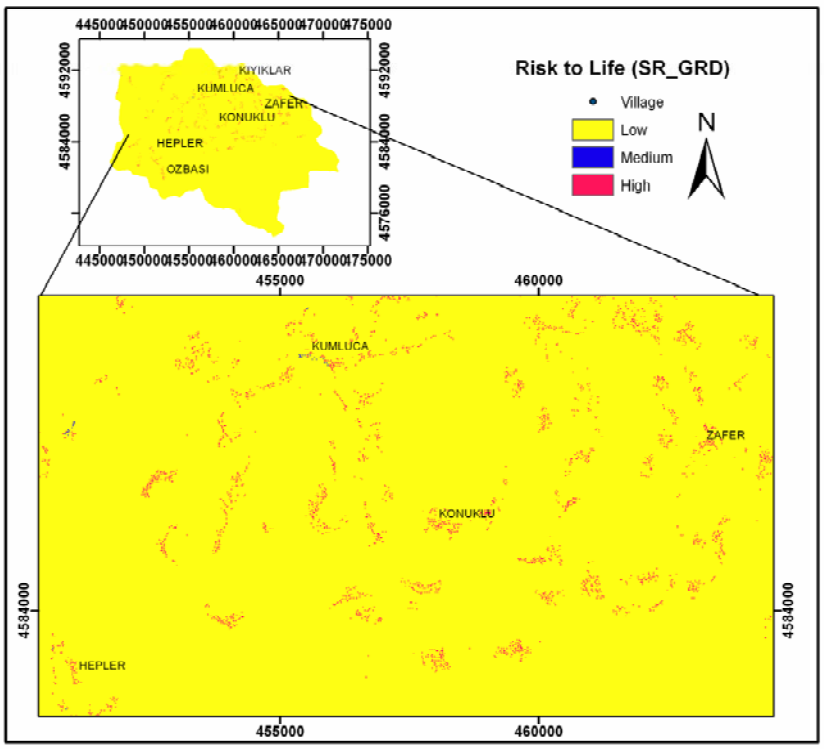

Figure D-6. Risk to life for SR model and grid-based mapping unit (SR_GRD)

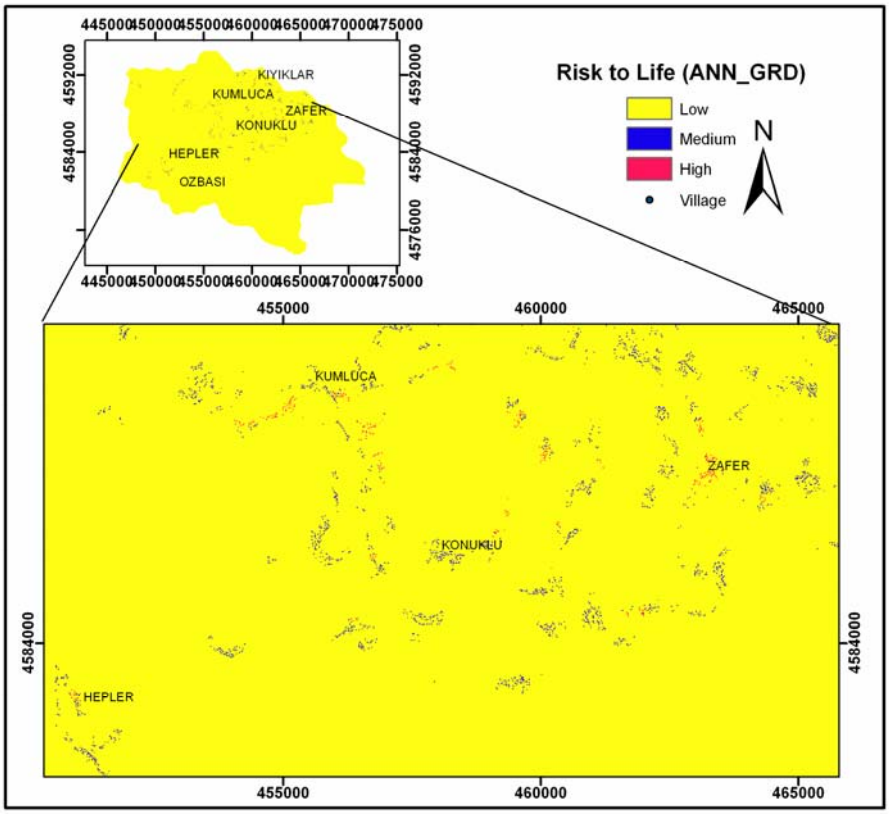

Figure D-7. Risk to life for ANN model and grid-based mapping unit (ANN_GRD)

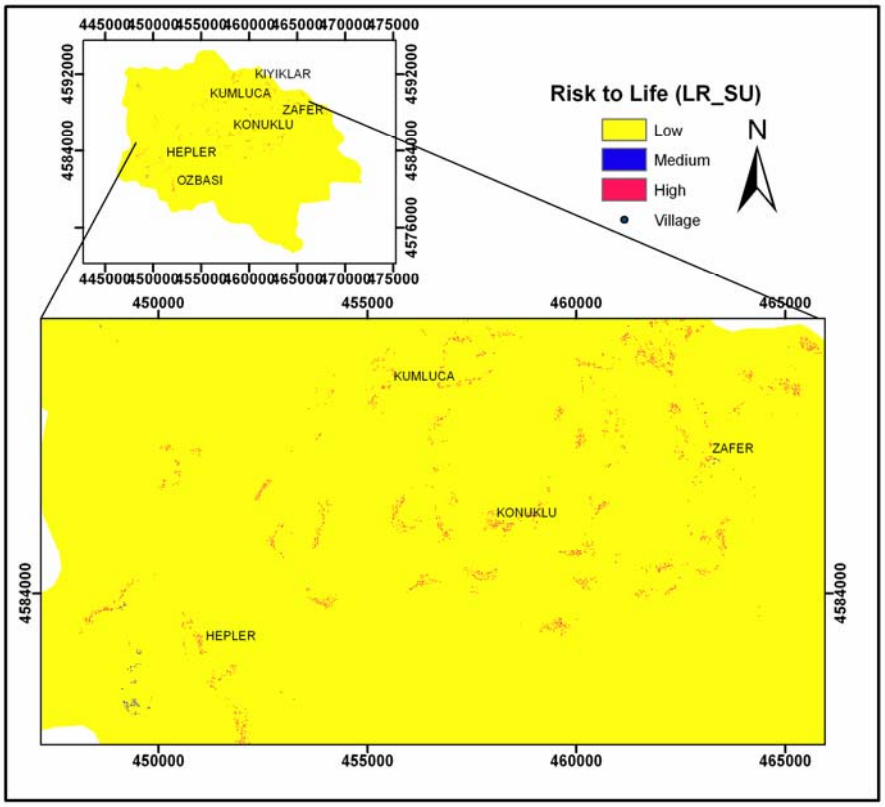

Figure D-8. Risk to life for LR model and slope unit-based mapping unit (LR_SU)

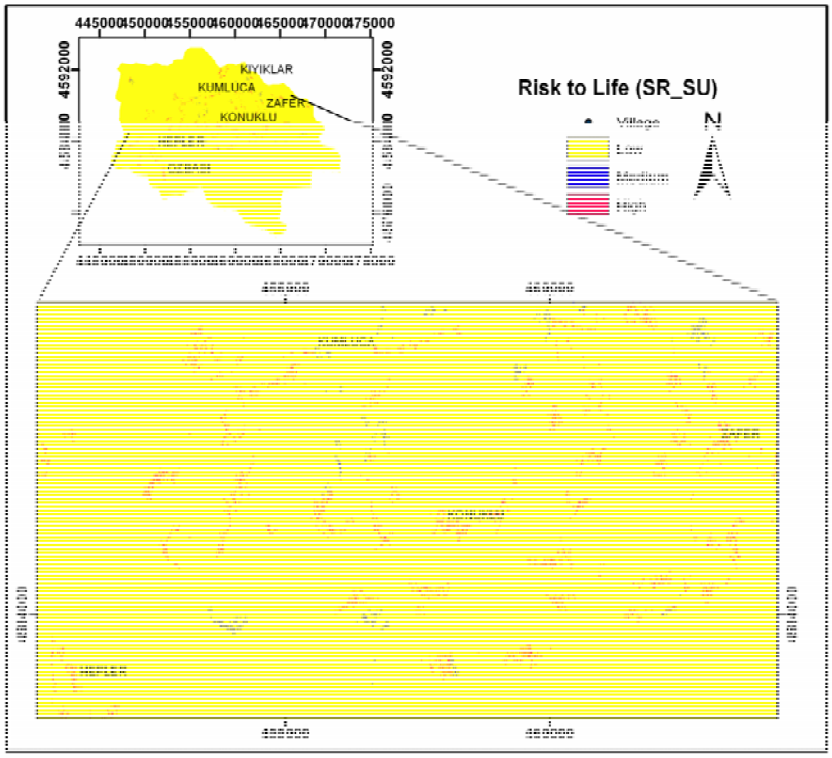

Figure D-9. Risk to life for SR model and slope unit-based mapping unit (SR_SU)

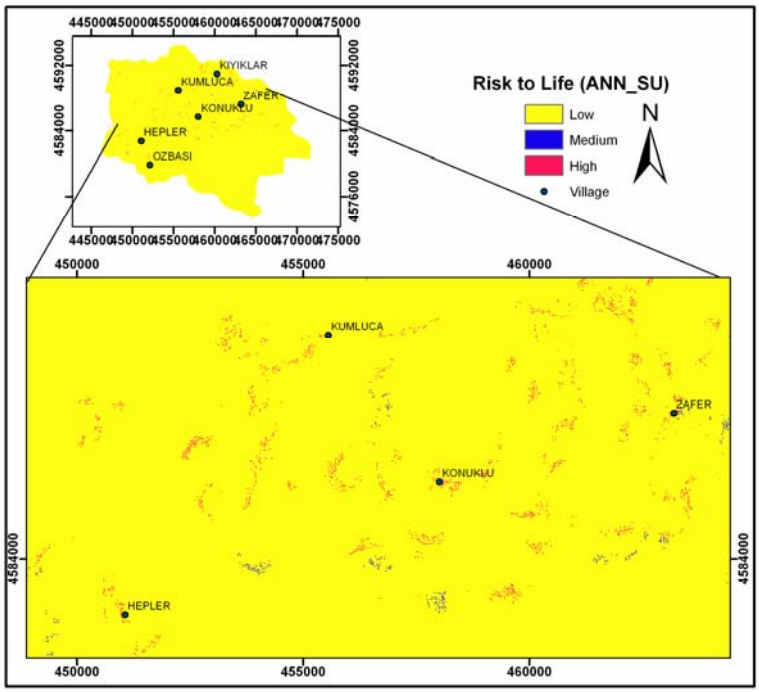

Figure D-10. Risk to life for ANN model and slope unit-based mapping unit (ANN_SU)

APPENDIX E

Table E-1. Overland Flow Manning's n Roughness Value. [1]Adapted from COE, 1997

Surface	n-value
Dense turf	0.17 - 0.80
Bermuda and dense grass, dense vegetation	0.17 - 0.48
Shrubs and forest litter, pasture	0.30 - 0.40
Average grass cover	0.20 - 0.40
Poor grass cover on rough surface	0.20 - 0.30
Short prairie grass	0.10 - 0.20
Sparse vegetation	0.05 - 0.13
Sparse rangeland with debris 0% cover 20 % cover	 0.09 - 0.34 0.05 - 0.25
Plowed or tilled fields Fallow - no residue Conventional tillage Chisel plow Fall disking No till - no residue No till (20 - 40% residue cover) No till (60 - 100% residue cover)	 0.008 - 0.012 0.06 - 0.22 0.06 - 0.16 0.30 - 0.50 0.04 - 0.10 0.07 - 0.17 0.17 - 0.47
Open ground with debris	0.10 - 0.20
Shallow glow on asphalt or concrete (0.25" to 1.0")	0.10 - 0.15
Fallow fields	0.08 - 0.12
Open ground, no debris	0.04 - 0.10
Asphalt or concrete	0.02 - 0.05

RISK MAPS AT LOCAL SCALE for LOSS of PROPERTY

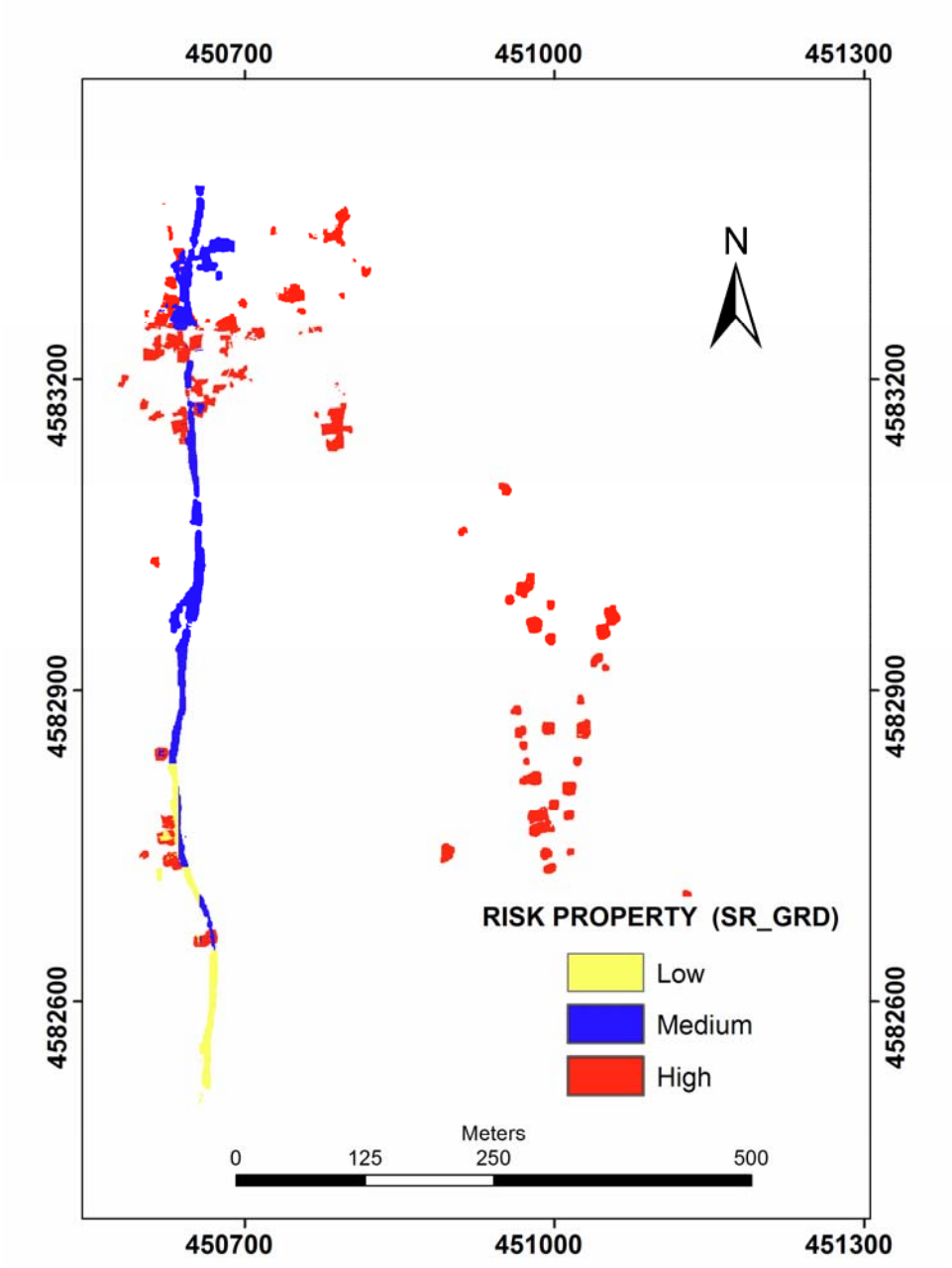

Figure E-1. Risk to property map created based on the SR model at grid-based mapping unit (SR_GRD)

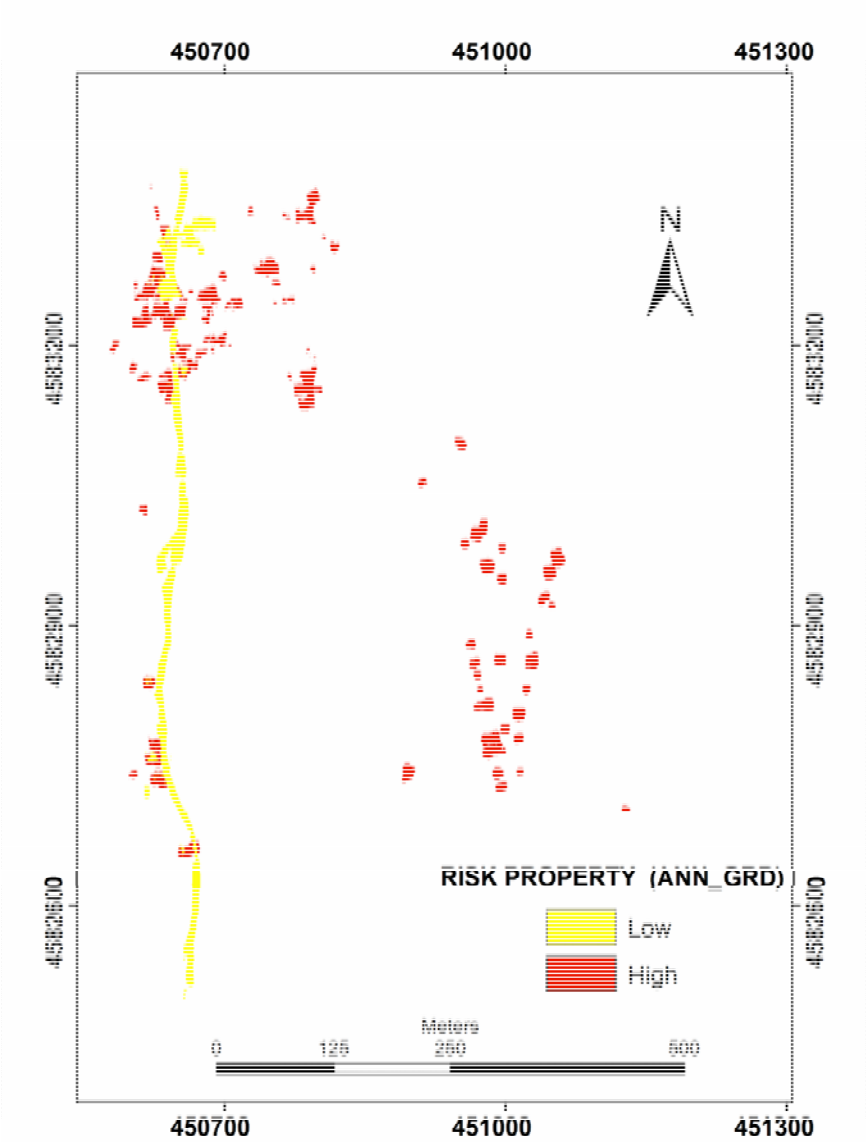

Figure E-2. Risk to property map created based on the ANN model at grid-based mapping unit (ANN_GRD)

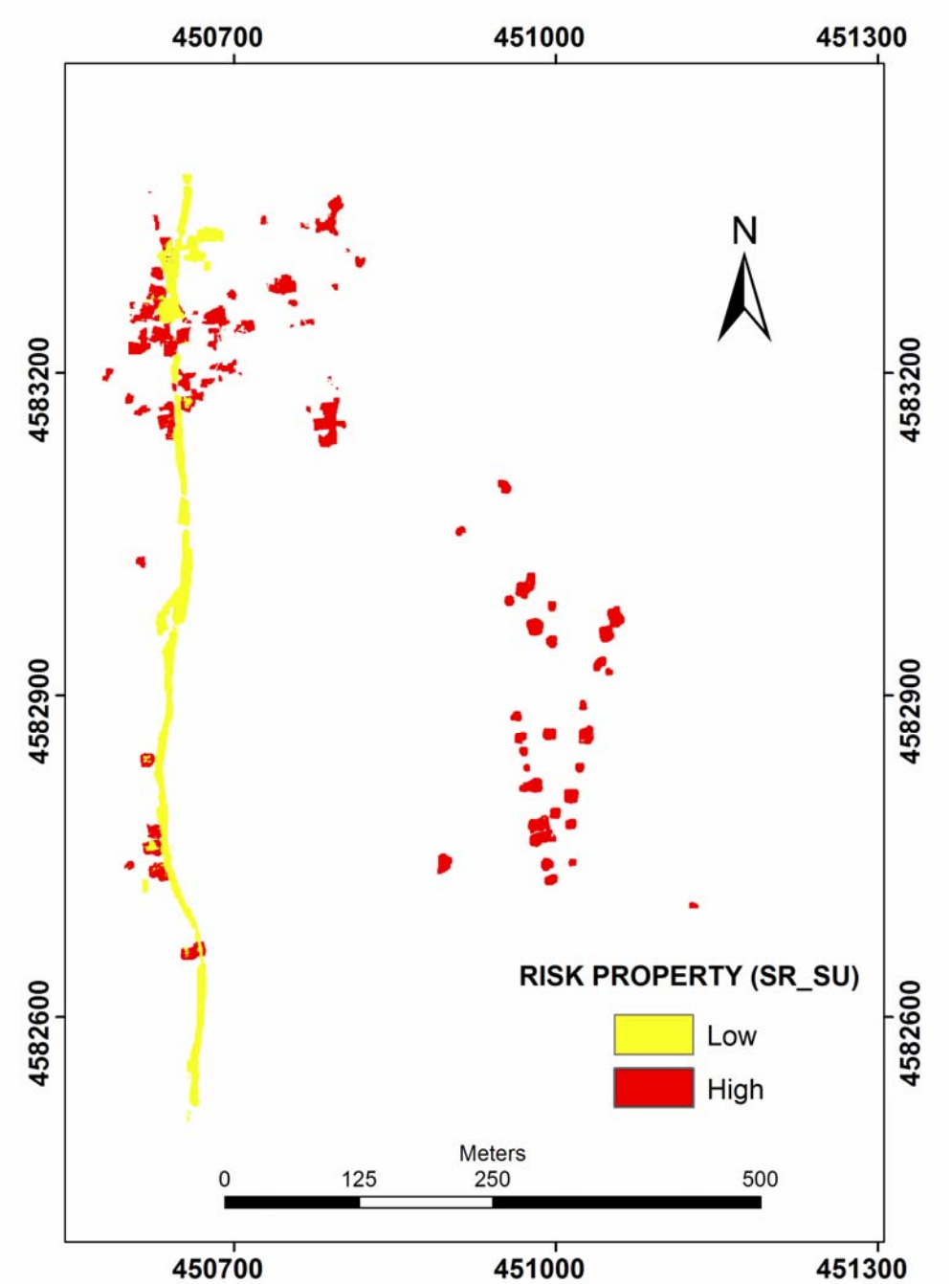

Figure E-3. Risk to property map created based on the SR model at slope unit-based mapping unit (SR_SU)

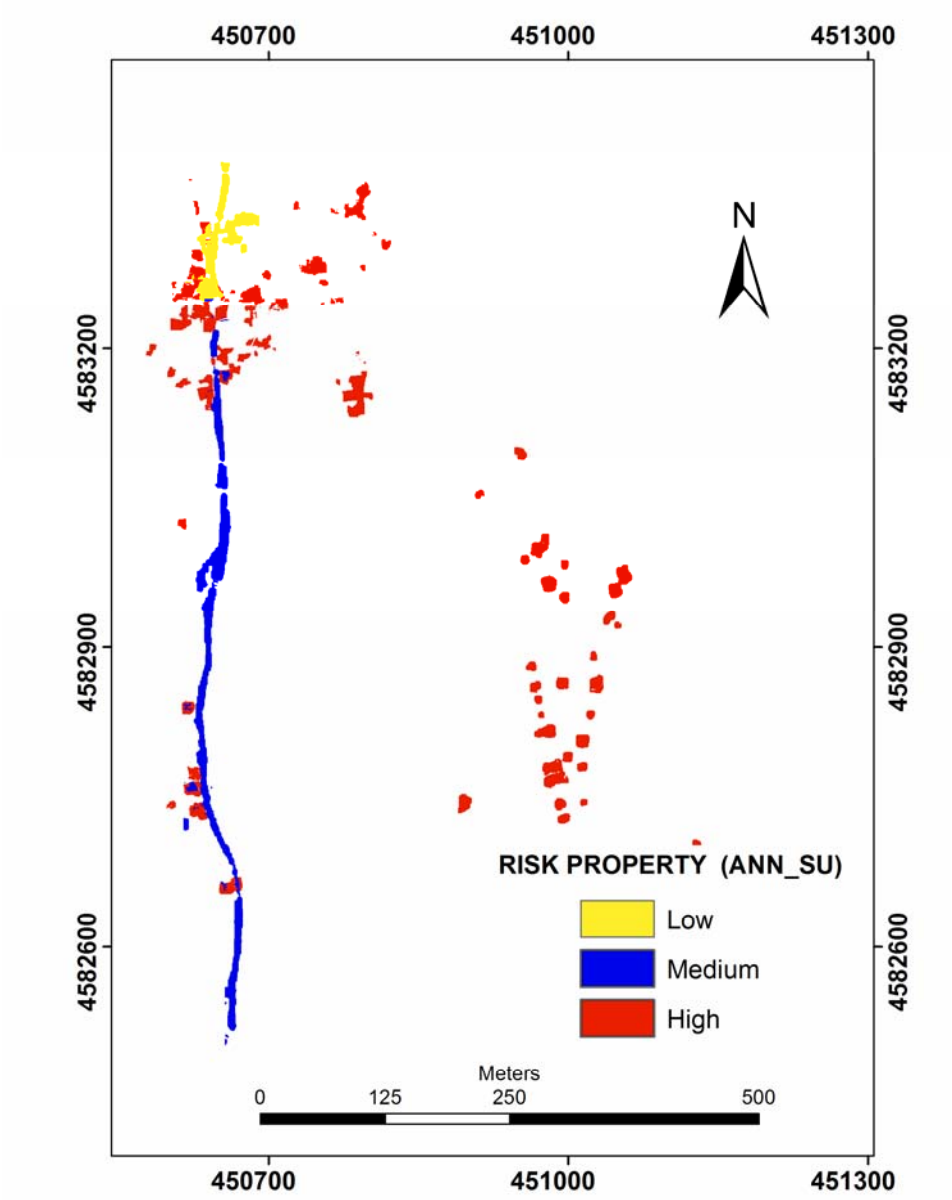

Figure E-4. Risk to property map created based on the ANN model at slope unit-based mapping unit (ANN_SU)

COMPARISON of RISK MAPS AT LOCAL SCALE for LOSS of PROPERTY

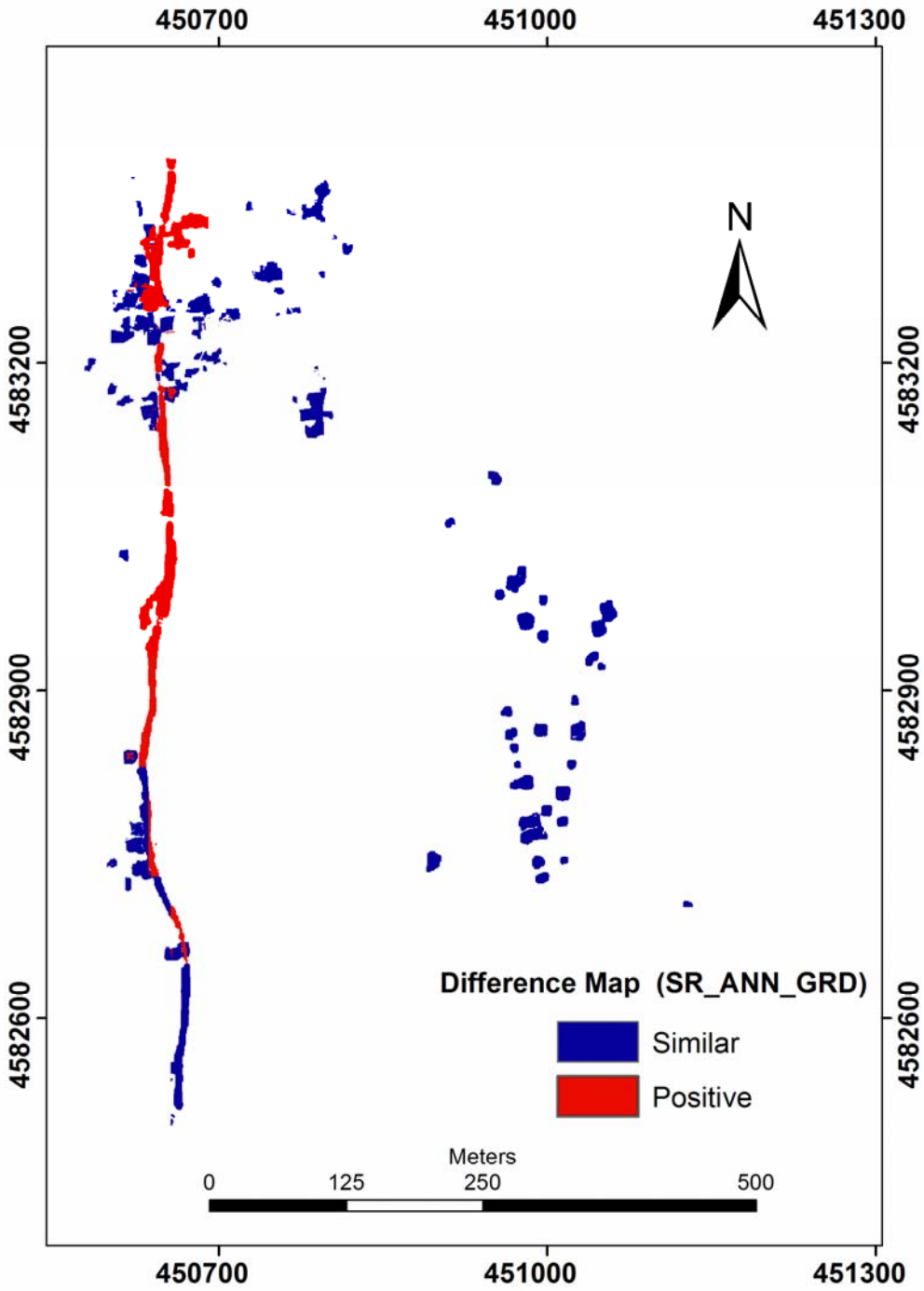

Figure E-5. Difference of risk to property maps between SR and ANN models at grid-based mapping unit (SR_ANN_GRD)

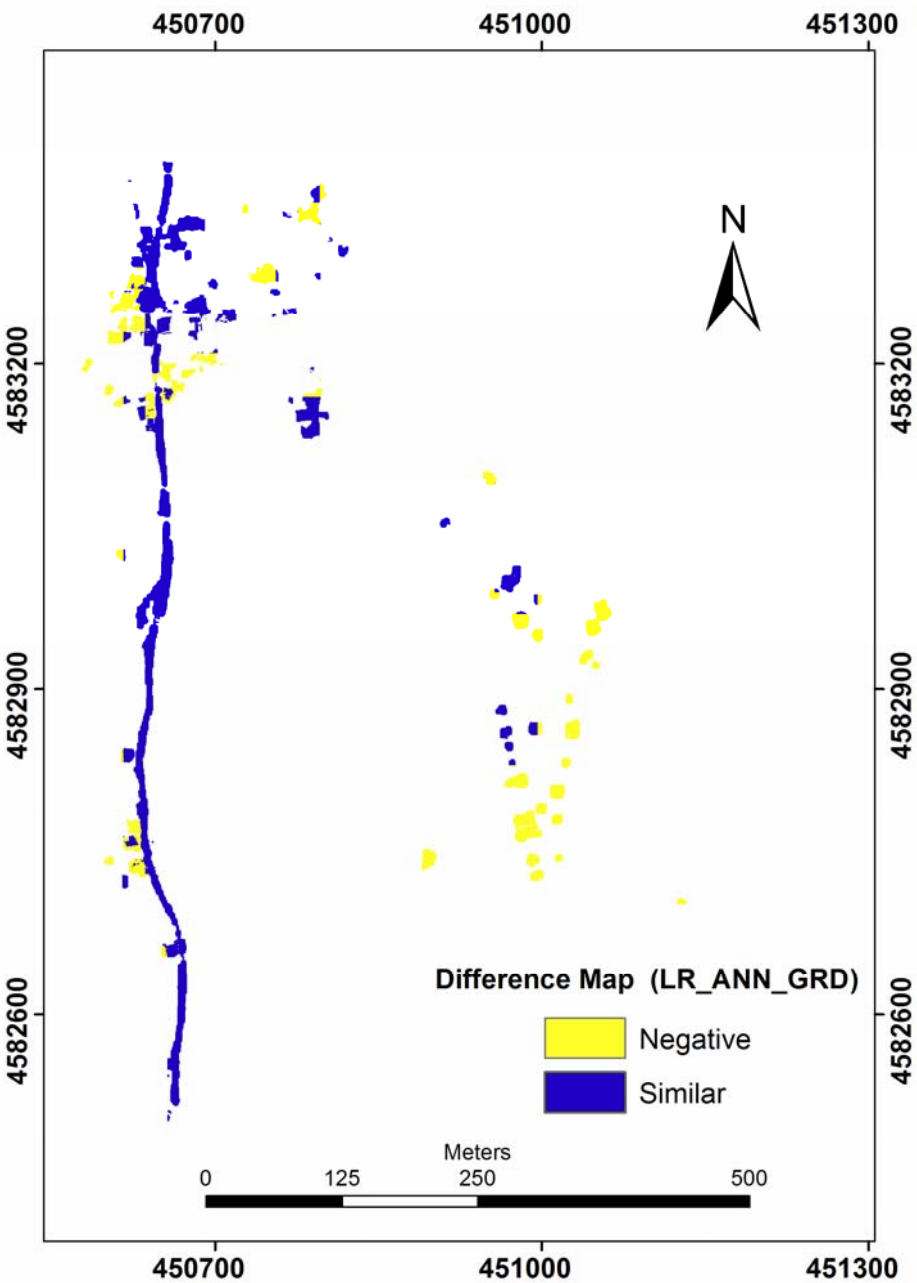

Figure E-6. Difference of risk to property maps between LR and ANN models at grid-based mapping unit (LR_ANN_GRD)

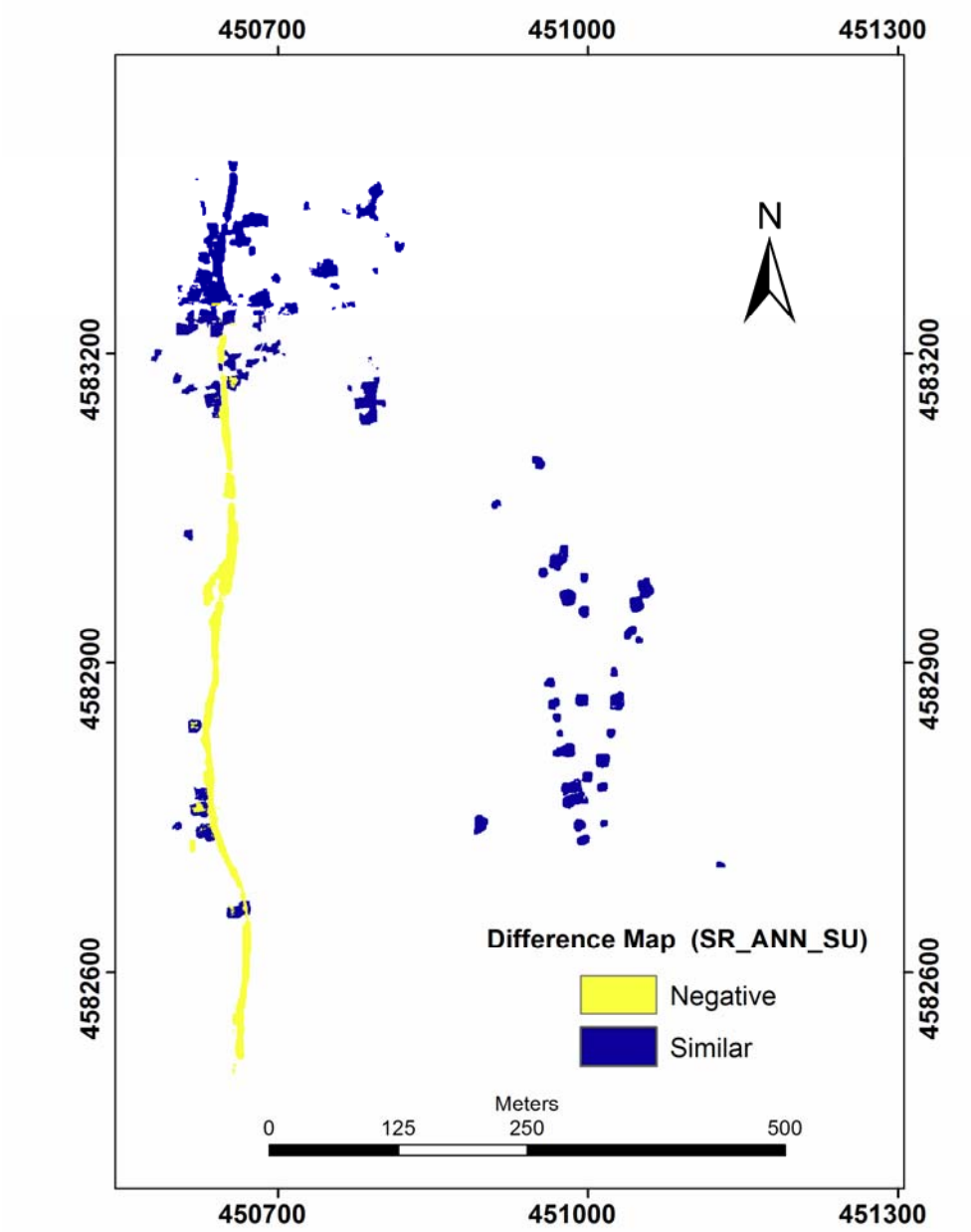

Figure E-7. Difference of risk to property maps between SR and ANN models at slope unit-based mapping unit (SR_ANN_SU)

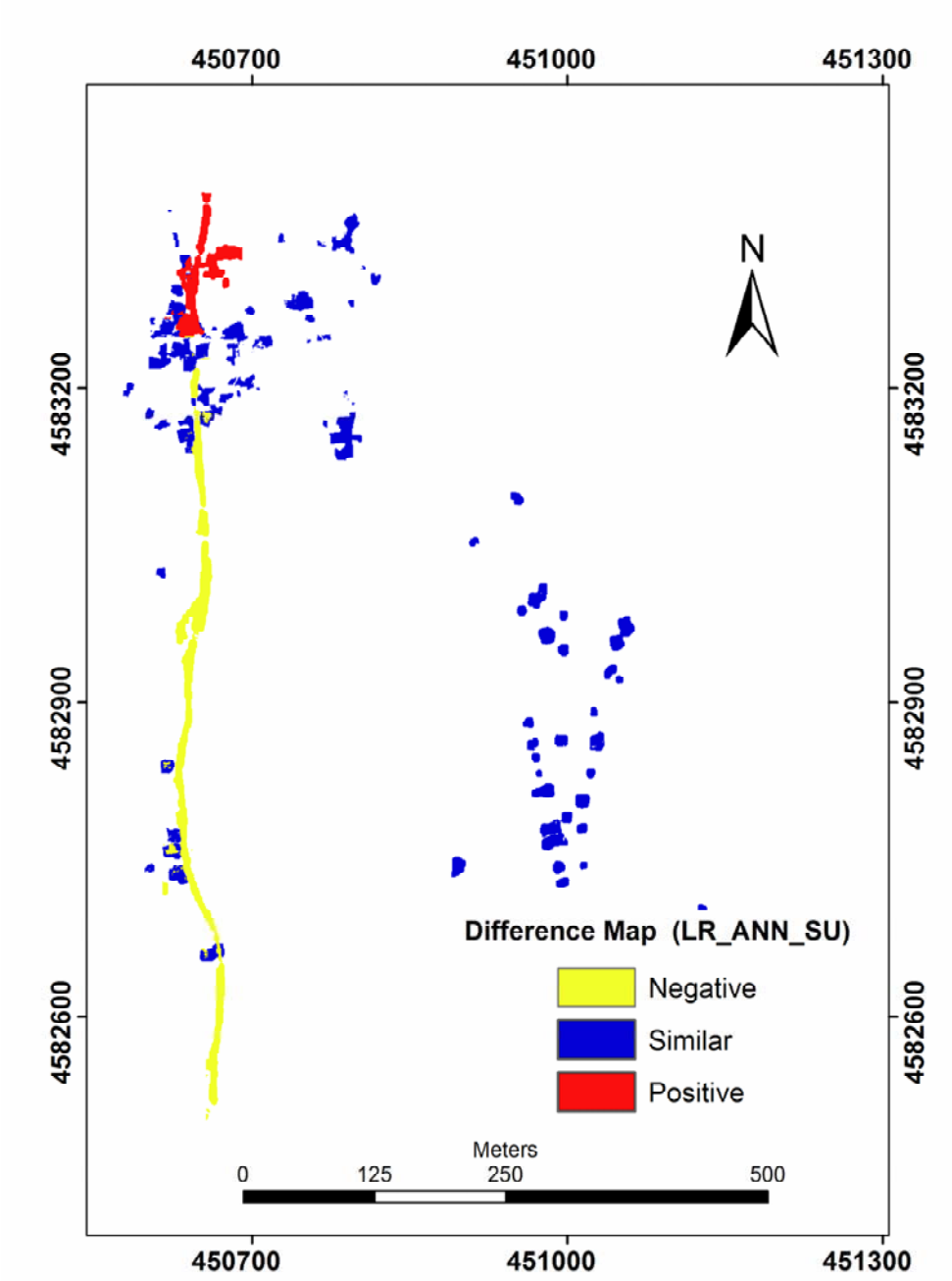

Figure E-8. Difference of risk to property maps between LR and ANN models at slope unit-based mapping unit (LR_ANN_SU)

RISK MAPS AT LOCAL SCALE for LOSS of LIFE

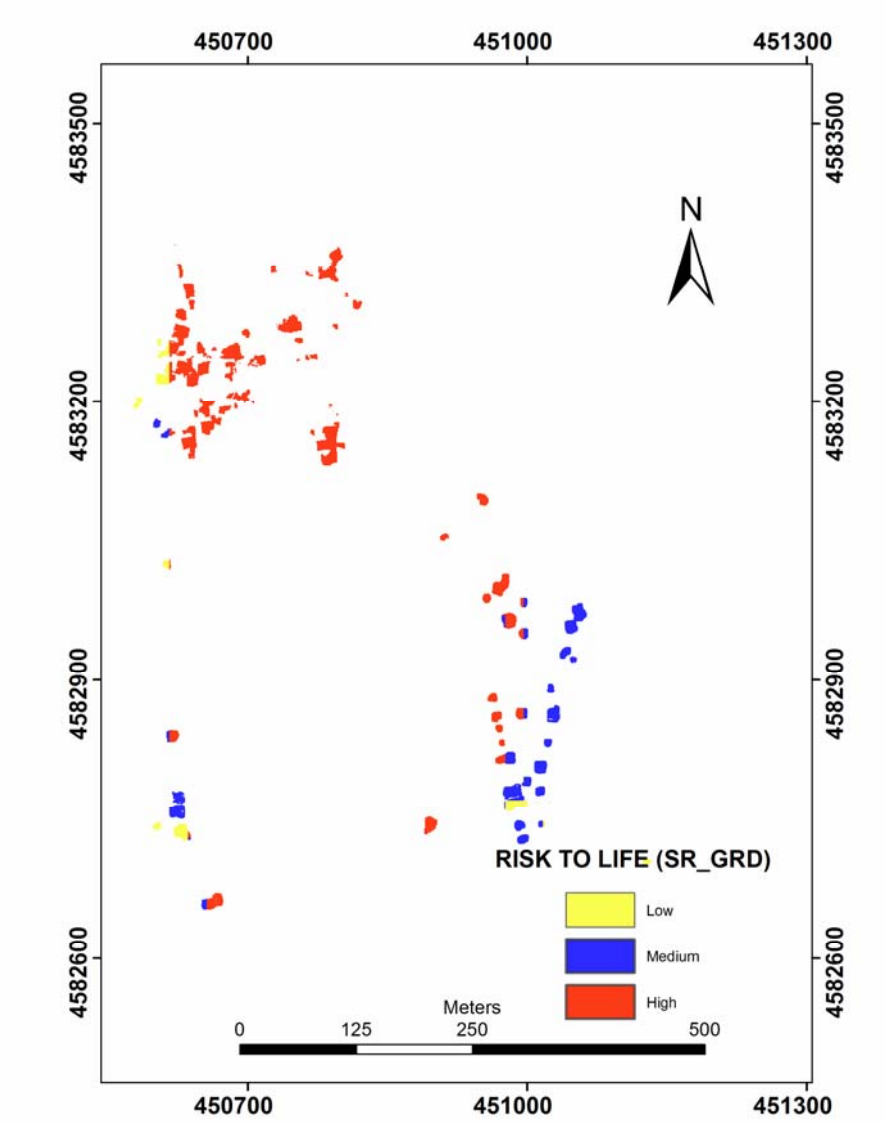

Figure E-9. Risk to life map created based on the SR model at grid-based mapping unit (SR_GRD)

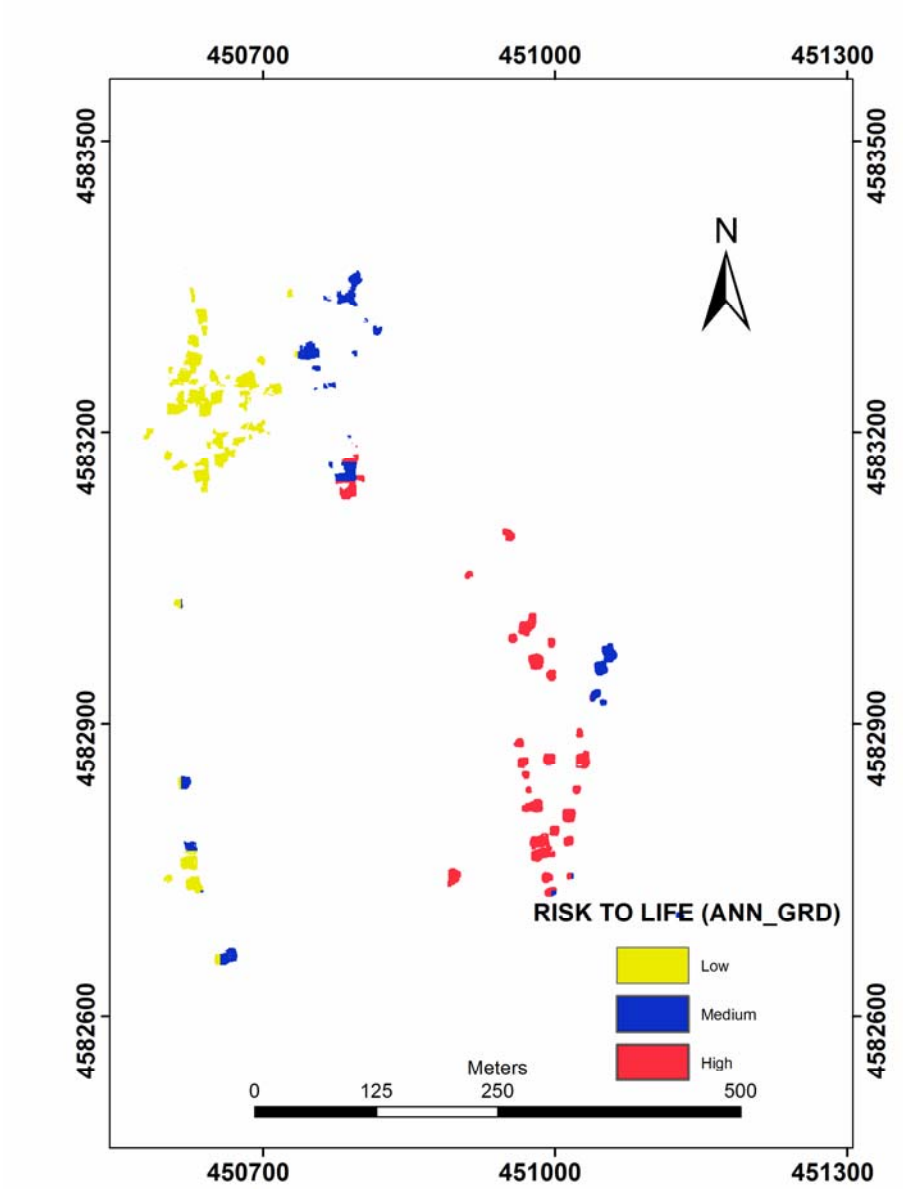

Figure E-10. Risk to life map created based on the ANN model at grid-based mapping unit (ANN_GRD)

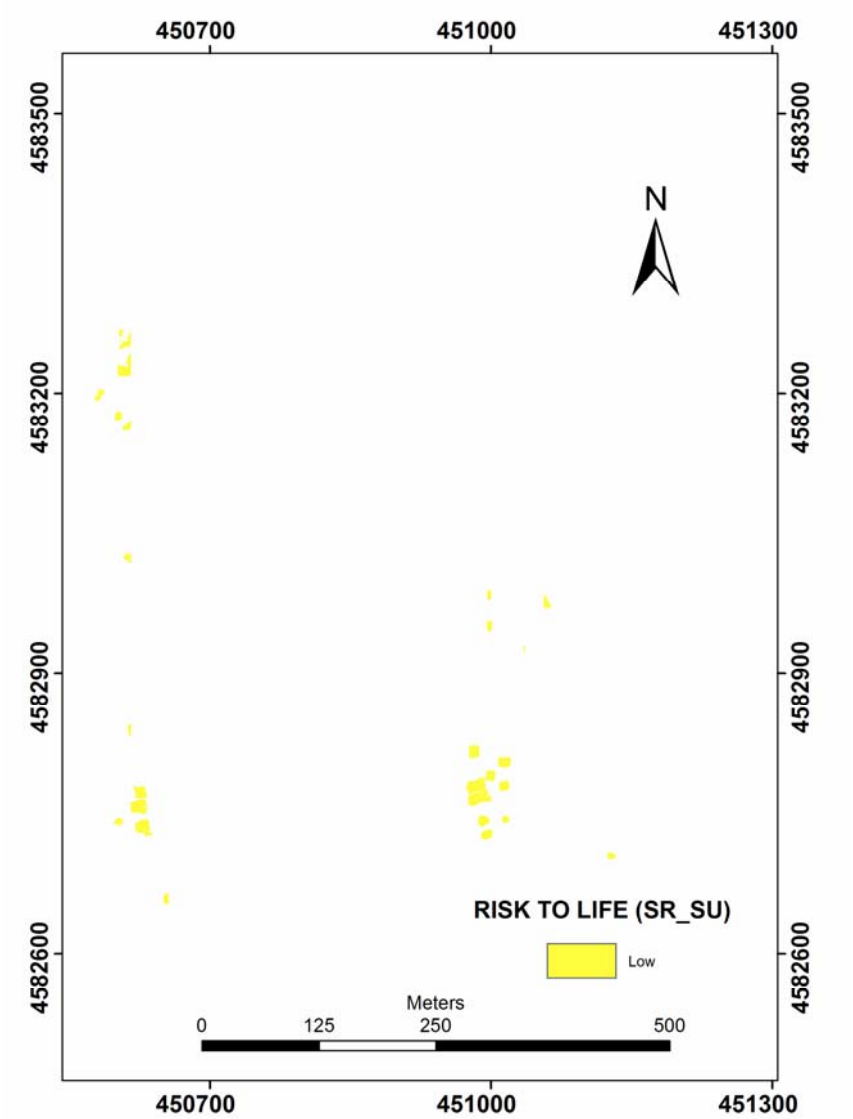

Figure E-11. Risk to life map created based on the SR model at slope unit-based mapping unit (SR_SU)

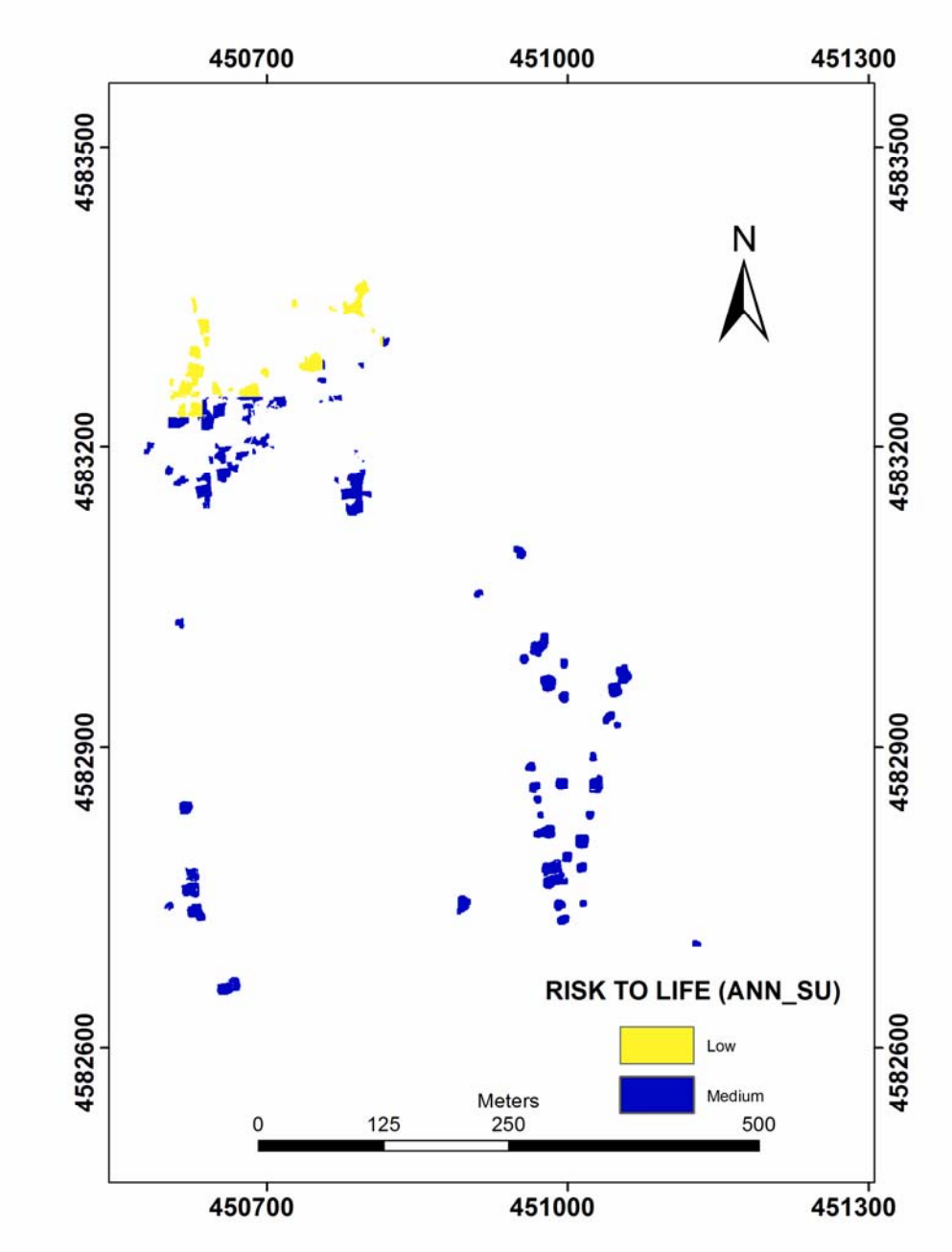

Figure E-12. Risk to life map created based on the ANN model at slope unit-based mapping unit (ANN_SU)

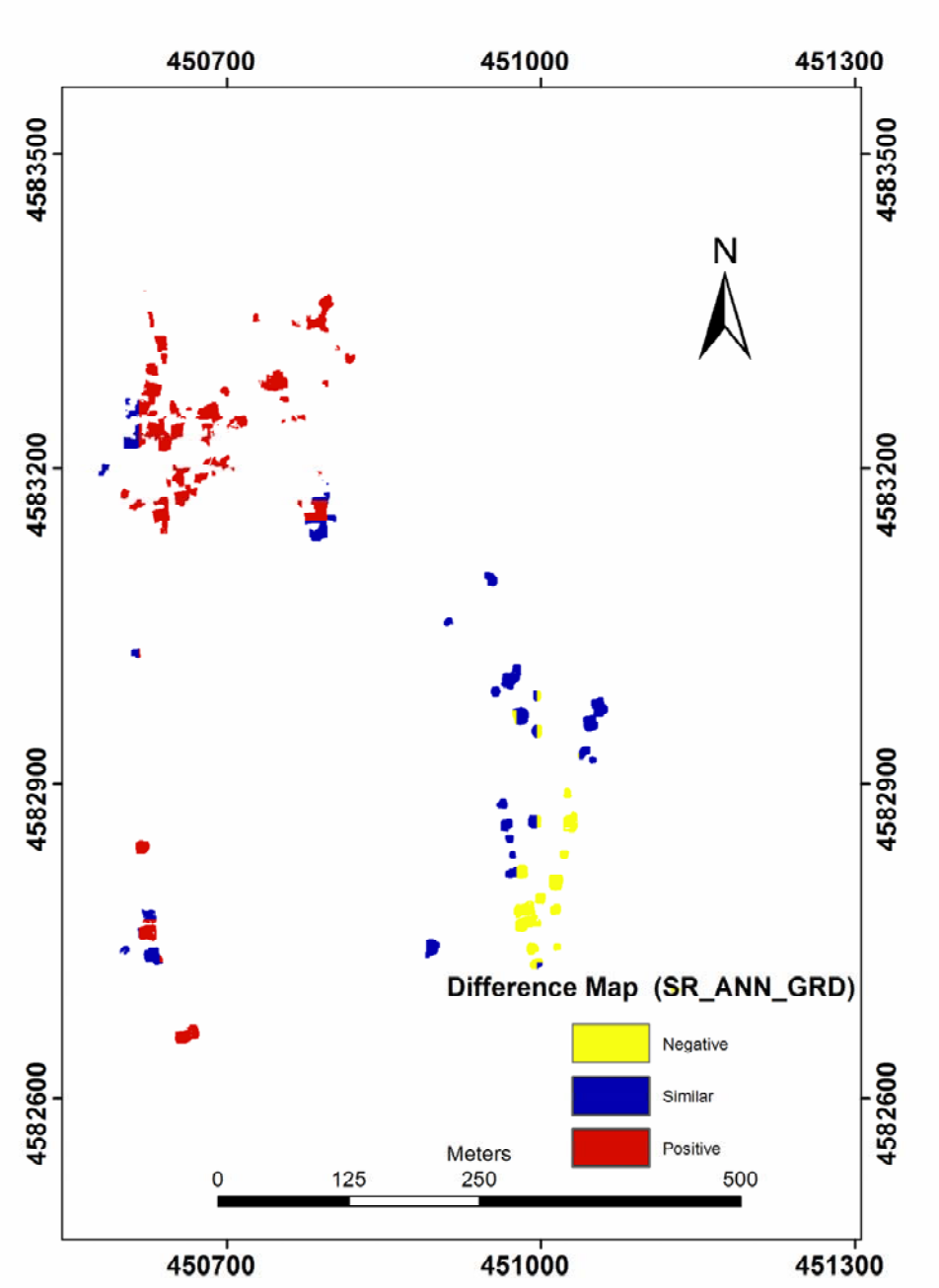

Figure E-13. Difference of risk to life maps between SR and ANN models at grid-based mapping unit (SR_ANN_GRD)

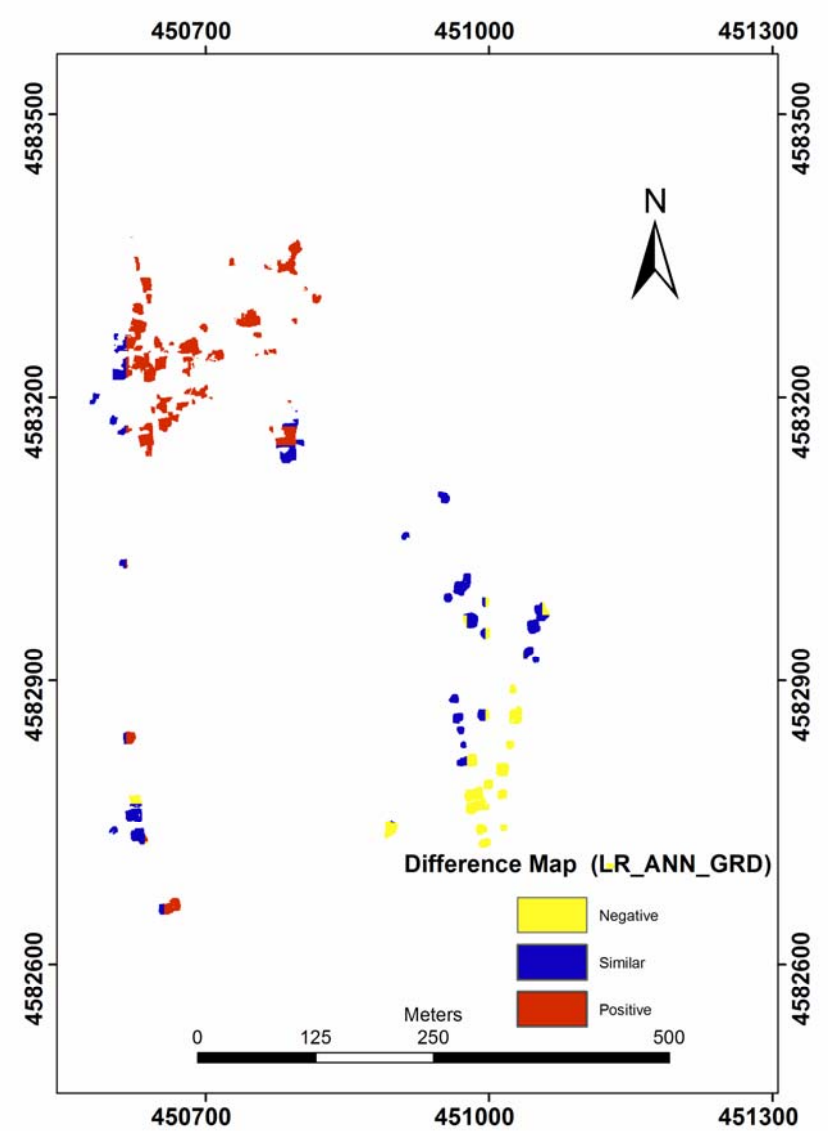

Figure E-14. Difference of risk to life maps between LR and ANN models at grid-based mapping unit (LR_ANN_GRD)

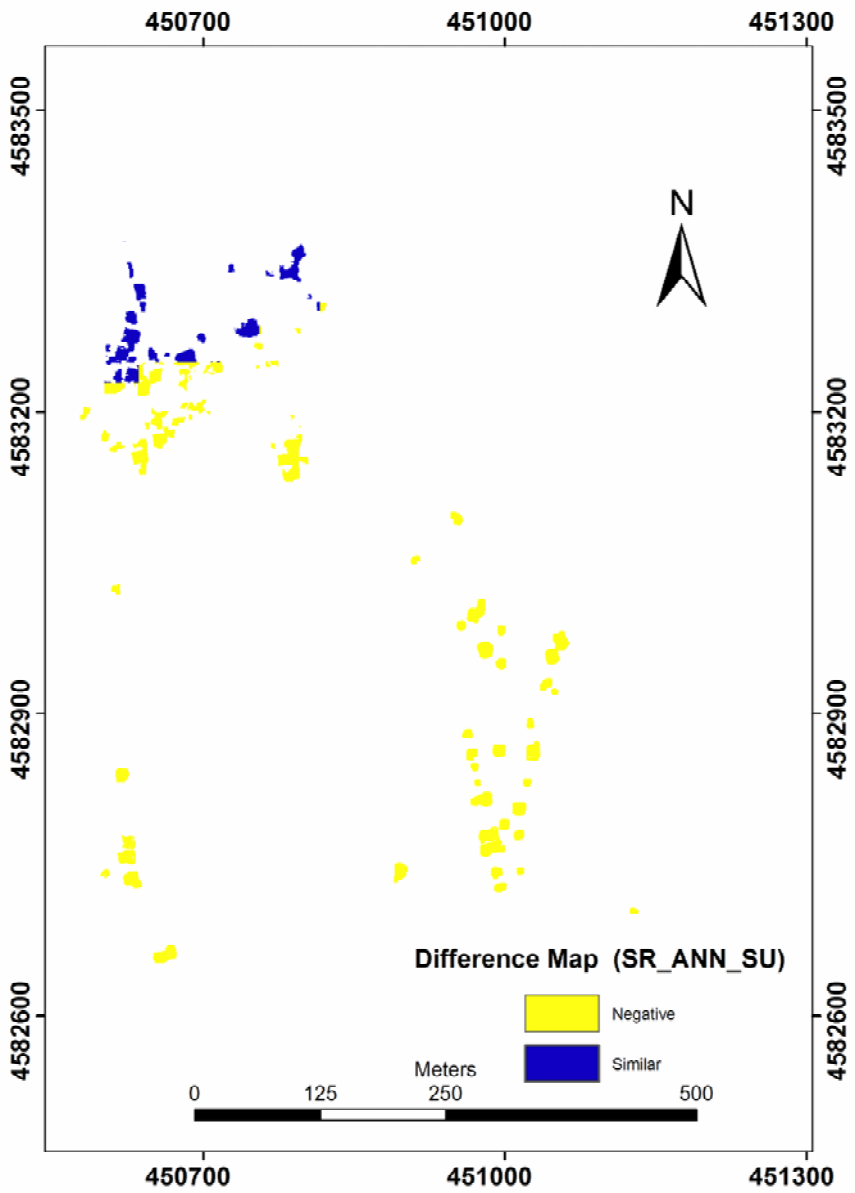

Figure E-15. Difference of risk to life maps between SR and ANN models at slope unit-based mapping unit (SR_ANN_SU)

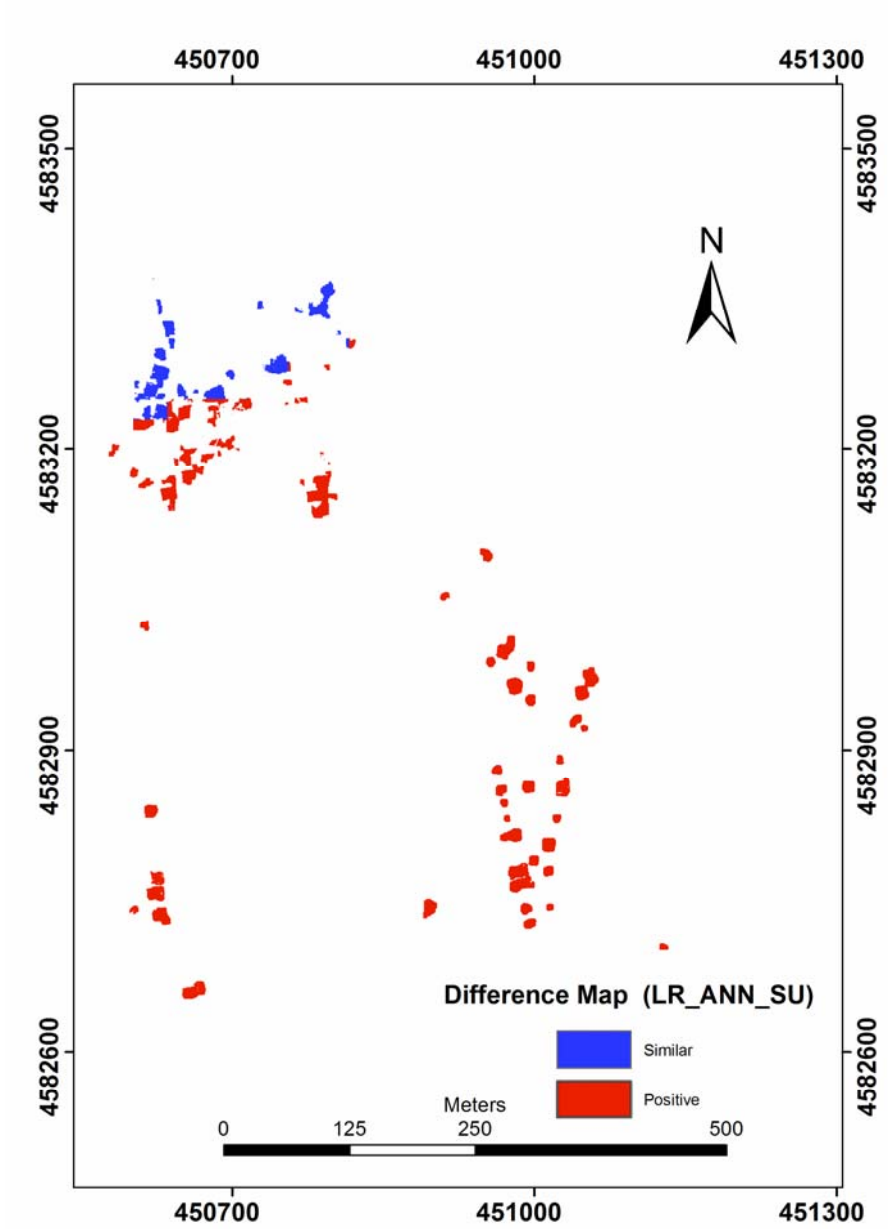

Figure E-16. Difference of risk to life maps between LR and ANN models at slope unit-based mapping unit (LR_ANN_SU)

LIST OF ABBREVIATIONS

ACF	Autocorrelation Function
ANN	Artificial neural networks
ANN_GRD_HAZ	Hazard map obtained by the ANN based susceptibility model for grid-based mapping unit
ANN_GRD_RISK_PROP	Risk maps for property obtained by ANN based susceptibility method for grid-based mapping unit
ANN_GRD_SUSCP	ANN model based susceptibility maps created for grid-based mapping unit
ANN_SU_HAZ	Hazard map obtained by the ANN based susceptibility model for slope unit -based mapping unit
ANN_SU_SUSCP	ANN model based susceptibility maps created for slope unit-based mapping unit
ANN_SU_RISK_PROP	Risk maps for property obtained by ANN based susceptibility method for slope unit -based mapping unit
ANN_SU_RISK_POP	Risk maps for loss of life obtained by ANN based susceptibility method for slope unit-based mapping unit
AR	Autoregressive
ASTER	Advanced Space borne Thermal Emission and Reflection Radiometer
Asp	Aspect
BMNN	Back propagation neural network learning algorithm
C	Consequence
CDR	Central Damage Ratio
CSR	Conditional Spatial Regression
Curv	Curvature
DEM	Digital Elevation Model
DensRoad	Density of Road Network
DensStrm	Density of Stream Network
DisttoFault	Distance to Fault
DisttoRoad	Distance to Road
DisttoStrm	Distance to Stream Network
DTM	Digital Terrain Model
EAR	Elements at risk
Elev	Topographical Elevation
EM-DAT	Emergency Disaster Database
E_{pe}	Number of people in each building
E_ M	Erosion Middle
E_ L	Erosion Less
E_ S	Erosion Severe
E_VS	Erosion Verysevere
FP	False Positive
FN	False Negative
GDDA	General Directorate of Disaster Affair

Geo_ Allv	Alluvial Geological Formation
Geo_ And	Andesite Geological Formation
Geo_ C	Conglomerate Geological Formation
Geo_ M	Marl Geological Formation
Geo_ L	Limestone Geological Formation
Geo_ SM	Sandstone_Mudstone Geological Formation
GPS	Global Positioning System
GIS	Geographic Information Systems
GWR	Geographically Weighted Regression
GWR_GRD_SUSCP	GWR model based susceptibility maps created for grid-based mapping unit
GWR_GRD_SUSCP	GWR model based susceptibility maps created for slope unit-based mapping unit
H	Hazard
HSDT	High Season Day Time
HSNT	High Season Night Time
I	Intensity
ID	Intensity-Duration
InvDEM	Inverse DEM
JTC-1	Joint Technical Committee on Landslides and Engineered Slopes
LR	Logistic Regression
LR_ANN_GRD	The difference between ANN and LR susceptibility model based results for grid-based mapping unit
LR_ANN_SU	The difference between ANN and LR susceptibility model based results for slope unit-based mapping unit
LR_GRD_HAZ	Hazard map obtained by the LR based susceptibility model for grid-based mapping unit
LR_GRD_RISK_PROP	Risk maps for property obtained by LR based susceptibility method for grid-based mapping unit
LR_GRD_SUSCP	LR model based susceptibility maps created for grid-based mapping unit
LR_GRD_RISK_POP	Risk maps for loss of life obtained by LR based susceptibility method for grid-based mapping unit
LR_SU_HAZ	Hazard map obtained by the LR based susceptibility model for slope unit -based mapping unit
LR_SU_RISK_PROP	Risk maps for property obtained by LR based susceptibility method for slope unit-based mapping unit
LR_SU_RISK_POP	Risk maps for loss of life obtained by LR based susceptibility method for slope unit-based mapping unit
LR_SU_SUSCP	ANN model based susceptibility maps created for slope unit-based mapping unit
LSDT	Low Season Day Time
LSNT	Low Season Night Time
LU_ DF	Land Use Dryfarming
LU_ F	Land Use Forest

LU_ RD	Land Use Rock_And_Debris
LU_ RF	Land Use RiverfloodingRegions
LU_S	Land Use Settlement
M	Magnitude
MA	Moving Average
MAP	Mean Annual Precipitation
MDR	Mean Damage Ratio
MF	Missing Factor
MTA	General Directorate of Mineral Research and Exploration
NDVI	Normalized Difference Vegetative Index
PACF	Partial Autocorrelation Function
PCA	Principle Component Analysis
P_f	Probability of failure
Plan_Curv	Plan curvature
Prof_Curv	Profile curvature
P(H)	Annual probability of landslide event
$P_l \mid P_t$	Conditional probability of having a landslide given that rainfall triggers exceed a certain threshold value for a given time period
P(S|H)	Spatial Impact
P_s	Spatial Probability
P_t	Probability of trigger that exceeds a certain threshold
PBD	Percent of feature determination
QP	Quality Percent
RDR	Range of Damage Ratio
RMSE	Root-mean-square error
R(LOL)	Loss of Life
R(LOP)	Loss of Property
ROC	Relative Operating Characteristics
R_S	Risk Specific
R_t	Risk Total
RS	Remote Sensing
S	Scale
SAR	Simultaneous auto regression
SF	Split Factor
SPD	Probability of observing damage state for the given temporal condition
SR	Spatial Regression
SR_LR_GRD,	The difference between SR and LR susceptibility model based results for grid-based mapping unit
SR_ANN_GRD	The difference between SR and ANN susceptibility model based results for grid-based mapping unit
SR_LR_SU	The difference between SR and LR susceptibility model based results for slope-based mapping unit
SR_ANN_SU	The difference between SR and ANN susceptibility Model based results for slope unit-based mapping unit
SR_GRD_HAZ	Hazard map obtained by the SR based susceptibility model for grid-based mapping unit

SR_GRD_RISK_PROP	Risk maps for property obtained by SR based susceptibility method for grid-based mapping unit
SR_GRD_SUSCP	SR model based susceptibility maps created for grid-based mapping unit
SR_GRD_RISK_POP	Risk maps for loss of life obtained by SR based susceptibility method for grid-based mapping unit
SR_SU_RISK_PROP	Risk maps for property obtained by SR based susceptibility method for slope unit-based mapping unit
SR_SU_RISK_POP	Risk maps for loss of life obtained by SR based susceptibility method for slope unit-based mapping unit
SR_SU_HAZ	Hazard map obtained by the SR based susceptibility model for slope unit -based mapping unit
SR_SU_SUSCP	SR model based susceptibility maps created for slope unit-based mapping unit
S_ Allv	Alluvial Soil
S_ BFS	Brown Forest Soil
S_ BFSWL	Brown Forest Soil without lime
S_ Collv	Colluvial Soil
S_ GBPdz	Grey Brown Podzolic Soil
Slp	Slope
SD_ D	Soil Depth Deep
SD_ S	Soil Depth Shallow
SD_ VD	Soil Depth Verydeep
SD_ VS	Soil Depth Veryshallow
TFNW	Trapezoidal fuzzy number weighting
TP	True Positive
TIN	Triangular Irregular Network
TN	True Negative
TÜİK	Turkish Statistical Institute
TWI	Topographic Wetness Index
2-D	Two-dimensional
3-D	Three-dimensional
UTM	Universal Transverse Mercator
V	Vulnerability
Veg	NDVI
V(P|S)	Vulnerability of the property
WLC	Weighted linear combination model
WOL	Worth of Loss
Wtns	Topographic wetness index

CURRICULUM VITAE

PERSONAL INFORMATION

Surname, Name	:	Erener, Arzu
Email	:	erener@metu.edu.tr
Title	:	Research Assistant
Nationality	:	Turk
Date of Birth	:	5 May 1976
Marital Status	:	Married
Address	:	ODTU Ins. Müh. Bol. Su Kaynaklari Lab. K4-123, 06531 Ankara Turkey
Phone	:	+90- 312-2414326 (Home) +90- 312-2105471 (Work) +90- 312-2107956 (Fax)

ACADEMIC QUALIFICATIONS

Degree	Institude	Year of Graduation
Ph.D	METU, Geodetic and Geographic Inf. Tech. Dept.	2002-
MS	KTU, Geodesy and Photogrammetry Eng. Dept.	2000 – 2002
BS	ITU, Geodesy and Photogrammetry Eng. Dept.	1994- 1999

EMPLOYEMENT

Year	Place	Enrollment
2002 -	METU, Geodetic and Geographic Inf. Tech. Dept.	Research Assistant
2000-2002	KTU, Geodesy and Photogrammetry Eng. Dept.	Research Assistant
1998 – 2000	Turkish Airlines	Cabin Assistant

PUBLICATIONS:

National Conferences

1. Gökalp, E. and Erener, A., 2003. "Hidrografik Ölçmelerde GZK (Gerçek Zamanlı Kinematik) GPS Ölçü Yönteminin Kullanımı ve Dalga Etkisinin İncelenmesi", 9. Harita Bilimsel ve Teknik Kurultayı, Ankara, Turkey

2. Erener, A. and Düzgün, HSB., 2007. "Heyelan Analizlerinde Coğrafi Ağırlıklandırılmış Regrasyon (CAR) Metodu", Türkiye Harita Bilimsel ve Teknik Kurultayı (Oral presentation)

3. Erener, A. and Kaynia, A.M., 2007, *"İsveç'te LilleEdet şehrinde CBS kullanılarak Heyelan Duyarlılık Haritalaması Uygulaması"* ",TMMOB Harita ve Kadastro Mühendisleri Odası Ulusal Coğrafi Bilgi Sistemleri Kongresi, KTÜ, Trabzon

4. Erener, A. and Lacasse**,** S., 2007. "Heyelan Duyarlilik Haritalamasi için CBS Kullanımı **",**TMMOB Harita ve Kadastro Mühendisleri Odası Ulusal Coğrafi Bilgi Sistemleri Kongresi, KTÜ, Trabzon (Oral presentation)

5. Sarp, G., and Erener A., 2008. "Litolojik Birimlerin Farklı Sınıflandırma Yöntemleri ile Uydu Görüntülerinden Belirlenmesi" 1.Ulusal Jeolojik Uzaktan Algılama Sempozyumu 22-23 Mayıs. Sivas. (Oral Presentation) (Extended abstract published in PDf form)

6. Erener A., Sarp, G., and Düzgün, HSB., 2008. "Görüntü Sınıfladırmasında Doku (Texture) Parametrelerinin Etkisinin Incelenmesi" UZAL-CBS2008 2. Uzaktan Algılama ve Coğrafi Bilgi Sistemleri Sempozyumu-2008 13-14 Ekim 2008, Kayseri,1. oturum, pp.64 (Oral Presentation) (Full Paper)

7. Erener,A., Sarp, G., and Düzgün HSB., 2008. "Hücre Tabanlı Heyelan Duyarlılık Haritalarının Oluşturulması" TMMOB Harita ve Kadastro Mühendisleri Odası Ankara Şubesi I. CBS Günleri Sempozyumu 2008 19 – 21 Kasım 2008, Ankara. (Oral Presentation) (Full Paper)

8. Sarp, G. and Erener, A., 2008. "Yüksek Çözünürlüklü Uydu Görüntüsünden Binaların Belirlenme Doğruluğunun Artırılması" TMMOB Harita ve Kadastro Mühendisleri Odası Ankara Şubesi I. CBS Günleri Sempozyumu 2008 19 – 21 Kasım 2008, Ankara. (Oral Presentation) (Full Paper)

9. Erener A. and Düzgün, HSB. 2009. Siyah Beyaz Hava Fotoğraflarından Doku Parametreleri Kullanılarak Bilgi Çıkarımı. Türkiye Ulusal Fotogrametri ve Uzaktan Algılaa Birliği V. Teknik Sempozyumu. Fotogrametri ve Uzaktan Algılama Uygulamaları. TUFUAB 2009.4-6 Şubat 2009, syf. 45-48. (Oral Presentation) (Full Paper)

International Conferences

1. Arzu Erener and Ertan Gökalp, 2004 "Mapping the Sea Bottom Using RTK GPS and Lead-Line in Trabzon Harbor, FIG Working Week 2004 Workshop – Hydro, WSH3 – Vertical Reference Frame & Marine Construction/Dredging, Athens, Greece

2. Erener, A. and Düzgün, HSB., 2006. "Comparison of Statistical Landslide Hazard Assessment Methods at Regional Scale" International Disaster Reduction Conference (IDRC), Davos, Switzerland , Vol: 3 (2006), pp.164

3. Erener, A., Lacasse, S., and Kaynia, A.M., 2007. Landslide Hazard Mapping by using GIS in the Lilla Edet province of Sweden, 28th Asian Conference on Remote Sensing ACRS2007, Kuala Lumpur, Malesia. 12 – 16 November 2007 (Oral Presentation)

4. Erener, A. and Lacasse, S., 2007. Landslide Susceptibility Mapping Using GIS, 28th Asian Conference on Remote Sensing ACRS2007, Kuala Lumpur, Malesia. 12 – 16 November 2007

5. Erener, A., Lacasse, S., and Kaynia, A.M., 2007. Hazard Mapping in quick clay area using GIS, Joint CIG / ISPRS Conference, "Geomatics for Disaster and Risk Management", Toronto, Canada

6. Erener, A. and Lacasse, S., 2007. "Landslide Susceptibility Mapping Using GIS" 28th Asian Conference on Remote Sensing ACRS2007 , Kuala Lumpur, Malesia

7. Erener A. and Düzgün HSB., 2008. Analysis of Landslide Hazard Mapping Methods: Regression Models Versus Weight Rating; XXIst ISPRS Congress 2008; 3-11 July. Beijing,China. Commission VIII papers, Vol. 37, Part B8, ISSN 1682-1750

8. Akagündüz E., Erener A., Ulusoy l., Sebnem H. S.B. Düzgün, (2008). Deliniation of Slope Units Based on Scale and Resolution Invariant 3D Curvature Extraction; 2008 IEEE International Geoscience & Remote Sensing Symposium 2008; 6-11 July. Boston, Massachusetts, U.S.A. WE4.107.2: Geospatial Based Analysis.

9. Sarp, G. and Erener A., 2008. "Land Use Detection Comparison From Satellite Images With Different Classification Procedures" XXI ISPRS Congress 3-11 Jul. Beijing, CHINA (Poster Presentation) (Full Paper is published in PDF form)

10. Aytekin, Ö. Erener, A., Ulusoy, İ., and Düzgün, HSB., 2009. Automatic and Unsupervised Building Extraction in Complex Urban Environments from Multi Spectral Satellite Imagery. International Conference on Recent Advances in Space Technologies RAST 2009 11-13 June 2009, İstanbul, TURKEY

11. Erener, A. and Düzgün, HSB., 2009. Prediction of Population in Urban Areas by Using High Resolution Satellite Images. International Conference on Recent Advances in Space Technologies RAST 2009. 11-13 June 2009, İstanbul, TURKEY.

Journal Papers

1. Erener A. and Düzgün H.Ş., 2009. A methodology for land use change detection of high resolution pan images based on texture analysis. Rivista Italiana di Telerilevamento - 2009, 41 (2): 47-59. Italian Journal of Remote Sensing - 2009, 41 (2): 47-59

2. Erener A. and Düzgün HSB. Improvement of Statistical Landslide Susceptibility Mapping by Using Spatial and Global Regression Methods in the case of More and Romsdal (Norway). Landslides. (Accepted, UnderPress)

OTHER EXPERIENCE

Year	Place
2000 May- 2000 September	English Summer Course in Guilford Collage, UK
2006 October - 2007 May	Research Scholarship from Norwegian Geotechnical Institude (NGI)